GEORGIA INSTITUTE OF TECHNOLOGY
OFFICE OF CONTRACT ADMINISTRATION
SPONSORED PROJECT INITIATION

A016

Date: November 29, 1976

Project Title: Partial Support for "Second International Conference on Submillimeter Waves and Their Applications."

Project No: B-479

Project Director: Mr. J. J. Gallagher

Sponsor: U. S. Army Research Office; Research Triangle Park, N. C. 27709

Agreement Period: From 10/15/76 Until 12/31/76

Type Agreement: Purchase Order No. DAAG29-77-M-0016

Amount: $5,000.00 (Fixed Price)

Reports Required: Conference Proceedings

Sponsor Contact Person (s):

Technical Matters

Contractual Matters (thru OCA)

Contracting Officer
U. S. Army Research Office
P. O. Box 12211
Research Triangle Park, N.C. 27709

Defense Priority Rating: None

Assigned to: Electromagnetics Laboratory (School/Laboratory)

COPIES TO:

- Project Director
- Division Chief (EES)
- School/Laboratory Director
- Dean/Director—EES
- Accounting Office
- Procurement Office
- Security Coordinator (OCA)
- Reports Coordinator (OCA) ✓
- Library, Technical Reports Section
- Office of Computing Services
- Director, Physical Plant
- EES Information Office
- Project File (OCA)
- Project Code (GTRI)
- Other

CA-3 (3/76)

GEORGIA INSTITUTE OF TECHNOLOGY
OFFICE OF CONTRACT ADMINISTRATION

SPONSORED PROJECT TERMINATION

Post 69
Acct
OAL - No Prop. Letters

Date: March 18, 1977

Project Title: *Partial Support for "Second International Conference on Submillimeter Waves and their Applications"*

Project No: *B-479*

Project Director: *Mr. J. J. Gallagher*

Sponsor: *U. S. Army Research Office; Research Triangle Park, N.C. 27709*

Effective Termination Date: *31 December 1976 (End Performance Period)*

Clearance of Accounting Charges: *N.A. - Fixed Price*

Grant/Contract Closeout Actions Remaining:

- *x* Final Invoice ~~and Closing Documents~~ *ASAP.*
- _ Final Fiscal Report
- _ Final Report of Inventions
- _ Govt. Property Inventory & Related Certificate
- _ Classified Material Certificate
- _ Other _____

- Project Director provide OCA Reports Coordinator w/two (2) copies Conference Proceedings (Final Report) and transmittal document/letter.

Assigned to: *Electromagnetics Laboratory* (School/Laboratory)

COPIES TO:

- Project Director
- Division Chief (EES)
- School/Laboratory Director
- Dean/Director—EES
- Accounting Office
- Procurement Office
- Security Coordinator (OCA)
- Reports Coordinator (OCA) ✓
- Library, Technical Reports Section
- Office of Computing Services
- Director, Physical Plant
- EES Information Office
- Project File (OCA)
- Project Code (GTRI)
- Other _____

CA—4 (3/76)

SECOND INTERNATIONAL CONFERENCE AND WINTER SCHOOL ON SUBMILLIMETER WAVES AND THEIR APPLICATIONS

DECEMBER 6-11, 1976
Puerto Rico Sheraton Hotel
San Juan, Puerto Rico

CONFERENCE DIGEST

S. Perkowitz, Editor

Sponsored by

IEEE Society on Microwave Theory and Techniques

International Commission for Optics

Optical Society of America

U.S. Army Research Office

with the cooperation of

The Joint IEEE/OSA Council on Quantum Electronics

IEEE CAT NO. 76 CH 1152-8 MTT

FOREWORD

SUBMILLIMETER II

This five-day winter conference in San Juan is a risky experiment. We are trying to cope with the amazing international growth and progress in submillimeter waves and their applications. If we have good weather and not too much rain, we may succeed!

Some effort had to be made to gather together a maximum number of world-wide participants to hear and to evaluate the unmanageable number of claims that have been scattered through the literature. For example, in the case of optically pumped lasers, 500 to 1000 emission lines have been tabulated in the wavelength range between 10 micrometers and several millimeters but no standards of power output have been established. Power output claims have been startling: 250 kilowatts peak power in pulses at wavelengths between 300 micrometers and 1.22 millimeter. The continuous-wave output of optically-pumped "waveguide lasers" is even more valuable for general research purposes so that many delegates will want to know how hundreds of milliwatts of fundamental single-mode CW power can be obtained from these step-tunable sources.

Therefore, one feature of this "experimental" meeting is the Winter School consisting of invited lectures composing six seminars, in all. We are sure that the invited lecturers will provide background and perspective in the major areas. We are also experimenting with some discussion sessions to be held in the morning on Fisherman's Terrace. If these discussion sessions become too large, they will not accomplish the purpose; therefore, please work out any difficulties among yourselves. Do not assume that there is any "management" that would presume to "organize" a discussion among scientists!

But it is in this way that we hope to cover the subjects of grating spectroscopy, interferometry, lasers, detectors, electron beam sources, cosmic, solar and atmospheric physics, propagation, plasma interactions and spectroscopy of solids, liquids, gases and molecules in an orderly, well-organized fashion.

The chaos will become noticeable when we encounter the sessions of contributed papers each evening and on Saturday morning. There are 135 papers arranged into three parallel sessions, usually. It is strongly suggested that you do not try to cope with this situation. You have seen the abstracts in your Preliminary Program several weeks ago. There is enough information in this Digest to help you to choose your favorite topic. There will be more complete papers published in the Proceedings and in other journals. Try, for once, to enjoy yourself and your friends and we shall learn everything soon enough.

FUTURE PLANS

Our first conference, SUBMILLIMETER I, held in Atlanta in June, 1974 was followed by CIRP I, held in Zürich in August, 1975 under the guidance and organization of F.K. Kneubühl. The participation and the quality of contributions exceeded expectations. Therefore, the present meeting, SUBMILLIMETER II, was expanded to five days to include a "winter school" consisting of five sessions of afternoon lectures (and the special Wednesday morning sesssion) in our six principal specialties. The unexpected large number of contributed papers forced us to extend the program into Saturday morning, 11 December, and then to expand again to three parallel sessions, all of which are quite full.

It is important now that both the CIRP and the SUBMILLIMETER series must retain their international participation. This can be done only if we hold our meetings in the winter time to take advantage of very low trans-oceanic air fares and low hotel rates. Also, the meetings must be held alternately on different continents as we have done so far. Therefore, SUBMILLIMETER III and CIRP II will be held in Europe, SUBMILLIMETER IV in San Juan, The Bahamas or Florida (10-15 December 1979) and SUBMILLIMETER V in Europe again in March, 1981.

SUBMILLIMETER III will be held in England, 29 March to 1 April, 1978 under the guidance of George W. Chantry and his colleagues. Its location in Surrey at the University of Guildford is less than 30 minutes southwest of London's Waterloo Station. The European locations of CIRP II and SUBMILLIMETER V have also been chosen and will be announced as soon as Prof. Kneubühl has completed the arrangements for the facilities. Every effort will be made by the North American Committee to make inexpensive trans-Atlantic air fare available. We hope that a large number of North Americans will notice these travel bargains to Europe and participate in these winter meetings. Perhaps a Japanese committee can make a similar effort.

TECHNOLOGY FORECASTING

In the 1974 Foreward, I brashly remarked, "One can easily see that the future offers excellent prospects for those working in submillimeter waves ... we have a prospect for sources of radiation that are better than some of the other regions of the spectrum that are quite fully developed." In this 1976 Foreward, it is appropriate to go on to point out that our next area of rapid growth is in Implementation and Application. It is typical that scientists and engineers put their innovations to work in their own laboratories first and this might be called Implementation.

As you glance through this program, you can visualize that Interferometry, Spectroscopy using laser sources and the Cosmic, Solar and Atmospheric Physics will be coming forth to dominate the Guildford program in 1978. It is certain now that Applications with financial support for submillimeter wave development will follow quickly, with measurements of plasma interactions in Tokamak machines leading the way. Anyone who doubts that we have reached that stage in submillimeter waves must be asked to recall the popular question of the early 1960's, namely, "Well, these optical lasers are very interesting devices but what will you ever use them for?" The answers to a question like that about submillimeter waves will surely begin to appear in the 1978 Guildford program.

We are still in a stage of development where we must build almost all of our own apparatus with the single exception of the excellent commercial Fourier transform Michelson interferometers that are very useful for some measurements. Commercial components are beginning to appear that perform quite reliably and well but some others of these components perform somewhat less effectively than one could expect from one's own laboratory model. This sort of situation delays the development of Implementation and Application because who knows whether to waste the time to build a system or waste the money to buy the system? I can imagine that some of the new faces that will appear at the Guildford conference in 1978 will be looking toward us for the answer to that question. For most major systems, the answer to be given at San Juan is, "Build it yourself".

PROCEEDINGS OF SUBMILLIMETER II

The Proceedings of the Atlanta Conference (June, 1974) were published in the IEEE Transactions on Microwave Theory and Techniques as they will again for this San Juan Conference. The Proceedings are being expanded, however, by publishing some of the optics-oriented papers in the Journal of the Optical Society of America and the IEEE Journal of Quantum Electronics. To some extent the authors and referees have a choice of journal but, clearly, not all can publish in one journal. It is economically impossible for one journal to publish 500 pages of a proceedings because the cost is well over $100 per page, the page charges covering no more than half this actual cost. As the forthcoming conference organizations progress, additional effort will be given to the plans for publication of the Proceedings. Perhaps we can get a financial grant. Somehow, we hope to become established with one journal. Nevertheless, we shall always use the type of scholarly journal which is collected and bound by most libraries so that these papers can be properly referenced, abstracted, indexed and located.

ACKNOWLEDGMENTS

We are grateful to our friends in the IEEE Microwave Theory and Techniques Society and the Optical Society of America who have encouraged the organization of this series of conferences on far infrared and submillimeter waves. We are also very pleased to acknowledge the support of the U.S. Army Research Office through Robert Lontz. We wish particularly to thank Anthony J. DeMaria and Bruce W. Steiner (OSA Technical Council), G.P. Rodrigue and Lawrence R. Whicker (IEEE-MTT Administrative Committee), Jarus W. Quinn and Jon Hagan (OSA), Don Parker (Editor, IEEE-MTT Transactions), J.N. Howard and P.R. Wakeling (Applied Optics), A.G. Fox and P.D. Coleman (IEEE Quantum Electronics Council) and D.C. Sinclair (Editor, JOSA). We also are greatly indebted to those many individuals who performed the arduous task of referee in selecting the manuscripts to be acceptable to the Proceedings publications. It is a pity that they must remain unidentified.

Kenneth J. Button
Program Chairman

SECOND INTERNATIONAL CONFERENCE ON
SUBMILLIMETER WAVES AND THEIR
APPLICATIONS

CONFERENCE COMMITTEE

General Chairman:
James J. Gallagher
Georgia Institute of Technology

Program Chairman:
Kenneth J. Button
Massachusetts Institute of Technology

Executive Secretary:
J. W. Dees
Georgia Institute of Technology

Treasurer:
R. G. Shackelford
Georgia Institute of Technology

Publications Chairman:
S. Perkowitz
Emory University

Conference Secretary:
Susan Harden

International Advisory Committee

G. W. Chantry, NPL, Teddington
L. Genzel, Stuttgart
A. Hadni, Nancy
F. Kneubuhl, ETH, Zurich
G. Landwehr, Wurzburg
W. Low, Jerusalem
D. H. Martin, Queen Mary College, London
A. M. Prokhorov, Moscow
K. Shimoda, Tokyo
H. Yoshinaga, Osaka

North American Advisory Committee

K. M. Evensen, NBS, Boulder
T. Hartwick, Los Angeles
D. P. Hutchinson, Oak Ridge
R. Lontz, Army Research Office, Durham
F. W. Quelle, ONR, Boston
G. P. Rodrigue, Atlanta
S. P. Schlesinger, Columbia Univ., New York
P. E. Tannenwald, Lincoln Lab., Lexington
L. R. Whicker, NRL, Washington

Program Committee

T. J. Bridges, BTL, Holmdel
P. D. Coleman, Illinois Univ., Urbana
V. L. Granatstein, NRL, Washington
E. D. Palik, NRL, Washington
S. Perkowitz, Emory Univ., Atlanta
P. L. Richards, U. Calif., Berkeley
E. A. Vinogradov, Lebedev, Moscow

TECHNICAL PROGRAM

SECOND INTERNATIONAL CONFERENCE ON SUBMILLIMETER WAVES AND THEIR APPLICATIONS

Puerto Rico Sheraton Hotel, San Juan, Puerto Rico

MONDAY AFTERNOON, DECEMBER 6, 1976
1300 -1620 Hours

ANNOUNCEMENTS
WELCOMING REMARKS

REVIEW OF SUBMILLIMETER WAVE RESEARCH
(Invited Lectures) North Ballroom
Presider: E. D. Palik

THE RUBENS' ERA
E. D. Palik, Naval Research Lab., Washington, D.C.

THE GRATING ERA, 1930 to 1960
N. Ginsburg, Syracuse Univ., Syracuse,NY

HISTORY OF FAR IR AND SUBMILLIMETER RESEARCH, 1950 TO PRESENT INTERFEROMETRY
L. Genzel, Max-Planck-Institute, Stuttgart, GFR

CRITIQUE OF PRESENT AND FUTURE PROBLEMS IN THE FAR INFRARED
P. D. Coleman, U. of Illinois, Urbana, IL

MONDAY EVENING, 1915 Hours

Session M-1: Fourier Transform Interferometry
Riolama Room
Presider: D. H. Martin

M-1-1 19:15 PROGRESS IN FOURIER SPECTROMETRY: A REVIEW OF PRESENT ACHIEVEMENT AND FUTURE POSSIBILITIES (Invited)
D. H. Martin, Queen Mary College, London, UK

M-1-2 19:35 DOUBLE BEAM FOURIER SPECTROSCOPY WITH INTERFEROMETRIC BACKGROUND COMPENSATION
L. Genzel, Max-Planck-Institut, Stuttgart, GFR

M-1-3 19:55 PRECISE DIELECTRIC MEASUREMENTS OF LOW LOSS MATERIALS AT MILLIMETER AND SUBMILLIMETER WAVELENGTHS
M. N. Afsar & G. W. Chantry, National Physical Laboratory, Teddington, UK

M-1-4 20:15 POLARIZED TWO-BEAM INTERFEROMETRY: REVIEW AND ASSESSMENT
D. H. Martin, E. Puplett, B. Carli and R. Hughes, Queen Mary College, London, UK

M-1-5 20:35 DISPERSIVE FOURIER TRANSFORM SPECTROMETRY WITH VARIABLE THICKNESS, VARIABLE TEMPERATURE LIQUID CELLS
M. N. Afsar, National Physical Lab., Teddington, UK, D. D. Honijk and W. F. Passchier, Rijksuniversiteit Leiden, The Netherlands, and J. Goulon, Universite de Nancy, France

M-1-6 20:55 MEASUREMENTS OF THE OPTICAL CONSTANTS OF LIQUID H_2O AND D_2O UP TO 450 cm^{-1}
M. N. Afsar & J. B. Hasted, National Physical Lab., Teddington, and Univ. of London, UK

Session M-2: Lasers
Surf Room
Presider: F. W. Quelle

M-2-1 19:15 TRANSVERSELY EXCITED FAR-INFRARED WAVEGUIDE LASERS
Ch. Sturzenegger, B. Adam & F. Kneubuhl, ETH Zurich, Switzerland

M-2-2 19:35 INCREASE IN THE OPTICAL PUMPING EFFICIENCY OF A TEA CO_2 LASER BY LONGITUDINAL MODE CONTROL
P. Mathieu & J. R. Izatt, Universite Laval, Quebec, Canada

M-2-3 19:55 TUNABLE DIODE LASER SPECTROSCOPY
H. Flicker, N. Nereson & J. P. Aldridge, Los Alamos Scientific Lab., NM

M-2-4 20:15 APPLICATION OF SUBMILLIMETER WAVE TECHNIQUES TO ISOTOPE SEPARATION
R. W. McMillan, R. G. Shackelford & J. J. Gallagher, Georgia Tech, Atlanta, GA

M-2-5 20:35 TIME RESOLVED COLLISION FREQUENCY MEASUREMENTS IN HIGH PRESSURE GLOW DISCHARGES
T. V. George, L. J. Denes & L. E. Kline, Westinghouse Research Labs., Pittsburgh, PA

M-2-6 20:55 THE ROLE OF FIR EMISSION IN AN OPTICALLY PUMPED MULTI-LINE NH_3 LASER
S. M. Fry, Hughes Labs., Malibu, CA

M-2-7 21:15 DEVELOPMENT OF A SUBMILLIMETER BROADBAND TUNABLE SOURCE
R. Bonnefoy, ESTEC, Noordwijk, The Netherlands, and G. Kantorowicz and P. Palluel, Thomson-CSF, Velizy-Villacoublay, France

Session M-3: Optically Pumped Lasers
Carnival Room
Presider: K. M. Evenson

M-3-1 19:15 THE USES OF OPTICALLY PUMPED SUBMILLIMETER LASERS FOR ABSOLUTE FREQUENCY MEASUREMENTS AND LASER MAGNETIC RESONANCE SPECTROSCOPY (Invited)
K. M. Evenson, D. A. Jennings, J. J. Jiminez & J. A. Mucha, National Bureau of Standards, Boulder, CO

M-3-2 19:35 HIGH POWER OPERATION AND SCALING BEHAVIOR OF CW OPTICALLY PUMPED FIR WAVEGUIDE LASERS
D. T. Hodges, F. B. Foote & R. D. Reel, Aerospace Corp., Los Angeles, CA

M-3-3 19:55 INTERNAL CAVITY, OPTICALLY PUMPED MOLECULAR LASER
H. R. Fetterman, MIT, Cambridge, & H. R. Schlossberg, RADC, Hanscom AFB, MA

M-3-4 20:15 CO_2 - FIR LASERS WITH COMMON RESONATOR
G. A. Koepf, NASA Goddard Center, Greenbelt, MD

M-3-5 20:35 FREQUENCY MEASUREMENT OF 496μm CH_3F FIR LASER LINE
F. Strumia, Univ. of Colorado, Boulder, CO, R. Benedetti, M. Inguscio, P. Minguzzi, M. Tonnelli, E. Bava, A. Demarchi & A. Godone, IEN, Torino, Italy

M-3-6 20:55 DESIGN CRITERIA FOR FIR WAVEGUIDE LASERS
G. A. Koepf and N. McAvoy, NASA Goddard Center, Greenbelt, MD

M-3-7 21:15 ASSIGNMENTS OF THE HIGH POWER OPTICALLY PUMPED CW LASER LINES OF CH_3OH
E. J. Danielewicz, Jr. & P. D. Coleman, Univ. of Illinois, Urbana, IL

M-3-8 21:35 ASSIGNMENT OF FIR LASER LINES IN OPTICALLY PUMPED CH_3OH
J. O. Henningsen, Univ of Copenhagen, Denmark

M-3-9 21:55 IDENTIFICATION OF METHYL HALIDE SUBMILLIMETER LASER PUMP LINES
J. M. Martin & W. T. Smith, Martin Marietta Corp., Orlando, FL

TUESDAY MORNING, 0940 Hours

FORMAL DISCUSSIONS

Tu-D1 SCHOTTKY BARRIER DIODES
Fisherman's Court
G. T. Wrixon, Univ. College, Cork, Ireland (Discussion Leader)

Tu-D2 INTERFEROMETRY FOR PLASMA DENSITY MEASUREMENTS
Fisherman's Court
D. Veron, Centre d'Etudes Nucleaires, Fontenay-aux-Roses, France (Discussion Leader)

Tu-D3 SIGNAL PROCESSING EQUIPMENT AND TECHNIQUES FOR LOW LEVEL DETECTION
Fisherman's Court
L. G. Rubin, MIT, Cambridge, MA (Discussion Leader)

TUESDAY AFTERNOON, 1300 to 1620 Hours

LASERS AND DETECTORS
(Invited Lectures) North Ballroom
Presider: H. Yoshinaga

OPTICALLY PUMPED WAVEGUIDE LASERS
M. Yamanaka, Osaka Univ., Japan

WAVEGUIDES FOR SUB-MM LASERS
F. K. Kneubuhl, ETH Zurich, Switzerland

SCHOTTKY BARRIER DIODES FOR SUBMILLIMETER HETERODYNE DETECTION
B. J. Clifton, Lincoln Lab., Lexington, MA

RATE EQUATIONS AND THEORY OF OPTICALLY-PUMPED SUBMILLIMETER LASERS
R. J. Temkin, MIT National Magnet Lab., Cambridge, MA

TUESDAY EVENING, 1915 Hours

Session Tu-1: Components
Riolama Room

Tu-1-1 19:15 NARROWBANDPASS FILTERS FOR THE FAR INFRARED (Invited)
G. D. Holah & N. D. Morrison, Heriot-Watt Univ., Edinburgh, Scotland

Tu-1-2 19:35 THEORY OF AN EFFICIENT ELECTRONIC PHASE SHIFTER EMPLOYING MULTI-LAYER DIELECTRIC WAVEGUIDE STRUCTURE
A. B. Buckman, Univ. of Texas, Austin, TX

Tu-1-3 19:55 SWITCHES AND MODULATORS EMPLOYING FRUSTRATED TOTAL INTERNAL REFLECTION
R. R. Selleck, E. W. McDonald & J. C. Wiltse, Martin Marietta Corp., Orlando, FL

Tu-1-4 20:15 OPTICAL PROPERTIES OF METALLIC FILMS IN THE INFRARED
B. Carli, Univ. of Florence, Italy

Tu-1-5 20:35 FIR FRESNEL PRISM USED AS A QUARTER WAVE PLATE
U. O. Farrukh, Phoenix Corp., McLean, VA, and G. A. Koepf, NASA Goddard Center, Greenbelt, MD

Tu-1-6 20:55 ANALYSIS OF SUBMILLIMETER WAVE FABRY-PEROT INTERFEROMETERS MADE OF FOUR WIRE GRIDS
R. W. McMillan & J. B. Langley, Georgia Tech, Atlanta, GA

Tu-1-7 21:15 FREE STANDING WIRE GRIDS: THEIR MANUFACTURE, PERFORMANCE AND USE AT MILLIMETER AND SUBMILLIMETER WAVELENGTHS
A. E. Costley, K. Hursey, G. F. Neill, and J. W. M. Ward, National Physical Lab., Teddington, UK

Tu-1-8 21:35 SUBMILLIMETER MONOCHROMATIC SPECTROSCOPY AND ONE-DIMENSIONAL WIRE GRIDS (Invited)
E. A. Vinogradov, N. A. Irisova, and A. M. Prokohorov, P.N. Lebedev Institute, Moscow, USSR

Session Tu-2: Detectors
Surf Room
Presider: L. G. Rubin

Tu-2-1 19:15 RECENT ADVANCES IN FAR INFRARED DETECTORS FOR ASTRONOMY IN THE 1-1000μm RANGE (Invited)
K. Shivanandan, Naval Research Lab., Washington, DC

Tu-2-2 19:35 DEVELOPMENT OF THIN PYROELECTRIC DETECTORS FOR THE FAR INFRARED
A. Hadni, R. Thomas, and C. Erhard, Univ. of Nancy, France

Tu-2-3 19:55 MATERIALS FOR LOW NOISE SCHOTTKY-BARRIER CONVERTERS AT SUBMILLIMETER WAVELENGTHS
G. T. Wrixon, University College, Cork, Ireland, & M. D. Blue, Georgia Tech, Atlanta, GA

WEDNESDAY MORNING, 0940 Hours

TUTORIAL REVIEW

SUBMILLIMETER SOURCES BASED UPON RELATIVISTIC ELECTRON BEAM PHENOMENOLOGY
(Invited Lectures) Carnival Room
Presider: T. Godlove

MECHANISMS FOR COHERENT SCATTERING OF ELECTROMAGNETIC WAVES FROM RELATIVISTIC ELECTRON BEAMS
V. L. Granatstein, Naval Research Lab., Washington, DC

FRENCH ACTIVITY IN RELATIVISTIC ELECTRON BEAMS AND SUBMILLIMETER WAVES
H. J. Doucet, Ecole Polytechnique, Palaiseau, France

THE ELECTRON CYCLOTRON MASER--AN HISTORICAL SURVEY
J. L. Hirshfield, Yale Univ., New Haven, CT

PANEL DISCUSSION PERIOD
J. L. Hirshfield, Yale Univ., New Haven, CT (Moderator)

WEDNESDAY MORNING, 0940 Hours

FORMAL DISCUSSIONS

W-D1 FOURIER SPECTROSCOPY
Fisherman's Court
R. Geick, Universitat Wurzburg, GFR (Discussion Leader)

W-D2 POWER AND ENERGY MEASUREMENTS OF THE EMISSIONS OF SUBMILLIMETER WAVE LASERS
Fisherman's Court
F. K. Kneubuhl, ETH Zurich, Switzerland (Discussion Leader)

WEDNESDAY AFTERNOON, 1300 to 1700 Hours

COSMIC AND ATMOSPHERIC PHYSICS AND APPLICATIONS
(Invited Lectures) North Ballroom
Presider: P. L. Richards

COSMIC BACKGROUND RADIATION
P. L. Richards and D. P. Woody, Univ. of Calif. and Lawrence Lab., Berkeley, CA

SUBMILLIMETER WAVE ASTRONOMY
M. W. Werner, California Institute of Technology, Pasadena, CA

SUBMILLIMETER WAVE SPECTROSCOPY OF THE ATMOSPHERE
J. E. Harries, National Physical Lab., Teddington, UK

OBSERVATIONS OF COSMIC BACKGROUND RADIATION THROUGH THE FAR INFRARED ATMOSPHERIC WINDOWS AT THE ARCTIC STATION AT SKYBOT
A. Coletti, Istituto di Fisica Dell'Atmosfera, Rome, Italy, V. Decosmo, Istituto di Fisica, Firenze, Italy, and B. Melchiorri, F. Melchiorri, V. Natale, and S. Sivertsen, Auroral Observatory, Tromsoe, Norway

ABSOLUTE HIGH RESOLUTION FAR INFRARED MEASUREMENTS OF ATMOSPHERIC CONSTITUENTS
B. Carli, University of Florence, Italy, J. E. Harries, National Physical Lab., Teddington, and D. H. Martin and E. Puplett, Queen Mary College, London, UK

INFRARED OPTO-ACOUSTIC SPECTROSCOPY OF THE ATMOSPHERE AND STRATOSPHERE
C. K. N. Patel, Bell Labs., Murray Hill, NJ

WEDNESDAY EVENING, 1915 Hours

Session W-1: Cosmic, Solar and Atmospheric Physics
Riolama Room
Presider: H. A. Gebbie

W-1-1 19:15 NEW MOLECULAR ABSORBERS IN THE EARTH'S ATMOSPHERE AND THEIR SUB-MILLIMETER SPECTRA (Invited)
H. A. Gebbie, Appleton Lab., Slough, UK

W-1-2 19:35 ATMOSPHERIC ABSORPTION OF FAR INFRARED LASER RADIATION
N. McAvoy and V. G. Kundy, NASA Goddard Center, Greenbelt, MD, and A. S. Milman, U. O. Farrukh, and G. L. Mader, Phoenix Corp., McLean, VA

W-1-3 19:55 FABRY-PEROT SPECTROSCOPY OF THE WATER MOLECULE IN SUBMILLIMETER ATMOSPHERIC WINDOWS
R. W. McMillan & J. J. Gallagher, Georgia Tech, Atlanta, GA and G. T. Wrixon, University College, Cork, Ireland

W-1-4 20:15 SUBMILLIMETER WAVE NOISE INTERACTION WITH RAINY ATMOSPHERES
G. Schaerer, NASA Goddard Center, Greenbelt, MD

W-1-5 20:35 SUBMILLIMETER WAVELENGTH APPLICATIONS OF LASER RADAR FOR ATMOSPHERIC PROBING
J. A. Cooney, Drexel Univ., Philadelphia, PA

W-1-6 20:55 CALCULATIONS OF ANTENNA TEMPERATURE AND HORIZONTAL PATH ATTENUATION DUE TO THE 320 GHz ABSORPTION LINE OF WATER VAPOR
R. W. McMillan, J. J. Gallagher & A. M. Cook, Georgia Tech, Atlanta, GA

W-1-7 21:15 THE SOLAR BRIGHTNESS TEMPERATURE IN THE FAR-INFRARED
J. Rast & F. Kneubuhl, ETH Zurich, and E. A. Muller & D. Huguenin, Geneva Observatory, Switzerland

W-1-8 21:35 MILLIMETER RADIOMETRY IN THE 75 GHz-300 GHz BAND
K. Shivanandan & D. P. McNutt, Naval Research Lab., Washington, DC

W-1-9 21:55 A QUASI-OPTICAL RADIOMETER
J. J. Gustincic, Consulting Engineer, Marina Del Rey, CA

W-1-10 22:15 APPLICATIONS OF SUBMILLIMETER TECHNIQUES TO ATMOSPHERIC REMOTE SENSING
J. W. Waters, California Institute of Technology, Pasadena, CA

Session W-2: Solid State Spectroscopy
Surf Room
Presider: R. G. Wheeler

W-2-1 19:15 FAR INFRARED PHOTO-RESPONSE OF SILICON INVERSION LAYERS (Invited)
R. G. Wheeler, Yale Univ., New Haven, CT

W-2-2 19:35 FIR MAGNETOSPECTROSCOPY OF Si INVERSION LAYERS (Invited)
T. A. Kennedy, Naval Research Lab., Washington, DC

W-2-3 19:55 COHERENT ACOUSTIC BEAMS AT THz FREQUENCIES
F. Keilman, Max-Planck-Institute, Stuttgart, GFR

W-2-4 20:15 FIR-ABSORPTION SPECTRA OF HIGH POLYMERS WITH DIFFERENT DEGREES OF CRYSTALLINITY
W. Frank, Universitat Ulm, GFR

W-2-5 20:35 INTERACTION OF MICROWAVE BIASED n-GaAs AND 337 μm RADIATION
P. J. Epton, W. L. Wilson, Jr., & F. K. Tittel, Rice University, Houston, TX

W-2-6 20:55 INFLUENCE OF THE BOUNDARY CONDITIONS ON THE INFRARED SPECTRAL BEHAVIOR OF LiF THIN FILMS AND KCl MICROCRYSTALS
R. Kalin & F. Kneubuhl, ETH Zurich, Switzerland

W-2-7 21:15 THE MEASUREMENT OF THE SURFACE RESISTIVITY OF EVAPORATED GOLD AT 890 GHz
R. J. Batt & G. D. Jones, Portsmouth Polytechnic, UK, and D. J. Harris, U.W.I.S.T., Cardiff, South Wales

W-2-8 21:35 THE TRANSVERSE OPTIC MODE ANHARMONIC SELF-ENERGY OF NaCl FROM MEASUREMENTS BY DISPERSIVE FOURIER TRANSFORM SPECTROSCOPY
K. F. Pai, A. Rastogi, N. E. Tornberg, T. J. Parker & R. P. Lowndes, Northeastern Univ., Boston, MA

W-2-9 21:55 GAMMA IRRADIATION INDUCED CHANGES IN THE FAR INFRARED RESTSTRAHLEN SPECTRUM OF SOME ALKALI HALIDES
T. L. Rome & N. Ginsburg, Syracuse Univ., NY

THURSDAY MORNING, 0940 Hours

Session Th-1: Submillimeter Sources Based On Relativistic Electron Beam Phenomenology
Carnival Room
Presider: R. L. Gullickson

THURSDAY AFTERNOON, 1300 - 1700 Hours

SOLID STATE SPECTROSCOPY
(Invited Lectures) North Ballroom
Presider: R. A. Stradling

SEMICONDUCTOR CYCLOTRON RESONANCE, TRANSPORT AND SURFACE PHENOMENA
G. Landwehr, Universitat Wurzburg, GFR

APPLICATION OF SUBMILLIMETER SPECTROSCOPY TO MAGNETIC EXCITATIONS
R. Geick, Universitat Wurzburg, GFR

DIELECTRIC MEASUREMENTS IN THE SUBMILLIMETER REGION
G. W. Chantry, National Physical Lab., Teddington, UK

INFRARED SPECTROSCOPY OF THE BOUND STATES OF THE SHALLOW IMPURITIES IN SEMICONDUCTORS
A. K. Ramdas, Purdue Univ., West Lafayette, IN

ANOMALOUS EXCITATIONS IN GLASSES IN THE FAR INFRARED
A. J. Sievers, Cornell Univ., Ithaca, NY

THURSDAY EVENING, 1915 Hours

Session Th-2: Optically Pumped Lasers and Their Applications
North Ballroom

Th-2-1 19:15 SUBMILLIMETER SPECTROSCOPY IN THE LIQUID AND SOLID STATE WITH A TUNABLE OPTICALLY PUMPED LASER
B. L. Bean & S. Perkowitz, Emory Univ., Atlanta, GA

Th-2-2 19:35 SERVO ELECTRONICS FOR OPTICALLY PUMPED FIR LASER
E. G. Reid, NASA Goddard Center, Greenbelt, MD

Th-2-3 19:55 DIFFRACTION LIMITED CW OPTICALLY PUMPED LASERS
M. Schubert, M. Durschlag & T. A. DeTemple, Univ. of Illinois, Urbana, IL

Th-2-4 20:15 MODE LOSSES IN WAVEGUIDE FAR-INFRARED LASERS
C. H. Ma, Univ. of Mississippi, University, MS

FRIDAY MORNING, 0940 Hours

FORMAL DISCUSSIONS

FRIDAY AFTERNOON, 1300 - 1620 Hours

PLASMA INTERACTIONS
(Invited Lectures) North Ballroom
Presider: R. E. Slusher

SUBMILLIMETER PLASMA DIAGNOSTICS IN CONTROLLED THERMONUCLEAR FUSION RESEARCH
D. R. Cohn, MIT National Magnet Lab., Cambridge, MA

THOMSON SCATTERING
D. E. Evans, Culham Laboratory, Oxford, UK

CYCLOTRON EMISSION FROM TOKAMAK PLASMAS
Alan E. Costley, National Physical Lab., Teddington, UK

SUBMILLIMETER SOURCES AND THEIR APPLICATION TO SCIENCE
Benjamin Lax, MIT National Magnet Lab., Cambridge, MA

FRIDAY EVENING, 1915 Hours

Session F-1: Liquid, Gaseous, Molecular, Raman Spectroscopy
North Ballroom
Presider: F. K. Kneubuhl

F-1-1 19:15 FAR-INFRARED GAS ANALYZER
W. Ehrfeld & G. Krieg, Universitat Karlsruhe, GFR

F-1-2 19:35 STIMULATED RAMAN EMISSION IN INFRARED EXCITED GASES
S. J. Petuchowski, A. T. Rosenberger & T. A. DeTemple, Univ. of Illinois, Urbana, IL

F-1-3 19:55 SUBMILLIMETER PRESSURE BROADENING MEASUREMENTS
J. J. Gallagher & W. M. Penn, Georgia Tech, Atlanta, GA and G. T. Wrixon, University College, Cork, Ireland

F-1-4 20:15 ABSORPTION MEASUREMENTS ON VERY DILUTE SOLUTIONS IN THE 10 TO 120 cm^{-1} RANGE
H. Kilp, Universitat Mainz, GFR

F-1-5 20:35 STARK SHIFT LASER SPECTROSCOPY AT SUBMILLIMETER WAVELENGTHS FOR CHEMICAL ANALYSIS
L. W. Hrubesh & D. C. Johnson, Livermore Lab., CA, and E. A. Rinehart, Univ. of Wyoming, Laramie, WY

F-1-6 20:55 EXTENSION OF ELECTRIC RESONANCE SPECTROSCOPY TO THE SUBMILLIMETER WAVELENGTH REGION
J. J. Gallagher & W. M. Penn, Georgia Tech, Atlanta, GA

F-1-7 21:15 SPECTROSCOPIC DETECTION OF METHOXY (CH_3O)
H. E. Radford, Harvard College and Smithsonian Observatories, Cambridge, MA, and D. K. Russell, Univ. of Cambridge, UK

F-1-8 21:35 COLLISION INDUCED FAR INFRARED ABSORPTION IN ARGON-HELIUM MIXTURES AND NITROGEN AT HIGH PRESSURE
R. P. Lowndes & A. Rastogi, Northeastern University, Boston, MA

F-1-9 21:55 STARK MEASUREMENTS OF H_2S IN THE MILLIMETER/SUBMILLIMETER WAVELENGTH REGION
R. E. Cupp, National Oceanic and Atmospheric Admin., Boulder, CO., and J. J. Gallagher, Georgia Tech, Atlanta, GA

Session F-2: Post Deadline Papers
Surf Room

SATURDAY MORNING, 0900 Hours

Session S-1: Plasma Diagnostics
Carnival Room
Presider: N. C. Luhmann, Jr.

S-1-1 09:00 PLASMA DENSITY MEASUREMENTS BY USING A MODULATED SUBMILLIMETER LASER INTERFEROMETER SYSTEM (Invited)
S. M. Wolfe, K. J. Button, J. Waldman & D. R. Cohn, MIT National Magnet Lab., Cambridge, MA

S-1-2 09:20 HCN INTERFEROMETER FOR ELECTRON DENSITY MEASUREMENT OF A TOKAMAK PLASMA
D. Veron, J. Certain & J. P. Crenn, Centre d'Etudes Nucleaires, Fontenay-aux-Roses, France

S-1-3 09:40 EVAPOROGRAPHIC AND PYROELECTRIC IMAGE RECORDING FOR TWO-DIMENSIONAL PLASMA INTERFEROMETRY IN THE FAR INFRARED
G. Dodel & W. Kunz, Universitat Stuttgart, GFR

S-1-4 10:00 CO_2 LASER SCATTERING FROM TURBULENCE IN TOKAMAKS
R. E. Slusher & C. M. Surko, Bell Labs., Murray Hill, NJ

S-1-5 10:20 CYCLOTRON RESONANT LASER INDUCED GAS BREAKDOWN AT 496 MICRONS
M. P. Hacker, R. J. Temkin & B. Lax, MIT National Magnet Lab., Cambridge, MA

S-1-6 10:40 QUARTZ BEAM SPLITTERS FOR FAR INFRARED (FIR) DIAGNOSTICS
A. M. Frank, Livermore Lab., Livermore, CA

Session S-2: Semiconductors
Riolama Room

S-2-1 09:00 A HIGH PRECISION STUDY OF EXCITED STATE TRANSITIONS OF SHALLOW DONORS IN SEMICONDUCTORS (Invited)
R. A. Stradling, Univ. of Oxford, UK

S-2-2 09:20 SURFACE POLARITON STUDIES IN THE FAR INFRARED (Invited)
R. T. Holm, Naval Research Lab., Washington, DC

S-2-3 09:40 FAR INFRARED PROPERTIES OF III-V AND IV-VI SEMICONDUCTOR SYSTEMS
P. M. Amirtharaj, B. L. Bean & S. Perkowitz, Emory University, Atlanta, GA

S-2-4 10:00 FAR INFRARED PROPERTIES OF SHALLOW IMPURITY STATES IN HEAVILY DOPED p-TYPE GERMANIUM
K. Yoshihiro, J. Kinoshita & C. Yamanouchi, Electrotechnical Lab., Tokyo, Japan

S-2-5 10:20 SPECTRAL RESPONSE VARIATIONS IN THE PHOTOCONDUCTIVITY FROM SHALLOW IMPURITY STATES IN SILICON AS A FUNCTION OF CONCENTRATION AND TEMPERATURE
P. Norton, Bell Labs., Murray Hill, NJ

S-2-6 10:40 FAR-INFRARED STUDY OF EXCITON, ELECTRON-HOLE DROP AND IMPURITY SYSTEMS IN GERMANIUM
E. Otsuka, T. Ohyama, H. Nakata & Y. Okada, Osaka University, Osaka, Japan

S-2-7 11:00 SUBMILLIMETER-CYCLOTRON RESONANCE OF ELECTRONS IN ACCUMULATION LAYERS ON INDIUM ANTIMONIDE SURFACES
M. v.Ortenberg & U. Steigenberger, Univ. of Wurzburg, GFR

S-2-8 11:20 LINE SHAPE OF CYCLOTRON RESONANCE IN n-TYPE GERMANIUM AT 337 μm IN THE TEMPERATURE RANGE 15-100K
F. Kuchar, Univ. of Vienna and Boltzmann Institut, Vienna, Austria

S-2-9 11:40 RAMAN LIGHT SCATTERING ON LANDAU LEVELS IN SEMICONDUCTORS
G. K. Vlasov, Academy of Sciences of the Ukranian SSR, Kiev, USSR

S-2-10 12:00 VOLTAGE TUNABLE FAR-INFRARED SOURCE BASED ON ELECTRONIC TRANSITIONS IN Si-INVERSION LAYERS
D. C. Tsui & E. Gornik, Bell Labs., Murray Hill and Holmdel, NJ

Session S-3: Propagation and Imaging
South Ballroom

S-3-1 09:00 SUBMILLIMETER SYSTEM FOR IMAGING THROUGH INCLEMENT WEATHER
R. L. Hartman, MICOM, Redstone Arsenal, AL, and P. W. Kruse, Honeywell Corp. Research Center, Bloomington, MN

S-3-2 09:20 SUBMILLIMETER LASER WAVE PROPAGATION
W. L. Gamble & B. D. Guenther, MICOM, Redstone Arsenal, AL

S-3-3 09:40 SPECKLE AND SPECULAR EFFECTS IN SUBMILLIMETER IMAGING
V. J. Corcoran, Institute for Defense Analyses, Arlington, VA

S-3-4 10:00 REFLECTIVITY OF COMMON MATERIALS IN THE SUBMILLIMETER REGION
M. D. Blue, Georgia Tech, and S. Perkowitz, Emory Univ., Atlanta, GA

S-3-5 10:20 SUBMILLIMETER WAVE PROPAGATION STUDIES - A COMPARISON WITH OTHER SPECTRAL REGIONS
R.W. McMillan, R. G. Shackelford, M. D. Blue & J. J. Gallagher, Georgia Tech, Atlanta, GA

S-3-6 10:40 INDIRECT INTERACTION FREQUENCY SHIFT OF RADIATION
J. A. Cooney, Drexel Univ., Philadelphia, PA

S-3-7 11:00 SUBMILLIMETER WAVE PROPAGATION MEASUREMENT TECHNIQUES
S. L. Johnston, Professional Engineer, Huntsville, AL

INDEX TO AUTHORS

Invited papers are denoted by (I). Papers without session numbers are invited tutorial lectures.

INDEX TO AUTHORS

INDEX TO AUTHORS

INDEX TO AUTHORS

INDEX TO AUTHORS

THE RUBENS ERA

E. D. Palik
Naval Research Laboratory
Washington, D.C. 20375

H. Rubens' spectroscopic work began in the near infrared and progressed in steps to the far infrared. The milestones along the way from 1892 to 1922 are in both the development of experimental techniques and equipment, and in the wide range of problems that were attacked with this equipment.

In the area of techniques and equipment, we must note 1) the discovery of reststrahlen rays in a large number of solids and their utilization to construct monochromators, 2) the measurement of the transmission properties of numerous materials with the development of prisms amd windows extending to longer and longer wavelengths, 3) the perfection of the transmission wire grating, focal isolation and the Fabry-Perot interferometer, 4) the search for and characterization of far-infrared sources including the high-pressure Hg lamp, 5) significant improvement in detectors, blackenings and galvonometer systems, 6) the invention of the echelette grating by R. W. Wood.

In the area of physics problems attacked, we note 1) the measurement of vibration and rotation bands of gases such as CO_2 and H_2O in the laboratory as well as the atmosphere, 2) the verification of Planck's black-body-radiation law (a problem Rubens, et al, work on throughout this era), 3) the study of lattice vibrations with the Lorentz-oscillator model (which is still with us), 4) the precise determination of the optical constants of many materials including birefringent crystals; index-of-refraction values are often in agreement with today's values to the second decimal place, 5) the connection between optical and electrical properties of metals; the test of the Drude model (which is still with us), 6) the polarization properties of wire gratings.

This thirty years of work in collaboration with about 20 people, including the American physicists, Nichols, Trowbridge and Wood, appeared in over 130 papers. Rubens appears as the sole author on 42 of these papers. This is indeed productivity considering that he was also director of the Physical Institute of the University of Berlin from 1906 to 1922. Inspection of these papers reveals that the same work was often published twice in identical or slightly different form in German journals such as Berl. Ber. (Sitzungsberichte der Königlich Preussischen Academie der Wissenschaften), Verhandl. Deut. Phys. Ges. (Verhandlungen der Deutsche Physikalische Gesellschaft) and Wied. Ann. (Wiedemann Annalen der Physik und Chemie, later to be Ann. Physik (Annalen der Physik)). Short letters on new research appeared in Phys. Zeit. (Physikalische Zeitschrift). Direct translations of important papers into English and French were sometimes made and appeared in Phil. Mag. (Philosophical Magazine) and Le Radium. Even this duplicate publishing (which we rarely do today!?) does not detract from the originality, wide scope, quality and quantity of topics studied by Rubens, et al.

The cost of research in 1910 was modest, indeed. Rubens was supported by the Institute and the Preussische Akademie der Wissenschaften with about 5000 gold marks per year. This amounted to about $1250. Assuming that this support was about constant for thirty years of research, we guess that a grand total of $37,500 supported this work; thus, the research cost $290 per paper. If we include that the cost of living today is at least six times what it was in 1910, this leads to the logical conclusion that far-infrared work today should cost about $1740 per paper. Therefore, a one-year grant for $37,500 should produce about 21 papers. This conclusion assumes that, in the custom of these times, neither professor (privatdozent) nor graduate student is paid for the work.

During Rubens' time nearly all the published far-infrared work not bearing his name (this amounts to about 15 papers) was done by scientists who had worked in his laboratory and then returned to their own laboratories to initiate new work. The foundations laid by Rubens, et al, were built upon by still greater numbers of researchers into the large active field we have today.

THE GRATING ERA, 1930 - 1960

Nathan Ginsburg
Department of Physics
Syracuse University
Syracuse, New York 13210

The Grating Era is rather an ill-defined period, since Rubens used them almost from the time of his first measurements in the far infrared, and they are still being used today in many commercial instruments. Thus, I will discuss principally the post-Rubens time, up to the advent of the modern interferometer and the laser. In actual time, that is from 1920 to 1960.

The first grating spectrometer not in Rubens' laboratory was that described by H. Witt in 1920 at the University of Lund. It was also the first reflection-grating instrument using concave gratings in a Rowland mount. The two gratings available to Witt were both approximately 60 cm radius of curvature and had spacings of either 1 or ½ mm. In 1925, Czerny published his classic paper on the rotational spectrum of HCl, made with another instrument using transmision gratings.

The first United States grating instrument was that of Badger (at Cal. Tech.), described in 1926. An improved version (1929, with Cartwright) was used to measure the rotational spectrum of ammonia. They did not achieve resolution of the doublet structure of that spectrum. Pfund, at Johns Hopkins, built a prism-grating instrument for use up to the 30 μm wavelength region, and in 1932, Barnes at Princeton built a transmission grating instrument, essentially a copy of the one of Czerny, with whom he had worked.

Also in 1932, the first really high-resolution instrument was described by Randall at the University of Michigan. There was already available a grating ruling engine for plane gratings up to 10" by 20" in size, and with the fortuitous acquisition of a 24" diameter paraboloid broken into two halves, the very large aperture spectrometer was constructed. It was with this spectrometer that the rotational doublets of ammonia were first observed (Wright and Randall, 1932) and the very detailed water-vapor spectrum was measured. It was with the latter work that I was associated (Randall, Dennison, Ginsburg and Weber, 1937). A resolution of about 0.3 cm^{-1} was obtained, which allowed a complete identification of all of the lower rotational energy levels (up to J - 11) of that asymmetric rotator.

There had not been much change in far infrared spectrometers from the time they were first built by Rubens until after World War II. The typical system used a Welsbach mantle as source, either burning gas or electrically heated. This illuminated the slit of the spectrometer, which was always a single-beam instrument, of the Littrow or Czerny-Turner type. The detector was a thermopile with blackened vanes. The voltage output from the thermopile was fed to a low-resistance galvanometer, which was read at distances of up to 5 meters, giving swings of not more than a few centimeters even at that distance. The noise limitation was the Brownian motion of the galvanometer mirror. Readings were taken with a stop-watch in hand, timing the reading to the period of the galvanometer, since drift often exceeded the reading by factors of up to five. The spectrometer shutter would be opened, timed appropriately, then closed and again timed. In order to approximate thermal equilibrium as required to reduce drift, I would turn on the mantle, and all electrical apparatus at about 8 PM, place a 60 or 100 watt bulb in the observer chair, depart for a movie, return at 11 PM or midnight, and take readings of the galvanometer swing, turn the grating by 10 or 20 seconds of arc between sets of reading, usually three at each grating position. It was also always necessary to find the central image of the grating before and after each set of readings in order to determine the wavelength accurately.

Some improvements in the detection system were made by Pfund, using a grid with photocell. That, with a Firestone resonant system, allowed the galvanometer swings to be recorded on photographic paper. This was the scheme used with the first recording far IR spectrometer with which the D_2O rotational spectrum was observed (Fuson, Randall and Dennison, 1939).

The real surge in far-infrared spectroscopy began after World War II. The main improvements were in the invention of the Golay detector, chopping with AC amplification and pen recorders. Also, of course, the great interest in semiconductors and solid-state physics in general, where optical properties were of such great importance in elucidating structure, provided the impetus for a world-wide period of construction of new instruments. In the United States, high resolution instruments were constructed at Ohio State and Syracuse, lower resolution spectrometers at Johns Hopkins, MIT, Purdue and Berkeley. In other countries in the early 1950's, far infrared research was being done at Osaka in Japan; Nancy, France; Freiburg, Germany; Queen Mary College in London; and at the Institute of Optics in Leningrad, USSR.

Essentially, the improvement in grating spectrometers since the earliest ones is due to the new detectors. Relatively cheap cryostats with carbon, doped germanium or superconducting bolometers or intrinsic photoconductors have raised detectivities by factors of 100 and more over thermopiles.

HISTORY OF FAR-IR AND SUBMILLIMETER RESEARCH. 1950 TO PRESENT INTERFEROMETRY

L. Genzel
Max-Planck-Institut für Festkörperforschung,
Stuttgart, Federal Republic of Germany

This paper is concerned with the history, the development and the important aspects of that part of interferometry which is known today as Fourier Transform Spectroscopy (FTS). An excellent review of the same topic with the development up to 1965 has been published by Loewenstein [6] .
The modern birthday of FTS was 1951 when Fellgett [16] showed in his thesis the multiplex advantage of two-beam interferometry over the sequential slit spectrometry. Already a few years earlier, it was shown by Jacqinot and Dufour [15] that axially symmetric interferometers have a throughput advantage of light-gathering over slit-instruments. It is fair to mention the work of Rubens and Wood [2] who already in 1913 first used the FTS in the far-IR but gave it up some years later because of the lack of digital computers. The years from 1952 to 1961 could be called the "exploration period of FTS". First interferometers of the lamellar and Michelson type were developed for the IR and mainly FIR. The great potential of digital computers for the multiplex FTS was appreciated while it was realized that analog computation is too troublesome to be competitive. The subjects of resolution, apodization and scanning function, interferogram sampling, filtering and digital recovering of the spectrum were worked out in this period. At the end of 1961 the thesis of J. Connes [4] appeared which covered almost all basic aspects of FTS including phase error problems and noise theory.
After 1961 the "elaboration period of FTS" started and is apparently continuing at present. It is astonishing how many new significant improvements could still be found. Among these are the dispersive or amplitude-phase FTS, double-beaming in the conventional (chopping) way or in the more sophisticated compensative (interferometric) way, furthermore the phase-modulated FTS, the polarizing interferometer and the development of high-resolution FIR-FTS. Since it seems impossible to mention in detail all the contributions to FIR-FTS in this paper, an extensive list of references is added.

References

Historical Articles

1. A.A. Michelson, Phil.Mag.(5),31,256,338(1891)
2. H. Rubens, R.W.Wood, Phil.Mag.21,249(1911)

Review Articles and Books

3. P.Jacquinot,Rept.Progr.Phys.XIII,267(1960)
4. J. Connes, Rev.Opt.40,45,116,171,231(1961)
5. L.Mertz, Transformation in Optics (John Wiley, New York) 1965
6. E.V. Loewenstein, Appl.Opt.5,845(1966),Ref. 12
7. G.A. Vanasse, H.Sakai, Progr. in Optics, VI, 261(1967)
8. L. Genzel, Plenarvorträge d. Deutschen Physikalischen Gesellschaft (B.G. Teubner, Stuttgart), p.128-178, 1968.
9. G.W. Chantry, Submillimeter-wave Spectroscopy (London, England, Academic Press) 1971.
10. R.J. Bell, Introductory Fourier Transform Spectroscopy, (Academic Press, New York and London), 1972.

Conferences

11. C.N.R.S. Bellevue Colloquium, J.Phys.Radium 19,187(1958).
12. C.N.R.S. Orsay Colloquium, J. de Physique 28, C2 (1967).
13. Aspen International Conference on Fourier Spectroscopy (1970) (Ed. G.A. Vanasse, A.T. Stair, D.J. Baker) AFCRL-71-0019.
14. International Conference on Infrared Physics, Zürich 1975, Infrared Physics 16, Nr.1/2(1976)

Multiplex and Throughput Advantage

15. P. Jacquinot, C.Dufour, J.Rech.C.N.R.S. Lab. Bellevue (Paris), 6,91(1948).
16. P.B. Fellgett, Thesis, Univ.of Cambridge 1951; Ref. 11 .
17. C.S. Rupert, Symp.Mol.Struct. and Spectr., Ohio State Univ.,1952.
18. J. Strong, Concepts of Classical Optics (W.H. Freeman, San Francisco) 1958.
19. P.L. Richards, J.Opt.Soc.Am.54 , 1474 (1964).
20. J. Connes, P. Connes, J.Opt.Soc.Am. 56, 896 (1966).

Scanning Function, Apodization and Resolution

21. B. Dossier, Rev.Opt. 33,57,147,267 (1954).
22. H.A. Gebbie, G.A. Vanasse, J.Strong, J.Opt. Soc. Am. 46, 377 (1956).
23. J. Connes, Ref. 11 , Ref. 4 .
24. H.A. Gebbie, Ref. 11 .
25. L. Genzel, R.Weber, Z.Angew. Phys. 10, 127, 195 (1958).
26. J. Strong, G.A. Vanasse, J.Opt.Soc.Am. 49, 844 (1959).
27. L. Genzel, J.Mol.Spectr. 4, 241 (1960).
28. H. Happ, L.Genzel, Infrared Physics 1, 39 (1961).
29. P.F. Parshin, Opt.Spectry. 13,418 (1962).
30. G.A. Vanasse, J.Opt.Soc.Am. 52, 472 (1962).
31. A.S. Filler, J.Opt.Soc.Am. 54, 762 (1964).

Digital Computation, Sampling and Filtering

32. H.A. Gebbie, G.A. Vanasse, Nature 178, 432 (1956).
33. J. Strong, G.A. Vanasse, Ref. 26 .
34. J. Connes, V. Nozal, J.Phys.Radium 22, 359 (1961).
35. P.L. Richards, Ref. 19 .
36. H. Yoshinaga, Appl.Opt. 3, 805 (1964).
37. J.W. Cooley, J.W. Tukey, Math. of Computation 19, 297 (1965).

38. S. Fujita et.al., Japan J.Appl.Phys. 4, Suppl. I, 429 (1965).
39. H. Yoshinaga et.al., Appl.Opt. 5, 1159 (1966).
40. J.E. Hoffman, G.A. Vanasse, Appl.Opt. 5,1167 (1966).
41. M.L. Forman, J.Opt.Soc.Am. 56, 978 (1966).
42. J. Connes, P. Connes, Ref. 12 .
43. J.N.A. Ridyard, Ref. 12 .
44. Various papers on computing techniques in Ref. 13 .

Analog Computation

45. J. Strong, G.A. Vanasse, Ref. 11 .
46. L. Genzel, R.Weber, Ref. 25 .
47. M. Tinkham, D.H. Martin, Ref. 12 .
48. J. Pritchard, H. Sakai, G.A. Vanasse, Ref. 12
49. R.F. Edgar et.al., Ref. 12 .
50. F. Lanzl, H.J. Mager, W.Waidelich, J.Opt.Soc. Am. 61, 1355 (1971).
51. H.J. Mager, Infrared Physics 13, 7 (1973).

Noise Considerations

52. J. Connes, Ref. 4 .
53. B.A. Kiselev, P.F. Parshin, Opt.Spectry. 12, 169 (1962).
54. P.F. Parshin, Opt.Spectry. 16, 275 (1964).
55. E.E. Bell, Infrared Physics 6, 57 (1966).
56. G. Roland, Thesis, Univ. de Liège 1966.
57. J.M. Dowling, Appl.Opt. 6, 1580 (1966).
58. H. Sakai, Ref. 13 .

Phase Errors

59. J. Connes, Ref. 4 , Ref. 13 .
60. E.V. Loewenstein, Appl.Opt. 2, 491 (1963).
61. J.E. Gibbs, H.A. Gebbie, Infrared Physics 5, 187 (1965).
62. M. Forman, W.H. Steel, G.A. Vanasse, J.Opt. Soc.Am., 56, 59 (1966).
63. A.S. Filler, Ref. 12 .
64. L. Mertz, Infrared Physics 7, 17 (1967).
65. L.W. Thorpe, Ref. 13 .
66. E.E. Bell, R.B. Sanderson, Appl.Opt. 11, 688 (1972), Appl.Opt. 12, 266 (1973).
67. Ph. Marteau et.al., Ref. 14 .

Beam Splitters

68. H.A. Gebbie, N.W.B. Stone, Infrared Physics 4, 85 (1964).
69. P. Vogel, L.Genzel, Infrared Physics 4, 257 (1964).
70. P.L. Richards, Ref. 19 .
71. C.H. Perry, R. Geick, E.F. Young, Appl.Opt. 5, 1171 (1966).
72. J.E. Chamberlain et.al., Infrared Physics 6, 195 (1966).
73. D.J. James, J. Ring, Ref. 12 .
74. E.V. Loewenstein, Ref. 12 .
75. A.G. Tescher, Ref. 13 .
76. D.H. Martin, E. Puplett, Infrared Physics 10, 105 (1969).

Dispersive (Amplitude-Phase) Fourier Spectroscopy

77. J.E. Chamberlain, J.E. Gibbs, H.A. Gebbie, Nature 198, 874 (1963), Infrared Physics 9, 185 (1969).
78. J.E. Chamberlain, F.D. Findlay, H.A. Gebbie, Appl.Opt. 4, 1832 (1965).
79. E.E. Bell, Japan J.Appl.Phys. 4, Suppl. I, 412 (1965); Infrared Physics 6, 57 (1966), Ref. 12,13 .
80. E.E. Russel, E.E. Bell, Infrared Physics 6, 75 (1966).
81. J.E. Chamberlain, H.A. Gebbie, Appl.Opt. 5, 393 (1966).
82. J. Chamberlain, Infrared Physics 12, 145(1972)
83. J. Gast, L. Genzel, Opt.Commun. 8, 26 (1973).
84. J. Gast, L. Genzel, U.Zwick, IEEE MTT-22, 1026 (1974).
85. T.J. Parker, W.G. Chambers, J.F. Angress, Infrared Physics, 14, 207 (1974).
86. T.J. Parker, W.G. Chambers, IEEE, MTT-22,1032 (1974); Infrared Physics 16, 349 (1976).
87. D.D. Honijk, W.F. Passchier, M. Mandel, M.N. Afsar, Ref. 14 .
88. U. Zwick, C. Irslinger, L. Genzel, Ref. 14 .
89. T.J. Parker, D.A. Ledsham, W.G. Chambers, Ref. 14 .
90. M.N. Afsar, J.B. Hasted, J. Chamberlain, Ref. 14 .

Double Beam Fourier Spectroscopy

91. R.T. Hall, D.Vrabek, J.M. Dowling, J.Opt.Soc. Am., 54, 1390 A (1964), Appl.Opt. 5, 1147 (1966).
92. D.H. Martin, E. Pupplett, Ref. 76 .
93. R. Hanel, M.Forman, T.Meilleur, R. Westcott, J. Pritchard, Appl.Opt. 8, 2059 (1969).
94. J.M. Dowling, Ref. 13 .
95. W.J. Burroughs, J. Chamberlain, Infrared Physics 11, 1 (1971).
96. F.J. Ahern, C. Pritchet,Appl.Opt. 13, 2240 (1974).
97. J. Kauppinen, Appl.Opt. 14, 1984 (1975).
98. G.A. Vanasse, R.E. Murphy, F.H. Cook, Appl. Opt. 15, 290 (1976).
99. H.R. Chandrasekhar, L. Genzel, J. Kuhl, Opt. Commun. 17, 106 (1976).
100. J.N. Willis, Ref. 14 .

Phase Modulated Fourier Spectroscopy

101. J. Chamberlain, Infrared Physics 11, 25(1971).
102. J. Chamberlain, H.A. Gebbie, Infrared Physics 11, 57 (1971).
103. J. Chamberlain, J.Haigh, M.J. Hine, Infrared Physics 11, 75 (1971)

High - Resolution Far Infrared Fourier Spectroscopy

104. R.T. Hall, D. Vrabec, J.M. Dowling, Ref. 91
105. J.M. Dowling, Ref. 13 .
106. R.B. Sanderson, H.E. Scott, Ref. 13 .
107. J.W. Fleming, IEEE, MTT-22, 1023 (1974).
108. J.W. Fleming, J. Chamberlain, Infrared Phyics 14, 277 (1974).
109. H. Mark, M.J.D. Low, Infrared Physics 15, 1 (1975).

CRITIQUE OF PRESENT AND FUTURE PROBLEMS IN THE FAR INFRARED

Paul D. Coleman
Department of Electrical Engineering
University of Illinois
Urbana, Illinois 61801

The coherent radiation history of the far IR began around 1960-62 with the extension of the Compagnie Générale de Telégraphie sans Fils O type Carcinotrons down to 500 μm wavelength and the extension of the He-Ne laser by Bell Telephone Laboratories first to 28 and later to 133 μm wavelength [1,2]. Less than a year later, the British Services Electronics Research Laboratory announced the first far IR molecular lasers (H_2O and HCN) operating at 78 and 337 μm wavelength [3].

This initial work demonstrated that sufficient population inversions could be obtained via glow discharge in atomic and molecular gases to achieve lasing and stimulated a renewed activity of research in the far IR. Unfortunately, few molecules could survive a high current glow discharge, as evidence by the fact that only a few (H_2S, SO_2, NH_3) more lasing molecules were reported [4,5]. Also, pulsed power levels above a few kilowatts were difficult to achieve [6,7].

Problems in analytical modelling of glow discharge, far IR molecular lasers were difficult, especially where the excitation was indirect. Hence, while the thrust of far IR molecular laser research was on glow discharge excitation from about 1964 to 1970, the area did not expand too rapidly in spite of numerous available coherent laser signals.

Coherent pumping of a three-level system goes back to the days (1956) of the microwave maser, typically pumped by a frequency tunable reflex klystron [8]. In spite of this well-developed maser art and science, coherent pumping of molecular gas far IR lasers was not reported until 1970 by Chang and Bridges with their work on CH_3F [9]. By 1975, some 50-60 papers a year were appearing on the optical pumping of far IR molecular lasers and the far IR area was experiencing its greatest development and activity [10].

Some of the fundamental problems encountered in this molecular laser effort were limited spectroscopic data on the molecules, data on dipole moments, relaxation rates, collisional energy exchange rates, etc. This situation made it difficult to make the first step of assigning laser energy levels in the molecules, especially if the lasing occurred in high lying energy states. Analytical modelling is dependent on knowing appropriate relaxation and rate constants.

As pump intensities in the optically pumped molecular lasers were increased to achieve higher output power, nonlinear (i.e., Raman) effects should have been observed but strangely have as yet not been reported. Intense outputs have been seen from molecular lasers with no feedback (i.e., no mirrors or optical cavity) [11]. The nature of this "superradiant" emission has not been explained. Is it amplified spontaneous or Raman radiation, or a form of Dicke superradiance?

A major challenge in the molecular laser area is that of obtaining a frequency tunable source. Mixing of two near IR coherent signals in a nonlinear crystal, four-wave interactions in atomic gases, spin flip lasers, current tunable diode lasers, pressure broadened gain curves, etc. techniques have achieved some success in this area but a real practical solution to the problems remains to be found. Perhaps the "right" molecule with the "right" properties remains to be discovered.

Pumping joules of pulsed CO_2 radiation into a far IR optical cavity, absorbing the radiation in the molecular gases, and coupling the far IR radiation out efficiently is not a trivial problem. Progress along this line has appeared during 1975-76 in the form of new cavity designs, transverse pumping arrangements, hybrid dielectric-metal mesh output couplers, metal and dielectric waveguide configurations, etc. [12,13]. However, many of the problems have only been partially solved and much remains to be done with high power systems.

While the major recent effort on far IR molecular lasers has been on optical pumping, chemical excitation, flash photolysis, and collisional energy exchange pumping have also had some success. New chemical laser systems are difficult to find, flash photolysis systems usually have slow repetition rates, and matching collision partners is a challenge [14,15,16]. However, this is an area of study that should expand further in the near future.

It would also appear that classical

electronics has not yet entirely vanished from the far IR picture and may appear in the visible. Gyrotron oscillators, with large CW capabilities, are breaking the 1000 μm barrier and Pantell at Stanford has been able to modulate an electron beam with a visible laser [17,18].

This paper will attempt to identify and discuss the key steps in the progress of the generation of coherent far IR radiation since 1962, the problems encountered and the directions the area appears to be taking in the near future.

References

1. Convert, D., et al., "Millimeter Wave O-Carcinotron", Polytechnic Institute of Brooklyn, Symposia Series IX on Millimeter Waves, p. 313, New York, 1959.

2. McFarlane, R. A., et al., "Gas Maser Operation at Wavelengths out to 28 Microns", Quantum Electronics, 3, 573, Columbia Press, New York, 1964.

3. Gebbie, H. A., et al., "A Stimulated Emission Source at 0.34 Millimeter Wavelength", Nature, 685, May 1964.

4. Hassler, J. C. and Coleman, P. D., "Far IR Lasing in H_2S, OCS, and SO_2", Appl. Phys. Lett., 14, 135, February 1969.

5. Akitt, D. P. and Wittig, C. F., "Laser Emission in Ammonia", J. Appl. Phys., 40, 902, February 1969.

6. Coleman, P. D., et al., "Device Aspects of a far IR H_2O Vapor Laser", IEEE Int. Electron Devices Meeting, 1967, Washington, D.C.

7. McFarlane, R. A. and Fritz, L. H., "High Power Operation of Pulsed H_2O Laser", Appl. Phys. Lett., 14, 385, June 1969

8. Bloembergen, N., "Three Level Maser Proposal", Phys. Rev., 104, 324, 1956.

9. Chang, T. Y. and Bridges, T. J., "Laser Action at 452, 496, and 541 μm in Optically Pumped CH_3F", Opt. Commun., 1, 423, April 1970.

10. Yamanaka, M., "Optically Pumped Gas Lasers", The Review of Laser Engineering - Japan, 3, 253, March 1976.

11. DeTemple, T. A., et al., "Intense Superradiant Emission at 496 μm from Optically Pumped Methyl Fluoride", Appl. Phys. Lett., 22, 644, June 1973.

12. Cohn, D. R., et al., "Development of an Efficient 9-KW 496 μm CH_3F Laser Oscillator", Appl. Phys. Lett., 27, 280, September 1975.

13. Danielewicz, E. J., et al., "Hybrid Output Mirror for Optically Pumped Far IR Lasers", Opt. Commun., 13, 366, April 1975.

14. Berry, M. J., "Chemical Laser Studies of Energy Partitioning into Chemical Reaction Products", Molecular Energy Transfer, Wiley, New York, 1975, J. Jortner and R. D. Levine, Editors.

15. Kildal, H. and Deutsch, T. F., "Optically Pumped Infrared V-V Transfer Lasers", Appl. Phys. Lett., 27, 500 November 1975.

16. Wittig, C., "Infra-Red Molecular Lasers Pumped by Electronic-Vibrational Energy Transfer", Appl. Phys. Lett., 27, 305, September 1975.

17. Zaystev, A. I., et al., "Millimeter and Submillimeter Wave Gyrotrons", Radio Eng. and Elect. Physics, 5, 103, 1974.

18. Pantell, R., et al., "Cerenkov Radiation as a Light Source for the 2000-620 Å Spectral Range", Appl. Phys. Lett., 28, 92, January 1976.

PROGRESS IN FOURIER SPECTROMETRY: A REVIEW OF PRESENT ACHIEVEMENT AND FUTURE POSSIBILITIES.

D. H. Martin
Physics Department
Queen Mary College
Mile End Road
London E1 4NS. England

Several important theoretical papers were published in 1960 or so stressing the advantages, in detector-limited circumstances, of two-beam interferometry as a method of spectroscopy. There followed several years of imaginative development of suitable laboratory systems for the submillimetre spectrum. Gradually the pitfalls of the method were identified and the many sceptics were slowly won over as greater reproducibility was achieved.

In terms of signal-to-noise ratio, rate of data acquisition and spectral resolution, the theoretical analysis promises yet more remarkable performance than has yet been widely achieved, however. The time is opportune for detailed assessment of the current limitations to performance in practice.

In terms of the possible modes of application (e.g., absolute radiometry, complex dielectric spectroscopy) too, more is possible in principle than is widely achieved in practice, and a detailed examination of the difficulties is called for.

The paper summarises the results of such assessments, and reviews the future potential of this well-established method of spectroscopy, including a comparison with the alternative methods promised for the future based on coherent sources and detection.

DOUBLE BEAM FOURIER SPECTROSCOPY WITH INTERFEROMETRIC BACKGROUND COMPENSATION

L. Genzel

Max-Planck-Institut für Festkörperforschung
Stuttgart, Federal Republic of Germany.

Double-beam spectroscopy for ratioing is not as easily achieved in Fourier interferometry as it is in conventional slit spectroscopy because the ratioing has to be done in the recovered spectrum and not in the interferogram. But double-beam differencing spectroscopy can be done successfully in the interferogram domaine of Fourier spectroscopy [1-10]. Such a technique is especially useful if a sample shows only small variations in absorptivity or reflectivity compared to a refence standard.

A slightly modified Michelson interferometer can have two accessible inputs and outputs each of which could be used for double-beaming. A possible version of such an interferometer is shown in Fig.1 [3] . Other versions have been described elsewhere [4-9] . Each input beam has an interferogram and an anti-interferogram output. Adding the intensities of these two outputs by detection with one detector results in a cancellation of the modulated parts of the interferogram and the anti-interferogram if the two beams are balanced. Introducing a sample and a reference standard in the two beams respectively causes an inbalance and yields a small interferogram-like modulation while all common features are still cancelled [9] . It can be shown that an interchanging of source and detector gives the same result provided the two input beams have equal spectral intensities.

If we describe the above mentioned properties more quantitatively we get for the output power $P_1 = |A_1|^2$ (Fig.1) in one spectral element at wavenumber ν

$$P_1 = p_1 2RT + p_2 (R^2+T^2) + (p_1-p_2)2RT\cos\varphi + p_2 4RT\cos\phi\cos(\varphi-\phi) \qquad (1)$$

where p_1 and p_2 are the two input powers respectively, R and T are the power reflectance and transmittance of the two identical beamsplitters, $\phi = \phi_r - \phi_t$ is the phase difference between beamsplitter reflection and transmission and $\varphi = 2\pi\nu\gamma$ is the phase shift due to the path difference γ introduced by the movable mirror P (Fig.1). The power P_2 of the second output is obtained from(1) by exchanging p_1 and p_2 and by replacing φ by $(-\varphi)$.

It is important to note that the expected double-beam properties are possible only if the fourth term in (1) is zero because this term causes a sine-modulation of the respective anti-interferogram which is not cancelled by adding P_1 and P_2. The fourth term can be made zero by using lossless beamsplitters, $R+T = 1, |\phi| = \frac{\pi}{2}$. We have then

$$P_1 = p_2 + (p_1-p_2)2RT(1+\cos\varphi) \qquad (2a)$$

$$P_2 = p_1 - (p_1-p_2)2RT(1+\cos\varphi) \qquad (2b)$$

and

$$P_1 + P_2 = p_1 + p_2 \qquad (3)$$

Equ. (3) shows the cancellation effect because the φ-dependence is dropped out. Fig.2 shows an actual result achieved with an instrument described earlier [9] but now used in the mode (b) shown in Fig. 3 instead of mode (a) as it was used then. In mode (b), care must be taken that the input beams from different but nearby solid angles of the source meet the condition $p_1 = p_2 = p$ for all wavenumbers of interest. A copper metal mesh proved to be a good approximation to a lossless beamsplitter in the selected spectral range below 100 cm^{-1}. If a sample (transmittance T_S) and a reference standard (transmittance T_R) is now introduced in the input beams of mode (b) a resulting interferogram is obtained given by

$$I(\gamma) = \int_0^\infty p(\nu)\left[T_S(\nu) - 2R(\nu)T(\nu)(T_R(\nu)-T_S(\nu))\right]d\nu - \int_0^\infty p(\nu)\,2R(\nu)T(\nu)\left(T_R(\nu)-T_S(\nu)\right)\cos(2\pi\nu\gamma)\,d\nu \qquad (4)$$

and which can be transformed to give $(T_R(\nu)-T_S(\nu))$ if $p(\nu)\cdot 2R(\nu)T(\nu)$ is measured separately by a background interferogram. It is seen from (4) that the modulated part in (4) can be small compared to the unmodulated part if T_R and T_S differ by a small amount. The large unmodulated part can give rise to strong noise effects in the recovered spectrum if source fluctuations are appreciable. A way to get rid of this is by using a chopping technique as shown in Fig.4 (a) and (b). Consider for instance mode (a) in Fig. 4. During one half-period of the chopper, say only p_1 is present and $p_2 = o$, the detector measures $P_1' + P_2'$. In the other half period, the detector sees $P_1" + P_2"$. Subtraction of these signals by phase sensitive electronics yields with $p_1 = p_2 = p$ the interferogram

$$I(\gamma) = \int_0^\infty p(\nu)\left(T_R(\nu)-T_S(\nu)\right)\left(1-4R(\nu)T(\nu)\right)d\nu - \int_0^\infty p(\nu)\left(T_R(\nu)-T_S(\nu)\right)4R(\nu)T(\nu)\cos(2\pi\nu\gamma)\,d\nu \qquad (5)$$

The same result follows if mode (b) of Fig.4 is used. Equ. (5) shows that the unmodulated part of $I(\gamma)$ is now small, especially if the beam splitter has a high efficiency 4RT and if T_R and T_S do not greatly differ.

It is worth noting that the two beams entering the detector in mode (a) of Fig. 3 and 4 at the same time must be inclined against another to average out interference fringes caused by the two coherent output waves A_1 and A_2. The mode (b)

(Fig.3 and 4) may therefore be preferable if small detector areas are used.

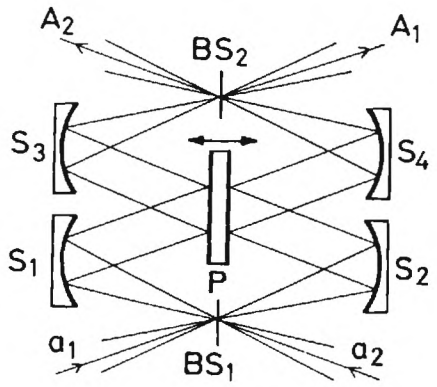

Fig. 1 A schematic of a double-input double-output interferometer. a_1, a_2 input amplitudes. A_1, A_2 output amplitudes. BS_1 and BS_2 beamsplitters. S_1-S_4 spherical mirrors. P movable plane double-mirror.

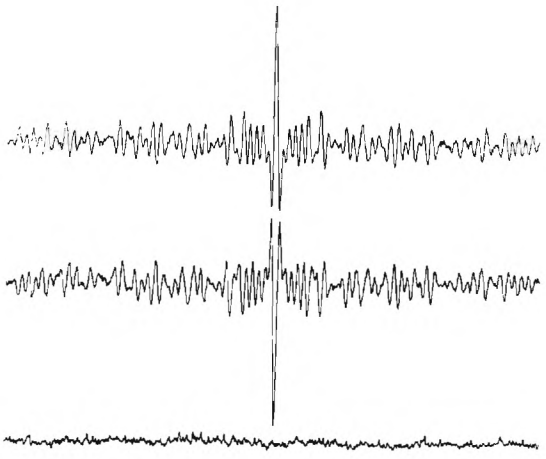

Fig. 2 Experimental results of double-input single-output set-up (Fig. 3b). Upper trace: Interferogram of p_1, p_2 closed. Middle trace: Anti-interferogram of p_2, p_1 closed. Lower trace: Both p_1 and p_2 open.

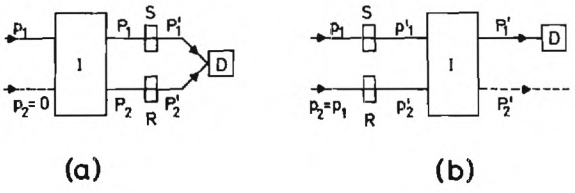

Fig. 3 A schematic of the (a) single-input double output mode, and (b) double-input single-output mode of operation. I interferometer. D detector. S sample. R reference standard.

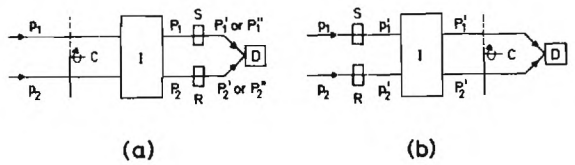

Fig. 4 A schematic of the (a) chopped-double-input double output mode and (b) double-input chopped-double-output mode of operation. C chopper. Remaining symbols as in Fig. 3.

References

1. R.T. Hall, D. Vrabek, J.M. Dowling, Appl. Opt. 5, 1147 (1966).
2. J. Kauppinen, Appl. Opt. 14, 1984 (1975).
3. L. Genzel, H.R. Chandrasekhar, J. Kuhl, appearing in Opt. Commun.
4. D. H. Martin, E. Puplett, Infrared Physics 10, 105 (1970).
5. W.J. Burroughs, J. Chamberlain, Infrared Physics 11, 1 (1971).
6. R. Hanel, M. Forman, R. Meilleur, R. Westcott, J. Pritchard, Appl. Opt. 8, 2059 (1969).
7. F.J. Ahern, C. Pritchet, Appl. Opt. 13, 2240 (1974).
8. G.A. Vanasse, R.E. Murphy, F.H. Cook, Appl. Opt. 15, 290 (1976).
9. H. R. Chandrasekhar, L. Genzel, J. Kuhl, Opt. Commun. 17, 106 (1976).
10. J.N. Willis, Infrared Physics 16, 299 (1976).

PRECISE DIELECTRIC MEASUREMENTS ON LOW-LOSS MATERIALS AT MILLIMETRE AND SUBMILLIMETRE WAVELENGTHS

M.N. Afsar and G.W. Chantry
Division of Electrical Science
National Physical Laboratory, Teddington,
Middlesex, United Kingdom

Summary

The first indication that non-polar materials might show dielectric absorption and dispersion in the high-frequency region came from the microwave work of Whiffen [1] on non-dipolar liquids such as carbon tetrachloride and benzene. Günthard and his colleagues [2] later detected the infrared "tail" of this absorption in the frequency region above 50 cm^{-1} but it was only with the work of Chantry et al. [3] and of Gabelnick and Strauss [4] that the absorption bands were completely characterised. They were then shown to be similar in profile to the bands observed for polar liquids [5] but about one order of magnitude weaker. Since that time much theoretical effort has been deployed in attempts to understand the origin of this absorption process. These theories are usually couched in terms of the complex relative permittivity $\hat{\varepsilon}' = \varepsilon' - i\,\varepsilon''$ whereas the quantity usually measured at submillimetre frequencies is the complex refractive index $\hat{n} = n - i\,\alpha/4\pi\tilde{\nu}$ where n is the refractive index, α is the power absorption coefficient (usually expressed in Neper/cm) and $\tilde{\nu}$ is the wavenumber (in cm^{-1}). The two systems are however readily related by Maxwell's celebrated equation

$$\hat{\varepsilon} = (\hat{n})^2$$

Apart from its theoretical interest, the absorption, in the submillimetre region by non-polar material is of great practical importance since transparent materials are required as transmissive media for high-frequency communication systems [7]. The simple theory of crystalline non-polar polymers, such as polypropylene $-[CH_2.CH(CH_3)]_n-$, just as does the theory of simple non-polar liquids, predicts no absorption in the millimetre wave region. However finite absorption is detected [6] for all practical polymers and it is now suspected that even were one able to make bulk specimens with 100% crystallinity, they too would show absorption in this band.

In the light of this we have over the last few years been developing techniques which permit us to make precise measurements of both n and α for low-loss liquids and solids. These involve the use of advanced Michelson type interferometric spectrometers used in the asymmetric or dispersive mode [8]. The Fourier transformation of the interferograms produced by these instruments gives both n and α directly [8,9]. The principal difficulty in measurements on low-loss materials is that the reflection losses and artefacts due to non-parallel radiation may easily exceed the absorptive loss in the specimen. However the fully developed dispersive method [10] permits a full treatment of all interface effects and results therefore in very accurate determinations. This is true provided the absorption is not so small that an impossibly thick specimen is required to give measurable absorption. In practice we can measure α values down to about 0.08 Neper cm^{-1} but this could be extended (with a consequent loss in precision) down to about 0.05 Neper cm^{-1} by going over to straight transmission methods. The absolute precision we can achieve is about ± 1% for α and ± 0.01% for n but this at the limit of our present technique.

The three most transparent liquids so far known in the submillimetre region are cyclohexane, and cis and trans decalin. Cyclohexane is the least absorbing at microwave frequencies but at 50-100 cm^{-1} (1.5-3 THz) the situation is reversed and both decalins are more transparent. Thus the peak of the submillimetre absorption band for cyclohexane reaches 0.68 Neper/cm (at a frequency of 2.5 THz) whereas the peaks for both decalins lie below 0.5 Neper cm. The reason for this is not at all clear. The spectra of cis and trans decalin at 26 °C are shown in Figs 1 and 2. The spectrum of polypropylene at 26 °C is shown in Fig. 3. The absorption levels so far achieved with hydrocarbon polymers are still too high for effective use of the materials in communication systems but they are low enough for them to be used as windows and in the fabrication of optical components such as lenses.

References

[1] Whiffen, D.H. Trans Faraday Soc. 45, 124, 1949.

[2] Wyss, H.R., Werder, R.D., and Günthard, Hs.H. Spectrochim Acta, 20, 573, 1964.

[3] Chantry, G.W., Gebbie, H.A., Lassier, B., and Wyllie, G., Nature, Lond., 214, 163, 1967.

[4] Gabelnick, H.S., and Strauss, H.L. J. Chem. Phys. 46, 396, 1967.

[5a] Chantry, G.W. and Gebbie, H.A. Nature, Lond. 208, 328, 1965.

[5b] Davies, M., Pardoe, G.W.F., Chamberlain, J., and Gebbie, H.A. Trans Faraday Soc. 66 273, 1970.

[6] Chantry, G.W., Fleming, J.W., Smith, P.M., Cudby, M., and Willis, H.A. Chemical Physics Letts. 10 (4), 483, 1971.

[7] Davies, G.J., and Haigh, J. Infrared Physics, 14, 183, 1974.

[8] Afsar, M.N., Hasted, J.B. and Chamberlain, J. Infrared Physics, 16 (1/2), 301, 1976.

[9] Afsar, M.N., Hasted, J.B., Zafar, M.S., and Chamberlain, J. Chemical Physics Letters, 36 (1), 69, 1975.

[10] Afsar, M.N. Accepted for publication, Physica.

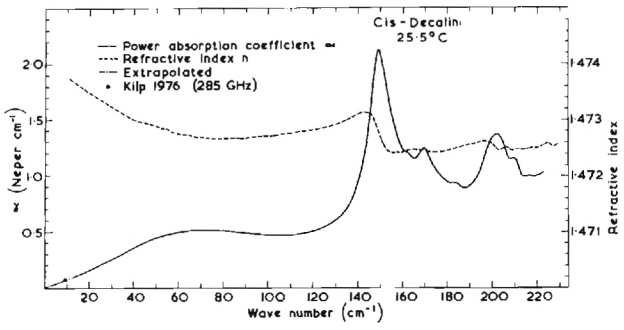

Figure 1. Power absorption coefficient and refraction spectra of cis-decalin at 25.5 °C.

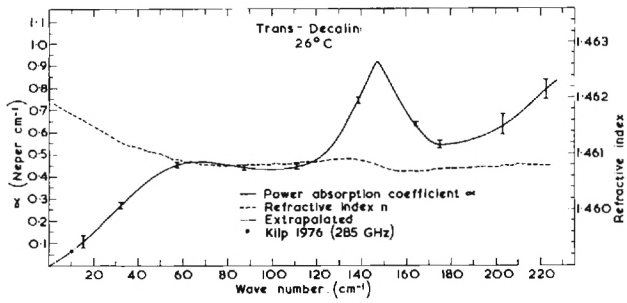

Figure 2. Power absorption coefficient and refractive index spectra of trans-decalin at 26 °C.

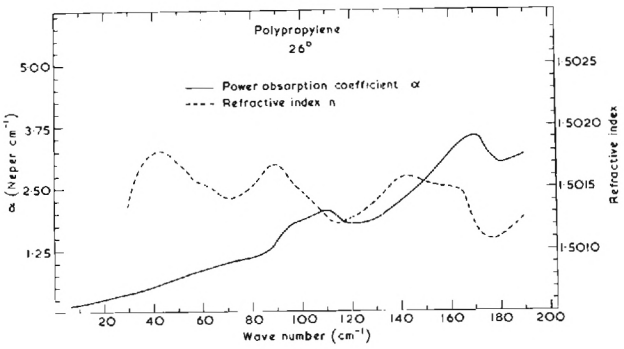

Figure 3. Power absorption coefficient and refractive index spectra of polypropylene at 26 °C.

POLARISED TWO-BEAM INTERFEROMETRY: REVIEW AND ASSESSMENT

D. H. Martin, E. Puplett, B. Carli, and R. Hughes
Physics Department
Queen Mary College
Mile End Road
London E1 4NS. England

The well-known advantages of two-beam interferometry over dispersive techniques of spectrometry refer to detector-noise limited circumstances. As detectors improve and much higher signal-to-noise ratios are expected, the advantages are gained only by fully exploiting other basic aspects of two-beam interferometry, namely the complementary natures of the two input ports and the two output ports. Conventional ways of doing this can lead to elaborate optical systems; the method of polarised interferometry is, however, a direct and simple method. This was first pointed out in 1969 [1]. Since then the method has been fully developed and used in a number of demanding applications, but has not been fully described in the literature.

In this method the two beams are orthogonally polarised and, on recombination, the interferometric information is in the ellipticity. It is then transferred to the intensity by transmission through or reflection from an output polariser. To give a non-zero output the input beam must be coded by transmission through, or reflection from, an input polariser. The two possibilities (transmission and reflection) define the two input and two output ports.

In the paper, the many ways of exploiting the easy access to all ports are reviewed, and examples of performance (e.g., 0.01 cm^{-1} resolution, in 10 minute scans, in the range 5-500 cm^{-1}) will be given.

[1] Martin, D. H., Puplett, E., 1969 Infrared Physics, 10, 105

DISPERSIVE FOURIER TRANSFORM SPECTROMETRY WITH VARIABLE THICKNESS, VARIABLE TEMPERATURE LIQUID CELLS

M.N. Afsar*, D.D. Honijk†, W.F. Passchier†
and J. Goulon‡

*Division of Electrical Science, National Physical Laboratory, Teddington, Middlesex, United Kingdom

†Gorlaeus Laboratoria, afd. Fysische Chemie, Rijksuniversiteit Leiden, Netherlands

‡Laboratoire de Chimie theorique, Universite de Nancy 1, France

Summary

Dispersive Fourier transform spectrometry (DFTS) of liquids [1] in the millimetre and submillimetre wave region has been extended to include precise measurement of the complex refractive index $\hat{n}$ or the complex relative permittivity $\hat{\epsilon}$ of medium loss as well as high loss volatile liquids over a wide temperature range (- 80 °C to 80 °C) by the use of variable thickness windowed cell in one active arm of the Michelson type two beam interferometer. In the past these measurements were restricted to liquids of relatively low vapour pressure because of the necessity to use a free layer of liquid. An excess of liquid vapour absorbs radiation and gives its own characteristic spectrum [2]. The free layer method and subtraction [3,4] and double subtraction [5] procedures enabled investigation of liquids of absorption coefficient α up to 250 Neper/cm. But as the absorption increases it becomes more and more difficult to produce a sufficiently thin plane parallel layer held freely under gravity. However for very absorbing liquids, like water, reflection DFTS [5,6] has been successfully used in which accurate determination of the phase shift and an extremely stable interferometric system are essential.

In order to overcome these difficulties two liquid cells with windows have been constructed, one at the University of Leiden, The Netherlands and the other at the University of Nancy 1, France in cooperation with the National Physical Laboratory, United Kingdom. These cells were used at the N.P.L. with an improved Michelson-type interferometric system. The ray diagram of the interferometer and the cell arrangement is shown in figure 1. The fixed mirror arm is mounted vertically upwards. The mirror can be moved up and down above the window to produce different thicknesses. The interferometer can be readily interchanged to either the dielectric beam splitter mode or the polarization mode [5]. The interferometer in the polarization mode with free standing wire grid beam splitters covers the frequency range between 3 and 220 cm^{-1} while the dielectric mode has been normally used between 100 and 600 cm^{-1}. The scanning mirror arm is bent at 45° with the use of a half cube. This half cube accommodates the phase modulator assembly. Extreme care has been taken for thermal stabilization of the interferometer by circulating thermostated liquid in its different parts.

The Leiden cell [7,8] comprises of a 40 mm diameter window (crystal quartz or hyperpure silicon) of thickness ~ 2.5 mm. The gold plated mirror is mounted under a cylinder which moves in another cylinder by difference in pressure. Thermal isolation is maintained by evacuating the space between the cylinders and the outer jacket. The displacement of the mirror can be measured with an accuracy of 0.1 μm by the use of slip gauges positioned in between a fixed rigid table and the rod mounted with the inner cylinder. A liquid thickness of 10 μm to 5 mm can be used.

A germanium or a T.P.X. (poly 4-methyl pentene-1) window of 75 mm diameter and 5 mm thickness has been used with the Nancy cell [9-11]. The front surface of a piston is polished and gold plated and acts as a mirror. This is mounted on a micrometer which allows displacement up to 10 mm thereby permitting liquid thicknesses between 10 μm and 10 mm. The displacement is measured using precision transducers. Thermal isolation is maintained by the use of nylon spacers.

Different evaluation methods [7-13] can be used with these cell techniques. Knowledge of the complex refractive index of the window $\hat{n}_w$ is required in all evaluation methods except the two thicknesses method. $\hat{n}_w$ is evaluated from the same set of measurements [7,8,14]. Details of these techniques together with some new results will be discussed at the conference. Comparisons of experimental results of different evaluative methods and the free layer method will also be shown.

Acknowledgements

The project was initiated in cooperation with the late Dr J. Chamberlain of the National Physical Laboratory. The authors wish to thank Professor M. Mandel of the University of Leiden, Professor Rivail of the University of Nancy, Mr J.R. Birch, Dr G.W. Chantry and Dr N.W.B. Stone of the National Physical Laboratory for their kind help.

References

[1] J. Chamberlain, J.E. Gibbs and H.A. Gebbie, Infrared Physics, 9, 185, 1969.

[2] W.F. Passchier, D.D. Honijk and M. Mandel, Infrared Physics, 16, 389, 1976.

[3] J. Chamberlain, M.N. Afsar and J.B. Hasted, Nature Phys. Sci., 245, 28, 1973.

[4] M.N. Afsar, J. Chamberlain and J.B. Hasted, Infrared Physics, in Press.

[5] M.N. Afsar, J.B. Hasted and J. Chamberlain, Infrared Physics, 16, 301, 1976.

[6] J. Chamberlain, M.N. Afsar, D.K. Murray, G.D. Price and M.S. Zafar, IEEE Trans. Inst. and Meas. IM 23, 483, 1974.

[7] D.D. Honijk, W.F. Passchier, M. Mandel and M.N. Afsar, Infrared Physics, 16, 257, 1976.

[8] D.D. Honijk, W.F. Passchier, M. Mandel and M.N. Afsar, Infrared Physics, in Press.

[9] J. Goulon and M.N. Afsar, to be published.

[10] M. Hollecker, Docteur de specialite, Thesis, University of Nancy - 1, France, 1975.

[11] M.N. Afsar and J. Goulon, to be published.

[12] D.D. Honijk, W.F. Passchier and M. Mandel, Physica, 68, 457, 1973.

[13] W.F. Passchier, D.D. Honijk and M. Mandel, Infrared Physics, 15, 95, 1975.

[14] W.F. Passchier, D.D. Honijk, M. Mandel and M.N. Afsar, to be published.

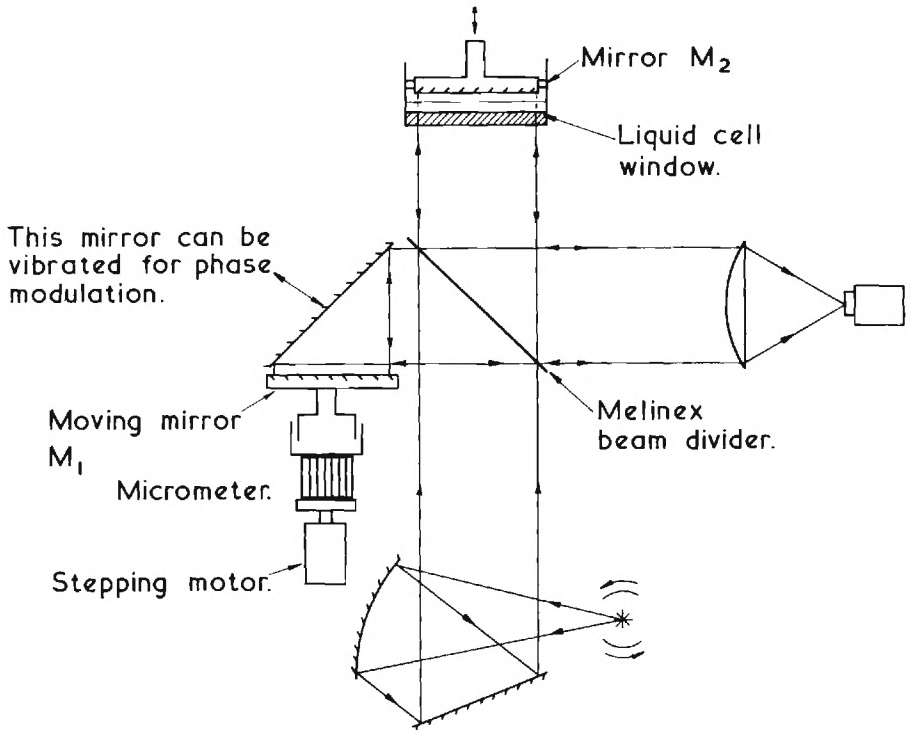

Figure 1. Ray diagram of the Michelson interferometer with the liquid cell in the dielectric beam splitter mode

MEASUREMENTS OF THE OPTICAL CONSTANTS OF LIQUID H_2O AND D_2O UP TO 450 CM^{-1}

M.N. Afsar and J.B. Hasted
Division of Electrical Science, National Physical Laboratory, Teddington, Middlesex, U.K., and Department of Physics, Birkbeck College, University of London, U.K.

Summary

Reflection dispersive Fourier transform spectrometric (DFTS) technique has been used to measure the optical constants of liquid water and heavy water at 19 °C over the frequency range $70 \leq \tilde{\nu} \leq 450$ cm^{-1}. A new liquid cell, with a single crystal hyperpure silicon window of thickness 2.45 mm, has been used. Its design is similar to that previously reported [1]. The interferogram signature $F_{WO}(x)$ obtained at the silicon-air interface is considered as a reference interferogram [2] instead of using a window-mercury reference. The complex insertion loss $\hat{\mathcal{L}}(\tilde{\nu})$ is given by

$$\hat{\mathcal{L}}(\tilde{\nu}) = \frac{\hat{r}_{WL}(\tilde{\nu})}{r_{WO}(\tilde{\nu})} = \frac{\mathcal{F}\{F_{WL}(x)\}}{\mathcal{F}\{F_{WO}(x)\}}$$

$$= \frac{[\hat{n}_L(\tilde{\nu}) - \hat{n}_W(\tilde{\nu})][1 + \hat{n}_W(\tilde{\nu})]}{[\hat{n}_L(\tilde{\nu}) + \hat{n}_W(\tilde{\nu})][1 - \hat{n}_W(\tilde{\nu})]}$$

where $f_{WL}(\tilde{\nu})$, $f_{WO}(\tilde{\nu})$ are the amplitude reflectivities respectively at window-liquid and window-air interfaces, $\mathcal{F}\{\}$ represents Fourier transform, $F_{WL}(x)$ is the interferogram signature obtained at window-liquid interface $\hat{n}_W(\tilde{\nu})$ and $\hat{n}_L(\tilde{\nu})$ are the complex refractive indices of the window and the liquid respectively. $\hat{n}_W(\tilde{\nu})$ is determined from the same measurements using transmission DFTS. [2,3]. Figures 1 and 2 represent the absorption and refractive index data for liquid water and heavy water.

Comparison of the present absorption data and our previous data [1,4] and that of Draegert et al [5] is reasonably satisfactory, but there is no recent refractive index data available beyond 200 cm^{-1} for comparison. The permittivity has been calculated from the data, and is plotted in the complex plane in Figure 3. Although the contribution from the principal relaxation is appreciable at low frequencies, its calculation and subtraction will be possible. There is a broad region of anomalously high refractive index, which might be associated with a molecular relaxation rather than a resonance process. The basic form of such a process plotted in this way should be a semi-circle. But a resonance process at 200 cm^{-1} and 600 cm^{-1} appears superposed on this broad region, and the significant feature of this data is the small curlecue around 200 cm^{-1}, which is displayed for the first time, and distinguishes this process from the semi-circular background.

References

[1] M.N. Afsar, J.B. Hasted and J. Chamberlain, Infrared Physics, 16, 1976, 301-310.

[2] D.D. Honijk, W.F. Passchier, M. Mandel and M.N. Afsar, Infrared Physics, 16, 1976, 257-262.

[3] W.F. Passchier, D.D. Honijk, M. Mandel and M.N. Afsar, To be published.

[4] J. Chamberlain, M.N. Afsar, J.B. Hasted, M.S. Zafar and G.J. Davies, Nature, 255, 1975, 319-321.

[5] D.A. Draegert, N.W.B. Stone, B. Curnette and D. Williams, Journal of the Optical Society of America, 56 (1), 1966, 64-69.

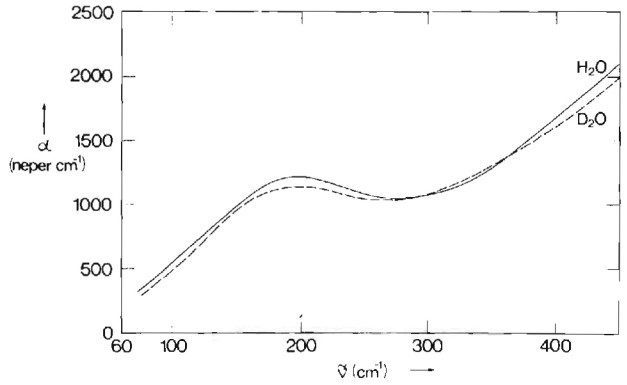

Figure 1 Power absorption coefficient $\alpha(\tilde{\nu})$ for liquid water and heavy water at 19 °C.

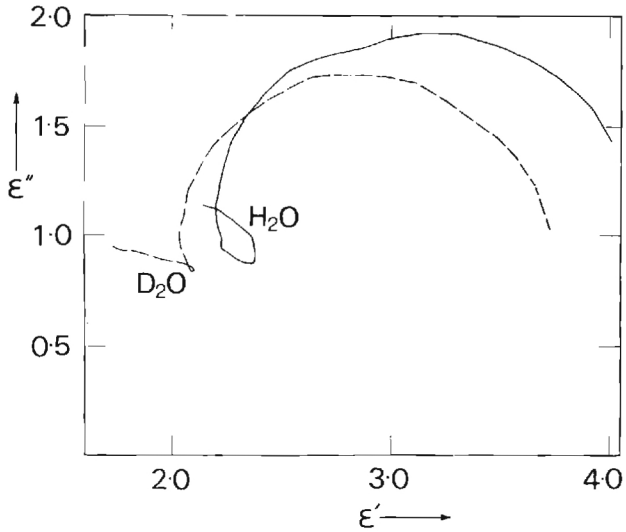

Figure 3 High frequency end of Cole-Cole diagram for liquid H_2O and D_2O calculated from the $\alpha(\tilde{\nu})$, $n(\tilde{\nu})$ data.

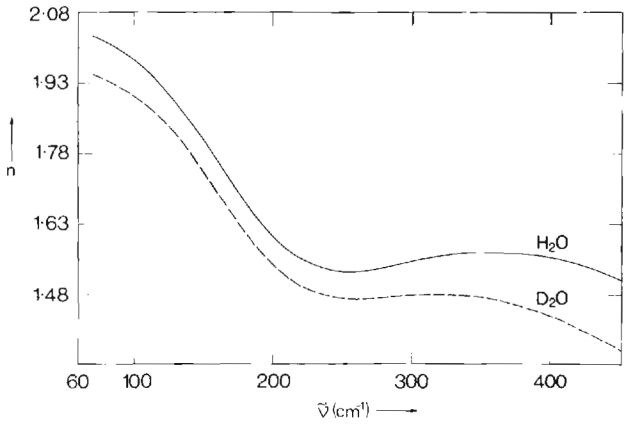

Figure 2 Refractive index spectra of H_2O and D_2O at 19 °C.

INCREASE IN THE OPTICAL PUMPING EFFICIENCY OF A TEA-CO_2 LASER BY LONGITUDINAL MODE CONTROL

Pierre Mathieu and Jerald R. Izatt
Laboratoire de recherches en optique et laser
Université Laval, Québec, P.Q. Canada

Introduction

Optical pumping of organic molecules at pressure < 10 Torr by a molecular infrared laser can produce strong coherent FIR radiation. The TEA-CO_2 laser is well suited for this purpose because of its high power and the large number of lines it produces. An apparent disadvantage is the linewidth discrepancy between the TEA-CO_2 laser emission and the absorption lines in the FIR laser medium, due to the large pressure difference. As a result of this mismatch the energy conversion efficiency is usually much lower than when a cw CO_2 laser is used as a pump. Thus, for example, only 6 FIR laser lines produced by pumping CH_3OH with a TEA-CO_2 laser have been reported to date, and the maximum reported energy conversion efficiency is $\sim 10^{-5}$ [1] , [2] . On the other hand, pumping CH_3OH with a cw CO_2 laser has produced over 80 FIR lines and the conversion efficiency for many of them is $\sim 10^{-3}$. In principal, the linewidth mismatch can be put to good use by restricting the bandwidth over which the TEA-CO_2 laser is allowed to oscillate. The homogeneously broadened gain curve then insures that the laser emission will still be fed by the total population inversion, and the width of the gain curve constitutes a frequency tuning range within which it should be possible to pump many closely spaced transitions in the FIR laser medium. In the experiment reported here a tiltable Ge etalon was introduced into the TEA-CO_2 laser cavity to accomplish this purpose. The result was a large increase in conversion efficiency for a number of pump lines, including cases which permitted the observation of 14 new FIR laser lines.

Theory

The gain coefficient g (ν) for a given TEA-CO_2 emission line has a Lorentzian profile,

$$g(\nu) = g(\nu_o)\left\{1 + [2(\nu-\nu_o)/\Delta\nu]^2\right\}^{-1} \qquad (1)$$

Here ν_o is the frequency at the center of the line and the linewidth (FWHM) is $\Delta\nu$.

With the Ge etalon in the laser cavity oscillation occurs when

$$\ell\, g(\nu) + \tfrac{1}{2}\ln(R_1 R_2) \geq -\ln T(\nu) \qquad (2)$$

Here ℓ is the cavity length, R_1 and R_2 are the reflectivities of the end mirrors, and T (ν) is the frequency dependent transmission of the etalon.

To calculate T (ν) it is necessary to consider reflection and scattering at the etalon surfaces, absorption within the Ge slab, and walkoff losses when the etalon is tilted. Neglecting the latter loss for the moment it can be shown that in the plane parallel wave approximation the transmission is given by

$$T'(\nu) = \frac{T^2}{(e^{\beta} - Re^{-\beta})^2 + 4R^2\sin^2\gamma} \qquad (3)$$

with

$$\gamma = 2\pi n' t \nu c^{-1}\cos\theta' . \qquad (4)$$

In Eq. (3) T is the surface transmissivity corrected for scattering losses, R is the surface reflectivity, and $\beta = t\alpha/2\cos\theta'$. The etalon thickness is t, α is the absorption coefficient and n' is the refractive index of the germanium. θ' is the angle between the rays inside the etalon and a normal to its surface. θ' is related to the tilt angle by Snell's law. Note that in the limit $\beta = \alpha = 0$, Eq. (3) reduces to the usual Airy formula.

The walkoff losses have been treated by Leeb [3] , and for our setup they do not exceed 4%. We therefore use T (ν) = .96T'(ν) in the following example, which has been chosen to facilitate comparison with our experimental results. We take R=0.5, T=0.49, $\alpha = 3.2\text{m}^{-1}$, t=7mm, n'=4, and we set the tilt angle at a value which places one of the transmission maxima 500 MHz from the center of the gain curve. The results are plotted in Fig. 1 for a laser line near 9.6μm. The solid line represents the left-hand side of Eq. (2) using g (ν_o)=.002cm^{-1} and $\Delta\nu$=3.6 GHz . The other parameters used in Eq. (2) were ℓ =200 cm, R_1 =.65 and R_2 =.80. The dashed line in Fig. 1 represents the right hand side of Eq. (2).

It can be seen from Fig. 1 that oscillation can occur over a bandwidth of $\sim$ 5 GHz when there is no etalon in the cavity. Introduction of the etalon reduces the oscillation bandwidth to $\sim$400 MHz . As the etalon is tilted the $\ln$T (ν) curve shifts in frequency, and Fig. 1 indicates that oscillation can continue to occur for a shift of $\sim$1 GHz on either side of the line center. The free spectral range of the etalon is 5.3 GHz , and this places the other minima of -$\ln$T (ν) beyond the region where the gain is sufficient to permit oscillation.

Experiment

Our FIR laser cavity consisted of a cylindrical metallic waveguide 2.5 cm in diameter and 90 cm long, closed on both ends by piston-type mirrors with central coupling holes [4]. The pump laser was a resistor-ballasted helical TEA-CO_2 laser with a 200 cm discharge section. It could be tuned by means of a plane intracavity grating to oscillate on all of the principal lines in the 9.6 μm and 10.6 μm bands. The gain bandwidth was estimated to be $\sim$ 3.6 GHz. The TEA-CO_2 laser pulses displayed sharply spiked multimode structure. The pulse envelope had a width (FWHM) of 0.2 μsec and the energy of a typical pulse was $\sim$ 0.2 joules. The peak gain was estimated to be $\sim .002$ cm^{-1} by introducing known losses into the cavity until lasing stopped. The TEA laser end mirrors had the reflectivities used in the example treated in the previous section.

Using this laser to pump CH_3OH in the FIR laser cavity we were able to observe 8 FIR emission lines before the etalon was introduced into the TEA laser cavity. The CH_3OH pressure was maintained at $\sim$ 1 Torr, so that the width of the absorption lines was $\sim$ 80 MHz.

We then inserted a Ge etalon into the TEA-CO_2 cavity which was 7mm thick and had dielectric coated faces with a reflectivity of 0.5. With this etalon in place all of the parameters used in the example of the previous section were closely reproduced. By observing the laser pulses with a photon drag detector and analyzing the greatly reduced pulse fine structure we estimated the oscillation bandwidth to be $\sim$ 200 MHz. By tilting the etalon we were able to tune the laser over 1.5 GHz for the highest gain lines. Thus the experimental results are in reasonable agreement with the calculations.

Some of the results obtained when this laser was used to pump the CH_3OH laser are shown in Table 1, which lists the ratio of the energy conversion efficienies observed with and without the intracavity etalon in place. Three previously unreported FIR lines are indicated by asterisks. The wavelengths were measured with a Fabry-Perot etalon with metallic mesh mirrors. Obviously a comparison of conversion efficiencies could not be made for the 14 new lines which could be observed only with the etalon in place.

Conclusion

Our results demonstrate that a significant increase in pumping efficiency can be achieved by restricting and tuning the frequency band within which the TEA-CO_2 laser oscillates. Indeed the energy conversion efficiency which we measured for the 55.8 μm line pumped by P (14) was $\sim 10^{-3}$, and while the calibration of the detectors used for the absolute measurements is not yet complete, it appears safe to conjecture that conversion efficiencies comparable to those achieved with a cw CO_2 laser pump can be realized by further development of this technique.

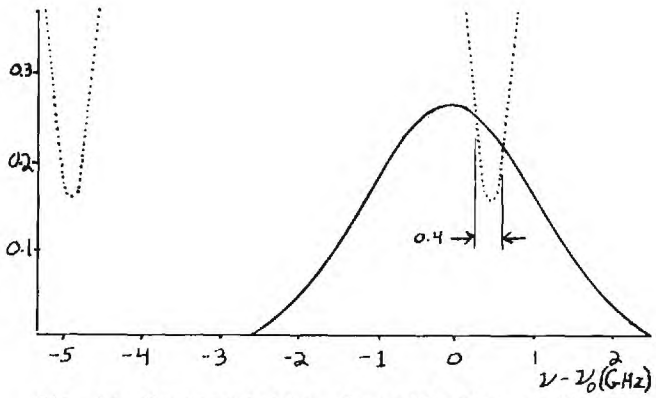

Fig. 1: Representation of oscillation condition for laser with intracavity etalon.

Table 1: Increase in efficiency obtained by using Ge etalon.

CO_2 Pump Lines 9.6 μm Band	CH_3OH Laser Wavelengths	Efficiency Ratio
R (18)	64.0 μm	2.1±.2
P (10)*	46.8	37 ± 4
P (12)*	46.4	23 ± 3
P (14)	55.8	23 ± 3
P (16)	570.5	3.6±.2
P (20)*	59.8	18 ± 2

REFERENCES

[1]. H.R. Fetterman, H.R. Schlossberg and J. Waldman, Opt. Commun. 6, 156, (1972).

[2]. J.R. Izatt, B.L. Bean and G.F. Caudle Opt. Commun. 14, 385, (1975).

[3]. W.R. Leeb, Appl. Optics 14, 1706, (1975).

[4]. D.T. Hodges and T.S. Hartwick, Appl. Phys. Lett. 23, 252, (1973).

APPLICATION OF SUBMILLIMETER WAVE TECHNIQUES TO ISOTOPE SEPARATION

R. W. McMillan, R. G. Shackelford
and J. J. Gallagher
Georgia Institute of Technology
Atlanta, Georgia

I. INTRODUCTION

With the extension of available laser wavelengths into regions of the spectrum previously unattainable, especially in the infrared [1], laser induced photochemistry is becoming a valuable approach for both analysis and synthesis of compounds. In the field of isotope separation [2], used for uranium enrichment, the advantage of laser photochemistry over earlier methods is especially marked, and results in order-of-magnitude cost savings over the next most cost effective method.

Unfortunately, since lasers generally operate at certain discrete wavelengths, with narrow tuning ranges, it is not always possible to match a laser wavelength to the desired transition in the material to be irradiated. Mixing of different lasers, or mixing of lasers with microwave sources [3], are approaches to this matching problem which have recently received considerable attention. The recent availability of relativistic electron beam (REB) microwave sources makes the laser/microwave mixing approach to tunability even more attractive. Peak power up to 10^9 watts in pulsewidths of 10^{-8} seconds have been observed and outputs to 100 cm^{-1} have been shown to be possible [4]. Such a source would be generally compatible in pulsewidth and peak power to, for example, a transversely excited (TEA) CO_2 laser, and should provide good efficiency, since mixing efficiencies are generally proportional to the powers of the constituent sources.

II. DISCUSSION

The laser/microwave mixing scheme provides a highly flexible mechanism for infrared tunability. This scheme can be employed throughout the IR if stable fixed frequency lasers and appropriate mixing media exist in the spectral regions of interest. Because of the power limitations imposed by nonlinear crystals, generally used for this type mixing, different mixing media are required, and this role may be filled by nonlinear effects in gases, which are currently being explored.

If an REB device were used in a frequency up-conversion process, it is estimated that considerable energy for isotope enrichment could be achieved, when mixed with a fixed frequency TEA laser operating in the spectral range of interest. In such a mixing configuration, powers on the order of 10^7W would be available from both sources with pulse widths on the order of 300 ns. Both mixing sources are capable of high efficiency; the REB efficiencies running as high as 40% while CO_2 TEA lasers have been on the order of 5%. With an efficient mixing medium, the economic requirements of the isotope enrichment process should be well satisfied, and an overall efficiency of 0.1% should be attainable.

In making predictions of the efficiency of four photon processes, it is assumed that the pump power density is limited by two-photon absorption of an intermediate non-allowed transition. The power density generated in a single coherence length at the sum (or difference) requency ω_s is given by [5]

$$\frac{P}{A}(\omega_s) = \frac{1}{2\pi^2}\, \eta\omega_s^2 \,|\, P(\omega_s) \,|^2 L_c^2 \qquad (1)$$

where $P(\omega_s)$ is the generated dipole moment, L_c = coherence length, and $\eta = (\mu/\varepsilon_o)^{1/2}$. For the energy level system such as that in Figure 1, the dipole moment and coherence length are approximated by

$$P(\omega_s) = \frac{N\mu_{01}\ \mu_{12}\ \mu_{23}\ \mu_{30}\ E_p^2\ E_t}{4h^3\ (\Delta\omega_1)\ (\Delta\omega_2 + 1/2\ j\delta\omega_2)\ \Delta\omega_3}\ , \qquad (2)$$

and

$$L_c = \frac{2\pi}{N}\ \frac{\hbar}{\eta}\ \frac{1}{\omega_s}\ \frac{\Delta\omega_3}{\mu_{03}^2}\ , \qquad (3)$$

where
- N = atomic (or molecular) density
- μ_{ij} = various dipole matrix elements
- $\Delta\omega_1 = \omega_p - \omega_{01}$
- $\Delta\omega_2 = 2\,\omega_p - \omega_{02}$
- $\Delta\omega_3 = 2\,\omega_p \pm \omega_t - \omega_{03}$
- $\delta\omega_2$ = half-power linewidth of ω_{02} transition
- E_p, E_t = electric field strenghts of pump and tunable microwave source

To employ the resonantly enhanced technique in the IR, energy level schemes must be investigated. In Figure 1, a pump laser at frequency ω_p is tuned or chosen so that the sum of two photons is equal to a non-allowed transition ω_{02}. The microwave source at frequency ω_t mixes with the pump signal to produce the sum or difference frequency $2\,\omega_p \pm \omega_t$. It has been shown that the process is particularly efficient if the generated frequency lies near an allowed transition ω_{03}. In Figure 1 n_0, n_1, n_2, and n_3 are energy levels in the mixing medium.

The use of an REB source in a resonant four photon process can be envisioned in several ways, two of which are shown in Figure 2. Figure 2a shows a Raman resonance energy level scheme in which a single photon of a TEA CO_2 laser (ω_1) is

mixed with two REB photons (ω_2) to produce a tunable output at ω_3, a frequency of interest to isotope enrichment. As an example, the CO_2 P(20) laser line of the 001-100 band (ω_1 = 944.19 cm^{-1}) mixed with two photons from an REB source at ω_2 = 60.6 cm^{-1} would yield an output at ω_3 = 823 cm^{-1}. Figure 2b demonstrates the 4-photon mixing process with 2-photon absorption. An example of this mixing process would consist of the CO_2 R(20) laser line of the 001-020 band (ω_1 = 1078.59 cm^{-1}) mixed with two REB photons at ω_2 = 40.705 cm^{-1} to give an output at ω_3 = 1160 cm^{-1}. The CO_2 laser is an excellent device to employ as a baseline laser for such mixing mechanisms. It is an efficient source, capable of high power, short pulses and narrow bandwidth. The frequencies of CO_2 transitions have been identified to 10^{-4} cm^{-1}, and this could be improved if required. The tunability of the REB can take advantage of the well-developed characteristics of the CO_2 laser by extending tunability as far as the spectral regions for uranium isotope enrichment.

A block diagram of the proposed experiment is shown in Figure 3. Microwave and laser sources are triggered simultaneously. A dichroic mirror makes the two beams collinear and they pass into the flowing gas mixing cell. At the output of the cell, the laser, microwave, and mixed components are separated by the monochromator and the mixed signal is sensed by the detector.

III. CONCLUSIONS

Because of recent advances in REB technology, and the attention being given gases as nonlinear mixing media, it is expected that this combination together with the CO_2 laser, will play an important role in future isotope enrichment efforts. Much work needs to be done in the areas of determination of dipole moments and energy levels, but efforts are being made in these areas which have already given fruitful results.

REFERENCES

1. J. J. Gallagher, M. D. Blue, B. Bean, S. Perkowitz, "Tabulation of Optically Pumped Far Infrared Laser Lines and Applications to Atmospheric Transmission," Infrared Phys. (to be published).
2. R. Jensen, J. Marinuzzi, P. Robinson, and S. Rockwood, "Prospects for Uranium Enrichment," Laser Focus, May 1976, p. 51.
3. V. J. Corcoran, J. J. Gallagher and R. E. Cupp, Applied Physics Lett. 16, 316, (1970).
4. J. J. Gallagher, H. A. Ecker, M. D. Blue and R. G. Shackelford, "Applications of Submillimeter Wave Gigawatt Sources," Final Report, ARPA Contract N00014-75-C-1011, September 1975.
5. S. E. Harris and D. M. Bloom, Applied Physics Lett. 24, 229, 1974.

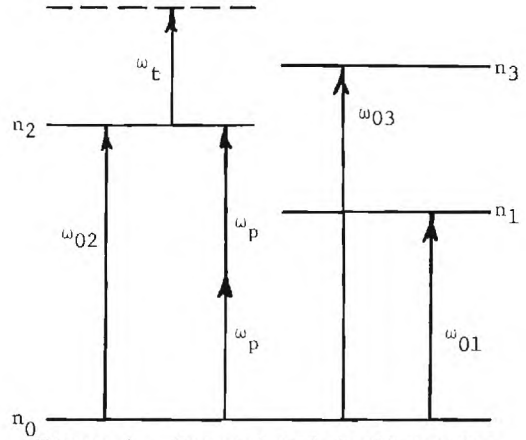

Figure 1. Energy Level Configuration for Resonantly Enhanced Two-photon Optical Mixing.

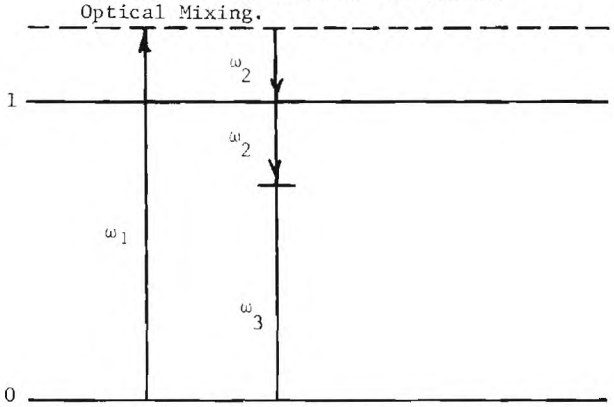

Figure 2a. Raman resonance energy level scheme. ω_1 = 955.19 cm^{-1}, ω_2 = 60.595 cm^{-1} ω_3 = 823 cm^{-1}.

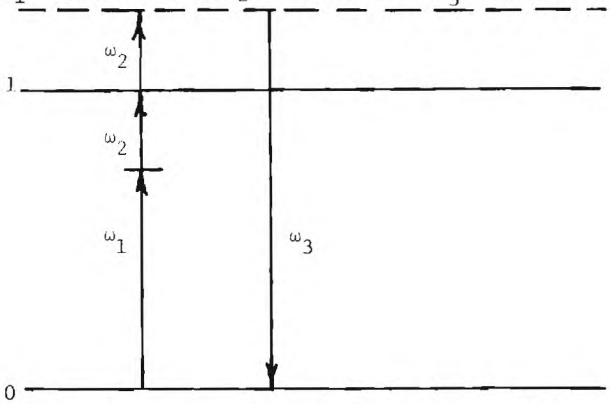

Figure 2b. Four-photon mixing process with two photon absorption. ω_1 = 1078.59 cm^{-1}, ω_2 = 40.705 cm^{-1}, ω_3 = 1160 cm^{-1}.

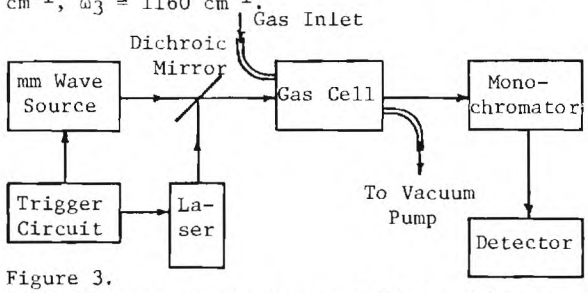

Figure 3.
Block Diagram of the Proposed Mixing Scheme.

TIME RESOLVED COLLISION FREQUENCY MEASUREMENTS IN HIGH PRESSURE GLOW DISCHARGES

T. V. George*, L. J. Denes and L. E. Kline
Westinghouse Research Laboratories
Pittsburgh, Pennsylvania 15235

Abstract

We have used the far infrared absorption techniques reported earlier [1] to measure the time resolved electron-neutral collision frequency in pulsed, high pressure glow discharges.

Theory

When an electromagnetic wave propagates through a weakly ionized high pressure glow discharge plasma, the wave undergoes attenuation according to the relation:

$$P_t = P_i \exp(-\alpha L) \tag{1}$$

where P_t is the transmitted power, P_i is the incident power, α is the absorption coefficient and L is the length of the absorbing plasma. The electron-neutral collision frequency, ν, is related to α by

$$\alpha = \sqrt{2}\,\frac{\omega}{c}\left\{\left[(1-R)^2 + (R\nu/\omega)^2\right]^{1/2} - (1-R)\right\}^{1/2} \tag{2}$$

where $R = \omega_p^2/(\nu^2 + \omega^2)$, ω is the radian frequency of the electromagnetic wave, c is the speed of light, and ω_p is the plasma frequency given by:

$$\omega_p^2 = ne^2/m\varepsilon \tag{3}$$

In Eq. (3) n, e and m are, respectively, the electron density, charge, and mass and ε is the permitivity of free space. In the present experiments $R \ll 1$. This relation and ω_p^2 from Eq. (3) can be substituted into Eq. (2) to give

$$n = (cm\varepsilon/e^2)[\nu^2 + \omega^2)/\nu]\alpha \tag{4}$$

An alternate expression for n as a function of the electron drift velocity, W and the current density, j is:

$$n = j/eW = jm\nu/e^2E \tag{5}$$

where we have used the expression

$$\nu/N = eE/mWN \tag{6}$$

In Eq. (6) E is the electric field in the discharge and N is the gas density.

By using Eqs. (4) and (5) to eliminate n and solving for ν we obtain:

$$\nu = \omega\{\alpha/[(j/c\varepsilon E) - \alpha]^{1/2} \tag{7}$$

which relates ν to measurable quantities since $j = I/A$, $E = V/d$ and $\alpha = -\ell n(P_t/P_i)/L$ from Eq. (1). I, V, A and d are, respectively, the discharge current, voltage, area and electrode spacing.

We have also calculated ν/N as a function of E/N following the procedure outlined by Lowke et al. [2]. First W was calculated as a function of E/N. Then the calculated values of W were substituted into Eq. (6). A calculated curve of ν/N vs. E/N for nitrogen is shown in Fig. 1.

Experimental Apparatus

Our experimental arrangement is described in [1]. The output of an HCN laser was focused at the center of the discharge chamber. The chopped transmitted beam was collected by a waveguide of 1.2 cm diameter and directed to an indium antimonide detector which was cooled to liquid-helium temperature and also subjected to a steady magnetic field of about 15 kG. The detector signal was amplified and displayed on an oscilloscope. This experimental configuration provided a spatial resolution of 0.5 cm and temporal resolution of 200 ns. The discharge was triggered twice so that the base line along with the electrical noise could be observed on the first trace, and the signal along with the same noise on the second trace. The ratio of the transmitted to the incident power was determined directly from the composite oscilloscope traces. Voltage and current traces corresponding to the same discharge conditions were also measured. Typical oscillograph traces are shown in Fig. 2. The dimensions of the discharge as established by time resolved framing photographs and the experimental geometry are: d = 1.3 cm, L = 10 cm and A = 26.5 cm^2. Substituting these dimensions and the values of the constants c and ε into Eq. (7) gives, for 337 μm radiation:

$$\nu = 5.59 \times 10^{12}\sqrt{\alpha/[18.49I/V)-\alpha]},\ \text{sec}^{-1} \tag{8}$$

Equation (8) was used together with the waveforms of V, I, P_t and P_i shown in Fig. 2, to determine measured values of ν as a function of time.

Results

Measured values and a calculated curve of ν vs. time for a discharge in 300 Torr nitrogen are shown in Fig. 3. The calculated curve was determined from the curve of ν/N vs. E/N shown in Fig. 1 and the measured E/N waveform which is

*Present address: ERDA, Washington, DC 20545

also shown in Fig. 3. The measured and calculated values of ν agree well except at early times when the measured value of P_t/P_i may be affected by the 200 ns time response of the detector and the discharge dimensions are not as well known.

We have also measured and calculated ν for discharges in helium and in three representative CO_2 laser mixtures. These results are compared in Table I which again shows good agreement.

Conclusions

We have shown that the electron-neutral collision frequency measured using the far infrared absorption technique described in this paper agrees well with the collision frequency calculated using the method of Lowke et al. [2]. The temporal variation of the collision frequency arises from the temporal variation of E/N in the discharge.

Acknowledgement

We wish to thank J. J. Lowke and A. V. Phelps for helpful discussions.

Mixture CO_2:N_2:He	E/N (Td)	ν/N, theory	10^{-7} cm^3 sec^{-1} experiment	
0:0:1	8.2	0.87	0.72	0.82
1:1:8	23	0.70	0.69	0.72
1:2:3	46	0.97	0.97	1.02
1:7:0	77	1.42	1.41	1.55

Table I Calculated and Experimental Collision Frequencies.

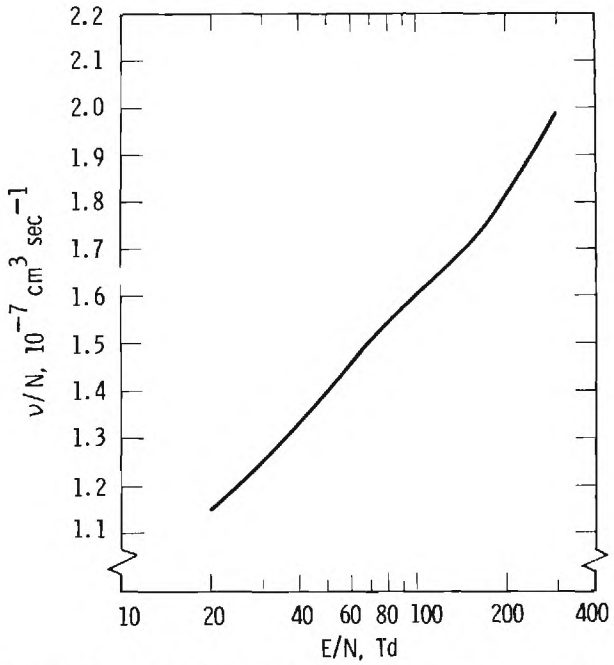

Figure 1. Calculated collision frequency vs. E/N.

References

[1] T. V. George and L. J. Denes, Applied Physics Letters 26, 1 (1975)

[2] J. J. Lowke, A. V. Phelps and B. W. Irwin, J. Appl. Phys. 44, 4664 (1973).

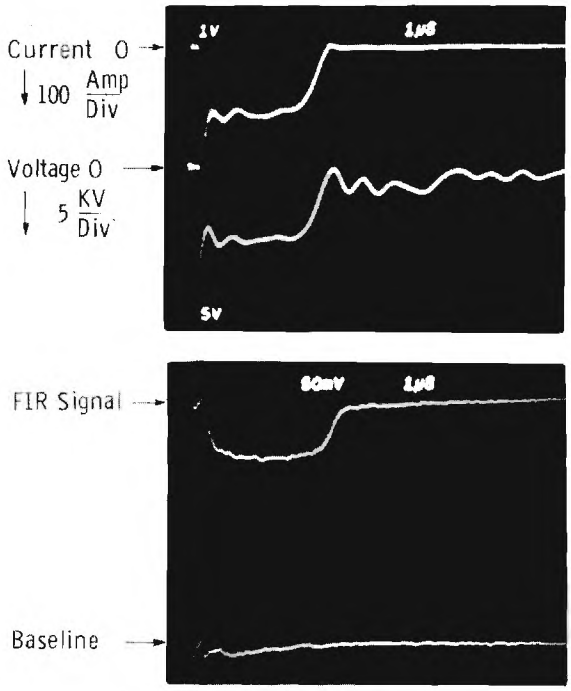

Figure 2. Measured FIR, voltage and current waveforms. Horiz. scale 1 μsec/div.

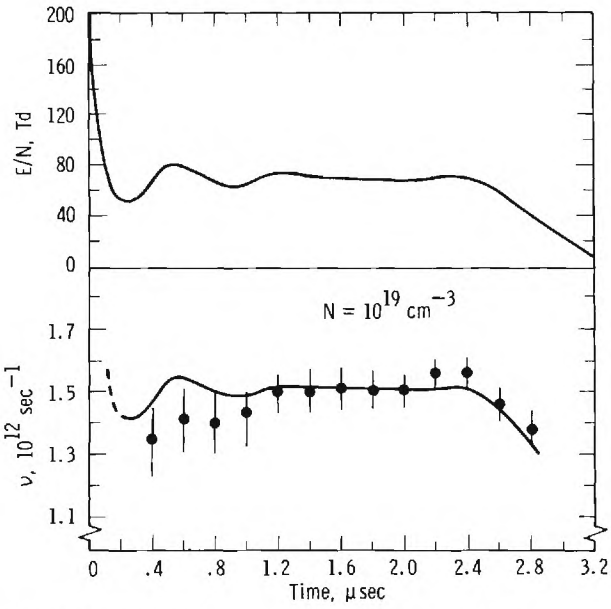

Figure 3. Measured voltage waveform and measured (points) and calculated (curve) collision frequencies, all vs. time.

THE ROLE OF FIR EMISSION IN AN OPTICALLY PUMPED MULTI-LINE NH_3 LASER

Stephen M. Fry
Hughes Research Laboratories,
Malibu, California 90265 USA

Abstract

We have observed more than 50 new laser lines in NH_3 pumped by a TEA CO_2 laser operating on the R(30) 9.2 μm transition. The new lines span the region from 9.3 μm to 13.8 μm. FIR cascade emission is responsible for energy transfer from the pumped antisymmetric to the lasing symmetric levels in the ν_2 band. A novel wedged transverse pumping scheme allows efficient use of pump energy and a compact device design. Application of this laser system to isotope separation of UF_6 is discussed.

Introduction

We are actively engaged in laser pumped laser research for generation of specific wavelengths required for isotope separation, laser photochemistry, high resolution spectroscopy, and air pollution measurements. Important parameters of the isotope separation laser are efficiency, tunability, and output at particular wavelengths (e.g., 7.7, 8.6, 12.2, and 15.9 microns) [1]. We have recently observed more than fifty new laser lines in $N^{14}H_3$ pumped by R(30) of the 001-020 CO_2 laser band, using a wedged transverse pumping scheme [2]. One of these lines is the closest to the 12.15 μm LIS wavelength yet found. Our initial studies show that many of the lines will lase at high buffer gas pressures, which Lorentz broaden the molecular transition linewidth to provide some tunability. If the laser can be made to lase at multi-atmosphere pressures, the rotational levels would merge into a band, allowing large fractional tunability.

With pumping from the antisymmetric ground state to the ν_2 symmetric band in NH_3, we observe both the ν_2^a to 0^s transition from the directly pumped level and the ν_2^a to 0^s transition into the pump depleted level. Most of the lines, however, arise from transitions between levels in the ν_2 symmetric band and the antisymmetric ground state. We believe that FIR cascade emission plays a crucial role in transferring population from the ν_2^a to the ν_2^s band. This FIR mechanism plus rotational relaxation induced by collisions at higher pressures (e.g., 100-800 torr) allows inversion of a large portion of the ν_2^s band, giving multi-line operation over a broad frequency range.

Experimental

The experimental arrangement is shown in Figure 1. The pump laser is a grating-controlled CO_2 TEA laser with a typical output energy of 1 Joule multi-mode and single line, in a 3-4 μS pulse. The beam enters the 20 cm long cavity transversely, and is reflected in a zig-zag fashion to the end of the cell. The gold-coated side mirrors are wedged so that the beam turns around at the end of the device and makes another transit through the gas, resulting in efficient absorption of the pump radiation and more uniform pumping. The gold-coated resonator mirrors are mounted internally near the edge of the gain section. The total reflector is flat, and the output mirror is spherical with a 1 m radius of curvature and a 1 mm output coupling hole. Auxiliary equipment includes the gas-handling station, 1/4-m grating monochromator, and various filters and detectors.

Results

Figure 2 shows a partial energy level diagram with the important mechanisms operating in the multi-line NH_3 laser. The CO_2 (R30) 9.2 μm line pumps the sR(5,K) transition. Lasing in pure NH_3 is observed on the sP(7,K) and sP(5,K) transitions [3]. In addition, some of the aP(6,K) lines are also observed in pure NH_3. The J=6 level in ν_2^a is connected to the J=5 level in ν_2^s by 64-67 μm FIR emission. The cascade lines of Figure 2 have all been reported previously [4]. The sP(7,K) transition at 12.08 μm is the strongest of all of the NH_3 laser lines observed, and is displaced less than 5 cm^{-1} from the 12.15 μm LIS wavelength. An optimum pressure of 3-4 torr is observed for this line [5].

With the addition of buffer gas (e.g., N_2 or He), other lines (dashed lines in Figure 2) are observed. Most of these lines are aP(J,K) transitions, with $\sim 3 \leq J \leq \sim 10$, and all allowed K values. These lines generally have an optimum buffer gas pressure on the order of 40-100 torr, and some are observed at buffer gas pressures greater than 1 Atm. Thus fractional bandwidths on the order of 0.2% should be realizable. Increased pumping in an optimized system will increase the operating pressure range and the potential tunability. Direct Stark tuning of the output should be a useful method for this laser; the corresponding tuning of the pump transition out of resonance with the CO_2 pump line in a scaled-up device would allow larger energy input before the molecular transition reaches saturation.

Conclusions

We have demonstrated multi-line lasing in NH_3. FIR cascade emission and rotational relaxation are important mechanisms in this laser. By

utilizing these mechanisms, design of laser pumped laser systems covering other wavelength ranges should be possible. The transverse wedged pumping scheme allows design of a simple, efficient, and compact device. Future work should yield many new laser transitions of interest for laser isotope separation, laser enhanced chemistry, spectroscopy, and other areas where matches must be made between available laser wavelengths and molecular absorptions.

References

1. Proceedings: Isotope Separation Laser Conference, April 13-14, 1976, Albuquerque, NM.

2. Paper submitted to Optics Comm. (8/76).

3. J. S. Garing, H. H. Nielsen, and K. Narahari Rao, J. Mol. Spectrosc. 3 (1959) 496.

4. K. Gullberg, B. Hartman, and B. Kleman, Physica Scripta, 8 (1973) 177.

5. The 12.08 μm line has recently been reported by two other groups. The author thanks T. Y. Chang and E. Malk for experimental information in advance of publication.

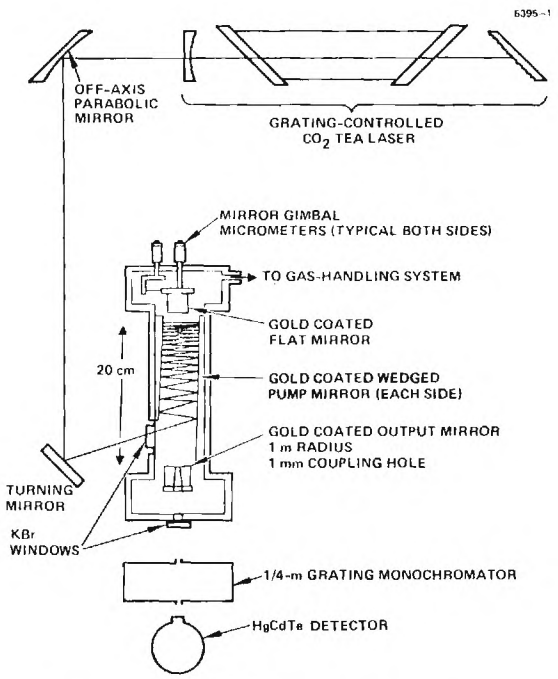

Figure 1. Experimental arrangement

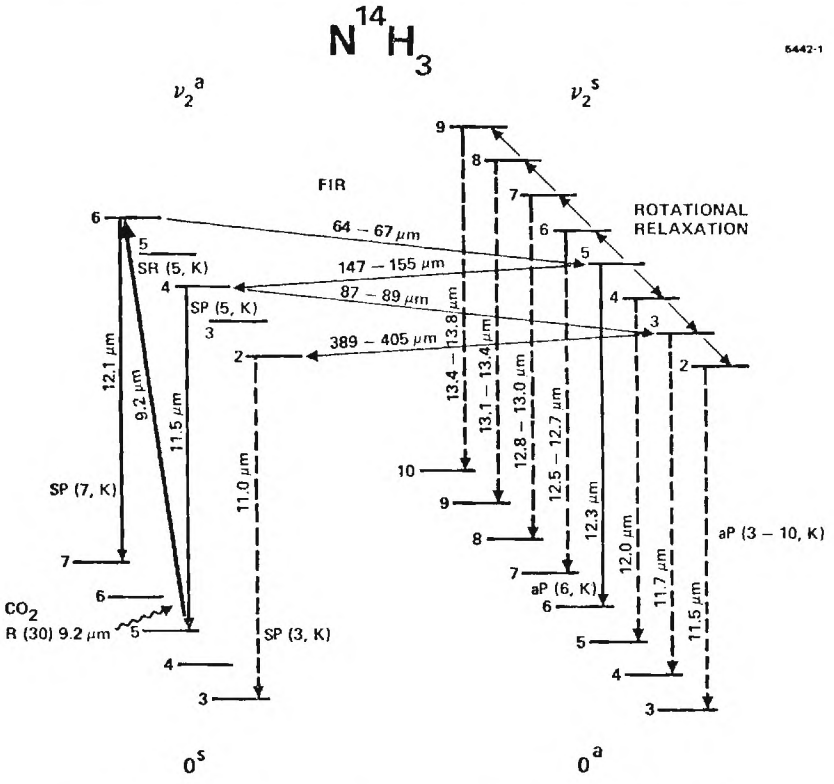

Figure 2. Energy level diagram and some of the energy transfer mechanisms in the NH_3 laser

DEVELOPMENT OF A SUBMILLIMETRE BROADBAND TUNABLE SOURCE

R. Bonnefoy
ESTEC, European Space Agency
Domeinweg, Noordwijk,
The Netherlands

and

G. Kantorowicz and P. Palluel
Electron Tube Division
Thomson - CSF
2 Rue Latécoëre
78140 Vélizy - Villacoublay, France

In the past few years, a growing interest has been shown by astronomers or astrophysicists for the possibility of observations in the submillimetre range. Should these observations be carried out on board a space platform (and therefore not limited by atmospheric transmission), the submillimetre range presents an even wider interest for the understanding of the universe.

As a consequence to this demand, the European Space Agency has initiated a research and development programme on components required for advanced astronomical submillimetre observations. In a first approach a study of technological requirements associated with infra-red (submillimetre) astronomy was achieved by Hawker Siddeley Dynamics Ltd. (United Kingdom). As a result, heterodyne detection was considered as a promising technique (high spectral resolution) and, amongst the suggestions of components needed for spaceborne heterodyne experiments, the Josephson Junction and the tunable electron-beam sources were selected for further investigation.

A contract has been awarded to National Physical Laboratory (United Kingdom) for the study and assessment of suitability of the Josephson Junction for heterodyne detection in the submillimetre range. The theoretical investigations of this device have been completed and NPL are presently involved in an experimental programme on point-contact Josephson Junction to determine parameters such as: intrinsic mixer noise, input coupling efficiency together with the conversion efficiency, the overall receiver noise,..... in the 0.5 - 0.8 mm range.

In parallel to this activity on the detector-mixer, attention has been paid to the local oscillator required in an heterodyne experiment. In a spaceborne equipment the major constraints are: mass, volume and power consumption. In order to cover the spectral range of interest for astronomers (between, say, 0.3 and 1 mm) with as few components as possible, large tunability is an asset for the local oscillator and, in this respect, tunable electron beam sources are believed to be the most adequate. In 1975, Thomson-CSF (France) has conducted a study, on behalf of ESA, on the possibilities to realize a tunable oscillator in the submillimetre range. Devices like Klystron, Orotron, Ledatron, Backward Wave Oscillator were reviewed and the latter was considered as the most promising. It is worth pointing out that, in the course of this work, tests on a 24-40 GHz phase-locked Carcinotron (trade name for the BWO manufactured by the Electron Tube Division of Thomson-CSF) have shown a frequency stability of 1 to 2 kHz.

The next step of development was then decided to be devoted to a new Carcinotron model with an extended bandwidth together with a sufficient output power in the 0.75 - 1 mm range. A design goal of 10 mW output power was selected in order not to limit unduly the choice of the detector/mixer, should other devices, such as Schottky barrier diodes, appear to be more attractive than the Josephson Junction. Theoretical studies were conducted and critical parameters (circuit dispersion, coupling impedance) were verified on a scaled-up (x 100) model of the circuit. The feasibility of the broadband Carcinotron being demonstrated, a model has then been manufactured, based on the existing CO-10 operating at 1.05 mm, but equipped with a longer delay circuit. Although every parameter has not been optimised, preliminary test results indicate a tunability of 20% with an output power higher than 10 mW (up to 50mW for various frequencies) in the range 0.75 - 0.9 mm. The power consumption is between 65 to 130 W: this figure represents a large improvement with respect to existing submillimetre tubes. More extensive tests (influence of the magnetic field, frequency stability.....) are under way and complete results will be available in the near future.

HIGH POWER OPERATION AND SCALING BEHAVIOR OF CW OPTICALLY PUMPED FIR WAVEGUIDE LASERS*

D. T. Hodges, F. B. Foote, and R. D. Reel

The Ivan A. Getting Laboratories
The Aerospace Corporation
P.O. Box 92957
Los Angeles, California 90009

ABSTRACT

Significant improvement in laser power and efficiency are reported throughout the 40 - 1222 μm region, using new waveguide laser geometries and output coupling schemes. Best performance is 400 mW at 118 μm at 20% of theoretical efficiency. Scaling laws for higher power are also described.

*This work was supported by the Aerospace Corporation.

Optically-pumped far-infrared (FIR) lasers are now commonly employed as sources in a variety of experimental applications. The cw laser, which has demonstrated output at the 1 - 10 mW level throughout the 40 μm - 1.5 mm[1] spectral region, has typically operated at only 1% of the maximum theoretical efficiency for converting infrared pump power into FIR power. This paper describes the results of a series of experiments which have increased the efficiency and output power of FIR lasers by as much as an order of magnitude and which have also helped to establish guidelines for scaling FIR lasers to higher cw powers.

Infrared pump power P_p at a frequency ν_p can be converted into FIR laser power P_{FIR} at frequency ν_{FIR} with a maximum theoretical efficiency expressed by

$$P_{FIR} = \frac{1}{2} \frac{\nu_{FIR}}{\nu_p} \delta P_p \qquad (1)$$

where δ is the fraction of the pump radiation absorbed in the gas, i.e.

$$\delta = (1 - e^{-N\alpha(\nu)L}) , \qquad (2)$$

$\alpha(\nu)$ is the absorption coefficient of the pump transition, L is the length of the laser resonator, and N is the number of passes through the laser cavity made by the pump before being dissipated through losses apart from absorption by the gas. For the highest power cw transitions such as 118 μm in CH_3OH[2] and 496 μm in CH_3F[3], $\alpha(\nu)$ is strongly saturated at the operating pressure of the cw laser,

$$10^{-4}\text{cm}^{-1} < \alpha(\nu) < 10^{-3}\text{cm}^{-1} . \qquad (3)$$

Thus a 1 meter laser cavity with N = 10 would imply a fraction of energy usefully absorbed to be in the range

$$0.1 < \delta < 0.6 . \qquad (4)$$

For the weaker cw transitions, the situation deteriorates rapidly; assuming a 10% typical absorption ($\delta = 0.1$), most of the pump energy is not utilized. Weak absorption (accompanied by strong saturation) at the low operating pressure of the cw laser is the major obstacle to the overcome in improving the efficiency of cw FIR lasers.[3,4] A number of conventional Fabry-Perot and waveguide laser resonators have been studied and compared in an effort to reduce the effect of this constraint. In addition to improving the operating efficiency, a laser geometry is desired that provides good output mode quality and permits operation over a wide spectral bandwidth. All these criteria are best satisfied by the hollow dielectric waveguide resonator.

The cavity arrangement developed in these experiments consists of a 38 mm dia. hollow dielectric waveguide with plane external reflectors at each end. Experiments in our laboratory have indicated that the output power dependence on waveguide diameter is very weak for hollow dielectric waveguides. A center coupling hole of 3.5 - 5 mm dia. in one mirrors allows the CO_2 pump radiation to be injected in a collimated beam using F/50 - F/200 optics while coupling out only a small amount (2 - 4%) of the FIR energy. This geometrical arrangement reduces the loss of the pump beam at the wall and also helps to selectively excite the lowest order FIR mode for the hollow dielectric waveguide, EH_{11}. This mode is linearly polarized and transforms very efficiently into the TEM_{00} gaussian free space mode. The efficient coupling permits the use of reflectors external to the waveguide, which simplifies laser construction with only a small additional penalty (1 - 2%) in fixed cavity losses. For the 38 mm dia. pyrex pipe used in these experiments, the calculated loss for the EH_{11} mode is < 1% at 496 μm and approximately 5%/m at 1222 μm.

This new geometry achieves a finesse of 3 - 5 at the pump wavelength in resonators up to 3 m in length and yields the high power performance summarized in Table I. Several output coupling techniques were actually tested, including inductive[5] and capacitive[6] mesh reflectors, silicon etalons and hole coupling. Initial experiments were performed with coupling holes in plane metal reflectors. However, improvement factors of 2 - 3 were achieved with a new output coupler which was used to produce the data in Table I (except for the lines below 100 μm). This new coupler consists of a silicon substrate which is first coated with a highly reflecting (98%) dielectric coating for the 9.5 - 10.5 μm region and is then masked and overcoated with

5000 Å of gold. The mask is removed leaving a center hole of the desired diameter. FIR radiation coupled out through the hole in the gold film is not measurably attenuated by the dielectric film at wavelengths greater than 100 μm. The silicon substrate provides some feedback (~50% of the FIR radiation), but the pump radiation is confined through reflection from the dielectric film. Relatively large hole sizes (8 - 20 mm dia.) still allow oscillation on the EH_{11} mode.

Given a satisfactory coupling scheme and a resonator geometry with reasonable efficiency and good mode quality, the question arises as to how these lasers can be scaled to deliver 100 - 1000 mW throughout the FIR. For examination of FIR scaling laws, a practical limit for single-line CO_2 pump power of 50 - 100 watts can be assumed. Optimum utilization of this power impacts the resonator dimensions. Dimensional changes in the length or diameter of the laser waveguide affect the pump intensity and optimum operating pressure; for example, we have found that the optimum operating pressure varies inversely with diameter over the 5 - 40 mm waveguide diameter range investigated, but the output power exhibits only a slight variation. The output power increases with length, but beyond 2 m the incremental increase is small, presumably because of the lowered circulating pump intensity. The data in Fig. 1 indicate the improvement accrued by increasing the resonator length from 1 m to 2 m for comparable pump power. However, a 3 m laser provides only a 10 - 20% improvement over the 2 m length. The tradeoffs between available pump power, the laser resonator dimensions, and the gas pressure and temperature will be discussed.

REFERENCES

1. M. Yamanaka, Rev. Laser Engr. (Japan) 3, 256 (1976).
2. C. O. Weiss, IEEE J. Quant. Electr. (to be published).
3. D. T. Hodges, J. R. Tucker, and T. S. Hartwick, Infr. Phys. 16, 175 (1976).
4. T. A. DeTemple and E. J. Danielewicz, IEEE J. Quant. Electr., QE-12, 40 (1976).
5. E. J. Danielewicz, T. K. Plant, and T. A. DeTemple, Opt. Comm. 13, 366 (1975).
6. S. M. Wolfe, K. J. Button, J. Waldman and D. R. Cohn, Appl. Optics, (to be published).

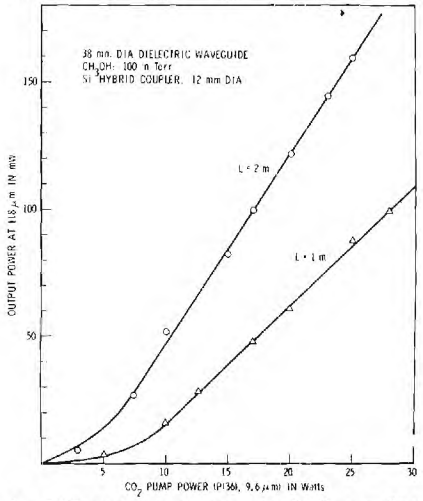

Fig. 1: CW output power at 118 μm for 1 and 2 m long, 38 mm dia. dielectric waveguide laser.

OUTPUT POWER (mW)	WAVELENGTH (μm)	DIA x LENGTH (mm x m)	MOLECULE	PUMP LINE (9.6μm)	PUMP POWER (W)	EFFICIENCY (%)
100	71	38 x 1.1	CH_3OH	P (34)	30	4.8
150	118		CH_3OH	P (36)	27	13.1
15	496		$C^{12}H_3F$	P (20)	30	5.0
10	1222		$C^{13}H_3F$	P (32)	30	8.3
400	118	38 x 2.0	CH_3OH	P (36)	60	15.7
40	496		$C^{12}H_3F$	P (20)	70	5.7
55	41.7	38 x 3.0	CH_3OH	P (32)	33	1.5
3.6	265		CH_3OH	P (34)	26	<1.0
2	570		CH_3OH	P (16)	25	1.0

Table I: CW performance data for 38 mm dia. dielectric waveguide lasers. Output power and efficiency are listed for single end only. Output coupling at 71 μm and 41.7 μm is provided by 5 mm dia. hole in plane metallic reflector. Remaining data were taken using Si hybrid output coupler with 12 mm dia. hole.

CO_2 - FIR Lasers with Common Resonator.

G. A. Koepf
NASA
Goddard Space Flight Center

Throughout the last years much progress has been made in the understanding of the mechanisms involved in coherently pumped FIR gas lasers. Diffusion of molecules to the tube walls have been found to be a dominant process for the relaxation to the ground state /1/. Unfortunately, this restricts the operating gas pressure as is evident from experiments and theoretical analysis, as well /1,2/. Since low gas pressures imply a low pump absorption coefficient and saturation parameter, saturation of the absorption transition occurs for relatively small values of pump irradiance. This in turn makes it difficult to achieve a high pump efficiency, i. e., to get most of the pump radiation absorbed in the FIR gas.

In order to increase the working pressure one has to find buffer gases with large vibrational heat content /3/; or one has to use smaller diameter laser tubes, keeping the product of pressure and tube diameter a constant. Since the pump saturation parameter then increases with 1/d, it takes a larger pump field circulating in the FIR cavity to saturate the absorption line. As the FIR tube diameter is decreased it becomes more difficult to achieve a high Q for the IR radiation, because of increasing wall losses and the increasing ratio of the input hole to the tube diameter. For example, pump efficiencies in the order of 80% are very hard to achieve when using a waveguide diameter of less than 2 cm.

Because of the small beam diameter and the high circulating power inside an IR pump laser, placing the whole FIR cavity inside the pump laser would appear to be an attractive alternative. Instead of the usual dielectric partial IR reflector a highly reflective mirror (metal or hybrid mirror) has to be used. The internal FIR tube diameter, in series with the IR plasma tube, can be made as small as the pump beam diameter. A coupling element between the two tubes is needed, which is transparent to the pump radiation but reflective to the FIR radiation. Since the circulating IR power is very sensitive to intra cavity losses, the pump efficiency is determined to a large extent by the losses of this coupling element.

To compare the pump efficiency in this case with the efficiency in the case of a FIR cavity external to the pump laser, we will define pump efficiency as the ratio of the pump power actually absorbed in the FIR gas and the output power of the same pump laser without the FIR cavity. Based on Rigrods power equation for a homogeneous line, simple estimates can be made concerning the efficiency and the pump power circulating in the cavities. It follows that efficiencies as high as 90% might be reached for FIR lines that are polarized perpendicular to the pump radiation. For parallel polarized lines, efficiencies up to 60% seem ralistic. At a first glance, the latter value does not compare favorably with efficiencies of external cavities. On the other hand, the circulating IR power is much higher and fairly small tube diameters can be used.

A variety of components may be suitable for coupling elements, because for the pump radiation a two way part is needed rather than an optical isolator as in the external case. The simplest element would be a hole in the FIR mirror next to the pump plasma tube. For perpendicular polarized lines, this might be the best solution with the hole also acting as coupling window for the FIR radiation. A metal mirror would be used at the other end of the FIR cavity and a Brewster angle window to separate the two beams. However, for parallel polarized lines the hole should be as small as possible to reduce FIR losses; a hybrid mirror would be used to couple out the FIR beam at the other end. In addition a lens might be needed to focus the pump beam through the coupling hole. The use of a specially blazed line selecting grating as one of the FIR mirrors and as a pump beam deflector at the same time is a possibility, although a grating with the high necessary diffraction efficiency may be difficult to fabricate.

A first experiment using the setup shown in the Figure is under way and operational results with the same FIR cavity used both internally and externally are under evaluation.

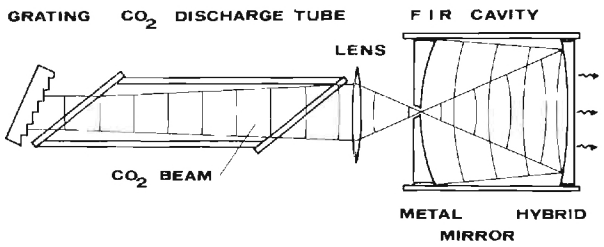

Experimental setup for common resonator FIR laser.

References

/1/ D.T. Hodges and J.R. Tucker, Appl. Phys. Lett., 27, 667, 1975.
D.T. Hodges, J.R. Tucker and T.S. Hartwick, Proceedings of the International Conference on Infrared Physics, Zurich 1975.

/2/ J.R. Tucker, Conference Digest, International Conference on Submillimeter Waves and Their Application, Atlanta, Ga., 1974.

/3/ T.Y. Chang and C. Lin, J. Opt. Soc. Am., 66, 362, 1976.

DESIGN CRITERIA FOR F I R WAVEGUIDE LASERS

G.A. Koepf
N. McAvoy
NASA
Goddard Space Flight Center

The low working pressures of FIR gas lasers and the associated low absorption per length of the pump radiation make it difficult to achieve an efficient use of the pump power available. Unwanted losses of pump power occur in the optics between pump laser and FIR cavity, in the coupling process, and at mirrors and walls inside the cavity. For the pump efficiency to be high the evacuated FIR cavity must have a high Q for the pump radiation.

Degeneracy signature

Disregarding first their properties for the FIR radiation, stable open optical resonators with two curved mirrors will be considered. Coupling of a coherent beam into such a cavity so it continues to travel back and forth can only be done practically through an injection hole in one of the mirrors. To keep the size of the hole as small as possible a beam waist has to coincide with the hole. Following the beam through a number of roundtrips one finds a periodical occurrence of beam waists, their separation depending on the curvatures of the mirrors and the cavity length d, but independent of the size and radial displacement of the injection hole. After a certain number of roundtrips the beam reproduces itself and is reflected out through the hole. As a ray trace analysis shows, each resonator can be described by two integer numbers N and K, where N is the number of roundtrips necessary for the ray to retrace itself, and K gives the number of beam waists over the whole path length of N roundtrips. In the terminology of Sinclair /1/ and Ramsey and Degnan /2/, N corresponds to the number of sets of degenerate transverse modes, i. e., modes with the same resonance frequency. A degeneracy signature diagram is shown in Fig. 1 for stable resonators with two mirrors of equal curvature, R. Degeneracies up to N=16 have been taken into consideration. The solid line in Fig. 1 connects points of lowest degeneracy while the dotted line represents cavities with equal K values. The diagram is valid for resonators with $d<R$, and $d>R$ as well, with the abscissas d/R and 2-d/R, respectively. A similar signature can be drawn for resonators consisting of one flat mirror and one curved mirror.

For cylindrical symmetriy of the pump beam inside the cavity a degeneracy N divisible by 4 is necessary, because only then do the vertices of the beam on the mirrors lie on a circle. This reduces the number of cavities exhibiting high pump efficiency considerably.

Waveguide lasers

Considering now circular waveguide FIR lasers; one finds the number of feasible cavities reduced again. Coupling losses of waveguide modes reflected at curved mirrors increase drastically as the mirror curvature decreases. Only resonators with $d<R$ and low d/R values are appropriate. Therefore, essentially the three cases indicated with circles in Fig. 1 and with d/R values of 0.034 for N=12, K=1, 0.076 for N=8, K=1 and 0.169 for N=16, K=3 are left.

Another criterion is the pump absorption per length of the laser gas at working pressure, which can be determined experimentally. Knowing this and the pump reflection losses at the mirrors (less than 2% when using hybrid mirrors) for a certain power efficiency and a certain N, the cavity length is determined. From the corresponding d/R value the radius of curvature of the mirrors follows. Except for the waveguide diameter 2a, now the cavity geometry is given.

Besides availability, there are three criteria for the optimum diameter at a given FIR wavelength: the waveguide FIR losses; the FIR mode coupling losses; and the injection hole size and position. The first two can be evaluated using data given in the literature. Assuming the diameter of the injection hole to be three times the gaussian beam waist radius w_o, one can calculate the maximum beam diameter of the pump beam traveling back and forth. It always occurs at the position of one of the mirrors. The product of maximum beam radius w_m and w_o turns out to be a constant for a given cavity. Considering again cavities with equal mirrors this parameter normalized to R is plotted over d/R in Fig. 2. The linear part of the curve corresponds to resonators in which the first beam diameter maximum occurs at the first reflection, i.e., after half a roundtrip. As one goes versus decreasing d/R values the consecutive curved sections show the increasing number of half roundtrips before the maximum radius, w_m is reached.

From this graph together with an assumption on the radial displacement of the injection hole r_o for any waveguide diameter 2a the diameter of the injection hole can be derived. r_o is identical to the radius of the circle the beam vertices form on the mirrors. Therefore, the maximum actual pump beam radius -- taken as 1.5 times w_m -- must be smaller than $a-r_o$. Generally, the size of the injection hole increases with r_o, but the case of axial pumping, from an efficiency standpoint, is a very bad case because the pump beam suffers considerable transmission and diffraction losses at each reflection.

A similar approach can be made for rectangular waveguide FIR lasers with curved mirrors, using pump beam traces in a plane. There is no restriction in degeneracy values in this case.

Open resonators

It is worthwhile to reexamine here open FIR resonators and utilize the above analysis to proviede efficient pumping.
Open FIR resonators offer single transverse mode operation together with lossless propagation and with reflections at the mirrors free of coupling losses. Of course, the FIR mode diameter is larger and there might be a serious loss of FIR gain due to reduction of molecule-wall collisions. However, for a close-to-confocal cavity configuration, as N=16, K=7 or N=16, K=5 the TEM mode diameter is not much larger than a lowloss mode in a dielectric waveguide at longer wavelengths. As in the waveguide case the whole mode volume can be filled with pump radiation by an appropriate choice of r_o and the hole size.

References

/1/ D.C. Sinclair, Spectra-Physics Laser Technical Bulletin Number 6 (April 1968).
/2/ I. A. Ramsay and J.J. Degnan, Appl. Opt. 9, 385, 1970.

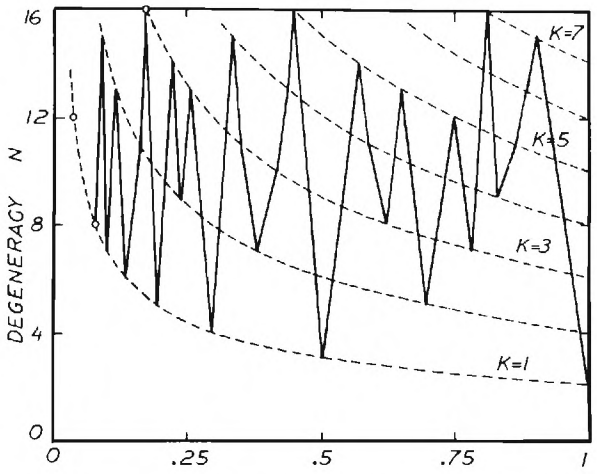

Fig. 1. Degeneracy signature for stable open optical resonators consisting of two mirrors with radius of curvature, R at distance, d. abscissa reading: d/R for d<R and 2-d/R for d>R.

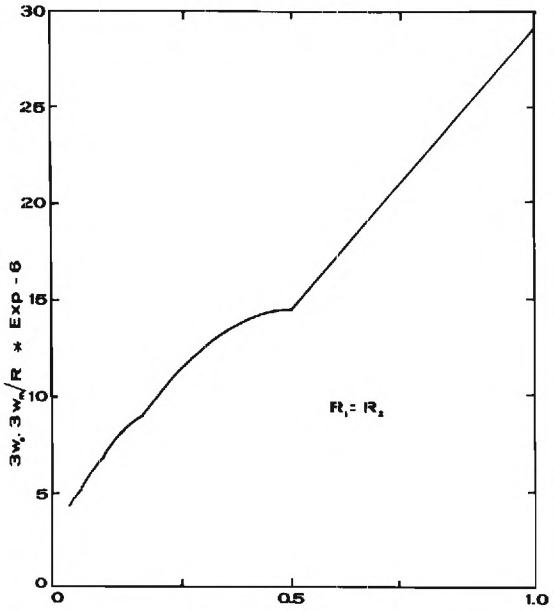

Fig. 2. Maximum gaussian beam diameter $3w_o$ normalized to $R/3w_o$; abscissa reading: d/R for d<R and 2-d/R for d>R.

ASSIGNMENT OF THE HIGH POWER OPTICALLY PUMPED CW LASER LINES OF CH_3OH

Edward J. Danielewicz, Jr. and Paul D. Coleman

Electro-Physics Laboratory
Department of Electrical Engineeiring
University of Illinois
Urbana, Illinois 61801

Introduction

Methyl alcohol (CH_3OH) and its deuterated varieties account for a total of 174 wavelengths or about 25 % of all of the optically pumped FIR laser lines.[1] In addition, the highest CW power, so far, of over 50 mW has been obtained from the 118.8 μm line of CH_3OH. Until now however, none of the transitions have been assigned except for a tentative identification by Chang[2] of the 570.57 μm line as a J' = 11 → 10 transition pumped via an R (10) absorption line. Accurate frequency measurements have recently been performed for a number of the stronger CW laser lines.[3] Combining this data with the high dispersion spectra of the CO stretch bands of normal and deuterated methanol,[4] we have been able to assign most of the high power CW laser lines of CH_3OH.

Theory

Methanol is one of the simplest asymmetric molecules capable of hindered internal rotation. It has one of the most complex, intense, and extensive rotational spectra, which has been studied. The complexity arises from the rotation of the hydroxyl group about the symmetry axis of the methyl group. It is intense because the molecule has a large permanent dipole moment (1.7 D.) with a large component perpendicular to the symmetry axis, namely, $\mu_\perp$ = 1.44 D. It is extensive, since the moment of inertia of the rotating OH component is small thus allowing the existence of high rotational frequencies.

A theory of the hindered-rotational-torsional spectrum of methanol was developed by Burkhard and Dennison.[5] Methanol is only slightly asymmetric (asymmetry parameter κ = -0.98) and the total rotational energy can be separated into an ordinary part described by the equations of a prolate symmetric top and a part arising from the internal rotation. The internal rotational energy is specified by 3 quantum numbers (n, τ, K). Here n corresponds to the torsional-vibrational quantum number, K is the component of the total angular momentum along the symmetry axis, and τ may assume the values 1,2 and 3 and is connected with the tunneling process of the OH group through the threefold potential. The threefold potential causes a splitting of the energy levels into 3 components. This is important, since it triples the chances that a CO_2 laser line will coincide with a CH_3OH absorption line.

Identification Procedure

The rotational fine structure in the IR-spectrum of the ν_5 CO stretch band of CH_3OH has been resolved by Woods.[4] His analysis of the spectrum yielded a set of molecular constants, which allowed R.M. Lees[6] to identify and measure several microwave transitions in the ground torsional state (n = 0) of the first excited CO stretch mode. Lees then determined the value of B_v' = 0.80089 cm^{-1} for the excited state rotational constant. The identification procedure we used was to first search for coincidences between the known CO_2 pump lines and the calculated absorption line frequencies. Each coincidence then specified the J' value of the upper laser level. Pure rotational transition frequencies of the symmetric top type (ΔK' = 0) were then calculated approximately using the J' value and the measured B_v' value. As an example, the partial energy level diagram in Figure 1 illustrates the identification of the 392.1 μm transition from J' = 16 → 15. The transition frequencies of a number of the stronger CW laser lines of CH_3OH have been measured with high precision.[3] Several transitions of the type associated with the parallel component of the dipole moment, such as the 392.1 μm line, were identified. The accuracy of the measured lines was sufficient to allow both J' and K' to be determined. By fitting the frequencies to the equation for a symmetric top rotational transition, a set of constants was calculated which could be used to accurately predict the frequencies of all other pure rotational transitions. Using the known selection rules, for radiative transitions, the frequencies of the transitions with ΔK' = ±1 could then be calculated, including the internal rotational energy terms. This led to the identification of the P,Q, and R branch lines associated with the changing dipole moment perpendicular to the symmetry axis, such as the important 118.8 μm and 170.6 μm lines as shown in Figure 1. The assignments also predicted other lines such as the 417.9 μm line in Figure 1 observed as a cascade from the 118.8 μm line.[2] The final criterion was that the polarization of the output lines had to be consistent with the polarization expected with the particular absorbing transition.[2] Similar assignments of other strong lines, including the 570.6 μm line, enabled us to calculate a complete set of constants for the excited CO stretching vibration.

References

1. Yamanaka, "Optically Pumped Gas Lasers - A Wavelength Table of Laser Lines", The Review of Laser Engineering, 3, 253-294 (1976).
2. T.Y. Chang, T.J. Bridges, and E.G. Burkhardt, "CW Submillimeter Laser Action in Optically Pumped Methyl Fluoride, Methyl Alcohol, and Vinyl Chloride Gases", Appl. Phys. Lett., 17, 249-251 (1970).

3. F.R. Peterson, K.M. Evenson, D.A. Jennings, J.S. Wells, K. Goto, and J.J. Jimenez, "Far Infrared Frequency Systhesis with Stabilized CO_2 Lasers: Accurate Measurements of the Water Vapor and Methyl Alcohol Laser Frequencies", IEEE J. Quantum Electron., QE-11, 838-843 (1975).
4. D.R. Woods, "The High Resolution Infrared Spectra of Normal and Deuterated Methanol between 400 cm^{-1} and 1300 cm^{-1}", Ph.D. Thesis, University of Michigan, Ann Arbor, Mich.(1970).
5. D.G. Burkhard and D.M. Dennison, "Rotation Spectrum of Methyl Alcohol", J. Mol. Spectroscopy, 3, 299-334 (1959).
6. R.M. Lees, "Torsion-Vibration-Rotation Interactions in Methanol. IV. Microwave Spectrum of CH_3OH in the Excited CO Stretching State", J. Chem. Phys., 57, 2249-2252 (1972).

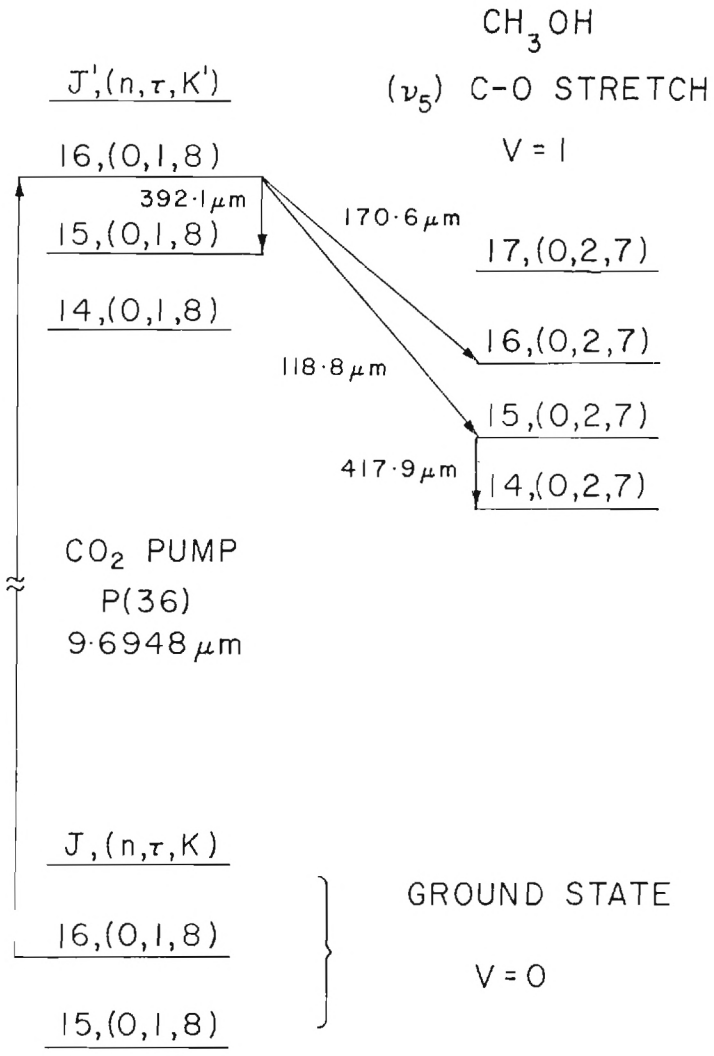

Figure 1. Partial energy level diagram for CH_3OH showing several laser line assignments.

ASSIGNMENT OF FIR LASER LINES IN OPTICALLY PUMPED CH_3OH

J. O. Henningsen
Physics Lab. I, H.C. Ørsted Institute
University of Copenhagen
Denmark

Since the advent of the optically pumped FIR laser, CH_3OH has been recognized as a source of many strong lines [1] . Till now, emission has been observed at 80 different wavelengths ranging from 34μm to 1217μm [2], but none of the lines have been assigned to specific transitions.

CH_3OH is a weakly asymmetric top with hindered internal rotation. Its energy levels are characterized by the quantum numbers J and K , supplemented by a torsional quantum number $n=0,1,2...$ describing torsional oscillations of the OH group in the 3-fold hindering potential. For infinite barrier height, each state would be triply degenerate, but the degeneracy is removed by tunnelling and the split states are labeled by $\tau=1,2,3$. Alternatively they may be labeled according to their symmetry under the point group C_3 as A, E_2 or E_1 states for $K+\tau = 3N+1$, $3N+2$ or $3N+3$ respectively, N being integral. The energy levels for the vibrational ground state are represented by the formula

$$E=W(n\tau K)+B^*(n\tau K)J(J+1)-D_{JJ}J^2(J+1)^2+\text{asym.}$$

W is the J-independent part of the internal rotation energy while B^* is an effective rotation constant which depends on the internal rotation state. The main effect of the asymmetry is to split the doubly degenerate A-states for $K\neq 0$ by an amount which decreases rapidly with increasing K . In addition, it adds to all states a term proportional to $J^2(J+1)^2$. This term depends in a nonsystematic way on the internal rotation state, and for small K it may be larger than the D_{JJ}-term.

Selection rules for transitions involving the axial component of the dipole moment are similar to those for a rigid symmetric top, i.e., $\Delta J=0,\pm 1$ and $\Delta K=0$. The perpendicular component leads to transitions between internal rotation states of same symmetry, with $\Delta K=\pm 1$, Δn arbitrary. In addition, each of these transitions has associated with it a P,Q and an R branch, corresponding to $\Delta J=1$, 0 or -1 respectively. Inspection of the electric dipole matrix element shows that unless K is small, transitions in which J and K change in the same direction are strongly favored over transitions where the change is in opposite directions.

The emitted radiation is linearly polarized, and if the change in J induced by the pump transition and the FIR transition are denoted ΔJ_1 and ΔJ_2 respectively, the relative polarization of the pump beam and the FIR beam follows the rule

$\Delta J_1+\Delta J_2$ even → ∥ polarization
$\Delta J_1+\Delta J_2$ odd → ⊥ polarization

For the vibrational ground state, W and B^* are given in terms of molecular moments of inertia, the usual centrifugal distortion coefficients, the height of the hindering potential barrier, and an expansion in internal rotation variables involving 10 so-called Kirtman coefficients. If the parameters are chosen suitably, calculated $\Delta K=0$ and $\Delta K\neq 0$ frequencies agree with experiments to within about 1 MHz and 25 MHz respectively. However, it turns out that no choice of coefficients can lead to a similar agreement for the vibrationally excited state. This observation has also been made in a study of the excited OH band, and it is attributed to the presence of resonance with other vibrational modes [3] . We have therefore used a crude model in which W, B^*, and asymmetry shifts are calculated from ground state coefficients and where B^* is subsequently reduced by 0.0087 cm^{-1} to account for the major effect of going to the excited CO band. The calculated and emitted vacuum wavelengths are listed in Table I and the assignments are shown graphically in Fig.1.

Table I

No.	pol.	emitted wavel. (μm)	calc.wavel. (μm)
1	∥	570.5686	570.4
2	∥	627.34	627.3
3	?	1217	1223
4	∥	369.1137	368.5
5	∥	223.5	220.3
6	⊥	392.0687	392.2
7	∥	170.5764	168.8
8	⊥	118.8341	118.0
9	⊥	417.8	418.2
10	∥	202.4	202.7
11	⊥	699.4226	698.2
12	⊥	70.51172	70.7[a]
13	?	40.2	39.9[a]
14	∥	264.6	257.8
15	⊥	185.5	182.7
16	∥	263.7	257.8
17	⊥	190.8	188.2
18	∥	253.6	250.0
19	∥	254.1	250.0
20	⊥	292.5	294.2
21	∥	237.6	237.4[b]

[a] assignment tentative since larger deviations are expected for $n=1\rightarrow 0$ transitions.

[b] $(134)\rightarrow(125)$, $J=9$ in vibrational ground state.

Table II

Pump line	abs.transition J	nτK	calc. vib.freq. (cm^{-1})
P(16')	10→11	010→010	1033.89
P(16")	16→17	013→022	1034.37
P(34)	9→9	125→125	1033.76
P(36)	16→16	018→018	1034.39

10 lines are emitted directly from the primary pumped level. The remaining ones are emitted from levels that are populated either by spontaneous emission from the primary pumped level or by collisional relaxation involving dipole-dipole interaction. The vibration frequencies derived from the 4 different pump lines are listed in Table II. The results may be compared with the value 1033.5 cm^{-1} obtained from IR spectroscopy.

[1] T.Y. Chang, T.J. Bridges, and E.G. Burkhardt Appl.Phys.Lett. 17, 249 (1970).

[2] M. Yamanaha, Rev.of Laser Eng., 3, 253 (1976).

[3] R.G. Lee, R.H. Hunt, E.K. Plyler and D.M. Dennison, J.Mol.Spectr. 57, (1975).

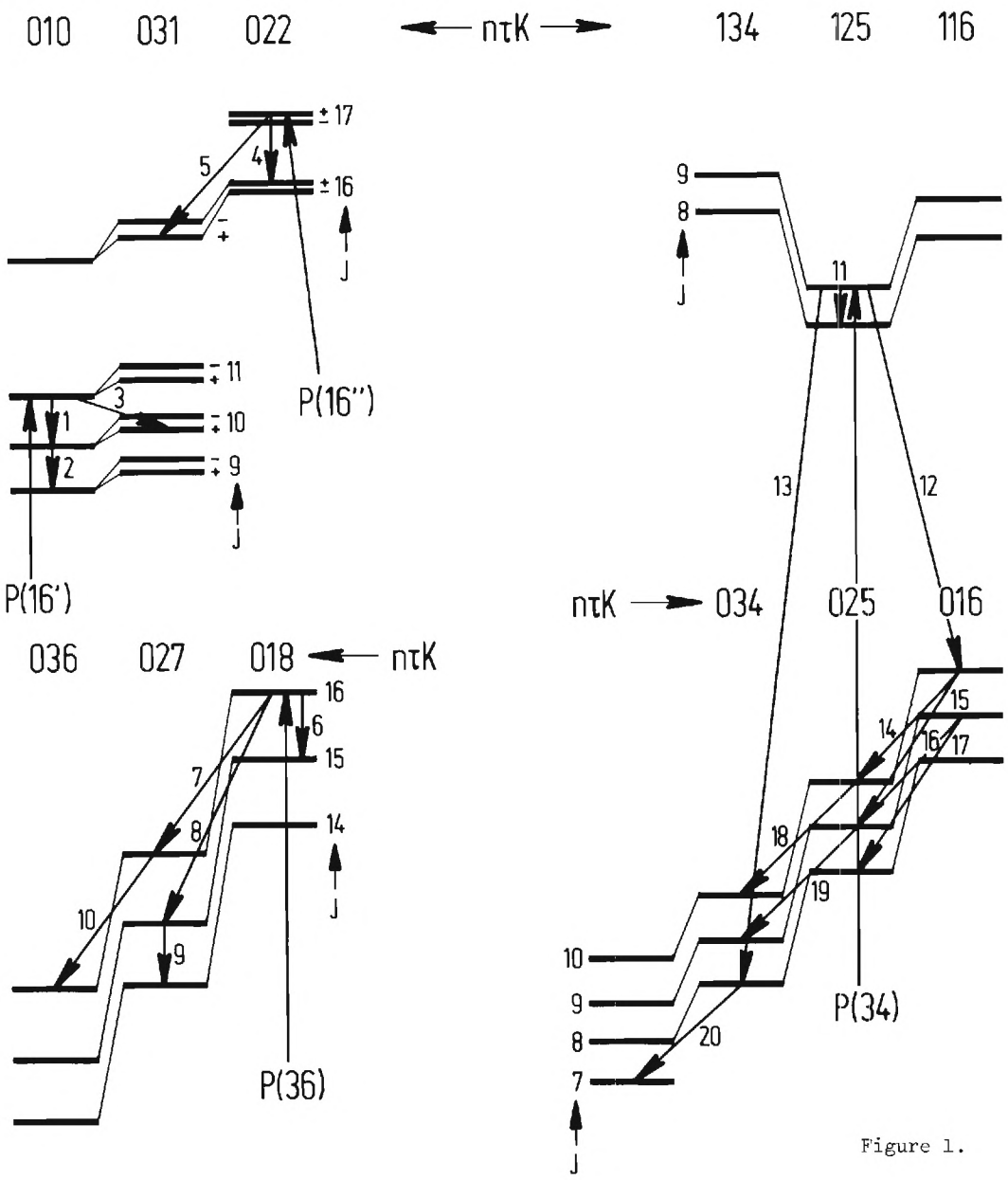

Figure 1.

OPTICALLY PUMPED WAVEGUIDE LASERS

Masanobu Yamanaka
Department of Applied Physics, Osaka University
Yamada-Kami, Suita, Osaka 565, Japan

ABSTRACT

The optically pumped waveguide gas lasers in the submillimeter and millimeter wave regions are simple, compact, rugged, efficient, practical, coherent sources. A number of new laser lines have been observed in these lasers. General considerations are given on the attenuation constants of waveguides and the rate equation models. Characteristics of these lasers are reviewed with output coupling, new laser line, mode, polarization, output power, stability, and compactness. Some applications are described briefly. Finally, future aspects are discussed.

Waveguide laser
Submillimeter wave laser
Optical pumping

I. Introduction

Since Chang and Bridges [1] have discovered the submillimeter wave lasing in CH_3F molecule, excited by the near-resonant absorption of P(20) CO_2 laser line at 9.55 μm, over 800 new laser lines have been reported in the wavelength region of 13 μm and 2 mm [2]-[4].

In 1968, Steffen and Kneubühl [5] introduced hollow dielectric waveguide modes to explain the transverse mode frequencies they observed with a submillimeter wave laser. The first experiments to clearly demonstrate waveguide gas laser action were made with a 0.6328-μm He-Ne laser system in 1971 by Smith [6]. Since that time waveguide gas laser operation has been observed with the He-Ne system at 3.39 μm, the CO_2 system at 10.6 μm, the CO system at 5 μm and the He-Xe system at 3.5 μm [7].

A waveguide laser can be distinguished from a conventional laser by the fact that the radiation is guided and does not obey the laws of free space propagation [8].

In 1973, Hodges and Hartwick [9] operated for the first time an optically pumped submillimeter CH_3OH laser in waveguide resonator structures. Since then the optically pumped waveguide gas lasers have become simple, compact, rugged, efficient, practical, coherent sources. About 90 new laser lines have been observed in these lasers [3]. Waveguide resonators constructed from hollow cylindrical dielectric or metallic tubing are most widely used, although parallel-plate [10] and rectangular [11], [12] metallic waveguide structures as well as rectangular metal-dielectric waveguide structure [12a] have also been successfully employed.

In this paper, progress in the optically pumped waveguide lasers since 1973 will be reviewed. General considerations will be given, firstly, on the attenuation constants of low-loss waveguides and, secondly, on the rate equation models. Thirdly, characteristics of these lasers will be oberviewed with output coupling, new laser line, mode, polarization, output power and compactness. Fourthly, some applications will be stated briefly. Finally, some future aspects of these lasers will be discussed.

A review paper on the waveguide lasers has been presented by Degnan [8] recently.

II. Attenuation Constants of Hollow Waveguides

Attenuation constants of some small-sized, low-loss waveguides for optically pumped waveguide lasers were calculated using existing theories [13]-[16]. Shown in Fig. 1 are the power attenuation constants for the lowest-loss modes, such as TE_{01} doughnut-shaped mode in hollow cylindrical copper guides, EH_{11} linearly polarized mode and TE_{01} doughnut-shaped mode in hollow cylindrical fused-quartz guides (both modes have almost same attenuation constants), TE_{10} linearly polarized mode in hollow tall-rectangular guides, and TE_1 linearly polarized mode in parallel-plate copper guides and in parallel-plate fused-quartz guides. It can be seen that an increasing degree of oversize in the much shorter wavelengths as compared to the cut-off wavelength results in a decreasing attenuation.

Both a cylindrical copper guide and cylindrical fused-quartz guide whose diameter is one order larger than that of the copper guide have almost the same attenuation constants for TE_{01} mode in the submillimeter wave region.

The attenuation constant of the TE_1 mode is less than that of the TE_{01} mode by a factor of about 6 regardless of wavelength and material when plate separation is equal to diameter [15], as shown in Fig. 1. Thus the parallel-plate waveguides for TE_1 mode have the very low losses.

In practice, the parallel-plate guide can not be realized because it requires infinitely wide plates. The tall guide, however, has a field configuration approaching that of the parallel plate guide and has very low losses in the submillimeter wave region. On the contrary, it has large losses in the sub-submillimeter wave region.

Figure 1 shows that the 10-mm ID fused quartz waveguide has very low losses in the wavelengths shorter than about 0.1 mm, and it may be suitable to get linearly polarized output power; however, it has large losses in the longer submillimeter wave region, which fact has been confirmed experimentally [17]. However, the 10-mm ID copper waveguide has negligible losses in the wavelength region of 0.01 and 1 mm, and even a 2-mm ID copper tubing may be usable in the shorter wavelengths than about 0.2 mm. Such small bore tubings may be attractive to enhance the vibrational deexcitation, which will be discussed next.

III. Rate Equation Models

The photon-conversion efficiency of the optically pumped open-resonator lasers has been found to be on the order of only a few percent or less. The rate equation model by Tucker [18] has pointed out that this low efficiency is largely caused by the combination of a rapid rotational relaxation rate and a much slower vibrational relaxation rate of the active molecules.

One highly effective way to improve the

performance of this type of laser is to increase the rate of vibrational deexcitation at the vessel wall (diffusion) by using a small-bore waveguide resonator [9], [17], [19]. (See Fig. 12.) This diffusion rate is proportional to $p^{-1}d^{-2}$, where p is the pressure and d is the waveguide diameter [18].

Hodges et al. [20] have concluded that the dramatic decrease (cut-off) in laser output power with increasing pressure is due to a diffusion limited rate of vibrational relaxation. This cut-off pressure p_c for a CW 496-μm CH_3F waveguide laser is given by $p_c = 1300/d(mm)$ in mTorr. The operation pressures tend to scale inversely with the diameter of the waveguide.

The small bore waveguide has also pump-beam confinement effect if the converged pump beam through input coupling hole is used [17], [19]. The waveguide wall may keep the active gas medium cool.

For any given wavelength, there is an optimum waveguide size for which the power conversion is maximum [17], [19]. Reducing the waveguide size below the optimum value will cause the submillimeter output power to drop due to the rapidly diminishing mode volume and the increasing waveguide loss when approaching the cut-off diameter which is calculated by using a cut-off wavelength.

Another possible way to enhance the vibrational deexcitation is to use a buffer gas, as tried by Chang and Lin [21]. The improvement of the submillimeter laser performance over and above that achieved by the use of a waveguide resonator can therefore be obtained by the simultaneous utilization of a buffer gas [21].

Rate equation models by Yamanaka et al. [22], Tucker [18], and Henningsen and Jensen [23] were concerned primarily with the qualitative aspects of the optically pumped submillimeter lasers. In contrast, DeTemple and Danielewicz [24] have presented a physically detailed rate equation model of the waveguide laser which exhibits a good quantitative agreement with their experiments.

VI. Characteristics of the Waveguide Lasers

1. Output Coupling——Most lasers utilize simple hole coupling [9], [10], which has the advantage of low loss in the submillimeter and operates over a broad spectral range. The inner mirror configuration can serve a very low-loss resonator [19], [25]. The output from a hole is highly diverging because of the small aperture and lacks a well-defined transverse intensity profile. It is not easy to optimize the laser output by changing the diameter of the coupling hole because the laser mode will distort or switch to a higher order transverse mode [26]. The output power can also be extracted transversely through a coupling hole on the side wall of waveguide [17], [27]. This coupling may be suitable for a very compact structure.

In contrast, metallic mesh mirrors, including inductive grid [19], [28], capacitive grid [29] and hybrid metal-mesh dielectric (MMD) mirror [26], [30], have a uniform reflectance and transmittance over the entire mirror. These mesh mirrors couple the total mode out of the laser, and the output beam has a minimum angular divergence because of the large aperture. By varying the mesh geometry, one can optimize the laser output [24].

There are other waveguide cavities, such as the mirrorless waveguide cavity in superradiant mode [31]-[33], and the waveguide amplifier for high-power experiments [34], [35].

2. New Laser Line——Since (a) the oversized waveguide has low propagation losses, (b) its wall has a pump-beam confinement effect and (c) it enhances diffusion to the wall, about 90 new laser lines have been observed in such waveguide lasers [31], [19], [36]-[40]. It may be concluded that the oversized metallic (e.g., copper) waveguide resonator with inner mirror having small coupling hole at the center is suitable in searching for new submillimeter laser lines having small gains [38].

Fetterman et al. [10] have found three new lines by Stark tuning of NH_3 into CO_2 pump resonance. This technique may greatly increase the number of stable CW submillimeter laser lines.

3. Mode and Polarization—— Some transverse mode patterns have been observed by employing mesh couplers, that is, TE_{01} and TE_{02} mode patterns in metallic guide [28], and EH_{11} and LP_{11} mode patterns in dielectric guide [28], [26]. The latter two modes have linear polarization. The EH_{11} linearly polarized mode is widely used [34], [29], [41], for it has the lowest losses among modes in a dielectric guide, and it has an intensity distribution consisting of a single circularly symmetric peak [14], [41].

A tall-rectangular guide has low-loss TE_{mo} linearly polarized modes [11]. In a parallel-plate guide used for Stark tuning, TE_m linearly polarized modes have very low losses [10], [12a].

4. Output Power and Stability——As described previously, the DeTemple and Danielewicz theory [24] is a most quantitative one so far for the optically pumped submillimeter waveguide lasers. However, it may be possible for us to find guide lines getting a high CW-output power in such a waveguide by means of a qualitative theory [22], [42].

We can summarize the ways to get a high CW-output power as follows:

(a) High operation pressures are recommended. If a small diameter waveguide is used, high operation pressures are allowed since the cut-off pressure is proportional to 1/d [20]. Waveguide has a pump beam confinement effect, resulting in high pump intensity and thus high operation pressures [19], [17], [27]. However, there is an optimum waveguide diameter due to the diminishing mode volume, the increasing waveguide loss (see Fig. 1) and the increasing coupling hole losses relative to the cross section of waveguide [17], [19], [27].

(b) Longer waveguides are suitable, for a large volume is obtained and the pump power is well absorbed [19], [40]. With a CW 81.5-μm NH_3 laser, a photon-conversion efficiency of 10% (40-mW output power for 3.1-W pump power) has been reported for a 1.6-m 12-mm ID copper waveguide resonator [19], [17], [27].

(c) Larger pump-powers are required. In this case, heating of the active gas by intense pump radiation may become troublesome [43]; then, cooling the gas by means of a cooled waveguide wall may be necessary. Hodges [44] has obtained a 0.2-W (12% photon-conversion efficiency) CW output power with 119-μm CH_3OH laser under a 20-W pump power.

(d) Optimum coupling must be employed [24], since optically pumped molecular lasers usually have very large gains [2].
And, (e) If a buffer gas, such as C_6H_{14}, is added, high operation pressures may be allowed, resulting in high output power [21], as discussed previously.

There is another novel way to get higher output power. Application of a high frequency (say, 100 KHz) modulation to Stark plates reduces saturation due to the hole burning and allows the entire velocity distribution in the initial state to be pumped. Although the pulsed output power is obtained, more than a tenfold increase in NH_3-laser output power has been obtained via this method [45].

It has been shown that the optically pumped waveguide laser is very stable when excited by an ultrastable frequency and output-power CO_2 laser [25], [12].

5. Compactness——Since the optically pumped laser has high gain and the metallic waveguide has low loss, the following very compact lasers have been constructed as handy submillimeter monochromatic sources [19], [27], [17].

With a 81.5-μm NH_3 laser, the 6-mm ID x 5-cm copper waveguide resonator could sustain the laser oscillation because of high gain. This is the most compact laser in the submillimeter wave region.
A practical compact waveguide laser consisting of 12-mm ID and 20-cm long copper tubing has been constructed. Its output power is about 0.1 mW at 81.5 μm of NH_3 laser when the pump power is about 3W. The threshold pump power of this laser is as low as 0.2W. Another example of compact waveguide laser consists of 6-mm ID and 17-cm long copper tubing. The output power of this laser is coupled out through a coupling hole on the side wall of the copper tube. The output power of 5 μW at 81.5 μm of NH_3 laser is obtained when the pump power is 2.5W.

Hodges and Hartwick [25], [2] have used a compact CO_2 waveguide laser as pump source, which will offer a handy submillimeter waveguide laser system.

V. Applications

Several hundreds of laser lines in the submillimeter wave region have been obtained. The optically pumped submillimeter waveguide lasers being simple, compact, stable, efficient, coherent sources have had many applications, among which are cyclotron resonance absorption [28], Tokamak plasma diagnostics [29], [31], [33]-[35], imaging [46], transmission and reflection measurement [46], and nonlinear effects by Stark switching [45]. In the near future, we may realize their value in the following areas : Stark spectroscopy of molecule [47], astronomy [37], communication [48], radar [48], calibration of detector [49] and spectrometer, and infrared-submillimeter double resonance.

VI. Future Aspects

Following are some of the future aspects of the optically pumped submillimeter waveguide lasers.
(a) Nishihara et al. [15], [50] have shown that the waveguide consisting of a parallel plate with a slight curvature has the important property that the light beam is self-focused toward the center, whose beam width is independent of the wavelength. If this slightly curved parallel-plate waveguide is used as a laser resonator, the cooled and fresh molecular gas can be flowed transversely through it, resulting in high output power.
(b) After Miles and Grow [51] have demonstrated the distributed feedback (DFB) CO_2 laser, DFB and DBR (distributed Bragg reflector) submillimeter lasers have been proposed by Affolter and Kneubühl [52] and by the author [53]. The DFB or DBR lasers will be operated in single line with single mode. Since the DBR has very narrow band width [52], its corrugation pitch has to be tuned very exactly to half the wavelength of interest [54].
(c) The waveguide laser can lase at higher pressures [19], thus the pressure tunable laser can be expected in the submillimeter region [31].
(d) The use of intense pump lasers will result in the finding of many new laser lines, such as CO_2 isotope lasers [55], new CO_2 laser [56] and visible through infrared tunable lasers [57].
(e) A Stark tunable 496-μm CH_3F laser using a tunable CO_2 laser has been proposed, which will have a tunability of about 1% of its center frequency [58].
(f) Since the Stark waveguide laser can produce new laser lines [10], Ueda [59] has proposed many new laser lines by Stark tuning of $^{14}NH_3$ and $^{15}NH_3$ into CO_2 pump resonance.
(g) High-power 16-μm waveguide lasers for UF_6 lisosepping [60] will be also achieved by optical pumping. Already, a 15.9-μm SF_6 laser has been reported in an open resonator [61].
(h) Sealed-off compact waveguide laser system may be realized in the near future for submillimeter researches [2].
(i) One-watt CW 50-100-μm lasers will be constructed for multiple beam CW interferometry for Tokamak plasma [29].

VII. Conclusion

Although the optically pumped submillimeter waveguide lasers are worldwidely being investigated and applied to many fields, more systematic and quantitative studies toward an ideal coherent source in the submillimeter and millimeter wave region should be made. By introducing more microwave techniques [16] into the optically pumped waveguide lasers, more useful lasers will be developed.

References

[1] T. Y. Chang and T. J. Bridges, Opt. Comm., 1 423 (1970).
[2] T. Y. Chang, IEEE Trans. Microwave Theory Thech., MTT-22, 983 (1974).
[3] M. Yamanaka, Rev. Laser Eng. (Japan), 3, 253 (1976); and references therein.
[4] M. Rosenbluh et al., Appl. Opt. (in the press).
[5] H. Steffen and F. K. Kneubühl, IEEE J. Quantum Electron., QE-4, 992 (1968).
[6] P. W. Smith, Appl. Phys. Lett., 19, 132 (1971).
[7] P. W. Smith, Laser Spectroscopy, eds. R. G. Brewer and A. Mooradian (Plenum Press-New York and London, 1974), pp. 247-262.
[8] J. J. Degnan, Appl. Phys. (1976). (in the press).
[9] D. T. Hodges and T. S. Hartwick, Appl. Phys. Lett., 23, 252 (1973).
[10] H. R. Fetterman et al., Appl. Phys. Lett., 23, 684 (1973).
[11] M. Yamanaka et al., Opt. Comm., 15, 426 (1975).
[12] D. T. Hodges, SPIE Meeting, San Diego, Aug. 1975.

[12a]M. S. Tobin and R. E. Jensen, Appl. Opt., 15, 2023 (1976).
[13] N. Marcuvitz (ed.), Waveguide Handbook, Boston Technical Publishers, Inc., 1964) pp. 56-72.
[14] E. A. J. Marcatili and R. A. Schmeltzer, Bell System Tech. J., 43, 1783 (1964).
[15] H. Nishihara et al., Appl. Phys. Lett., 25, 391 (1974).
[16] D. J. Kroon and J. M. Van Nieuwland, Spectroscopic Techniques for Far Infra-red, Submillimetre and Millimetre Waves, ed. D. H. Martin (North-Holland Publishing Company-Amsterdam, 1967), Ch. 7.
[17] A. Tanaka, Ph. D. Thesis (Osaka University, 1975); A. Tanaka et al., (to be published).
[18] J. R. Tucker, Conf. Dig., Int. Conf. on Submillimeter Waves and Their Applications, Atlanta, June 1974, Cat. No.74 CHO 856-5 MTT, p. 17.
[19] A. Tanaka et al., Japan. J. Appl. Phys., 13, 1491 (1974).
[20] D. T. Hodges et al., Infrared Phys., 16, 175 (1976).
[21] T. Y. Chang and C. Lin, J. Opt. Soc. Am., 66, 362 (1976).
[22] M. Yamanaka et al., Japan. J. Appl. Phys., 13, 843 (1974).
[23] J. O. Henningsen and H. G. Jensen, IEEE J. Quantum Electron., QE-11, 248 (1975).
[24] T. A. DeTemple and E. J. Danielewicz, IEEE J. Quantum Electron., QE-12, 40 (1976).
[25] D. T. Hodges and T. S. Hartwick, Conf. Dig., Int. Conf. on Submillimeter Waves and Their Applications, Atlanta, June 1974, Cat. No.74 CHO 856-5 MTT, p. 59.
[26] E. J. Danielewicz et al., Opt. Comm., 13, 366 (1975).
[27] M. Yamanaka and H. Yoshinaga, Conf. Deg., Int. Conf. on Submillimeter Waves and Their Applications, Atlanta, June 1974, Cat. No.74 CHO 856-5 MTT, p. 26.
[28] R. A. Wood et al., Infrared Phys., 16, 201 (1976).
[29] S. M. Wolfe et al., Appl. Opt. (in the press).
[30] E. J. Danielewicz and P. D. Coleman, Appl. Opt., 15, 761 (1976).
[31] F. Brown et al., Appl. Phys. Lett., 25, 394 (1974).
[32] T. K. Plant et al., IEEE Tran. Microwave Theory Tech., MTT-22, 988 (1974).
[33] M. P. Hacker et al., Phys. Lett., 57A, 328 (1976).
[34] A. Semet and N. C. Luhmann, Jr., Appl. Phys. Lett., 28, 659 (1976).
[35] T. K. Plant and T. A. DeTemple, J. Appl. Phys., 47, 3042 (1976).
[36] J. R. Izatt et al., Opt. Comm., 14, 385 (1975).
[37] H. E. Radfor, IEEE J. Quantum Electron., QE-11, 213 (1975).
[38] A. Tanaka et al., ibid., QE-11, 853 (1975).
[39] D. A. Jennings et al., ibid. QE-11, 637 (1975).
[40] F. R. Peterson et al., ibid. QE-11, 213 (1975).
[41] P. Belland et al., J. Phys. D, 8, 2113 (1975).
[42] J. R. Tucker (private communication).
[43] C. O. Weiss and G. Kramer, Appl. Phys., 9, 175 (1976).
[44] D. T. Hodges (private communication).
[45] H. R. Fetterman et al., Opt. Comm., 18, 10 (1976).
[46] T. S. Hartwick et al., Appl. Opt., 15, 1919 (1976).
[47] L. H. Johnston and R. P. Srivastawa, J. Mol. Spectrosc., 61, 147 (1976).
[48] H. R. Fetterman and H. R. Schlossberg, Microwave J., 17, 35 (1974).
[49] M. Daehler, Naval Research Laboratory Report 7976 (1976).
[50] H. Nishihara et al., Appl. Phys. Lett. (in the press).
[51] R. O. Miles and R. W. Grow, J. Opt. Soc. Am., 66, 292 (1976).
[52] E. Affolter and F. Kneubühl, Phys. Lett. (to be published).
[53] M. Yamanaka (unpublished).
[54] M. Yamanaka and S. Komatsubara (unpublished work).
[55] C. Feed et al., J. Mol. Spectrosc., 49, 439 (1974).
[56] J. Reid and K. Siemsen, Appl. Phys. Lett., 29, 250 (1976).
[57] M. J. Colles and C. R. Pidgeon, Rep. Prog. Phys., 38, 329 (1975).
[58] M. Inguscio et al., Conf. Dig., Int. Conf. Infrared Physics, Zurich, Aug. 1975, p. C229.
[59] Y. Ueda, Oyo Buturi, 45, 729 (1976). (in Japanese).
[60] J. W. Eerkens, Appl. Phys., 10, 15 (1976).
[61] W. E. Barch et al., Opt. Comm., 15, 358 (1975).

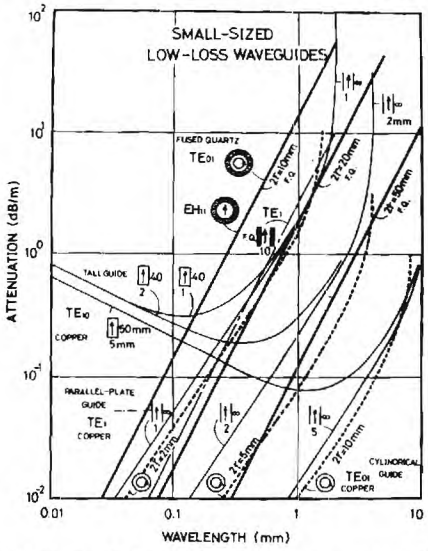

Fig. 1 Some small-sized, low-loss waveguides for optically pumped waveguide lasers.

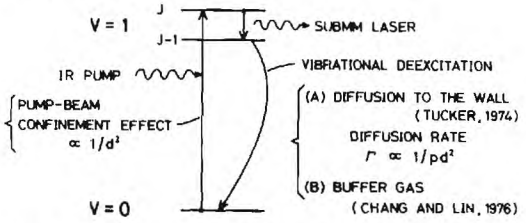

Fig. 2 Schematic of partial energy level diagram in CW optically pumped submillimeter waveguide laser.

WAVEGUIDES FOR SUBMM-LASERS

F.K. Kneubühl
Infrared Physics Group,
Solid State Physics Laboratory, ETH,
Hönggerberg, CH-8093 Zurich,
Switzerland

ABSTRACT

A review on the history and the present state of the art of waveguides for submillimeter wave lasers is presented. Theoretical and experimental aspects of waveguides for longitudinally and transversely excited as well as for optically pumped lasers are discussed. This is followed by a comment on investigations of periodic waveguide structures for distributed feedback submillimeter wave lasers.

In 1964 Marcatili and Schmeltzer [1] determined the field configurations and the propagation constants of the modes of hollow circular waveguides made of dielectric material or metal. They suggested to apply these waveguides for the construction of lasers in the wavelength region between 0.4 μm and 4 μm . A characteristic prerequisite for low-loss waveguide modes is a large ratio of the diameter versus the wavelength. Phase shift and loss per pass of a waveguide-laser resonator depend on the diameter of the tube and on the dielectric constant of the wall material, whereas those of a standard two-mirror laser resonator are dominated by the diffraction.

The first waveguide laser was realized by Steffen and Kneubühl [2] in 1968. It was not an optical or a near-ir laser as expected, but a longitudinally excited submillimeter-wave HCN-laser. The first infrared waveguide laser was constructed by Smith [3] in 1971 for the 10.6 μm CO_2-emission. Since the Doppler and the pressure broadening of the low pressure 337 μm HCN-emission are smaller than mode separation of a submillimeter-wave laser resonator, the mode structure of the above waveguide laser was tested by laser resonator interferometry [2]. In addition to the construction and operation of the waveguide HCN-laser, Steffen and Kneubühl had also calculated [2,4] the fields and losses of the modes of the circular hollow dielectric waveguide for their submillimeter-wave laser without knowledge of the paper by Marcatili and Schmeltzer [1]. Thus they labeled the hybrid "tube" modes by $T^{+/-}_{nm}$ instead of EH_{nm} . Further studies on the longitudinally excited waveguide HCN-laser were made recently by Belland et. al. [5] in order to optimize its performance and to minimize its size.

Since the initial calculations [1,2,4] on the circular hollow waveguides the theory has been improved and extended to other tube cross sections. Abrams and Chester developed a numerical technique for analyzing the modes of circular waveguide lasers with external mirrors [6]. They determined mode shapes, guide and coupling losses for waveguides with Fresnel numbers from 0.1 to 1 and with various values of mirror curvatures, as well as optimum resonator parameters for single mode operation. Batt et. al. [7] studied experimentally the performance of a modified H-guide as a low-loss waveguide in the far infrared. Adam and Kneubühl [9] calculated the fields and the propagation constants of the modes of a waveguide consisting of two parallel ideal conductors and dielectric side walls. Recently Laakmann and Steier [10] determined the characteristics of a rectangular hollow dielectric waveguide.

Hollow dielectric waveguides do not support guided waves in the usual sence. Due to the refraction of the waves at the interface separating the media, the guide is continuously losing power by radiation. The complete system of orthogonal modes of the hollow dielectric waveguide consists only of leaky modes, also called radiation modes, improper modes, pseudo-modes and quasimodes. A good description is given in reference [11]. The field distributions belonging to such modes indicate an exponentially increasing field transverse to the axis in the lossless dielectric with a real dielectric constant. Therefore they do not satisfy the condition of vanishing field at infinity. It can be shown [12] that also the usual treatment of Fabry-Pérot resonators does not give the proper modes of the structure.

Thus, neither the usual resonator nor the hollow waveguide has proper modes in the sense used in the literature, since they are open structures and therefore the fields do leak into space.

Under most experimental conditions however, the observed modes of a hollow dielectric waveguide are well described by the leaky modes mentioned above. This can be explained by losses in the waveguide wall described by a non-vanishing imaginary part ε'' of the dielectric constant $\varepsilon, = \varepsilon' + i\varepsilon''$. Even small losses in the wall material suppress the exponential increase of the field in the wall, as demonstrated by Adam and Kneubühl [9] for the waveguide structure mentioned above. In addition they were able to devise precise criteria for ε'' .

In 1973 Hodges and Hartwick [13] gave a new impetus on the research of submillimeter-wave waveguides resonators by using a waveguide for a far-infrared methyl alcohol laser optically pumped by CO_2 [14]. Subsequently Yamanaka et. al. [15] made important contributions to the study of optically pumped waveguide lasers.

Transverse electric excitation has proven effective for producing laser action in high pressure gas mixtures since the discovery of 10.6 µm CO_2 TEA-laser by Beaulieu [16]. Unfortunately, the standard electrode structure for transverse excitation strongly hinder the propagation of submillimeter waves. Therefore Adam and Kneubühl [8,9] succeeded 1973/75 in the first transverse excitation of submillimeterwave laser action at the 337 µm HCN emission only by using electrodes in the form of a waveguide. Research is continued along these lines by applying uv-preionization in order to produce HCN-laser active discharges in gas mixtures at 1 atmosphere [17].

The first proposal for a distributed feedback (DFB) laser with a waveguide resonator was made by Marcuse [18]. At the beginning of this year Miles and Grow [19] achieved the first operation of a DFB gas laser with the CO_2 10.6 µm emission. The DFB gives low laser thresholds and high mode selectivities. In the submillimeter-wave regions the DFB could therefore bring advantages for optically pumped lasers as well as for transversely excited lasers at high pressure. However, this would require waveguide structures with deep periodic corrugations. Affolter and Kneubühl [20] have studied the theory of such structures. For one specific type of waveguide they were able to calculate the dispersion relation, the threshold and the resonance condition. Unfortunately the numerial analysis of these complex equations by a computer is arduous. Furthermore the general theory of DFB lasers is still in a rudimentary state, since it is essentially the mathematics of the complex Hill's and Mathieu's equation [21]. First experimental attempts on distributed feedback and distributed Bragg reflectors in the submillimeter wave region were recently performed by Yamanaka [22].

Another possibility to obtain a good frequency selectivity and stabilization for optically pumped far-infrared lasers seems to consist of oversized helical waveguides used in the highest pass bands [23]. However the construction and tuning of suitable helical or corrugated waveguides encounters difficulties.

In the past years the study of hollow waveguides has strongly influenced the development of electrically excited and optically pumped submillimeter-wave lasers. The present state of the art indicates that these waveguides will also play an important role in the future.

The author wishes to acknowledge the support of the research on waveguides for submillimeter-wave lasers in his laboratory by the Schweizerischer Nationalfonds and the ETH Zurich.

References:

[1] E.A.J. Marcatili, R.A. Schmeltzer: Bell System Techn. Journal, 1783 - 1809, (1964)

[2] H. Steffen, F. Kneubühl: IEEE J. of Quantum Electronics QE-4, 992 - 1008, (1968)

[3] P.W. Smith: Appl. Phys. Letters 19, 132, (1971)

[4] H. Steffen, F. Kneubühl: Physics Letters 27A, 612 - 613, (1968)

[5] P. Belland, D. Véron, L.B. Whitebourn: J. Phys. D: Appl. Phys. 8, 2113 - 2122, (1974)

P. Belland, C. Pigot, D. Véron: Physics Letters 56A, 21 - 22,(1976)

[6] R.L. Abrams, A.N. Chester: Appl. Optics 13, 2117 - 2125, (1974)

[7] R.J. Batt, H.L. Bradley, A. Doswell, D.J. Harris: IEEE Transactions on Microwave Theory and Techniques MTT-22, 1089 - 1094, (1974)

[8] B. Adam, H.J. Schötzau, F. Kneubühl: Physics Letters 45A, 365 - 366, (1973)

[9] B. Adam, F. Kneubühl: Appl. Phys. 8, 281 - 291, (1975)

[10] K.D. Laakmann, W.H. Steier: Appl. Optics 15, 1334 - 1340, 2029, (1976)

[11] V.V. Shevchenko: "Continuous Transitions in Open Waveguides" The Golem Press. Boulder, Colorado, (1971)

[12] A.E. Karbowjak: Int. Symp. on El. Magn. Theory and Antennas, Copenhagen 1962, Pergamon Press (1973)

[13] D.T. Hodges, T.S. Hartwick: Appl. Phys. Letters 23, 252 - 253, (1973)

[14] T.J. Chang, J.D. McGee: Appl. Phys. Lett. 19, 103, (1971)

[15] M. Yamanaka, H. Yoshinaga: IEEE Trans. Microwave Theory and Techniques MTT-22, 1117, (1974)

M. Yamanaka, H. Tsuda, S. Mitani: Opt. Communications 15, 426 - 428, (1975)

[16] A.J. Beaulieu: Appl. Phys. Lett. 16, 504,(1970)

[17] Ch. Sturzenegger, B. Adam, F. Kneubühl: "Transversely Excited Far-Infrared Waveguide Lasers" this conference

[18] D. Marcuse: IEEE J. Quantum Electron. QE-8, 661, (1972)

[19] R.O. Miles, R.W. Grow: J. Opt. Soc. Am. 66, 292, (1976)

[20] E. Affolter, F. Kneubühl: Physics Letters, in print

[21] E. Affolter, F. Kneubühl: Meeting of the Swiss Physical Society Bern, April 8 - 9, (1976) ZAMP (J. of Appl. Math. & Phys.), in print

[22] M. Yamanaka: private communication, (1976)

[23] E. Affolter, F. Kneubühl: Physics Letters, in print

RATE EQUATIONS AND THEORY OF OPTICALLY-PUMPED SUBMILLIMETER LASERS*

R.J. Temkin

Francis Bitter National Magnet Laboratory†
Massachusetts Institute of Technology
Cambridge, Massachusetts 02139

ABSTRACT

Theoretical models for the operating characteristics of both pulsed and CW optically pumped submillimeter lasers are reviewed. The agreement between theoretical and experimental results for the absorption of pump radiation and the submillimeter laser gain is discussed. Rate equation models that have been used are found to be inadequate in several applications and, instead, the quantum mechanical treatment of a three level system must be employed.

---

*Work supported by National Science Foundation, Division of Engineering
†Supported by National Science Foundation

Since the discovery of the optically pumped, CH_3F laser by Chang and Bridges [1], much effort has gone into demonstrating a theoretical basis for the operating characteristics of both the CW and pulsed optically pumped submillimeter (SMM) laser [2-13]. These studies have provided theoretical expressions for both the absorption of pump radiation and the gain at the submillimeter laser wavelength. Such studies are particularly useful in designing submillimeter laser systems which efficiently convert pump laser radiation into submillimeter laser output.

The optically pumped submillimeter laser is a special case of the general three level laser system. Ordinarily, the optical pump excites molecules from a rotational state of the ground vibrational level (level 1) to an excited vibrational-rotational level (level 3). Lasing occurs at a submillimeter wavelength in a rotational transition from level 3 to another rotational level within the same excited vibrational state (level 2). The same fundamental theoretical considerations would apply to this three level system if the transition from level 3 to level 2 were a vibrational transition or even if level 2 were higher in energy than level 3, leading to absorption. In fact, it may be shown that a number of results of importance in analyzing optically-pumped submillimeter lasers have been previously derived for other applications, including double resonance spectroscopy of molecules (both photons absorbed).

An accurate theory for an optically pumped laser must correctly treat both the molecular dynamics of the gas, such as the relaxation rates, and the optical transitions of the gas at the pump and laser frequencies. The theoretical treatment will, however, require a number of assumptions based on the gas pressure, laser intensity, laser pulse length and other parameters. Most theoretical treatments are appropriate for either the case of a pulsed laser, with optical pumping by an intense, short pulse such as that of a CO_2 TEA laser; or a CW (or chopped) laser, with optical pumping by a CW (or chopped) CO_2 laser. These two cases differ in many respects. In the pulsed case, the rate of optical pumping is in equilibrium with the rate of rotational relaxation and stimulated emission within the excited vibrational level. In the CW case, the rate of optical pumping must be balanced by deexcitation from the excited vibrational level to the ground state. In the pulsed case, both the pump and emitting transitions are usually homogeneously (pressure) broadened, while at least the pump transition is Doppler broadened for the CW laser.

A rate equation model solution for the optically pumped submillimeter laser has been obtained for the pulsed case assuming homogeneously broadened transitions [8, 9]. Expressions have been derived for pump radiation absorption and SMM laser gain. Comparison of theoretical results with experimental data for CO_2 laser absorption in CH_3F has yielded good agreement [8, 9]. The comparison indicates that at high pressure, there is a measurable reduction in CO_2 absorption as the excited vibrational state becomes highly populated through optical pumping.

We have recently obtained experimental evidence that, for the pulsed laser case, the rate equation model does not adequately describe the SMM laser gain. Rather, a quantum mechanical treatment of the three level system, using the time dependent Schrödinger equation, is required. For the case of a weak SMM laser field, the SMM laser gain may be obtained from Javan's treatment of a homogeneously broadened three level system interacting with two laser (or maser) fields [14]. We have obtained analytic expressions for pump absorption and SMM laser gain in the general case of pump and SMM laser fields of arbitrary intensity interacting with a homogeneously broadened, three level system [15]. In the rate equation model, molecules make transitions from level 1 to level 2 by means of two successive single photon transitions. These transitions are only correlated through the change in population of level 3. In the quantum theory, such single photon transitions also occur, but there are, in addition, two photon transitions in which, simultaneously, a photon is absorbed at the frequency of the pump laser and a photon is emitted at the frequency of the SMM laser. As a consequence of the two photon term, the small signal gain of the SMM laser may be split into two symmetric peaks if either the pump laser field strongly saturates the pump transition or the pump laser frequency is very far off resonance. We have recently observed the splitting in the SMM laser gain spectrum for off resonance pumping in experiments with the 385 μm line of D_2O.

Several theoretical analyses of the CW, optically pumped laser have been undertaken using rate equation models [3, 4, 5, 7, 10, 12, 13]. A major problem

in analyzing the CW laser is to properly account for the equilibrium between the rate of optical pumping to the excited vibrational level and the rate of deexcitation back to the ground state via collisions or diffusion to the walls. This rate of deexcitation is a limiting factor in the pressure at which CW lasers may operate and results in a reduced laser efficiency. A simple expression for the cutoff pressure, above which the deexcitation rate in the gas limits the laser gain, has been derived by Tucker [4] and has been shown to have experimental validity [12]. A detailed model of the molecular relaxation processes has been developed by De Temple and Danielewicz to provide a quantitative analysis of the output of a CW CH_3F laser as a function of pressure [10]. The role of buffer gases in the deexcitation process has been studied by Chang and Lin [13], who have found good agreement between their theoretical model and experiments.

The theoretical treatments of the CW SMM laser have all employed the rate equation model. An accurate treatment of the system should, however, employ a quantum mechanical approach, as in the pulsed laser case. A quantum mechanical treatment of a three level system with Doppler broadened transitions has in fact been derived [16, 17]. The quantum treatment, which includes two photon transitions, should have a major effect on the expression for SMM laser gain when the pump field is strong enough to saturate the pump transition. Such saturation of the pump transition has already been demonstrated at low pressure in CH_3F [7] and HCOOH [18].

References

1. T.Y. Chang and T.J. Bridges, Opt. Commun. 1, 423 (1970).
2. A.L. Golger and V.S. Letokhov, Sov. J. Quant. Electron. 3, 15 (1973).
3. M. Yamanaka, Y. Homma, A. Tanaka, M. Takada, A. Tanimoto, and H. Yoshinaga, Japan J. Appl. Phys. 13, 843 (1974).
4. J.R. Tucker, Conference Digest, Int. Conf. Submillimeter Waves and their Applications, Atlanta, Ga., 1974 (IEEE, New York, 1974), Cat. No. 74 CHO 856-5MTT, p. 17.
5. J.O. Henningsen and H.G. Jensen, IEEE. J. Quant. Electron. QE-11, 248 (1975).
6. H.J.A. Bluyssen, R.E. McIntosh, A.F. van Etteger and P. Wyder, IEEE J. Quant. Electron. QE-11, 341 (1975).
7. D.T. Hodges and J.R. Tucker, Appl. Phys. Lett. 27, 667 (1975).
8. R.J. Temkin and D.R. Cohn, Opt. Commun. 16, 213 (1976).
9. J.R. Tucker, Opt. Commun. 16, 209 (1976).
10. T.A. De Temple and E.J. Danielewicz, IEEE J. Quant. Electron. QE-12, 40 (1976).
11. H.J.A. Bluyssen, R.E. McIntosh, A.F. van Etteger and P. Wyder, Infrared Phys. 16, 183 (1976).
12. D.T. Hodges, J.R. Tucker and T.S. Hartwick, Infrared Phys. 16, 175 (1976).
13. T.Y. Chang and C. Lin, J. Opt. Soc. Am. 66, 362 (1976).
14. A. Javan, Phys. Rev. 107, 1579 (1957).
15. R. Panock and R.J. Temkin (to be published).
16. M.S. Feld and A. Javan, Phys. Rev. 177, 540 (1969).
17. B.J. Feldman and M.S. Feld, Phys. Rev. A5, 899 (1972).
18. C.O. Weiss and G. Kramer, Appl. Phys. 9, 175 (1976).

NARROWBANDPASS FILTERS FOR THE FAR INFRARED

G.D. Holah and N.D. Morrison
Physics Department
Heriot-Watt University
Riccarton, Edinburgh, Scotland.

A technique is described which enables narrowbandpass filters to be made at any predetermined wavelength beyond 50μm and which operate efficiently at 77°K.

Discussion

In many infrared measurements, particularly those concerned with astronomical observations, it is often necessary to restrict the optical bandwidth to a small region centered about a particular wavelength. This has proved difficult to produce on anything approaching a routine basis. Previous techniques 1 have, in the main, relied on the use of metallic annuli to act as spacers between two or more pieces of metallic mesh. Even though such annuli can be prepared to within ± 1μ of any required thickness and flatness it is often found that the assembled filter does not have the peak at the correct wavelength and/or the parallelism has been degraded to such an extent that the filter profile is not adequate.

It is also one of the necessary requirements of many far infrared filters that they operate efficiently at low temperatures, ideally at 4°K or below.

The purpose of this paper is to report a method for making narrowband filters, halfwidths between 5 and 10% of the peak wavelength, and which function adequately at 77°K. At the time of writing they have not been tested at 4°K, however this is under investigation. The method avoids the need for metal spacers and the separation and parallelism of the meshes can be adjusted in situ. The rig is placed inside a Fourier Transform Spectrometer and consequently a continuous record of the adjustments may be made.

A photograph of the apparatus is shown in Figure 1. The two meshes are stretched and glued to aluminium rigs which are of different sizes such that they will slide one inside the other. The two rings are held in stepped collets one of which is attached to the linear (y) translation system through an x-z translation operating at right angles to the axis of translation, this allows for aligning the axes of both collets so that the mesh rings will telescope smoothly inside each other. The other collet is mounted on a fixed bridge through a kinematic mount utilising 120 TPI threader for coarse adjustment and piezoelectric transducers for fine adjustment of mesh parallelism, the separation and parallelism can be adjusted to 1/10μm. Unfortunately this does not represent the accuracy to which a particular wavelength may be selected since after these adjustments have been made the two meshes on their rings have to be glued together. Epoxy resin is used for this and it is often found that shrinkage occurs on setting, for the particular system discussed this varies between 1μm and 5μm, depending on the amount of adhesive. Although efforts are made to compensate for this, the accuracy in pitching the wavelength is usually ± 2μ. The parallelism is not usually affected sufficiently to degrade the filter profile.

To demonstrate how the method works a series of stages of development are shown in Figs. 2,3,4 and 5.

After two meshes, appropriately chosen for the wavelength of interest, have been placed in the jig, initial parallelism is obtained using the reflected diffraction patterns of a He-Ne laser from both meshes. The micrometer adjustments are used for this purpose, the position of the patterns are adjusted to overlap. It is then necessary to adjust the vertical and horizontal positions of one of the meshes to make certain the two rings slide smoothly inside each other. The initial separation of the meshes is then estimated and normally set at 2mm. The parallelism is then rechecked and the jig placed inside a Fourier Transform Spectrometer and the piezoelectric transducers, to give both tilt and separation are connected through vacuum seals to a stabilised d.c power supply. The interesting interferogram obtained for such wide spacings, and hence many Fabry-Perot orders, is shown in Figure 2 together with the transformed spectrum. The translation micrometer is then used to bring the separation to approximately the correct position, Figs. 3 and 4, showing intermediate stages. The final filter is obtained after fine adjustments using the piezoelectric transducers. Although this technique has a much higher success rate than those using metal spacers the time taken to make an adjustment and then obtain the effect on the filter profile is still considerable. Sometimes as many as 50 adjustments and correspondingly 50 transforms are needed, though this can be reduced by reading the interferogram for wide separations and only having a computer for the final stages. The final filter after gluing is shown in Figure 5.

Most of the filters made using this technique have shown no significant deterioration at 77°K.

References

1 Smith, S.D., Holah, G.D., Seeley, J.S., Evans, C. and Hunneman, R., Infrared Detection Techniques for Space Research, Eds. Manno and Ring, D. Reidel, Holland, 1972.

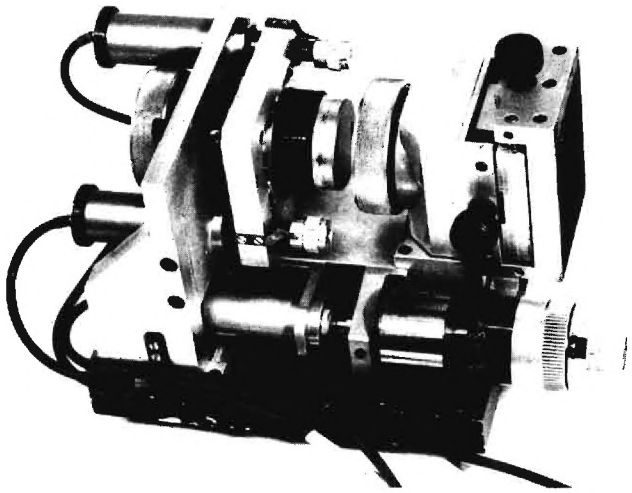

Fig. 1. Jig for making filters

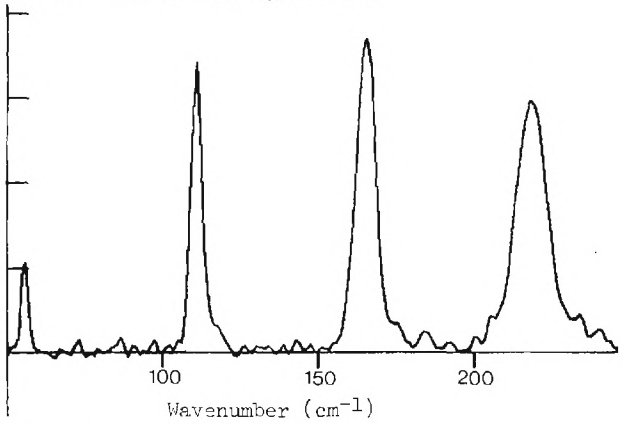

Fig. 3. Filter at intermediate stage

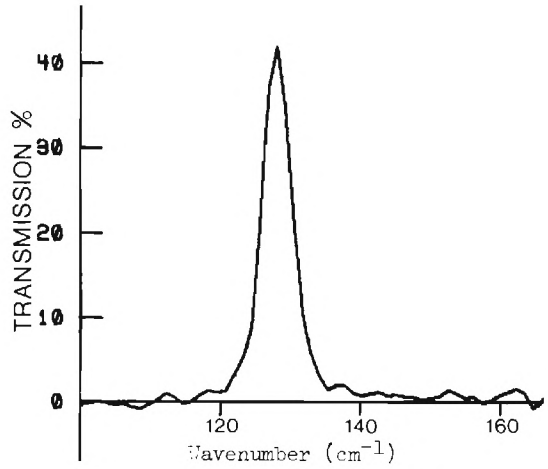

Fig. 5. Final filter after gluing and removal from jig

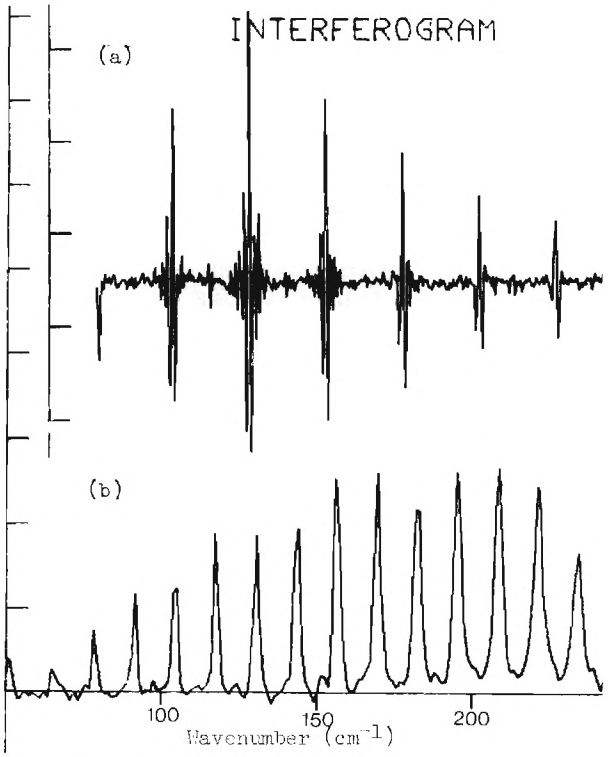

Fig. 2. (a) Interferogram
(b) Transform

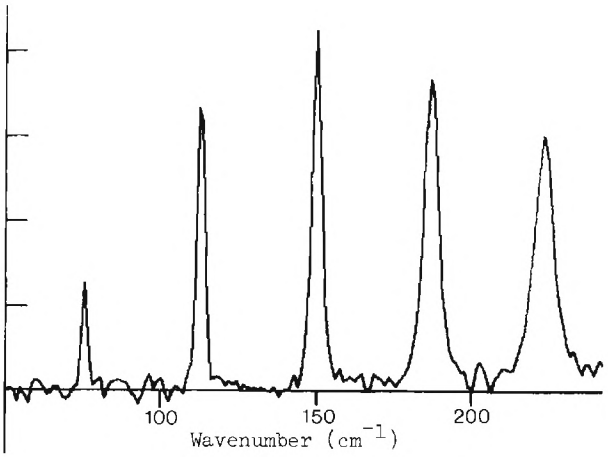

Fig. 4. Separation decreased further

THEORY OF AN EFFICIENT ELECTRONIC PHASE SHIFTER EMPLOYING MULTILAYER DIELECTRIC WAVEGUIDE STRUCTURE

A. B. Buckman
Electronics Research Center and Electrical Engineering Department
The University of Texas at Austin
Austin, Texas 78712

Introduction

The possibility of enhancing the modulation in an electrooptic single-slab dielectric waveguide by exciting high-order modes in thick slabs was first pointed out by Lotspeich [1]. Later, Buckman [2] showed that, for a three-layer dielectric slab structure, the modulation in the effective refractive index of a guided mode could be made to exceed that of the "bulk" refractive index of the active layer by up to a factor of n_g^2, where n_g^2 is the highest refractive index in the system. This enhancement in modulation of the effective refractive index $\bar{n}$, and hence of the propagation constant β, is critically dependent on the value of $\bar{n}$ in the absence of modulation, which is, in turn, dependent on the layer thickness.

In the mm region, the use of dielectric waveguides made of Si or GaAs has been proposed [3,4], and an electronic phase shifter driven by a PIN diode has been demonstrated experimentally [5], which exhibited a phase shift/unit length of $\sim 35°/cm$ at a drive current density of the order ~ 6 A/cm^2. The mechanism of operation of this device was interpreted to be control of the height of the guide by shifting a high-conductivity region toward its center. However, the absence of any drive current dependent losses in these devices, until the drive current was sufficient to heat the waveguides, suggests that free-carrier dispersion [6] rather than the movement of a metal-like wall, may be responsible for the observed phase shift. To obtain phase-shifts of this size in the sub-mm to far-IR region with "scaled-down" versions of the devices in Ref. [5] would be impossible, since the refractive index change, for a given material and injection current density, is proportional to ω^{-2}.

In this paper, the general theory of the sensitivity of a multilayer dielectric waveguide to small refractive index changes in one of the layers is applied to the design of a PIN diode-driven phase shifter for the sub-mm region. For particular materials, wavelengths and injection current densities, the usual figure of merit, the phase shift/unit length, is proportional to this sensitivity.

The Multilayer Waveguide

For simplicity, two assumptions will be made concerning the geometry of the waveguide and the PIN diode. The waveguide is assumed to have an aspect ratio sufficiently large so that TE- or TM-like modes propagate. If desired, this can be refined by using the effective refractive index to include the effects of lateral containment by boundaries [7]. The phase-shifts are only slightly affected. In addition, the PIN-diode current density, and hence the induced refractive index change Δn_a, is assumed uniform over the active region of the waveguide. The part of the device design involving the multilayer structure then reduces to obtaining a large magnitude for

$$\frac{\partial \bar{n}}{\partial n_a} = \frac{-n_g\,(\partial \xi/\partial n_g) + \xi \delta_{ga}}{\xi q/(1-q^2) + \partial q/\partial q} \qquad (1)$$

where n_g is the refractive index of the reference layer, ξ is the Kronecher delta, $q = \bar{n}/n_g$, and ξ is the sum of the phase shifts on total internal reflection at the boundaries of the reference medium. The value of q is determined by the modal equation,

$$4\pi\, n_g \frac{d_g}{\lambda} \sqrt{1 - q^2} = \xi(q) + 2m\pi, \quad m = 0,1,2 \qquad (2)$$

where d_g is the thickness of medium g and λ is the vacuum wavelength.

Two approaches to multilayer waveguide design for large $|\partial \bar{n}/\partial n_a|$ are considered here. The first, the resonantly coupled active layer, is shown in Figure 1. The active layer is in the form of a flat PIN diode, with P and N regions formed along opposite sides of the dielectric stripline guide. Atop this diode are the evanescent coupling and guide layers, in narrower strips occupying the space between the P and N regions. In this geometry a TE-like guided mode is weakly confined in the y-direction. Approximating this situation with a pure TE mode and following Ref [2] yields a maximum $|\partial \bar{n}/\partial n_a|$ of n_g^2, for values of $\bar{n}$ quite near n_a. In contrast, if the guide were made from a single slab of the active medium only, the maximum is n_g. Further, it occurs at infinite waveguide thickness, which would require intolerably large drive current. For single slab thicknesses up to 10-20 λ, $|\partial \bar{n}/\partial n_a|$ is usually $\lesssim 1$.

The second approach is synthesis of a four layer structure in which $\partial \xi/\partial q$ in (1) is negative and nearly offsets $\xi q/(1 - q^2)$ in a narrow range of q. In addition, the active layer is made as thin as practicable, to reduce the required drive

current to obtain a given Δn_a. This device is shown in Figure 2. The PIN diode is fabricated in the thin top layer. Confinement of the mode in the y-direction occurs by the same means as in Figure 1. For values of $\bar{n}$ within $\sim .005\ n_a$ of n_3, $|\partial\bar{n}/\partial n_a|$ can approach 10 for realistic thickness tolerance on d_a.

Limitations

Both designs take advantage of a resonance in $|\partial\bar{n}/\partial n_a|$ in (1), and hence dimensional tolerances are important in achieving the proper operating point, $\bar{n} \gtrsim n_3$, in both cases. For both designs, the range of q over which the resonance occurs is about 5×10^{-3} for refractive indices in the range 3-4. For the device in Figure 1, the most critical dimension is d_g/λ, and the maximum permissible error is $\sim 10^{-4}$. For $\lambda \gtrsim 100$ μm, this means ~ 100 Å thickness control, which is not out of the question using conventional film growth techniques.

The tight thickness tolerances for large phase shifts give these devices a frequency-selective behavior. If a spectrum of vacuum wavelengths are guided into the phase shifter, only that part of the spectrum very close to the design wavelength will undergo a significant phase shift.

References

[1] J. F. Lotspeich, J. Opt. Soc. Am. Vol. 65, p. 797 (1975).

[2] A. B. Buckman, J. Opt. Soc. Am. Vol. 66, p. 30 (1976).

[3] M. M. Chrepta and H. Jacobs, Fort Monmouth N.J. Tech. Rep. ECOM-3482, Sept. 1971.

[4] M. M. Chrepta and H. Jacobs, Fort Monmouth N.J. Tech. Rep. ECOM-3513, Nov. 1971.

[5] H. Jacobs and M. Chrepta, IEEE Trans., Microwave Theory Tech., Vol. MTT-22, p. 411 (1974).

[6] J. P. Woerdman and B. Boelger, Phys. Letters A, Vol. 30, p. 164 (1969).

[7] W. V. McLevige, Univ. of Ill.-Urbana Rep. R-673, Feb. 1975.

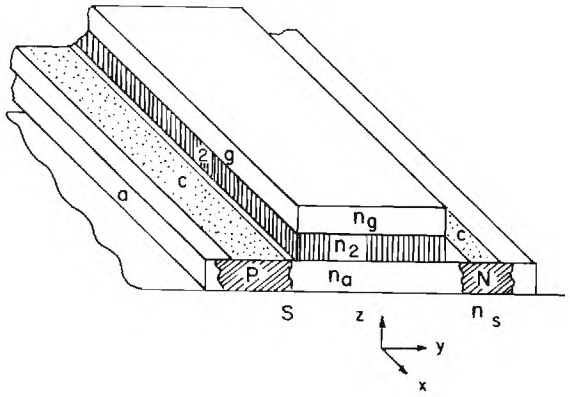

Figure 1. Resonantly coupled active layer phase-shifter. P, N: p- and n-type regions formed in intrinsic active layer, a. S: substrate. C: Metal contacts. 2: coupling layer. g: guide layer. S: substrate. $n_g > n_a > n_2 > n_s$.

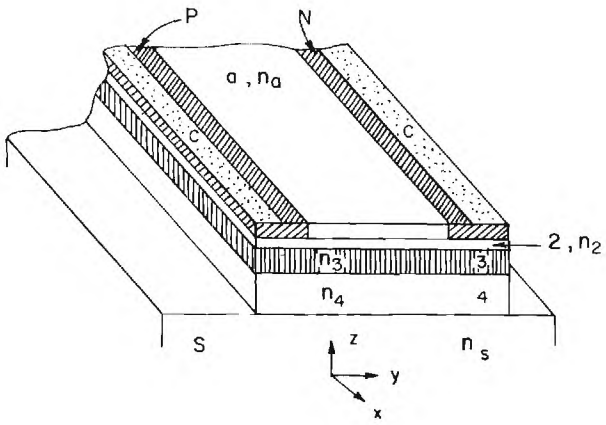

Figure 2. Four layer phase shifter designed for low drive current. P, N: p- and n-type regions formed in intrinsic active layer, a. S: substrate. C: metal contacts. 2, 3, 4: dielectric multilayer stack. $n_2 > n_a > n_4 > n_3 > n_s$.

SWITCHES AND MODULATORS EMPLOYING FRUSTRATED TOTAL INTERNAL REFLECTION

R. R. Selleck, E. W. McDonald, and J. C. Wiltse
Martin Marietta Corporation
P. O. Box 5837
Orlando, Florida 32805

Many aspects of the submillimeter region have led both microwave and infrared specialists to approach this regime from their respective fields. In overcoming the new technical difficulties, the standard existing techniques have been pushed from both ends to nearly their limit in order to accommodate this new domain. We would like to suggest the inclusion of one technique which has been used in both microwaves and infrared laser applications which has apparently been overlooked. The suggestion is to utilize FTIR type devices in order to achieve electro-optic effects without requiring electro-optic materials.

If radiation strikes a surface at an angle greater than the critical angle, it experiences total internal reflection as illustrated in Figure 1A. Should two surfaces of like index come into contact, the surface effects tend to disappear resulting in total transmission across the interface regardless of incident angle. This condition is shown in Figure 1B as adapted from the original case. There is a region where the transmission across the boundary is a function of the separation as suggested in Figure 1C. This region is where the Total Internal Reflection is Frustrated by coupling the radiant energy across the boundary by an evanescent wave.

Although the transmission response of the switch is a complex function of the refractive index of the prisms, the gap spacing, wavelength, and angle of incidence to the interface, a typical transmission curve for the FTIR switch will look similar to Figure 2. Note that the response is normalized to wavelength requiring only a fraction of a wavelength to switch states regardless of the wavelength involved. In general, the two polarizations have separate responses, however, there is always an angle for which the two polarization curves coincide. As the refractive index increases, the polarization independent curves shift to the left. As the angle of incidence increases from the polarization insensitive operating angle, the response curve splits into its two polarization components with both curves shifting to the left. (For decreasing angles, the two curves cross and shift to the right until the critical angle is reached.) By choosing the incident angle and refractive index of the prism material, a response curve of the general characteristic shape can be generated to meet a wide variety of specific amplitude modulation requirements.

By controlling the relative gap separation between the prisms, amplitude modulation of transmitted and reflected energy can be achieved. The implementation of this concept has been demonstrated in several devices throughout the radiation spectrum. Most of this activity has recently been in the infrared region directly associated with lasers [1]. Amplitude modulators and optical switches with responses in excess of 500 hertz have been built for use with both 5 and 10 micron sources. Because of the wide freedom of choice in the material used, these devices are typically capable of handling high power loadings. In this spectral region, several hundred watts are not uncommon. Here, piezo-electric transducers are used to control the gap separation by physically moving the prisms together and apart, as shown in Figure 3A, by applying an electrical signal proportional to the separation desired. Extinction ratios in excess of 100:1 are readily attainable and devices with apertures of 1½ inches have been made. Another implementation of the FTIR concept has been employed to accommodate a dynamic condition of a 1.06 micron Q-switch configuration. Here, an acoustic wave is launched into the prism material by an electrical impulse to a PZT mounted to the prism opposite the interface as suggested in Figure 3B. Upon reaching the dielectric interface gap, the prism deforms and dynamically changes the separation allowing an optical feedback to occur within the laser cavity which results in a Q-switched pulse. By choosing the prism material from a damage resistant criteria, this type Q-switch can handle much greater power levels without detrimental effects.

From the microwave end of the spectrum, static FTIR dual prism devices have been used in the past as beamsplitters, duplexers, and attenuators [2-6]. In extending this idea to the submillimeter wavelength region, two major differences immediately occur. The first naturally concerns the materials that are available for consideration. Most IR materials cut off before the 20 to 40 micron region. Although some of these, such as germanium and magnesium oxide, do have windows further out, primarily a new set of materials must be considered. Since the device requires no special characteristics of the material, any that transmit at the desired wavelength are possible candidates. Silica, Polystyrene, TPX, and Polyethylene are possible choices for the submillimeter region with others perhaps being better depending upon the exact wavelength in question [7].

The second influence in shifting to longer wavelengths is the drive requirement. Since the transmission response curve is normalized to wavelength, the motion required to achieve similar results will be essentially magnified by the increase in wavelength. This causes a substantial strain on PZT type implementation for most of the submillimeter wavelength region. Although different geometries can be used to help minimize

the drive requirement, with waves greater than 500 microns a new mechanism will most likely need to be employed. To date, most microwave and submillimeter wave applications have used micrometer or similar arrangements for control, however, for dynamic response an electro-mechanical implementation will have to be devised. This is not as difficult as might first be anticipated since the positioning tolerances have been reduced with the longer wavelength allowing for a more casual positioning. With this drive requirement in mind, perhaps a more promising utilization of the FTIR device for submillimeter work is to exploit the phase nature of the interaction. When light strikes a dielectric boundary at an angle greater than the critical angle, that light incurs a phase shift upon its total reflection. The amount of phase shift is determined by the incident angle, the polarization, and the relative refractive index across the boundary. By changing the boundary dielectric, the phase of the emerging wave can therefore be altered. The interesting fact is that whereas to change the amplitude states, a gap variation in the order of a wavelength is required; to change phase states, less than 1/10 wave gap motion is needed as illustrated in a typical phase plot of Figure 4. The two polarization responses here are always separate which can then be exploited as a variable wave plate or polarization switch when placed in a proper configuration. In this way, electro-optic effects can be achieved without the use of electro-optic materials. If used with only one polarization component, the device becomes a phase shifter for the entire incident beam.

This reduced motion requirement allows the submillimeter phase modulator drive mechanism to be similar to that of the infrared amplitude modulator which has given flexibility and versatility for random real time response.

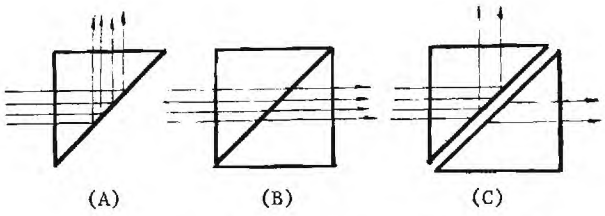

Figure 1. Principle of FTIR Operation

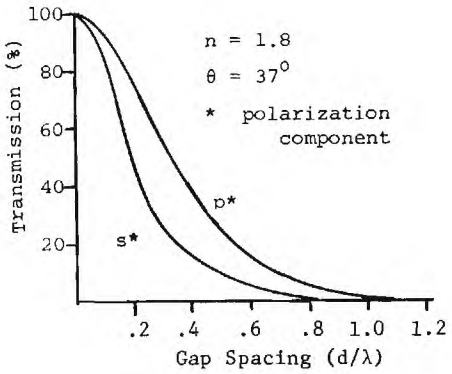

Figure 2. Typical FTIR Response

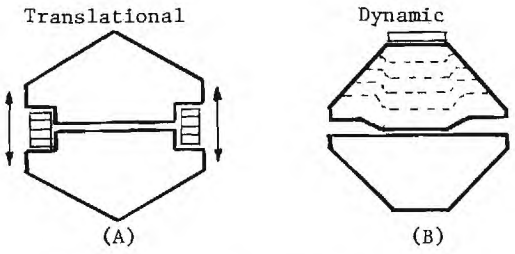

Figure 3. FTIR Operational Modes

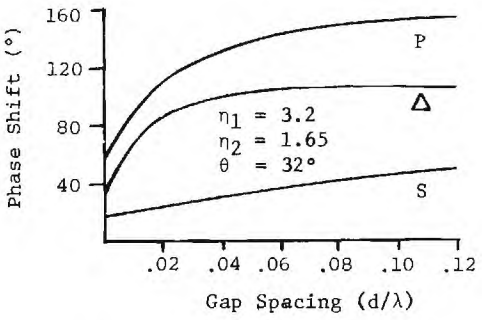

Figure 4. Typical FTIR Phase Response

References

1. R. R. Selleck, "High Power Infrared Modulator." Technical Report AFAL-TR-76-32; June, 1976.
2. M. Daenler, "A Submillimeter Michelson Interferometer with Frustrated-Total-Internal-Reflection Beamsplitter," Proceedings of First International Conference on Submillimeter Waves, pp. 126-127; June, 1974.
3. J. W. Dees, "Detection and Harmonic Generation in the Submillimeter Wavelength Region," Microwave Journal, Vol. 9, pp. 48-55; Sept., 1966.
4. H. D. Raker and G. R. Valenzuela, "A Double-Prism Attenuator for Millimeter Waves," IRE Trans., MTT, Vol. MTT-10, pp.392-393; Sept. 1962.
5. J. J. Taub and H. J. Hindin, "Design of Quasi-Optical Components," Microwaves, Vol. 3, pp. 20-29; January, 1964.
6. J. W. Dees, V. E. Derr, J. J. Gallagher, and J. C. Wiltse, "Beyond Microwaves," International Science and Technology, pp. 50-56; November, 1965.
7. G. W. Chantry, "Submillimeter Spectroscopy," Academic Press, New York; 1971.

OPTICAL PROPERTIES OF METALLIC FILMS IN THE INFRARED

B. Carli
Physical Institute
University of Florence
Florence 50154 Italy

When a metallic film is used as a reflector, its thichness need to be greater than the penetration depth $d = \lambda/(4\pi n\kappa)$ to ensure the maximum reflectivity. The penetration depth encreases with the wavelength and, in the infrared and in the millimetre region, the required thickness is usually greater than the standard thickness of reflectors. Costly procedures are often needed for this special requirement.

On the other hand, the maximum reflectivity of metallic films at long wavelengths is very high and for many applications the reflectivity obtained with metallic films of thickness h smaller than the penetration depth can be sufficient. To calculate the thichness h wich is actually needed for each application, a formula which gives the reflectivity R as a function of h is particularly useful. From classical calculations (M.Born and E.Wolf, "Principles of Optics" Fifth ed., sec. 13.4), Pergamon Press, Oxford 1975), for infrared and millimetre radiation, one obtains that the reflectivity R, the transmissivity T and the absorbtion A of a metallic film of thischness h($h \ll d$), electrical conductivity σ and resistance per square $r = 1/(h\sigma)$, surrounded by a medium of refractive index n, for an angle of incidence θ, are :

$$R = (f^*/(f^* + 1))^2$$

$$T = 1/(f^* + 1)^2 \qquad (1)$$

$$A = 2f^*/(f^* + 1)^2$$

where for TE waves $f^* = 188.5/(nr\cos\theta)$ and for TM waves $f^* = 188.5\cos\theta/(nr)$. The minimum thichness to obtain a reflectivity R is :

$$h_{min} = \frac{(1 + \sqrt{R})\sqrt{R}}{188.5\,(1 - R)\sigma}$$

and for $R \simeq 1$

$$h_{min} = 1/(1 - R)\,30\pi\sigma$$

As an example, if one wants to obtain the maximum possible reflectivity with silver at 1 mm ($R_{max} = 0.998$), a layer thicker than 570 Å is needed, but 80 Å are enough if a reflectivity of 0.98 is sufficient.

Formulae (1) can also be used to justify why in the far infrared interference filters (Fabry-Perot type) require the use of meshes and do not work if made with metallic films. The peak transmission of a Fabry-Perot filter is equal to

$$t = (1 - A/(1-R))^2$$

Using the values of reflectivity and absorption of a metallic film one obtains

$$t = 1/(1 + 2f^*)^2$$

and for $f^* \gg 1$, condition to have a filter with high finesse, the peak transmission is very small.

FIR FRESNEL PRISM USED AS A QUARTERWAVE PLATE

U. O. Farrukh
Phoenix Corp. 1311 Dolley Madison Blvd. McLean, VA 22101
G. A. Koepf
NASA Goddard Space Flight Center, Greenbelt, Md. 20771

Fresnel prisms were extensively studied and used in the optical region of the spectrum /1/. When radiation propagates in a medium towards a surface that separates the given medium from an optically less dense material, then total reflection may occur, when the angle of incidence is greater than the critical angle of the optically dense medium. Under conditions of total reflection, different components of the radiation field experience different amounts of phase shift and the relative phase shift is given by the well known expression

$$\tan \delta/2 = \sqrt{1 - 1/n^2 \sin^2\Theta} \ / \tan\Theta$$

where δ = relative phase shift
Θ = angle of incidence
n = ratio of the index of refraction of the medium to that of the optically less dense medium.

Fig. 1. is a plot of the index of refraction versus the angle of incidence at a constant phase shift. Checking the plots for a phase shift per reflection of 90° and 45 degrees we find that the minimum possible index of refraction to achieve the required phase shift is 2.4 and 1.5, respectively. Fresnel prisms are used if one reflection gives enough phase shift, while Fresnel rhombs are used when a greater phase shift is needed.

In the far infrared region for wavelength range of 100 to 1000 microns special problems arise when designing prisms or rhombs for such a wavelength. These are the large beam diameters and the relatively high absoption coefficients of most materials. Also, overlapping of incident and reflected beams must be avoyded by proper shaping the prism. For example, a prism is shown in Fig. 2., the total path length inside the prism is given by beam width w over $\tan\Theta$. To minimize losses, the path length must be made as small as possible. To eliminate truncation and aperturing effects then the prism input surface must be larger than the beam cross section, which in turn will increase the path length. When truncation is allowed the path length should be greater than the beam diameter squared over 4λ, otherwise the exit surface would fall in the near field region of diffraction with its associated central dark regions at certain positions which will increase the radiation losses.

The table shows a listing of some common materials with their index of refraction and the absorption coefficient. These values are obtained from data in the literature. They apply only to a wavelength of 300 microns.

As an example for using the phase shift of total reflection to produce a quarter wave element for FIR wavelengths, two materials will be choosen and the total losses will be calculated. Using germanium an angle of incidence of 53° gives a phase shift of 90° in one reflection. The path length results to be 1.1 cm if a 1cm * 1cm input aperture is assumed. The total losses resulting from reflections at both surfaces and from the absoption are calculated to be 86,5%. When using teflon, two total reflections are needed to accomplish the phase shift of 90 degrees. A path length of 2.65 cm and total transmission losses of 70% result.

References

/1/ M. Born and E. Wolf, Principles of Optics, Pergamon Press, New York, 1975.
/2/ U. Farrukh, "Diffraction and Focusing of Trancated Gaussian Beams", Ph.D. Thesis, Univ. of Southern Calif., June 1974.

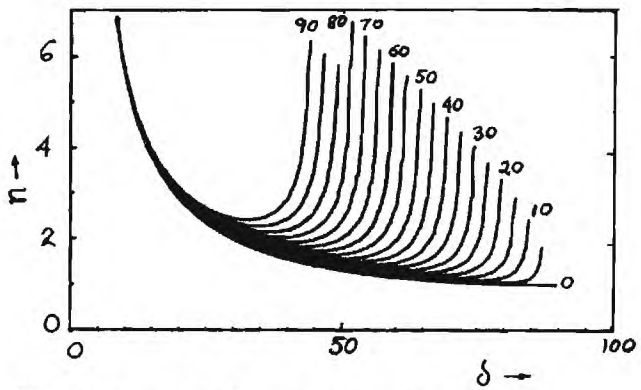

Fig. 1. Phase shift over index of refraction.

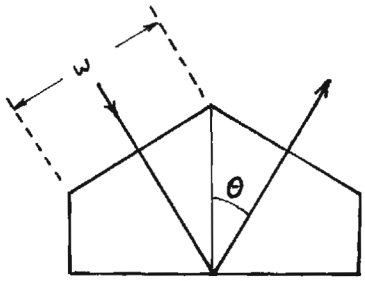

Fig. 2. Modified Fresnel prism.

Material	n	α(cm-1)
Polyethylene (high density)	1.44	0.30
TPX	1.425	0.70
Teflon	1.44	0.30
GaAs	3.6	0.50
Ge	4.005	1.05
Si	3.147	0.54
SiO2 (crystal)	2.10	0.35
Al2O3 (Saphire)	3.07	1.00

Table: Refractive index and absorption coefficient of some common materials.

ANALYSIS OF SUBMILLIMETER WAVE FABRY-PEROT INTERFEROMETERS MADE OF FOUR WIRE GRIDS*

R. W. McMillan and J. B. Langley
Engineering Experiment Station
Georgia Institute of Technology
Atlanta, Georgia 30332

Several workers [1,2,3] have successfully constructed Fabry-Perot interferometers for use in the microwave spectrum by using wire grid arrays. Recently Gustincic [4] was able to build such an interferometer which would effectively rotate the plane of polarization of a reflected wave and transmit without change the wavelength to which it was tuned. This configuration has application in microwave radiometers where it is generally difficult to couple the local oscillator into the mixer without considerable loss of power. Use of a Fabry-Perot interferometer also gives inherent single sideband operation and rejects local oscillator noise at the signal frequency. In this paper results of calculations on the performance of wire grid arrays are presented.

Consider the wire grid oriented as shown in Figure 1a. Assume that radiation polarized perpendicular to the wires is totally transmitted and that radiation polarized parallel to the wires is totally reflected. The latter assumption, expecailly, may not be valid for all grid spacings, but it is possible to construct grids for which it is essentially true. Under these conditions, the transmission and reflection for this grid are:

$$t_\Theta = \begin{pmatrix} \cos^2\Theta & \cos\Theta\sin\Theta \\ \sin\Theta\cos\Theta & \sin^2\Theta \end{pmatrix}, \quad r_\Theta = \begin{pmatrix} -\sin^2\Theta & \sin\Theta\cos\Theta \\ \cos\Theta\sin\Theta & -\cos^2\Theta \end{pmatrix}, \tag{1}$$

where Θ is defined in Figure (1a). It is further assumed that the phase shift on reflection is π. Multiplication of either of these matrices by a column vector $\begin{pmatrix} e_x \\ e_y \end{pmatrix}$ representing a given input polarization and amplitude gives a column vector representing the resulting output. In Figure 1b, a second grid, oriented at angle α is shown, along with a vector $\vec{e}$ at angle β representing an input signal. For this second grid, the transmission and reflection matrices are obtained by simply replacing Θ in Equations (1) with α.

Figure 1c shows the side view of a two-grid array formed by placing an α-grid behind a Θ-grid and separating them by a double pass phase shift ϕ_1. This phase shift for wavelength λ is:

$$\phi_1 = \frac{4\pi}{\lambda} nh. \tag{2}$$

where n is index of refraction and h is thickness. Using techniques used by Born and Wolf [5] it is possible to show that the transmitted amplitude $\vec{A}_T$ for this array is:

$$\vec{A}_T = \cos\gamma \frac{1-e^{i\phi_1}}{1-e^{i\phi_1}\cos^2\gamma} \cdot \begin{pmatrix} \cos\alpha\cos\Theta & \cos\alpha\sin\Theta \\ \sin\alpha\cos\Theta & \sin\Theta\sin\alpha \end{pmatrix} \begin{pmatrix} e_x \\ e_y \end{pmatrix} \tag{3}$$

where $\gamma = \Theta - \alpha$. The reflected amplitude is:

$$\vec{A}_R = \left[\begin{pmatrix} -\sin^2\Theta & \sin\Theta\cos\Theta \\ \cos\Theta\sin\Theta & -\cos^2\Theta \end{pmatrix} - \frac{\sin^2\gamma e^{i\phi_1}}{1-e^{i\phi_1}\cos^2\gamma} \cdot \begin{pmatrix} \cos^2\Theta & \cos\Theta\sin\Theta \\ \cos\Theta\sin\Theta & \sin^2\Theta \end{pmatrix} \right] \begin{pmatrix} e_x \\ e_y \end{pmatrix}. \tag{4}$$

Now let $e_x = e\cos\beta$ and $e_y = e\sin\beta$. The transmissivity T and reflectivity R of this array are then:

$$T = \frac{1}{e_o^2} \vec{A}_T^* \cdot \vec{A}_T$$

$$= \frac{2\cos^2\gamma(1-\cos\phi_1)\cos^2(\Theta-\beta)}{1 - 2\cos\phi_1\cos^2\gamma + \cos^4\gamma}, \tag{5}$$

$$R = \frac{1}{e_o^2} \vec{A}_R^* \cdot \vec{A}_R = \sin^2(\Theta-\beta)$$

$$+ \frac{\sin^4\gamma\cos^2(\Theta-\beta)}{1 - 2\cos\phi_1\cos^2\gamma + \cos^4\gamma}. \tag{6}$$

Using Equations (5) and (6) it has been verified that $T + R = 1$.

Now consider two pairs of grids arranged as shown in Figure (2). The indicated phase shifts are double pass relative as before. This configuration is symmetrical, so that the direction of the incident radiation is unimportant. Using Equations (3) and (4), the transmitted and reflected amplitudes A_{TF} and A_{RF} for this arrangement have been determined to be

$$\vec{A}_{TF} = \frac{\cos^2\gamma(1-e^{i\phi_1})^2}{(1-e^{i\phi_1}\cos^2\gamma)^2 - \sin^4\gamma e^{i\delta}}$$

(equation continued on next page)

$$\cdot \begin{pmatrix} \cos^2\theta & \sin\theta\cos\theta \\ \sin\theta\cos\theta & \sin^2\theta \end{pmatrix} \begin{pmatrix} e_x \\ e_y \end{pmatrix}, \qquad (7)$$

$$\vec{A}_{RF} = \left\{ \begin{pmatrix} -\sin^2\theta & \sin\theta\cos\theta \\ \sin\theta\cos\theta & -\cos^2\theta \end{pmatrix} - \frac{\sin^2\gamma e^{i\phi_1}}{1-e^{i\phi_1}\cos^2\gamma} \cdot \begin{pmatrix} \cos^2\theta & \sin\theta\cos\theta \\ \sin\theta\cos\theta & \sin^2\theta \end{pmatrix} \cdot \left[1 + \frac{\cos^2\gamma e^{i\phi_3}(1-e^{i\phi_1})^2}{(1-e^{i\phi_1}\cos^2\gamma)^2 - \sin^4\gamma e^{i\delta}} \right] \right\} \begin{pmatrix} e_x \\ e_y \end{pmatrix}, \qquad (8)$$

where $\delta = 2\phi_1 + \phi_3$.

Expressions for transmitted and reflected power for the configuration of Figure 2 have also been derived, but have proven to be almost intractable from the point of view of reducing them to expressions which provide insight into their workings. It has proven easier to substitute values into Equations (7) and (8) and square the results to obtain power.

Using these results, it is possible to show that the polarization of microwave signals may be effectively manipulated by using a wire grid Fabry-Perot interferometer. This manipulation is in addition to the filtering effects normally given by interferometers of this type. These devices have applications in those areas where it is necessary to mix local oscillator and signal microwave frequencies with minimum loss of local oscillator power.

References

* This work was supported by NASA Grant NSG-5012

1. W. Culshaw, "Reflectors for a Microwave Fabry-Perot Interferometer," NBS Report 5527 (1957).
2. W. Culshaw, IRE Trans. Microwave Theory and Techniques, MTT-8, (1960) 182-180.
3. R. Ulrich, K. F. Renk and L. Genzel, IEEE Trans. Microwave Theory and Techniques, MTT-11 (1963) 363-371.
4. J. J. Gustincic, Private Communication.
5. M. Born and E. Wolf, Principles of Optics, Pergamon Press, New York (1965) 323-333.

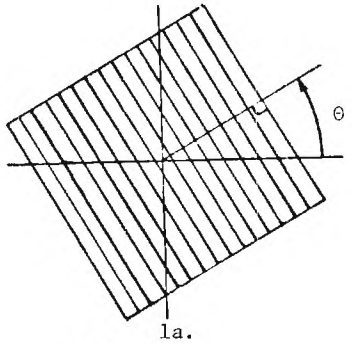

1a.

$\vec{e} = \vec{e}_x + \vec{e}_y$

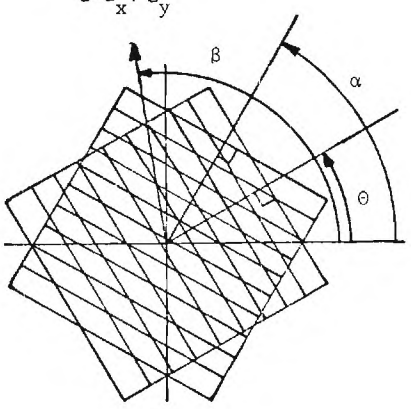

1b.

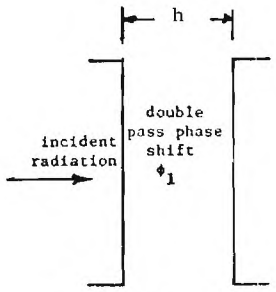

θ grid α grid

1c.

Figure 1. Definition of Wire Grid Parameters

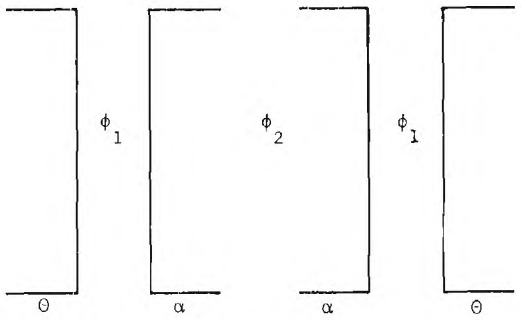

Figure 2. Two Pairs of Grids Forming an Interferometer

SUBMILLIMETER MONOCHROMATIC SPECTROSCOPY AND ONE-DIMENSIONAL WIRE GRIDS

E.A. Vinogradov, N.A. Irisova, A.M. Prokhorov

P.N. Lebedev Institue
Moscow, USSR

Highly sensitive spectrometers based on using backward-wave tubes with a resolution of $\frac{\Delta\lambda}{\lambda} \sim 10^{-5}$ in the wave range 4 mm ± 0.2 mm has been designed. The quasioptical measuring circuits of spectrometers based on using instruments with one-dimensional wire grids.

Amplitude and original phase investigations of the characteristics of the one-dimensional grids with wire spacing $\ell << \lambda$ has been conducted as well as the characteristics of the quasioptical instruments.

The method investigations of the field distributions in the quasioptical lines and open resonators by using thermosenstivity luminofor has been proposed.

RECENT ADVANCES IN FAR INFRARED DETECTORS FOR ASTRONOMY IN THE 1-1000μm RANGE

K. Shivanandan
E.O. Hulburt Center for Space Research
Naval Research Laboratory
Washington, D. C. 20375

ABSTRACT

The increasing interest in the application of bolometers and photoconductors in infrared astronomy has stimulated considerable research effort during the past few years in improving the sensitivities of these detectors under low and high background conditions. A review of these detectors will be given and their applications in photometry and spectroscopy with ground based and airborne infrared astronomical systems will be discussed.

Introduction

There are three types of incoherent detectors which are being used in infrared astronomy. They are:

a) Thermal detectors such as the germanium or silicon bolometers operating at 2.2°K and n-type InSb at 4.2°K.

b) Intrinsic photoconductive and photovoltaic devices operating at 77°K.

c) Extrinsic photoconductive detectors such as shallow impurity doped germanium and silicon detectors operating at 4.2°K.

For astronomical purposes, the most relevant basis for comparison of detectors is the minimum value of the noise equivalent power (NEP) which is defined as the input signal power which produces unity signal to noise ratio when the noise is measured as the rms value in unity bandwidth. Photometric measurements of astronomical sources are calibrated against a planetary object with a known brightness temperature and expressed in terms of spectral flux density which is defined in units of Jansky (1 Jansky (J) = 10^{-26} w-m^{2}Hz).

Characteristics of Infrared Systems

Infrared photometers are limited by noise associated with background fluctuation within the optical components of the telescope and from sky emission. For ground based telescopes, sky noise dominates over other sources and restricted fields of view, typically a few seconds of arc are used for observing small sources. The background is reduced by use of spatial differential chopping, the technique is to move the optical beam by wobbling the secondary mirror of a telescope from the source to the nearby sky, and to amplify only the difference in signal with an AC amplifier and coherent detector. Statistically the signal to noise ratio increases with the square root of the observing time, and typically for one hour of integration sources as faint as 5×10^{-5} Jansky at 2μm and 2.5×10^{-3} Jansky at 10μm have been measured with 2.3 meter telescope. Airborne systems such as the NASA C-141 Airborne Infrared Observatory and balloon borne telescopes are used for far infrared measurements with increased field of view and unlimited wavelength range. Conventionally germanium bolometers have been used and detector N.E.P. sensitivities of 10^{-14}WHz$^{-\frac{1}{2}}$ at 100μm have been achieved. This limit is conditioned by the background. Multicolor photometry have been developed for airborne systems and have produced remarkable results on the structure of the Galactic center.

Liquid helium cooled telescopes have been flown on sounding rockets with microsecond response time photoconductive detectors and amplifiers with N.E.P. of 10^{-15}WHz$^{-\frac{1}{2}}$ under low background conditions and only basic limit to signal-to-noise ratio is the photon counting statistics of the sources being studied.

Detector Technological Improvements

Developmental programs in the 1 to 30μm region pursued by the military over the last decade have resulted in detectors with theoretical limits of sensitivity under a wide range of background conditions. Array technology developed with a large number of detector elements produced on a single solid state chop and integrated with signal conditioning and readout electronics will permit infrared images to be produced similar to visual photographs, and resolutions limited only by the telescope optical system.

Most of the far infrared astronomy (30μm to 1mm) of the last decade has been done with bolometer detectors operating at 1-2K. Composite and metal film bolometers are being developed to improve the radiative coupling and also decreasing the operating temperature to 0.3K so as to improve the sensitivity.

Photoconductive detectors such as beryllium doped germanium (Ge:Be) sensitive to 60μm and gallium doped germanium (Ge:Ga) sensitive to 125μm are being developed for low background environment in liquid helium cooled satellite experiments. These detectors are presently limited by contact noise and material non-uniformities. Application of state-of-the-art solid state techniques developed for near infrared detectors are being used with the long wavelength doped germanium detectors, which will result in a very substantial improvement

in their performances.

Recent discoveries in physics have created a new technology that depends on long-range quantum effects in superconductors. A new device which shows promise in infrared astronomy is the Superconducting Link Electromagnetic Detector (SLED) which is formed by a point contact between two superconductors. The SLED is an optimum detector for the wavelength region from 100μm to 8 millimeters and it offers high sensitivity, subnanosecond response time and insensitive to near infrared and visible radiation, a problem in bolometric and photoconductive detectors where filters are required to eliminate the near infrared.

Recent developments on up-conversion, permitting conversion of infrared photons to optical photons which can then be detected with sensitive optical detectors, will provide a unique type of spectrometer for line emission studies in H_2 regions and planetary nebulae.

Finally, extrinsic photoconductors such as arsenic doped silicon and gallium doped germanium, under conditions of low background photon flux, can have impedances greater than 10^{10} ohms. In order to minimize microphonics and shunt capacitance, the load resistor and MOSFETS for impedance matching are placed directly adjacent to the detector element in the cryogenic environment. Low noise MOSFET devices with low drain current at liquid helium temperatures are being developed as voltage and current mode amplifiers.

Conclusion

The development of better detectors - photoconductors and bolometers - including two-dimensional detector arrays, together with low noise cryogenically cooled preamplifiers in a reduced background environment, will yield large advancements in infrared astronomy and in the development of instruments for future space missions.

DEVELOPMENT OF THIN PYROELECTRIC DETECTORS FOR FAR INFRARED

A. HADNI, R. THOMAS and C. ERHARD
University of Nancy I
Nancy, France

Description of a new method to grow very thin single crystals (0.5 μm thick) on a metal surface with the right orientation to make far Infrared pyroelectric detectors.

We have shown that by evaporation of any saturated solution it is possible to get on any metallic film a number of microscopic flat and very thin single crystals (i.e. thickness smaller than 1 μm), the orientations of which are parallel [1]. The metallic film has to be deposited on a single crystal of the same material contained in the solution. The micro-crystals are either separated (fig.1) or closely jointed (fig.2) according to the thickness of the metallic film. In that case we have got a quasi single crystal film. An explanation is given in terms of submicroscopic holes in the film (fig.3). There is first epitaxial germination in the holes then a growth at the surface of the film.

Pyroelectric detectors made in this way have a high detectivity at frequencies up to 20 Mcps.

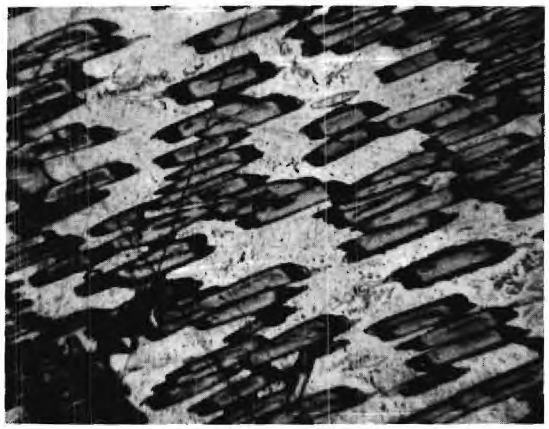

Fig.1. TGS single crystals obtained by evaporation of a TGS solution on a silver layer R_c = 10 ohms.

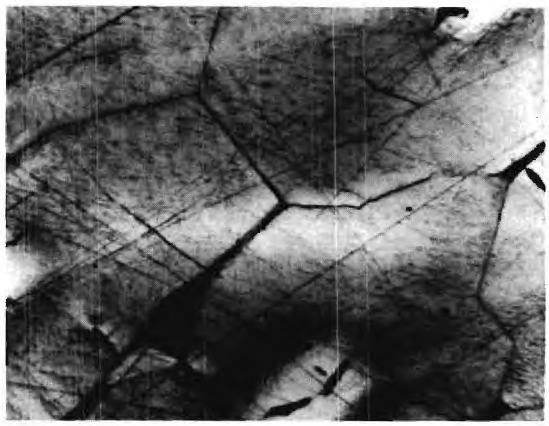

Fig.2. Flat TGSe single crystals covering the whole surface of a silver layer R_c = 0.05 ohm.

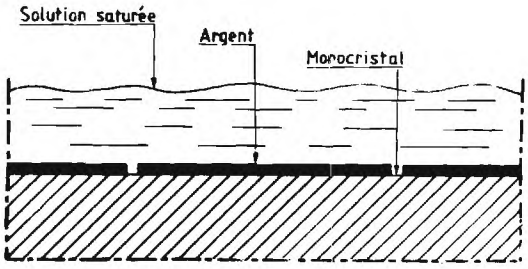

Fig.3. Sub-microscopic holes in the silver layer.

References

[1] A. HADNI, R. THOMAS et C. ERHARD - Cristallisation par germination epitaxique Compte Rendu Acad. Sci. Paris (Sept.1976).

MATERIALS FOR LOW NOISE SCHOTTKY-BARRIER CONVERTERS AT SUBMILLIMETER WAVELENGTHS

G. T. Wrixon
University College, Cork, Ireland
and
M. D. Blue
Georgia Institute of Technology, Atlanta, Georgia

Abstract

The prospects for realization of low noise coherent detectors in the 25 μm - 100 μm region are critically assessed. Use of high efficiency Schottky-barrier converters can be extended to the submillimeter region through the use of appropriate diode materials.

Summary

We analyze the effect of material parameters on mixer noise temperature for Schottky-barrier devices with a view toward optimizing performance at submillimeter wavelengths. A low noise temperature and high frequency cut-off are desired. Small diameters are of limited value due to current crowding. Thin layer expitaxial technology will be essential to extract maximum performance for a given material. Expected performance of such a submillimeter receiver should provide a lower NEP than is obtainable from cryogenic bolometers.

Introduction

The high frequency performance of Schottky-barrier diodes is limited by the barrier capacitance, C_j, and the series resistance, R_s. The barrier or depletion-layer capacitance effectively shunts the non-linear diode resistance R_j. In an epitaxial diode, the resistance R_s arises from the undepleted portion of the epilayer under the metal plus the spreading resistance of the bulk material, and is in series with the parallel combination of R_j and C_j. Thus C_j allows current to by-pass R_j, while R_s is a source of signal and LO power dissipation, heat production, and excess diode noise.

For a diode radius r_D, the dependences of C_j and R_s are $C_j \sim r_D^2$, $R_s \sim r_D^{-n}$ where $1 < n < 2$ depending on thickness of the epitaxial layer and the diode diameter. The diode cut-off frequency $f_c = (2\pi R_s C_j)^{-1}$ has been found to be a reliable indicator of high frequency performance if $R_s < 10\ \Omega$. Under this condition, $f_c \sim r_D^{-m}$ where typically $0.5 < m < 1$ depending again on material and epilayer properties.

The I-V characteristic of a Schottky diode for $I >> I_s$ may be written [1]

$$I = I_s \exp (V/V_o) \tag{1}$$

where
$$V_o = (E_{oo}/q) \coth (E_{oo}/kT) \tag{2}$$

and
$$E_{oo} = q\hbar (N/4\varepsilon m^*)^{1/2} \tag{3}$$

where N is the semiconductor carrier concentration, m^* is the carrier effective mass, and ε is the relative dielectric constant.

Under the most operating conditions, the principal source of noise from a Schottky diode is shot noise. For this case, the available noise power for bandwidth B is

$$P_N = qIR_jB/2$$

where
$$R_j = (dI/dV)^{-1} \sim V_o/I.$$

The equivalent noise temperature of the diode limited by shot noise may be shown to be

$$T_{eq} = qV_o/2k \tag{4}$$

It can be seen from equations (2) and (4) that reducing the diode's physical temperature will reduce T_{eq} until V_o becomes temperature independent at $V_o = E_{oo}/q$. At this temperature field emission dominates the conduction process giving a minimum noise temperature of

$$T_{eq} = E_{oo}/2k = (q\hbar/2k)\ [N/4\varepsilon m^*]^{1/2} \tag{5}$$

Schottky-Barrier Diode Parameters

The parameters of interest are T_{eq} from (5), C_j, R_s, and f_c given by

$$C_j = (\pi r_D^2)\ [q\varepsilon N/2V_B]^{1/2} \tag{6}$$

$$R_s = (Nq\mu)(4r_D)^{-1} \tag{7}$$

$$f_c = (2\pi R_s C_j)^{-1} \tag{8}$$

where V_B is the barrier potential, and μ is the carrier mobility. Equation (7) refers to bulk material, and does not include the influence of an epitaxial configuration.

For GaAs, an electron concentration of 2×10^{17} cm^{-3} is near optimum giving $T_{eq} = 23°K$. For a 2μm diameter diode, $C_j = 4 \times 10^{-15}$ F and $R_s = 16\Omega$. This value of series resistance is undesirably high, and may be reduced with a 2×10^{17} cm^{-3} epitaxial layer on a substrate with an electron concentration of 2×10^{18} cm^{-3}. For layer thickness of 0.1μm and a transition region of similar thickness, a value of $R_j = 7\Omega$ can be obtained [2], giving $f_c = 4$ THz or 75μm cut-off wavelength.

For a smaller diode diameter, current crowding raises R_s and raises the barrier temperature. Increasing the perimeter-to-area ratio can help [3], but further improvement will require another material.

Table I shows calculated performance for several materials. We have calculated series resistance using equation (7) and estimated the series resistance of an epitaxial device, R_ϵ, from the results for GaAs. The most promising new material is InSb, where useful device technology is in existance. Potentially better performance is offered by HgCdTe diodes, but the absence of experimental information and the lack of developed material technology mean higher risk.

TABLE 1. Calculated Parameters For Schottky-Barrier Diodes

Diode Material	Doping cm^{-3}	T_{eq} °K	C_B pF	R_s Ω	R_ϵ Ω	f_c Hz	λc μm
GaAs	$2x10^{17}$	23	.004	17	7	$4x10^{12}$	75
Si	10^{17}	21	.003	250	100	$0.5x10^{12}$	560
GaP	10^{17}	34	.002	1600	650	$0.1x10^{12}$	2500
InSb	$3x10^{16}$	40	.004	9	4	$10x10^{12}$	30
HgCdTe	10^{16}	28	.003	4.7	2	$27x10^{12}$	11

Conclusion

Our results indicate the potential for extending ultra-low noise Schottky-barrier mixer technology into the submillimeter wavelength region and perhaps to the LWIR. A well developed technology will be required for high quality epitaxial layers (or ion implanted layers), effective surface passivation, and low leakage currents.

A receiver incorporating such diodes offers high sensitivity and wide bandwidth in a wavelength region currently dominated by thermal detectors. The present situation is summarized in Figure 1. where sensitivities of coherent and incoherent detectors are compared. The curve for Schottky-barrier devices was obtained from data in the current literature. A factor of three increase in frequency for a given sensitivity is sufficient to provide a NEP of better than 10^{-15} W/Hz throughout the submillimeter region. The optimum operating temperature for a submillimeter converter appears from (2), (5), and Table I to lie between 20°K and 50°K. Temperatures near that of liquid helium will not be required.

This work was supported in part by NASA Goddard Space Flight Center and the Army Research Office.

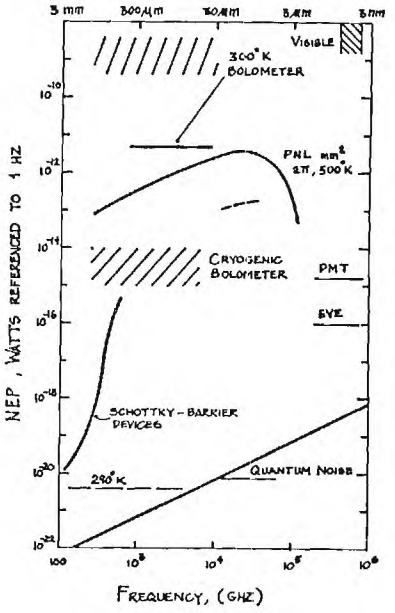

Figure 1. A comparison of coherent and incoherent detectors in the extreme infrared-submillimeter region. Thermal noise at 290°K and quantum noise limitations are shown at the bottom of the figure. The photon noise limit for 1 mm^2 detector viewing a 500°K black body is also shown for comparison. Schottky-barrier converters offer the potential of high sensitivity in this region. The dashed line at 10μm refers to an MOM diode at 10.6μm[4].

References

1. F. A. Padovani and R. Stratton, Solid State Electronics 9, 695 (1966).

2. Gerard T. Wrixon, IEEE Trans. on Microwave Theory and Techniques, to appear Nov. 1976.

3. Gerard T. Wrixon, IEEE Trans. on Microwave Theory and Techniques, MTT-22, 1159 (1974).

4. R. L. Abrams and W. B. Gandrud, Applied Physics Letters 17, 150 (1970).

SUBMILLIMETER-WAVE DETECTION WITH SUBMICRON SIZE SCHOTTKY BARRIER DIODES*

M. McColl, D. T. Hodges and W. A. Garber
The Ivan A. Getting Laboratories
The Aerospace Corporation
El Segundo, CA 90245

ABSTRACT

Video detection and heterodyne mixing with ultra-small Schottky diodes are observed between 70 and 1222 μm and the results characterized in terms of key diode parameters. The implications of these data for optimum design of submillimeter-wave diodes are discussed with reference to recent analytical work.

*This work was supported by The Aerospace Corporation.

The Schottky barrier diode can be characterized in terms of the equivalent circuit in Fig. 1. The element R represents the nonlinear junction resistance which provides the rectifying volt-ampere behavior necessary for detecting and mixing. The spreading resistance R_S is the resistance in the bulk of the semiconductor which results from the crowding of the current near the metal contact. R_S and the junction capacitance C are parasitic elements and are the primary cause of the degradation in performance of the diode as the frequency is increased. Both elements are unavoidable, but they can be minimized by choosing the proper materials and geometries. The exact design of the diode for optimum performance depends to a large degree on the mount in which the diode is situated.

The measurements reported below were performed on Schottky diodes mounted in an open type of structure. Such a mount has no provision for tuning-out the effect of the junction capacitance C, and consequently, at short wavelengths where typically $\omega RC >> 1$, diode performance is dominated by C. That is, a reduction in C increases the diode response and sensitivity. Since junction capacitance is proportional to junction area, a reduction in diode size increases its performance. For submillimeter operation, diode diameters less than 1 μm are preferred.

Table I summarizes our video detection data for a 0.5 μm diameter Schottky diode. Mixing was also observed at these same wavelengths. The video data at wavelengths of 119 μm and 496 μm are comparable to values previously reported [1,2]. Our 70.5 μm measurements represent the shortest wavelength for a Schottky barrier detector yet reported.

The diodes consisted of plated Pt contacts 0.5 μm in diameter on uniformly-doped, non-epitaxial 5×10^{18} cm^{-3} n-type GaAs. The size and doping of the structure yields a calculated zero-bias capacitance C_O of 1.3×10^{-15} F. This value and a measured dc series resistance R_S of 19 ± 3 ohms yields a calculated figure of merit cut-off frequency $f_c = (2\pi R_S C_O)^{-1}$ of 9×10^{12} Hz (a wavelength of 34 μm). Because of the higher plasma frequency, freedom from transit-time limitations, and lower parasitic losses, this choice of doping portends a higher frequency capability than an epitaxial structure. Our plans call for a comparison of both uniformly doped and epitaxial structures at 70 μm and shorter wavelengths.

The ultra-low capacitance junctions were obtained by fabricating submicron size junctions using electron lithographic techniques [3]. Relatively large arrays of 2500 Å diameter diodes as shown in Fig. 2 can be produced routinely. On a limited basis, contact diameters of 1000Å have been achieved.

To utilize the submicron diodes in a low noise receiver, a 600 GHz tunable single-mode mount is being assembled in our laboratory. With a tunable mount, performance is strongly effected by both R_S and C, and consequently, the requirements placed on the diode are more complex than those on a diode in an open mount. For instance, the conversion loss L_c of a mixer is given by the product of two terms:

$$L_c = L_0 L_1 \qquad (1)$$

where L_0 is the intrinsic loss associated with the frequency conversion process that occurs in the nonlinear resistance and L_1 is the parasitic loss arising from R_S and C. Typically, L_0 and L_1 behave oppositely with respect to diode area. The standard method of minimizing L_1 is by reducing the diode size, but L_0 generally increases as its size is reduced [4]. These competing effects can be resolved by the use of a multiple contact structure. For an array of independent diodes connected in parallel, the L_1 of the array is identical to the L_1 for a single diode of that array. However, the L_0 of the array is identical to the L_0 appropriate to the sum of the areas of each diode. Hence, a multiple contact structure consisting of a large number of very small diodes achieves the best compromise between L_0 and L_1, and consequently, for L_c. Figure 3 shows an example of an 8 x 8 square array of diodes with diameters of approximately 0.3 μm. Optimum multiple contact geometries for minimizing L_c will be described, as well as the impact of these structures on the development of sensitive FIR receivers.

REFERENCES

1. H. R. Fetterman, B. J. Clifton, P. E. Tannenwald, and C. D. Parker, Appl. Phys. Lett. 24, 70 (1974).
2. H. R. Fetterman, B. J. Clifton, P. E. Tannenwald, C. D. Parker, and H. Penfield, IEEE Trans. Microwave Theory Tech. MTT-22, 1013 (1974).

3. M. McColl, W. A. Garber and M. F. Millea, Proc. IEEE 60, 1446, (1972).

4. M. McColl, to be published in IEEE Trans. Microwave Theory Tech. MTT-25, Jan. 1977.

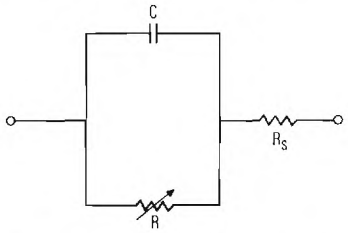

Fig. 1 Equivalent circuit of a Schottky barrier diode.

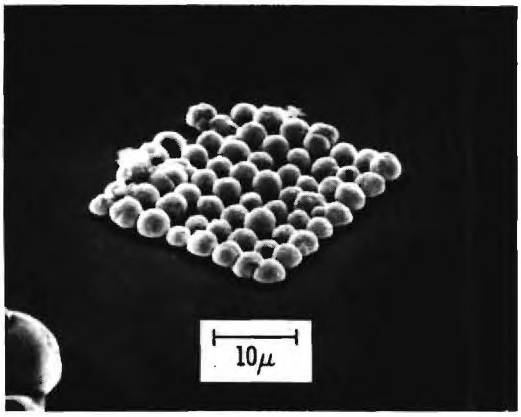

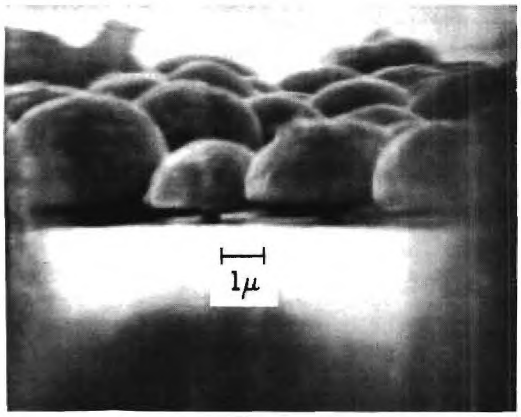

Fig. 3 SEM photographs of a plated 8 x 8 square multiple contact structure. The insulating layer normally present has been stripped away. The bottom photograph is a shot of the base of the structure.

Table 1

WAVELENGTH (μm)	RESPONSIVITY (V/W)	NEP ($W/Hz^{1/2}$) AT 5×10^3 Hz
70.5	0.04	2.5×10^{-6}
118.8	0.4	1.5×10^{-7}
496	10.0	1×10^{-8}
1222	10.0	1×10^{-8}

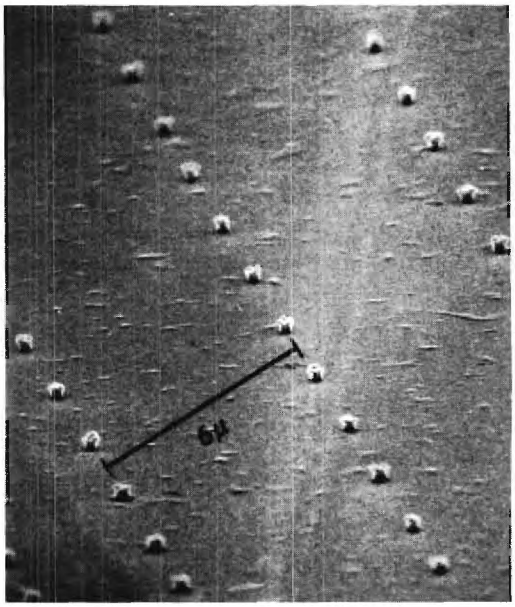

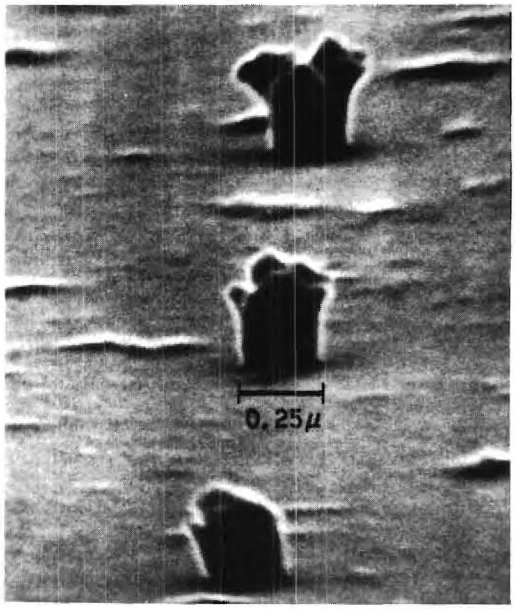

Fig. 2 SEM photographs of plated Schottky diodes. The insulating layer normally present has been stripped away. The photographs were taken at steep angles from normal incidence to show the dimensions of the diodes at their base. The bottom photo is a magnified shot of three of the diodes shown in the upper photo.

COMPOSITE BOLOMETERS FOR SUBMILLIMETER WAVELENGTHS

P. L. Richards, J. Clarke
G. I. Hoffer, N. S. Nishioka, D. P. Woody, N.-H. Yeh
Department of Physics, University of California
and
Molecular and Materials Research Division
Lawrence Berkeley Laboratory
Berkeley, California 94720

We have developed two types of ^{4}He temperature composite submillimeter wave bolometers which use metal film absorbing elements. Dark electrical noise-equivalent-powers of 2×10^{-15} W/$\sqrt{\text{Hz}}$ and 3×10^{-14} W/$\sqrt{\text{Hz}}$ have been measured in large area bolometers with superconducting and semiconducting thermometers, respectively. Experiments confirm the theoretically predicted frequency independent absorptivity of $\sim$ 0.5 in a single pass.

The conventional low temperature doped semiconducting bolometer uses a single element as throughput (mode) limiter, absorber, and thermometer. When operated without special coatings, these bolometers have dielectric reflectivities of 36 percent (for Ge at normal incidence). The absorption coefficient usually decreases with increasing wavelength so that the fraction of the incident power which is absorbed in a thin bolometer at 10 cm^{-1} can be very small.

Developers of submillimeter wave bolometers have begun to separate the functions of absorber and thermometer to obtain better performance. Systems used have included a coating of black paint on semiconducting bolometers, black paint on metal foil with a semiconducting thermometer, and a lossy dielectric (doped Si) absorber with a semiconducting thermometer. This last approach can be made resonant to absorb efficiently at a chosen frequency.

We have developed several composite bolometers based on an absorbing element made from a transparent dielectric layer coated on the back side with a thin metal film. This type of infrared absorber is well known from its use in the Golay cell, but had apparently not been applied to bolometers before it was used by (some of) the authors [1]. It provides an efficient absorbing surface which is reproducible, is easily tailored to a chosen application, and which can have extremely low heat capacity per unit area.

The dielectric layer should be thin and strong, have good thermal conductance, and a high Debye temperature (θ_D). We have used sapphire (θ_D = 600 K) sheets 30-135 μm thick, but diamond (θ_D = 2200 K) would be better. The design calculations for the absorber are straightforward. For frequency independent absorption, the surface resistance of the metal film should be $R_\square = 2Z_b/(n+1)$ where Z_o is the impedance of free space, and n is the index of refraction of the substrate. The predicted absorption of $\simeq$ 50 percent in a single pass through a sapphire substrate coated with a 200 Ω/□ Bi film has been experimentally verified by transmittance measurements and (less precisely) by direct optical calibration of a working submillimeter bolometer. If metal films with different resistances are used, the absorption spectrum contains Fabry-Perot resonances. These can give $\sim$ 90 percent absorption over a band whose width and center frequency can be varied by selecting the appropriate thickness of film and substrate.

Because of the extremely low heat capacity per unit area available from this technique, the bolometer designer can find himself in the limit in which the electrical NEP of the (dark) bolometer is relatively independent of the bolometer area. In this case, the figure of merit $D^* = \sqrt{\text{Area}}/\text{NEP}$ must be used with caution.

To obtain high sensitivity in practice it is critical to control the background radiation which reaches the bolometer. When the heat capacity of a bolometer is independent of its area, there can be advantages in the use of an external structure to limit the modes (throughput) which enter the system to those which contain signal information, and to illuminate the bolometer with radiation whose angular spread is independently adjusted to obtain high absorption efficiency.

We have used, for example, a primary concentrating element, a cooled aperture stop and a collimating element. This could be done with image forming components such as lenses or mirrors, but we have found it convenient to use two conical metal Winston [2] light concentrators, back-to-back. The partly collimated portion of the beam which follows the mode limiting structure can be a convenient place to install cold spectrometers [3], or transmission filters. Scattering or diffraction from these elements and from any reflecting surfaces placed behind the bolometer cannot affect the field of view of this system. Since the elements we use for spectral definition often require well collimated radiation, we generally reconcentrate the light onto the bolometer. The solid angle at which the bolometer is fed is chosen by considering the dependence of the heat capacity of the bolometer on its area, and the angular dependence of its absorptivity. For most of our applications, this is not a difficult optimization, since the absorption in the broad band sapphire-Bi system described above is essentially independent of angle out to $\sim$ 60 degrees from normal incidence. Our use of the Winston concentrator is different from one which has been proposed for bolometers whose heat capacity is proportional to their area [4].

The design of a bolometer intended for de-

tecting small signals depends critically on the background power P_B which will be incident on it. Once this background power is known, the background fluctuation limit $NEP_B = \sqrt{2kTP_B}$ of an ideal detector can be computed. Two requirements set lower limits to the value of the thermal conductance G between the bolometer element and the heat sink: The temperature rise of the element above the sink temperature, due to Joule heating and P_B, must be acceptably small. Also, the system requirements for response speed, and the noise power spectrum of the bolometer set limits on the thermal relaxation time $\tau = C/G$. The heat capacity C is often a limiting factor in this optimization. Once G is selected, the thermal fluctuation noise $NEP_{TF} = \sqrt{4kT^2GB}$ further limits the best performance available from a bolometer with given C, P_B, and system speed requirement. Since C is a sensitive function of operating temperature, the detailed optimization is quite complicated. We have found digital computer calculations to be helpful.

We have developed two types of composite bolometer which use the metal film absorber, but different thermometers. One type which we use in applications with moderate values of P_B is similar to that first constructed by the Caltech group [5]. It uses a small Ge thermometer glued to the sapphire substrate. We support the substrate with a cradle of 15 μm nylon threads, and make electrical and thermal contacts to it with metal wires (Cu or brass) soldered with In to the Ge thermometer element. This bolometer is easily made in laboratories where conventional Ge bolometer technology is available, and uses a conventional FET amplifier. Properties of a typical bolometer are shown in Table I.

Parameter	Semiconducting Bolometer	Superconducting Bolometer
Area (cm^2)	0.16	0.08
Time constant (ms)	25	50
Thermal conductance G (W/K)	1×10^{-7}	3.4×10^{-8}
Heat capacity C (J/K)	2.5×10^{-9}	1.7×10^{-9}
Dark electrical NEP ($W/\sqrt{Hz}$)	3×10^{-14}	2×10^{-15}
Specific Detectivity D* (cm $W/\sqrt{Hz}$)	1.3×10^{13}	1.4×10^{14}

Table I. Properties of ^{4}He temperature composite bolometers with semiconducting and superconducting thermometers.

The dominant source of noise is current dependent noise in the Ge thermometer. This troublesome type of noise has a 1/f power spectrum and is present in all semiconducting bolometers which we have made or purchased. It is not changed when the thermometer is attached to the bolometer substrate. This noise can arise from the soldered contacts and may thus depend on the techniques of etching and soldering. Four terminal measurements have suggested that there is also a residual current dependent noise which arises from the bulk of our Ga:Ge thermometer material.

A second type of bolometer has been developed [6] for extremely low background applications in which bolometers with small G and small (dark) NEP can be used. These use an Al film operated on its superconducting transition edge as a very low heat capacity thermometer. This superconducting transition-edge bolometer has comparable sensitivity to the superconductor-normal metal-superconductor bolometer previously reported [1], but is easier to fabricate and use. Electrical and thermal contact is made through superconducting In films evaporated on the 15 μm nylon threads which provide the mechanical support. The bolometer is AC biased at 50 KHz and uses a cooled resonant step-up transformer in front of the room temperature FET amplifier. The rectified output is fed back to the bolometer mount to stabilize the operating temperature at the ∿ 1.4 K transition temperature of the Al film. One unusual feature of this system is that 1/f noise becomes important only at frequencies well below 1 Hz. Properties of a typical bolometer are given in Table I. Thermal fluctuation noise contributed most of the noise in this bolometer.

The measured bolometer properties given in Table I were obtained using 135 μm thick sapphire substrates. Significant improvement is expected when bolometers are constructed using the 30 μm thick substrates which have recently become available to us.

Work supported in part by the USERDA.

References

1. Clarke, J., Hoffer, G. I., and Richards, P. L., Rev. Phys. Appl. 9, 69 (1974).

2. Winston, R., J. Opt. Soc. Am. 60, 245 (1970).

3. Woody, D. P., Mather, J. C., Nishioka, N. S., and Richards, P. L., Phys. Rev. Lett. 34, 1036 (1975).

4. Harper, D. A., Hildebrand, R. H., Stiening, R., and Winston, R., Appl. Opt. 15, 53 (1976).

5. Werner, M. W., Elias, J. H., Gezari, D. Y., Hauser, M. G., and Westbrook, W. E., Astrophys. J. 199, 1185 (1975).

6. Clarke, J., Hoffer, G. I., Richards, P. L., and Yeh, N.-H., A superconducting transition edge bolometer. "Low Temperature Physics - LT14", Krusius, M., and Vuorio, M., Eds. (American Elsevier, New York, 1975), Vol. 4, p. 226; (and to be published).

A THEORETICAL COMPARISON OF DC- AND MICROWAVE-BIASED EXTRINSIC GaAs PHOTOCONDUCTORS

J. N. Crouch, Jr.
E-Systems, Inc.
Greenville, Texas 75401

Introduction

High resistivity extrinsic gallium arsenide photoconductors are well-known detectors for the 100-400 micron region. Such detectors are usually operated in a dc series circuit with a matching load resistor [1-3]. Feedback amplifier techniques are sometimes used to reduce the total capacitance, thus increasing the electrical bandwidth [4]. In general, such devices have reduced sensitivity when operated with wide electrical bandwidths.

In an effort to provide a sensitive yet wide electrical bandwidth detector, microwave-biased GaAs photoconductors are being investigated [5]. Here the photoconductor is placed in the high electric field region of a microwave cavity. This results in a large gain-bandwidth product device [6] which is capacitively-coupled to its bias field.

In this paper, the theoretical performance of dc- and microwave-biased GaAs photoconductors are compared under a variety of conditions. The primary variables are the electrical bandwidth (1 KHz to 10 MHz) and the background photon irradiance (1E8 to 1E16* ph/sec. cm^2). Experimental results taken from the literature are also compared to the theoretical performance.

Analysis Procedure

The high resistivity GaAs photoconductor is assumed to be 0.3 cm X 0.3 cm X 250 microns thick. The donor concentration is 2E14 cm^{-3}, and the residual acceptor concentration is 1E14 cm^{-3}. The photoconductor is operated at 4.2°K and is assumed to have an 18 percent quantum efficiency. Improvements to the quantum efficiency due to integrating chambers are not included. Semiconductor parameters are those of sample #2 in Reference [2], and the peak wavelength is 282 microns. Furthermore, a 4 nsec recombination lifetime is assumed, and the photoconductor is operated with an applied electric field of 5 V/cm.

The performance of the GaAs photoconductor, regardless of the bias frequency, is calculated in terms of the D* (cm $Hz^{\frac{1}{2}}$/W) figure of merit. Two D* terms are calculated, each the result of a particular noise source. The two noise sources are the background noise and the Johnson noise due to the appropriate load resistor/photoconductor resistance combination. The individual D* values are combined by recognizing that the noise sources are uncorrelated.

The dc-biased GaAs photoconductor is assumed to be operated in a series circuit with a variable load resistor and a low-capacitance feedback amplifier. The load resistor and the amplifier are also cooled to 4.2°K. The load resistor is determined by the required electrical bandwidth and the assumed amplifier input capacitance of 2 picofarads [4]. For example, an electrical bandwidth of 1 MHz corresponds to a maximum load resistance of 175 KΩ.

The microwave-biased GaAs photoconductor is assumed to be operated in a 10 GHz microwave cavity having a characteristic impedance of 50 ohms. The microwave receiver used to process the signal has an input impedance of 50 ohms. The loaded cavity quality factor is allowed to be a variable which is set by the required electrical bandwidth. For example, an electrical bandwidth of 1 MHz corresponds to a loaded cavity quality factor of 10,000 and an equivalent cavity resistance of 1 MΩ.

---

* 1E16 = 1 X 10^{16} This notation is used throughout the summary.

Summary and Conclusions

The theoretical performance of dc- and microwave-biased GaAs photoconductors at the extremes of the conditions considered herein is shown in Figure 1. Experimental values taken from the literature are also listed in Figure 1.

The dc-biased GaAs photoconductor is seen to be Johnson noise limited at low backgrounds and/or wide electrical bandwidths. The microwave-biased GaAs photoconductor is seen to be capable of near background noise limited performance under nearly all conditions considered.

References

1. G. E. Stillman, et. al., Appl. Phys. Ltrs., Vol. 13, 1 August 1968.
2. G. E. Stillman, et. al., Symposium on Submm. Waves, Polytechnic Institute of Brooklyn, 1970.
3. K. Shivanandan, et. al., Proc. SPIE, Vol. 67, 1975.
4. L. W. Kunz and J. M. J. Madey, First Int. Conf. on Submm. Waves, Atlanta, Georgia, 1974.
5. J. D. Crowley, et. al., IR Phys., Vol. 16, 1976.
6. J. N. Crouch, Jr., Int. Conf. on IR Phys., Zurich, Switzerland, 1975.

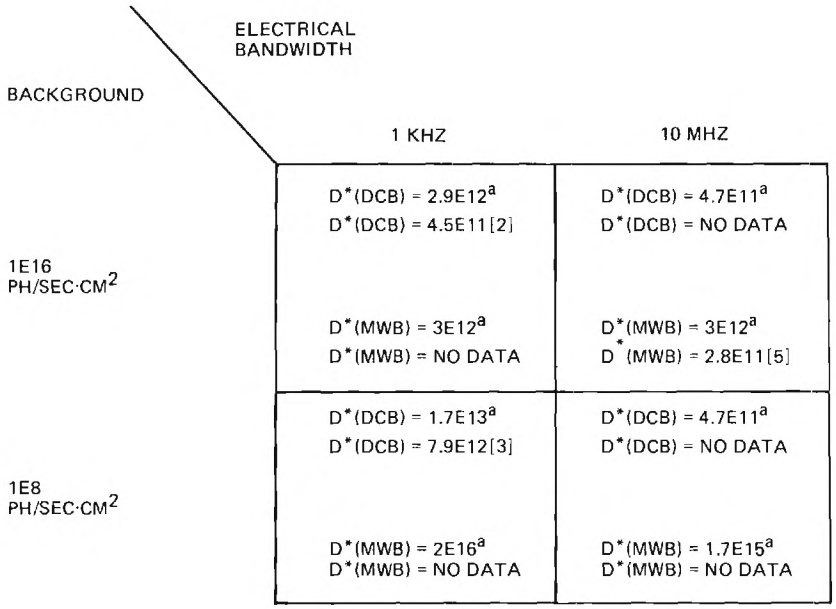

Figure 1. Theoretical/Experimental Performance of DC- and Microwave-Biased Extrinsic GaAs Photoconductors

LOW BACKGROUND OPERATION OF GALLIUM-DOPED GERMANIUM PHOTOCONDUCTORS

W. J. Moore
Naval Research Laboratory
Washington, D. C. 20375

Gallium-doped germanium detectors for use at wavelengths as long as 130 μm have been tested with low optical backgrounds characteristic of the space environment. These tests were performed in order to determine the limits on the performance of well-behaved submillimeter photoconductors for space use.

The measurements performed included: Current-voltage characteristic as a function of infrared background, signal responsivity to a cold blackbody source, and noise.

Two separate calibration systems were used. The simpler was designed to allow quick calibration without transferring liquid helium coolant into a laboratory container. It consists of three concentric stainless steel tubes carrying the detector, a blackbody, apertures, a filter, and a cooled MOSFET preamplifier. The entire assembly passes through the neck of a standard helium storage vessel. Calibration is accomplished by determining the detector conductance and noise as a function of blackbody radiance as the blackbody temperature is varied from room temperature to about 50K. This calibration does not require a chopper.

The second, more accurate, calibration system consists of a liquid helium container with a cooled blackbody, tuning fork chopper, and apertures and a filter to limit the radiation falling on the detector. Experimental results acquired with these two systems give results which agree within a factor of approximately two.

These results were analyzed in order to determine the detector characteristics including: Noise equivalent power (NEP), responsivity, carrier mobility, and device temperature. Signal responsivity was calculated in two ways: (1) The total signal power in the 50 - 130 μm spectral range was used to determine the average sensitivity in that range and, (2) the integrated product of the blackbody and detector spectral curves was used to determine the peak sensitivity at 100 μm.

This analysis indicates that the best device measured was thermal generation-recombination (g-r) noise limited at the operating temperature, irrespective of the method of determining signal power. The detector characteristics required for consistency in all measurements are given for the best device tested in Table I.

TABLE I

Characteristics of a Ge:Ga detector with dimensions 1.6 x 1.8 x 6.6 mm operated at 3.0 V/cm. The hole lifetime is assumed to be 1.7×10^{-7} sec.

		Folded Spectrum	Power Inband
NEP	(watts $Hz^{-1/2}$)	1.8×10^{-15}	3.2×10^{-15}
η		1.0	0.56
R_V	(volts $watt^{-1}$)	5.5×10^{9}	3.2×10^{9}
R_I	(amps $watt^{-1}$)	3.4	2.0
R_G	(Ω^{-1} $watt^{-1}$)	1.9	1.1
μ	(cm^2 $volt^{-1}$ sec^{-1})	6.0×10^{4}	6.2×10^{4}
g		4.6×10^{-2}	4.8×10^{-2}
S_o	(cm^{-3} sec^{-1})	5.6×10^{12}	5.4×10^{12}
T	(Kelvins)	~ 4.7	~ 4.7

Submillimeter photoconductors possess several characteristics which are not commonly encountered in detectors for use at shorter wavelengths. These characteristics include: Low impact ionization breakdown electric field ($E < 3$ V cm^{-1}), low photoconductive gain ($g < 1/2$), g-r noise lower than the simple shot noise in a device carrying the same bids current, thermal g-r noise limited performance at temperatures near that of liquid helium, a markedly non-ohmic current-voltage characteristic even at low bias, a low optimum impurity concentration ($N_A \leq 2 \times 10^{14}$ cm^{-3}), and unique electrical contacting requirements. These characteristics and their effect on device performance and system design will be described.

The existence of high performance thermal g-r noise limited devices at 4.7K suggests that even more sensitive devices capable of detecting infrared signals of the order of a few times 10^{-16} watts should be possible with smaller detectors or a lower operating temperature.

STANNIC-OXIDE, A NEW F I R DETECTOR MATERIAL ?

M. v.Ortenberg, J.Link
University of Würzburg
D-8700 Würzburg, GFR

and

R. Helbig
University of Erlangen
D-8520 Erlangen, GFR

Abstract:

We report of the strong photo-conductivity response of doped stannic oxide single crystals for submillimeter radiation. As confirmed up to 120 kG the magnetic field dependence of the photo-conductivity response is negligible. This fact admits in a magneto-transmission experiment the stannic-oxide detector to be positioned directly behind the investigated sample in the presence of the external magnetic field. Design and operation of the detector system are discussed in detail.

Submillimeter-magneto spectroscopy is a fundamental tool in the investigation of the electronic properties of semiconductors. One of the most important experimental methods is the measurement of the relative transmission of submillimeter radiation of fixed frequency through a sample as function of the magnetic field intensity. A typical experimental arrangement is shown in fig.1 [1]. The light-pipe system leads the electromagnetic radiation to the sample. The transmitted part of the radiation is measured by the FIR detector system. Since all of the so far known detector systems are very sensitive to the presence of an external magnetic field,

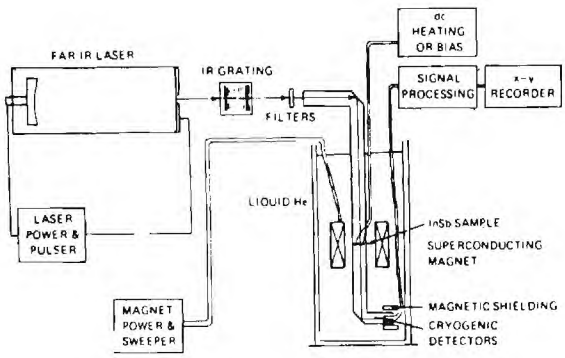

Figure 1. FIR-laser-magneto spectrometer with the detector system outside the magnetic field as used by ref.[1].

the detector has to be placed well outside the field and special shielding procedures have to ensure that the sensitivity is not affected by a magnetic field sweep. Because of the extended light-pipe system from sample to detector, including the reflecting mirror system, there is generally a considerable loss of intensity.

We are now proposing a cryogenic FIR-detector system which avoids these complications because its sensitivity is almost independent of any external magnetic field. The response is comparable to the sensitivity of a Ge-bolometer. As FIR sensitive bolometer-material we used doped stannic-oxide [2]. In fig.2 we have plotted by the solid line the temperature dependence of the reduced bolometer-resistance of a doped stannic-oxide detector.

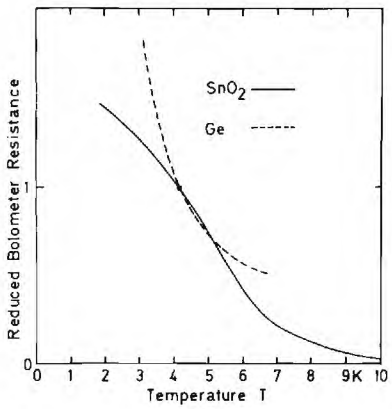

Figure 2. From the two curves of the temperature dependence of the reduced bolometer resistance for stannic-oxide and germanium can be seen that the differential change at 4.2 K is comparable for both materials.

There is a strong increase of the bolometer resistance with decreasing temperature. For comparison we have plotted in the same figure by the broken curve the temperature dependence of a Ge-bolometer crystal as used by Zwerdling et al. [3]. From the two different curves can be seen that the differential change of the reduced bolometer resistance at a temperature of 4.2 K is comparable for both materials.

In fig.3 we demonstrate the independence of the magnetic field for the stannic

oxide-bolometer signal using 118 μm and 337 μm wavelength radiation. The FIR-response is to very good approximation independent of the magnetic field intensity.

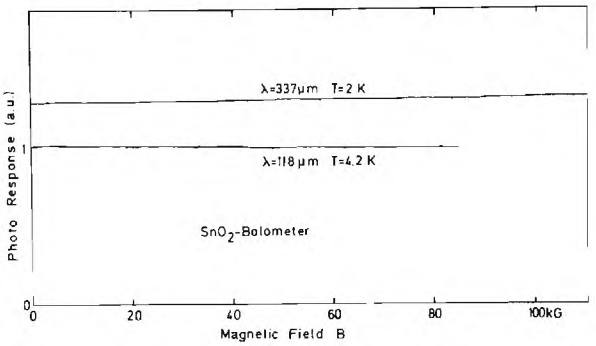

Figure 3. The straight lines of the photo response of the stannic-oxide detector versus magnetic field intensity exhibit the independence of the magnetic field.

To prove the practical applicability of the proposed detector system we have plotted in fig.4 the spectra of the relative transmission of 337 μm wavelength radiation through a pure n-type indiumantimonide sample as function of the magnetic field intensity. The transmission curves exhibit the cyclotron-resonance absorption of free electrons. The spectrum in the left part of this figure was recorded by use of the proposed stannic-oxide detector

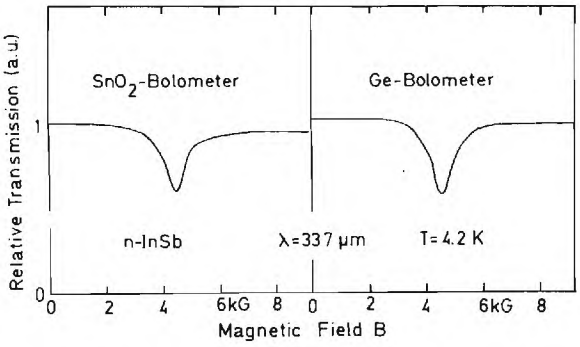

Figure 4. The cyclotron resonance of electrons in InSb as recorded by the stannic-oxide detector in the left part in comparison with the corresponding spectrum by the Ge-bolometer in the right part.

mounted directly below the indiumantimonide sample. The temperature of both sample and detector was 4.2 K. For comparison we have plotted in the right part the corresponding spectrum as recorded by use of a Ge-bolometer well outside the external magnetic field at a temperature of 4.2 K. For both detector systems the current has been chosen to provide maximum signal. It should be noticed that the crystal of the stannic-oxide detector has not yet been optimized because the system is still in the experimental stage of development, whereas the Ge-bolometer crystal is the product of a long experience.

References

[1] J.R. Apel, T.O. Poehler, C.R.Westgate, and R.I. Joseph, Phys.Rev. B4, 436 (1971)

[2] B. Thiel and R. Helbig, Journal of Crystal Growth 32, 259 (1976)

[3] S. Zwerdling, R.A. Smith, and J.P. Theriault, Infrared Physics 8, 271 (1968)

QUANTUM COUNTER FOR FAR-INFRARED RADIATION

H. Lengfellner and K.F. Renk
Institut für Angewandte Physik, Universität Regensburg
8400 Regensburg, W-Germany

Quantum counters converting infrared radiation to visible light have been proposed by Bloembergen [1] and were realized for the near infrared [2].

We report on a quantum counter converting far-infrared radiation to visible light. The principle is shown in Fig. 1. The FIR-radiation is absorbed by transitions between the excited states $\bar{E}$ and $2\bar{A}$ in optically pumped ruby. This leads to an increase of the population of level $2\bar{A}$ which is monitored by the R_2-fluorescence radiation (see Fig. 1). In a magnetic field parallel to the crystal c-axis the 29 cm^{-1} spaced $\bar{E}$ and $2\bar{A}$ levels split according to the g-values $g_{||}(\bar{E}) = 2.445$ [3] and $g_{||}(2\bar{A}) = 1.46$. For the 891 GHz-radiation of an HCN laser, detector response is expected at two magnetic fields B_1 and B_2 (see Fig. 1).

The experimental arrangement is shown in Fig. 2. The ruby crystal is pumped by a Hg-Xe-lamp. In order to avoid thermal occupation of the $2\bar{A}$ level the crystal is cooled with liquid Helium. The R_2-fluorescence radiation is separated from the strong R_1-line by several R_2-interference filters and registered with a photomultiplier. For FIR-source we use an HCN laser (10^{-2} Watt power entering the crystal). By chopping of the FIR, lock-in technique can be used.

In our measurements we obtain two detector signals at two magnetic fields B_1 and B_2. The signal at the field $B_1 \simeq 5$ kG is shown in Fig. 2. From the signal-halfwidth of 130 G we find for the bandwidth of the quantum counter (given by the linewidth of the transition $\bar{E} \simeq 2\bar{A}$) the value $\Delta\nu = 360$ MHz (0.012 cm^{-1}). From this value we obtain for the lifetime of the $2\bar{A}$ level $T_1 < 1/2\pi\Delta\nu = 4 \cdot 10^{-10}$ s indicating a strong relaxation to level $\bar{E}$. The same values for $\Delta\nu$ and T_1 are obtained from the detector signal at the field $B_2 \simeq 20$ kG. This signal has similar strength and line shape to the signal at the field B_1. From the value of T_1 we conclude a response time of less than 10^{-9} s for this detector.

We find a quantum efficiency (signal output power to FIR input power) of 10^{-6}. In our arrangement the minimum detectable FIR signal was in the order of 10^{-6} Watt. The detector sensitivity was limited by noise of the R_2-radiation which is generated by the pump process. It should be possible, however, to increase the sensitivity by several orders of magnitude by direct optical pumping of level $\bar{E}$ with a dye laser.

The peak-response of the detector can be tuned around 29 cm^{-1} with 1 cm^{-1}/Tesla.

[1] N. Bloembergen, Phys.Rev.Lett. 2, 84 (1959).

[2] M.R. Brown and W.A. Shand, Adv. Quantum Electron. 1, 2 (1970); L. Esterowitz, J. Schnitzler, J. Noonan and J. Bahler, Appl.Opt. 7, 2053 (1968); K.G. Sewell and W.B. Volz, Appl.Phys. Lett. 23, 104 (1973); M. Gundersen, Appl.Phys.Lett. 24, 591 (1974).

[3] S. Geschwind, R.J. Collins and A.L. Schawlow, Phys.Rev.Lett. 3, 545 (1959).

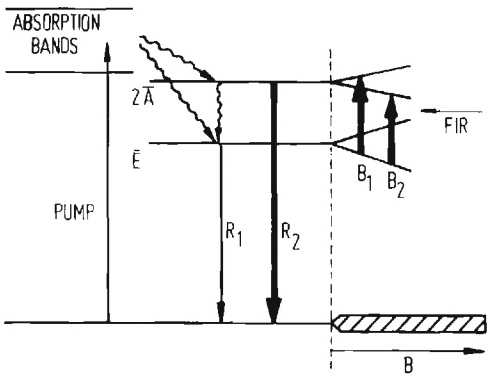

Figure 1. Principle of the ruby quantum counter (energy levels not to scale).

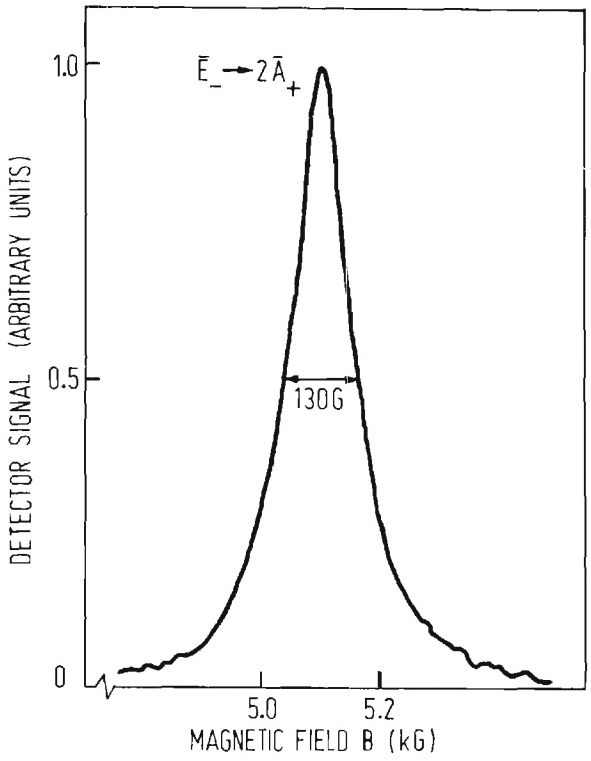

Figure 3. Quantum counter response for the 891 GHz radiation of an HCN laser as a function of the magnetic field in the region of $B_1 \approx 5$ kG.

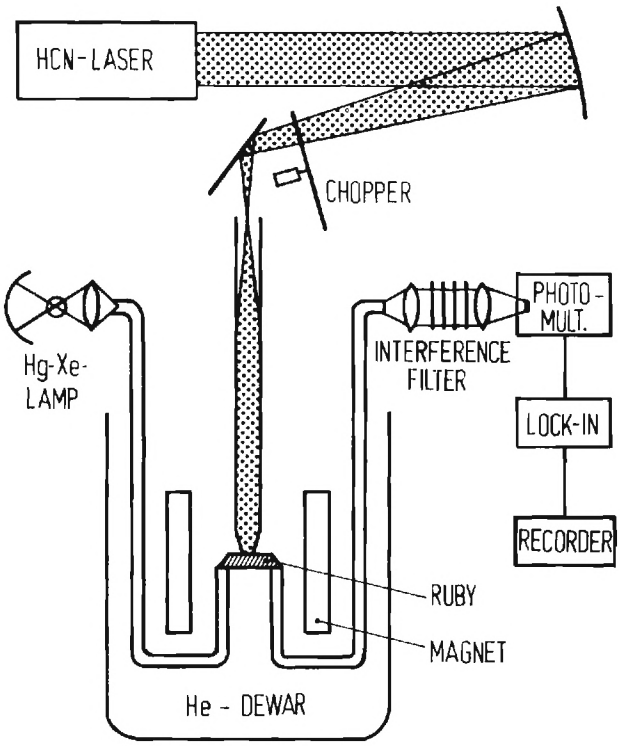

Figure 2. Experimental arrangement.

HIGH POWER OPTICALLY PUMPED SUBMILLIMETER LASER SYSTEMS*

Z. Drozdowicz, P. Woskoboinikow, K. Isobe†, D.R. Cohn,
R.J. Temkin, K.J. Button, and J. Waldman‡

Francis Bitter National Magnet Laboratory‡
Massachusetts Institute of Technology
Cambridge, Massachusetts 02139

ABSTRACT

The production of high power submillimeter radiation by 200 MW level CO_2 laser pumping of various gases such as CH_3F and D_2O has been studied. A number of cavity and amplifier configurations were used to produce narrow linewidth radiation. A 384.6 μm D_2O oscillator amplifier system was used to produce a 12.7 millijoule, 195 kW, 70 MHz wide single mode beam in 60-70 nsec pulses.

---

*Work supported by U.S. E.R.D.A.
†Visiting Scientist, Nippon Electric Company
‡Also University of Lowell
‡Supported by the National Science Foundation

Various means of producing high power submillimeter (SMM) radiation of narrow linewidth for tokamak diagnostics[1-3] are being investigated. CH_3F oscillator and oscillator-amplifier systems, pumped by 10 MW of 9.55 μm CO_2 radiation and operating at 496 μm were described previously[4,5]. They produced up to 9 kW of predominantly, but not fully, single mode radiation. A larger, 10 cm diameter system has been constructed using a 200 MW CO_2 oscillator-amplifier laser as a pump. A 1.25 m long SMM oscillator is pumped by the CO_2 beam in a zigzag fashion, and a 2.8 m long amplifier is pumped by the CO_2 beam parallel to the SMM radiation. This system produced about 130 kW peak power SMM output with a 70-80 MHz FWHM linewidth. A Fabry-Perot scan indicated that the narrow linewidth peaks were resting on a broader background of superradiant emission from the amplifier. The output of the oscillator consisted always of at least two longitudinal modes, the exact number depending on gas pressure and pump intensity.

We have recently investigated D_2O gas[6] pumped by 9.26 μm, CO_2 laser radiation and lasing on a 384.6 μm line and on a weaker 359.3 μm cascade line. A short, 36 cm cavity was used to achieve single longitudinal mode operation. This cavity and an 8 m long amplifier, both longitudinally pumped, produced a peak power of 195 kW on the 384.6 μm line in a 65 nsec FWHM pulse. The linewidth was about 70 MHz FWHM and the peaks were resting on a superradiant background, as shown in Fig. 1. Different delay times between the pumping of the oscillator and the amplifier were tried, none of which solved the problem of superradiance.

Because a wide superradiant background is unacceptable for plasma diagnostics, we have tried several novel systems in an attempt to eliminate superradiance. In one such system, a single mode beam from the 36 cm oscillator was injected, using a mesh beam splitter, into a 1.55 m long cavity which normally oscillated on 3 to 5 longitudinal modes. With proper tuning of the two cavities to the same frequency, one of the modes of the 1.55 m long cavity became strongly dominant but the others, though smaller, were always present, as shown in Fig. 2. This dominance was observed at injected beam intensities as small as a few watts/cm^2. Total power levels of 100 kW were achieved with this system.

A total power level of about 100 kW was also achieved when all of the CO_2 energy, about 10 J, normally split 20%-80% between the oscillator and the amplifier, was directed into the 36 cm oscillator alone. Only about 1/3 of the CO_2 laser energy was actually effective in pumping the oscillator due to the losses in transmission through two copper meshes. The CO_2 pump beam was slightly focused with a 10 m f.l. mirror. The oscillator consisted of 5 m focal length mirror and 40% reflecting mesh. A Fabry-Perot scan of its output revealed at least two transverse modes and signs of an extra longitudinal mode. It was possible to achieve a single longitudinal and transverse mode oscillation by replacing the curved mirror with a flat one and using unfocused CO_2 beam as a pump. The total power output of this flat-flat oscillator was 67 kW of which about 50 kW was in a single mode of the 384.6 μm transition and the rest of the power was due to the 359.3 μm cascade transition. Figure 3 shows the linewidth to be less than 25 MHz FWHM, since the instrumental linewidth of the Fabry-Perot contributes to the total linewidth. The linewidth is still less than 100 MHz at the 10 db point. The SMM pulses were 60 nsec FWHM long and the half angle of beam divergence was only 2 milliradians. This system appears to be particularly promising, in that it achieves a single longitudinal and transverse mode output with good efficiency and with a superradiant background at least two orders of magnitude weaker than the main mode. A larger aperture short cavity may be the best means of generating turly narrow linewidth, high power SMM radiation.

References

1. D.L. Jassby, D.R. Cohn, B. Lax and W. Halverson, Nucl. Fusion 14, 745 (1974).

2. D.E. Evans, and M.L. Yeoman, Phys. Rev. Lett. 33, 76 (1974).

3. D.R. Cohn, R.R. Parker, and D.L. Jassby, Nucl. Fusion 16, 1 (1976).

4. D.R. Cohn, T. Fuse, K.J. Button, B. Lax, and Z. Drozdowicz, Appl. Phys. Lett., 27, 280 (1975).

5. Z. Drozdowicz, R.J. Temkin, K.J. Button, and

D.R. Cohn, Appl. Phys. Lett. 28, 328 (1976).

6. P. Woskoboinikow, Z. Drozdowicz, K. Isobe, D.R. Cohn, and R.J. Temkin (submitted for publication).

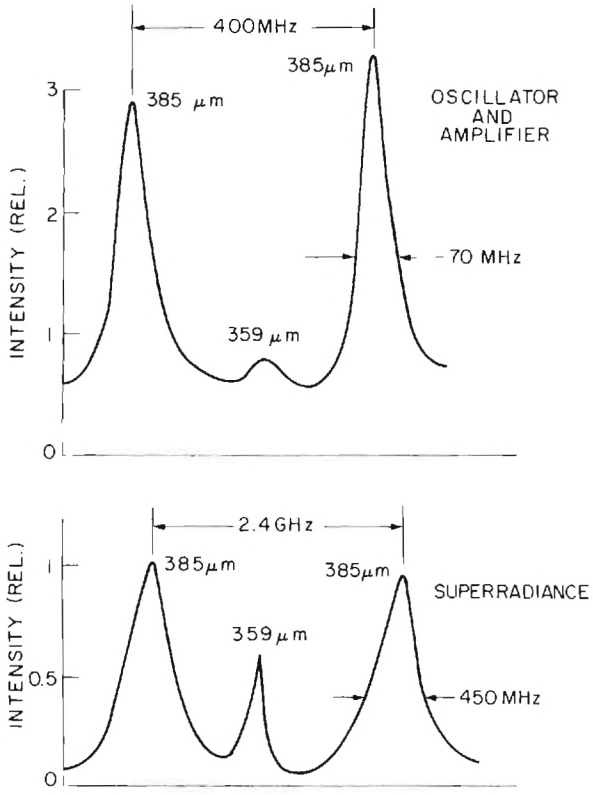

Figure 1. Spectral output of a D_2O oscillator-amplifier system.

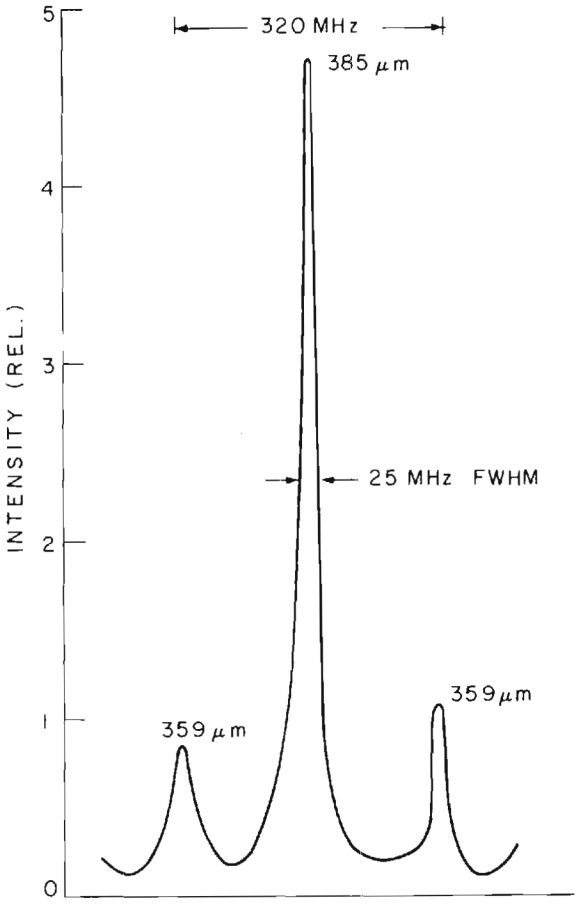

Figure 3. Spectral output of the 67 kW, 36 cm long D_2O cavity.

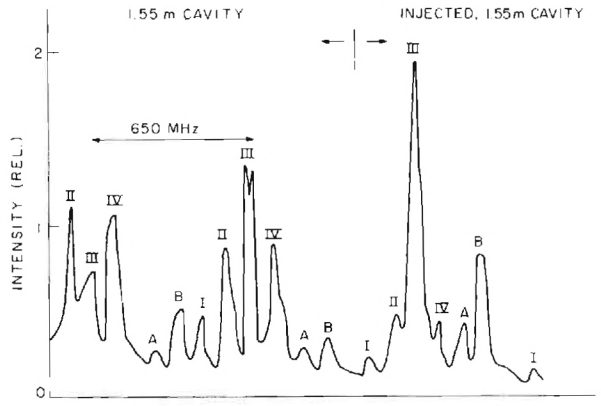

Figure 2. Effects of injection of single mode radiation on the operation of a multimode D_2O cavity. Roman numerals mark the modes of 384.6 μm line, capital letters mark the modes of 359.3 μm line.

WAVEGUIDE LASER AMPLIFIER OPERATION IN THE SUBMILLIMETER WAVELENGTH REGION*

T. A. Galantowicz
Department of Electrical Engineering
Union College
Schenectady, New York 12308

Abstract

An optically pumped, submillimeter wavelength, waveguide laser has been designed to operate as a regenerative amplifier. Small-signal gains of 9 dB have been measured for cw operation on the 372.8 μm transition of CH_3CN. System design and operating characteristics of the oscillator-amplifier configuration are described.

Introduction

The development of lasers operating on rotational transitions of optically pumped molecular systems [1] has resulted in convenient radiation sources covering the submillimeter wave region. The additional refinement of waveguide resonator design [2] enables efficient, low-threshold, continuous wave operation of milliwatt level devices in a compact package. An investigation of the amplifier mode of operation is a natural extension of the development of these lasers for application in increasing transmitted signal intensity and as a sensitive low-noise narrow-band receiver preamplifier. The experimental method described below is used to investigate the operation of a regenerative amplifier which is maintained below oscillation threshold both by limiting pump power and by varying output mirror-reflectivity. A small-signal gain of 9 dB has been obtained for the 372.8 μm transition in CH_3CN yielding a calculated gain coefficient of 0.8 m^{-1}.

Experimental Apparatus

Amplifier Design

The amplifier waveguide is an 89.1 cm long 13.3 mm diameter copper tube enclosed in a vacuum jacket. CO_2 pump radiation enters the vacuum jacket through a KCℓ Brewster window and is focused through a 2 mm hole in a nickel coated flat which forms one end mirror of the cavity. The opposite end of the cavity which acts as both input and output port for the submillimeter signal is composed of two parallel dielectric-coated mirrors spaced approximately 3 cm apart. These mirrors act as an interferometer to vary mirror reflectivity and are fabricated from multilayer coatings of Ge and ZnSe on crystal quartz substrates comparable to the hybrid mirror described in [3] but without the mesh grids. Each mirror has 98% reflectivity for the pump radiation and signal reflectivity near 60%. The interferometer spacing can be adjusted to cover a range of 7:1 in reflectivity. The amplifier can be adjusted to oscillate at the 372.8 μm transition in CH_3CN with pump power below five watts. For operation as an amplifier the reflectivity was set to its lowest value of 35%.

Amplifier-Oscillator Configuration

Amplifier measurements were made using the set-up shown in Fig. 1. The pump beam from a single source is used to power both the amplifier and oscillator. Pump intensity to the amplifier is controlled over a 2:1 ratio by varying the angular orientation of a ZnSe plate. The submillimeter wave signal from the oscillator is collimated by a polyethylene lens and incident on the amplifier signal input port. A wire mesh beamsplitter directs the amplifier output onto a Golay cell detector.

Results

Amplifier operation was obtained by adjusting the amplifier for oscillation, then reducing pump power by rotating the ZnSe plate to a point just below oscillation threshold. A signal gain of 9 dB could be obtained using CH_3CN gas at 40 mTorr pressure with a pump power of 3.5 watts on the P(20) line of the 10.6 μm band of a CO_2 laser. This pump power is measured internal to the cavity. Stable values of gain were difficult to maintain since the gain is sensitive to variations in pump power and frequency drift, gas pressure and mirror spacing. Knowing the output mirror reflectivity R = 35%, the net gain G = 9 dB and the cavity length ℓ, it is possible to estimate the gain coefficient α from [4]:

$$G = (1 - R)^2 e^{2\alpha\ell}/(1 - Re^{2\alpha\ell})^2$$

For the measured values we find $\alpha = 0.8\ m^{-1}$.

*This work supported by the National Aeronautics and Space Administration under Contract NGR 33-032-004.

References

1. T. Y. Chang and T. J. Bridges, Opt. Commum. 1, 423 (1970).
2. D. T. Hodges and T. S. Hartwick, Appl. Phys. Lett. 23, 252, 1973.
3. E. J. Danielewicz, T. K. Plant, and T. A. DeTemplé, Opt. Commun. 13, 366, 1975.
4. V. N. Smiley, Proc. IEEE. 51, 120, 1963.

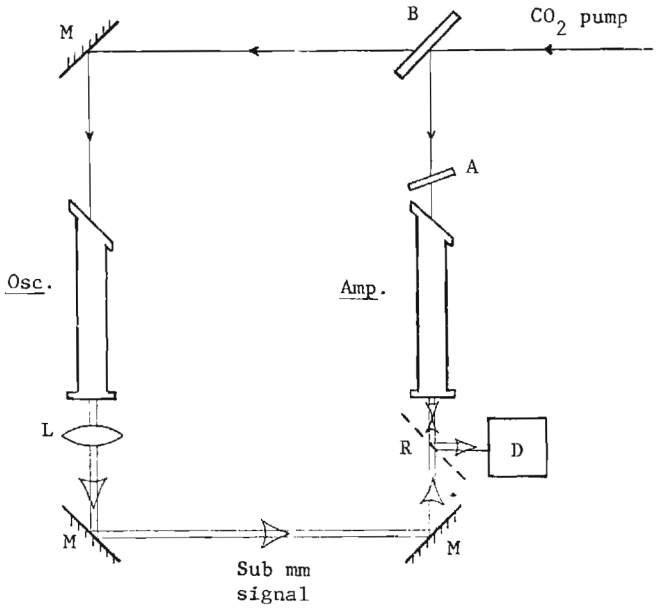

Fig. 1. Amplifier experimental arrangement.
Mirrors-M; Beamsplitter B; Lens-L;
Mesh reflector-R; plate attenuator-A;
Golay detector-D

DEVELOPMENT OF PULSED HIGH POWER LASERS IN THE 50-2000 μm BAND

A. Semet and N. C. Luhmann, Jr.
Electrical Sciences and Engineering Department
University of California
Los Angeles, California 90024

ABSTRACT. Performance and scaling of our high-power narrow-line pulsed 496μm laser is under investigation [1]. In addition, the performance of other high-power lasers in the 50-2000μm band is being studied.

High power levels (∿200 kW) at 496μm have now been obtained from several pulsed FIR laser configurations using CH_3F pumped by the P(20) 9.55μm line of CO_2 [1,2,3]. In particular, the UCLA system described previously has produced more than 150 kW with a bandwidth less than 40 MHz when pumped by an 8 J CO_2 laser [1]. The measured energy conversion efficiency of 0.1% (10% of theoretical maximum efficiency) has remained constant as the CO_2 pump has increased. Therefore, sufficiently high FIR power levels for Thomson scattering determination of Tokamak ion temperatures should be obtainable with a 100J CO_2 laser. Performance and scaling of our CH_3F oscillator-amplifier is presently being studied with a 20-50 J CO_2 pump.

Although the search for CW FIR lines has yielded hundreds of lines, surprisingly few have been found to operate at high power in the pulsed mode. This is unfortunate as a FIR lasing transition of increased efficiency over CH_3F would relax the CO_2 laser constraint necessary to obtain MW levels of narrow line FIR. Furthermore, a transition of slightly longer wavelength would eliminate the FIR receiver development problem as mixers with sufficiently low noise temperature for scattering purposes exist for $\lambda \gtrsim 570\mu m$ [4]. We have therefore designed an additional oscillator-amplifier to test promising gases with both parallel and perpendicular lasing transitions (relative to the pump polarization). The system is depicted schematically in Fig. 1. The output of a grating tuned CO_2 TEA laser enters the FIR vacuum envelope through a NaCl window. The 1m long FIR cavity consists of a dielectric waveguide (32 mm i.d. glass tubing) and Nickel mesh mirrors. The FIR oscillator output exits through a TPX window and is reflected from an additional mesh mirror into the FIR amplifier tube.

Table 1 lists the more promising gases which we have investigated in the oscillator section of our system together with the CO_2 pump line, expected FIR wavelength, pressure at maximum FIR output, maximum pyroelectric detector signal, FIR cavity mirrors used, and finally, the super-radiant energy (no output mirror) and CO_2 pump energy absorption at the pressure for maximum FIR oscillator output. The second number in the column on mirror mesh constants refers to the oscillator output mirror. The CO_2 pump energy within the FIR cavity was held constant at ∿0.5 J for all cases listed in Table 1. For purposes of comparison, a 600 mV pyroelectric detector signal from CH_3F at 496μm corresponds to a 10 kW pulse of ∿100 nsec duration. The expected FIR laser wavelengths listed in Table 1 are taken from the tabulation by Yamanaka [5]. Our present work is concerned with the study of the amplification properties of the above mentioned gases including pure $C^{13}H_3F$ at 1.22 mm in this system.

References

*Work supported in part by NSF Grant (ENG-75-14452) and in part by US ERDA Contract E(11-1)Gen.10 P.A. 26.

[1] A. Semet and N. C. Luhmann, Jr., Appl. Phys. Lett. 28, 659 (1976).
[2] D. Cohn, private communication.
[3] D. E. Evans, L. E. Sharp, W. A. Peebles and G. Taylor, to be published.
[4] N. Erickson, private communication.
[5] M. Yamanaka, Rev. of Laser Engin. (Japan) 3, 256 (1976).

TABLE I

PULSED FIR OSCILLATOR RESULTS

Molecule	CO_2 Pump (μm)	FIR λ (μm)	Mirror Mesh Constants (μm)	Oscillator Signal (mV)	Pressure (Torr)	Superradiant Signal (mV)	Pump Absorption (%)
CH_3F	P(20), 9.6	496	50.8,169	600	2.5	170	90
			50.8,317	300	2.5		
	R(32), 10.2	193	50.8,169	400	6	200	80
	P(32), 9.3	1222 from nat. ab. of $C^{13}H_3F$, lasing not observed				-----	very weak
D_2O	R(22), 9.3	385	50.8,169	1100	3.5	48	86
			12.5,50.8	100	5		
	P(32), 9.7	66	12.5,50.8	4000	4	150	37
	R(12), 9.3	94-114	12.5,50.8	6	3	-----	41
			12.5,100	10	4		
HCOOH	R(22), 9.2	414	50.8,100	5	1		
	R(20), 9.2	428	50.8,100	150	2		
			50.8,317	40	2		
		745?		-----			
	R(18), 9.2	400	50.8,100	30	1.5		
	R(16), 9.2	388	50.8,100	.1	.5		
	R(24), 9.3	534	50.8,100	2	.5		
	R(26), 9.3	670	50.8,100	-----			
	R(28), 9.3	512	50.8,100	100	1.5		
NH_3	P(32), 10.7	151	50.8,169	150	7	25	∿100
CH_3OH	P(36), 9.7	118	50.8,169	1	2		
CH_3I	P(32), 10.7	1253	50.8,169	.75	2		
	P(18), 10.6	447	50.8,169	8	5		
	P(34), 9.6	508	50.8,169	.3	5		
	P(38), 10.8	1063	50.8,169	-----			
CH_3Br	R(20), 10.2	661	50.8,169	.4	2		
	P(38), 10.7	545	50.8,169	.3	1		
	R(14), 10.4	749	50.8,169	.4	2.5		
	R(4), 10.4	1310	50.8,169	-----			
CH_3Cl	P(26), 9.6	1887	50.8,169	1	5		
			50.8,317	-----			
CH_3CN	P(20), 10.6	373	50.8,169	12	2.5		
	P(6), 9.4	494	50.8,169	.4	.15		
CH_3CCH	P(14), 10.5	648	100,none		4	-----	20
$C_2H_2F_2$	P(22), 10.6	890	50.8,169	1.5	1.5		
			50.8,100	2	1.5		
			50.8,317	-----			
	P(24), 10.6	568	50.8,169	.3	1.4		
	P(14), 10.5	554	50.8,169	.2	.5		
$C_2H_4F_2$	P(20), 10.6	458-533	50.8,169	-----			
CH_3OCH_3	P(20), 10.6	375	50.8,169	.2	.8		
	P(12), 10.5	495	50.8,169	2	2		
	P(34), 10.7	492	50.8,169	-----			

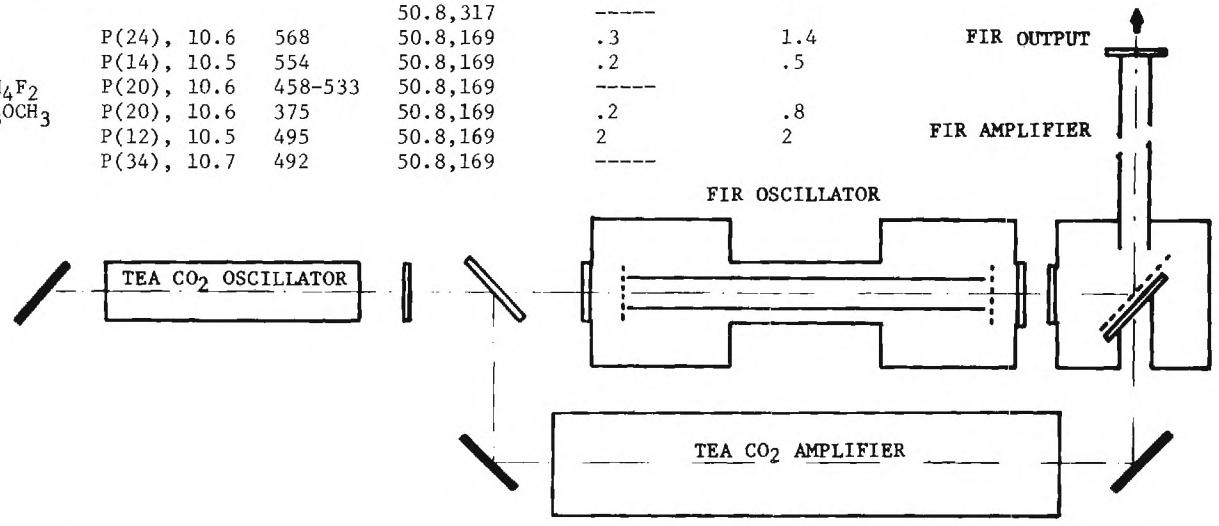

Figure 1. FIR oscillator-amplifier system which can be used for any FIR relative polarization.

DESIGN OF A HIGH POWER SUBMILLIMETER OSCILLATOR-AMPLIFIER SYSTEM

D. P. Hutchinson and K. L. Vander Sluis
Oak Ridge National Laboratory*
Oak Ridge, Tennessee 37830

A submillimeter laser source for an ion-temperature diagnostic of a thermonuclear plasma will require approximately a one megawatt narrow-linewidth pulse with a duration of 150-300 nsec [1]. An oscillator-amplifier system optically pumped by a CO_2 TEA laser system of the type developed by Chang and Bridges is being constructed for this purpose [2]. To meet these requirements a wavelength insensitive submillimeter oscillator, based on an unstable resonator cavity design, is being developed to drive a large volume submillimeter amplifier. The oscillator will be optically pumped by a 15 joule TEA CO_2 laser and the amplifier is to be pumped by a 150 joule TEA CO_2 laser. Presently, the oscillator characteristics are being determined by using the 496 μm CH_3F line and the 447 CH_3I line.

The basic requirements for the oscillator call for a large volume to provide sufficient absorption of CO_2 energy at the low operating pressures needed to achieve long pulse duration and a configuration to discriminate against high-order tranverse modes. The unstable resonator cavity offers a unique solution to these simultaneous requirements [3]. The oscillator design chosen for our application is a positive-branch resonator, based on the work by Krupke and Sooy [4]. The cavity is formed by a 15 cm diameter 15 m radius concave mirror and a 10.6 m radius convex 10 cm diameter mirror separated by an adjustable length set at 234 cm for our initial experiments. The mirrors are Pyrex with a 5000 A gold coating. The 15 cm concave mirror has a 5.0 cm hole in the center to provide for injection of the CO_2 pump beam on the optical axis of the resonator. The 5 cm hole is filled with a 15 m radius concave anti-reflection coated germanium window. This window transmits the CO_2 pump beam while reflecting 40% of the submillimeter radiation striking it from inside the cavity. The combination Ge-gold coated 15 cm mirror has an effective reflectivity of approximately 95% for submillimeter radiation. The radiation is coupled out of the resonator in an annulus around the 10 cm mirror. This configuration yields an effective output coupling of 50% and, hence, an effective feedback of 50% for regeneration. This output coupling technique produces, in the far-field, a central Gaussian profile surrounded by a series of diffraction rings. The fraction of power in the central peak is equal to the fractional output coupling, which is 50% for our case.

The output of the oscillator will be directed through a TPX window into a large volume submillimeter amplifier. The input to the amplifier consists of a X-cut natural quartz disk 15 cm in diameter set at a 45° angle to the incident FIR beam. One side of the quartz has a 98% reflective dielectric coating for CO_2 radiation. The submillimeter beam passes through the quartz and the CO_2 150 joule pump beam reflects off the coated side so as to spatially combine the 10 cm diameter beams in the amplifier. This type of beam combiner has been developed by Cohn *et al.* at MIT [5]. In order to combine large volume and short amplifier length, a necessity to minimize superradiance, the combined FIR-CO_2 beam is then expanded by a coaxial "Cassegrainian" type set of gold-coated aluminum parabolic mirrors to a diameter of 54 cm. The beams are compressed by an identical set of mirrors at the opposite end of the 100 cm long amplifier and the amplified FIR beam exits through a hole in the final 59 cm mirror and a TPX vacuum window. The volume of the amplifier is approximately 230 liters, which should be sufficient to absorb the entire 150 joule pump beam. The amplifier is symmetrical about the central plane between the beam expanders and may be extended by the insertion of an additional length of pipe to provide additional volume if necessary.

References

*Operated by Union Carbide Corporation for the U.S. Energy Research and Development Administration.

[1] Oak Ridge National Laboratory Report ORNL-TM-5071.

[2] T. Y. Chang and T. J. Bridges, "Laser action at 452, 496, and 541 μm in optically pumped CH_3F," *Optics Communications*, vol. 1, no. 9, p. 423, April 1970.

[3] A. E. Siegman and R. Arrathoon, "Modes in unstable optical resonators and lens waveguides," *J. Quantum Electronics*, vol. QE-3, no. 4, p. 156, April 1967.

[4] W. F. Krupke and W. R. Sooy, "Properties of an unstable confocal resonator CO_2 laser system," *J. Quantum Electronics*, vol. QE-5, no. 12, p. 575, Dec. 1969.

[5] Daniel Cohn, private communication.

AN OPTICAL PREAMPLIFIER FOR FIR RECEIVER SYSTEMS*

F. L. Merat, P. C. Claspy, and Yoh-Han Pao
Department of Electrical Engineering and Applied Physics
Case Western Reserve University
Cleveland, Ohio 44106

Abstract

An optically pumped amplifier suitable for use in a far infrared receiver system has been constructed and evaluated. Relevant parameters, including gain and noise characteristics, have been studied and are reported.

Introduction

The development of carbon-dioxide laser pumped FIR lasers has represented a major breakthrough in submillimeter wave sources [1]. Unfortunately, no corresponding major breakthroughs have occurred in the area of submillimeter wave detectors--current detectors operating at room temperature are characterized by slow response times and/or poor sensitivity. Cryogenically cooled detectors are sensitive and fast but have the inconveniences accompanying all such cooled detectors, and, in the case of liquid helium cooling, the high cost of the coolant. A reasonable alternative to cryogenically cooled detectors would be to extend the gain-bandwidth product of a suitably fast room temperature detector such as a pyroelectric detector. This paper describes the performance of a carbon-dioxide laser pumped optical preamplifier for use with a corresponding carbon-dioxide laser pumped FIR laser.

Experimental

The preamplifier is a gold-plated lightguide terminated at each end with crystal quartz windows. A hold in the side of the lightguide permits transverse pumping of a gas such as methanol with a carbon-dioxide laser. The lightguide itself is a standard Advanced Kinetics product 12.5 mm in diameter and 57.5 cm long. The guide diameter is reduced to 10 mm diameter at each end by a highly polished brass taper 7 mm long (see Figure 1). This taper is terminated in a 1 mm thick piece of crystal quartz to transmit only FIR radiation. The carbon-dioxide pump laser radiation is admitted through a zinc-selenide window at a shallow angle relative to the longitudinal axis of the preamplifier (see Figure 1).

The FIR laser source is a waveguide design similar to that of Hodges and Hartwick [2]. The pump laser beam is admitted through a 1.2 mm diameter hole and the FIR output is taken through a 2 mm diameter hole. Both mirrors are flat and FIR plunger fashion into a 70 cm section of Advanced Kinetics 25.4 mm diameter lightguide.

A shallow pumping angle for the preamplifier was chosen in preference to the conventional longitudinal pumping of FIR lasers to maintain a large clear apeture through the preamplifier and to keep the design as simple as possible. Ideally, one would like total absorption of the pump radiation by the preamplifier gas; in practice, much of the radiation is absorbed by the walls. This is particularly true in the case of transverse pumping. For the pump radiation entering the preamplifier at angles greater than 30 degrees most of the pump radiation is absorbed by the walls within a few centimeters of the entrance apeture. A pumping angle of 18 degrees has been used in these experiments both for experimental convenience and to reduce wall losses over larger angles.

Results

Preliminary results have been obtained for a preamplifier using CH_3OH pumped by a CO_2 laser operating at 9.6948 microns. Preamplifier gains of 50-500% have been measured, where preamplifier gain is defined as the ratio of the FIR signal passed through the preamplifier with optical pumping of the preamplifier gas to that without optical pumping. These results are consistent with the high gain of optically pumped FIR lasers [3].

References

1. For a review see: T. Y. Chang, "Optically Pumped Submillimeter Wave Sources", IEEE Transactions on Microwave Theory and Techniques, Vol. MTT-20, No. 12, December 1974, pp. 983-988.

2. D. T. Hodges and T. S. Hartwick, "FIR Waveguide Laser Performance in the 40 μm-1 mm Spectral Region", in Proceedings International Conference on Submillimeter Waves and Their Applications (Atlanta, Ga.), June 5-7, 1974, pp. 26-27.

3. T. Y. Chang and T. J. Bridges, "Laser Action at 452, 496 and 541 μm in Optically Pumped CH_3F", Optics Communications, Vol. 1, No. 9, April 1970, pp. 423-426.

*This work has been supported in part by a grant from the National Aeronautics and Space Administration.

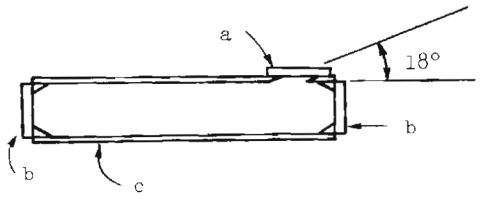

Figure 1. Preamplifier Configuration

a. zinc selenide window
b. 1 mm thick crystal quartz
c. lightguide (57.5 cm long, 12.5 mm diameter

QUANTUM MECHANICAL FEATURES OF OPTICALLY PUMPED FIR C.W. LASERS*

J.R.R. Leite**, D. Seligson, J.J. Mickey, M. Ducloy+, A. Sanchez and M.S. Feld§
Physics Department and Spectroscopy Laboratory
Massachusetts Institute of Technology
Cambridge, Massachusetts 02139

Generation of far infrared (FIR) laser radiation by means of optical pumping of molecules has received increasing attention over the past few years [1]. In the course of the development of FIR sources two important features have been largely neglected; (i) the assignment of the pump and FIR transitions; (ii) the detailed tuning behavior of the FIR emission. Knowledge of these two points is essential for a complete understanding of the optical pumping mechanism, and for assessing the full potential of various FIR laser sources and their extension to new spectral ranges. The assignment of CH_3OH transitions is presented in another talk. This communication discusses the frequency characteristics of the FIR emission.

Analysis of the optical pumping process is usually based on rate equations (RE) [2]. However, it is well known that two-quantum Raman-type processes, which are not accounted for in RE treatments, play an important role in three level systems of the type employed in FIR optical pumping [3]. For instance, these processes give rise to a directional anisotropy in the reemission of radiation. The way in which Raman-type processes manifest themselves depends on whether the transitions are homogeneously or inhomogeneously broadened. For these different cases, we will analyze the frequency dependence of the linear gain at the FIR 0-1 transition (frequency ω_1) when the excited level 0 is optically pumped via the 2→0 transition (ω_2) [$\omega_2>\omega_1$].

1. Fully Doppler-broadened systems

This case is now well understood [3]. For weak pump intensities, the gain curve is Lorentzian, narrower in forward emission ($\varepsilon=+1$) than in backward emission ($\varepsilon=-1$), and is centered at frequency $\omega_1 \times (1+\varepsilon\delta_2/\omega_2)$, where δ_2 is the frequency detuning of the pump.[2] The full widths at half maximum (FWHM) are respectively $\gamma(\pm)=\gamma_0+\gamma_1+\omega_1(\gamma_2+\gamma_0)/\omega_2$, where γ_j is the decay rate of level j [4]. In addition, the peak forward gain is greater than the backward gain, so that the "areas" under the two Lorentzians are equal. The forward-backward anisotropy increases with ω_1/ω_2. For large pump intensities the forward reemission line splits in two components because of the dynamical Stark splitting. The line splitting is given by $2\beta\,\omega_2^{-1}\sqrt{\omega_1(\omega_2-\omega_1)}$, where β is the Rabi nutation frequency on the 0-2 transition ($\beta=\mu E/\hbar$). The splitting in maximum for $\omega_1=\omega_2/2$.

2. Systems in which only the pump transition is Doppler-broadened

This is the case in which the Doppler effect at the FIR frequency is negligible compared to the pressure-broadened linewidth, but the pump transition is still Doppler-broadened. Then the single-quantum 2-0 transition and the double-quantum transition have the same Doppler shift, causing the forward-backward anisotropy to disappear. Furthermore, the gain curve is centered at the FIR molecular frequency. Only its overall amplitude depends on the detuning of the pump frequency. The lineshape of the gain curve is given by

$$g = \beta^2 (2\gamma_2 Q)^{-1} \times$$

$$\mathrm{Re}\left[\frac{\gamma_{12}+\gamma_{02}Q+\frac{\gamma_0}{2}(1-Q)+i\delta_1}{(\gamma_{01}+i\delta_1)(\gamma_{12}+\gamma_{02}Q+i\delta_1)+\beta^2/4}\right]$$

where γ_{ij} is the relaxation rate of the i-j coherence, δ_1 is the FIR frequency detuning and the saturation parameter is $Q=(1+\beta^2/\gamma_0\gamma_2)^{1/2}$. When phase-changing collisions are absent [$\gamma_{ij}=(\gamma_i+\gamma_j)/2$], the lineshape is a Lorentzian of width $\gamma_1+\gamma_0 Q$ (FWHM). The linewidth increases with increasing pump intensity, and, at high intensities, the gain saturates ($g\to 1$). The RE approximation corresponds to making γ_{12} infinitely large in Eq. (1), in order to cancel the 1-2 coherence (absence of Raman-type processes). Thus, for weak pump intensities RE gives the correct result, but not for an intense pump, where RE predicts a gain curve whose width does not power broaden (FWHM=$2\gamma_{01}$) and whose peak increases linearly with β. The correct behavior [Eq. (1)] is a direct consequence of the occurrence of two-quantum transitions. Notice also the absence of dynamical Stark splitting, which vanishes in the velocity integration.

3. Homogeneously-broadened systems

When the Doppler effect is negligible for both transitions the gain curve reverts to the well-known results observed in microwave-microwave and microwave-RF double resonance experiments. In particular, at high pump intensities the FIR line splits in two resonances, the splitting depending on the pump intensity and the detuning of the pump frequency [5].

4. Experimental observations

The experimental study of the FIR tuning behavior for different cases is under way. The sample is a methyl alcohol cell placed

inside a 1m waveguide cavity and optically pumped by a 10W c.w. CO_2 laser. Preliminary studies of c.w. FIR emission at λ= 120 μm [pump λ=9.7 μm, P(36) line], λ= 70 μm [P(34) pump] and other wavelengths are in progress. The emission frequency is tuned with a PZT mounted on one of the FIR cavity mirrors. At both 70 μm and 120 μm, for low (∿100 mTorrs) pressures (case 1), two narrow bands of FIR emission are observed when the CO_2 pump frequency is detuned from the CH_3OH center frequency. These correspond to forward and backward reemission components of the standing-wave FIR field, and are symmetrically located around the FIR transition frequency. Due to the small values of ω_1/ω_2 (0.08∿ 0.12), the forward-backward asymmetry is weak, and is most pronounced in Fig. 1c, where the backward signal has nearly fallen below the laser oscillation threshold. Cases (2) and (3) will be studied by going to higher pressures and longer FIR wavelengths (λ≈ 500 μm). Observation of transient FIR emission, obtained when the pump laser is suddenly turned on or off, is also under way, in order to check the theoretical predictions of a previously performed analysis [6].

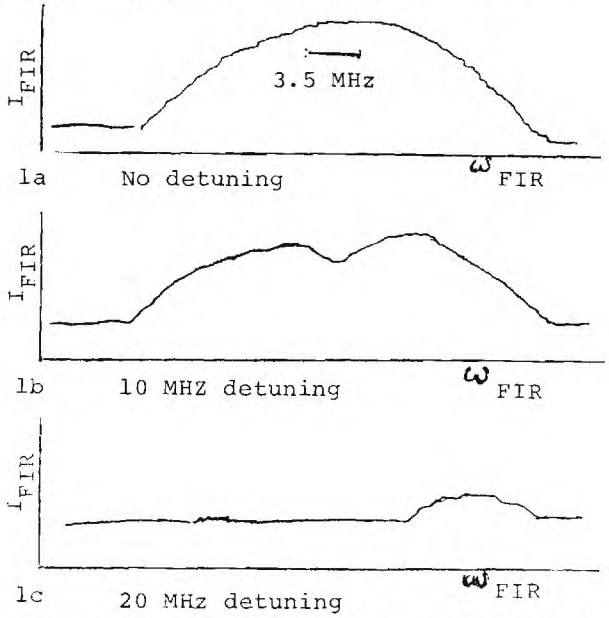

Figure 1 Observed features of FIR emission By optical pumping of CH_3OH with the 9.7μm P(34) line of a CO_2 laser (6 watts cw), we obtain lasing in the FIR at 70.6μm. The FIR emission lineshapes are given as the pump frequency is tuned away from the CH_3OH line center. Both pump and FIR transitions are Doppler broadened (see **1**. above). The difference in gain of the forward and backward signals is most clear in 1c, where the backward signal has nearly fallen below the laser oscillation threshold.

References

1. T.Y. Chang, IEEE Trans. Microwave Theory and Tech., MTT-22 (1974), 983.
2. e.g., J.R. Tucker, ibid, MTT-22 (1974), 1117.
3. For a review on three-level spectroscopy, see M.S. Feld in Fundamental and Applied Laser Physics, edited by M.S. Feld, A. Javan and N.A. Kurnit (Wiley, New York 1973), pp. 369-420.
4. For simplicity of this discussion, phase-changing collisions are not taken into account in this section.
5. S.H. Autler and C.H. Townes, Phys. Rev. 100 (1955), 703.
6. M. Ducloy and M.S. Feld, Journal de Physique-Lettres 37 (1976), L-173; M. Ducloy, J.R.R. Leite and M.S. Feld, Phys. Rev. A, to be published.

* Work supported by Army Research Office (Durham).

** Partially supported by Universidade Federal de Pernambuco and CNPq-Brazil.

+ Present address: Laboratoire de Physique des Lasers, Université Paris Nord, Av. J.B. Clément, 93430, Villetaneuse (France).

§ Alfred P. Sloan Fellow.

SATURATED ABSORPTION SPECTROSCOPY OF CH_3OH*

J.R.R. Leite**, A. Sanchez, M. Ducloy+ and M.S. Feld§
Physics Department and Spectroscopy Laboratory
Massachusetts Institute of Technology
Cambridge, Massachusetts 02139

Up to now methyl alcohol has been the most fertile molecule for generating far infrared laser radiation via CO_2 laser optical pumping [1]. Nevertheless, of the numerous CH_3OH submillimeter emission lines and their corresponding pump transitions, most of the spectroscopic assignments have yet to be made. Detailed knowledge of the quantum numbers, relaxation rates and dipole matrix elements is essential for assessing further potential of these lasers as sources and for new fundamental studies of the physics of three level systems.

In what follows we report some high resolution spectroscopic studies on two CH_3OH infrared transitions in near coincidence with the CO_2 P(34) and P(36) 9.7 μm lines. Their special interest lies in the fact that both can be pumped with a low power (∿3W) CW CO_2 laser to emit strong CW submillimeter radiation. In the experiments saturated absorption resonances (Lamb dips) were observed in a low pressure CH_3OH cell using a stable CO_2 laser, from which precise measurements of the pressure broadening coefficients, linear absorption coefficients and frequency detunings between the CO_2 and CH_3OH lines were obtained. In subsequent experiments a Stark field was applied, leading to partial assignment of the transitions.

The experimental set up used to observe the Lamb dips [2] is shown in Fig. 1. The CO_2 laser, with linearly polarized emission, was set at 100 mW power level to eliminate power broadening effects. A piezoelectric crystal, on which the laser mirror was mounted, permitted a 90 MHz tunability of each CO_2 line. An NaCl beam splitter was used to divide the laser output into two components, one intense (saturating beam) and one weak (probe beam), which were passed through the 1.5m CH_3OH sample cell in opposite directions. The Lamb dip occurs as a decrease in probe absorption as the laser is tuned across the CH_3OH line center. By measuring the frequency separation between the Lamb dip and the center of the CO_2 emission profile, the CH_3OH transition frequency could be obtained with a resolution much better than its 50 MHz Doppler width. For the P(34) CO_2 line, the methanol transition lies 38±5 MHz above the CO_2 center frequency. The transition overlapping the P(36) line lies 25±5 MHz above the corresponding CO_2 line center. The absence of Lamb dips for the P(32) and P(38) CO_2 lines indicates that the corresponding CH_3OH transitions are detuned by at least 45 MHz.

The linear absorption coefficient for the P(34) overlapping line is $\alpha=3.1\pm.5 m^{-1} Torr^{-1}$. By observing the linewidth of the Lamb dip with increasing pressure, the collision broadening coefficient was found to be $\gamma=18\pm4$ MHz/Torr (HWHM). The respective numbers for the P(36) overlapping line are $\alpha=1.6\pm.3\ m^{-1} Torr^{-1}$ and $\gamma=26\pm5$ MHz/Torr.

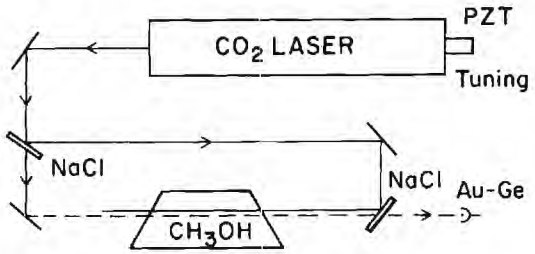

Figure 1. Experimental set up.

From early low-resolution studies [3] it could be established that the CO_2 9.7μm band overlaps the Q branch of the C-O parallel stretching mode of CH_3OH. However, the rotational quantum numbers for the various coincidences were unknown. Their identification was the subject of our Stark effect experiments. Applying a static electric field to the CH_3OH gas sample splits the magnetic (m) sublevels of the rotational manifold. Consequently, each Lamb dip will split into a series of dips, reflecting the character of the Stark effect (linear or quadratic) and the level degeneracy (J value). In our experiments P(34) and P(36) coincidences both exhibited linear Stark effect. The following discussion is valid only in this case. When the polarization of the saturating field is parallel to the Stark field and the probe field polarization is perpendicular to it, the Lamb dip splits into two multiplets, the strucutre of which are not resolved if $\Delta e-\Delta g$ is small compared to γ [$\Delta e(\Delta g)$ is the splitting between adjacent m-states in the excited (ground) levels]. The separation between the two components is then $\Delta=(\Delta e+\Delta g)/2$. This relation results from the fact that the saturating field is inducing $\Delta M=0$ transitions while the probe couples to the $\Delta m=\pm1$ transitions.

If, on the other hand, both probe and saturating beams are polarized along the Stark field, the Lamb dip splits into a series of 2J+1 components, separated by $\delta=|\Delta e-\Delta g|$. Figure 2 shows the Stark patterns obtained for the P(34) and P(36) coincidences. In these traces a 30 V/cm, 10 kHz modulation was added to the static (∿300 V/cm) Stark field, Es, and phase sensitive detection was used. In conse-

quence, the observed signal occurs as the derivative of the Lorentzian dips, and the central component is absent. The J value of the transition follows directly from the number of dips. From data like Fig. 2 taken at different values of Es and both polarization configurations we obtain for the P(34) coincidence: J=1, Δ=28±3MHz/(kV/cm), δ=3.3±.3MHz/(kV/cm). The corresponding values for the P(36) coincidence are J=7, Δ=25±3 MHz/(kV/cm) and δ=3.5±.3 MHz/(kV/cm).

Further work is under way to complete the assignments. Preliminary estimates for the transition dipole matrix element, using symmetric top partition functions, are $\sim$.03 Debye for both transitions. Definitive values will be obtained after the K± quantum numbers have been determined. As for the permanent dipole moments, we can conclude from δ/Δ that the vibrationally excited and ground state values differ by $\sim$10%.

Experiments are also in progress to assign the submillimeter emitting transitions and study their properties. These experiments employ a low pressure CH_3OH sample cell, saturated by the pump laser and probed by the submillimeter emission of an optically pumped CH_3OH laser. Both steady state and transient experiments are planned.

* Work supported by U.S. Army Research Office (Durham).

** Partially supported by Universidade Federal de Pernambuco and CNPq-Brazil.

+ Present address: Laboratoire de Physique des Lasers, Université Paris Nord, Av. J.B. Clément 93430 Villetaneuse (France).

§ Alfred P. Sloan Fellow.

Figure 2a. Lamb dip Stark splitting of $CO_2P(34)$-CH_3OH coincidence.

References

1. M. Rosenbluh, R.J. Temkin and K.J. Button, "Submillimeter Laser Wavelength Tables" to be published in Applied Optics, Nov. 1976.

2. See for example, P.E. Toschek in "Spectroscopie sans Largeur Doppler de Systèmes Moleculaires Simples" (Colloque No. 217-CNRS-Paris, 1974), pp. 13-27.

3. A Borden and E. F. Barker, J. of Chem. Phys. 6 553, 1938.

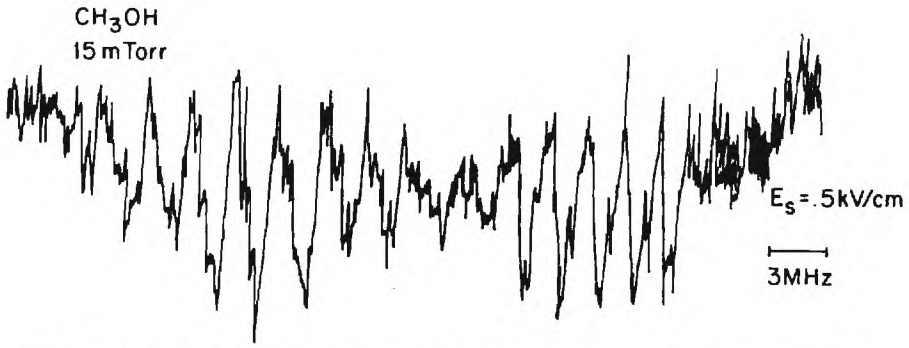

Figure 2b. Lamb dip Stark splitting of $CO_2P(36)$-CH_3OH coincidence.

MECHANISMS FOR COHERENT SCATTERING OF ELECTROMAGNETIC WAVES FROM RELATIVISTIC ELECTRON BEAMS

V. L. Granatstein
Naval Research Laboratory
Washington, D. C. 20375

I. Introduction

In 1968, Pantell et al. [1] proposed that strong submillimeter radiation could be produced by coherent scattering of a microwave signal from a counterstreaming relativistic electron beam. The merit of this proposal is clear since it involves the conversion of incident photons at a low frequency, ω_o, into an output of scattered photons at a high frequency, ω_s, via the Doppler effect. Thus, according to the Manley-Rowe relationship, the ratio of output wave energy to incident wave energy can be as large as $W_s/W_o = \omega_s/\omega_o$ and good device efficiency is possible. This may be contrasted to the case of optically pumped submillimeter lasers which convert high frequency photons into lower frequency photons and thus produce an output wave that is much weaker than the pump wave so that efficiency is inherently low.

II. Stimulated Scattering

Coherent scattering of an incident pump wave (ω_o, $\underset{\sim}{k}_o$) by a beam of electrons may be realized when the electrons are made to form into bunches along an axis parallel to $\underset{\sim}{k}_o$. Such an electron density modulation is generated by a beam instability in the presence of a strong pump wave.

Let us consider some features of this process in the reference frame where the electron streaming velocity is zero. In this reference frame, quantities will be primed as in Fig. 1.

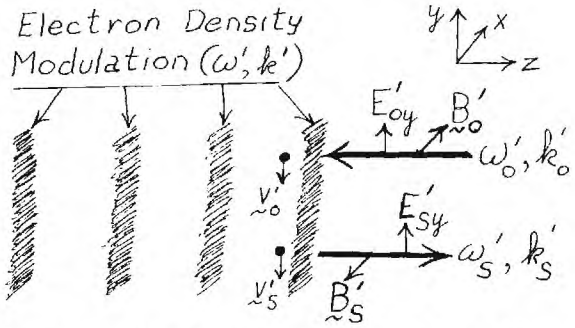

Figure 1. Stimulated scattering in beam frame.

The incident electromagnetic wave (ω_o', k_o') has a transverse electric field E_{oy}' which excites a transverse oscillation of the electrons with velocity $v_o' = -(e/m)E_{oy}'/\gamma'\omega_o'\hat{e}_y$, where

$$\gamma' = \left[1 - (v_o'/c)^2\right]^{-1/2}.$$

In the presence of an incipient scattered wave with magnetic field $B_s'\hat{e}_x$, an axial force, $ev_o'B_s'\hat{e}_z$, is exerted on the electrons. This type of coupling between the scattered electromagnetic wave and the incident wave thus produces a pondermotive force (radiation pressure force) which leads to a low frequency density modulation of the electrons (ω', k'). The pondermotive force is given by $\underset{\sim}{F} = -e(\underset{\sim}{v}_o' \times \underset{\sim}{B}_s' + \underset{\sim}{v}_s' \times \underset{\sim}{B}_i')\hat{e}_z$.

The growth of the density modulation gives increasing coherence to the scattering process resulting in a growing scattered wave. The rate of growth of this instability depends strongly on the strength of the pump wave.

III. The Doppler Shift

In the beam frame, the frequency and wavenumber of the electron density modulation satisfies the following conservation laws:

$$\omega' = \omega_o' - \omega_s'; \quad k' = k_o' + k_s'. \tag{1}$$

Typically the frequencies of the electromagnetic waves are much larger than the frequency of the density modulation, and thus Eq. (1) implies

$$\omega_o' \approx \omega_s'. \tag{2}$$

To obtain the relationship between the wave frequencies in the laboratory reference frame (quantities unprimed), one uses the following Lorentz transformations

$$\omega_o' = \gamma_\parallel(\omega_o + k_o v_z), \text{ and } \omega_s' = \gamma_\parallel(\omega_s - k_s v_z) \tag{3}$$

where v_z is the streaming velocity of the electron beam in the z direction and $\gamma_\parallel = (1 - v_z^2/c^2)^{-1/2}$. Substituting these transformations into Eq. (2) yields $\omega_s - k_s v_z \approx \omega_o + k_o v_z$. Then with $k_s = \omega_s/c$ and $k_o = \omega_o/c$, the relationship between the wave frequencies becomes

$$\omega_s \approx \omega_o(1 + v_z/c)/(1 - v_z/c) = (1 + v_z/c)^2\gamma_\parallel^2\omega_o.$$

It should be appreciated that the frequency conversion factor $(1 + v_z/c)^2\gamma_\parallel^2$ can be large. For example, if electron streaming energy is 2 MeV, $\gamma_\parallel = 5$ and $v_z/c \approx 1$ so that $\omega_s/\omega_o \approx 100$. Thus, a 3 cm pump wave would produce a 300 μm scattered wave.

IV. Magneto Resonant Stimulated Raman Scattering

When the electron beam is sufficiently dense and cold, its Debye length can be much smaller

than the pump wavelength i.e.

$$k_D' = \omega_p'/v_{TH}' \gg k_o' \qquad (4)$$

where k_D' is the Debye wave number, ω_p' is the beam plasma frequency and v_{TH}' is the electron mean thermal velocity. In that case, the electron density modulation takes the form of a collective oscillation at the plasma frequency; i.e.

$$\omega' = \omega_p'. \qquad (5)$$

Then the stimulated scattering is known as stimulated Raman scattering and has a number of noteworthy properties.

First of all, Eqs. (4) and (5) imply that the magnitude of the density wave phase velocity is much larger than the thermal velocity; i.e.

$$\omega'/k' \approx \omega_p'/2\,k_o' \gg v_{TH}'.$$

This situation is depicted in Fig. 2.

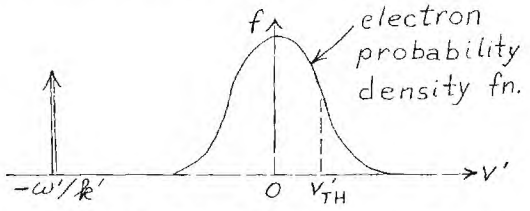

Figure 2. Stimulated Raman scattering.

In such a situation, the entire electron distribution participates in the density wave and the growth of the instability is faster than when $\omega'/k' \approx v_{TH}$.

The growth rate may be further increased when an external constant magnetic field, $B_o\hat{e}_z$, is present, and its strength is adjusted so that $\omega_o' \approx \Omega_o$, where $\Omega_o = eB_o/m$ is the cyclotron frequency. The transverse electron velocity then becomes

$$v_o' = \frac{-e}{m}\,\frac{E_{oy}'}{\gamma'}\,\frac{\omega_o'}{\omega_o' - \Omega_o}\,\hat{e}_y .$$

The temporal growth rate for the stimulated Raman scattering instability in the presence of a constant magnetic field has been derived in the beam frame as [2]

$$\Gamma' \approx \frac{1}{2}\,\frac{v_o'}{c}\,\omega_s'\left(\frac{\omega_p'}{2\,\omega_s' + \Omega_o}\right)^{1/2}. \qquad (6)$$

Laboratory frame calculations [3] have been carried out for the following set of parameters: $\omega_o/2\pi$ = 14 GHz, E_{oy} = 8 x 10^4 v/cm; B_o = 16 kG; $\gamma_{\parallel}$ = 5.3 and $\omega_p'/2\pi$ = 3.5 GHz. The predicted growth rate for the scattered wave at 440 μm wavelength was $\Gamma = 10^{10}$ sec^{-1}, implying an e-folding length for the submillimeter radiation of 3 cm.

In a recent experiment [4], employing an intense relativistic electron beam, parameters similar to those cited in the above example were realized. A 400 μm output wave was measured to have a power level of 1 megawatt when the length of the stimulated scattering region was 50 cm. Lastly, it should be noted that numerical simulation studies are underway with the goal of understanding the nonlinear behavior of this type of instability [5].

V. Stimulated Compton Scattering, and the Use of a Rippled Magnetic Field as a Pump Wave

The Raman scattering experiment described above employed a very intense electron beam with a current of tens of kiloamperes. In more conventional electron beams with lower current levels, it is difficult to achieve the condition in Eq. (4). In that case, rather than having $\omega'/k' \gg v_{TH}'$ it is more usual to have $\omega'/k' \approx v_{TH}'$. The phase velocity of the electron density modulation then overlays the electron probability density function as shown in Fig. 3, and only those electrons with $v' \approx \omega'/k' = (\omega_o' - \omega_s')/(k_o' + k_s')$ participate in the scattering process.

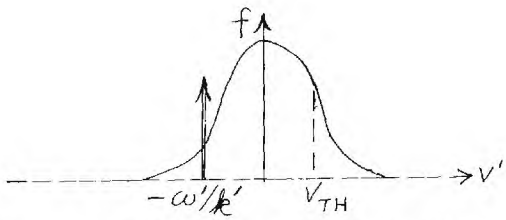

Figure 3. Stimulated Compton scattering.

This type of scattering is known as stimulated Compton scattering. Its potential for generating submillimeter waves was first investigated theoretically by Pantel et al. [1]. Elaboration was subsequently furnished by Sukhatme and Wolff who considered boundary effects and magnetization [6].

Both Pantel et al. and Sukhatme and Wolff used a quantum mechanical formalism. However, the process yields to an equivalent classical analysis. Such an analysis has been carried out [7] and the following expression has been derived for the growth rate

$$\Gamma' \approx \frac{\omega_p'^2}{\omega_s'}\left|\frac{v_o'}{v_{TH}'}\right|^2 . \qquad (7)$$

This may be compared with the Raman scattering expression in Eq. (6). Unlike the Raman case, the Compton growth rate depends on the electron thermal velocity and varies as $v_o'^2$ rather than linearly as v_o'.

An experiment which may be amenable to interpretation as stimulated Compton scattering has been carried out at Stanford University [8]. Instead of using a fast electromagnetic wave as a laboratory pump wave, the electron beam was passed through a region of periodically rippled magnetic field which we represent in simplified form as $b_r \hat{e}_x$. Such a rippled field may be regarded as a slow electromagnetic wave with $\underset{\sim}{E} = 0$, $\underset{\sim}{B} = b_r \hat{e}_x$, $\omega_o = 0$, and $k_o = 2\pi/L$ where L is the ripple period. In the beam frame, the quasiwave will have an electric field $E_y' = \gamma_\parallel v_z b_r$ and a frequency $\omega_o' = \gamma_\parallel v_z k_o = \gamma_\parallel v_z 2\pi/L$.

Then, all the considerations for the occurrence of stimulated scattering apply. From Eqs. (2) and (3) a scattered wave is expected at a laboratory frame wavelength

$$\lambda_s \approx L \Big/ \left[(1 + v_z/c)(v_z/c)\gamma_\parallel^2 \right] .$$

In the Stanford University experiments, a 70 mA, beam of 24 MeV electrons was passed through a helical, 2.4 kG, magnetic field of period 3.2 cm and length 5.2 m. A 10.6 μm signal was amplified in this system with a gain of 7% per pass. The gain was found to be independent of the power density at 10.6 μ over a range of 100 to 1.4×10^5 W/cm^2. Numerical simulation studies of this process are also in progress [9].

VI. Other Scattering Mechanisms

The examples given above in Sections IV and V by no means exhaust the possible coherent scattering mechanisms that can yield submillimeter radiation by upconversion of a relatively long wavelength incident wave. Schneider and Spitzer [10] have suggested a synergistic effect which combines stimulated Compton scattering with coherent Cerenkov radiation. A group at the Naval Research Laboratory [11] is studying scattering of an incident electromagnetic wave by the moving refractive index discontinuity represented by the front of an intense relativistic electron beam; in a preliminary experiment, a 3 cm incident wave at 150 kW was scattered to produce an 8 mm wave at 300 kW. The potential for having simultaneously both power gain and frequency conversion is likely to draw forth other suggestions for coherent scattering mechanisms in the future.

References

1. R. H. Pantell, G. Soncini, and H. E. Puthoff, IEEE J. Quantum Electronics QE-4, 905 (1968).

2. P. Sprangle and V. L. Granatstein, Appl. Phys. Lett. 25, 377 (1974).

3. P. Sprangle, V. L. Granatstein, and L. Baker, Phys. Rev. A, 12, 1697 (1975).

4. V. L. Granatstein, S. P. Schlesinger, M. Herndon, R. K. Parker, and J. Pasour, "Production of Megawatt Submillimeter Pulses by Stimulated Magneto-Resonant Raman Scattering," in this conference digest.

5. A. Drobot, "Results of Numerical Simulations of Submillimeter Radiation from Relativistic Electron Beams," in this conference digest.

6. V. P. Sukhatme and P. E. Wolff, J. Appl. Phys. 44, 2331 (1973); also, IEEE J. Quantum Electronics QE-10, 870 (1974).

7. A. Hasegawa, K. Mima, P. Sprangle, H. H. Szu, and V. L. Granatstein, Appl. Phys. Lett. (to be published).

8. L. R. Elias, W. M. Fairbank, J. M. J. Madey, H. A. Schwettman and T. I. Smith, Phys. Rev. Lett. (to be published).

9. T. Kwan, J. M. Dawson, and A. T. Lin, "The Free Electron Laser," Report PPG-267, Dept. of Physics, U.C.L.A. (1976).

10. S. Schneider and R. Spitzer, Nature 250, 643 (1974).

11. V. L. Granatstein, P. Sprangle, R. K. Parker, J. Pasour, M. Herndon and S. P. Schlesinger, Phys. Rev. A 14, 1194 (1976).

THE ELECTRON CYCLOTRON MASER--AN HISTORICAL SURVEY

J. L. Hirshfield
Yale University, New Haven, Connecticut

It has taken nearly twenty years for practical development of the electron cyclotron maser. The initial theoretical notions were understood by R. Q. Twiss in 1957, but the first clear experimental demonstration did not occur until 1964. Today, in the Soviet Union, these devices are being built which deliver kilowatt level cw power at submillimeter wavelengths, with high efficiency. This paper traces these developments, particularily during the first decade; after this Western activities in this field became rather somnolent, as the initiative passed to the Soviet scientists.

Theoretical Developments

It seems that the Australian astrophysicist R. Q. Twiss was the first to recognize an amplifying mechanism for free-electron gyroradiation [1]. He derived the general formula for the absorption coefficient α_ω for monochromatic radiation of angular frequency ω traversing an ionized medium undergoing free-free electronic radiative transitions.

$$\alpha_\omega = -(h\omega)^2 \int dE Q_\omega(E) \partial F(E)/\partial E \qquad (1)$$

Here F(E) is the energy distribution function for the ensemble of electrons and $Q_\omega(E)$ is the effective transition probability for stimulated emission. Eq. 1 is valid for $h\omega << \bar{E}$, where $\bar{E}$ is the mean energy. In (1), h is Planck's constant over 2π.

Twiss showed that the two necessary conditions which had to be simultaneously satisfied to produce negative absorption (i.e., amplification) are

$$(I)\quad \partial F/\partial E > 0; \quad \text{and} \quad (II)\quad \partial Q_\omega/\partial E < 0$$

over some joint range of the energy E. Condition (I) is the familiar population inversion requirement; condition (II) can be traced to a requirement for either an energy-dependent level width or an energy-dependent level spacing for the quantized free electron states.

While Twiss did not actually evaluate Eq. 1 for conditions appropriate to an amplifying device, he did point out that the formula predicts amplification for Cerenkov radiation and for cyclotron radiation, but not for bremsstrahlung in a fully ionized plasma.

Then in 1959, evidently without knowledge of Twiss's work, Schneider [2] and Gaponov [3] each published calculations which specifically treated the stimulated emission of relativistic monoenergetic electrons in a magnetic field; Schneider's approach was quantum-mechanical, while Gaponov's was classical. Schneider's result allowed one to estimate the experimental conditions required for stimulated emission to exceed absorption, albeit for monoenergetic electrons not drifting along the magnetic field.

But how can one understand physically the mechanism discovered by these workers which underlies the cyclotron resonance maser? If one takes a quantum-mechanical view, the free electron in a uniform static magnetic field B behaves as an anharmonic oscillator with quantized energy levels

$$W_n = mc^2[1 + 2(n + \tfrac{1}{2})h\Omega_o/mc^2]^{1/2} - mc^2 + p^2/2m$$

neglecting spin, where Ω_o is the rest electron gyrofrequency eB/mc and where p is the unquantized momentum along the magnetic field (hereafter neglected). Transitions between states n+1 and n will occur at frequency $\omega_n = (1 - nh\Omega_o/mc^2)\Omega_o$ for $nh\Omega_o << mc^2$; we note that ω_n decreases as n increases. Now, if a system is prepared with a higher population in state n+1 than in state n, photons at frequency ω_n will induce a greater number of downward transitions n+1 → n, than upward ones n → n+1. It is the unequal level spacing which reduces the probability for absorptive transitions n+1 → n+2, since $\omega_{n+1} < \omega_n$, thus allowing stimulated emission to exceed absorption, with a concomitant increase in the photon number. A similar effect can occur if the width of the level n+1 exceeds that of level n; this can be brought about if the radiating electrons suffer (elastic) phase-interrupting collisions (say with neutral atoms) with a sufficiently strong energy-dependent crossection [4].

The classical picture of cyclotron maser action emerges by considering the phases of electrons rotating about the magnetic field. The orbiting charge radiates as an individual electric dipole (and as a higher-order multipole when relativistic effects are properly included). For a system of monoenergetic electrons, originally distributed randomly in phase, the essential question for explaining coherent emission is to find a phase bunching mechanism, since N dipoles rotating in phase will give radiation which is about N^2 more intense than for N dipoles with random phases. For even slightly relativistic electrons this bunching does in fact occur: electrons absorbing radiation will become more "massive" and slip back in phase; electrons emitting radiation will become less "massive" and advance in phase. The ultimate phase distribution is such as to favor emission over absorption, thus enhancing the intensity of the incoming wave. Detailed trajectory calculations by Coccoli [5] have reinforced this view. The classical picture holds for the orbiting electron as a "soft-spring" oscillator in a general

theory of the maser developed by Lamb [6], and as discussed in an extensive review by Gaponov, Petelin, and Yulpatov [7].

Perhaps a better view of the theoretical requirements for achieving amplification is afforded by study of the detailed form of Eq. 1, as analyzed by Bekefi, Hirshfield, and Brown [8], and by Wachtel [9].

$$-\alpha_\omega = \frac{2\pi(2m)^{3/2}\omega_p^2}{3\Omega_o^2 c}\int dE\frac{\partial F}{\partial E}\{E^{3/2}\Omega(E)\,\mathrm{Im}[\Omega(E)-\omega+i\nu]^{-1}\}$$

where $\omega_p^2 = 4\pi Ne^2/m$ is the plasma frequency squared, F(E) is only a function of energy and is thus isotropic in momentum; and the aforementioned quantity $Q_\omega(E)$ is that part of the integrand in { }. For $\nu(E)$ the collision frequency taken as constant, $\partial Q_\omega/\partial E < 0$ only via $\Omega(E)$ and negative absorption is possible for $\omega < \Omega_o$. For $F(E) \sim \delta(E-E_o)$, the case discussed by Schneider, $\alpha_\omega \sim (1+x^2)^{-2}(1+x^2+ax)$ where $x = [\omega-\Omega(E_o)]/\nu$ and $a = 4E_o\Omega(E_o)/3mc^2\nu$; amplification results for $a > 2$. The presence of a phase-randomizing collision frequency ν requires sufficient relativistic phase bunching in a time ν^{-1} so that the attendant collisional absorption can be overcome by the stimulated coherent emission.

The possibilities for amplification when $\overline{E}$ is totally negligible with respect to mc^2, but when $\nu = \nu(E)$ was referred to above and discussed in refs. [8] and [9]. Experimental verification of this collision-induced cyclotron maser action has been obtained [10] when low energy electrons undergo elastic collisions in low pressure Xenon. But further discussion of this fascinating subject would carry us too far afield in this review [11].

Experimental Developments

Early experimental studies of the interaction of radiation with orbiting electrons in a static magnetic field were a natural outgrowth in the development of the traveling-wave tube, in all its variations. But since the interaction we have been discussing does not involve space-charge waves in any form, one may eliminate slow-wave interactions altogether in examining the early experiments. It was probably R. H. Pantell who, in 1959, reported the first results which could have involved the cyclotron maser interaction [12]. He described a device which oscillated at frequencies between 2.5 and 4.0 GHz, as the magnetic field into which a 3 μP electron beam at 1000 volts drifted was varied. The radiation propagated along an S-band waveguide and Pantell claimed that the radiation arose from synchronism between the backward cyclotron wave and the waveguide TE_{11} mode. These results were later extended by Chow and Pantell [13] who showed in fact how axial bunching could result from the combined forces due to the rf electric and rf magnetic fields.

In 1964, I. B. Bott of the Royal Radar Establishment reported the generation of radiation [14] between 2.2 and 0.95 mm using a 10 kV, 50 ma beam in a spatially converging pulsed magnetic field of up to 100 kG. Bott's radiation propagated within a 0.5 inch diameter internally silvered glass tube, was coupled out through a quartz end window, and was detected with an InSb detector. The gain mechanism briefly mentioned as being responsible for the emission was an axial bunching, similar to that discussed by Chow and Pantell; a cyclotron radiation mechanism was stated to only give incoherent emission. Still, as with Pantell's work, there was--in retrospect--no clear way to rule out the cyclotron maser gain mechanism in Bott's initial experiment.

These first experiments studied steady-state oscillators, where presumably non-linear effects have entered to saturate the gain, and thus to put the interaction out of reach of the linear theory which was outlined earlier. Moreover, the unknown mode properties of Bott's waveguide, and the clear possibility of coupling to the transverse rf magnetic fields in Pantell's devices, both left open questions as to whether cyclotron maser action had in fact been observed. (To be sure, neither author had claimed this.) For, in either case, had an axial synchronism condition been satisfied, it was demonstrably possible to explain the results without appeal to the cyclotron maser interaction [7].

In order to unequivocally establish the validity of the cyclotron maser mechanism an experiment was needed satisfying at least two requirements: (I) the apparatus should operate below the start oscillation condition, so that the predictions of linear theory could be checked in detail; and (II) the rf fields in the interaction region should be such that any axial bunching or axial synchronism would be prevented.

Both of these requirements were met in an experiment reported in 1964 [15], in which 5 keV electrons drifted along an axial magnetic field through a concentric high-Q TE_{011} cylindrical cavity. The beam was prepared using a low perveance gun and a combination of a twisted transverse static magnetic field ("corkscrew") and a magnetic hill; the electrons could then be injected into the cavity with most of their energy transverse to the magnetic field. Near the cavity axis negligible axial bunching is predicted, since the transverse rf magnetic field vanishes there. The beam current was kept below the value where the cavity would break into oscillations, and the external magnetic field was swept over a narrow interval about the cyclotron resonance value. Under appropriate conditions cavity loading curves (proportional to the change in reciprocal Q) were observed with a shape as predicted above, namely $(1+x^2)^{-2}(1+x^2+ax)$. When the beam current was increased oscillations occured just where the negative loading had previously been observed. It would seem that this experiment provided the first clear test of the validity of the cyclotron maser mechanism, and resulted in the first publication in which the moniker "electron cyclotron maser" was applied. Later, a two-cavity experiment was reported [16] which showed that an amplifier configuration was possible based fundamentally on the same phase bunching mechanism, only here the bunching is allowed to pile up between

cavities as the electrons move on free-streaming orbits. A theoretical efficiency of 34% was shown to be possible for this type of amplifier.

But Bott's work moved along. In 1965 he published a letter [17] describing experiments with an apparatus similar to that described earlier in [15], but with a 50 kG superconducting magnetic field. In these experiments continuous oscillations at watt levels were observed from 2 to 4 mm. Even second harmonic radiation of about 10 mW was seen down to 1.06 mm. Although Bott took note of the cyclotron maser mechanism in this paper, the uncertainties discussed above would still make an unequivocal identification of the gain mechanism difficult. Still, it seems unlikely that axial bunching could have occured in this apparatus due to the overlap of several axial waveguide modes in Bott's waveguide.

Finally, in 1968, L. C. Robinson [18] placed a tube built by the author into the high magnetic field facility at the Francis Bitter National Magnet Laboratory at MIT. An overmoded resonator was used so that, as in Bott's device, continuous tuning could be achieved by adjusting the magnetic field. Radiation at power levels up to 100 mW was observed in the wavelength range 5.82 mm - 725 μm. Second harmonic power of about 2 μW was detected at 488 μm. The cyclotron maser had penetrated the submillimeter regime!

But cyclotron maser device development had by the late '60's reached a low ebb in Western laboratories. The first decade of rather exciting discovery was to be followed by a second decade of careful engineering development, but this time in the laboratories of the Soviet Union. For in two electrifying papers [19,20] workers from the Gork'ii laboratory of Academician A. V. Gaponov were to announce millimeter and submillimeter cyclotron resonance masers (dubbed "gyrotrons") with extraordinary characteristics; but these Soviet accomplishments are the subject of another paper at this Conference. There is a resurgence of interest in the basic maser mechanism in explaining enormous bursts of radiation from intense relativistic beam devices; this subject is dealt with in papers by V. L. Granatstein and others at this Conference.

---

[1] R. Q. Twiss, Australian J. Phys. 11, 564 (1958). This paper was submitted on July 28, 1958, but in an earlier work in the same volume (Twiss and J. A. Roberts, submitted on February 27, 1958) reference is made to an amplifying mechanism; it may be fairly surmised that Dr. Twiss understood cyclotron masers in 1957.

[2] J. Schneider, Phys. Rev. Letters 2, 504 (1959).

[3] A. V. Gaponov, Izv. VUZ. Radiofizika 2, No.5, 836 (1959). This work is a brief Letter to the Editor and is basically an addendum to an earlier paper (ibid. No. 3, 450). The main paper derives the dispersion relation for waves on a thin beam in a waveguide; the electrons obey a non-relativistic equation of motion but may experience longitudinal or transverse bunching; instability for fast waves is predicted. The addendum (submitted October 19, 1959) briefly notes that the equation of motion used earlier should more properly include relativistic effects. If a uniform magnetic field is present, Gaponov identifies an additional gain mechanism based on "azimuthal grouping" since "... the gyromagnetic frequency ω_H depends on velocity ..." Gaponov acknowledged that the suggestion for including relativistic effects came from V. V. Zhelznyakov. Can we surmise that Dr. Zhelznyakov understood cyclotron masers in 1959?

[4] G. Bekefi, J. L. Hirshfield, and S. C. Brown, Phys. Fluids 4, 173 (1961).

[5] J. D. Coccoli, RLE QPR 67, MIT, Oct. 15, 1962 (unpublished).

[6] W. E. Lamb, Jr. Course Lecture Notes on "The Theory of the Optical Maser", Les Houches 1966.

[7] A. V. Gaponov, M. I. Petelin, and V. K. Yulpatov, Izv. VUZ. Radiofizika 10, No. 9-10, p. 1414 (1967).

[8] c.f., ref. [4].

[9] J. M. Wachtel, "Negative Cyclotron Resonance Absorption", thesis, Yale University 1967 (unpub.)

[10] J. M. Wachtel and J. L. Hirshfield, Phys. Rev. Letters 19, 293 (1967).

[11] Negative collision-induced absorption could have been predicted years earlier, since the eqn. for α_ω can be derived (at least for B = 0) from H. Margenau's microwave conductivity formula [Phys. Rev. 69, 508 (1946); 109, 6 (1958)]. Unfortunatly the formula's progenitor threw many off the track by originally disclaiming this quirk of his theory [E.A. Desloge, S. W. Matthysse, and H. Margenau, Phys. Rev. 112, 1437 (1958)]. Later, of course, he disclaimed the disclaimer [P. Mallozzi and H. Margenau, Astrophys. J. 137, 851 (1963)].

[12] R. H. Pantell, Proc. IRE 47, 1146 (1959).

[13] K. K. Chow and R. H. Pantell, Proc. IRE 48, 1865 (1960).

[14] I. B. Bott, Proc. IEEE 52, 330 (1964).

[15] J. L. Hirshfield and J. M. Wachtel, Phys. Rev. Letters 12, 533 (1964). This paper was submitted on March 26, 1964. Also see J. L. Hirshfield, I. B. Bernstein, and J. M. Wachtel, IEEE J. Quantum Electronics 1, 237 (1965).

[16] J. M. Wachtel and J. L. Hirshfield, Phys. Rev. Letters 17, 348 (1966).

[17] I. B. Bott, Phys. Letters 14, 293 (1965).

[18] L. C. Robinson, "Physical Principles of Far-Infrared Radiation", Academic Press, N.Y. 1973.

[19] N. I. Zaytsev, et al, Radiotekhnika i Elektronika 19, No. 5, 1056 (1974).

[20] D. V. Kisel', et al, ibid, No. 4, 95 (1974).

COSMIC BACKGROUND RADIATION

P. L. Richards and D. P. Woody
Department of Physics, University of California
and
Molecular and Materials Research Division
Lawrence Berkeley Laboratory
Berkeley, California 94720

Introduction

The existence of essentially isotropic homogeneous cosmic background radiation with the spectrum of a 3 K blackbody places important limits on cosmological speculations. This radiation has been the subject of intensive experimental investigation for more than a decade. Current research centers around measurements of the spectrum of the cosmic background radiation at submillimeter wavelengths, and measurements of the anisotropy of this radiation from centimeter to submillimeter wavelengths. In this talk we will discuss some of the difficulties of making these measurements and summarize the present status of the field.

In 1948, Alpher and Herman [1] reported theoretical investigations of "big bang" cosmological models in an effort to explain the abundance of the chemical elements. They concluded that their model universe was filled with isotropic homogeneous blackbody radiation with a characteristic temperature of a few degrees Kelvin. This radiation was emitted by the $\sim$ 3,000 K cosmic plasma and has not interacted with matter since the plasma cooled sufficiently to form hydrogen. Because of the subsequent expansion of the universe, this radiation has cooled to the present temperature of $\sim$ 3 K.

Spectrum

The first observation of the cosmic background radiation was made in 1965 by Penzias and Wilson [2] who measured the sky temperature at a wavelength of 7.4 cm. Their observation was immediately interpreted by the Princeton group [3] as evidence for the primordial plasma. Microwave measurements were subsequently made at seven different wavelengths between 74 cm and 3 mm. These measurements were generally made by switching a heterodyne receiver between a narrow beam on the sky and a cold blackbody. At the longer wavelengths, care was necessary to avoid contributions from galactic synchrotron sources. At the shorter wavelengths, data were measured in windows between atmospheric emission lines. Residual atmospheric contributions were substracted by measuring the flux as a function of zenith angle θ and fitting the data to the sec θ dependence expected from a horizontally stratified, unsaturated atmosphere. In the Rayleigh-Jeans limit, these procedures are relatively straightforward since ambient temperature black objects emit only $\sim$ 100 times more strongly than the 3 K cosmic background radiation.

Measurements at frequencies beyond the peak of the 3 K blackbody curve at $\sim$ 6 cm^{-1} become rapidly more difficult for three main reasons: (1) Heterodyne radiometers with low noise temperatures are not available for submillimeter wavelengths. (2) The emissivity of the atmosphere increases rapidly with frequency in the submillimeter range. (3) The flux in the Planck blackbody spectrum decreases nearly exponentially with frequency, while the emission from ambient temperature black objects increases as frequency squared. At 15 cm^{-1}, for example, an ambient temperature black object radiates 30,000 times more strongly than a 3 K blackbody.

More than ten different groups from many nations have attempted measurements of the spectrum of the cosmic background radiation in the submillimeter region with varying degrees of success. In a recent experiment by Coletti, Decosmo, Melchiorri, Natale, and Sivertsen [4] which will be described at this conference, the narrow band techniques used at lower frequencies have been extended to submillimeter wavelengths. Band-pass filters and bolometer detectors were used to explore unsaturated windows between atmospheric lines from a high dry site. This procedure can give valid results if great care is taken with all aspects of the measurement. In particular, the side-lobes of the antenna pattern must be carefully controlled to insure that the measurement of the cold callibrator, and of the sky flux as a function of zenith angle, are not influenced by the much larger flux from the earth and from ambient temperature portions of the apparatus.

Many groups have used balloon and rocket platforms to carry various types of broad band submillimeter wave radiometer or spectrophotometer above (much of) the atmosphere. Rockets can reach altitudes at which atmospheric emission near the zenith is no longer a problem, but observing times are limited to a few minutes. Balloon flights can give many hours of observing time, but the residual atmospheric effects at balloon altitudes are still very important, and must be measured by zenith angle or spectral scans. Spectral scans have some advantage in that data can be obtained at the particular zenith angle which minimize side-lobe response from the earth or the balloon hardware.

The most successful measurement of this type was reported in 1975 by Woody, Mather, Nishioka, and Richards. In this experiment, the radiation was collected in a conical metal antenna which was carefully designed and exhaustively evaluated to minimize the uncertainty due to side-lobe response. The portions of the antenna which were fully illuminated with radiation that reached the detector were cooled to helium temperatures to minimize their emission. The effectiveness of this cooling was tested by varying the temperature of the an-

tenna during the flight. The window which covered the antenna during ascent was removed to avoid emission from that source. Flowing helium gas was used to prevent residual atmospheric gases from freezing onto the cool antenna. The spectrum of the radiation accepted by the antenna was measured with a helium temperature polarizing interferometer which was operated as a Fourier transform spectrometer. A Ga:Ge bolometer was used for the radiation detector. The scale factor for the absolute calibration was obtained by using external ambient temperature blackbodies.

The spectrum of the night sky measured from an altitude of 40 km was dominated by the atmospheric emission lines from oxygen, ozone, and water. Since the parameters of these lines are well-known, it was possible to develop a model of the line emission with only two unknown parameters (the column densities of ozone and water). The column density of oxygen was obtained from the measured pressure at float altitude. Since the spectra of ozone and water are very different from that expected from the cosmic background radiation, it was possible to fit the model of the atmospheric emission to the data and then subtract it to obtain the spectrum of the cosmic background radiation shown as a cross-hatched region in Fig. 1. Due to an improvement in the analysis procedure, these data are somewhat better than those published originally [5]. Fig. 1 also shows a selection of microwave and interstellar molecular data.

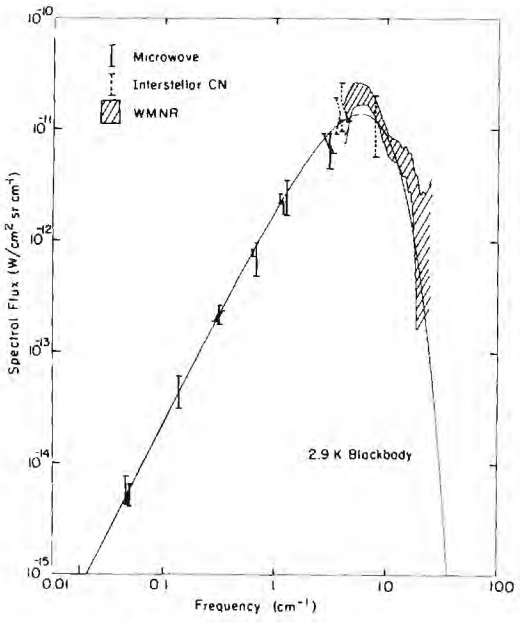

Figure 1. Plot of the microwave, interstellar CN, and Berkeley submillimeter measurements of the cosmic background radiation.

Composite submillimeter wave bolometers will be described at this conference [6] which can improve the ratio of signal to noise in this experiment by more than one order of magnitude. A larger balloon can reduce the contribution from the atmosphere by a factor of order three. Improvements in the antenna have been made to reduce errors in the measurement due to earthshine. An improved spectral measurement should therefore be possible in the near future.

The Planck curve for a 2.9 K blackbody is clearly in good qualitative agreement with the data shown in Fig. 1. This agreement provides strong evidence that the expected remnant of the big-bang is indeed being observed. The blackbody temperature which best fits the Berkeley submillimeter data is $2.99 \begin{smallmatrix} + 0.07 \\ - 0.14 \end{smallmatrix}$. This somewhat higher than the value 2.72 ± 0.16 K which best fits the microwave data for wavelengths longer than 3 mm. Although there are theoretical reasons to expect small deviations from a Planck curve which correspond to a higher temperature at shorter wavelengths, a detailed statistical analysis indicates that all of the observations are consistent with a single temperature of $\sim 2.90 \pm 0.08$ K.

Anisotropy

The standard cosmological models assume that the universe is homogeneous and isotropic. In these models there is a preferred local reference frame in which the cosmic background radiation appears to be isotropic. Any deviation from isotropy would therefore provide important cosmological information. Two types of anisotropy may be distinguished. Small scale anisotropy, with angular sizes of minutes of arc or less, might have resulted if the universe had begun to condense into clusters of galaxies at the time when the radiation was emitted. Very stringent limits have been set on the small-scale anisotropy at microwave wavelengths, but nothing has yet been done at submillimeter wavelengths. Larger scale anisotropies could have resulted from an anisotropic expansion of the universe. Anisotropy of the form $\Delta T = T_0[1 + (v/c)\cos\phi]$ must exist. Here ϕ is the angle between the observation direction and the velocity v of the earth relative to that reference frame in which the radiation is isotropic. The motion of the solar system in the universe is thought to contribute a term with $v \simeq 10^{-3}$ c. The orbital and spin motion of the earth make smaller contributions.

The anisotropy of the cosmic background radition is most easily observed at a wavelength of $\sim$ 1 cm. At longer wavelengths the galactic synchrotron background is much larger than any expected anisotropy in the cosmic background. At shorter wavelengths, atmospheric emission is a severe problem. Several current measurements which have not yet been described in the published literature are being made from platforms above most of the atmosphere. Corey and Wilkinson have a balloon experiment at 19 GHz. Gorenstein, Alvarez, Aymong, Muller, Smoot, and Tyson have an experiment at 33 GHz which is being flown on a U-2 aircraft. Boynton and Partridge have an experiment at

a similar frequency which has recently been flown on a transatlantic balloon. Muelhner and Weiss have flown a balloon apparatus to measure the anisotropy of the cosmic background radiation in the submillimeter wavelength range.

The measurement technique most commonly employed in anisotropy experiments includes the use of two horn antennas directed about 45° from the zenith, but 180° apart in azimuth. The signals from these antennas are alternately fed to a single sensitive receiver. The antenna system is rotated slowly in order to cancel differences between the antennas, and to survey the anisotropy. There are many possible sources of spurious anisotropy which must be careful evaluated and subtracted out. It is especially important to have information about radio interference signals, tilt in the axis of rotation relative to the horizon, and anisotropy in the residual atmosphere. Information on the latter effect can be obtained if the apparatus can also obtain data at a frequency at which atmospheric emission is very large. In one microwave experiment, two separate heterodyne radiometers are used, each with its pair of antennas. In the MIT submillimeter wave experiment, filters are used in front of bolometer detectors to divide the submillimeter waveband into two frequency regions.

The present measurements of the large scale anisotropy are consistent with a velocity towards the Virgo cluster of several hundreds km/s [7], [8], [9]. This result is somewhat surprising since it is opposite in sign to the effect expected from the rotation of our own galaxy. Because several good experiments are now in operation, improved data can be expected in the near future.

Work supported in part by the USERDA.

References

1. For a review of the history of the cosmic background radiation see Alpher, R. A., and Herman, R., Proc. Am. Phil. Soc. 119, 325 (1975).

2. Penzias, A. A., and Wilson, R. W., Astrophys. J. 142, 419 (1965).

3. Dicke, R. H., Peebles, P. J. E., Roll, P. G., and Wilkinson, D. T., Astrophys. J. 142, 414 (1965).

4. Coletti, A., Decosmo, V., Melchiorri, B., Melchiorri, F., Natale, V., and Sivertsen, S. (Paper C-10); Dall'Oglio, G., Fonti, S., Melchiorri, B., Melchiorri, F., Natale, V., Lombardini, P., Trivero, P., and Sivertsen, S., Phys. Rev. D13, 1187 (1976).

5. Woody, D. P., Mather, J. C., Nishioka, N. S., and Richards, P. L., Phys. Rev. Lett. 34, 1036 (1975). This experiment is more fully described in the Ph.D. theses of Mather and Woody which are available on request from P. L. Richards.

6. Richards, P. L., Clarke, J., Hoffer, G. I., Nishioka, N. S., Woody, D. P., and Yeh, N.-H. (Paper C-41).

8. Conklin. E. K., Nature 222, 971 (1969).

9. Muehlner, D. (private communication).

SUBMILLIMETER WAVE ASTRONOMY

M. W. Werner*
California Institute of Technology
and Hale Observatories
Physics Department
Pasadena, California 91125

Scientific Overview

Astronomical observations at submillimeter wavelengths, between 40 μm and 1 mm, study astrophysical sources and problems which differ from and complement those accessible at other wavelengths. Although a few nonthermal sources are known, most of the radiation observed in this spectral band from astronomical sources outside of the solar system comes from extended clouds of gas and dust with temperatures in the range 10-500 K and densities between 10 and 10^6 atoms cm^{-3}. The submillimeter radiation consists of both continuous emission from the sub-micron sized dust particles, which make up $\sim$ 1% of the total mass, and line emission from atomic and molecular species in the gas. The energy radiated at submillimeter wavelengths is generally supplied to such a cloud in the form of ultraviolet, optical, or near infrared radiation from stars or other luminous objects which is absorbed by the dust and goes into heating the dust and gas. Since only a small amount of dust is required to convert ultraviolet and optical radiation into submillimeter radiation, there are many astronomical sources from which most or all of the observed energy lies in this spectral region, although the objects which heat the dust and gas differ from one submillimeter source to another. Thus intense submillimeter radiation is seen from the center of our Galaxy [1] and from diffusely distributed matter within the galactic plane [2], where the heating is probably due to normal stars; from the nuclei of several other galaxies [3], where exotic heating sources may be important; and from shells of dust and gas which are expelled from and heated by evolving stars [4].

By far the most numerous, brightest, and best-studied submillimeter sources now known, however, are dense clouds of dust and gas within which stars appear to be forming in our Galaxy [5]. Most of the luminosity of the young and forming stars within such a region goes into heating the dust and is radiated away at submillimeter wavelengths, with a smooth, blackbody-like spectrum typically peaking between 50 μm and 200 μm. The gas in this type of region is studied by the microwave emission lines from numerous simple molecular species, including CO, HCN, H_2CO, etc. [6]. These observations supply information about the composition, density, temperature, and state of motion of the gas. The existence of this type of region has been known for less than a decade; however, observations of these regions have already provided a much clearer picture of the conditions under which stars form, and of the properties of newly formed stars, than was available previously. A conspicuous example of such a cloud is that associated with the well-known Orion Nebula [7]. This cloud is 10 light years in extent, contains 10^3 solar masses of gas and dust, and has a total submillimeter luminosity of 2 to 3 $\times$ 10^5 times the total luminosity of the sun. This cloud is heated from within by a cluster of stars which have recently formed within it and which are not yet visible at optical wavelengths.

Techniques and Instrumentation

Submillimeter astronomical observations are severely hampered and complicated by atmospheric water vapor. Wavelengths between 40 μm and 350 μm are inaccessible from any ground-based sites, and observations are carried out from airplane-, balloon-, and rocket-borne telescopes. The largest of these instruments have apertures $\sim$ 1 m, so that the spatial resolution of the observations is no better than 15 to 20 arcseconds, which is much poorer than can be attained at shorter wavelengths on large ground-based telescopes. In the poor atmospheric windows around 350 μm, observations can be carried out on an irregular basis from a very few mountain top observatories which are at altitudes in excess of 10,000 ft. Finally, in the 1 mm region, the water vapor absorption is sufficiently low that many large optical telescopes can be used effectively.

Most of the observations to date have been carried out using broad band detectors, including bolometers and photoconductors, and a number of types of filters and spectrometers which define spectral bands having $(\nu/\Delta\nu)$ between 1 and 100. These low resolution observations are mainly sensitive to the continuous emission from the dust in submillimeter sources and provide information about the luminosity of such regions and about the gross distribution of matter within them. The limiting fluxes which can be attained with existing telescopes and detectors are in the range 1 to 10 $\times$ 10^{-26} Watts m^{-2} Hz^{-1} throughout the submillimeter region.

Coherent detection techniques have not yet been used at wavelengths shortward of 1 mm, although several groups have reported observations of the CO J = 2 $\rightarrow$ J = 1 rotational transition at 1.3 mm (260 GHz) using Schottky barrier [8] and InSb mixers [9], and plans are now under way to extend these observations to the J = 3 $\rightarrow$ J = 2

line of CO at 390 GHz. Because of the large amount of information concerning the physical conditions and composition of a region which they provide, spectral line observations are essential to a detailed understanding of any astrophysical system. The submillimeter line observations will complement and extend the information already available from extensive spectral line observations at millimeter wavelengths.

Future Prospects and Requirements

In the next few years, several developments should give continued impetus to submillimeter astronomy. These include:

(A) Construction of major telescopes optimized for, and dedicated to, submillimeter observations, including the 10 m dishes being fabricated by R. B. Leighton at Caltech.

(B) Extension of coherent detection techniques into this spectral region.

(C) Development of more sensitive broad band detectors, including both photoconductors and bolometers.

(D) Performance of the first unbiased surveys of the sky in this spectral region, includint both balloon-borne investigations (P. L. Richards; F. J. Low) and that carried out from the joint American-Dutch-UK Infrared Astronomical Satellite. The submillimeter observations carried out to date have concentrated heavily on regions known from other observations to be of interest and are thus subject to a number of selection effects. The unbiased surveys will be crucial in establishing the true scope and promise of submillimeter astronomy.

Many of the parameters required for the interpretation of submillimeter observations, including, for example, the cross-sections for the excitation of molecular emission and the electromagnetic properties of likely interstellar grain materials, are at best only approximately known. Similarly, some of the observed properties of submillimeter sources, including, for example, the widths and profiles of the molecular emission lines, have not been interpreted satisfactorily. Thus the instrumental advances cited above will have to be accompanied by advances in theoretical and laboratory work if they are to be fully exploited.

*Work supported by National Aeronautics and Space Administration grants NGL 05 002 207 and NGR 05 002 281.

References

[1] Harvey et al., Astrophys. J. 205, L69, 1976.
[2] Fazio and Stecker, Astrophys. J. 207, L49, 1976.
[3] Telesco et al., Astrophys. J. 203, L53, 1976.
[4] Campbell et al., Astrophys. J. 208, 396, 1976.
[5] Werner et al., Science, to be published, 1977.
[6] Zuckerman and Palmer, Ann. Rev. Astron. Astrophys. 12, 279, 1974.
[7] Werner et al., Astrophys. J. 204, 420, 1976.
[8] Goldsmith et al., Astrophys. J. 196, L39, 1975.
[9] Phillips et al., Astrophys. J. 186, L19, 1973.

SUBMILLIMETRE WAVE SPECTROSCOPY OF THE ATMOSPHERE

J.E. Harries
Division of Quantum Metrology
National Physical Laboratory
Teddington, Middlesex
United Kingdom

Introduction

The paper which will be read at this conference will be a review paper in the sense that it will discuss recent and current research in submillimetre atmospheric spectroscopy within an historical framework. This Digest is intended as a guide to the topics which will be considered in the paper.

Historical Background

A survey of the relatively short history of the study of the submillimetre wavelength spectrum of the Earth's atmosphere must begin with the brief but classic paper by H.A. Gebbie in 1957 entitled "Detection of Submillimetre Solar Radiation" [1]. In this pioneering work Gebbie, who was then at the Johns Hopkins University, used a large aperture lamellar grating interferometer and a Golay detector to measure the solar absorption spectrum between 10 and 35 cm^{-1} at a resolution of 0.2 cm^{-1}. Many of the absorption lines detected were identified as due to H_2O, and others were provisionally assigned to O_3, though the basic spectroscopic data (strengths, positions, half-widths) required to make the O_3 assignments definite were not then available. Many O_3 lines were indeed later positively confirmed following experimental and theoretical investigations, as were lines due to magnetic dipole transitions in molecular oxygen, rather an unexpected result at the time of Gebbie's spectrum.

Gebbie's work was carried out at the Jungfraujoch observatory in the Swiss Alps, because he had rightly decided that the very intense spectrum of water vapour would totally obscure the solar spectrum at lower levels where water vapour column densities were, of course, much higher. Indeed, the intense pure rotation band of H_2O is the major characteristic of the submillimetre spectrum, and is now well known to all students of the subject. The strong H_2O lines dominate the spectrum at all levels within the troposphere and indeed well into the lower stratosphere.

Historically, these first mountain observations were followed, slowly at first but then with increasing frequency as awareness of the submillimetre spectrum grew, by other observations from ground-based sites (mostly from mountains, though some astronomers were detecting 0.9 mm radiation at sea level). With the realisation that to make measurements from aircraft which were capable of flying into the relatively very dry stratosphere would open up good transmission windows throughout the whole of the submillimetre region, several groups carried out studies from aircraft from the mid-1960's onwards, using aeroplanes ranging from small military and civil ones through large airliners (Convair 990, Comet 2) to the supersonic Concordes.

In a way, the history of submillimetre atmospheric research can be described as an attempt to get ever higher in the atmosphere. And so the numerous series of aircraft observations led on in some cases to balloon flights. The motivation for this desire to get ever higher is two-fold: for the astronomer, it is the wish to get above the nasty atmospheric emission lines which interfere with and mask radiation from his extra-terrestrial sources. In the case of the atmospheric scientist, however, it is the prospect of opening up many new windows containing lots of lovely sharp lines which can give him information about atmospheric composition that is the attraction.

The attempt to reach ever greater altitudes with a submillimetre spectrometer is not yet ended, as we shall discuss below. Before coming to that, though, we shall touch on some details of the spectrum and what it can tell us.

The Spectrum

Gebbie's spectrum [1] did in fact show features due to the three most important absorbing constituents of the atmosphere H_2O, O_3 and O_2. The other major atmospheric gases do not have permanent dipole moments and so are not "submillimetre-active". As indicated earlier, at sea level, mountain level and indeed at any level within the troposphere, H_2O is without exception the dominant absorber. In the stratosphere, however, all three are equally important, and above about 20 km O_3 takes on a major role. This is easily understood when the vertical distributions of concentration are considered: while the mixing ratio (concentration relative to air) of H_2O drops dramatically with height (at least in the troposphere), that of O_2 stays constant, while that of O_3 increases (in the lower stratosphere).

It was realised very early on that because of its spectral dominance, H_2O could be easily measured from the submillimetre spectrum, and, moreover, it could be measured easily at very high levels where more conventional meteorological

instruments, for example, were not sufficiently sensitive. At this point atmospheric spectroscopy became more than an academic exercise; it also became capable of practical application. Methods of measuring water vapour and ozone concentrations were developed.

In around 1970 the spectral resolution which was typically being obtained was of the order of 0.25 cm^{-1}. Then liquid helium-cooled detectors and more efficient versions of the basic Michelson interferometer became widely available and an immediate jump to 0.05 cm^{-1} meant that much more detailed atmospheric information became available from the spectrum. This coincided well with the dramatic increase in interest in stratospheric composition through the problem of stratospheric pollution and ozone depletion. Spurred on by these combined impetuses spectroscopists began to ask whether other much more weakly absorbing gases could be detected. Today it is still not certain just how many can be detected, but various authors have claimed to identify emission lines due to HNO_3, NO_2, N_2O, CO and other species including perhaps HCl and SO_2.

The information content of the submillimetre spectrum has still to be defined precisely, therefore, but most would probably agree that given certain improvements in experimental sensitivity, and in supporting laboratory (including theoretical) spectroscopy, lines from many other atmospheric gases than just the "big three" will be identified. The paper will deal in some detail with the current situation.

Future Developments

Already spectral resolutions of 0.01 cm^{-1} have been achieved, as conference attendees will learn. Instrumental developments (larger apertures, more sensitive and faster detectors, cooled instruments) will permit higher resolutions, using the now-conventional submillimetre tool, the Michelson interferometer in all its various forms.

Other, somewhat more speculative, techniques such as heterodyne spectroscopy offer even greater hopes for the very highest spectral resolutions of 10^{-4} cm^{-1} or better.

If such developments go hand-in-hand with a continuous improvement in the basic spectroscopic parameters which we need in order to interpret the atmospheric spectra, then the future is indeed hopeful that much more atmospheric information can be obtained from the submillimetre spectrum.

A fundamental limit will eventually be reached which is in a way rather peculiar to the submillimetre region. That is, blending. Because molecular rotation spectra are not as well-separated as in the "vibrational" infrared, the submillimetre atmospheric spectrum is by definition a large "pile" of spectra, one on top of the other. When resolution reaches line widths, we are limited by blending in a far more profound or complicated way than at shorter wavelengths where bands are usually well separated by their different vibrational frequencies.

One further thought must clearly be at the front of many of our minds. As I stated earlier, we have not stopped climbing yet: and the next step must surely be space. An exciting prospect indeed for astronomers, astrophysicists, terrestrial and planetary atmosphere scientists alike. And with Spacelab coming, with its ability to carry liquid helium and large aperture payloads the future surely is going to be as exciting as the past.

Reference

[1] H.A. Gebbie, Phys. Rev. 107, 1194, 1957.

ABSOLUTE HIGH RESOLUTION FAR INFRARED MEASUREMENTS OF ATMOSPHERIC CONSTITUENTS

B. Carli*, J.E. Harries**, D.H. Martin***, E. Puplett***

* Now at Physical Institute
University of Florence
Florence 50154, Italy

** National Physical Laboratory
Teddington, Middlesex, U.K.

*** Department of Physics
Queen Mary College,
London E1 4NS, U.K.

In the frame of the ASSESS-1 mission, a polarising interferometer (D.H.Martin, E. F.Puplett, Infrared Physics, 10, 105, 1970) has been flown on a NASA CV990 aircraft at the lower limit of the stratosphere, with the purpose of measuring sky emission in the spectral range 3-40 cm^{-1}. Due to the proximity of the tropopause during flight, limb sounding measurements were not practicable and the scientific objectives were limited to the exploration of the spectral assignments and concentrations of ozone and minor constituents of the atmosphere and in so doing to test developments of technique. Previous experiments (J.E.Beckman, J.E.Harries, Appl. Opt., 14, 470, 1975) had shown the need for improved techniques that would give a resolution of at least 0.01 cm^{-1} unapodised so that over-lapping emission lines from different constituents are resolved, that would allow an interferogram to be recorded in no more than a few minutes because significant changes can occur in the atmospheric signal observed from an aircraft in such time intervals, and that would give measurements of emission in absolute terms in order to make possible quantitative estimates of constituents. The changes required in the instrumentation to give these improvements were the introduction of a fast data acquisition system, the adoption of the polarised interferometric method both to suppress the effects of signal fluctuations and to allow continuous reference to black-body calibration sources (B.Carli, IEEE Trans., HTT-22, 1094, 1972), and the incorporation of greatly improved germanium bolometric detectors (P.A.R. Ade and S. El-Atawy, personal communication).

A servo-controlled imput mirror driven by the aircraft's inertial guidance system ensured the maintenance of a constant elevation of 14° during the recording of an interferogram.

The emission was continuously compared with that from a black-body cavity; to give absolute calibration two black-body cavities were used, one at ice temperature and the other at liquid-nitrogen temperature. More than 100 interferograms were recorded. Each interferogram was recorded in 8 minutes. The Fourier transform was linearly apodised to give a resolution of 0.02 cm^{-1}.

The position of lines of several constituents of the upper atmosphere was unambiguously identified by comparison with synthetic spectra and laboratory measurements (J.W.Fleming, private communication), and evaluation of the concentration of a number of minor components has been obtained.

ATMOSPHERIC ABSORPTION OF FAR INFRARED LASER RADIATION

Nelson McAvoy
V.G. Kundy
Goddard Space Flight Center
Greenbelt, Maryland 20771

A.S. Milman
U.O. Farrukh
G.L. Mader
Phoenix Corporation
1311 Dolley Madison Blvd.
McLean, Va. 22101

The low spectral emission of black bodies in the FIR and the heretofore unavailability of oscillators or other active networks has resulted in very little knowledge of atmospheric characteristics. This paper describes the beginning of a program for theoretical and experimental measurements of the atmosphere.

Theoretically, a transmittance model has been developed for high spectral resolution of atmospheric constituents such as H_2O, O_3, and CO_2. The below figure is a plot of transmittance according to this model for a complete atmospheric path with 0.1 mm of equivalent H_2O vapor plus the predicted O_3 concentration (1). The sharp line absorption is due to the O_3 while all the broader lines are due to H_2O at the higher pressures and temperatures existing near the earth.

Experimentally, the output of a FIR laser is matched into an 80 cm aperture telescope. A 70 cm aperture flat reflecter, 0.6 km away, provides a horizonal path of 1.2 km. Absorption measurements of water vapor in this path will be made. These measurements will provide experimental verification on only the broadband absorption. Measurements of the sharp O_3 absorption will be made later using an heterodyne radiometer and an heliostat tracker.

1. V.G. Kundy and W.C. Maguire: J. Quant. Spectrosc. Radiat. Transfer.; Vol. 14, pp. 803-817, Pergamon Press, Great Britian.

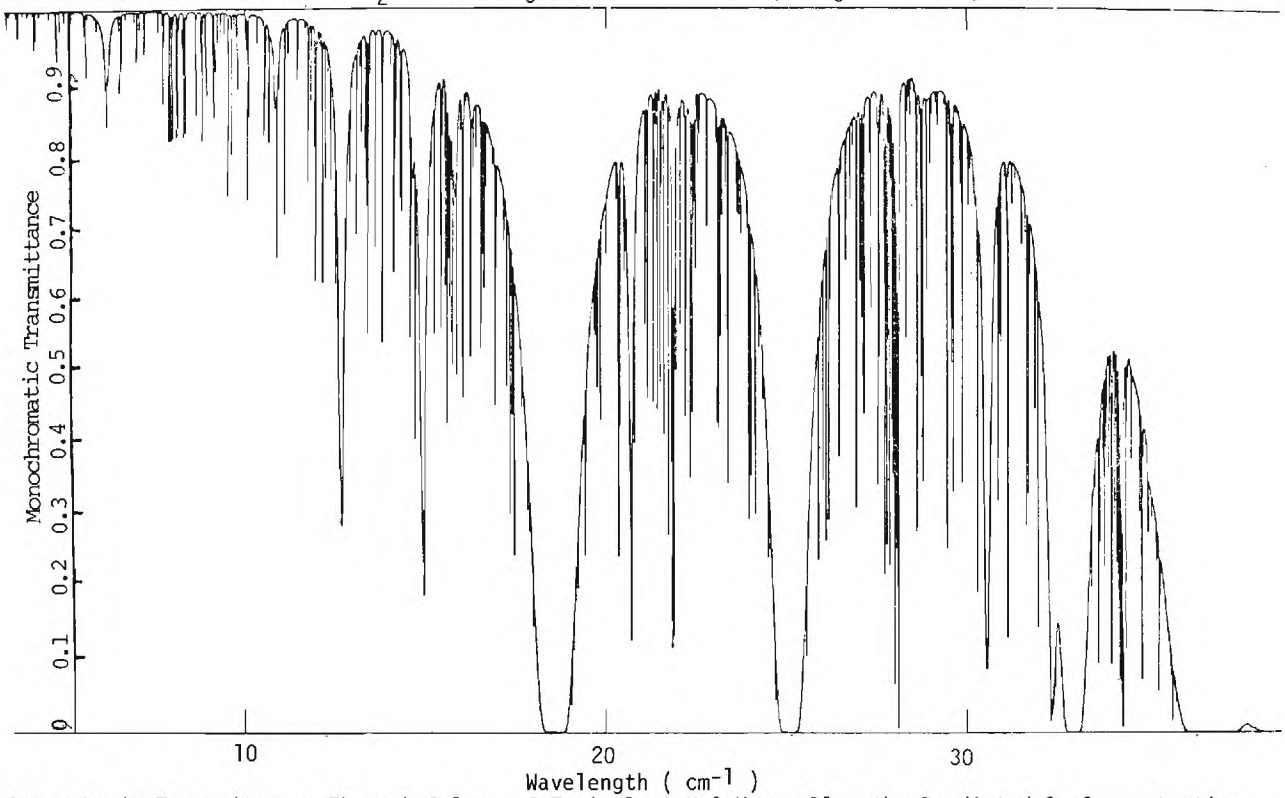

Atmospheric Transmittance Through 0.1 mm of Equivalent H_2O Vapor Plus the Predicted O_3 Concentration.

SUBMILLIMETER WAVE NOISE INTERACTION WITH RAINY ATMOSPHERES

G. Schaerer
Goddard Space Flight Center
Greenbelt, Maryland 20771

Introduction

The thermal radiation from the atmosphere is an unwanted contribution of noise from the standpoint of communications, whereas it may provide valuable information about various atmospheric parameters from a remote sensing standpoint. The monitoring of this radiation by spaceborn sensors has been done successfully at microwave and infrared wavelengths. The submillimeter region is still essentially untouched and could give further insight into atmospheric parameters although the interaction of these waves and the troposphere is highly complex and not yet completely described. An estimation of the noise levels for rainy atmospheres is a first step in this direction and shows some of the inherent limitations.

Emission Properties of a Clear Atmosphere

The noise emission from a clear atmosphere is dominated by the many strong water vapor absorption lines below 1.7 mm wavelength. Some discrepancies between measurements and theory within the submillimeter and millimeter windows were substantially reduced only recently [1, 2]. Figure 1 gives the maximum possible tropospheric influence on the noise on the basis of this model for some atmospheric windows and resonance lines. The abscissa gives the maximum possible drop in equivalent noise temperature which would occur if a layer from sea level to a height h were completely shielded. This drop can be written by

$$\Delta T(h) = T_\infty(O) - T_\infty(h)$$

$$B[T_\infty(h)] = \int_h^\infty B[T(x)] \exp[-t]\, dt$$

$$t = \int_x^\infty S(x')\, Q_{ext}(x')\, dx'$$

B = Planck function

S = density

T = temperature

Q_{ext} = extinction coefficient

A change in atmospheric noise can therefore not be expected with rain for wavelengths below 0.8 mm. However, there is a substantial influence due to clouds at 4-8 km height above sea level.

Interaction with Clouds and Rain

Water droplets of different sizes and densities are the sole kind of interaction with submillimeter waves considered here. The interaction with the droplets is assumed to obey the Mie-theory [3]. The dielectric data of water at submillimeter waves are sparse and do not fit the widely used Debeye relation. The modification introduced by Malyshenko predicts accurately, however, the measured dielectric data [4]. The cloud models used are those given by Fraser [5], with a Deirmendjian dropsize distribution.

$$N(r) = \alpha r^{C_1} \exp[-\beta r^{C_2}]$$

where α and β are functions of the empirical parameters C_1, C_2, the mass density of the cloud m and the 'mode' radius r_c (see Figure 2). For the rain a Marshall-Palmer dropsize distribution was assumed [6]. Scattering and extinction cross sections are numerically integrated over the different distributions. The scattering albedo ω_0 and extinction coefficient given in Figure 2 show some extreme values.

The radiative transfer equation [7] given by

$$\mu \frac{dI}{dt}(t, \hat{s}) = I(t, \hat{s}) - (1 - \omega_0)\, B[T(t)] - \omega_0 \int p(\hat{s}, \hat{s}')\, I(t, \hat{s}')\, d\Omega'$$

where p = scattering phase function
I = intensity in direction $\hat{s} = (\psi, \eta, \mu)$

has been solved by a straightforward iterative technique [8]. For a chosen set of atmospheric parameters, the atmosphere is divided into many optically thin layers. The up-and-downwelling intensities are then computed first without scattering and then in the following iteration steps by using the intensities of the previous iteration for the scattering term. Figure 2 shows a typical rain rate-brightness temperature relationship. The raindrops are assumed to be distributed equally from sea level to a 4 km height in a tropical atmosphere.

The interaction with some rain bearing cumulus and cumulonimbus clouds, ranging from sea level to a height h, is also shown in Figure 2. The density of 8 gm^{-3} is near the upper limit found in the atmosphere. The computations with the artificial suppression of the scattering show the weak effect of the scattering compared with any strongly scattering microwave situation [9]. This is due to the following:

1. the higher atmospheric gas absorption
2. the stronger forward versus backscatter. This

is due to the small values of the dielectric constant at submillimeter waves and is in contrast to the microwave region (much larger dielectric constant), where the backward scattering may exceed the forward scattering considerably.

References

[1] Waters, J., NASA Jet Propulsion Laboratory, private communication.

[2] Fulde, J., 'Theoretische und numerische Grundlagen fuer die Mikrowellen-Spektro-Radiometrische Untersuchung der atmosphaere, University of Bern, Ph.D. Dissertation, 1976.

[3] Mie, G., 'Beitraege zur Optik trueber Medien', Annalen der Physik 26, 597, 1908.

[4] Malyshenko, Yu., et al., 'Calculation of permittivity of water in sub mm range', Ukrainskiy Fizicheskiy Zhurnal, Vol. 15, No. 9, 1496, 1970.

[5] Reeves, R. G., 'Manual of Remote Sensing', American Society of Photogrammetry, Vol. 1, p. 209, Falls Church, 1975.

[6] Marshal, J. S., et al., 'The distribution of raindrops with size', T. Meteor., 5, 165, 1948.

[7] Chandrashekar, S., 'Radiative Transfer', New York, Dover, 1960.

[8] Herman, B. M., et al., 'The effect of atmospheric aerosols on scattered sunlight', J. Atm. Sci. 28, 419, 1971.

[9] Wilheit, T. T., et al., 'A satellite technique for quantitatively mapping rainfall rates over the oceans', to be published in J. Atm. Sci.

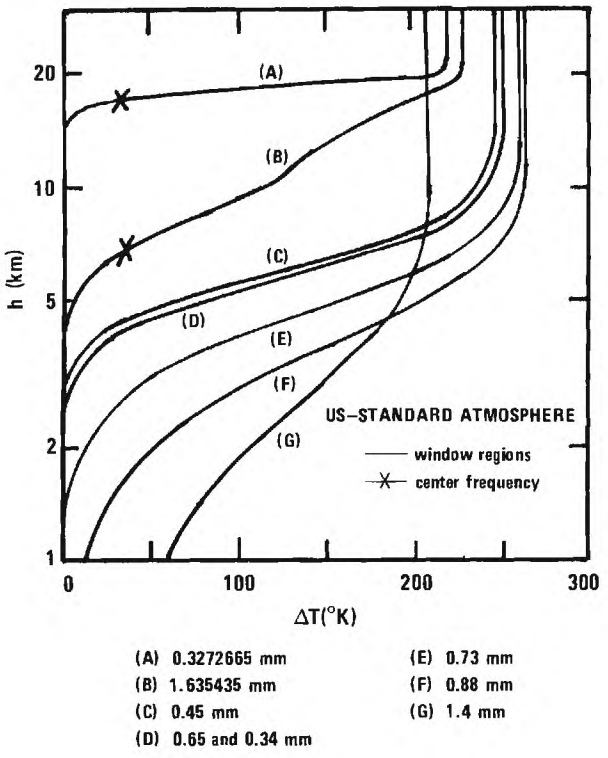

Figure 1. Maximum temperature drop due to a perfect shielding of the atmospheric layer from sea level to a height h.

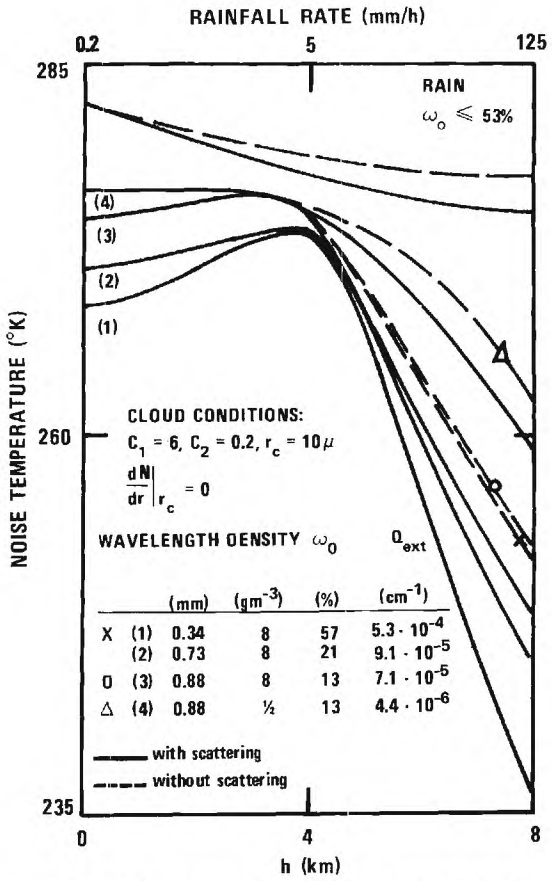

Figure 2. Actual noise temperature due to different cloud and rain conditions.

CALCULATIONS OF ANTENNA TEMPERATURE AND HORIZONTAL PATH ATTENUATION DUE TO THE 320 GHz ABSORPTION LINE OF WATER VAPOR*

R. W. McMillan, J. J. Gallagher, and A. M. Cook, Jr.

Engineering Experiment Station
Georgia Institute of Technology
Atlanta, Georgia 30332

A. Absorption Calculations

Van Vleck and Weisskopf [1], have shown that the attenuation coefficient α, at frequency ν, for a collision broadened absorption line centered at frequency ν_o, with linewidth parameter $\Delta\nu$, is given by

$$\alpha = \frac{8\pi^2 Nn|\mu|^2\nu^2 e^{-E_i/kT}}{3c\ kT\ G} F(\nu) \qquad (1)$$

where the other parameters are determined as discussed below. The parameter N is the number of molecules per unit volume and is

$$N = \frac{N_A \rho}{M}, \qquad (2)$$

in which N_A is Avogadro's number, ρ is the density of molecules, and M is the number of grams in a gram molecular weight. For water, this number is $N = 3.346 \times 10^{16}\ \rho$ where ρ is measured in g/m^3. The factor $|\mu|^2$ is the square of the dipole matrix element between transition states and is equal to $\Sigma|\phi|^2\mu_o^2$, where μ_o^2 is the electric dipole moment. The factor $\Sigma|\phi|^2$ is the line strength parameter determined by King et al. [2], and μ_o^2 is 3.39×10^{-36} esu from Van Vleck [3]. The statistical weighting factor n which accounts for nuclear spin is unity [4] for even rotational states and 3 for odd rotational states. In the exponential term, E_i is the energy of the lower transition state, k is Boltzmann's constant, and T is the absolute temperature at which the attenuation is measured. The partition function G has been calculated by Van Vleck [3] to be 170 at 293°K and varies with temperature as

$$G = KT^{3/2}. \qquad (3)$$

Evaluation of the constant K from the above values gives $G = 0.0339T^{3/2}$.

For these calculations, the line shape factor $F(\nu)$ was replaced by a factor calculated by Gross [5], which has been found to give better agreement with absorption cell measurements.

$$F(\nu) = \frac{4\nu\ \nu_0\ \Delta\nu}{(\nu_0^2 - \nu^2)^2 + 4\nu^2\Delta\nu^2}, \qquad (4)$$

in which the parameters are defined as before.

Since the attenuation calculations were made as a function of altitude, and because radiometric calculations must consider altitude, the altitude dependence of terms in Equation (1) must be considered. The density varies with altitude according to a relation given by Croom [6,7], who based his altitude dependence on U.S. Weather Bureau data. This dependence for height Z is as follows:

$$\begin{aligned} &Z < 17 \text{ km} && \rho = \rho_0\ [10^{-0.2286Z}], \\ &17 \text{ km} < Z < 26 \text{ km} && \rho = (3.611 \times 10^{-5})\ (10^{0.09155Z}), \\ &Z > 26 \text{ km} && \rho = 0.3\ (10^{-0.05914Z}). \end{aligned} \qquad (5)$$

Barrett and Chung [8], based on U.S. Air Force data, give the temperature variation as:

$$\begin{aligned} &Z < 12 \text{ km} && T = T_A - 5.83Z, \\ &12 \text{ km} < Z < 25 \text{ km} && T = 216^oK \\ &Z > 25 \text{ km} && T = 3.08Z + 139^oK, \end{aligned} \qquad (6)$$

and the pressure dependence

$$P = 760\ [10^{-3.05Z/50}]. \qquad (7)$$

Also from Barrett and Chung, the linewidth parameter is

$$\Delta\nu = \frac{(2.714 \times 10^9)\ \frac{P}{760}\ (1 + .0046\rho)}{\left(\frac{T}{318}\right)^{0.625}}, \qquad (8)$$

which gives $\Delta\nu = 3.00 \times 10^9$ Hz for P = 760 mm, $\rho = 7.5\ g/m^3$, and T = 286°K.

Using these parameters with the indicated altitude, density, and temperature dependence, the attenuation in db/km due to contributions from all of the water absorption lines below 1000 GHz were calculated in the wavelength region from 290 GHz to 360 GHz. The result of this calculation at sea level is shown in Figure 1.

B. Sky Temperature Calculations

The background sky temperature T_b measured by a radiometer at altitude h with an infinitesimally narrow beamwidth looking upward at zenith angle Θ is [6,7,8]

$$T_b = T_s \exp\left(-\int_h^\infty \alpha(Z)\sec\Theta dZ\right) + \int_h^\infty \alpha(Z)T(Z)\exp\left(-\int_h^Z \alpha(\acute{Z})\sec\Theta\, d\acute{Z}\right)\sec\Theta\, dZ, \qquad (9)$$

in which T_s is the sun temperature, and T(Z) is the temperature of a stratum of atmosphere of thickness dZ located at altitude Z. In this equation, the first term is seen to be the brightness of the sun as viewed through the atmosphere, and the second term is the emission of the atmosphere. The sum of these two terms is the temperature that would be measured if the sun were viewed as a

source through the atmosphere. Using the value of α given by Equation (1), this equation was integrated numerically up to an altitude of 50 km. In order to get good accuracy and minimize computer time, the stratum width was varied as follows:

$Z < 1.0$ km	$\Delta Z = 2.5$ m
1.0 km $< Z < 4.0$ km	$\Delta Z = 5.0$ m
4.0 km $< Z < 8.0$ km	$\Delta Z = 10.0$ m
8.0 km $< Z < 16.0$ km	$\Delta Z = 20.0$ m
16.0 km $< Z < 50.0$ km	$\Delta Z = 50.0$ m

The computer was programmed to read out emission temperature of the atmosphere, which is the temperature that would be measured by a radiometer pointing away from the sun; sky temperature, measured when the sun is viewed as a source; and zenith attenuation. The contributions of all of the water absorption lines between 100 GHz and 1000 GHz to these temperatures were included in the calculations. The result of calculating emission temperature near 325 GHz with the antenna pointing to the zenith is shown in Figure 2. Emission temperature calculated with the sun viewed as a source is shown in Figure 3.

* This work was supported by NASA Grant NSG-5012 and by the U. S. Army Research Office, Durham N.C.

REFERENCES

1. J. H. Van Vleck and V. F. Weisskopf, Rev. Mod. Phys. 17, 2 & 3 (1945) 227-236.
2. G. W. King, R.M. Hainer, P. C. Cross, Phys. Rev. 71, 7, (1947), 433-443.
3. J. H. Van Vleck, Phys. Rev. 71, 7 (1947) 425-433.
4. C. H. Townes and A. L. Schawlow, Microwave Spectroscopy, McGraw-Hill Book Company, New York (1955), p. 104.
5. E. P. Gross, Phys. Rev. 97, 2, (1955) 395-403.
6. D. L. Croom, J. Atmos. & Terr. Phys. 27 (1965) 217-233.
7. D. L. Croom, Ibid, 235-243.
8. A. H. Barrett and V. K. Chung, J. Geophys. Res., 67, 11 (1962) 4259-4266.

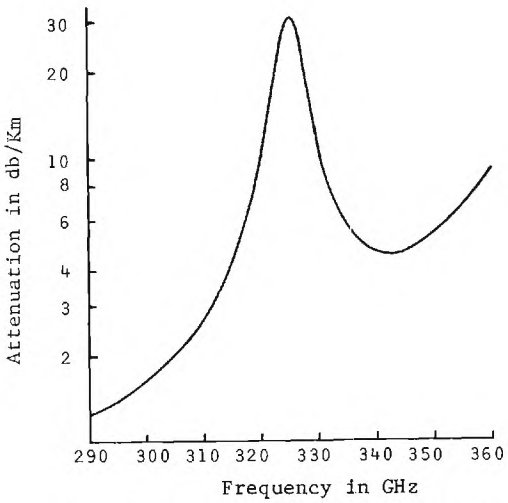

Figure 1. Sea Level Horizontal Path Attenuation Near 325 GHz for 300°K and 7.5 g/m^3 H_2O.

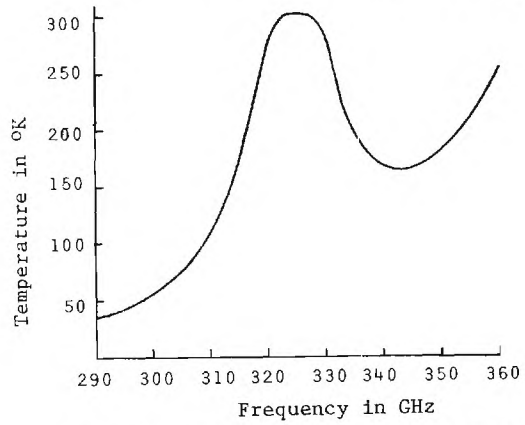

Figure 2. Zenith Emission Temperature for 300°K and 7.5 g/m^3 H_2O.

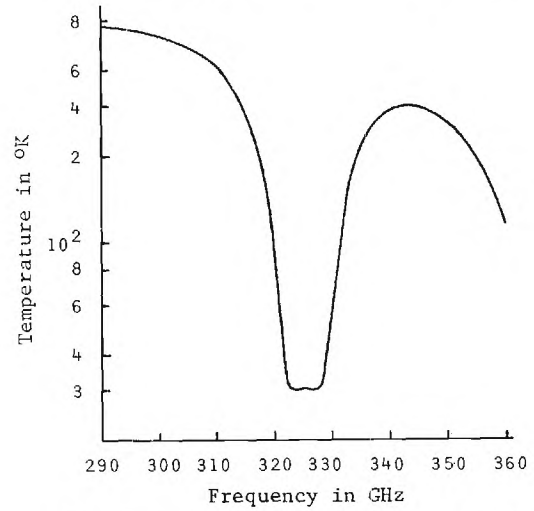

Figure 3. Sun Temperature Near 325 GHz for 300°K and 7.5 g/m^3 H_2O.

A QUASI-OPTICAL RADIOMETER

J. J. Gustincic
Consulting Engineer
13121 Mindanao Way
Marina Del Rey, CA 90291

Introduction

There has been a recent impetus to develop submillimeter spectral line receivers for the study of the upper atmosphere. This paper describes the present status of a program sponsored by the Jet Propulsion Laboratory to develop room temperature superheterodyne spectral line receivers with equivalent noise temperatures of approximately one thousand degrees in the range from 100 to 1000 GHz, suitable for flight applications. The program plan involves initial development at the lower frequencies with the objective of direct scaling of the devices up to the shorter wavelengths. The first step in this program was the construction of a complete 1.5 mm receiver based on quasi-optical techniques utilizing presently available klystron local oscillator sources and Schottky diode mixing elements. The central components in the receiver front end are the local oscillator injection circuitry and the quasi-optical mixer mount which are discussed in the following.

The Local Oscillator Injection System

The local oscillator injection system is shown in Figure 1. The novel scheme amounts to a

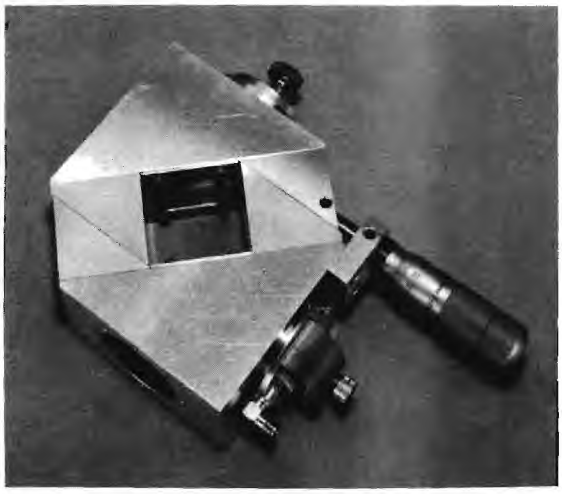

Figure 1. The quasi-optical L.O. injection circuit.

Quasi optical analog of the ring-hybrid local oscillator injection systems which are commonly realized in waveguide at millimeter frequencies. In the quasi-optical system, energy from the local oscillator source is collimated by a teflon lens 1" in diameter and this energy impinges on a Folded Fabry-Perot resonator at a 45° incidence angle. The resonator can be seen in the Figure as the square cavity in the center of the device. The Folded Fabry-Perot behaves in a fashion similar to the waveguide ring hybrid. The local oscillator energy resonates around the four walls of the cavity and finally exits into the quasi-optical mixer via a second teflon lens. At the signal frequency the cavity is anti-resonant and the signal energy bounces off the cavity entering the mixer with very small loss. The Folded Fabry-Perot cavity is tuned by mechanically increasing its diagonal dimension. The cavity in Figure 1 was designed for an I.F. frequency of 1.42 GHz.

The Quasi-Optical Mixer

The quasi-optical mixer consists of a gallium arsenide Schottky barrier diode chip mounted at the apex of a biconical horn antenna. The chip has 2.5 micron dots and was fabricated by R. J. Mattauch at the University of Virginia. The radiation pattern of the bicone was made suitable for the illumination of the collimating lens by surrounding the bicone with a curved short circuit which reflects energy back into the bicone everywhere but at a circular aperture in the face of the mixer mount. The aperture and bicone can be seen in Figure 2. The reactive whisker at the

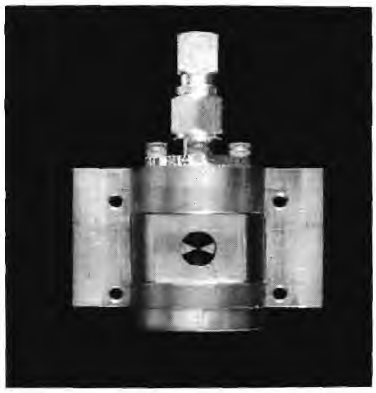

Figure 2. The quasi-optical mixer.

apex of the bicone is resonated by a movable section at the back of the short which serves to tune the mixer. Choke grooves are cut directly into the cylindrical extensions which support the bicone and no additional filtering was needed to isolate the I.F. output. An impedance level of approximately 8 ohms is measured looking into the mixer output port at the I.F. frequency when the mixer has the appropriate R.F. bias.

Receiver Component Performance

The local oscillator injection efficiency was investigated by placing waveguide feed horns at the L.O. and mixer ports and measuring the insertion loss between the waveguide inputs. Values ranging between 6 and 3 db were measured at 190 GHz. These values decreased a minimum of an additional 15 db as the cavity was tuned off resonance indicating a good figure for the local oscillator noise rejection and signal reflectivity at the other end of the cavity. Single sideband system noise temperatures of 2300 K were measured with room temperature waveguide mixers fabricated by A. R. Kerr of the Goddard Institute for Space Studies at 170 GHz with an I.F. amplifier having a noise temperature of 180 K and with a klystron local oscillator.

The quasi-optical mixer is presently under evaluation and is yielding noise figures comparable with waveguide mixers at 185 GHz.

An evaluation of the quasi-optical injection system and mixer at 245 GHz is presently under way with local oscillator power provided by a Methel Fluoride, CO_2 pumped laser supplied by D. Hodges of the Aerospace Corporation. Preliminary results to date are highly encouraging with every indication that the quasi-optical system is capable of system temperatures of several thousand degrees at these frequencies.

The Airborne Radiometric Receiver

The aircraft radiometer front end utilizing the quasi-optical components is shown in Figure 3.

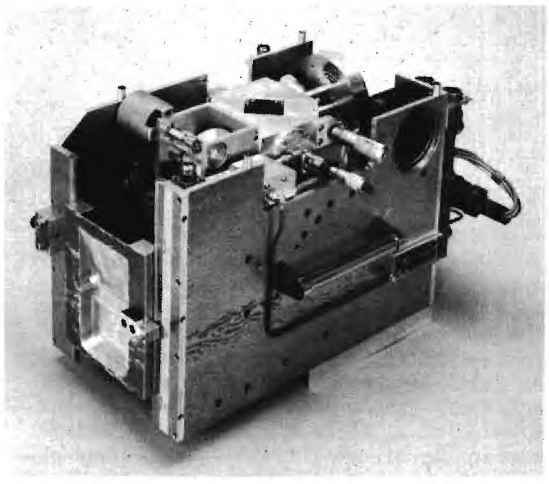

Figure 3. The aircraft radiometer.

The instrument is presently being flown on the NASA C-141 and CV-990 aircraft for spectral line measurements in the range 160-190 GHz. Klystron local oscillator sources are employed. The klystron energy is divided between the Folded Fabry-Perot resonator and a phase lock detector by means of a polarization sensitive reflector and an appropriate rotation of the klystron with its feed horn thus eliminating the need for waveguide components in the form of directional couplers and attenuators.

The instrument receives horizontally polarized signal energy in a beam with a 3 db width of approximately 5°. Reference switching is accomplished by means of a nutating mirror. Calibration is achieved with LN_2 reference loads and heated loads which are contained within the instrument.

FAR INFRARED PHOTO-RESPONSE OF SILICON INVERSION LAYERS

Robert G. Wheeler
Department of Engineering and Applied Science
Yale University
New Haven, CT. 06520

The photo response induced by far infrared radiation interacting with electrons in silicon inversion layers at 4.2°K can be associated with at least five distinct processes. Of these, four can be attributed directly to the physics of the quasi-two dimensional electron system. The response can be either photoresistive or photoconductive, each type characterized by a distinct response time, magnitude and temperature dependence as well as a resonant or broad band response with respect to photon energy. It is now accepted that as the electron density is increased, initially an electron localization occurs as evidenced by a thermally activated conductivity. In high mobility samples at electron densities greater than $\sim 5\times10^{11}$ electrons/cm^2 the conductivity becomes metallic in nature. The observed responses manifest both of these conditions as well as the quantization induced by the electric field perpendicular to the surface.

The Metallic Regime

Electric Subband Transitions

One of the interesting aspects of the two dimensional inversion layer is the existence of electric subbands whose energy is strongly dependent upon the variable electron density n_s [1]. This variability allows tuning of the system resonantly with far infrared laser produced photons. The response is resistive, reflecting the fact that in a three terminal field effect transistor one measures the conductivity of the electrons in the ground state subband [2]. The photoelectron resides for a time τ in a low mobility state, hence the resistive nature of the response. An example of this response is seen in fig. 1. The response is of resonant character with a one to one correlation between electron density n_s and photon energy over the range of $h\nu$ = 8 mev to 40 mev. Other characteristics are response times in the range of 10^{-4} to 10^{-3} second which is n_s dependent, and a very strong temperature dependence such that signals are not observable above 10°K.

Models [3-6] of the energy level variation with n_s are in reasonably good agreement with both absorption [7] and photoresponse measurements [2]. The detailed nature of the interaction of photons with the inversion layer must include screening of the infrared field by the inversion layer which shifts the frequency at which absorption occurs from the subband level differences [8]. A microscopic model of the recombination dynamics operative in photoconductivity has been suggested by Döhler [9]. The essential features are elastic scattering of the photoelectron by coulomb impurities to the ground state of a second subband ladder. The second ladder arises due to the anisotropic nature of the conduction band described by the six equivalent minima in silicon. Due to the surface quantization along a [001] direction, these minima are not equivalent, which give rise to two sets of subband levels [1]. He has estimated that the scattering times, involving large changes in crystal momentum, from this state to the lowest ground state is in general agreement with the observed response time.

Fermi Gas

In connection with defining the nature of the interaction of electromagnetic radiation with the inversion layer electrons, Allen and Tsui have shown that in the metallic regime and for photons whose energy is less than the subband energy difference the layer can be described as Drude like [10]. Hence the character of the response will be that of a two dimensional Fermi gas [11,12]. For a two-dimensional Fermi gas with a single band occupied and assuming simple isotropic scattering processes the conductivity is to first order in temperature

$$\sigma = \frac{e^2}{m^*} N(E) \left\{ E_F \tau + \frac{\pi^2}{6} (KT)^2 \left[E_F \frac{\partial^2 \tau}{\partial E_F^2} + 2 \frac{\partial \tau}{\partial E_F} \right] \right\} \quad (1)$$

where N(E) is the band density of states, a constant for a single two-dimensional band, E_F the Fermi level only a function of n_s and τ the scattering time. High precision conductivity measurements (4 significant figures) has allowed as to determine the scattering time of derivatives, where the first derivative is negative and the second derivative nearly a positive constant. The photoresponse due to the heating of the Fermi gas, reflects the nonresonant character expected and is photoresistive over the large range of n_s where the first derivative dominates. In figure 1 the low background observed at high gate voltage where $h\nu <$ subband splitting is due to this phenomena. The response time is less than 5×10^{-6} which is set by the maximum speed of our mechanical chopper. Since the specific heat of the Fermi gas is

$$C = \frac{\pi^2}{3} K^2 T N(E) \quad (2)$$

differential conductivity measurements with a pulsed megahertz source which allows higher precision than far infrared has determined a response time of the order of 10^{-9} seconds. In comparative magnitude this phenomena is about 1% of the subband photoresistive response.

Localized Regime

The experimental situation in this regime is more complicated since the conductivity is very temperature sensitive and the scattering time derivatives associated with the highly mobile electrons is an extremely strong function of electron density. However, the localized states probably have associated with them an energy width. To date we have been able to attribute most of the response which is photoconductive with $h\nu <$ subband energy splitting, to the bolometric effects. Search for distinctive resonant response due to excitation of localized electrons into the conduction subband have been unsuccessful.

As pointed out by Stradling [13] at photon energies above about 40 mev, photoconductive processes in the bulk of the silicon due to photoionization of neutral donors and negatively charged acceptors in the depletion layer will contribute to any response as measured in a field effect transistor. All responses as a function of gate voltage or n_s will reflect the basic mobility of the electrons in the channel which itself is a strong function of electron density. Thus all responses must be so modified in order to extract information regarding competitive processes.

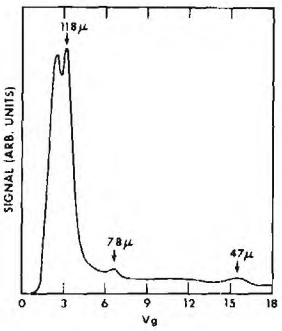

Figure 1. The photoresistive response as a function of gate voltage V_g when three laser wavelengths are simultaneously incident upon the field effect structure. The signal does not go to zero between resonances due to the Fermi gas heating, since the highest intensity line is that due to 118μ. This apparent background is present at all gate voltages beyond about 8 volts.

References

1. Stern, F. and Howard, W.E., Phys. Rev. 163, 816 (1967).
2. Wheeler, R.G. and Goldberg, H.S., I.E.E.E. Trans. on Elec. Dev. ED-22, 1001 (1975).
3. Stern, F., Phys. Rev. Letters 30, 278 (1973).
4. Stern, F., CRC. Crit. Rev. Solid State Sci. 4, 499 (1974). A comprehensive theoretical review up to mid 1974.
5. Vinter, B., Phys. Rev. Letters 35, 598 (1975).
6. Ando, T., Phys. Rev. B, 13, 3468 (1976).
7. Kamgar, A., Kneschawrek, P., Dorda, G. and Koch, J.F., Phys. Rev. Lett. 32, 1251 (1974).
8. Allen, S.J. Jr., Tsui, D.C. and Vinter, B., to be published.
9. Döhler, G.H., Solid State Communications 18, 633 (1976).
10. Allen, S.J. Jr., Tsui, D.C. and DeRoser, R., Phys. Rev. Letters 35, 1359 (1975).
11. Ziman, J.M., Principles of the Theory of Solids, Cambridge Univ. Press (1964), pgs. 182-208.
12. ter Haar, D., Elements of Statistical Mechanics, Rinehart and Company, Inc. New York (1954), pgs. 235-239.
13. Nicholas, R.J., von Klitzing, K. and Stradling, R.A. To appear in Solid State Communications.

COHERENT ACOUSTIC BEAMS AT THz FREQUENCIES

F. Keilmann, Max-Planck-Institut für Festkörperforschung
7000 Stuttgart 80, Germany

Abstract

Experiments are presented of launching THz acoustic waves by converting photons of a high-power, optically-pumped FIR laser into isoenergetic phonons at the surface of suitable crystals, thus making possible ultrasonics in the frequency range of acoustic dispersion.

An extension of hypersound methods beyond the microwave frequency range seems very attractive for solid state physics, since it is at submillimeter frequencies that sound approaches its minimum possible wavelength, i.e. the interatomic distance in a solid. Investigation of velocity dispersion, surface reflection, spontaneous decay etc. of such short wavelength acoustic phonons are expected to reveal new information on Lattice structure and dynamics.

The extension of traditional acoustics to frequencies beyond 100 GHz has not been successful for at least three reasons: (i) due to the short sound wavelength, resonant transducers for coupling e.m. radiation and sound field are very hard to build, (ii) coherent detection gets very ineffective with severe wavefront distortion encountered at short wavelengths from crystal imperfections, thus leaving only incoherent detection, (iii) submillimeter light sources suitable for launching submillimeter-frequency sound waves did not exist.

It was only in 1975 that the Heidelberg group headed by O. Weis succeeded in a first experiment clearly demonstrating the feasability of Terahertz acoustics (1). They used a polished quartz crystal at low temperature which they illuminated with short pulses of HCN- and H_2O-laser radiation. Due to the piezoelectric effect, collimated THz sound is generated at the surface and propagates through the bulk of the crystal (2) much as the mechanical analog of a laser light beam. Due to the smallness of piezoelectric coupling, the intensity in the sound beam was calculated to be six orders of magnitude smaller than the exciting laser's intensity (3). Detection was by a superconducting tin bolometer evaporated on the opposite crystal face. The monochromaticity could be ascertained by a measurement of the sound velocity, whereas the collimation of the sound beam was checked by laterally displacing the generating site.

Subsequent work on THz acoustics has been concerned with increasing observability and time resolution of the sound signal, e.g. by using (4) high-power optically-pumped FIR lasers (5) or by suggesting optically resonant transducers (6). In our own approach (7) we have shown a way of how to make use of a high-power optically pumped FIR laser without having the disadvantage of a deteriorating effect encountered at high light intensities: under these conditions enough incoherent phonons are generated in the bulk of the quartz crystal by two-phonon absorption so that the coherent phonon beam is scattered by phonon-phonon interaction. This can be greatly avoided by totally reflecting the laser beam from the quartz surface. The light thus can not penetrate the bulk of the crystal, but enters far enough for effectively launching the coherent acoustic beam.

References

1) W. Grill and O. Weis, Excitation of Coherent and Incoherent Terahertz Phonon Pulses in Quartz Using Infrared Laser Radiation, Phys. Rev. Letters 35, 588-591, 1975.

2) E.H. Jacobsen, Sources of Sound in Piezoelectric Crystals, J. Acoust. Soc. Amer. 32, 949-953, 1960.

3) O. Weis , Surface Excitation of Hypersound in Piezoelectric Crystals by Plane Electromagnetic Waves, Z. Physik B21, 1-10, 1975.

4) W.E. Bron, Indiana University, private communication.

5) T.Y. Chang, Optically Pumped Submillimeter-Wave Sources, IEEE Trans. Microwave Theory and Techn., MTT - 22, 963-988, 1974.

6) R. Ulrich, Dielektrische Wellenleiter zur wirksamen Anregung kohärenter THz-Phononen, unpublished.

7) F. Keilmann, B.C. Lehr and W.Schwerzel, Evanescent Wave Coupling for Piezoelectric Excitation of Coherent THz Acoustic Phonons, Sol. State Comm. 18, 1465-1466, 1976.

FIR-ABSORPTION SPECTRA OF HIGH POLYMERS WITH DIFFERENT DEGREE OF CRYSTALLINITY

W. Frank
Abteilung Exp. Physik III
Universität Ulm
Oberer Eselsberg
D-7900 Ulm (Donau), Germany

The volumn fraction w^c of crystallized substance in a bulk polymer influences the shape as well as the intensities of the absorption spectrum. The spectra of poly-(ethyleneterephthalat), polyethylene and similar linear polymers are reported and discussed.

Poly-(ethylene) (PE)

Samples of different crystallinity, thermal treatment and orientation were investigated (fig. 1). The absorption spectra show a very strong band at 73 cm^{-1} at room temperature and a weak one near 108 cm^{-1} observed below 100 K. They are assigned to transversal lattice modes of the unit cell by Krimm et al. (1). A dichroism at oriented samples following from the band assignement was measured (Frank and Rabus (2)). The temperature dependence of the maximum absorption frequency of the 73 cm^{-1} band at linear PE has been investigated (fig. 2). The changes in frequency shift at 237 K and 100 K are discussed in terms of anisotropic thermal expansion of the unit cell. The Grueneisen constant of the vibration is calculated.

Poly-(ethyleneterephthalat) (PET)

The absorption spectra of partially crystallized PET show 4 relatively strong bands at 83, 104, 139 and 186 cm^{-1}. Their intensities (fig. 3) grow with increasing degree of crystallinity. From this it is concluded that the spectra are caused by elastic waves in the crystalline parts of the polymer. Attempts to interprete this spectral region by in-plane vibrations of the monomeric unit as well as by torsional vibrations of the single chain are discussed. A new model is proposed to explain the spectrum involving lateral coupling of torsional modes. Benzene-ring, carbonyl- and ethyl-group perform torsional vibrations around the c-axis as rotational axis. The dispersion relations of the model are computed using the torsional force constants as fitting parameters. The boundary frequencies at $\Delta\phi = 0$ as well as π were assigned to the absorption peaks and related to the measured frequencies with good agreement. Conclusions of the model proposed concerning the spectrum of amorphous substance are discussed. The spectra of other polymers containing benzene rings are discussed.

(1) Tasumi, M and S. Krimm, J. Chem. Phys. 46, 755 (1967)

(2) Frank, W. and G. Rabus, Colloid & Polymer Sci. 252, 1003 (1974)

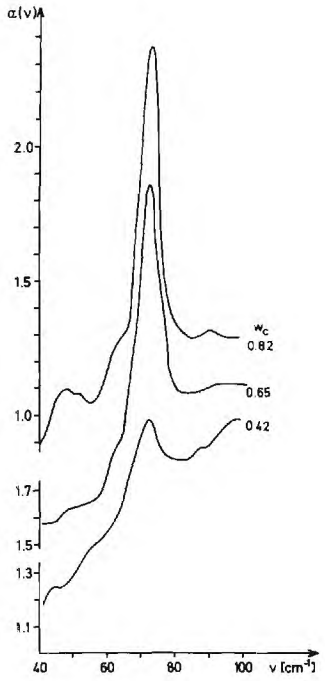

Fig. 1 FIR absorption spectra for PE samples with different degree of crystallinity w^c.

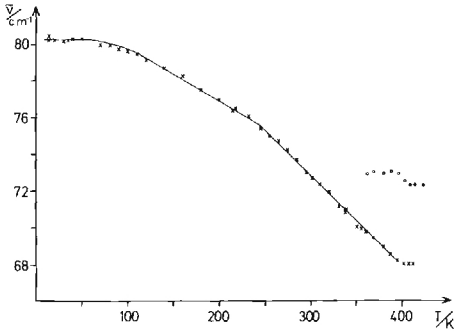

Fig. 2 The frequency shift of the band of fig. 1 as a fuction of temperature for linear PE (6011 L)

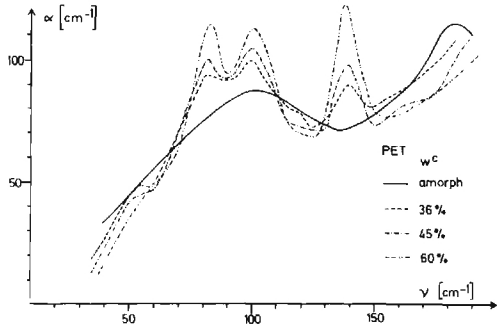

Fig.3 Absorption spectra of PET-samples, amorphous and partially crystallized.

INTERACTION OF MICROWAVE BIASED n-GaAs AND 337 μm RADIATION*

P.J. Epton, W.L. Wilson, Jr., and F.K. Tittel
Department of Electrical Engineering
Rice University
Houston, Texas

Abstract

n-GaAs cooled to 4.2°K is impact ionized with X-band microwave pulses. Fast rise-time modulation of 337 μm radiation is observed. The GaAs is less absorptive in the ionized state than in the un-ionized state.

The development of submillimeter devices has received considerable interest in recent years. In this paper, we describe details of a new type of GaAs impact ionization modulator for submillimeter radiation. High purity n-GaAs cooled to 4.2°K is well known as an extrinsic photoconductive detector of submillimeter radiation [1-3]. At bias fields above 5 V/cm, however, its response falls off due to impact ionization of the frozen out donors. In the present work, this breakdown is the basis for modulation of submillimeter radiation. Upon breakdown, there is an increase in the amount of light transmitted through the device. This effect is in contrast to the Ge absorption modulator reported previously [4].

The modulator, described elsewhere as a microwave-biased submillimeter detector [3], is a piece of high purity epitaxial n-GaAs grown on an insulating substrate. The epilayer is 100 μm thick, with donor and acceptor concentrations of $N_d=4.61\times10^{14}cm^{-3}$ and $2.45\times10^{14}cm^{-3}$, respectively. The device is placed within a microwave cavity immersed in liquid helium. Submillimeter radiation from a 337 μm HCN laser is incident on the modulator through a ½" stainless steel light pipe and dielectric cone condenser. After traveling through the modulator, the light passes through a polyethylene support and then out a hole in the bottom of the microwave cavity to a second piece of GaAs, used here as a DC-biased detector (see Figure 1.). A relatively low value load resistor is used to decrease the RC time constant of the detector, at the expense of responsivity. Microwave power from a pulsed klystron followed by a traveling-wave-tube amplifier is used to impact ionize the device. An adjustable coupling probe permits impedance matching of the modulator cavity to the microwave source at low microwave powers, where the resonant frequency is about 9.3 GHz. Above the .2 mW ionization threshold, microwave power is absorbed over a several hundred megahertz range centered around 9.8 GHz.

In operation, the cavity is tuned to match at a low microwave power level. The klystron is then set to an operating frequency in the avalanche region, typically f=9.8 GHz, and square wave modulated. The detector signal is measured with a lock-in amplifier. For absorbed microwave power up to about 10 times the ionization threshhold, there is no observable modulation signal. As the power continues to increase, a signal corresponding to an increase in the 337 μm radiation is observed. This signal goes through several maxima and minima within the range of the available microwave power. It is ultimately limited by the thickness of the GaAs epilayer, which in the unbiased state is still partially transparent. The risetime of the modulator is studied by using a pulse generator to modulate the klystron and a pulse amplifier and oscilloscope to measure the signal. A detector-limited risetime of less than 1 μs is observed. In addition, the pulse data indicate that heating of the GaAs has an effect on the modulation level. With a low duty cycle, the signal increases by a factor of four relative to that seen with a 50% duty cycle square wave.

The observed transmission increase is explained by the relative cross sections for shallow donor and free carrier submillimeter absorption. As shown by Stillman, et.al. [5], the shallow donor mechanism for 337 μm light involves a resonant 1s-2p transition between hydrogen-like impurity states. The free carrier absorption that dominates under avalanche conditions is a much weaker effect, so modulation appears as an increased transmission. Oscillations in the modulation level with microwave power can be explained in part by variations in the submillimeter propagation constant. The limit on peak amplitude for square wave modulation results from the partial thermal ionization of the donors in the unbiased state. Expected risetime

*Work supported by the National Science Foundation.

of the GaAs modulator should approach the 5 ns free carrier lifetime reported in reference 1, provided that the impact ionization and ionized impurity capture cross sections are equal, as proposed by Ryder, et.al. [6]. The experimentally observed 1 μs risetime is limited by the DC-biased GaAs detector.

References

1. Stillman, G.E., C.M. Wolfe, I. Melngailis, C.D. Parker, P.E. Tannenwald, & J.O. Dimmock, Appl. Phys. Lett. 13, 83 (68)

2. Bosomworth, D.R., R.S. Crandall, & R.E. Enstrom, Phys. Lett. 28A, 320 (68)

3. Crowley, J.D., W.L. Wilson, Jr., F.K. Tittel, & T.A. Rabson, Infared Phys. 16, 225 (76)

4. Melngailis, I., & P.E. Tannenwald, Proc I.E.E.E. 57, 806 (69)

5. Stillman, G.E., C.M. Wolfe, & J.O. Dimmock, Solid State Commun. 7, 921 (69)

6. Ryder, E.J., I.M. Ross, & D.A. Kleinman, Phys. Rev. 95, 1342 (54)

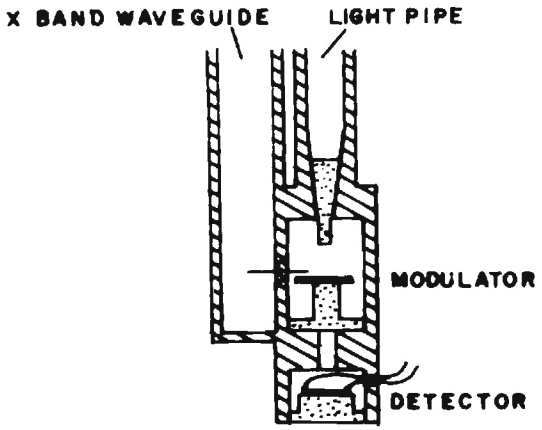

Figure 1. Detail of Modulator and Detector Assembly

INFLUENCE OF THE BOUNDARIES ON THE INFRARED SPECTRAL BEHAVIOUR OF LiF THIN FILMS AND KCl MICROCRYSTALS

R. Kälin and F. Kneubühl
Solid State Physics Laboratory, ETH, Hönggerberg
CH-8093 Zurich, Switzerland

ABSTRACT

The influence of the finite size of LiF and KCl crystals on the infrared spectrum was investigated by measuring the spectral thermal emissivity. A series of radiative modes were detected in thin layers and in microcrystals of various shapes.

The far infrared vibrational modes of LiF slabs and KCl microcrystals were determined by observation of the spectral radiative emission at temperatures of 250 C and 300 C . The emissivity was determined by comparing the sample radiation to that of a black body at the same temperature. This method is especially well suited for the determination of the angular dependence of radiative vibrational modes in thin films. Preliminary results of this work were reported at the Int. Conf. on Submm Waves and Their Applications, Atlanta 1974 [1] and are published to some extent [2]. A detailed treatment of this subject will be published in the future [3].

The infrared spectrum of thin films of ionic crystals is influenced by the boundary conditions. On both sides of the "Reststrahlenband" exist radiative emission modes. Their number and frequencies depend on the thickness of the films. The frequency position is also subject to the emission angle and the polarization direction. We measured the infrared emission spectrum of a series of LiF films with different thicknesses on the low frequency side of the "Reststrahlenband". The measured spectra were compared with the detailed free film theory by Fuchs and Kliewer [4]. The films were produced on a metallic substrate. Not all radiative modes existing in a free film are allowed in this case. The different boundary conditions produce a quenching of some of the free layer modes. The remaining modes coincide with a subset of solutions of the free slab of twofold thickness. A comparison of the experimental spectra of the films with the theoretical calculations shows a very good coincidence of the emission modes for both polarization directions over the whole angular range from 0° to 87° . All emission peaks can be assigned to definite theoretical radiative modes. The assumption of a constant damping in the dielectric function $\varepsilon(\omega)$ does not agree with the measured intensities. A calculation of a frequency dependent damping function from the experimental data results in a curve similar to that found by Klier and Genzel [5] on bulk crystals. Yet the values of the damping are considerably larger than in the bulk crystals. This is due to the fact that the samples are polycrystalline and the measuring temperature was rather high.

The infrared spectrum of alkali halide microcrystals depends on additional parameters, which play no rôle for macroscopic crystals. These parameters are the shape and the size of the microcrystals, the covering density on the sample surface and the spatial distribution of the microcrystals in the sample. Irregular distribution and mutual touching of the particles result in complicated scattering. Two of these parameters were investigated in some detail: The production of the cubic, octahedral and irregularly shaped crystals allowed a study of the influence of different shapes on the infrared spectrum. By varying the covering density of the cube-shaped crystals the influence of different covering densities was analysed. The experimental results can be partly explained by existing theories for spheres and cubes, yet there are additional structures in the experimental spectra, which cannot be explained by the present theories. All spectra of different crystal shapes show a dominant emission peak in the frequency domain of the "Reststrahlenband". The frequency of this peak is only weakly dependent on the crystal shape. This mode agrees with theoretical expectations and is explained as a surface polariton. Beside this dominant resonance there exists a secondary structure in all spectra. In the case of the cubes, a comparison with the recently developped theory by Fuchs [6] for irregularly shaped

crystals indicates, that at least one second emission peak can be assigned to a shape induced emission mode. A further identification of the experimental structure in the "Reststrahlenband" frequency region with theoretical shape induced radiative modes is doubtful, because the variation of the size and of the shape of the microcrystals and the forming of clusters cause a broadening and overlapping of the resonance peaks.

A rather complicated behaviour was detected near the frequency ω_{TO} of the transverse-optical phonon. KCl particles with a diameter of about 1 µm should not exhibit an emission mode at this frequency. On the contrary the actual spectra for cubes possess a resonance, the relative strength of which is a function of the covering density. A high covering density of the particles on the sample surface produces a marked peak at this frequency. Investigations with an electron microscope demonstrate that with a high covering density the particles tend to form clusters and chains. The limiting cases of these forms, the compact layer and the long cylinder, show an emission mode at this frequency. Therefore it seems possible that clusters and chains of microcrystals can induce an emission peak near ω_{TO} . The spectra of octahedral particles exhibit a pronounced peak also, at ω_{TO} even for rather small covering density. As the size of the octahedra is of the order of 10 µm, this peak can be explained by the theory for small spheres, which gives for intermediate particle diameters radiative bulk modes at this frequency. All spectra of KCl particles show an additional small emission peak near 200 cm^{-1} for which the theories of microcrystals give no explanation. However, single crystals also have peaks in this spectral region. These peaks are due to higher order phonon-photon interactions.

For discussions and suggestions we wish to thank Proff. Dr. R. Fuchs and K.L. Kliewer, Ames, Iowa, USA and Dr. H.P. Baltes, Zug, Switzerland.

This work was supported by the Schweizerischer Nationalfonds.

References:

[1] R. Kälin and F. Kneubühl: Int. Conf. on Submm Waves and Their Applications, 1974, Conference Digest, p. 191

[2] R. Kälin and F. Kneubühl: Sol. St. Comm. 15, 371 (1974)

R. Kälin and F. Kneubühl: Sol. St. Comm. 16, 405 (1975)

[3] to be published in Infrared Physics

[4] K.L. Kliewer and R. Fuchs: Phys. Rev. 150, 573 (1966)

R. Fuchs, K.L. Kliewer and W.J. Pardee: Phys. Rev. 150, 589 (1966)

[5] L. Genzel and M. Klier: Z. Physik 144, 25 (1956)

M. Klier: Z. Physik 150, 49 (1958)

[6] R. Fuchs: Phys. Rev. B 11, 1732 (1975)

R. Fuchs: Phys. Lett. 48 A, 353 (1974)

THE MEASUREMENT OF THE SURFACE RESISTIVITY OF EVAPORATED GOLD AT 890 GHz

R.J. Batt and G.D. Jones,
Department of Electrical and
Electronic Engineering,
Portsmouth Polytechnic,
Anglesea Road,
Portsmouth,
Hants, England.

D.J. Harris,
Department of Physics, Electronics
and Electrical Engineering,
U.W.I.S.T.,
Cardiff,
South Wales.

Abstract

A modified pyroelectric detector is used to measure the surface resistivity of evaporated gold at 890 GHz. The value of 0·65 Ω per square yields a ratio of measured-to-theoretical surface resistivity of approximately 2·2.

Introduction

The power absorbed by a conducting surface when it reflects an incident electromagnetic wave is largely determined by the surface resistivity of the reflector. The attenuation of a metal waveguide is determined also by the surface resistivity of the wall of the guide. However theoretical waveguide loss predictions using surface resistivity figures, which are derived from d.c. values of bulk resistivity, seriously underestimate the actual waveguide losses for frequencies greater than about 10 GHz.

This apparent anomaly in surface resistivity has been investigated by many workers [1] for various waveguide materials such as copper, gold, silver and brass in the microwave region, up to frequencies of about 200 GHz. The reported ratios of measured-to-theoretical loss of up to 2·5 imply similar variations of effective-to-theoretical surface resistivity. These variations appear to be dependent on a number of factors including frequency, surface condition and measurement uncertainty.

The reported loss measurements only indirectly determine absorbed power. They either require correction for other system losses e.g. coupling factor losses in cavity measurements, or they rely on the small difference between two relatively large measured quantities e.g. low loss transmission and reflection methods. A direct method avoiding these degradations is preferable. A direct measurement of absorbed power in evaporated gold films in the submillimetre region is reported here.

The Measurement Technique

The measurement of surface resistivity involves independent determinations of the incident radiation power P_i and the absorbed power P_a in the surface of the gold film.

The power absorbed in the surface results from the induced current and for low loss reflection this surface current may be assumed to be $J = 2 H_i$ where H_i is the incident magnetic field vector. The absorbed power density is then given by $P_a = J^2 R_s$ where R_s is the surface resistivity. The incident power $P_i = 120\pi H_i^2$ which gives a ratio for absorbed to incident powers of $\frac{P_a}{P_i} = \frac{R_s}{30\pi}$. Hence a value for the surface resistivity of the gold film may be deduced from measurement of the absorbed and incident powers. The incident power is measured using a thermopile and the absorbed power is determined using a modified pyroelectric detector.

The pyroelectric detector element has the gold film to be investigated, evaporated onto the front surface. Other modifications allow a low frequency current to be passed through the film and its heating effect to be compared to that of the absorbed power resulting from the incident chopped radiation. Thus the absorbed power is determined in terms of low frequency current and voltage measurements.

The Experimental Arrangement

The pyroelectric detector element described above has its normal front coating of nichrome overlaid with the evaporated gold to a thickness much greater than the skin depth at 890 GHz. The surface dimensions of the element are 4 x 2 mm, and a number of electrical contacts are made along each short edge for the voltage and current leads, as shown in Figure 1. A single contact is made to the back face and connected to an FET input amplifier. The low frequency heating circuit, shown in Figure 2, arranges for a virtual earth in the centre of the film.

This modified pyroelectric detector may now be used in the normal way to produce a pyroelectric voltage proportional to the absorbed power from the chopped incident radiation. This signal may then be compared with the heating effect of a low frequency current at half the chopping frequency.

Experimental Results

Some initial measurements at 890 GHz on evaporated gold films give an experimental value for surface resistivity of 0·65 Ω per square with a spread of ± 20%. This is to be compared with the theoretical surface resistivity of 0·29 Ω per square obtained from the normal expression $R_s = (\pi f \mu_r \mu_o \rho)^{\frac{1}{2}}$ where ρ is the d.c. bulk

resistivity, taken to be $2{\cdot}4 \times 10^{-8}$ ohm-metre for gold, f is frequency and μ_r is taken to be unity. This gives a ratio of measured-to-theoretical surface resistivity of approximately 2·2.

Improvements in instrumentation and experimental techniques now in progress will be reported and are expected to reduce the spread of the results. The technique should also be applicable for reflection loss measurements and power measurements from the short millimetric to optical wavelengths, and these possibilities are being investigated.

Acknowledgements

We wish to acknowledge the cooperation of the National Physical Laboratory and the Allen Clark Research Laboratory (Plessey Ltd.). This work was supported by the U.K. Science Research Council.

References

1. Benson, F.A., "Millimetre and Submillimetre Waves" (Iliffe, London, 1969), Chapter 14.

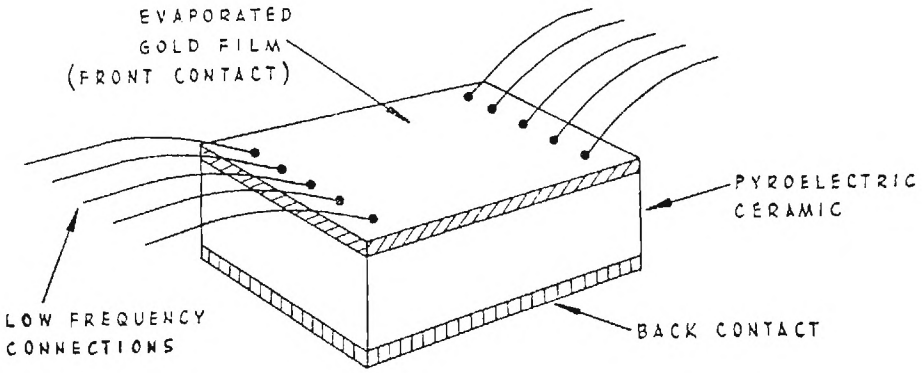

Figure 1 Modified pyroelectric detector element showing front contact connections

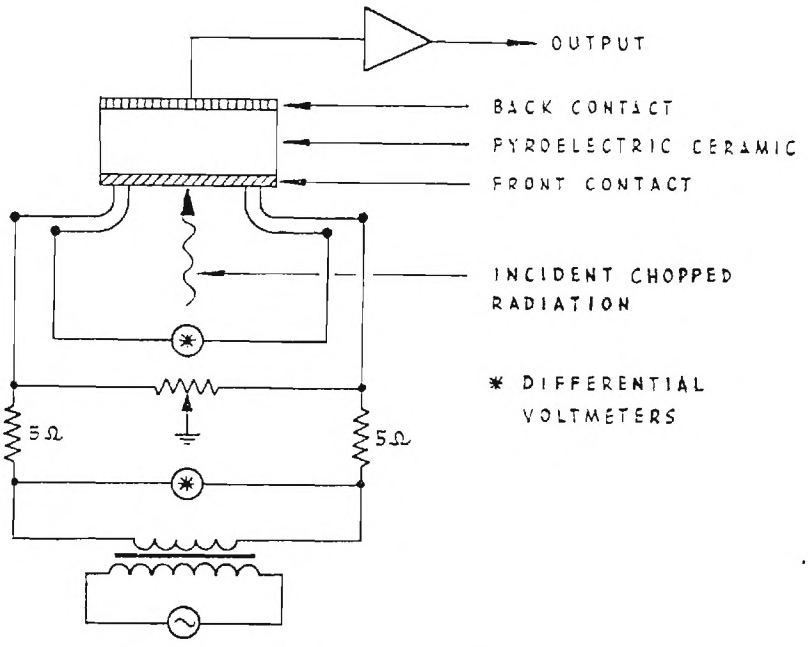

Figure 2 Circuit for low frequency heating of the evaporated gold film

THE TRANSVERSE OPTIC MODE ANHARMONIC SELF-ENERGY OF NaCℓ FROM MEASUREMENTS BY DISPERSIVE FOURIER TRANSFORM SPECTROSCOPY†

K.F. Pai, A. Rastogi, N.E. Tornberg, T.J. Parker* and R.P. Lowndes
Department of Physics
Northeastern University
Boston, Massachusetts 02115

The interatomic forces in a crystal are usually strongly dependent on the interatomic spacing and consequently the lattice potential energy for a crystal can generally be written as a power series in the displacements of the atoms from their equilibrium positions. If such an expansion is terminated at the quadratic terms, then this constitutes the so-called harmonic approximation. In the harmonic approximation the lattice vibrations are true normal modes such that if energy is channeled uniquely into any one lattice mode, then it will remain undissipated in that mode. The harmonic approximation would therefore predict, for instance, that the spectral profiles of lattice vibrations would be a set of undamped, temperature-independent resonances. These and other such predictions are, of course, in marked discord with experimental evidence. As a result, the anharmonic terms in a lattice potential must be considered if a full understanding of many of the physical properties of solids is to be achieved.

The inclusion of the anharmonic terms in a lattice potential has two main consequences. First, the phenomenon of thermal expansion is now allowed. Second, the anharmonicity allows interactions between the normal modes. The net effect of these interactions is to open up channels for the decay of phonons which lead to changes in the phonon energies together with the appearance of finite lifetimes for the phonons. The temperature dependence of each phonon energy in the Brillouin zone therefore arises in two separate ways from lattice anharmonicity. First, the thermal expansion arising from the anharmonicity creates a temperature-dependent shift of each phonon energy from the harmonic normal mode value. Second, the anharmonic interactions between phonons cause a further temperature-dependent shift for the phonon energies which can be distinguished from the effects of thermal strain because the former effect gives rise to a temperature dependence of the phonon self-energies that takes place even when the crystal is held under isochoric conditions.

The determination of these anharmonic self-energies has proved to be no easy matter on either theoretical or experimental grounds. Theoretical descriptions of anharmonic self-energies involve many-body thermodynamic Green's-function approaches, and quantitative theoretical estimates require complex calculations which need significant computational times. As a result, reports of such calculations have been somewhat limited and these have been confined to a few simple ionic compounds. Because of their complicated form and the need to separate out the effects of the thermal strain, experimental measurements do not lead straightforwardly to determinations of the anharmonic self-energies. Lowndes and Martin [1] have suggested an experimental approach using high-pressure and variable-temperature measurements to overcome these problems and have utilized it via dielectric-constant measurements to make first estimates of the low-frequency anharmonic self-energies of the $q \approx 0$ transverse-optic phonons in simple ionic solids. In a later series of experiments Lowndes [2,3] and Lowndes and Rastogi [4] have used a similar approach to determine first estimates of the anharmonic self-energies of the $q \approx 0$ transverse optic phonons in simple ionic solids at the transverse optic phonon frequency. But the anharmonic self-energies are frequency dependent and their full frequency dependence needs to be determined in order to more fully test current anharmonic theories. Although the procedure outlined by Lowndes and Martin [1] lends itself to such a measurement the technical difficulties increase significantly for measurements at other than isolated frequencies. The main difficulties have been the need to accurately determine the complex dielectric response throughout the region of the far infrared dispersion and to separate out the thermal strain contribution to the dielectric response. Dispersive Fourier transform spectroscopy [5] allows precise measurements of the dielectric response but, until recently, such measurements were confined to room temperatures because of the difficulty of accurately measuring the phase spectrum over a wide temperature range. Two solutions to this problem have recently been described [6-8]; in the method of Parker and Chambers [7,8], which has been used in the present work, part of the sample surface, suitably metallized, is used as a convenient phase reference surface. A number of authors have used dispersive Fourier transform spectroscopy [8-11] to obtain preliminary estimates of the real and imaginary parts of the complex anharmonic self-energies of transverse optic modes in ionic crystals but in all cases the measurements of the real part of the anharmonic self-energies are not well determined because the thermal strain contribution has not been separated out. The thermal strain contribution is most directly determined via high pressure spectroscopic studies on specific phonons but the technical problems associated with maintaining reasonable signal-to-noise levels in passing radiation from the comparatively weak far infrared or neutron sources through a high pressure cell have proved difficult to overcome. Nevertheless, Lowndes and Rastogi [4] have recently overcome these problems and have reported

on the thermal strain contributions to the anharmonic self-energies of the transverse optic mode in a number of ionic materials.

In this paper we report measurements of the complex far infrared dielectric response associated with the $q \approx 0$ transverse optic mode in NaCℓ for temperatures in the range 100-300 K determined using dispersive Fourier transform spectroscopy. We use these results together with the results of Lowndes and Rastogi to determine first estimates of the full frequency dependence of the anharmonic self-energy of this mode and show that these results are in reasonable agreement with theoretical calculations.

Acknowledgment

We wish to thank Professor E.H. Bellamy for permission to borrow the dispersive Fourier transform spectrometer from Westfield College, University of London, and we would also like to thank Dr. W.G. Chambers for providing the Fourier transform computer programs.

[+]Research supported by a grant from the Army Research Office and by a grant from the Research Corporation.

[*]On leave of absence from Westfield College, University of London during 1975-76.

[1] R.P. Lowndes and D.H. Martin, Proc. Roy. Soc. A316, 351 (1970).
[2] R.P. Lowndes, Phys. Rev. Lett. 27, 1134 (1971).
[3] R.P. Lowndes, Phys. Rev. B6, 1490 (1972).
[4] R.P. Lowndes and A. Rastogi, Phys. Rev. (in press 1976).
[5] J. Chamberlain, J.E. Gibbs and H.A. Gebbie, Nature 198, 874 (1963).
[6] J. Gast and L. Genzel, Opt. Commun. 8, 26 (1973).
[7] T.J. Parker and W.G. Chambers, I.E.E.E. Trans. MTT-22, 1032 (1974).
[8] T.J. Parker and W.G. Chambers, Infrared Phys. 16, 349 (1976).
[9] E.E. Bell, Infrared Phys. 6, 57 (1966).
[10] E.E. Russell and E.E. Bell, Infrared Phys. 6, 75 (1966).
[11] K.W. Johnson and E.E. Bell, Phys. Rev. 187, 1044 (1969).

GAMMA IRRADIATION INDUCED CHANGES IN THE FAR INFARED RESTSTRAHLEN SPECTRUM OF SOME ALKALI HALIDES

T. L. Rome* and N. Ginsburg
Department of Physics
Syracuse University
Syracuse, N.Y. 13210

This study investigates the modifications in the mid-infrared transmission and far infrared reflectivity of polar crystals that have been colored by ionizing radiation.

Using a Beckman IR-7 spectrophotometer the post irradiation transmission in the normally transparent region was compared to that prior to the irradiation. A large variety of crystals were investigated. Gamma ray dosages from 3.6×10^6 R. to 8.1×10^8 R. were used at a typical rate of 5×10^5 R/hr. Some crystals were also exposed to X-rays from a 50kV. 20 ma. tungsten source for times up to 23 hr. No modification in transmission was found in any of the crystals. In particular, we did not reproduce the strong absorption in LiF reported by Akhvlediani and Politov [1]. This was so even though our doses were equal to or greater than theirs and our crystals much thicker than theirs.

Three effects were found in the reflectivity spectra. The irradiation produced a substantial decrease in the reflectivity throughout the main reststrahlen band and in its short wavelength side band. Secondly, the reflection peaks and the band itself manifested a slight radiation induced shift to shorter wavelength in a number of the crystals. Third, both the preceding effects decayed with time.

The reduction in reflectivity is associated with a decrease in phonon lifetime. This latter is attributable to the scattering caused by the reduction in translational symmetry arising from the interstitial clusters [2] created by the coloring process.

The small shifts to shorter wavelength were just within the resolution of our spectrometer and were manifested by a number of crystals. No such shift was observed for NaCl. We connect this with two other characteristics of NaCl: the stability of the F^- center at room temperature [3] and the short-lived exponential rise in F-center absorption immediately after irradiation is terminated [4]. From this we speculatively attribute the wavelength shifts to the influence of F-center aggregates.

Some measurements were made on the decay of the reflectivity decrease with time. The half life of this decay was calculated for some crystals on the assumption that the decay was a simple exponential one. Our half lives for NaCl and KCl correlate nicely with measurements of post irradiation decay of F-center absorption in the visible region [4,5].

The reflectivity reductions in NaI and NaI:Tl were also compared. Our samples showed that the thallium doping significantly decreased the radiation induced reflectivity reduction and also appeared to stabilize it. The former is consistent with thallium's short circuiting the excitonic creation of color centers by its own fluorescence [6,7].

The above far infrared effects decay rather quickly while the crystal maintains a marked long term visible coloring. This suggests that the lattice conditions co-existing with the long term coloring are not significantly different from those of an uncolored crystal in thermal equilibrium. Hence, the long term coloring may be associated with lattice defects that exist in or close to thermal equilibrium. Decaying phonon effects associated with the short term coloring indicate that the lattice condition associated with the short term coloring is a non-equilibrium one and hence different from that accompanying the long term coloring.

*present address: 100 W. 92nd St., New York, N. Y. 10025

References

1. Z. G. Akhvlediani and N. G. Politov, Optics and Spectr. 25, 86, 1968.

2. L. W. Hobbs, A. E. Hughes and D. Pooley, Proc. R. Soc. Lond. A332, 167, 1973.

3. E. Sonder and W. A. Sibley, in Point Defects in Solids (J. H. Crawford and L. M. Slifkin, eds.), vol. 1, General and Ionic Crystals, Plenum, New York, 1972, p. 238.

4. P. L. Mattern, K. Lengweiler, and P. W. Levy, Solid State Commun. 9, 935, 1971.

5. P. W. Levy, P. L. Mattern, and K. Lengweiler, Phys. Rev. Lett. 24, 13, 1970.

6. P. H. Yuster and C. J. Delbecq, J. Chem. Phys. 21, 892, 1953.

7. W. J. Van Sciver, Phys. Rev. 120, 1193, 1960.

PRODUCTION OF MEGAWATT SUBMILLIMETER PULSES BY STIMULATED MAGNETO-RESONANT RAMAN SCATTERING

V. L. Granatstein, S. P. Schlesinger,* M. Herndon, and R. K. Parker
Naval Research Laboratory
Washington, D. C. 20375

J. A. Pasour
North Carolina State University
Raleigh, North Carolina 27607

Introduction

In previous experiments with an intense, relativistic, electron beam in an external magnetic field, [1] negative mass instability lead to coherent, electromagnetic radiation ('cyclotron maser'). Large radiated power levels were produced at wavelengths of several centimeters corresponding to the fundamental cyclotron frequency, and also at mm wavelengths corresponding to harmonics. However, the process was not expected to result in coherent submillimeter radiation; the largest harmonic number at which the cyclotron maser process produces coherent radiation is predicted [2] to be $n = W_\perp/\Delta W_\perp \leq 10$ for an intense beam (where $\Delta W_\perp/W_\perp$ is the fractional spread in electron transverse energy). Nevertheless, in experiments employing a cyclotron maser geometry strong submillimeter radiation was observed [3].

The explanation offered was that centimeter wavelength radiation produced by the cyclotron maser mechanism was spuriously reflected back onto the electron beam; it then interacted with the beam in such a way as to produce a scattered wave upshifted in frequency to submillimeter wavelengths via the Doppler effect.

A scattering mechanism which was calculated to be sufficiently strong was magneto-resonant Raman scattering [4]. In this process, a powerful pump wave at frequency ω_o is scattered into both a plasma oscillation of the electron beam at the plasma frequency ω_p, and a backscattered electromagnetic wave at a frequency

$$\omega_s = \gamma_{oz}(1 + \beta_o)\left[\gamma_{oz}(1 + v_o/v_{ph})\omega_o - \omega_p\right]$$

(where β_o is the axial beam velocity,

$$\gamma_{oz} = (1 - \beta_o^2)^{-1/2}$$

and v_{ph} is the axial phase velocity of the counterstreaming incident wave). It is easily verified for small ω_p and for an easily achievable value of $\gamma_{oz} = 4$ that $30 \leq \omega_s/\omega_o \leq 60$, and a 2 cm incident wave would yield a scattered submillimeter wave.

We are in the process of carrying out an experiment aimed at testing the above model and maximizing the submillimeter radiation.

Experiment

The experimental arrangement is shown in Fig. 1. A 60 nanosecond, 2 megavolt, voltage pulse is applied to a cold, field-immersed, cathode. A resultant 30 kA, annular electron beam is injected axially into an evacuated drift tube along the field lines of the externally applied magnetic field. The beam passes through a region where the magnetic field is periodically rippled along the axis and this converts a large fraction of the electron streaming energy into motion transverse to the axis. The electrons with large transverse energy then enter a homogeneous field region, L_1, where a negative mass instability occurs and transfers the electron transverse energy into electromagnetic radiation that attains a peak value of several hundred megawatts at $\omega_o/2\pi = 14$ GHz [3]. This 2 cm radiation propagates along the drift tube into a conical section where it is reflected from a brass plate that terminates the cone. The reflected wave backstreams up the drift tube where it can interact again with the electron beam. The interaction which will produce a scattered wave at the highest frequency takes place in region L_2 where the axial component of electron velocity is largest.

The submillimeter scattered wave is monitored through a series of tubes passed through the brass plate. The tubes have an i.d. = 1.1 cm and are displaced radially by 3.8 cm. By measuring the submillimeter power in each tube a radial profile can be deduced, and the total submillimeter radiation striking the brass plate can then be calculated. Each tube passes the radiation through a wave filter [5] with passband 390-540 μm and into a pyroelectric detector having a sensitivity of 0.15 mV/W and a rise time of 5 ns.

Results

Total radiation striking the brass plate in the 390-540 μm passband was found to be ~ 1 megawatt when the applied magnetic field was adjusted to 13 kG and when the position of the magnetic ripple structure was optimized. To verify that the radiation was in the designated passband, the reflector surface in the submillimeter output line was covered with absorber overlaid with wire screens of various mesh constant ϵ. It is expected that radiation with wavelength

$$\lambda \geq \epsilon(\sin i + 1)$$

(where the angle of incidence $i = 45^o$) will be well reflected, while shorter wavelength radiation will be poorly reflected. The results of this wavelength verification is shown in Fig. 2

where power to the pyroelectric detector is plotted vs ϵ for the various meshes. A break in the data occurs when $\epsilon \approx 250$ μm indicating that $\lambda \approx 400$ μm.

Dependence of the submillimeter radiation on the position of the ripple structure was studied. As the ripple structure was moved downstream from the cathode, region L_1, in which the cyclotron maser process operates, was shortened, while simultaneously lengthening the scattering, region L_2. Results are shown in Fig. 3 where the total power striking the brass plate in the 390-540 μm passband is plotted vs L_2. We do not yet understand the detailed structure of the curve in Fig. 3. However, the general tendency of the power to increase as L_2 is made longer adds plausibility to the model of submillimeter wave production by stimulated scattering from fast streaming electrons in the L_2 region.

References

1. e.g. V. L. Granatstein, P. Sprangle, R. K. Parker, and M. Herndon, J. Appl. Phys. 46, 2021 (1975).

2. G. Bekefi, J. L. Hirshfield, S. C. Brown, Phys. Rev. 122, 1037 (1961).

3. V. L. Granatstein, M. Herndon, R. K. Parker, and S. P. Schlesinger, Trans. IEEE, MTT-22 (1974).

4. P. Sprangle and V. L. Granatstein, Appl. Phys. Lett. 25, 377 (1974); also P. Sprangle, V. L. Granatstein, and L. Baker Phys. Rev. A 12, 1697 (1975).

5. S. P. Varma and K. D. Moller, Appl. Opt. 8, 2151 (1969).

* Also Columbia University.

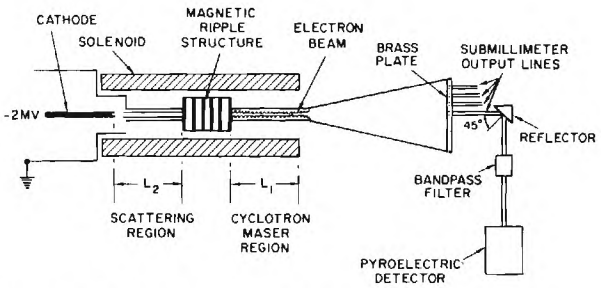

Figure 1. Experimental arrangement. (Annular electron beam has o.d. = 3.6 cm, i.d. = 3.2 cm)

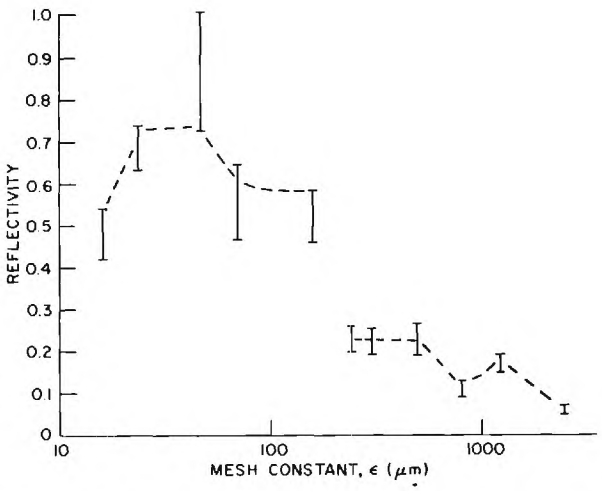

Figure 2. Power measured by pyroelectric detector vs mesh constant of metal screens reflecting the radiation.

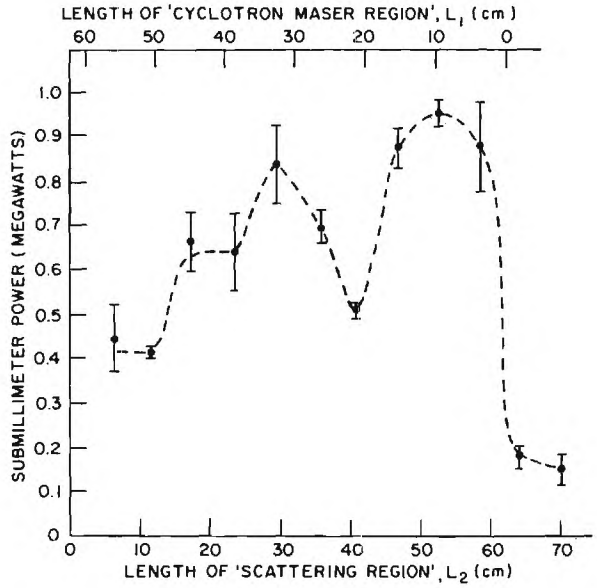

Figure 3. Total radiated power in the 390-540 μm passband vs length of 'Scattering' region.

STIMULATED COLLECTIVE SCATTERING FROM A MAGNETIZED RELATIVISTIC ELECTRON BEAM

P. Sprangle
Naval Research Laboratory, Washington, D. C. 20375

and

A. T. Drobot
Science Applications Inc., McLean, Virginia 22101

Abstract

Stimulated scattering of electromagnetic radiation off a magnetized relativistic electron beam is shown to be effective as a frequency conversion mechanism. Enhanced scattering results if the pump frequency is approximately equal to the electron's cyclotron frequency.

Introduction

It has been recognized that intense submillimeter radiation can be produced by scattering electromagnetic radiation off an intense relativistic electron beam. [1-3] When the characteristic Debye length in the beam is much shorter than the wavelength of the scattered radiation then the process of scattering is dominated by collective plasma effects. In such cases the incident wave scatters off plasmons instead of individual electrons. In the presence of an external magnetic field the growth rates for collective scattering can be greatly enhanced by cyclotron resonance effects.

In addition to scattering incident electromagnetic radiation efficiently a relativistic electron beam also upshifts the frequency of the reflected waves. This is the result of the relativistic Doppler effect and can result in large frequency conversion factors. For highly relativistic beams with $\gamma \gg 1$, where $\gamma = [1-v_o^2/c^2]^{-\frac{1}{2}}$, an incident wave with frequency ω_o will produce a scattered wave with $\omega_s = \omega_o 4\gamma^2$. With currently available electron beams as enhancement factor greater than 100 can be achieved. This scattering process can be used to construct tunable submillimeter microwave sources by selecting either the beam energy or the frequency of the incident radiation.

The theory of stimulated scattering including relativistic and magnetic effects has previously been done for cold beams. [4-5] We have extended the treatment to include finite beam temperature. Using the Vlasov equation we have derived the dispersion relation for the scattering of a right-circularly polarized electromagnetic pump wave off an intense magnetized electron beam.

The Frequency Upshift

The frequency upshift which results when an electromagnetic wave is scattered by a beam of electrons may be appreciated from the following one dimensional configuration. In the laboratory frame one considers an electromatnetic pump wave of frequency ω_o and wave number k_o propagating antiparallel to a beam of electrons travelling with a velocity v_o. Considering just the back scattered wave (ω_s, k_s) and performing the calculation in the beam frame, the pump wave has a frequency and wave number;

$$\omega_o' = \gamma\,(\omega_o + v_o k_o)\,,$$

$$k_o' = \gamma\,(k_o + v_o \omega_o/c^2).$$

The scattered wave then has frequency and wave number $(\omega_s', k_s') = (\omega_o', -k_o')$. When this is recalculated in the laboratory frame using the Lorentz transformation

$$\omega_s = \gamma^2 \omega_o \left[1 + 2\, v_o \frac{k_o}{\omega_o} + \frac{v_o^2}{c^2}\right].$$

If the incident wave is close to luminous, $k_o c \sim \omega_o$, and the beam highly relativistic, then

$$\omega_s \cong 4\,\gamma_o^2\,\omega_o$$

is the resulting scattered frequency. The additional factor that is important in this interaction is that the energy in the scattered wave is also enhanced by the conversion factor $4\gamma^2$. This can be surmized from the conservation of action; $W_o/\omega_o = W_s/\omega_s$ where W_o and W_s are the respective energies of the incident and scattered waves.

The upshift as derived would apply to reflection of radiation from a perfect mirror. In the case of a magnetized electron beam the scattered radiation results from a three-wave process. If the incident electromagnetic pump scatters off plasma oscillations then it is possible to prove that the frequency of the scattered wave is

$$\omega_s = \gamma_o^2\,\left(1+\frac{v_o}{c}\right)\left[\left(1+\frac{v_o k_o}{\omega_o}\right) - \frac{\omega_p}{\omega_o \gamma}\right]\omega_o$$

where ω_p is the plasma frequency. Again, if the pump wave (ω_o, k_o) is close to luminous and $\omega_p/\omega_o\,\gamma \ll 1$ then for a highly relativistic beam the perfect mirror result is approached. In this collective process however, there is a further restraint imposed. The scattered radiation must satisfy the linear dispersion relation and the two conditions

$$\omega_s = \omega_o \pm \omega_p$$

$$k_s = k_o \pm k_p$$

where k_p is the wave length of the plasma oscillations. It is possible to achieve this situation in the case of a magnetized plasma as indicated in Fig. 1. The Figure shows the scattering of a RHCP pump wave in the beam frame. The super luminous RHCP pump wave decays into a plasma oscillation and into a LHCP cyclotron mode which would have the upshifted frequency in the laboratory frame. The pump wave can also undergo

forward scattering which would produce a wave with a down shift in frequency.

The Dispersion Relation

In approaching this problem from the Kinetic Vlasov equation there are in the least two options. The first is to determine the particle orbits in the presence of the incident pump wave, construct an equilibrium and then find the first order perturbations to the distribution function in terms of the scattered fields. In the relativistic case with the inclusion of a guide magnetic field the particle orbits are sufficiently complicated that it becomes difficult to evaluate the integrals in the Laplace transform over the time variable. A second approach, that we have used here, is to consider both the pump wave and the scattered waves as perturbing quantities. The perturbed distribution function is then determined to second order about a simple equilibrium where the beam electrons only execute drift and gyro motion. In the resulting equations we recognize that the pump amplitude is a large quantity compared to the scattered field amplitudes and so terms of second order in the scattered field amplitudes are neglected. This results in a set of linear coupled equations for the scattered field amplitudes from which the dispersion relation can easily be obtained.

For a pump wave with frequency ω_o, wave number k_o and amplitude E_o the pump dispersion relation that must be satisfied is $T^{\pm}(\omega_o,k_o) = \frac{c^2k_o^2}{\omega_o^2}$ where

$$T^{\pm}(\omega,k) = 1 - \frac{\omega_b^2}{\omega^2}\int_{-\infty}^{\infty} du\, \frac{f_o(u)\psi(k,\omega)}{\gamma\Lambda^{\pm}(k,\omega)},$$

$$\psi(k,\omega) = \omega - cku/\gamma,$$

$$\Lambda^{\pm}(k,\omega) = \psi(k,\omega) \pm \Omega/\gamma,$$

ω_b is the beam plasma frequency, $\Omega = |e|B_o/mc$ the cyclotron frequency, $u = v_z\gamma$, and $f_o(u)$ is the beam distribution function. Denoting the longitudinal plasma oscillations with $_{//}$'s and the scattered electromagnetic waves with $_{\perp}$'s we find that the coupled equations for the pump wave decay products are:

$$\epsilon(k_{//},\omega_{//})\tilde{E}_z(k_{//},\omega_{//}) = \frac{i}{2}M^{\pm}\tilde{E}_s^{\pm}(k_{\perp},\omega_{\perp})$$

$$\left[T^{\pm}(k_{\perp},\omega_{\perp}) - \frac{k_{\perp}^2c^2}{\omega_{\perp}^2}\right]\tilde{E}_s^{\pm}(k_{\perp},\omega_{\perp}) = -iM^{\pm}\tilde{E}_s(k_{//},\omega_{//})$$

where $k_{//} = k_{\perp} \pm k_o$, $\omega_{//} = \omega_{\perp} \pm \omega_o$,

$$\epsilon(k_{//},\omega_{//}) = 1 - \omega_b^2\int \frac{du f_o(u)}{\gamma^3\psi_{//}^2},$$

and

$$M^{\pm} = \frac{\omega_b^2}{\omega_{\perp}\omega_o}\,\frac{|e|E_o}{mc}\,\frac{du}{\gamma^3}\int\frac{f_o(u)}{\Lambda_{\perp}^{\pm}}$$

$$\times\left\{\frac{ck_{\perp}\omega_o - \omega_{\perp}k_oc}{\gamma\psi_{//}^2} \pm \frac{(u\omega_{\perp}-\gamma k_{\perp}c)\psi_o}{\psi_{//}\Lambda_o^-}\right\}$$

We have so far examined these equations in the limit that $f_o(u) = \delta(\gamma-\gamma_o)$ and have recovered the cold beam dispersion relation of reference [5].

References

[1] R. H. Pantell, G. Soncini, and H. E. Puthoff, IEEE J. Quantum Electron. QE-4, 905 (1968).

[2] V. P. Sukhatme and P. E. Wolf, J. Appl. Phys. 44, 2331 (1973).

[3] V. P. Sukhatme and P. E. Wolf. IEEE J. Quantum Electron. QE-10, 870 (1974).

[4] P. Sprangle and V. L. Granatstein, Appl. Phys. Lett. 25, 7 (1974).

[5] P. Sprangle, V. L. Granatstein and L. Baker Phys. Rev. A 12, 4 (1975).

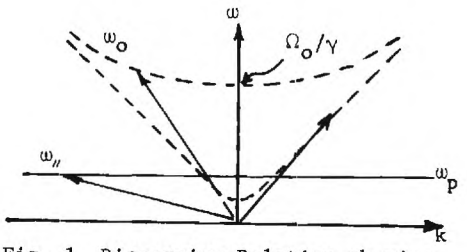

Fig. 1 Dispersion Relation showing decay of a pump wave in the beam frame.

RESULTS OF NUMERICAL SIMULATION OF SUB-MILLIMETER RADIATION FROM RELATIVISTIC ELECTRON BEAMS

A. T. Drobot
Science Applications Inc.
McLean, Virginia 22101

Introduction

We have recently concentrated our theoretical effort on two methods of producing submillimeter radiation with intense relativistic electron beams. The cyclotron maser instability and the magneto-resonant scattering of electromagnetic radiation by an electron beam both appear to be viable mechanisms for the generation of submillimeter radiation. The linear theories of the two instabilities have been derived and analyzed [1-4] but to answer the natural question of how efficient the two mechanisms are one has to develop an understanding of the nonlinear behavior. The methods of computer simulation developed for studying plasma phenomena are particularly useful for an analysis of the nonlinear development of the two instabilities we are concerned with.

As part of the work on the nonlinear theory of the cyclotron maser instability P. Sprangle and this author have run a large number of single wave simulations which have lead to an understanding of the nonlinear saturation mechanisms. The computer work also included a parametric study of the cyclotron maser instability which indicates the theoretical efficiency of that device can be greater than $\sim 60\%$. [4]

In the case of magneto-resonant scattering we have completed only a limited number of runs. These snow recovery of the linear results and saturation by mechanisms that we have not fully explored. A description of these runs is included.

Numerical Approach

In the case of the cyclotron maser the solution of the field equations can be approximated by a single wave. The amplitude and phase of the wave can in principle be found from Maxwell's equations where the current sources are determined by the electron dynamics which in turn depend on the fields. There seems to be no practical analytic way of attacking this highly nonlinear problem. From a computational point of view the problem is greatly reduced because both the field equations and the particle orbits can be integrated numerically. In practice it is not necessary to follow the orbits of all the particles in the electron beam, but only a representative number of test particles. We have found that 50-100 particles is a sufficient number. A computer program for this problem was written using a fourth order integration scheme and was vectorized to run on the Naval Research Laboratory's ASC-7 computer. It was possible to conduct a run for a single case using less than a minute of computer time.

Simulations of the magneto-resonant scattering were done with a particle in cell code called RECRAD. Several text books now exist detailing this approach and so we shall include just a brief summary. [5]. In finding the interaction of electrically charged particles where the dynamics are determined by long range forces rather than Coulomb collisions the tedious and extremely expensive method of finding the forces at each particle's position by summing contributions from all the other particle positions can be circumvented. In the space of interest a grid is established on which the Maxwell equations are computed in difference form. If the charge and current densities are known on the grid then the field equations on the grid can be integrated in time. The particle contributions to the densities can be computed from their positions and the positions then advanced in difference form by following the equations of motion and using fields interpolated from the grid. This permits fast and accurate computation of the interaction by integrating the fields on the grid and using the results to simultaneously follow the particle trajectories. A computer program of this type is run with typically 10,000 particles in a one dimensional problem and with an integration step per particle taking ~ 50 μsec of computer time. A run may consist of several thousand timesteps.

The Cyclotron Maser

In the single wave simulations we followed the evolution of test particles in the velocity phase space $(v_\perp, \varphi)$, where, using the notation of reference [4]

$$v_x = v_\perp \cos(\varphi),$$

$$v_y = v_\perp \sin(\varphi).$$

We found that at saturation there could be two configurations of particles in the velocity phase space. The interpretation of this is that there are two saturation mechanisms with the one actually occurring determined by initial beam conditions.

When the perpendicular beam velocity is close to the critical value for onset of the instability then saturation occurs by free energy depletion. The phase space configuration for this is shown in Fig. 1(a). When the initial beam energy is well above the critical value then saturation is caused by particle trapping in velocity phase space as shown in Fig. 1(b). The trapping dynamics can be related to a simple constant of the motion fully detailed in reference [4].

From the parametric study of the cyclotron maser instability we have found that high efficiencies can be achieved. The results are presented in Fig. 2 where the efficiency in the beam frame is shown as a function of perpendicular energy for various beam densities. We note, that even though the cyclotron maser instability is relativistic in origin, the highest efficiencies occur at moderate perpendicular energies.

Magneto-Resonant Scattering

The initial simulation of this problem was done in one dimension with a constant amplitude pump wave and zero wave number, $k_o' = o$, as viewed in the beam frame [6]. In the early stages of the instability the scattered electromagnetic and plasma waves grew with the linear growth rate and reproduced the spectral dependence predicted by linear theory. The parameters for this run were; $\omega_o'/c = 4.657$ cm^{-1} as the pump frequency in the beam frame, $\Omega_o/c = 4.0$ cm^{-1}, $\omega_p/c = 1.75$ cm^{-1} and the pump amplitude was chosen to give the beam electrons on oscillation velocity, $Vos/c = 0.2$. The simulation was run with 8192 test particles. The theoretically predicted growth rate was $\Gamma/c = 1.3$ cm^{-1} while the simulation yielded $\Gamma/c \cong 1.2$ cm^{-1}. The instability saturated when the energy in the scattered waves was 2-3 times the pump energy. At saturation the beam electrons exhibited both trapping in the phase space (x,v_x), where x would have been the direction of the beam in the laboratory frame, and thermalization in the perpendicular oscillation velocity. From these results it was difficult to pinpoint the exact reason for saturation.

A finite amplitude pump simulation, where pump depletion was included self-consistently, was also run. In this run the beam was allowed to have a finite drift velocity corresponding to a case where $\gamma_o = 2$, the pump wave was chosen to be at cutoff with $k_o' = o$, $\omega_o'/c = 1.515$ cm^{-1}. The pump amplitude was selected to give an oscillation velocity $Vos/c = 0.2$ while $\omega_p/c = 1.25$ cm^{-1} and $\Omega_o/c = 2.0$ cm^{-1}. In this particular case the interaction was not quite at the cyclotron resonance thereby reducing the growth rate. Unfortunately for a case such as this the pump wave decays into a broad spectrum that ranges in wave number from zero to $\sim 2\gamma_o^2\,\omega_o$. This was shown by the simulation with the linear growth rates again corresponding to those of linear theory. At saturation 8% of the beam energy was converted to electromagnetic radiation. It appears that the reason for saturation in this case was thermalization of the perpendicular oscillation velocity.

Before a complete picture of the nonlinear behavior of magneto-resonant scattering is achieved more simulations coupled with analytic work need be done. The parameter space for these instabilities is large and only a small piece of that has been examined.

ACKNOWLEDGMENTS

I would like to thank Dr. P. Sprangle for his invaluable contribution to this work and Dr. Roswell Lee for his involvement in the magneto-resonant scattering simulations. This work was supported by the Office of Naval Research.

References

1. P. Sprangle and V. L. Granatstein, Appl. Phys. Lett. 25, 7 (1974).
2. P. Sprangle, V. L. Granatstein and L. Baker, Phys. Rev. A 12, 4 (1975).
3. E. Ott and W. M. Manheimer, IEEE Trans. Plasma SC. Vol. PS-3, 1 (1975).
4. P. Sprangle and A. T. Drobot, to be published. See also these proceedings.
5. Vol. 9 and Vol. 16, Methods of Computational Physics, Academic Press. Fourth Conference on Numerical Simulation of Plasmas, Naval Research Laboratory, Washington, D.C., 1970.
6. Roswell Lee, P. Sprangle and V. L. Granatstein, Bull. Am. Phys. Soc. 20, 584 (1975).

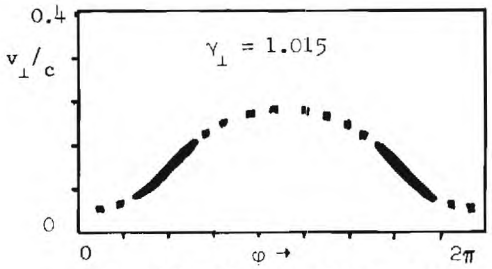

Fig. 1(a) Velocity phase space at saturation for energy depletion.

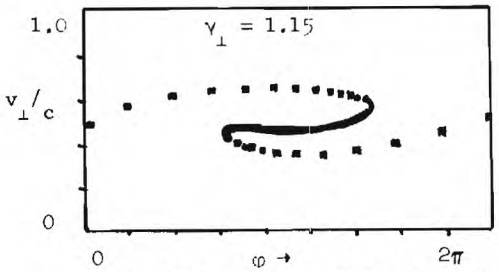

Fig. 1(b) Velocity phase space for saturation by trapping.

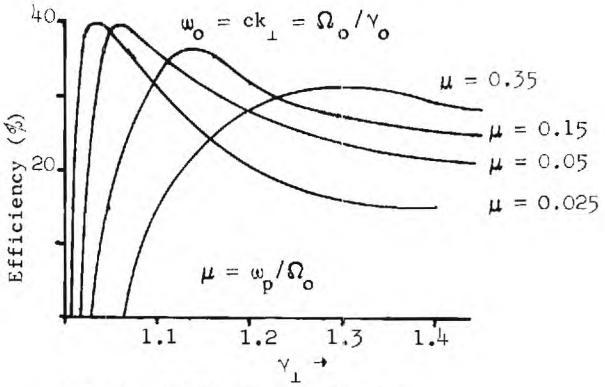

Fig. 2. Efficiencies for the cyclotron maser.

SUBMILLIMETER WAVE GENERATION THROUGH STIMULATED SCATTERING WITH AN INTENSE RELATIVISTIC* ELECTRON BEAM AND ZERO FREQUENCY PUMP

M.R. Mross, T.C. Marshall, P. Efthimion and S.P. Schlesinger
Plasma Physics Laboratory
Columbia University
New York, New York 10027

Introduction

We report a configuration of pulsed, intense, relativistic electron beam and rippled magnetic field which shows promise for production of electromagnetic energy in the wavelength range below 1 mm. The technique has been studied theoretically [1] and experimentally [2] in the microwave regime and a similar mechanism has been proposed as a means of generating shorter wavelength radiation [3]. Our apparatus has produced radiation at wavelengths in the 1-2 mm range at power levels of roughly 50 kW.

When an electron moves along a rippled line of magnetic field, it experiences in its rest frame a high frequency pump field. Since the transverse component of the magnetic field perturbation, $\delta B_\perp$, in the lab frame transforms into the fields,

$$\delta B_\perp' = \gamma \delta B_\perp \quad (1a)$$
$$\delta E_\perp' = \gamma \delta B_\perp \quad (1b)$$

in the electron rest frame, one can calculate the perturbation of the electron zero-order motion as if it were illuminated by an intense beam of electromagnetic radiation. If γ is 2.5 and $\delta B_\perp$ is a few hundred gauss, the equivalent intensity is roughly 50 MW/cm^2. Such an intense field yields an electron quiver velocity $\tilde{v} = 0.05C$. Accordingly, we may expect a parametric pumping process to occur in which the pump field interacts with the beam modes to generate a new, growing disturbance in the elctron rest frame [4]. In the lab frame, the disturbance with phase velocity parallel to the beam is doppler shifted to a frequency

$$f_p = 2\gamma^2(v_\parallel/\ell) \quad (2)$$

where ℓ is the ripple period and $v_\parallel$ is the electron axial velocity. The anti-parallel component will have approximately

$$f_a = v_\parallel/\ell \quad (3)$$

in the lab frame. Since the scattered waves must be normal modes of the system, the "space frequency," $v_\parallel/\ell$, is, by design, near the cut-off of the wave guide in which the interaction takes place. We thus expect radiation at roughly 30 and 300 GHz.

Apparatus

The electron beam is generated by a Physics International Pulserad 105 device, which supplies a -700 kV, 15 nsec pulse to a small, graphite-typed cathode. The cathode is in a foilless diode configuration immersed in a strong (~10kG), axial magnetic field (Fig. 1).

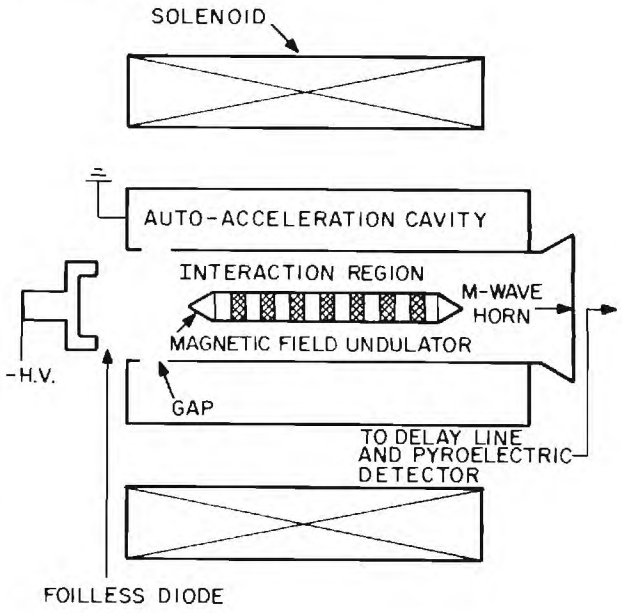

Figure 1. Schematic of the experiment.

A hollow beam having γ of 2 and a current of approximately 5 kA can be produced ($v/\gamma < 0.2$). To increase the beam energy we employ a concentric TEM cavity which auto-accelerates [5] the beam, boosting the γ to 2.5 (γ is measured by observing the frequency of a Cerenkov instability [6] when the field undulator is replaced by a dielectric rod). The beam then propagates over a tapered cone which joins a section of conducting pipe which serves as center conductor of the coaxial waveguide. The inner and outer radii are 0.635 and 1.11 cm respectively, giving 31.5 GHz for the TM_{01} cut-off frequency. Inside the center conductor is a 50 cm stack of alternating iron and teflon rings (period, ℓ, 0.75 cm). This undulator produces a 5% perturbation of the applied, axial magnetic field in the vicinity of the beam. To insure only a small, adiabatic perturbation of the electron zero-order motion, the ripple frequency ($v_\parallel/\ell$ = 30 GHz) has been designed to be well away from the cyclotron resonance ($\frac{\omega_c}{2\pi\gamma} \simeq$ 11 GHz).

The radiation passes through a polyethylene window in a horn. The low frequency component is observed using a dispersive 8 mm line. The high frequency radiation is detected with a carefully

shielded, calibrated pyroelectric detector (Molectron P3-00). The radiation is passed through 0.4 mm and/or 1 mm window metal meshes to provide a crude wavelength determination. The detector is enclosed in a thick brass casting to eliminate microwave and discharge noise interference. Signals are recorded in a screen room which contains attenuators, crystal detectors and fast oscilloscopes.

Experimental Results

Shown in Figure 2 are plots of total power of the high and low frequency radiation emitted from the system versus applied magnetic field. The frequency of the low frequency component is between 30 and 33 GHz (measured with delay line) as expected. The high frequency radiation has wavelength in the 1-2 mm range. We expect about 0.8 mm if $\gamma = 2.5$.

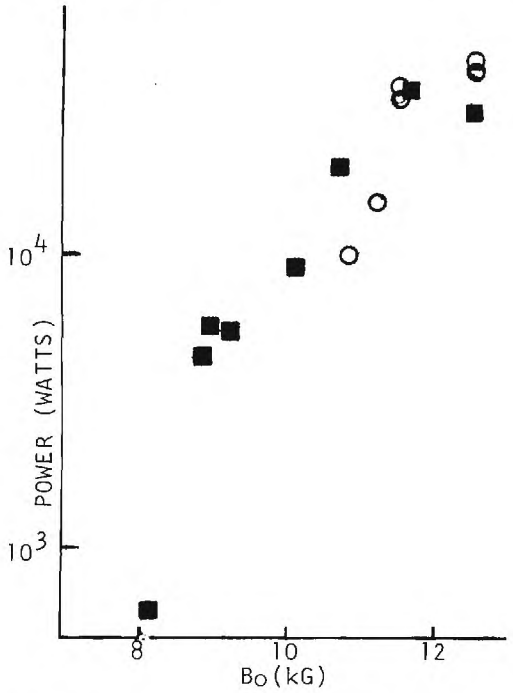

Figure 2. Radiated power versus applied magnetic field (■- 10 mm, ◘ - 1 mm).

The threshold with increasing applied field is associated with the increase in pump power seen by the beam. the pump power in the beam frame is proportional to $(\delta B_\perp)^2$ which is in turn proportional to B_0^2.

Discussion

The results given above demonstrate that the mechanism is worth investigating as a submillimeter source. The power levels attained are not indicative of the ultimate efficiency attainable in such a device since the instability has not saturated in the 50 cm interaction region, and further, since little attempt has been made to optimize the beam parameters. Estimates made by others [3] indicate conversion efficiencies on the order of 30% for this type pf mechanism.

We have also under consideration an experiment in which the outer wall of the waveguide is loaded with an array of alternating conducting and insulating discs. Such slow wave structures are known [7] to give substantial microwave radiation. In this configuration, however, there is also a periodic force on the beam electrons which propagate near such a wall due to the periodic variation of the beam's self electric and magnetic fields, and radiation at millimeter wavelengths can be expected.

* Work supported by AFOSR, F44620-75-C-0055

1. W. Manheimer and E. Ott, Phys. Fluids 17, 463 (1974)
2. P. Efthimion and S.P. Schlesinger, Bull.Am. Phys. Soc. 20, 1290 (1975)
3. T. Kwan, J.M. Dawson and A.T. Lin, UCLA, PPG-267, July (1976)
4. R.E. Kidder in Proc. Enrico Fermi School, Course XLVIII, Physics of High Energy Density (Academic Press, New York, 1971), p. 306.
5. M. Friedman, Appl. Phys. Lett. 26, 366 (1975)
6. J.E. Walsh, T.C. Marshall and S.P. Schlesinger (submitted to Phys. Fluids, August, 1976)
7. John A. Nation, Appl. Phys. Lett. 17, 491 (1970)

RELATIVISTIC ELECTRON BEAM GENERATED COHERENT SUBMILLIMETER WAVELENGTH, CERENKOV RADIATION*

J.E. Walsh
Department of Physics and Astronomy
Dartmouth College
Hanover, New Hampshire 03755

and

T.C. Marshall, M.R. Mross and S.P. Schlesinger
Department of Physics
Columbia University
New York, N.Y. 10027

Introduction

A cylindrical wave guide lined with thin dielectric layer can be used as a slow wave structure. As the dielectric filling factor becomes arbitrarily small and as the dielectric constant of the load material approaches unity the wavelength at which the phase velocity of the guide modes become less than the speed of light becomes arbitrarily short. The azimuthally symmetric TM modes of this structure will couple to an axially propagating electron stream and the resulting linearized dispersion relation has roots which correspond to exponentially growing waves.

Relativistic electron beams will permit operation at millimeter wavelengths without resorting to high loss dielectric loads. The intensity of the available beams is such that high power operation can be expected. Intense relativistic electron beams propagating in structures of the type described above have already been used to make coherent sources at wavelengths in the 5mm range [1,2].

Dispersion Relation of a Dielectric Loaded Electron Beam Driven Waveguide

A straightforward but lengthy calculation will yield the roots of the dispersion relation of the dielectric loaded guide. The results will be summarized here.

The axial wave number k, for which the beam line, $ck\beta$, ($c\beta$ - beam velocity) intercepts the unperturbed (by the beam) guide mode ω_{ok} is given by

$$k = p/(\beta^2 - \eta^2)^{1/2}, \qquad (1)$$

where p is the transverse mode number of the loaded guide, $\eta = 1 + d(1/\varepsilon - 1)/a$ is the slow-factor, ε is the dielectric constant of the load, d is the shell thickness and a is the diameter of the hole in the dielectric load.

The growth rate, Γ, of a synchronous TM mode, divided by the frequency of the wave is:

$$\Gamma/\omega_R \simeq 1.2\nu^{1/3} (1 - \eta^2/\beta^2)^{2/3}/\gamma\eta^{1/2} \qquad (2)$$

where ν is the beam strength parameter (electrons/cm times the classical electron radius) and $\gamma m_o c^2$ is the beam energy.

The theoretical predictions were obtained by assuming that the beam flow was essentially one dimensional and that the beam energy distribution was monoenergetic. We find that they are in good agreement with the experimental results in the long wavelength (3cm - 5mm) region of the spectrum. Extension of these devices into the submillimeter regime will, however, raise a number of further questions and will be convenient for the purpose of discussion to divide these questions into those related to the suitability of the resonant structure and those concerned with suitability of the available electron beams.

Requirements for Submillimeter Wavelength Operation

The 5mm radiation was obtained in a structure for which the wavelength at synchronism was about one fifth of the cutoff wavelength and the thickness of the loading shell was of the order of the free space wavelength. If we assume that a similar scaling is not unreasonable operation similar structures designed to operate at about one mm will represent a practical limit. In addition to the simple extension of the design of the 5mm structure to shorter wavelengths a number of modifications can be considered. We will discuss one of these, the thin dielectric shell, in some detail. Estimates of the resonant frequency and beam coupling for several modifications of the basic structure will be given.

The properties that the electron beam must possess if high frequency operation is to be obtained must also be considered. The assumption that the beam distribution is monoenergetic will become progressively less realistic as the operating wavelength becomes shorter finally reaching a limit where the beam energy spread measured in frequency units will span many modes. Expressions for the growth rate and resonant frequency in this limit will be given.

Finally we will consider modification of the beam electron orbits by the growing waves and saturation of the instability. An estimate of the power output expected from the dielectric resonators will be discussed.

References

1. J.E. Walsh, T.C. Marshall, and S.P. Schlesinger, Bull. Am. Phys. Soc. 21, 692 (1976).

2. J.E. Walsh, T.C. Marshall, and S.P. Schlesinger, Phys. Fluids, Submitted for publication.

* Work supported by AFOSR Grant F44620-75-C-0055.

STIMULATED ELECTROMAGNETIC SHOCK RADIATION

S. Schneider
26628 Fond du Lac Road
Palos Verdes Peninsula, California 90274

R. Spitzer
High Energy Physics Laboratory
Stanford University
Stanford, California 94305

We consider a basically new effect that to our knowledge has not as yet been observed, only calculated [1,2,3]. It involves the production of frequency shifted narrowband electromagnetic radiation by the scattering, in a suitable medium, of coherent electromagnetic waves from relativistic charged particles. The frequency of the scattered wave can be either upshifted or downshifted relative to that of the incident wave. Only the upward shift is considered here; the down shift will be covered in the following paper [4]. We first argue that the effect is to be expected on very general physical grounds and then present the solution to Maxwell's equations for a model that exhibits its salient features.

Stimulated electromagnetic shock radiation (SESR) involves two distinct and well established phenomena. The physical mechanisms underlying both of them are very general, and when conditions for both phenomena are satisfied simultaneously they will act synergistically to produce a basically new effect.

The first of the phenomena that underlie SESR is the Doppler shift in frequency of radiation scattered in vacuum from relativistic charged particles. When a relativistic charged particle of energy γmc^2 is accelerated in vacuum by an electromagnetic wave, the frequency ω of scattered radiation is shifted relative to the frequency ω_o of the incident wave by γ^2 times a factor that depends on the collision and scattering angles:

$$\omega = \gamma^2 (1-\beta \cos\theta)(1 + \beta \cos\theta')\omega_o \qquad (1)$$

For backscattered waves from nearly head-on collision, the angle-dependent factor is of order unity, and the scattered wave is upshifted in frequency by γ^2. The additional energy of the radiated wave is provided by the charged particle. This well known result is the first one that bears on the new effect.

The second basic phenomenon that underlies SESR is also well known. It has long been recognized that basically new effects arise, in wave phenomena of completely different nature, when a material body moves in a medium with speed greater than that of the waves it produces in the medium. In the field of acoustics the basic effect is a shock wave at supersonic velocities. For a charged particle moving through a medium with constant speed greater than a critical speed, the effect is Cerenkov radiation. The Cerenkov field vanishes outside the Mach cone, is sharply peaked in intensity on the surface of the cone, and decreases in intensity in the region away from the inside edge of the cone. This focusing by a medium of waves produced by a particle that satisfies the Mach condition is the second effect underlying SESR.

The focusing can now be put together with the frequency shift in Compton scattering to give the new effect. The basic difference between the mechanisms for the Cerenkov effect and for SESR has to do with the nature of the field of the incident particle producing the coherent response of the medium. Cerenkov radiation is medium response to the Coulomb field of the incident particle, and SESR is medium response to the radiation field of the incident particle. This difference has important consequences for the characteristics of the radiation in the two effects. For one, the frequency spectrum of the medium response will be characteristically different. Cerenkov radiation has a broad frequency spectrum. In SESR the medium response will be peaked about the specific frequency of the backscattered radiation. Moreover this frequency is continuously tunable because of its dependence on the electron energy and incident-wave frequency, both of which can be varied continuously, and on the medium properties.

The two effects are also distinguished by their relative magnitudes. The power emitted into SESR depends quadratically on the interaction distance compared to linear dependence of the Cerenkov effect. This difference can also be traced back to the difference in their mechanisms.

The SESR mechanism also differs fundamentally from that for the laser, which is based on the excess of stimulated emission over stimulated absorption from a nonequilibrium distribution. The basic mechanism for SESR involves energy conversion from the electron into radiation, but no appreciable change in the equilibrium distribution of level populations of the medium.

The existence and properties of this Mach-type radiation are confirmed by an exactly soluble model [1] that contains the essential elements of the physical mechanism underlying SESR and which exhibits the expected characteristics. The model consists of an unterminated electron beam of velocity $\vec{u}$ and an unterminated monochromatic electromagnetic wave of amplitude $\vec{E}_o$ and frequency ω_o interacting in either parallel or antiparallel flow in an infinite, isotropic, homogeneous, nonmagnetic medium with linear response of the medium

to incident wave and constant susceptibility χ, $\epsilon = 1 + \chi$. The solution of Maxwell's equations for the portion of the field of interest is, to leading order in $\vec{E}_o$,

$$\vec{E}(\rho,z)=2\vec{E}_o \frac{r_o}{\omega_o}\frac{\gamma_s}{\gamma} \cdot\frac{\partial}{\partial t}\left\{\theta(\tau)\theta(\gamma_s u\tau-\rho)\cos(\Omega t - Kz)\frac{\cos(\alpha Q)}{Q}\right\} \quad (2)$$

where (ρ,z) are cylindrical coordinates, r_o is the classical electron radius, $\theta(x)$ is the unit step function, and

$$\gamma_s \equiv (\beta^2\epsilon-1)^{-\frac{1}{2}}, \quad \tau\equiv t-z/u, \quad Q\equiv(\gamma_s^2u^2\tau^2-\rho^2)^{\frac{1}{2}}$$

$$\Omega\equiv\gamma_s^2\omega_o(1-\vec{\beta}\cdot\hat{k}_o\sqrt{\epsilon}), \quad K\equiv(\Omega/u)(1+\gamma_s^{-2}),$$

$$\alpha\equiv\Omega\sqrt{\epsilon}/c, \quad \vec{\beta}\equiv\vec{u}/c, \quad k_o=\omega_o\sqrt{\epsilon}/c. \quad (3)$$

The field is confined to a conical region and is infinite on the surface of the cone, where the parameter Q vanishes. The dependence of Q on time indicates a propagating singularity, that is, a shock wave. The oscillatory dependence of the field shows explicitly the shifted frequency. Thus the model substantiates the main qualitative properties of SESR expected on the basis of general arguments.

The case of frequency-dispersive media [2,3] turns out to be considerably richer in physical content, with the radiation showing unexpected new properties. A spatially dispersive medium should exhibit still other features. SESR in dispersive media is covered in the following paper [4].

1. S. Schneider and R. Spitzer, Nature 250 (1974) 643.

2. S. Schneider and R. Spitzer, Stimulated Electromagnetic Shock Radiation in Frequency-Dispersive Media; submitted to Science.

3. S. Schneider and R. Spitzer, Frequency Conversion and Amplification by Stimulated Electromagnetic Shock Radiation (SESR); submitted to Applied Physics.

4. S. Schneider and R. Spitzer, Application of Stimulated Electromagnetic Shock Radiation to the Generation of Intense Submillimeter Waves; paper C-EB-6, this Conference.

APPLICATION OF STIMULATED ELECTROMAGNETIC SHOCK RADIATION (SESR) TO THE GENERATION OF INTENSE SUBMILLIMETER AND FAR INFRARED WAVES

S. Schneider
26628 Fond du Lac Road
Palos Verdes Peninsula, California 90274

R. Spitzer
High Energy Physics Laboratory
Stanford University
Stanford, California 94305

The excitation of intense, tunable submillimeter and far infrared waves by the interaction, through the mechanism described in the preceding paper (1), of microwave and infrared sources with relativistic electron beams in frequency-dispersive media is discussed. The possibility of using artificial dielectrics (spatially dispersive polarizability) is then described.

The frequencies of electromagnetic waves produced by the SESR mechanism can be shifted up or down from that of the incident wave. Coherent microwaves counterflowing against the electron beam in the polarizable medium can readily produce the higher-frequency millimeter, submillimeter and far infrared waves, which are more difficult to generate. In weakly-dispersive media (2) the upward frequency shift becomes larger as $\beta^2\varepsilon \to 1$; ε is the dielectric constant at the SESR frequency, $\beta = u/c$, where u is the electron speed. The downshift is enhanced for $\beta^2\varepsilon >> 1$ and even more strongly for parallel beams. When the dielectric constant ε_i at the incident frequency differs significantly from the value ε at the SESR frequency, expression (3) for Ω in (1) has to be modified to $\Omega = \gamma_s \omega_o (1 - \hat{\beta}\cdot\hat{k}_o \sqrt{\varepsilon_i})$. It is clear that for parallel beams ($\hat{\beta}\cdot\hat{k}_o = \beta$), and an attendant downshift, the value of the dielectric constant at the frequency of the incident wave takes on added significance. Under suitable conditions, electron energy loss in the medium is dominated by radiation reaction due to SESR emission, the process will be self-limiting, and high efficiencies are expected. It is emphasized again that power emitted into SESR depends quadratically on the interaction distance, compared to linear dependence of the Cerenkov effect. The frequency spread of the predominant radiation is dictated by the velocity spread of the electron beam.

The study was extended to frequency-dispersive media (3,4). The susceptibility was modelled as a sum of Lorentzian functions corresponding to different atomic and molecular resonance frequencies of the medium. Associated with each resonance frequency are two SESR frequencies, i.e., two shock fronts. These occur below the resonance frequency at thermal equilibrium of the medium and above the resonance frequency when the populations of the corresponding two levels are inverted. There is in addition a much smaller amount of radiation with a continuous spectrum of frequencies in bands containing each SESR frequency. This radiation lies within the shock cone. When the SESR frequency lies far from the resonant frequency, the two SESR frequencies coalesce to yield the formulae of the weakly dispersive calculation (2). For a medium with an inverted population the SESR pattern has gain associated with it, as the stored energy of the medium is released during the process. In equilibrium there is a small loss as the medium absorbs radiation. The loss associated with SESR emission can be minimized by tuning the output frequency to lie far from any resonance frequency.

The SESR frequencies can be varied continuously by changing, separately or in any combination, the incident-wave frequency, the electron velocity, and the medium density. Additional new output frequencies can be generated at shifted frequencies by changing the energy-level populations of the medium from their equilibrium values. The attainable submillimeter and far infrared frequencies <u>are not limited</u> to the forbidden transitions of the medium, as they are in the laser mechanism.

The SESR process can also be used as a pump, to prepare a medium in a negative-temperature state and for laser action. Furthermore, the possibility exists of sustained pumping by an SESR frequency that has shifted dynamically from below to above a resonant frequency as the populations of the two energy levels associated with this resonance frequency become inverted. The upper level associated with this resonance need not be metastable because as this level is depleted by the allowed transition, the SESR process would be continuously replenishing it, with the energy being derived from the electron beam. Thus the energy in the electron beam is transduced into radiation at a selected frequency. The resulting new SESR/laser synergism (frequency transducer), not being limited to frequencies tied to the metastable levels on which the laser mechanism by itself is dependent, would make available new lines. Moreover, far intrared lasers are presently confined to low-temperature operation to avoid depletion of the higher level by collisional deactivation. The continuous additional pumping provided by the SESR process may help mitigate collisional deactivation and allow for higher-temperature operation.

The SESR process can also be generated in artificial dielectrics, such as a dielectric-loaded waveguide or periodic arrays of dielectric or conducting obstacles. The system then exhibits, in addition to possible frequency dispersion, additional wave-number dependence of the polarizability arising from the geometrical properties of the loadings and cavity. The additional degrees

of design freedom in artificial dielectrics, e.g., design anisotropy and frequency filtering by the array, are expected to enhance the SESR effect even further. By choosing a geometry for which the constructive-interference properties of the array (Bragg effect) are made compatible with the spatial characteristics of only one of the shock patterns produced by the SESR effect, further enhancement of the intensity in the chosen mode as well as more precise control of the monochromaticity and directionality of the stimulated output is expected.

The possibility of the interacting electron beam passing through an evacuated but loaded structure without any contact with it offers the potential of eliminating collision degradation entirely. Velocity loss by the electron would then be due solely to radiation reaction incurred by emission of SESR itself. The monochromaticity, spatial coherence and intensity of the output of the effect should then be even further enhanced compared to when then process is self-limiting in a gas.

1. S. Schneider and R. Spitzer, Stimulated Electromagnetic Shock Radiation; paper C-EB-5, this Conference.

2. S. Schneider and R. Spitzer, Nature 250 (1974) 643.

3. S. Schneider and R. Spitzer, Stimulated Electromagnetic Shock Radiation in Frequency-Dispersive Media; submitted to Science.

4. S. Schneider and R. Spitzer, Frequency Conversion and Amplification by Stimulated Electromagnetic Shock Radiation (SESR); submitted to Applied Physics.

THE LINEAR AND SELF CONSISTENT NONLINEAR THEORY OF THE CYCLOTRON MASER INSTABILITY

P. Sprangle
Naval Research Laboratory, Washington, D.C., 20375

and

A. T. Drobot
Science Applications Inc., McLean, Virginia 22101

Introduction

We have found that it is possible to produce submillimeter microwaves with the cyclotron maser instability at reasonable efficiencies and high power levels. The configuration used to study the instability is shown in Fig. 1. For simplicity we have chosen a parallel plate geometry in which electrons travel along a guide magnetic field and execute gyro orbits in the direction perpendicular to the magnetic field. It is the perpendicular energy which is responsible for the maser instability. The gyrating electrons interact and feed energy to the electromagnetic TE_{on} modes between the parallel plates. This instability is a relativistic effect and we discuss it in more detail in the section on the Physical Mechanism.

From the linear theory we have found that the growth rate of the cyclotron maser instability maximizes when the beam drift velocity equals the wave group velocity. Since we are interested in the fastest growing mode this permits us to do the analysis in the beam frame, where k_z the parallel wave number vanishes, greatly simplifying the analysis. The linear theory also indicates that there is a minimum perpendicular energy necessary for the onset of the instability.

In the nonlinear theory we self consistently relate the particle dynamics to the amplitude and phase of the excited electric field in the single wave approximation. This is detailed in the section on the formalism. As a result of the nonlinear approach we have found two distinct mechanisms which saturate the cyclotron maser instability. Competition between the two mechanisms leads to an optimum value of beam energy for efficient transfer of power to the electromagnetic waves. We have found maximum efficiencies $\eta \geq 60\%$.

The cyclotron maser is particularily promising for the generation of submillimeter radiation[1-4]. In this part of the electromagnetic spectrum conventional electron devices are limited in both power and efficiency and require slow wave structures that are difficult to fabricate. The cyclotron maser does not have these drawbacks and can in addition be operated as an amplifier as well as an oscillator.

Physical Mechanisms

In the presence of a small amplitude electric field, $E_y = E_o \cos(\omega_b t)\hat{e}_y$, the gyrating electrons shown in Fig. 1 will be either gaining or losing energy depending on their phase relative to the electric field. If the frequency of the field is slightly greater than the electron gyro frequency, $\Omega_o/\gamma_\perp = |e|B_o/mc\gamma_\perp$, where $\gamma_\perp$ is the relativistic factor $[1-v_\perp^2/c^2]^{-\frac{1}{2}}$, then roughly half the electrons will be gaining energy and half losing it. Because the gyro frequency is energy dependent, those particles that have lost energy will tend to spend a longer time in phase with the field than the particles that are gaining energy. The particles that have gained energy will gyrate more slowly and will eventually come into phase with the field and also start losing energy. It is the effect of the relativistically dependent cyclotron frequency then, that leads to the instability and the bunching of the electrons in their orbits in phase with the electric field. The free source of energy is in the gyrational motion of the electrons and is transferred to the exciting electromagnetic field.

Linear Theory

The linear theory of the cyclotron maser instability has been previously derived[5]. In doing the nonlinear theory the aspects of the linear dispersion relation that are important are:

i) The existence of a critical condition for the onset of instability[7] $\gamma_\perp > \gamma_{\perp,crit}$ where $\gamma_\perp = [1-v_\perp^2/c^2]^{-\frac{1}{2}}$.

ii) The coincidence of the beam and cutoff frames when the growth rate maximizes. This permits a greatly simplified analysis in the beam frame with $k_z = 0$.

iii) The condition that the unstable wave must satisfy $\omega - \Omega_o/\gamma_\perp = \Delta\omega > o$, where $\Delta\omega$ is the linear phase shift. The phase shift is important in roughly determining the expected saturation level when $\gamma_{\perp o} \gg \gamma_{\perp,crit}$.

iv) The linear theory also predicts a narrow growth rate spectrum so that the analysis can be done in the single wave approximation.

Nonlinear Formalism

The particle equations of motion and Maxwell's equations from a self consistent nonlinear description of the time evolution of the field phase and amplitude. In the single wave approximation it is possible to reduce the equations to a form where an analytical and numerical treatment can be used to study the equations.[5,6]

It is a good approximation to assume that the cyclotron maser instability excites a single wave guide mode for which we express the E_y field as $E_y = -E_o(t)\cos(\omega_o t + \alpha(t))\sin(k_n(x-a))$ where $E_o(t)$ is the field amplitude, α is the nonlinear frequency shift and the spatial form satisfies the boundary conditions for the TE_{on} mode. By performing spacial and temporal averages over the nonlinear period we find that the equations governing the nonlinear growth rate and time shift are:

$$\left\{\omega_o^2 - c^2k_n^2 + (\omega^2 + c^2k_n^2)\frac{\dot{\alpha}}{\omega_o}\right\} E_o = \frac{4\pi|e|\sigma_o}{a}\frac{\omega_o}{2\pi}\langle\langle v_y(\phi_o,t')\sin(\omega_o t' + \alpha) \sin(k_n(x(\phi_o) - a))\rangle\rangle .$$

$$(\omega_o^2 + c^2k_n^2)\frac{\dot{E}_o}{\omega_o} = \frac{4\pi|e|\sigma_o}{a}\frac{\omega_o}{2\pi} \langle\langle v_y(\phi_o,t')\cos(\omega_o t' + \alpha) \sin(k_n(x(\phi_o) - a))\rangle\rangle .$$

where, $\langle\langle\ \rangle\rangle$ indicates an average over the initial electron phases ϕ_o and the nonlinear time period $2\pi/(\omega + \dot{\alpha})$, a is half the distance between the plates while σ_o is charge per unit area of the sheet beam in Fig. 1.

These equations can be solved by numerically integrating contributions from the particle orbits on the right hand side. The assumption built into these equations is that the growth rate and time derivative of the phase shift change little over a wave period.

Saturation Mechanisms

From the study of the nonlinear equations governing the maser instability we have found that there are two mechanisms responsible for saturation.

Energy depletion. When the perpendicular beam energy $\gamma_{\perp o} \geq \gamma_{\perp,crit}$ is close to the critical energy for onset of the instability we find that the beam loses energy until $\gamma_\perp \cong \gamma_{\perp,crit}$ at which time the system is linearly stable.

Phase trapping. When the original perpendicular beam energy $\gamma_{\perp o} \gg \gamma_{\perp,crit}$ the instability saturates because of phase trapping in the cyclotron orbits. In this case we find that the energy given up by the beam is $\gamma_{\perp o} - \gamma_\perp = \Delta\omega/\omega_o$, where $\Delta\omega$ is the linear phase shift.

The implication of the two saturation mechanisms is that there exists an optimum energy for transferring energy from the beam to the electromagnetic waves. In Fig. 2 we show the actual efficiency $\eta = (\gamma_\perp - \gamma_\perp)/(\gamma_{\perp o} - 1)$, and in dashed lines the expected efficiencies from depletion and trapping.

In the phase trapping case the final efficiency can be further increased by contouring the magnetic field. We have found that saturation occurs when $\omega - \Omega_o/\gamma_\perp = \Delta\omega \to 0$. This can be prevented by changing the magnetic field so that $\Omega_o/\gamma_\perp = \text{const}$, in which case efficiencies greater than 60% can be realized.

References

[1] V.L. Granatstein, M. Herndon, P. Sprangle, Y. Carmel and J. A. Nation, Plasma Physics 17, 23 (1975).

[2] V.L. Granatstein, P. Sprangle, M. Herndon, R. K. Parker and S. P. Schlesinger, JAP 46, 3800 (1975).

[3] N. I. Zaytsev, T. B. Pankratova, M. I. Petelin and Va. A. Flyagin, Radiotekhnika i Electronica 19, 1056 (1974).

[4] D.V. Kisel', G. S. Korablev, V. G. Navel'yeV, M. I. Petelin and Sh. E. Tsimring, Radio Engineering and Electronic Physics 19, 95 (1974).

[5] E. Ott and W. M. Manheimer, IEEE Trans. Plasma SC., Vol. PS-3, 1 (1975).

[6] P. Sprangle and W. M. Manheimer, Phys. Fluids 18, 224 (1975).

[7] P. Sprangle and A. T. Drobot, to be published.

Acknowledgment

This work was supported by BMDATC and MAVMAT.

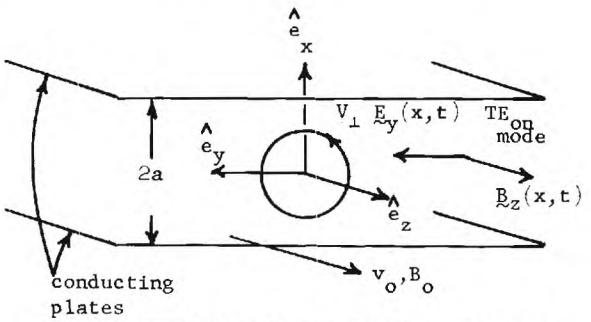

Fig. 1 Cyclotron Maser in Plane Geometry.

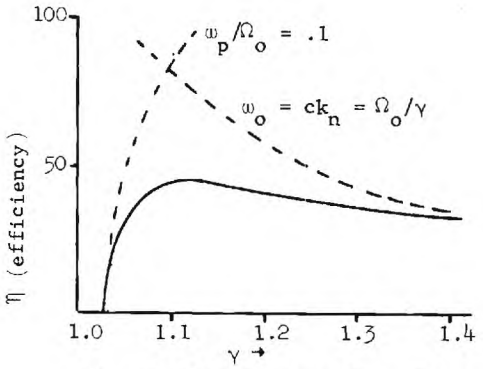

Fig. 2 Efficiency vs Beam Energy

COHERENT MILLIMETER RADIATION FROM RELATIVISTIC BEAM-PLASMA INSTABILITIES

G. Benford, S. Robertson, C. Roberson, and D. Tzach
Physics Department, University of California
Irvine, California 92717
and
V. Granatstein
Naval Research Laboratory, Washington, D. C.

I. Introduction

We have explored the possibilities of producing mm and sub-mm radiation by using basic features of relativistic beam-plasma interaction. Our projected (idealized) beam geometry is shown in Fig. 1. After it is launched from a cathode, the beam passes through a cusped field, which makes it spin with $v_\theta > v_z$. This differs from the usual straight propagation of beams, used earlier to produce cm radiation. More importantly, the beam passes through a dense background plasma. The beam gains coherence, not because of a rippled guide field or other external agency, but rather because of the intrinsic beam-plasma instabilities. Thus the low-energy plasma fixes the radiated frequency, but the high energy-beam actually does the radiating. This means the energy budget is concentrated where it can be used for radiation. This approach has several advantages:

1. Arbitrarily high beam currents can be propagated when beam charge and current neutralization are provided by the background plasma. Contrast this with the unneutralized beam radiation schemes, which are limited to lower currents, and thus lower radiated power.

2. The radiated power for a rotating beam should peak at a wave number

$$k = \sqrt{\omega_p^2 + \Omega_p^2}\,/c = \omega/c \qquad (1)$$

where ω_p is the plasma frequency and Ω_p is the cyclotron frequency in the background plasma, and most radiation occurs at millimeter wavelengths.

3. Since $\omega > \omega_p$ at the peak of radiated power, the radiation is not screened by the plasma. This overcomes the primary limitation on most coherent beam-plasma radiation schemes.

4. The coherence depends on readily adjustable parameters, such as background plasma frequency, ambient magnetic field, and the pitch of the rotating beam imparted by cusp magnetic field.

5. The theory is formulated in a quite general manner, applicable to a wide range of laboratory, magnetospheric and astrophysical plasmas. This allows checking of the theory by comparison with already known (but largely not understood) sources of coherent radiation, such as pulsars.

6. Since we use a rotating beam with large pitch angle to preferentially excite the upper hybrid mode ($\omega^2 = \omega_p^2 + \Omega_p^2$), the beam spends much longer in the drift tube than if it had been propagating straight through, and so loses much more of its energy to radiation.

7. Simply increasing ω_p pushes the peak emission into the sub-mm region. The condition for maximum emission at ω_p

$$\gamma^3 \Omega_b = \gamma^2 \Omega_p \geq \sqrt{\omega_p^2 + \Omega_p^2} \qquad (2)$$

can be satisfied for higher ω_p by using higher γ, which also increases the emission rate. (Here Ω_b is the beam cyclotron frequency.)

II. Theory

We already carried out preliminary theoretical studies for laboratory experiments; here we briefly sketch our ideas. We have also completed a quite general analysis of relativistic coherent radiation, which is described later.

Since radiated power increases rapidly with beam relativistic energy factor , we consider cases in which the curvature frequency $\bar{\omega} = \gamma^3 c/\rho$ exceeds the cyclotron frequency Ω_b. (Here c is light speed and ρ the radius of curvature of a particle orbit. ρ need not be a cyclotron radius, for example, when the particles follow helices.) Particles moving along general curved orbits radiate at harmonics of $\gamma^{-1}\Omega_b$ up to $\bar{\omega}$; this is the single particle spectrum. To increase the radiated power the beam particles must act coherently, in which case radiated power exceeds the single-particle power by N, where N is the number of beam electrons cooperating in collective motions.

Consider a beam injected into a cylindrical background plasma and then passed through a cusp, so that the beam rotates. This rotation is important, because it allows us to adjust ρ to our liking. Coherence is forced on this beam because there is a resonance between beam charge oscillations and the plasma hybrid wave at $(\omega_p^2 + \Omega_p^2)^{\frac{1}{2}}$. The beam bunches due to this instability, and since we expect the background plasma frequency ω_p to exceed Ω_p by an order of magnitude, the bunching wavenumber is $k \gtrsim \omega_p / c$.

The experiment is shown schematically in Fig. 1. A typical beam electron spends about 20 nsec. in the drift tube after it leaves the cusp,

unless a mirror at the end reflects it (which will be so, in later experiments).

Because the beam electrons are bunched, they emit curvature radiation coherently. There are several bunches inside each segment of the annulus which emits into the local radiation cone, which has angular width $\sim \gamma^{-1}$. These bunches radiate in a plane nearly normal to B_o, when the beam is propagating with $v_z \sim c/10$ and $v_\theta \simeq c$. A detailed calculation shows that the effect of coherence is to give a strongly peaked maximum at $\omega = (\omega_p^2 + \Omega_p^2)^{\frac{1}{2}}$ when $\omega = \bar{\omega}$. Thus we get the most power when $\gamma^3 c/\rho \geq (\omega_p^2 + \Omega_p^2)^{\frac{1}{2}}$. There will also be radiation at frequencies below $\bar{\omega}$. (However, absorption by the plasma will cut off the spectrum rather quickly below ω_p). See Fig. 2.

As an example, with a beam density of $10^{11} cm^{-3}$, $\gamma = 3$, and assuming the cusp has produced an annular beam of radius 5 cm., annular width 1 cm., we find that a minimum of 50 megawatts are radiated. Contrast this with a single-particle power of 10 watts. Radiation peaks between 0.5 and 1.0 cm. We assume saturation of the beam instability by trapping of beam electrons in wave troughs.

There is no intrinsic reason why comparable or higher radiated powers cannot be produced by increasing γ or beam currents. Raising γ and plasma density will also shift the maximum radiated power to higher frequencies, producing powerful sources in the mm and sub-mm range.

The type of coherent emission we describe here can be distinguished from other mechanisms by noting whether radiation increases significantly as the beam pitch angle is increased smoothly (shot to shot) from zero. This will serve to separate the transverse coherence (k_θ) we seek from the longitudinal coherence (k_z), which undoubtedly exists but which for the numbered reasons given in the Introduction will probably be a less efficient radiator.

III. Experiments

A rotating beam-plasma interaction experiment is currently in operation. Typically, we inject a 1 MeV, 70 kA annular beam of 6 cm. mean diameter and 1 cm. thickness through a magnetic cusp and into a hydrogen plasma of variable density. The emission of Ka band (26-40 GHz.) radiation is detected and resolved in frequency using a dispersive line technique.[1]

No detectable signal is found for $\omega_p/2\pi > 50$ GHz. However, when ω_p is reduced below this value, there is a sharp onset of Ka band emission with a maximum at $\omega_p/2\pi \approx 30$ GHz.

When the magnetic cusp field is increased so as to increase the rotation velocity of the electron beam, the Ka band emission rises sharply until beam propagation through the cusp is shut off. The dependence of the Ka band radiation on the electron rotational velocity as well as on the background plasma density is consistent with the model of coherent curvature radiation presented above.

Total radiated power in Ka band is on the order of one megawatt in contrast to the few watts of single particle synchrotron radiation. In a preliminary determination, the frequency spectrum appears to consist of a series of sharp maxima with a spacing ~ 2 GHz.

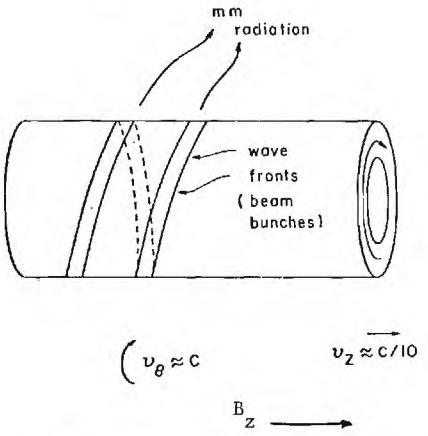

Figure 1. Schematic of the rotating, annular beam after it has passed through the cusp fields. Instability wave fronts are pitched forward by angle v_z/v_θ.

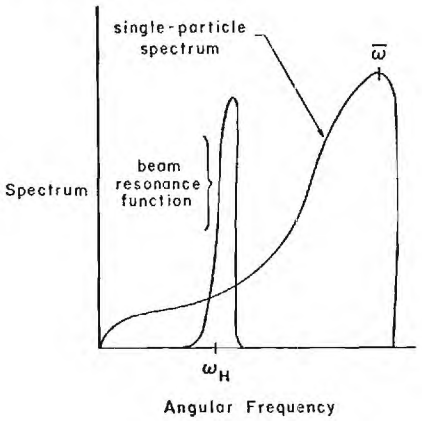

Figure 2. Radiated spectrum is given by product of the single particle spectrum, which peaks at $\bar{\omega} = \gamma^3 c/\rho$, times the beam resonance function, peaked at ω_H and having width $2\pi\, v_\theta/s_o$. Here s_o is the beam coherence length. For most efficient radiation, $\omega_H \approx \bar{\omega}$.

Work supported, in part, by ERDA.

[1] e.g., V. L. Granatstein, P. Sprangle, R. K. Parker, and M. Herndon, J. Appl. Phys. 46, 2021 (1975).

THE GENERATION OF HIGH-FREQUENCY RADIATION BY THE BACK-SCATTERING OF MICROWAVES FROM THE FRONT OF AN INTENSE, RELATIVISTIC ELECTRON BEAM†

J. A. Pasour
North Carolina State University
Raleigh, North Carolina 27607

R. K. Parker, V. L. Granatstein, M. Herndon, and S. P. Schlesinger*
Naval Research Laboratory
Washington, D. C. 20375

Introduction

The reflection of electromagnetic radiation from a relativistic mirror has several intriguing properties. The backscattered radiation is Doppler shifted to a higher frequency, and with efficient interaction its energy and power are also increased. As the mirror velocity approaches that of light, these effects become substantial. In a recent publication [1], preliminary experimental observations are reported which are in agreement with a simple theory of microwave reflection from the front of an intense, relativistic electron beam. Since the original work was performed, refinements have been made in the theory and experiment. These refinements will be discussed after briefly reviewing the earlier work.

Theory

Consider a uniform, magnetically-confined, relativistic electron beam which propagates at speed $\bar{v}$ within a cylindrical waveguide. An electromagnetic wave of frequency ω_i is incident on the beam. The reflected wave frequency is then given by

$$\omega_s = \gamma^2(1 + \beta^2 + 2\,\beta\beta_g)\omega_i \qquad (1)$$

where $\beta = \bar{v}/c$, $\gamma = (1 - \beta^2)^{-1/2}$, and β_g is the normalized group velocity of the incident wave. Similarly, the energy of the reflected wave is

$$W_s = \gamma^2(1 + \beta^2 + 2\,\beta\beta_g)RW_i \qquad (2)$$

where R is the reflection coefficient of the beam front in the beam frame. Clearly large energy gains require that R approach unity. By time compression, the power is enhanced even more:

$$P_s = \gamma^4(1 + \beta^2 + 2\,\beta\beta_g)^2 \frac{\beta_{gs}}{\beta_g} RP_i \qquad (3)$$

where β_{gs} is the group velocity of the backscattered wave.

To determine the conditions under which reflection occurs, the dispersion relations, shown in Fig. 1, were computed for the beam in this finite geometry. The dashed line represents the dispersion relation for the empty waveguide. In the beam-filled waveguide, the dispersion curve is separated into two branches (solid lines) by the Doppler-shifted cyclotron beam line, $\omega = \bar{v}k_z + \Omega_o/\gamma$, where $\Omega_o = eB/m_o$ is the cyclotron frequency. A stop band appears near the intersection of the empty-waveguide mode and the cyclotron line. Reflection occurs when the incident wave frequency lies in a narrow region just above this intersection, as represented by point c. The reflected wave then propagates at point c'. Waves incident at points a or b continue to propagate into the beam, but with a shift in frequency and wavenumber as denoted by points a' and b', respectively. Thus for a given incident wave frequency, a magnetic field and beam velocity can be chosen such that reflection will occur.

Since the accelerating voltage pulse has a finite rise time, the electron velocity at the beam front increases as the beam traverses the drift tube. Since the incident wave frequency and magnetic field are fixed in the experiment, this variation in beam-front velocity limits the length of the reflecting region. The finite rise time further complicates the interaction by introducing velocity and density gradients in the beam front. With these gradients, the refractive index can become infinite or zero at some point near the beam front. Budden has shown by using a WKB analysis that absorption of the incident wave can occur at a singularity, whereas reflection occurs at a zero [2]. The net effect of these considerations is that the beam-wave interaction evolves through three phases as the beam propagates. When the beam front first enters the drift tube, the electron velocity is so low that the beam is transparent. As the front continues to propagate and its velocity increases, the beam-wave interaction passes through an absorption phase. Further along the drift tube, the conditions necessary for reflection are finally achieved. If the voltage rise time could be reduced, the beam front would reach a high, relatively constant velocity more quickly and the length of the reflecting region would, therefore, be increased.

Experiment

The improved experimental configuration is shown in Fig. 2. The beam is generated by applying a 1 MV voltage pulse to a foilless field-emission diode [3]. The electrons are injected into an evacuated, 1 m-long drift tube which also serves as the waveguide for the counterstreaming microwave pulse (f_i = 9.3 GHz). The high-frequency output radiation passes through holes drilled in the sidewall of a 90° bend, which acts as a high-pass filter. A 12 mm-diameter, gold-plated pipe which cuts off all signals with f < 14 GHz transports the radiation to a detector, in this case a multichannel grating spectrometer.

The configuration shown in Fig. 2 includes two major improvements over the original experiment discussed in Ref. 1. First, the spectrometer has replaced a mesh-filter, pyroelectric detector combination. The spectrometer provides much greater resolution ($\lambda/\Delta\lambda \approx 20$) than could be obtained previously, and it can cover the region from $\lambda = 2$ mm to $\lambda = 8$ mm with two gratings. The second refinement is the inclusion of a pulse-sharpening switch in the diode. The switch is a length of dielectric inserted into the cathode shank, and is designed to break down when the voltage across it approaches 1 MV. Preliminary measurements indicate that this switch shortens the rise time from $t_R \geq 10$ nsec to $t_R \leq 5$ nsec. Figure 3 demonstrates the effects of decreasing the rise time of a 1 MV diode pulse from 10 nsec to 2.5 nsec. Normalized beam-front velocity is plotted as a function of distance from the cathode. Note that for $t_R = 10$ nsec the beam-front electrons have $\beta \approx 0.6$ over most of the drift tube. This is consistent with the observed Doppler shift in the original experiment, in which the reflected wavelength $\lambda_s \approx 8$ mm.

The other experimental results are also consistent with our theoretical model of beam-front scattering. As expected, the output pulse is very short compared to the 50 nsec beam duration. Also, a strong output signal is observed only when the magnetic field lies within a narrow band centered about 5 kG. This result agrees well with theoretical predictions when $f_i = 9.3$ GHz and $\beta = 0.6$. Finally, in the original experiment, the output power was about 300 kW, or twice the incident power.

With the inclusion of the pulse-sharpening switch and spectrometer, it should be possible to detect a variation in output frequency as well as a shift in the magnetic resonance as the beam rise time is changed. These experiments are now underway and results will be reported at the conference. In the present experiments, wavelengths no shorter than ~ 3 mm are anticipated. However, further decreases in the rise time coupled with increased peak accelerating voltage should extend this output into the submillimeter range.

References

1. V. L. Granatstein, P. Sprangle, R. K. Parker, J. Pasour, M. Herndon, S. P. Schlesinger, and J. L. Seftor, Phys. Rev. A 14, 1194 (1976).

2. K. G. Budden, in "Physics of the Ionosphere: Report of Phys. Soc. Conf. Cavendish Lab.," p. 320, Phys. Soc., London (1955).

3. M. Friedman and M. Ury, Rev. Sci. Instrum. 41, 1334 (1970).

† Work partially supported by the Air Force Office of Scientific Research.

* Also Columbia University.

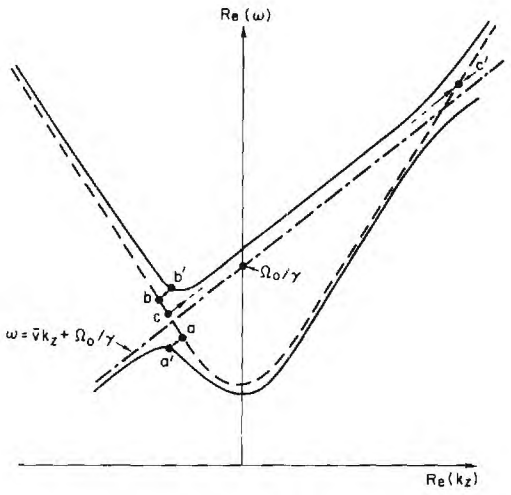

Figure 1. Dispersion curves for the magnetized beam.

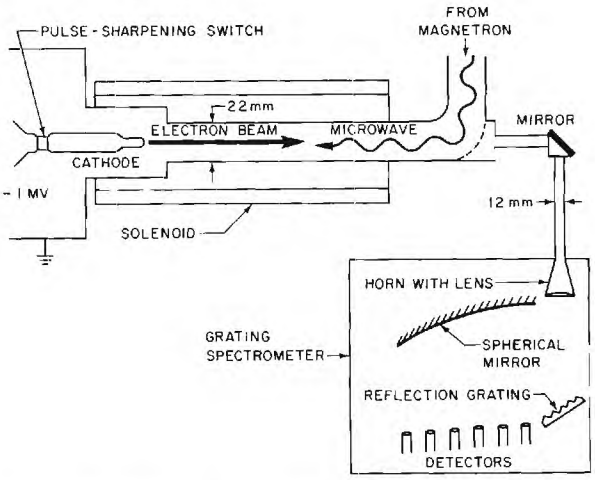

Figure 2. Improved experimental configuration.

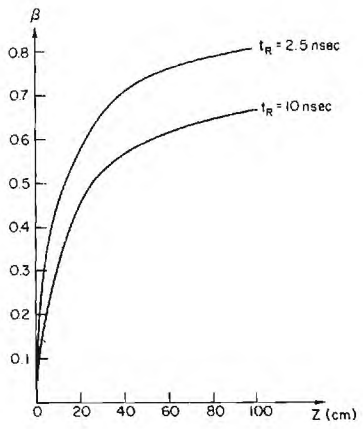

Figure 3. Variation of beam front velocity with axial position.

PRODUCTION OF MICROWAVES WITH AN INTENSE RELATIVISTIC SHEET ELECTRON BEAM*

G. Providakes, J. A. Nation and M. E. Read
Laboratory of Plasma Studies, Cornell University, Ithaca, NY 14853

There has been a great deal of interest in the production of high power microwaves in the mm and sub mm bands using high current relativistic electron beams. Coherent radiation from the cyclotron maser configuration has been produced at powers in excess of 100 MW in the Ku band [1], 8 MW in the Ka band, and 1 MW in the V band [2]. We report here on an investigation into the radiation produced by the interaction of an intense REB with a slow wave structure. In this case, both the beam and the structure are of rectangular cross section. The structure is open at the sides; thus the dispersion characteristics of the guide are independent of its width. This allows an arbitrary choice for the structure and beam width, and makes possible a reduction in the usual scaling of power with the frequency from $P \tilde{\alpha} 1/f^{5/2}$ to $P \tilde{\alpha} 1/f^{3/2}$.

In the experiment the electron beam was generated by a Marx-Blumlein accelerator. The beam produced had a energy of 300-500 keV, a current of 500 to 2000 amps, and a pulse width of 70 ns. Its cross section was approximately 5 x 0.2 cm. The slow wave structure was formed by a ridge loaded parallel plate waveguide 5 cm wide and 40 cm long (see figure 1). The beam entrance to the structure was tapered to assure reflection of the backward wave for coupling of the radiation out of the system. The Brillouin diagram for the structure and a slow space charge wave is shown in figure 2 [3]. The period and transverse dimensions of the guide were chosen in order to have the system act as a backward wave oscillator on the fundamental harmonic in the K (18-26 GHz) band. A second, similar, structure was designed to operate in the Ka (26-40 GHz) band by reduction of the ridge depth from 2.8 mm to 1.9 mm. The structure was situated in a 7.5 cm diameter metal tube, which served as a return path for the beam and a vacuum chamber (see figure 3). The pressure in the drift region was kept below 10^{-3} Torr. The drift region was immersed in a uniform 10 kGauss magnetic field oriented along the axis. This field was necessary to guide the unneutralized beam. Damage patterns of the beam taken downstream of the structure show no gross breakup or filamentation of the beam at these fields.

The beam voltage and current were measured conventionally. Measurements of the microwaves were accomplished with standard crystal detectors, with the different band waveguides forming high-pass filters. The bands monitored were Ku, K, Ka and V. All of the detectors except the V band crystal were calibrated for absolute power measurements.

Results were obtained from both structures. The deep ridge structure produced up to 2.5 MW (total output power) in the K band and 8 kW in the Ka band. The shallow ridge guide produced about 100 kW in both the K and Ka bands. The frequency expected with the deep ridge guide is about 20-22 GHz. These frequencies are slightly below the cutoff for the Ka band waveguide, and the signal reaching the Ka detector should be strongly attenuated. With the second structure the expected frequency is about 26-28 GHz, well above the Ka band cutoff, and agreement of the K and Ka band powers is expected. The reduced power observed with the shallow ridge guide may be due to a difference in the construction of the two structures. The deep ridge structure was machined from solid brass, while the shallow ridge one was built up with non conductors and coated with conducting paint. This is quite likely very lossy.

Some activity was seen in the V (50-75 GHz) band. This band coincides with the passbands of the second harmonic of the two structures, and the intersection of the beam and guide dispersion curves indicate that BWO operation is possible. No absolute power calibration was available for this detector but the signal was at least 25 db above the background noise.

Little variation of output power with the beam voltage or current was observed. A minimum structure length for oscillation was found (with the deep ridge guide) to be 15 cm. This is in reasonable agreement with a simple calculation for the turn on condition given by Heffner [4]. An optimum plate separation was found for power output. In the shallow ridge guide this was 6.5 mm. Reduction of this gap to 5.9 mm caused an 8 db drop in power, possibly due to the wave having a lower group velocity and the associated higher wall losses. Larger gap spacings also produced reduced powers, most likely due to a larger ridge to beam spacing. Complete removal of the lower (unloaded) plate caused a > 40 db drop in power. Shorting the ridges by a thin aluminum foil produced a similar drop. There was no dependence of the power on the magnitude of the magnetic field as long as the beam retained its shape. With these indications and the estimates of the frequency of the radiation it is evident that the system was operating as a BWO.

Future experimentation will be directed at the improvement of the output power by increase of the system width. Beam widths of up to 50 cm seem possible, enabling a power increase to 20 MW. Better construction of the device to reduce wall losses and minimize chance of breakdown may produce additional increases in power. In the scaling of the device width, questions of beam stability and uniformity and wave coherence will have to be addressed. Successful scaling in the

present bands points the way to work at higher frequencies where the advantage of the strip geometry is even greater. We note also that it seems probable that high power mm wave generation using other physical mechanisms can profit from the strip beam configuration. Specifically, we believe that the Ubitron, cyclotron maser, and gyrotron configurations may also scale with width, although some gain may be lost due to the sheet geometries requiring operation in modes more lossy than the TE_{01} (circular) mode in which these devices normally operate.

References

1. V. L. Granatstein, M. Herndon, R. K. Parker, and S. P. Schlesinger, IEEE Trans. on Microwave Theory and Tech., MTT 22, 12 (1974).

2. M. Friedman, and M. Herndon, Phys. Fluids 16, 11 (1973).

3. A. W. Lines, G. R. Nicoll, and A. M. Woodward, Proc. IEE 97 III, 904 (1950).

4. H. Heffner, Proc. IRE 42, 930 (1954).

*Work supported by AFOSR Contract #F44620-75-C-0054.

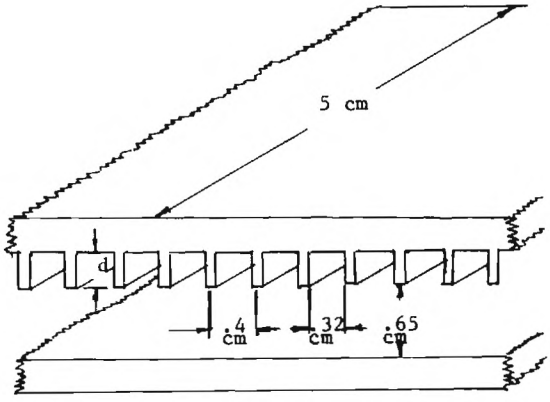

Figure 1. Diagram of the slow wave structure. d=2.8mm and 1.9mm for the deep and shallow ridge structures, respectively.

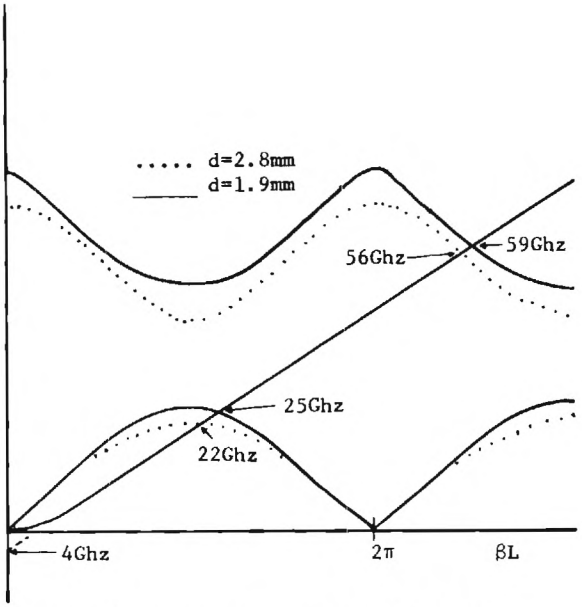

Figure 2. Dispersion curves for the two structures and the slow space charge wave.

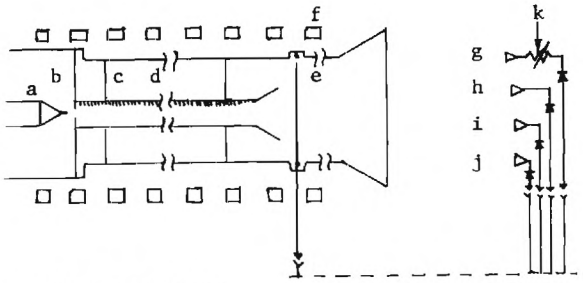

a Carbon Cathode
b Brass Anode
c Brass Spacer
d Ridged Structure
e Rogowski
f Magnetic Coils
g-j Ku,K,Ka,V Detectors
k Attenuators with Waveguide

Figure 3. Schematic of the experiment.

REFLECTION OF ELECTROMAGNETIC WAVES FROM A MOVING IONIZATION FRONT

M. Lampe, E. Ott*, W. M. Manheimer, S. Kainer
Naval Research Laboratory
Washington, D. C. 20375

(Work supported by Naval Surface Weapons Center)

Abstract

The Doppler shift and reflection coefficients are calculated for reflection of an EM wave from a moving ionization front in a stationary gas. It is suggested that this process can be used to upshift microwaves to submillimeter waves.

Introduction

An ionization wave can be propagated through a gas in many ways, e.g. a strong electromagnetic pulse, an ionizing shock, a propagating electron beam, or a laser or electron beam sweeping across the gas. Similarly, a finite time after such an ionizing pulse has passed, a recombination wave will move across the plasma. In this paper, we consider the reflection of an electromagnetic wave, incident from the neutral gas side, by such a moving ionization or recombination front. It would appear that an electron density which will render the plasma overdense to microwaves can be attained with relatively modest means. We suggest, therefore, that the Doppler shift which occurs upon reflection can be used to upshift microwaves to the submillimeter wave range [1].

For specificity, we assume that the ionization or recombination front is planar, and that the EM wave is normally incident. The velocity U of the front can be relativistic, or can even exceed the speed of light (e.g. if the ionization is created by a laser sweeping across the gas). However we shall be discussing the case $|U| < c$, except for some comments on the supraluminous case in the last section. In the present calculations, the plasma is treated as cold and collisionless. The calculations are most easily performed in the frame of reference in which the ionization or recombination front is stationary (i.e. the electron density $n(z)$ is time-independent), and the gas/plasma is streaming at velocity U. The situation in this frame is illustrated in Fig. 1.

The reflection process under consideration has some similarities to and some differences from the process of reflection by a moving mirror. A relevant example of the latter is upscattering of microwaves by reflection from a relativistic electron beam [2]. In both cases, reflection is from a critical electron density surface, rather than from individual particles, and thus the frequency ω_r of the reflected wave is Doppler shifted relative to the incident ω_i,

$$\omega_r/\omega_i = (1 + \beta)/(1 - \beta), \qquad (1)$$

where $\beta = U/c$. In both cases, the duration τ_r of the reflected pulse is similarly related to that of the incident pulse,

$$\tau_r/\tau_i = (1 - \beta)/(1 + \beta). \qquad (2)$$

However the plasma itself is moving in the case of the moving mirror (e.g. relativistic electron beam) but is stationary in the case under consideration here. This introduces a difference in the wave dispersion properties in the plasma which, in the case of an oncoming ionization front ($U > 0$ in Fig. 1), reduces the reflection coefficient as compared to what it would be for a moving mirror. Indeed it is obvious that this must be true, since the pulse reflected from a moving mirror has more energy than the incoming pulse, the extra energy being supplied by the kinetic energy of the mirror; in the case of reflection from a moving ionization front in a stationary gas, this energy source is not available. It turns out, however, that the reflection coefficient from a receding recombination front is exactly the same as that from a receding mirror.

While reflection from an oncoming ionization front is less efficient than from an oncoming overdense electron beam, an ionization front device has advantages with respect to size and cost.

Analysis

Working in the frame of reference in which the ionization front is stationary (Fig. 1), the oscillating transverse electron velocity is determined by the linearized momentum conservation equation,

$$n\frac{\partial \underline{v}}{\partial t} + nU\frac{\partial \underline{v}}{\partial z} + U\underline{v}\frac{\partial n}{\partial z} = -\frac{e}{m}(\underline{E} + \frac{1}{c}\underline{U}\times\underline{B}) + \underline{R}. \qquad (3)$$

For the case of a recombination front ($U < 0$), $\underline{R} = \gamma U\underline{v}(dn/dz)$ represents the loss of electron oscillating momentum upon recombination; for the case of an ionization front ($U > 0$), $\underline{R} = 0$, since electrons are born with $\underline{v} = 0$. Using Eq. (3) and Maxwell's equations for curl $\underline{E}$ and curl $\underline{B}$, assuming time dependence $\exp(-i\omega t)$, and performing some algebraic manipulations, we find the wave equations

$$(c^2D^2 + \omega^2 - \omega_p^2)(-i\omega + UD)\,E = 0, \quad U > 0, \qquad (4a)$$

$$(-i\omega + UD)\omega_p^{-2}(c^2D^2 + \omega^2 - \omega_p^2)\,E = 0, \quad U < 0, \qquad (4b)$$

where $D \equiv d/dz$, $\omega_p^2 \equiv 4\pi n(z)e^2/m\gamma$, and $\gamma^{-2} \equiv 1-\beta^2$. Note that ω is related to the incident frequency in the laboratory frame by $\omega = (1+\beta)^{1/2}/(1-\beta)^{1/2}\,\omega_i$, and ω_p is numerically the same as the plasma frequency in the laboratory frame.

In the gas (assumed to have the dielectric properties of the vacuum), the solutions are of course the incident and reflected EM waves, $k = \pm\,\omega/c$. In the plasma, well behind the ionization front, where ω_p is constant, there are three solutions: (if $\omega_p^2 > \omega^2$) the evanescent and purely growing waves, $k = \pm\, i(\omega_p^2 - \omega^2)^{1/2}/c$,

and a propagating wave $k = \omega/U$ which connects with the plasma. The first two waves have exactly the same dispersion relation as in a stationary plasma. The third wave would reduce to a time-independent magnetic field $\underline{B} = B_0 \hat{y} e^{ikz}$, in a stationary plasma, but in a moving plasma it is a genuine transverse EM wave, transporting energy at the plasma velocity U. We shall refer to it as the "magnetic wave".

We now solve Eqs. (4) for the reflection coefficient, considering first the case $U < 0$. For $z \to +\infty$, where ω_p becomes constant, one of the three independent solutions is proportional to $\exp(i\omega z/U)$, i.e. represents the magnetic wave. This solution must be excluded, since, for $U < 0$, it transports energy in from $z = +\infty$. The other two solutions satisfy

$$[d^2/dz^2 + (\omega^2 - \omega_p^2)/c^2]\, E = 0, \qquad (5)$$

which is identical to the wave equation for a stationary ionization front in a stationary plasma (i.e. a mirror). The solution to (5) is thus, for $\omega_p^2 > \omega^2$ behind the front, evanescent wave in the plasma, and total reflection, i.e.

$$E(z) = E_i[\exp(i\omega z/c) + \exp(-i\omega z/c + i\theta)], \qquad (6)$$

in the gas. The ratio of reflected to incident power (still in the frame of the recombination front) is

$$P_r/P_i = |E_r|^2/|E_i|^2 = 1. \qquad (7)$$

Lorentz transforming back to the laboratory frame, where the plasma is stationary but the recombination front is receding, we have for reflected power

$$P_r^*/P_i^* = (1 - |\beta|)^2/(1 + |\beta|)^2, \qquad (8a)$$

and for total energy (integrated over the pulse)

$$\mathcal{E}_r^*/\mathcal{E}_i^* = (1 - |\beta|)/(1 + |\beta|). \qquad (8b)$$

Equations (8a,b) are compatible because the reflected pulse is elongated according to Eq. (2). Equations (5-8) are all identical to those for a receding mirror.

We now consider the case of an oncoming ionization front, $U > 0$. E is a solution of Eq. (4a) if

$$E = \int_{\infty}^{z} dz' \exp[i\omega(z-z')/U] g(z'), \qquad (9)$$

and g is a solution of Eq. (5). Using the solution (6) ($\omega_p^2 > \omega^2$) in (9), we find, in the gas, $E \propto \exp(i\omega z/c) + \{(1-\beta)/(1+\beta)\}\exp(-i\omega z/c + i\theta)$. Thus the reflected power is given by

$$P_r/P_i = (1 - \beta)^2/(1 + \beta)^2. \qquad (10)$$

Transforming back to the laboratory frame, we find, for the reflected power,

$$P_r^*/P_i^* = 1, \qquad (11a)$$

but the total reflected energy is less than the incident energy,

$$\mathcal{E}_r^*/\mathcal{E}_i^* = (1 - \beta)/(1 + \beta). \qquad (11b)$$

The reflected pulse is shortened according to (2). Equations (11) differ from those for a moving mirror, which would be

$$P_r^*/P_i^* = (1 + \beta)^2/(1 - \beta)^2, \qquad (12a)$$

$$\mathcal{E}_r^*/\mathcal{E}_i^* = (1 + \beta)/(1 - \beta). \qquad (12b)$$

In the limit of a sharp ionization front (i.e. narrower than a wavelength), the wave equations (4) can be solved explicitly. For $U > 0$, we find that both the evanescent wave and the magnetic wave are excited, and the latter transmits into the plasma that portion of the incident energy which is not reflected. (In the laboratory frame it would be more correct to say that magnetic energy and transverse electron kinetic energy is left behind in the plasma as the front moves on.) In the opposite limit of a broad front, the magnetic wave vanishes, but the same amount of energy convects into the plasma, totally in the form of electron kinetic energy. It can be shown that overall energy and momentum are conserved in this way. It is interesting to note that, in either case, wave energy penetrates into an overdense plasma.

For the recombination front case, $U < 0$, oscillating electron kinetic energy is carried toward the neutral gas, and is ultimately released as recombination radiation. Again, it can be shown that energy and momentum are conserved. The magnetic wave is never excited, since it would carry energy in from $z = +\infty$.

It is obvious physically that EM waves cannot be reflected from an oncoming ionization front moving faster than c, since the front would instantaneously overtake the wave. It is reassuring that this result also emerges from the mathematics. In the superluminous case, the evanescent and growing waves in the plasma both become (in the laboratory frame) propagating waves. Both of these are excited, rather than one reflected wave and one evanescent wave.

Finally, we reiterate our main conclusions: a microwave reflected from an approaching ionization front will be Doppler up-shifted, the reflection coefficient, given by Eqs. (11), becomes small in the relativistic limit $\beta \to 1$, but the effect may be useful nonetheless, because the investment in energy and equipment needed is modest compared to other methods of up-shifting microwaves, e.g. Ref. 2.

References and Footnotes

*Permanent address: Cornell University.

1. Downshift of an IR laser beam off a moving recombination front may also prove useful.

2. P. Sprangle, V. Granatstein, and L. Baker, Phys. Rev. A12, 1697 (1975).

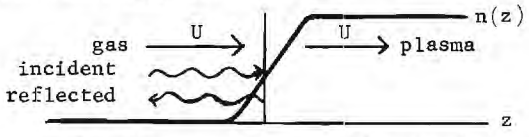

Figure 1. The scattering problem in the frame of reference of the ionization front.

SEMICONDUCTOR CYCLOTRON RESONANCE, TRANSPORT AND SURFACE PHENOMENA

G. Landwehr

Physikalisches Institut der Universität Würzburg
8700 Würzburg, Germany

Cyclotron resonance in bulk semiconductors

The use of submillimeter waves in cyclotron resonance experiments with semiconductors has the advantage that due to the higher frequency (in comparison with microwaves) either the $\omega\tau$ (ω = cyclotron frequency eB/m, τ = relaxation time) values can be increased or materials with lower mobility can be explored. Usually transmission-type spectrometers in the Faraday configuration with molecular lasers are employed. Due to the small wavelengths a number of problems arise which must be kept in mind.

A plane-parallel sample can behave like a Fabry-Perot cavity; and interference effects can substantially change the shape of the cyclotron absorption line.

Plasma effects (f. i. helicon-like excitations) can be observed when the electron or hole density in the specimens is not too low.

Not all transmission minima in a magneto-transmission experiment can be assigned to cyclotron resonance absorption. A very pronounced structure can be caused by impurity transitions. This is shown in Fig. 1 where the relative transmission for tellurium as a function of a magnetic field is plotted for temperatures of 2.6 K (top), 5.4 K, 9.2 K and 13 K (bottom). The magnetic field is parallel to the trigonal axis and the free hole concentration is $4 \cdot 10^{13}/cm^3$. The structure which is recorded at 2.6 K at magnetic fields below 3 T disappears when the temperature is raised to 13 K and can be attributed to impurity transitions. The transmission minimum at about 3.5 T can be assigned to cyclotron resonance absorption. To distinguish impurity and cyclotron resonance transitions it can be helpful to take data at different frequencies.

The possible complications in cyclotron resonance experiments will be discussed by choosing tellurium as an example. In this semiconductor the magneto-transmission has been studied rather thoroughly during the last few years /1/. For tellurium it can be demonstrated how rather complex absorption spectra can be caused by a complicated band structure. In general, a close

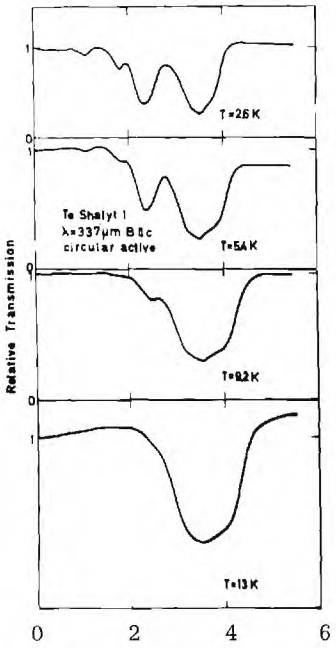

Fig. 1:

interaction between theory and experiment is necessary to explain magneto-transmission data on a quantitative basis.

In order to study cyclotron resonance and impurity transitions in pure semiconductors, it can be advantageous to use a Fourier transform spectrometer in which the sample is used as a photocunductive detector. The method is extremely sensitive and especially useful for experiments in regions of high absorption close to a reststrahlen band and for very pure crystals with low absorption.

Submillimeter investigations in two-dimensional systems

In the last few years a substantial amount of work has been devoted to the investigation of the properties of space charge layers in semiconductors. Submillimeter waves have played an essential role in this area. Semiconductor in-

version- or accumulation layers with a surface charge density up to $10^{13}/cm^2$ can be generated by field strengths up to 10^6 V/cm. The thickness of the potential well parallel to the surface can be of the order of 100 Å or less. This confinement leads to quantum effects because the carriers are not free to move perpendicular to the surface. Due to the boundary quantization the quasi-continuous levels are grouped into electric subbands. Because the carriers are free to move parallel to the surface, they behave as a quasi-twodimensional electron gas.

Cyclotron resonance experiments with carriers confined to narrow space charge layers have been performed for silicon /2/, tellurium /3/, InSb /4/ and germanium /5/. The activity in this area has been quite large during the last few years. A number of special features have been observed. Superimposed on the cyclotron absorption line is a quantum structure which was first predicted by Ando /6/. These superimposed oscillations are not Shubnikov-de Haas oscillations. Not only the main absorption peak has been observed for silicon, but also subharmonic structure. A very unusual temperature dependence was found for the electron cyclotron resonance in silicon (100) surfaces /7/. The absorption peak shifted quite substantially to higher magnetic fields with increasing temperature. The effect is not yet fully explained. Anomalous behaviour was also discovered for surface carrier concentrations below $10^{12}/cm^2$ where an apparent shift in cyclotron mass has been attributed to localization effects.

In p-type silicon inversion layers the cyclotron mass m_c depends substantially on the surface electric field E, m_c increases with increasing E values. Recent cyclotron resonance experiments /8/ have confirmed previous data which were derived from the Shubnikov-de Haas effect /9/.

Whereas the silicon data were obtained with MOS devices (metal-oxide-semiconductor), the experiments on Te, InSb and Ge have been performed with the MIS configuration (metal-insulator-semiconductor). In this case the insulator consisted of a Mylar foil. The Te-results are of special interest in so far that up to now it has been impossible to produce extrinsic n-type tellurium and that consequently the information about electrons at low temperatures is very scarce.

The cyclotron resonance transition in space charge layers occur between different Landau levels which belong to a particular electric subband. It is, however, possible to study transitions between different subbands without a magnetic field. In this case the transmission or its derivative is studied as a function of the surface electric field at a fixed laser frequency. By employing various frequencies the difference in energy between two subbands may be determined /10/. Because the charge carrier density in the surface layer can be quite large (up to $10^{19}/cm^3$), plasma effects have to be taken into account /11/. Also, it has been suggested that an exciton-like interaction plays a role /12/. It has become clear that many-body-effects like exchange interaction and correllation are significant in semiconductor space charge layers. The experimental data on the subband energies can only be explained when many-body-effects are taken into account /13/.

A wealth of information has been obtained from the submillimeter spectroscopy in semiconductor space charge layers. Although many features of the data are rather well understood, some aspects are not understood at all. Undoubtedly the activities in this field will continue for some time to come.

Cyclotron resonance in the Azbel-Kaner geometry

Transmission-type cyclotron resonance experiments in the Faraday geometry are restricted to materials with low carrier concentrations. In semiconductors with high carrier density the penetration depth of submillimeter radiation is very small. In this case a technique can be employed which has been successfully used in metal physics, the Azbel-Kaner technique /14/. The interaction between carriers and the radiation occurs within the skin depth. Experiments are performed by constructing a TE-moded strip line and by recording the transmitted submillimeter wave intensity. The distance between two sample surfaces is small in comparison to the wave length. In order to calculate the attenuation, Maxwell's equations have to be solved under the appropriate boundary conditions which can be quite cumbersome. It turns out that the strip line transmission depends essentially on the component ε_{zz} of the dielectric tensor. Typical data for PbSe are shown in Fig. 2 for various temperatures /14/.

The relative transmission has been plotted for 337 µm radiation for a strip line with a PbSe sample of (100) orientation. Clearly the signal decreases in amplitude with increasing temperature. Because the valence band maxima in PbSe are located along the (111) axis of the Brillouin zone, only a single transmission mi-

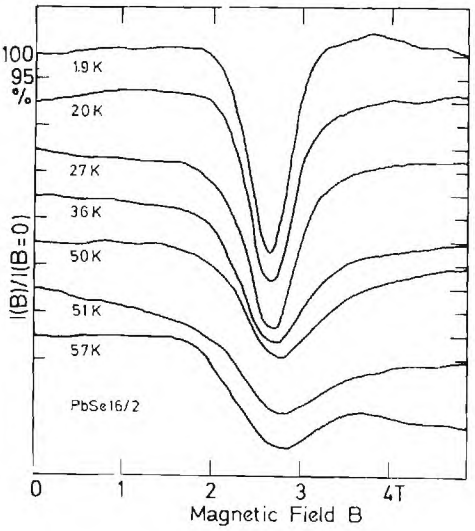

Fig. 2

nimum occurs. These and additional data for other orientations can be fitted with the mass parameters $m_T = 0.0626\ m_o$, $m_L = 0.111\ m_o$.

Experiments of this type have also been performed for PbTe, $Pb_{1-x}Sn_xTe$ /15/ and for HgSe /16/. Additional structure has been observed, the possible origin of which will be discussed.

In conclusion it can be stated that submillimeter cyclotron resonance spectroscopy has continued to be a valuable tool to elucidate the band structure of semiconductors and the subbands in semiconductor space charge layers.

References

/1/ M. von Ortenberg, K. J. Button, G. Landwehr and D. Fischer, Phys. Rev. B 6, 2100 (1972)
M. von Ortenberg, IEEE Transactions on Microwave Theory and Techniques MTT 22, 1081 (1974)

/2/ See, f.i. G. Abstreiter, J.P. Kotthaus, J.F. Koch and G. Dorda, Phys. Rev. B 14, in print

/3/ M. von Ortenberg and R. Silbermann, Solid State Comm. 17, 617 (1975)

/4/ A. Därr, J.P. Kotthaus and J.F. Koch, Solid State Comm. 17, 455 (1975)

/5/ W. Weber, G. Abstreiter and J.F. Koch, Solid State Comm. 18, 1397 (1976)

/6/ T. Ando, Phys. Rev. Lett. 36, 1383 (1976)

/7/ J.P. Kotthaus, in Lecture Notes on "The Application of High Magnetic Fields in Semiconductor Physics", Physikalisches Institut der Univ. Würzburg, p. 663 (1976)

/8/ J.P. Kotthaus, to be published and ref. /7/

/9/ G. Landwehr, Festkörperprobleme XIV (Advances in Solid State Physics), p. 49, Pergamon-Vieweg 1975

/10/ A. Kamgar, P. Kneschaurek, W. Beinvogl and J.F. Koch, Proc. 12th Conf. on the Physics of Semiconductors, Stuttgart 1974, p. 709 (B.G. Teubner, Stuttgart)

/11/ W.B. Chen, Y.J. Chen and E. Burstein, Surface Science 58 (1976), in print

/12/ T. Ando, to be published

/13/ T. Ando, Phys. Rev. B 13, 3468 (1976)
B. Vinter, Phys. Rev. Lett. 35, 598 (1975)

/14/ M. von Ortenberg, K. Schwarzbeck and G. Landwehr, Physique sous Champs Magnétiques Intenses, Grenoble 1974, p. 305 (CNRS)

/15/ J.Q. Ramage, R.A. Stradling, R.J. Tidey and J.R. Burke, Proc. 12th Int. Conf. on the Physics of Semiconductors, Stuttgart 1974, p. 531 (B.G. Teubner, Stuttgart)

/16/ M. von Ortenberg, K. Schwarzbeck, G. Landwehr and R.R. Galazka, Proc. of the 13th Int. Conf. on the Physics of Semiconductors, Rome 1976, in print

APPLICATION OF SUBMILLIMETER SPECTROSCOPY TO MAGNETIC EXCITATIONS

R. Geick
Physikalisches Institut der Universität Würzburg
D-8700 Würzburg, West Germany

1. Introduction

Magnetic excitations are the collective modes of a system of spins or magnetic moments which are usually observed in the ordered ferromagnetic or antiferromagnetic state of the system. The frequencies of these excitations fall in the microwave range and in the far infrared or submillimeter spectral region, up to 1000 cm^{-1}.

The study of magnetic excitations is of current interest since the dominating exchange interaction between the magnetic ions may be 3-dimensional or may be restricted to 2 or 1 dimensions even though the crystal is an ordinary 3-dimensional one, but with an anisotropic structure. The properties of such systems, i.e. susceptibility, excitations, specific heat etc., are of particular interest with respect to the theory of phase transitions and critical phenomena. Some materials are compiled as examples in table 1.

Table 1: Examples of 1-, 2- and 3-dimensional magnetic materials

Dominating exchange interaction		
1-dimensional	2-dimensional	3-dimensional
← pure materials →		
$CsNiF_3$ /26/	K_2MnF_4 /16, 22/	MnF_2 /1/
$CoCl_2\ 2H_2O$ /7, 20/	K_2NiF_4 /11, 13/	NiF_2 /4, 18, 21/
$CoCl_2\ 6H_2O$ /28/	Rb_2MnF_4 /16/	CoF_2 /3, 18/
	$CoCl_2$ /5/	$KMnF_3$ /19/
	$FeCl_2$ /5, 17/	NiO /2/, CoO /9, 10/
← doped materials, mixed crystals →		
	$K_2MnF_4:Ni^{2+}$ /14, 22/	$MnF_2:Fe^{2+}$ /6, 8/, $MnF_2:Co^{2+}$ /8, 24/
		$MnF_2:Zn^{2+}$ /12, 15/, $CoF_2:Mn^{2+}$ /23/
		CoO/NiO /25, 27/

Among the great number of existing materials of each kind, those have been selected which were actually studied by means of submillimeter spectroscopy, and the references refer mostly to these investigations.

Materials with rather isotropic structures (cubic rocksalt, cubic perovskite and rutile structure) are generally 3-dimensional ferro- or antiferromagnets. In materials with perovskite-type layer structures such as K_2NiF_4, the interlayer exchange interaction is partly cancelled and is much weaker as compared to the intralayer interaction. And in hexagonal $CsNiF_3$ and monoclinic $CoCl_2 \cdot 2H_2O$ for example, the spins are predominantly coupled along linear chains. Thus, these magnetic materials represent very realistic model system in one, two or three dimensions. In most cases, the isotropic Heisenberg-model seems to be adequate to describe the properties. In systems with Co-ions, however, the Ising-model or an X-Y-model may be more appropriate. It should be noted, that two types of dimensionality enter these consideration, namely the lattice dimensionality already discussed and the spin dimensionality (Heisenberg, X-Y, or Ising model).

2. Experimental technique

Magnetic excitations can be studied by means of inelastic neutron scattering, by Raman

scattering and by submillimeter spectroscopy. Due to wavenumber conservation, the two optical methods allow only the determination of the q = 0 modes of the spin wave spectrum, apart from broad two-magnon bands, while there is no such restriction for the neutron scattering technique. The present paper is to review the role that submillimeter spectroscopy played in studying magnetic systems, and the other two methods and their results will not be further mentioned in detail here. Indeed, submillimeter spectroscopy is a rather direct method to study the q = 0 spin wave excitations or the antiferromagnetic and ferromagnetic resonance in antiferromagnets and ferromagnets, respectively. For such investigations, various techniques have been employed:

1) conventional grating monochromator
2) Fourier transform spectrometer
3) FIR-laser spectroscopy
4) Microwave techniques

In the frequency range 15 - 100 cm^{-1}, grating spectrometers have been widely used for the investigation of magnetic excitations, especially for the early work on 3-dimensional antiferromagnetics /1, 2, 7/. As a broad-band source, the mercury high pressure arc is usually employed. Low temperature carbon, silicon or germanium bolometers improved as detectors the signal-to-noise ratio considerably. In the last decade, an increasing number of investigations was performed with the method of Fourier transform spectroscopy /3, 4, 6, 8, 11, 12, 15, 17, 22, 25-27/. For the range above 15 cm^{-1}, the Michelson interferometer and a bolometer at 4.2 K may be used. Below 15 cm^{-1}, however, it is necessary to increase the interferometer efficiency by using a lamellar grating beam divider and to increase the signal-to-noise ratio by means of a ^3He cooled detector /6, 8, 17, 22, 26/.

In most cases, the frequency of the q = 0 magnon (antiferromagnetic resonance) is not only determined in zero magnetic field but also as a function of an external static magnetic field. And with grating or Fourier transform spectrometers, the transmission of the sample is usually measured as a function of wavelength or frequency at fixed magnetic field. In the microwave region on the other hand, it is the usual magnetic resonance technique to measure the transmission of the sample as a function of applied magnet field at a fixed frequency which is provided by a microwave source (klystron, carcinotron etc.). This technique is of advantage at rather low frequencies and has been used there frequently /1, 13, 16, 18, 21, 23, 28/. The frequencies range from 20 GHz to 600 GHz. For higher frequencies, no microwave sources are available. But there are a number of molecular laser sources in the submillimeter range which have been used for submillimeter spectroscopy, e.g. the HCN-laser (29.7; 32.2 cm^{-1}), the DCN-laser (51.4; 52.7 cm^{-1}), the H_2O (127.5 cm^{-1}) and the D_2O-laser (118.7 cm^{-1}) /20, 24/. And it seems that lasers will be used increasingly in future since a great number of frequencies is available from a variety of molecular lasers which can conveniently be pumped by powerful CO_2-lasers.

3. Experimental Results

In this section, the results of studying magnetic excitations will be reviewed and discussed with respect to their contribution to the understanding of the properties of magnetic materials.

3.1. Three-dimensional pure materials

For a simple 3-dimensional easy-axis antiferromagnet like MnF_2, the antiferromagnetic resonance (AFMR) frequency

$$\omega_{AFMR} = \gamma \left[\sqrt{H_A (2H_E + H_A)} \pm H_0 \right] \qquad (1)$$

(with the gyromagnetic ratio $\gamma = g\mu_B/\hbar$) depends not only on the isotropic exchange interaction ($H_E = \frac{1}{\gamma} 2 z S J = 49$ cm^{-1}, S = 5/2, number of next nearest neighbours z = 8) but also on the anisotropy field ($H_A \hat{=} 0.75$ cm^{-1}) which, in the case of Mn^{2+}-ions, arises mainly from magnetic dipole-dipole interactions /1/. In an external magnetic field H_0 parallel to the easy axis, the doubly degenerate mode splits and varies linearly with H_0. As a function of temperature, the AFMR-frequency is proportional to the sublattice-magnetization and approaches zero as the temperature approaches the Néel-temperature T_N (cf. Fig. 1).

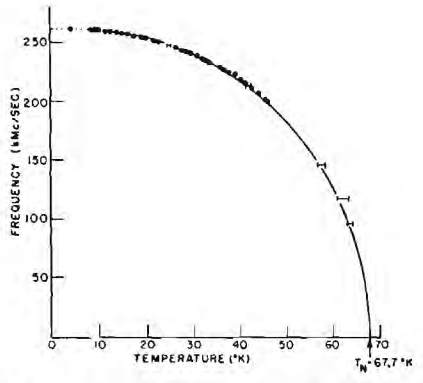

Fig. 1: AFMR frequency of MnF_2 versus temperature ( ) as compared to the appropriate Brillouin curve $B_{5/2}(T/T_N)$ (solid curve)/1/

In this 3-dimensional magnetic material, the variation of ω_{AFMR} with temperature is reasonably well described by the appropriate Brillouin-function $B_{5/2}(T/T_N)$ [solid curve in Fig. 1]. In CoF_2, this simple picture has to be somewhat modified (cf. Fig. 2).

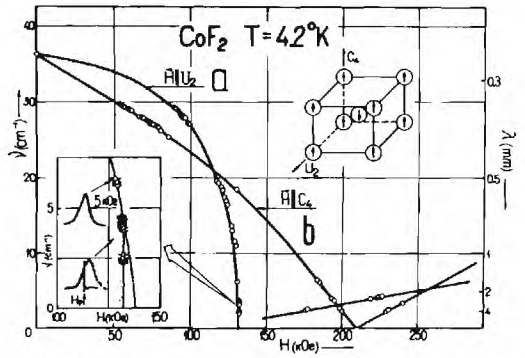

Fig. 2: AFMR frequency versus magnetic field for CoF_2 /18/

For H_o c, i.e. parallel to the easy axis, the variation of $_{AFMR}$ with magnetic field is no longer linear. The more complicated behaviour of $_{AFMR}$ versus H_o can be described in terms of the Dzyaloshinski-interaction (parameter H_D) and by including higher order terms in the spin hamiltonian /18/. With the Dzyaloshinski-interaction, the AFMR frequency is

$$\omega^2 = \gamma^2 (2H_E H_A - H_D^2)\left[1 - \frac{(H_A^2 + H_D^2) H_o^2}{(2H_E H_A - H_D^2)^2}\right] \qquad H_o \| a$$

$$\omega^2 = \gamma^2 \left[\left(\sqrt{2H_E H_A} \pm H_o\right)^2 - H_D^2\right] \qquad H_o \| c \qquad (2)$$

Physically, the Dzyaloshinski-interaction means additional terms of single ion anisotropy or anisotropic exchange. Since in the case of Co^{2+} the orbital angular momentum is not quenched, both effects are expected to be considerable in the case of Co^{2+}. When the AFMR-mode softens and its frequency approaches zero, magnetic phase transitions occur (cf. Fig. 2), e.g. the spin flop transition at 210 KOe.

3.2. Two-dimensional pure materials

In the 2-dimensional material K_2MnF_4, each magnetic ion is coupled to its 4 nearest in-plane neighbours by exchange. The interplanar exchange is negligible. And there should be no transition to an ordered magnetic state for $T_N > 0$ according to theory. However, the small anisotropy field (dipole interactions!) causes a transition to an ordered antiferromagnetic state at T_N = 42.1 K (K_2MnF_4). But the spin waves are essentially those of two-dimensional layers with practically no interlayer coupling. These properties are reflected in the variation of the AFMR-frequency (and of the sublattice magnetization with temperature which deviate substantially from the Brillouin-curve (cf. Fig. 3).

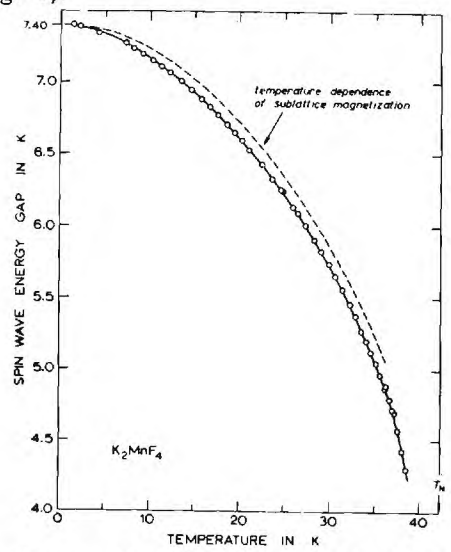

Fig. 3: Temperature dependence of AFMR frequency in K_2MnF_4 (o) and sublattice magnetization as determined by ^{19}F-NMR-spectroscopy /16/

Due to the modified density of states in 2 dimensions, there is a rather large zero point spin deviation of nearly 20 % in these materials ($\sim$ 2 % in MnF_2). Therefore, the so-called Oguchi corrections /30/ are often taken into account in the spin wave theory:

$$\omega_{AFMR} = \gamma\sqrt{H_A(2H_E + H_A)} - \frac{g(0)\gamma H_E}{2SN}\sum_k \left(g(k) - 1\right) \qquad (3)$$

$$\text{with } g(k) = \left(H_E\left[1 - \gamma_k^2\right] + H_A\right)\left(\left[H_E + H_A\right]^2 - H_E^2\gamma_k^2\right)^{-\frac{1}{2}}$$

$$\text{and } \gamma_k = \cos\left(\frac{k_x a}{2}\right)\cos\left(\frac{k_y a}{2}\right)$$

The second term of Eq. (3) is the Oguchi-correction for T = 0. For calculating spin wave frequency and eventually sublattice magnetization as a function of temperature, the corrections are essential. For $T \approx 0$, however, H_E and H_A are often determined from experimental data by means of Eq.(1) instead of Eq.(3) (H_E = 60.3 cm^{-1}, H_A = 0.22 cm^{-1}). The values with Oguchi cor-

rection are $H_E^o = 58.5\ cm^{-1}$ and $H_A^o = 0.23\ cm^{-1}$ /16, 22, 29/.

3.3. One-dimensional pure materials

For the hexagonal compound $CsNiF_3$, it has been found by neutron scattering experiments that the dominant exchange interaction is along linear chains. Above the 3-dimensional antiferromagnetic ordering temperature ($T_N = 2.61$ K), there exists a 1-dimensional short range order along the chains and ferromagnetic spin waves were observed up to 20 K. The antiferromagnetic resonance frequency is for a 1-dimensional easy-plane ferromagnet /26/:

$$\omega_{FMR} = \gamma \sqrt{H_o (H_A + H_o)} \qquad (4)$$

where H_o is the external field applied perpendicular to the chains and $H_A = 3.3\ cm^{-1}$ is the anisotropy field, respectively. In Fig. 4, the FMR frequency is shown versus temperature at fixed

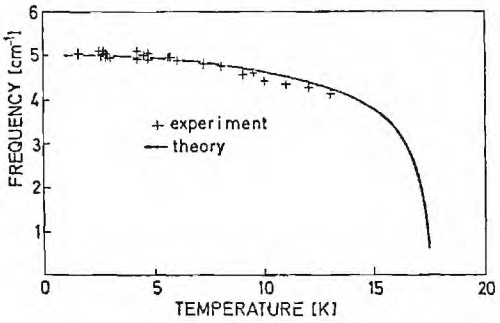

Fig. 4: FMR frequency of $CsNiF_3$ versus temperature (+). The solid line is calculated by means of spin wave renormalization /26/

external field $H_o = 2.675$ T. The solid line in Fig. 5 has been calculated by means of a spin wave renormalization. The agreement between experimental and calculated data is quite good. $CoCl_2 \cdot 2H_2O$ is also a 1-dimensional magnetic material. Its peculiar property is that the excitations in this material derived by submillimeter-spectroscopy can well be approximated by a 1-dimensional Ising-model /7, 20/.

3.4. Doped materials and mixed crystals

In the last section, let us consider the properties of 3-dimensional materials doped with impurities. If an isolated impurity is subject to an effective field $H_{eff} = H_E + H_A$ (exchange and anisotropy field) and if the frequency $\omega = \gamma H_{eff}$ is above the spin wave band, a localized spin wave mode will occur. This happens for MnF_2:Fe^{2+} ($\nu_{Local} = 94.8\ cm^{-1}$) and for MnF_2:Co^{2+} ($\nu_{Local} = 123.5\ cm^{-1}$) /6, 7, 24/. If, on the other hand, $\omega = \gamma H_{eff}$ is smaller than ω_{AFMR}, a local mode will occur below the spin wave band. This is the case for CoF_2:Mn^{2+} (cf. Fig. 7) /23/.

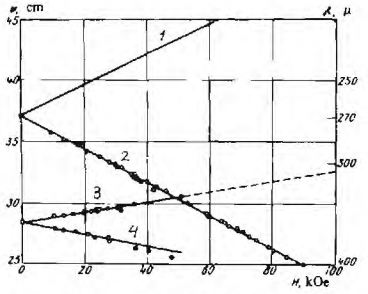

Fig. 5: Dependence of AFMR frequencies and impurity mode frequencies on magnetic field /23/

At a magnetic field of $H_o \approx 50$ KOe, the frequencies of one AFMR-mode ( ) and of one impurity mode ( ) coincide. For $H_o > 50$ KOe, the local mode is no longer observed because it is incorporated in the spin-wave-band and is no longer localized. If MnF_2 is doped with the diamagnetic impurity Zn^{2+}, the exchange field is drastically reduced /12, 15/.

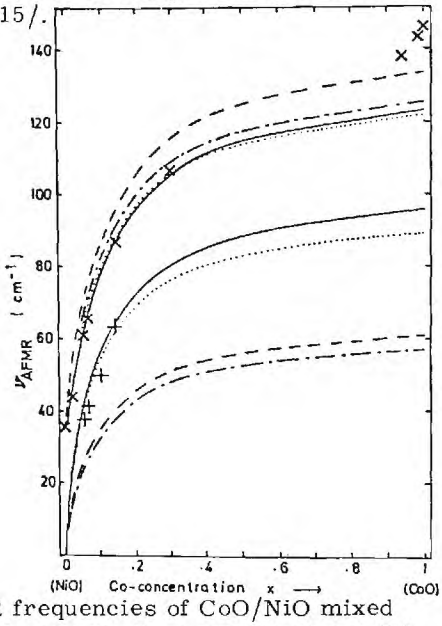

Fig. 6: AFMR frequencies of CoO/NiO mixed crystals versus Co-concentration x (X). The curves have been calculated by means of a four-sublattice-model for various parameter combinations /27/

NiO and CoO are antiferromagnets with the rocksalt structure /2, 9, 10/. The AFMR of CoO/NiO mixed crystals has been studied for various concentrations. By means of model considerations, it was shown that the drastic variation of ω_{AFMR} at the Ni-rich side is due to the rotation

of the preferred spin direction in NiO ($<11\bar{2}>$) to that of CoO ($\approx$ $<33\bar{8}>$) as a consequence of the much larger anisotropy of the Co-ions. The drastic variation on the Co-rich side is attributed to collective effects of the Co-ions /25, 27/. Thus, the AFMR of the mixed crystals provides detailed information about the Co-ion anisotropy energy.

References

/1/ F.M. Johnson and A.H. Nethercot, Phys. Rev. 114, 705 (1959)
/2/ A.J. Sievers and M. Tinkham, Phys. Rev. 129, 1566 (1963)
/3/ P.L. Richards, J. Appl. Phys. 35, 850 (1964)
/4/ P.L. Richards, Phys. Rev. 138, A 1769 (1965)
/5/ L.S. Jacobs, S. Roberts, and P.E. Lawrence, J. Appl. Phys. 36, 1197 (1965)
/6/ R. Weber, Phys. Rev. Lett. 21, 1260 (1968)
/7/ J.B. Torrance and M. Tinkham, Phys. Rev. 187, 595 (1969)
/8/ R. Weber, J. Appl. Phys. 40, 995 (1969)
/9/ M.R. Daniell and A.P. Cracknell, Phys. Rev. 177, 932 (1969)
/10/ I.S. Austin and E.S. Garbett, J. Phys. C 3, 1605 (1970)
/11/ R.J. Birgeneau, F. de Rosa, and H.J. Guggenheim, Sol. State Comm. 8, 13 (1970)
/12/ H. Mitlehner, R. Geick, W. Lehmann, R. Weber, G. Dietrich, and H. Schoenherr, Sol. State Comm. 9, 2059 (1971)
/13/ H. Yamazaki, K. Watanabe, and H. Abe, J. Phys. Soc. Japan 32, 862 (1972)
/14/ W. Lehmann and R. Weber, Phys. Letters 45 A, 33 (1973)
/15/ M. Buchanan, W.J.L Buyers, R.J. Eliott, R.T. Harley, W. Hayes, A.M. Perry, and I.D. Savilles, J. Phys. C 5, 2011 (1972)
/16/ H.W. de Wijn, L.R. Walker, S. Geschwind, and H.J. Guggenheim, Phys. Rev. B 8, 299 (1973)
/17/ K.C. Johnson and A.J. Sievers, Phys. Rev. B 7, 1081 (1973)
/18/ E.G. Rudashevsky, A.S. Prokhorov, and L.V. Velikov, IEEE Transactions MTT-22, 1064 (1974)
/19/ K. Saiki, J. Phys. Soc. Japan 38, 373 (1975)
/20/ D.F. Nicoli, and M. Tinkham, Phys. Rev. B 9, 3126 (1974)
/21/ L.V. Velikov, L.A. Prozorova, A.S. Prokhorov, E.G. Rudashevsky, and A.I. Smirnov, Sov. Phys. - JETP 41 567 (1975) /Zh. Eksp. Teor. Fiz. 68, 1145 (1975)/
/22/ W. Lehmann, F. Macco, and R. Weber, Physica 80 B, 27 (1975)
/23/ A.S. Prokhorov, and E.G. Rudashevsky, JETP Lett. 22, 99 (1975) /Pisma Zh. Eksp. Teor. Fiz. 22, 214 (1975)/
/24/ U. Dürr, and K.J. Button, Sol. State Comm. 16, 695 (1975)
/25/ C.R. Becker, Ph. Lau, R. Geick, and V. Wagner, phys. stat. sol. (b) 67, 653 (1975)
/26/ R.J. Grill, U. Dürr, and R. Weber, Proc. Int. Conf. on Magnetism, Amsterdam 1976, to be published
/27/ G. Geis, R. Geick, C.R. Becker, and V. Wagner, Proc. Int. Conf. on Magnetism, Amsterdam 1976, to be published
/28/ W. Ghidalia, J. Tuchendler, J. Magarino, Proc. Int. Conf. on Magnetism, Amsterdam 1976, to be published
/29/ W. Lehmann, and R. Weber, J. Phys. C 1976, to be published
/30/ T. Oguchi, Phys. Rev. 117, 117 (1960)

DIELECTRIC MEASUREMENTS IN THE SUBMILLIMETRE REGION

G.W. Chantry
Division of Electrical Science
National Physical Laboratory
Teddington, Middlesex U.K.

The anomalous dispersion of polar liquids in the radio-frequency and microwave regions was considered theoretically by Debye in 1913 long before any accurate measurements were possible [1]. The whole problem of treating the frequency dependent complex polarizability of an ensemble of interacting dipoles was (and still is!) intractable but Debye with the characteristic courage of a great mind cut through the Gordian knots of the theoretical sticking points and came up with a simple theory which gave, in restricted frequency regions, a reasonable account of the dispersion. From the late thirties onwards, when measurements became possible this Debye equation

$$\frac{\hat{\varepsilon}(\omega)-\varepsilon_\infty}{\varepsilon_s-\varepsilon_\infty} = \frac{1}{1+i\omega\tau} \qquad (1)$$

where $\hat{\varepsilon}(\omega) = \varepsilon'(\omega)-i\varepsilon''(\omega)$ is the complex relative permittivity, ε_s and ε_∞ its values at zero and infinite frequency and τ a characteristic relaxation time, was extensively used to give some insight into the microdynamics of polar liquids. One consequence of this equation is that since it may be written [2]

$$\left[\varepsilon' - \left(\frac{\varepsilon_o+\varepsilon_\infty}{2}\right)\right]^2 + \left[\varepsilon''\right]^2 = \left(\frac{\varepsilon_o-\varepsilon_\infty}{2}\right)^2, \qquad (2)$$

a plot of ε'' versus ε' should be a semi-circle and such plots (often called Cole-Cole plots) feature strongly in the literature. The Cole-Cole plot for chlorobenzene is shown, as an example in Fig 1.

Debye was very careful to point out that his approximate equation should not be used at frequencies ω greater than τ^{-1} for in that region inertial effects would become significant and these are expressly excluded in the derivation of the equation. Equation (1) taken as it stands leads (via the relationship $\alpha \approx \varepsilon''\omega/c(\varepsilon')^{\frac{1}{2}}$) to a limiting high frequency absorption coefficient α_∞ given by $\alpha_\infty = (\varepsilon_s-\varepsilon_\infty)/c\tau\varepsilon^{\frac{1}{2}}_\infty$. This implies that all polar liquids would be opaque throughout the infrared and optical regions in conflict, of course, with observation. Numerous theoretical attempts to overcome this difficulty have been made from time to time but these were given a boost by the experimental determinations of submillimetre spectra which began at the NPL in the middle sixties [3]. These spectra showed, for the first time the broad additional absorption ("Poley" absorption) now known to be characteristic of the liquid state. Experimental results for chlorobenzene are shown in Fig 2 along with the "plateau" extrapolation of the Debye equation.

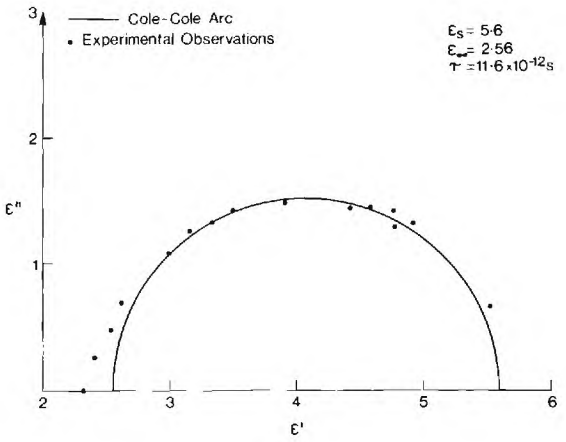

Figure 1. Cole-Cole arc for liquid chlorobenzene at 25 °C.

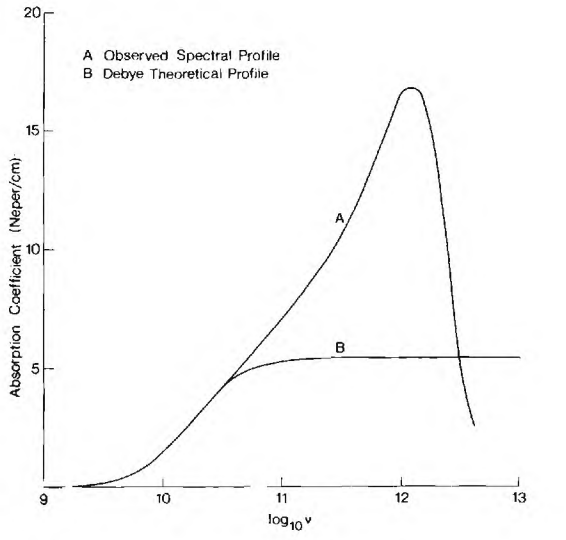

Figure 2. Observed high frequency spectrum of liquid chlorobenzene.

The theoretical explanations of the Poley absorption have taken two paths. Firstly there have been attempts to propose specific molecular models and to derive the expected spectrum from an analysis of the model:- typical of this approach is the work of Lassier and Brot [4]. Secondly there have been more abstract approaches in which general mathematical-physical concepts are used to constrain the theory and thus produce equations with a finite number of parameters. This latter approach came basically from Sack [5] with earlier input from Rocard and E.P. Gross. The modern versions use the correlation function, the memory function and such ideas as frequency dependent viscosity and are associated with the names of Kubo and Mori. In all these an integral equation is solved by means of taking Laplace transforms and one finishes up with a continued fraction of which the type

$$\frac{\hat{\varepsilon}-\varepsilon_\infty}{\varepsilon_s-\varepsilon_\infty} = 1 - i\omega\tau\gamma/i\omega\tau\gamma+\gamma/1+i\omega\tau\gamma+2\gamma/2+i\omega\tau\gamma+ \text{ etc.} \quad (3)$$

where $\gamma = I/\tau^2 kT$, is typical. It will be seen that the various truncations (i.e. the convergents) of this continued fraction give successively some familiar results. Thus one has

$$\frac{\hat{\varepsilon}-\varepsilon_\infty}{\varepsilon_s-\varepsilon_\infty} = 1, \quad \frac{1}{1+i\omega\tau}, \quad \frac{1}{(1+i\omega\tau)(1+i\omega\tau\gamma)} \text{etc.} \quad (4)$$

The absorption coefficient calculated from the higher truncations does go to zero at sufficiently high frequency and one has the desired recovery of transparency but this approach does not explain the additional "Poley" absorption, an explanation for which has to lie in terms of intermolecular interactions. At the moment opinions are divided on the question of how far the semi-classical approach can be pushed before quantum ideas have to be introduced.

The most modern approach is to side-track these interpretational difficulties by calculating the correlation function by direct Fourier transformation of the observed submillimetre and radio-frequency spectrum [6]. However for this approach to give meaningful answers the original spectral data has to be of very high quality. The efforts of the experimentalists is therefore being directed towards improving precision and eliminating sources of systematic error [7]. The submillimetre spectra are obtained from the Fourier transformation of the output of a Michelson interferometer used in either the conventional mode or else in the asymmetric (i.e. the dispersive) mode. Since their introduction by Gebbie and his colleagues in the late fifties these interferometers have been steadily improved and modern interferometers feature temperature stabilization, constant-current stabilized sources, phase modulation, high grade mechanical construction and last but by no means least cryogenically cooled low-noise solid-state detectors. These advanced interferometers coupled with the radically new designs of specimen cell which are emerging are opening up new realms of precision. Computational techniques are likewise being refined to the point where all the potential sources of error - even the most subtle have to all intents and purposes been eliminated. The present situation is that the experimentalists can guarantee absolute precision of ± 1% in α and ± 0.1% in n and it now remains to be seen whether these levels of accuracy are sufficient for the theoreticians to extract meaningful information or whether still more accuracy will be required.

References

(1)cf.Debye, P. "Polar Molecules" Chemical Catalogue Co. New York 1929.

(2) Cole, K.S. and Cole, R.H. Jour. Chem. Phys. 9 341 1941.

(3) Chantry, G.W. and Gebbie, H.A. Nature (London) 208 378 1965.

(4) Lassier, B. and Brot, C. Chem. Phys. letters 1 581 1968.

(5) Sack, R.A. Proc. Phys. Soc. B70 402, 414, 1957.

(6) Evans, M.W. Advances in Molecular Relaxation Processes. To be published 1976.

(7) Afsar, M.N., Chamberlain, J., Chantry, G.W., Finsy, R. and Van Loon, R. Proc. IEE. To be published.

INFRARED SPECTROSCOPY OF THE BOUND STATES OF THE SHALLOW IMPURITIES IN SEMICONDUCTORS

A.K. Ramdas

Department of Physics, Purdue University
West Lafayette, Indiana, 47907, U.S.A.

The electronic excitation (Lyman) spectra and the photo-ionization thresholds of many imperfections in semiconductors occur in the far infrared as a result of the small binding energies of the charge carriers bound to them. Group V donors and group III acceptors in Si and Ge are the classic examples and represent solid state analogs of the hydrogen atom. The paper will review the results on absorption, photoconductivity, and photothermal ionization spectra obtained with high resolution grating spectrometers, interferometers, and lasers, and discuss the effects of external perturbations on such spectra.

ANOMALOUS EXCITATIONS IN GLASSES IN THE FAR INFRARED*

A. J. Sievers
Laboratory of Atomic and Solid State Physics
and
Materials Science Center
Cornell University
Ithaca, New York 14853

An intriguing feature of amorphous dielectrics is the presence of low frequency anharmonic modes, these are qualified as "anomalous" since they contribute to large deviations from the expected crystalline behavior. The first clear evidence that these anomalous modes represented a general phenomenon in glassy materials was obtained from the low temperature specific heat and thermal conductivity measurements of Zeller and Pohl[1]. For a variety of glassy materials they found a linear temperature dependence of the specific heat and a thermal conductivity whose temperature dependence and magnitude were the same for all glasses. Extensive measurements of the specific heat [2] of a large number of glasses have confirmed the presence of anomalous excitations in the energy range below a few cm^{-1}. Additional evidence for such low frequency excitations comes from ultrasonic attenuation experiments [3]. Finally the observation of boundary scattering in small glass fibers has shown that Debye-like phonons carry the heat (as in a crystalline solid) and that the excess excitations observed in specific heat measurements do not themselves carry heat through the crystal [4]. To account for these special modes a localized tunneling model [5,6] has been proposed in which atoms, ions or groups of particles quantum mechanically tunnel between two or more equivalent sites. The linear dependence of the specific heat has been obtained from this model by including a statistical distribution of barrier heights and asymmetries for the local potential. One straightforward prediction which this model makes is that the temperature dependence of the far infrared absorption coefficient should be determined by the occupation numbers of a small number of energy levels associated with the tunneling manifold. For example a distribution of infrared-active two-level systems will produce an infrared absorption which decreases with increasing temperature in a well-defined way. In this talk, we shall discuss a variety of measurements of the temperature-dependent absorption coefficient of amorphous dielectrics in the far infrared. In one restricted temperature and frequency regime a decrease in absorption coefficient with increasing temperature is observed as expected while in another temperature and frequency range the absorption coefficient increases with increasing temperature [7]. A complete mapping of the absorption coefficient versus frequency and temperature for a number of glasses demonstrates that both ground state and excited state transitions are observed in the far infrared. In addition the results are consistent with the presence of widely spaced manifolds of energy levels. All of these results can be explained with an asymmetric tunneling potential model. At frequencies above 10 cm^{-1} a modest temperature dependence indicates that resonant mode transitions are being measured. Apparently the spatial inhomogeneities in glass provide a natural habitat not only for Debye-like phonons but also for localized modes, resonant modes and tunneling states - excitations which in the past were associated exclusively with slightly perturbed single crystals [8].

* Work supported in part by Energy Research and Development Administration, Grant No. E(11-1) 3151.

1. R.C. Zeller and R.O. Pohl, Phys. Rev. B4, 2029 (1971).
2. R.B. Stephens, Phys. Rev. B8, 2896 (1973).
3. W. Arnold, S. Hunklinger, S. Stein and K. Dransfeld, J. Non. Cryst. Solids 14, 1972 (1974).
4. R.O. Pohl, W.F. Love and R.B. Stephens, in Amorphous and Liquid Semiconductors, J. Stuke and W. Brenig, eds. (Taylor and Francis, 1974), pg. 1121.
5. P.W. Anderson, B.I. Halperin and C.M. Varma, Phil, Mag. 25, 1 (1972).
6. W.A. Phillips, J. Low Temp. Phys. 7, 351 (1972).
7. K.K. Mon, Y.J. Chabal and A.J. Sievers, Phys. Rev. Letters 35, 1352 (1975).
8. A.S. Barker, Jr. and A.J. Sievers, Rev. Mod. Phys. 47 Suppl. 2 (1975).

SUBMILLIMETER SPECTROSCOPY IN THE LIQUID AND SOLID STATE WITH A TUNABLE OPTICALLY PUMPED LASER*

B. L. Bean and S. Perkowitz
Physics Department
Emory University
Atlanta, Georgia 30322

The recent development of optically pumped far infrared (FIR) lasers has resulted in relatively powerful, quasi-tunable sources whose applications are just beginning to be explored. This paper reports on the use of such a laser to make transmission measurements in liquid H_2O, the semiconductor GaAs, and the high temperature superconductor V_3Si. The laser results are compared to other methods.

A block diagram of the FIR laser spectrometer is shown in Fig. 1. The 15-20 W of radiation from the CO_2 laser pumped the FIR metal waveguide laser [1]. The movable mirror M_6 and the Fabry-Perot interferometer provided wavelength tuning and measurement. After detection and lock-in amplification the transmitted and reference signals were ratioed in a digital ratiometer. This method gave very good data without requiring long term stability from the FIR laser. Further details are given in Ref. [2].

As a first test of this system the transmission of distilled liquid H_2O was measured at six wavelengths [2]. Methyl alcohol was pumped to obtain lines at 96.5, 118.8, 163.0, 232.9, and 570.5 μm, and 1,1-difluoroethylene provided a line at 375 μm. The measured absorption coefficient is shown in Fig. 2 to agree well with previous results [3]. The power levels of 0.5 to 3 mW obtained in the FIR lines gave a satisfactory signal-to-noise ratio with water pathlengths greater than 300 μm.

In a first solid state application a sample of GaAs (carrier concentration 5×10^{15} cm^{-3}) was examined with the methyl alcohol lines already mentioned as well as lines at 699.5 and 1217 μm. The laser data are compared to Fourier transform data [4] in Fig. 3 and are seen to have much smaller errors, and to agree very well except for transmissions below about 1%. A reasonable explanation is that stray light is important in the Fourier spectrometer, where the power is low and where the mercury arc lamp has broad band output. In the laser system only the lowest measured value at 570.5 μm is dubious because of stray light. That the value of 0.04% measured at 232.9 μm is valid is shown in Fig. 4. According to semiconductor optical theory the reciprocal of the free carrier absorption should be quadratic in frequency [4]. The new laser value at 232.9 μm falls on the same straight line established by the data at shorter wavelengths.

In a second solid state measurement the methyl alcohol lines from 96.5 to 1217 μm were used to examine a thin film (300 Å) of V_3Si deposited on a sapphire substrate. The measured relative transmission (T(film + substrate)/T (substrate)) is compared to Fourier results in Fig. 5. The laser data were superior in terms of random noise but they agree with only some of the Fourier results. The theoretical fit [5] shows that the Fourier data are approximately correct. The probable explanation here is that the flat and polished substrate produces interference fringes in the laser system but not in the Fourier spectrometer, where the broad-band character of the radiation tends to suppress fringes. Line widths of FIR lines have not been widely measured but estimates made from the literature [1,6] are less than the fringe spacing of 3 cm^{-1} that the substrate would generate. With the additional narrowing provided by the interferometer FP such lines would give clear interference effects.

These exploratory efforts in FIR pumped laser spectroscopy show that in practice the high power offers improved signal-to-noise ratios, increased penetration power, and reduced stray light problems. The monochromaticity of the laser lines eliminates the broad band mercury arc radiation which can be undesirable in certain solid state and biological applications. This same monochromaticity can lead to interference effects which can complicate some measurements but may provide additional information in others. The FIR lasers do have the disadvantage of being only quasi-tunable. The results here show, however, that even a handful of lines from only two pumped media is enough to make useful measurements, and many more lines are available.

*This work was partially supported by grants from the Emory University Research Committee and the NIH Biomedical Sciences Support Program, NSF Grant No. DMR75-13917, and ONR Contract No. N00014-76-C-0429.

References

1. D. T. Hodges and T. S. Hartwick, Appl. Phys. Lett. 23, 252 (1973).
2. B. L. Bean and S. Perkowitz, Appl. Opt., Nov. 1976 (to be published).
3. H. D. Downing and D. Williams, J. Geophys. Res. 80, 1656 (1975).
4. S. Perkowitz, J. Phys. Chem. Solids 32, 2267 (1971).
5. R. E. Glover and M. Tinkham, Phys. Rev. 108, 243 (1957).
6. D. E. Evans, B. W. James, W. A. Peebles, and L. E. Sharp, Infrared Phys. 16, 193 (1976).

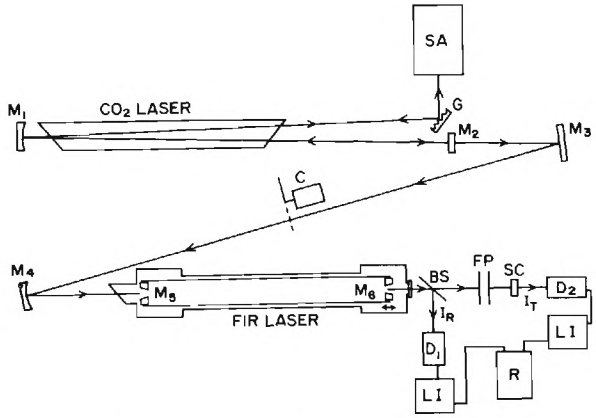

Fig. 1. Block diagram of the FIR laser spectrometer. M, mirrors; G, grating, SA, spectrum analyzer; C, chopper; BS, beamsplitter; D, detectors; FP, Fabry-Perot interferometer; SC, sample cell; LI, lock-in amplifier; and R, digital ratiometer.

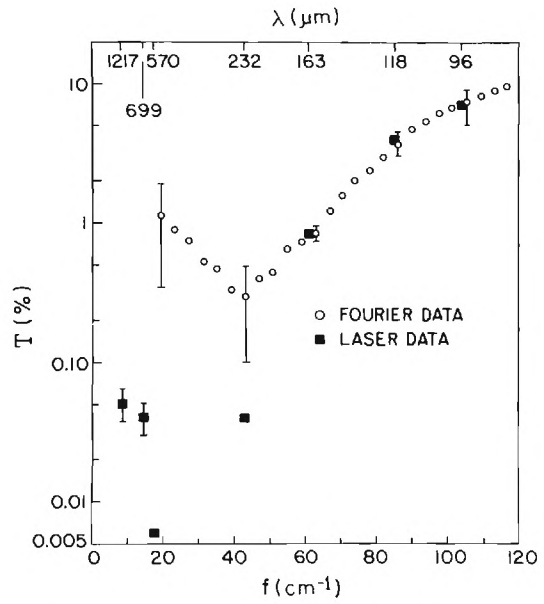

Fig. 3. Percent transmission of 0.054 cm thick GaAs. The FIR laser wavelengths are marked at the top of the figure.

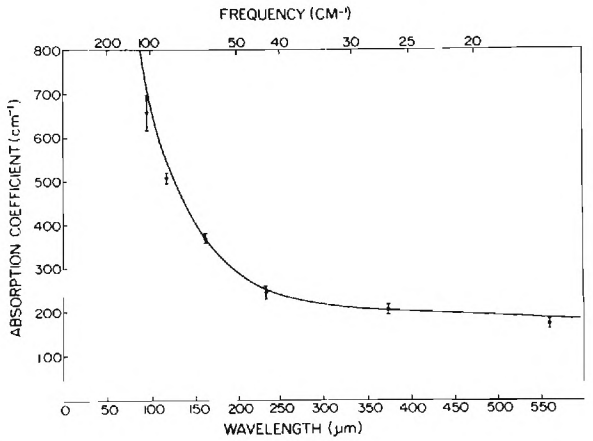

Fig. 2. Measured values of the absorption coefficient of liquid H_2O at six wavelengths. The solid curve was generated from experimental data in Ref. 3.

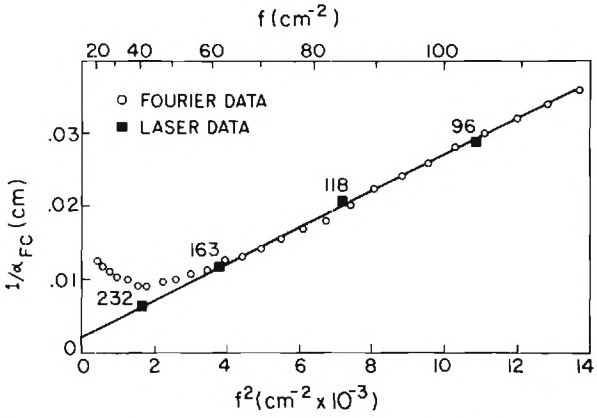

Fig. 4. Graph of the reciprocal of the free carrier absorption for GaAs versus the frequency squared. The solid curve shows the linear nature of the laser data.

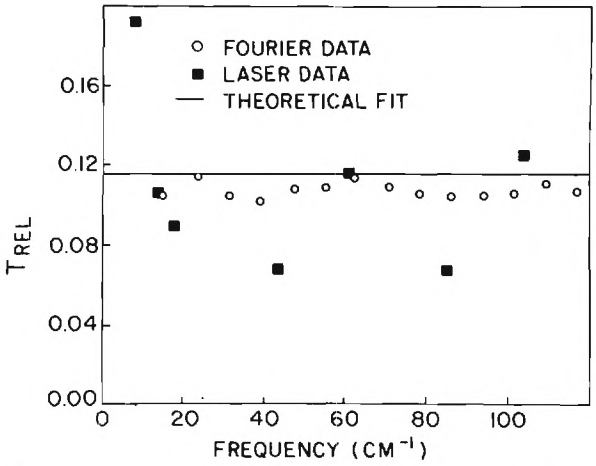

Fig. 5. Relative transmission of a V_3Si film at 300 K.

Servo Electronics for Optically Pumped FIR Laser

Ed G. Reid

Electro Optics Branch
Goddard Space Flight Center
Greenbelt Maryland 20770

Instabilities in CO_2 lasers and FIR lasers necessitate an automatic means of control in order to achieve stable FIR output power over a long period of time. The digital control circuit described maybe one solution to the problem,(fig.1)

An 8 bit binary coded decimal A to D converter is used to convert the output of a FIR detector into a digital format. The AtoD output is fed into two registers that are clocked at a rate f_1 of 0.5 to 5pps in such a way that the output of one is delayed in time from the other by one sampling step. Outputs of the two registers then go into a comparator whose output is dependent on an increase or decrease of the original FIR signal. The comparator output can be used for theservo loop of the FIR cavity and the servo loop of the CO_2 cavity as well.

At each sampling time from the discriminated signal a command is derived to drive a stepping motor clockwise or counter-clockwise. The number of steps that the motor makes at each sampling time can be varied, thus allowing for different gear ratios. The direction of rotation of each command step is also determined by the direction of the last movement.

Any time a power increase has been measured, the motor is moved in the same direction as before. A reverse movement is made when a power decrease has been measured. This is accomplished by a feed back loop which consists of an AND gate and two inverters.

The much slower drift of the pump frequency is also controlled by the discriminator signal, but at a 10-20 times slower sample rate. Therefore this signal has to be stored over a time peroid of $1/f_2$. The delayed signal is thencompared with the undelayed signal of the next sampling time. The comparator output is fed into a high-voltage operational power supply to drive a piezeo-electric-transducer and to adjust for frequency drift.

The servo loops can be switched on separately after a manual adjustment of the cavities has been accomplished.

This servo loop is presently being tested and quantative results will be given.

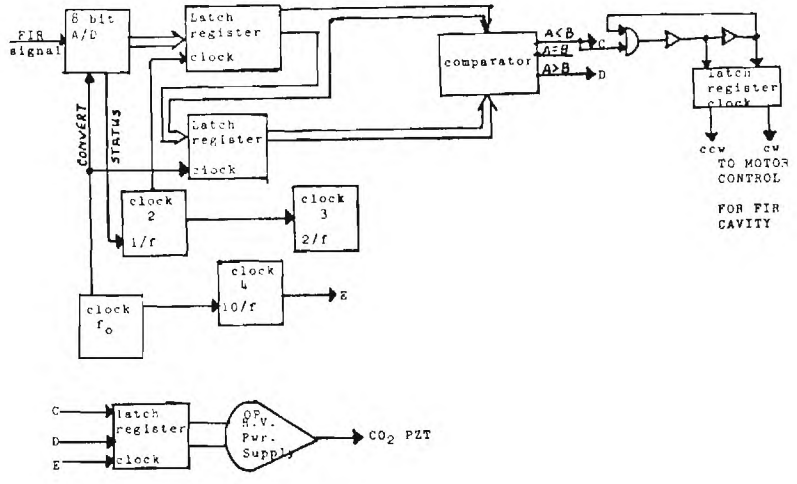

fig. 1 Block diagram of Servo Electronics.

DIFFRACTION LIMITED CW OPTICALLY PUMPED LASERS*

M. Schubert, M. Durschlag and T. A. DeTemple
Department of Electrical Engineering
University of Illinois
Urbana, Illinois 61801

ABSTRACT

Using hybrid capacitive and inductive mesh mirrors, the characteristics of optically pumped FIR lasers were investigated in the range 70 μm to 1.2 mm and found to produce single mode EH_{11} outputs at the mW level.

A CW optically pumped FIR waveguide laser utilizing a hybrid metal mesh dielectric (MMD) mirror and a dielectric waveguide has been shown to produce a diffraction limited output beam at the mW level at 496 μm [1]. We report here on the characteristics of a laser utilizing this configuration with an extended spectral range.

Certain improvements have been implemented on the original mirror which extend the spectral coverage and reduce the loss in the FIR [2]. Specifically, the new mirrors are in the configuration Si substrate, IR dielectric mirror and FIR mesh mirror which now places the IR films partially outside the FIR cavity. The IR mirror is composed of a three-layer pair of Ge-ZnS which is low loss at wavelengths greater than 50 μm and is 98% reflecting at 10 μm. The FIR mesh mirror is either of the capacitive or inductive type allowing a high reflectivity to be obtained from ∿ 50 μm to the mm range.

Table I summarizes the lines obtained to date using the MMD mirrors. No detailed attempt has been made to optimize the output for each wavelength so some improvements might be expected. For example, using only a dielectrically coated substrate, the output at 118 μm in CH_3OH increased by 30%. Constructive techniques and detailed IR and FIR spectral data will be presented on the MMD mirror used for these data.

The transverse modes were investigated by scanning the beam across a detector-pinhole combination in the far field. In Fig. 1 is shown some of the linearly polarized modes obtained from CH_3OH at 118 μm. As in the case of the 496 μm line in CH_3F, the EH_{11} mode is the fundamental [1].

The side-lobes of the EH_{11} mode barely visible in Fig. 1 were found to be approximately a factor of 10 larger than predicted by theory [3]. In addition, the LP_{11} mode, although observed, is not strictly allowed in this waveguide configuration. Finally there are unidentified modes such as that shown in the bottom of Fig. 1 which appeared to be EH_{11} in one direction and EH_{12} like in the orthogonal direction. These observations suggest that lens effects may be present in the medium and are playing a role in controlling the allowable cavity modes.

There are at least three contributions which could produce lens-like effects: a) ground state molecular gradients caused by kinetic cooling or heating, b) radial gain variation caused by the known diffusion dominance, and c) radial variation in the pump intensity [4,5]. The relative contribution of these is not known at this time however it is thought that a combination of a) and b) are most likely producing the lens.

Finally, mention should be made of a rather interesting behavior associated with HCOOH at 393 μm and CH_3OH at 118 and 170 μm. Under certain conditions (cavity tuning, pressure, pump power) the normally CW output breaks up into a periodic pulsed output reminiscent of relaxation oscillation. Peak power enhancement of ∿ 2, pulse width of ∿ .5-5 μsec and periodicities of 25-50 μsec have been observed suggesting that the effect may be a convenient means of producing periodic short pulses.

*Supported in part by the National Science Foundation, Army Research Office, and the University of Illinois Industrial Affiliates Program.

References

1. E. J. Danielewicz, T. K. Plant and T. A. DeTemple, Optics Comm., 13, 366 (1975).

2. E. J. Danielewicz and P. D. Coleman, Appl. Optics, 15, 761 (1976).

3. J. J. Degnan, Appl. Optics, 12, 1026 (1973).

4. F. Grabiner, D. R. Siebert and G. W. Flynn, Chem. Phys. Lett., 17, 189 (1972).

5. T. A. DeTemple and E. J. Danielewicz, IEEE J. Quan. Elec., QE-12, 40 (1976).

Table I. CW Waveguide Laser Species.

MOLECULE	λFIR μm	FIR POWER mW[a]	MESH MIRROR[b]	θ_D mr[c]
CH_3OH	70.6	1.5	750C	
CH_3OH	96.48	4.5	500C	
CH_3OH	118.8	30.	500C	8
CH_3NH_2	143.5	.35	750C	
CH_3OH	170.6	3.7	750I	9
HCOOH	393.6	3.5	750I	22
HCOOH	419.6	4.5	750I	
HCOOH	432.5	4.5	750I	
HCOOH	458.	.33	750I	
$C^{12}H_3F$	496.	6.	333I	24
HCOOH	512.8	.5	750I	
CH_3OH	570.	.1	750I	
HCOOH	743.	.1	750I	
$C^{13}H_3F$	1221.8	.5	333I	

[a] Typical pump power of 25W.

[b] Mesh elements/inch, I = inductive, C = capacitive.

[c] Divergence half-angle at e^{-2} power point for EH_{11} mode.

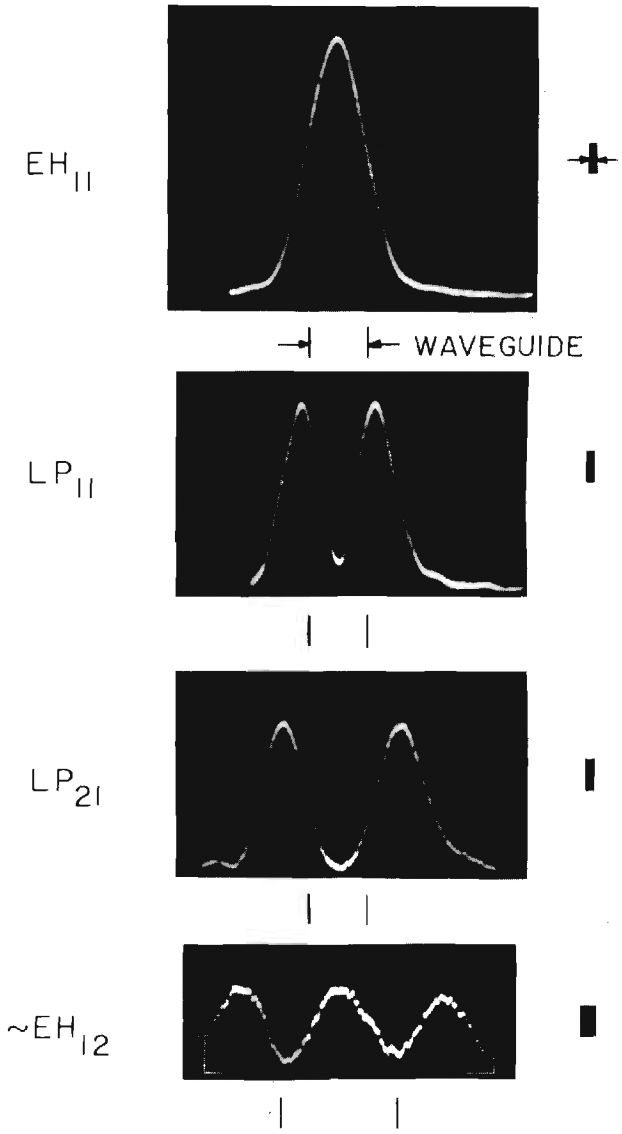

Figure 1. Far field transverse modes.

MODE LOSSES IN WAVEGUIDE FAR-INFRARED LASERS

C. H. Ma
Department of Electrical Engineering
University of Mississippi
University, MS 38677

The mode losses in hollow-circular waveguide resonators for far-infrared lasers are studied. Theoretical formalisms have been developed for the waveguide resonator which consists of both dielectric and metallic tubes with dielectric films and metallic grids deposited on mirrors and waveguide walls. Both propagation loss and the coupling loss for low-loss modes, circular magnetic and electric modes, and hybrid modes are investigated theoretically. A computer program was written to solve the equations numerically.

Initially, the losses of conventional dielectric and metallic waveguide resonators are calculated to verify the accuracy of this technique. In this case, resistive losses in metallic waveguide walls determine the propagation losses, and the radiative losses dominate the dielectric tube propagation loss. The results are compared with experimental and theoretical data reported in the literature [1 - 9]. It is found that the results are in good agreement throughout the range of investigation.

The mode losses of dielectric and metallic waveguides with the newly developed hybrid output mirror for optically pumped far-infrared lasers [10] are studied next. This mirror has dielectric films for infrared reflection and metallic films in the form of grids for far-infrared reflection. The far-infrared reflectivity are investigated for various grid parameters and the results are compared with the reported experiments [11].

Several new waveguide structures with both dielectric and metallic waveguide walls with and without metallic grids are proposed. The mode losses of those resonators are computed. The results are summarized in plots of mode losses and relative far-infrared power as function of waveguide and mirror parameters and the performance characteristics of those lasers are discussed.

References

1. E. A. J. Mareatili and R. A. Schmeitzer, "Hollow metallic and dielectric waveguides for long distance optical transmission and lasers," Bell Syst. Tech. J., vol. 43, pp. 1783 - 1869, 1964.

2. D. T. Hodges and T. S. Hartwick, "Waveguide laser for the far infrared (FIR) pumped by a CO_2 laser," Appl. Phys. Lett., vol. 23, pp. 252 - 253, 1973.

3. R. L. Abrams, "Coupling losses in hollow waveguide laser resonators," IEEE J. Quantum Electron,. vol. QE-8, pp. 838 - 843, Nov. 1972.

4. Arthur N. Chester and Richard L. Abrams, "Mode losses in hollow-waveguide lasers," Appl. Phys. Lett., vol. 21, pp. 576, Dec. 1972.

5. T. Y. Chang, "Optically pumped submillimeter-wave sources," IEEE Trans. Microwave Theory Tech. (Part I of Two Parts: Special Issue on the Proc. 1st Int. Conf. Submillimeter Waves and Their Applications), vol. MTT-22, pp. 983 - 988, Dec. 1974.

6. a) M. Yamanaka and H. Yoshinaga, "Compact waveguide lasers in the submillimeter and millimeter wave regions," presented at the Int. Conf. Submillimeter Waves and Their Applications, Atlanta, GA, June 1974, Paper III-4. b) M. Yamanaka et al., "On the transverse mode in an optically pumped far-infrared NH_3 laser," Japan. J. Appl. Phys., vol. 13, pp. 843 - 850, 1974.

7. J. R. Tucker, "Theory of a FIR gas laser," presented at the Int. Conf. Submillimeter Waves and Their Applications, Atlanta, GA, June 1974, Paper I-3.

8. J. O. Henningsen and H. G. Jensen, "The optically pumped far-infrared laser: Rate equations and diagnostic experiments," IEEE J. Quantum Electron, vol. QE-11, pp. 248 - 252, June 1975.

9. D. T. Hodges and T. S. Hartwick, "FIR waveguide laser performance in the 40 μm-1mm spectral region," presented at the Int. Conf. Submillimeter Waves and Their Applications, Atlanta, GA, June 1974, Paper IX-2.

10. E. J. Danielewicz, T. K. Plant, and T. A. DeTemple, "Hybrid output mirror for optically pumped far-infrared lasers," Opt. Commun., vol. 13, pp. 366 - 369, 1975.

11. Thomas A. DeTemple and Edward J. Danielewicz, "Continuous-wave CH_3F waveguide laser at 496 μm: theory and experiment," IEEE J. Quantum Electron., vol. QE-12, no. 1, pp. 40 - 47, Jan. 1976.

OBSERVATION OF DICKE SUPERRADIANCE IN FAR INFRARED EMISSION FROM CH_3F*

A. T. Rosenberger and S. J. Petuchowski
Department of Physics
University of Illinois
Urbana, Illinois 61801

and

T. A. DeTemple
Department of Electrical Engineering
University of Illinois
Urbana, Illinois 61801

ABSTRACT

Dicke superradiance has been observed in far infrared pulses from homogeneously broadened CH_3F optically pumped by a CO_2 TEA laser. The superradiant character of the emission has been verified by the pressure dependence of the height, width, and delay of the pulses.

Delayed far infrared pulses have been observed from CH_3F (methyl fluoride) gas optically pumped by a pulsed CO_2 TEA laser. The delay, pulse width, and pulse height have been studied as a function of CH_3F pressure and seem to indicate that a superradiant process [1] (cooperative spontaneous emission) is taking place at a wavelength of 496 μm on a pure rotational transition in methyl fluoride.

The apparatus used is shown in Fig. 1. The pump pulse is produced by a grating-tuned CO_2 TEA (transverse excitation atmospheric) laser which contains an intercavity low-pressure CW CO_2 cell to limit the output to a single longitudinal mode [2]. The resulting output is a temporally smooth pulse about 150 nsec wide, of 1 MW power, with a spectral purity of better than 1 MHz [3]. This pulse is passed through an optical breakdown switch which causes a sharp cutoff of the pump pulse on command, allowing clean separation of the pump (IR) and far-infrared (FIR) pulses. This switch consists of a small surface dielectric spark gap, driven by a Marx bank triggered by a gold-doped germanium detector downstream from the switch. [4,5]. Clean N_2 is flowed through the spark gap, which is located between a pair of Ge lenses which focus and collimate the CO_2 laser beam; the nitrogen gas breaks down when electrons are produced by the ionizing ultraviolet radiation from the spark, and a plasma then forms very rapidly, cutting off the pulse in < 100 psec [5]. The pulse enters the CH_3F cell and is reflected down the cell by a coated silicon window; some intensity is transmitted by this window and serves to trigger the Marx bank. The coated Si window is labeled in Fig. 1 as a low-feedback input coupler because it is used with the pump pulse polarized in the plane of the window; since the FIR pulse is polarized perpendicular to the pump pulse, any backward FIR wave will pass through the window and can then be absorbed to minimize feedback and help insure that we observe spontaneous rather than stimulated emission [6]. The output from the FIR cell consists of IR and FIR radiation, since little of the pump pulse is actually absorbed at our working pressures; this is incident upon a coated Si wafer which transmits most of the FIR and reflects most of the IR, the latter focused onto a photon drag detector and the former incident on a new phosphorus-doped silicon detector which has a respose time of ~ 2 nsec when cooled to 2.3 K [7].

Typical pulses are shown in Fig. 1; the FIR pulse is seen to be delayed, beginning ~ 50 nsec after the pump pulse has ended. This delay indicates that the system is prepared in a certain excited state and then evolves without the perturbation of continuing excitation, a condition that other experiments have been able to realize only for the longest delays [8,9]. Existing theories predict that this delay should be approximately inversely proportional to pressure, and the data in Fig. 2a qualitatively verify this dependence; similarly, the FIR pulse width in Fig. 2b is inversely proportional to pressure, as predicted. The pulse height should be proportional to the square of the pressure, and our data are consistent with this, as seen in Fig. 2c.

A quantitative comparison with existing theories is not straightforward at this time because CH_3F is not a simple two-level system, because the action of the pump pulse is not completely understood, and because the decay times of the polarization and of the population inversion (T_2 and T_1) are not long on the time scale of the delay and emission. In addition, the length of our sample is on the order of a cooperation length, so we

should expect oscillatory rather than pure superradiance [10]. Nevertheless the results so far are promising; we seem to be observing Dicke superradiance for the first time in a homogeneously broadened system.

The significance of this study is that we now have a system in the homogeneously broadened limit in which theory and experiment can be compared most easily. It should also be possible to study this system in the swept-gain mode (which effectively removes the cooperation length limitation) and compare the results with predictions [11]. It is interesting that this method, originally proposed for excitation of an x-ray laser, may prove to be useful for short pulse generation in the far infrared.

*Sponsored by Army Research Office - Durham and University of Illinois Industrial Affiliates Program.

References

1. Charles M. Bowden, International Conference on Submillimeter Waves and Their Applications, Atlanta, June 1974.
2. T. A. DeTemple and A. V. Nurmikko, Optics Comm., 4,321 (1971).
3. R. I. Rudko, IEEE J. Quant. Elec., QE-11, 54D (1975).
4. E. Yablonovitch, Phys. Rev. A, 10, 1888 (1974).
5. H. S. Kwok and E. Yablonovitch, Appl. Phys. Lett., 27, 583 (1975).
6. T. K. Plant and T. A. DeTemple, J. Appl. Phys., 47, 3042 (1976).
7. P. Norton, J. Appl. Phys., 47, 308 (1976); Phys. Rev. Lett., 37, 164 (1976).
8. N. Skribanowitz et al., Phys. Rev. Lett., 30, 309 (1973).
9. M. Gross et al., Phys. Rev. Lett., 36, 1035 (1976).
10. R. Bonifacio and L. A. Lugiato, Phys. Rev. A, 11, 1507 (1975).
11. R. Bonifacio et al., Phys. Rev. A, 12, 256 (1975).

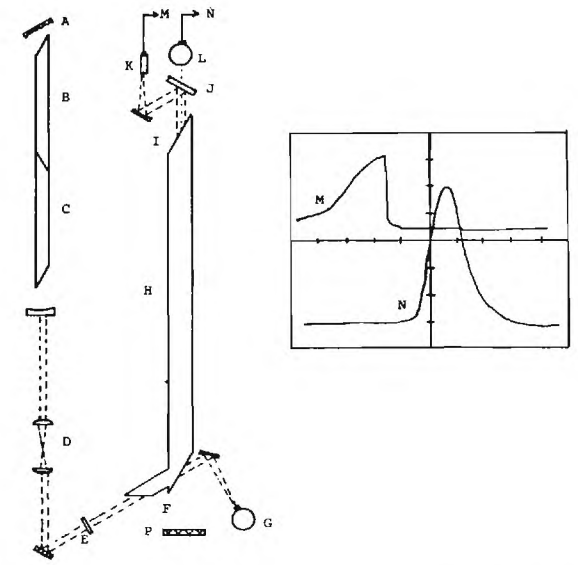

Figure 1. Apparatus and typical pulses. A, grating; B, CO_2 TEA laser; C, single mode cell; D, breakdown switch; E, quarter-wave plate; F, low-feedback input coupler; G, Ge:Au trigger; H, 3.5-m CH_3F cell; I, Si Brewster window; J, IR-FIR filter; K, photon drag detector; L, Si:P detector; M, IR pulse and N, FIR pulse, also shown in synchronized oscilloscope traces, 50 nsec/division; P, absorber.

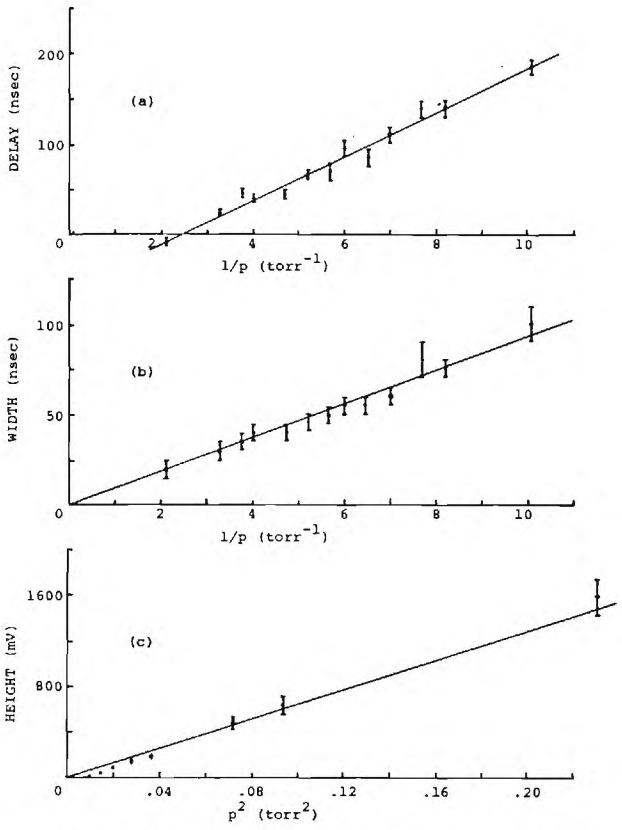

Figure 2. (a) FIR peak delay from pump cutoff and (b) pulse width vs. inverse pressure; (c) FIR pulse height vs. pressure squared.

STARK EFFECT ON FIR WAVEGUIDE LASER ACTION

M. S. Tobin and R. E. Jensen
Naval Surface Weapons Center
White Oak Laboratory
Silver Spring, Maryland 20910

Abstract. A rectangular metal-dielectric waveguide has been constructed to observe the Stark effect on a CO_2 laser pumped FIR laser. AC and dc Stark effects will be discussed.

Introduction

All of the optically pumped FIR molecular lasers emitting on a pure rotational transition must have an electric dipole moment and should exhibit the Stark effect. The simplest type of molecular interaction with an external electric field E_S, occurring for symmetric top molecules, is the linear Stark effect. The shift of an energy level is given by

$$\Delta E = -\mu MKE_S/J(J+1) \qquad (1)$$

where μ is the electric dipole moment and J,K,M, are the angular momentum quantum numbers. Asymetric molecules may have a second order Stark effect depending on E_S^2. For slightly asymmetric top molecules, an intermediate type of Stark effect results. Frequently these molecules have pairs of nearly degenerate levels, with a resultant first-order Stark effect for sufficiently large fields and small molecular asymmetry. [1]

The Stark effect in an FIR laser has a number of possible applications. It may be used to bring an absorbing transition into resonance with a pump line to produce new lasing lines, as has been experimentally demonstrated in CO_2 laser pumped NH_3 by Fetterman, et.al. [2] For some existing lasers the Stark effect may result in an increase in output power as we reported in reference 3. A. C. fields can be used to modulate the laser. The possibility exists for frequency tuning the FIR laser as theoretically predicted for CH_3F by Inguscio, et. al. [4].

Experimental Details

The experimental arrangement is shown in Fig. 1. The cw commercial CO_2 laser has power capability to 20 watts on the strongest CO_2 lines. Both CO_2 and FIR laser cavities incorporate invar rods for stability. The vacuum integrity of the FIR laser is maintained by a two inch glass pipe, permitting easy interchange of waveguide. For this Stark experiment, a 79 cm long rectangular metal-dielectric guide (Fig. 2) is used as previously described [3]. The aluminum coated plate glass walls serve as the Stark plates. An uncoated section of 1 cm length was left at each end of the glass strips to provide electrical insulation from the gold coated end mirrors. The sidewalls are of Teflon. One mirror is located directly at the end of the guide and the second mirror is located several millimeters from the other end and can be adjusted to tune the FIR laser. Pump laser input and FIR output are accomplished by hole coupling. The FIR output is observed with a golay cell or a pyroelectric detector. Wavelengths are determined with a metal mesh Fabry-Perot interferometer. To observe ac effects an ac signal is superimposed on a dc ramp voltage.

Results and Discussion

The effect of a dc Stark field on the output of the 118.8μm CH_3OH line is demonstrated in Fig. 3. Both the pump frequency and the FIR cavity length were set for optimum FIR output at zero field. CO_2 pump radiation was introduced into the waveguide polarized parallel to the metal walls, and the resultant FIR radiation was also observed to be polarized parallel to the walls. CH_3F similarly showed an increase in output power with about 100 volt/cm Stark field. CH_3F is well understood spectroscopically and exhibits a linear Stark effect making it an attractive molecule to study. Low frequency modulation of the 118.8μm CH_3OH line is demonstrated in Fig. 4. The entire signal was chopped to determine the magnitude of the modulated output relative to the cw background. The dc bias, 235 volt/cm, permits operation on the most sensitive portion of the intensity curve of Fig. 3. The detector sensitivity dropped rapidly beyond 1 kHz; however, modulation was detectable to 40 kHz. This technique should also work for a number of gases in the longer wavelength window regions. Stark modulation may have application for a cheap and simple modulation technique for a short range FIR communications system.

References

1. W. G. Penney, "The Stark effect in band spectra", Phil. Mag., Vol 11, pp. 602-609, 1931.

2. H. R. Fetterman, H. R. Schlossberg and C. C. Parker, "CW submillimeter laser generation in optically pumped Stark-tuned NH_3", Appl. Phys. Lett., Vol 23, pp. 684-686, 1973.

3. M. S. Tobin and R. E. Jensen, "Far IR laser with metal-dielectric waveguide to observe the Stark effect", Appl. Optics (lett), Vol. 15, pp. 2023-2024, 1976.

4. M. Inguscio, P. Minguzzi and F. Strumia, "Stark tunability of a CH_3F laser", Infrared Phys., Vol. 16, pp. 453-456, 1976.

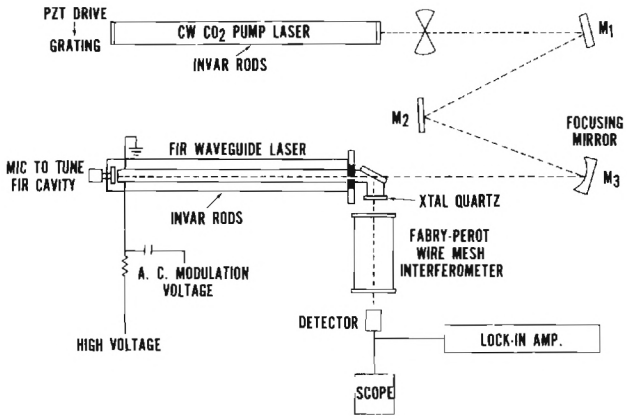

Fig. 1 Schematic of experimental apparatus

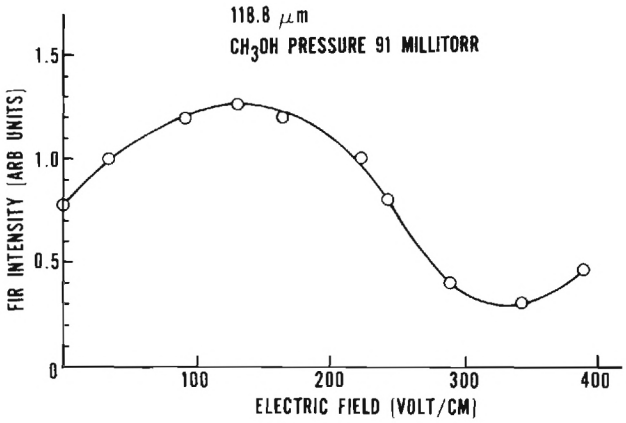

Fig. 3 FIR intensity vs. electric field

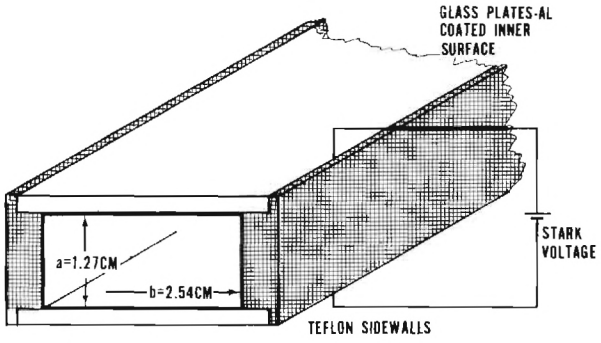

Fig. 2 Metal-dielectric waveguide

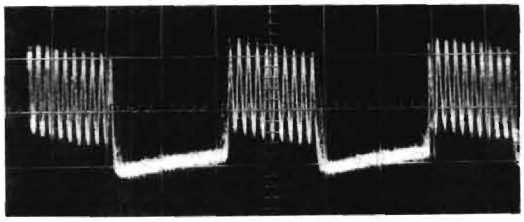

Fig. 4 Modulated FIR output, sweep rate = 2 msec/div, E_{bias} = 235 volt/cm, E_{ac} = 100 volt/cm at 3 kHz, λ = 118.8μm, CH_3OH pressure = 140 millitorr

STARK MODULATION OF SUBMILLIMETER RADIATION

J.A. Jenkins, W.L. Wilson, Jr., F.K. Tittel
Department of Electrical Engineering
Rice University
Houston, Texas 77001

Abstract: A Stark cell containing methanol at pressures around 200μm Hg has been used to modulate 119μm submillimeter radiation generated by a methanol waveguide laser. Applying an electric field across the cell shifted the absorption band of methanol away from the laser frequency.

We report here the modulation of 119μm radiation from an optically-pumped methanol waveguide laser by Stark shifting the rotational-vibrational energy levels of methanol gas in an absorption cell. The waveguide laser was made from a 2 m length of precision-bore tubing (OFHC copper: I.D. - 1.4 cm) with a polished Cu mirror at each end of the tube. Infrared 9.6um (P(36)) radiation from a diffraction grating-tuned CO_2 laser was focused through a coupling hole (1.27 mm) in the center of one mirror and 119um submillimeter radiation was coupled out the other end of the tube through a 2.49 mm hole in the output mirror. A peak power submillimeter output of 4 mW could be obtained with 8 W CO_2 pump input and a methanol operating pressure in the neighborhood of 125μm Hg.

The Stark cell was constructed from a 32.5 in. (82.55 cm.) length of copper x-band waveguide, the ends of which were cut at 55.5° in order to accommodate polyethylene Brewster windows (0.0125 in. thick). The output from the CO_2 laser was oriented with a polarization in the horizontal direction. The methanol laser however, rotates the 119 μm output 90° from the pump polarization. Thus, it was necessary to align both the Brewster windows, as well as the Stark electric field, for a vertically polarized submillimeter wave. A brass septum (0.0625 in. thick, 0.8125 in. wide) was inserted down the entire length of the cell, dividing the smaller cross-sectional dimension of the waveguide in half. Supporting the septum and electrically insulating it from the waveguide walls were two narrow teflon strips. Teflon has a relatively low absorption coefficient in the far-infrared and so helped cut down on the insertion loss of the cell. A rectangular brass collar was soldered to each end of the cell and provided support for gas inlet and outlet ports and electrical feedthroughs. A thermocouple tube was used to monitor the pressure in the cell.

Figure 1 shows the experimental setup which was used to monitor the change in submillimeter radiation absorbed by the Stark cell as a function of the electric field applied across the cell. CO_2 radiation at 9.695 μm (P(36)) was focused into the waveguide laser with a germanium lens (10 in. focal length). The 118.8 μm light generated by the waveguide laser was then passed through the Stark cell and into a photoconductive GaAs detector cooled to liquid helium temperatures (4.2°k)

A square wave modulated high voltage signal was applied between the center plate and the walls of the Stark cell. With the aid of a pulse amplifier, approximately 700 volts, with a rise time less than 1 msec was available at the Stark terminals. A DC signal, proportional to the pulse height was applied to the x-axis input of an a-y recorder. The output of a DC biased GaAs detector was fed into a phase sensitive detector synchronized with the pulser. The PSD output was then displayed on the y-axis of the recorder.

As the results in Figures 2 and 3 show, increasing the voltage across the Stark cell allowed more submillimeter radiation to reach the detector. Figure 2 illustrates the pressure-broadening of the absorption line as the amount of methanol in the Stark cell is increased from 90 μm to 400 μm.

It was observed that maximum modulation occurred for a Stark cell pressure of about 300 μm with the effect dying off completely at pressures above approximately 600 μm. In Figure 3 note that as the cell pressure is increased from 90 μm to 290 μm, the modulation amplitude increases, an effect attributable to the larger number of absorbing molecules at higher pressures.

Assuming a Lorentzian shape for the absorption line, we found that the closest fit to the experimental results occurred for a first-order (linear) Stark coefficient of 2.88×10^{-3} cm/volt. Since methanol, neglecting the hindered rotation of the OH group around the axis of the CH_3 group, has the structure of a rigid asymmetric top, we expected to observe a second-order (quadratic) Stark effect. Hughes, Good and Cole have reported[2] similar results for work with methanol at microwave frequencies. The explanations they present are that the K-type doubling may be too small to resolve, making the molecule appear to have a first-order Stark effect, or a very close degeneracy may exist accidentally. In this latter explanation a linear Stark effect will occur when two "interacting" levels lie rather close together -- considerably closer than the energy spacing between either one and any third level[3].

The authors would like to acknowledge the numerous suggestions and guidance received by R.F. Curl during the course of this work.

References

[1] T.Y. Chang, T.J. Bridges, and E.G. Burkhardt, Appl. Phys. Letters 17, 249 (1970).

[2] R.H. Hughes, W.D. Good, and D.K. Coles, Phys. Rev. 84, 418 (1951).

[3] C.H. Townes and A.L. Schawlow, Microwave Spectroscopy (1955) pp. 252.

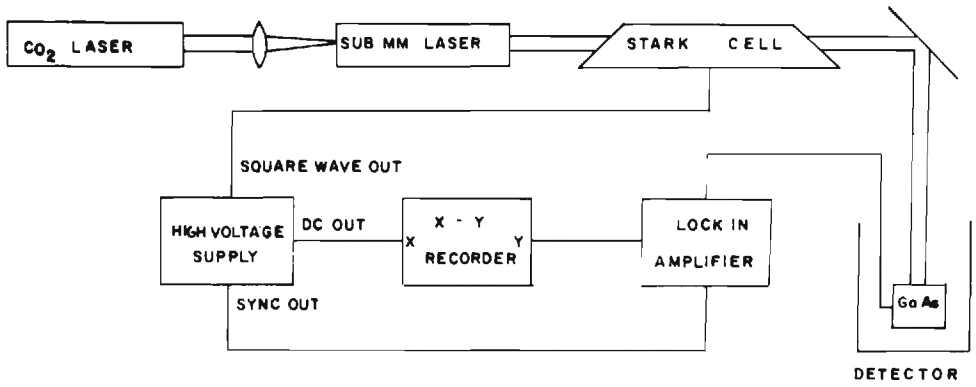

Figure 1. Diagram of the experimental set-up

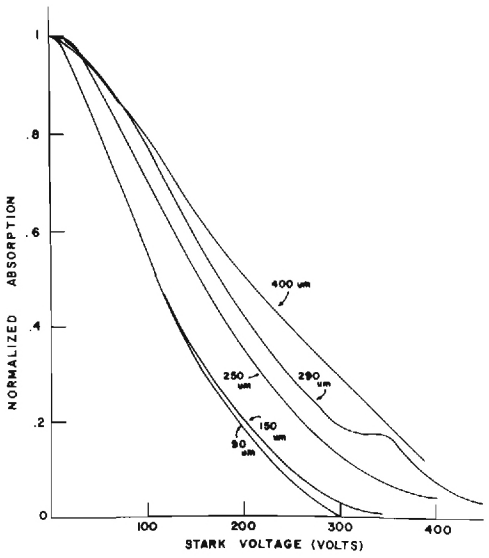

Figure 2. Normalized absorption as a function of Stark voltage for various pressures of methanol.

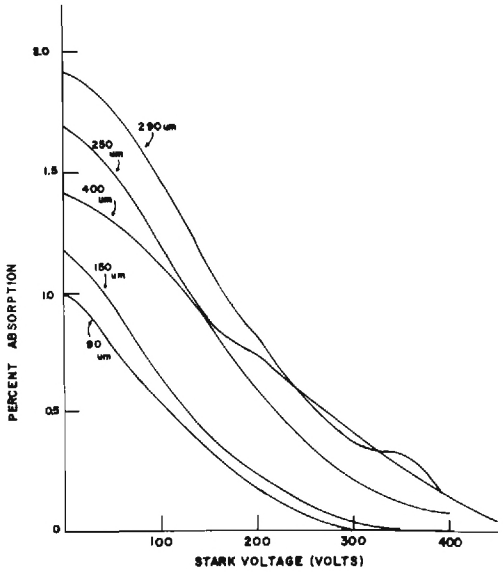

Figure 3. Percent absorption as a function of Stark voltage for various pressures.

Work supported by the National Science Foundation.

STARK EFFECTS IN OPTICALLY PUMPED FIR LASERS*

K. P. Koo and P. C. Claspy
Department of Electrical Engineering and Applied Physics
Case Western Reserve University
Cleveland, Ohio 44106

Abstract

Low electric field Stark effects on an optically pumped FIR waveguide laser have been investigated. Modifications of output characteristics produced by DC and AC Stark fields are discussed.

Introduction

Many of the far infrared (FIR) laser gases, which can be optically pumped by CO_2 laser lines, have shown infrared Stark effects both from Stark modulation studies [1] and Stark spectroscopy studies [2]. By the same token, Stark effects on these FIR laser system are expected and in fact have been observed [3,4]. A goal of our investigation [2] has been to produce usable Stark effects in FIR lasers operating at the typical optimal pressure of a few hundred mTorr. Our observed Stark effects on a CH_3OH FIR laser pumped by the P(36) 9.4μ CO_2 laser line are: (1) enhancement of FIR output by a DC Stark field; (2) Stark modulation of FIR output and (3) selective FIR laser line enhancement.

Experiment

Our optically pumped FIR laser system consists of a grating-tuned CO_2 laser pumping a waveguide FIR laser. The waveguide is formed by a pair of Stark plates with dielectric spacer. The flowing gas CO_2 pump laser has an output power 6-10 watts, depending on the transition to which it is tuned. The peak power mode structure is typically TEM_{01}. The FIR laser is made up of a two inch diameter pyrex vacuum envelope which houses a pair of parallel stainless steel Stark plates 68 cm long, 3.8 cm wide and 0-1.5 cm adjustable plate separation. The FIR laser cavity mirrors are commercially made micro-lapped aluminum mirrors with a 1 mm diameter hole in the center. These mirrors are placed ∿1 mm away from the Stark plates which form the FIR laser guide. Both mirrors are connected to the vacuum envelope through flexible metal bellows so that they can be externally adjusted for mirror alignments. In addition, the FIR laser output mirror can be translated axially by a hollow differential micrometer (21 μm per turn). The CO_2 radiation is coupled into the FIR cavity through a NaCℓ Brewster window and the 1 mm hole in the mirror by a 25 cm focal length lens. The FIR radiation is coupled out through the 1 mm hole in the FIR laser output mirror and a quartz window. A pyroelectric detector or a Golay cell is used to detect the FIR laser signal while the CO_2 pump laser is cavity (i.e., linewidth) scanning.

Discussion

We have chosen CH_3OH vapor and the P(36) 9.4μ CO_2 pump laser line for our study. The Stark plate spacing is 1/4 inch (6.35 mm). FIR lasing action is observed over the pressure range from ∿80 mTorr to ∿300 mTorr, with maximum FIR output occurring at around 200 mTorr using a 6 watts pump power. With a Stark field perpendicular to the pump laser polarization ($\Delta M=1$) the FIR output signal increases with increase of DC Stark field up to ∿180 v/cm beyond which the FIR output rolls off as shown in Fig. 1. At least two FIR laser lines are observed to be lasing over different portion of the CO_2 pump laser linewidth although one line is stronger than the other. A DC Stark field of ∿400 v/cm tend to suppress the weaker FIR line.

When an AC Stark field is used, modulation of FIR output is observed as shown in Fig. 2. The characteristics of the FIR laser modulation phenomenon are very similar to those of Stark modulation of a CO_2 laser by a Stark absorption cell. 180° phase shift and frequency doubling of FIR modulation relative to the Stark modulating signal have been observed. The specific nature of the modulation is a function of the DC Stark field which is superimposed on the AC Stark field [5].

The Stark effects we have observed indicate that significant low E-field Stark tuning of an optically pumped waveguide FIR laser is possible. This means that the FIR laser can still operate at its normal optimal pressure and coincidence between absorption line and CO_2 pump laser line can be increased.

References

1. See for example, P. C. Claspy and Yoh-Han Pao, "Basic Characteristics of High Frequency Stark Effect Modulation of CO_2 Lasers", J-QE 7, No. 11, pp. 512-519, November, 1971.

2. See for example, P. C. Claspy and K. P. Koo, "Stark Effect Applicable to Optically Pumped Far Infrared Laser", to be published in J-QE, October 1976.

* This work has been supported in part by a grant from the National Aeronautics and Space Administration.

3. H. R. Fetterman, H. R. Schlossberg and C. D. Parker, "CW Submillimeter Laser Generation in Optically Pumped Stark-Tuned NH_3", Appl. Phys. Lett. 23, No. 12, pp. 684-686, 15 December 1973.

H. R. Fetterman, C. D. Parker and P. E. Tennenwald, "Enhancement of Optically Pumped Far Infrared Lasing by Stark Modulation", 9th International Quantum Electronics Conference at Amsterdam, 14-18 June 1976.

4. M. S. Tobin and R. E. Jensen, "Far ir Laser with Metal-Dielectric Waveguide to Observe the Stark Effect", Applied Optics 15, No. 9 pp. 2023-2024, September 1976.

5. "Laser Technology for Communications", Case Western Reserve University Semi-annual Technical Progress Report 1, NASA Grant 36-027-014, Feb.-July 1970.

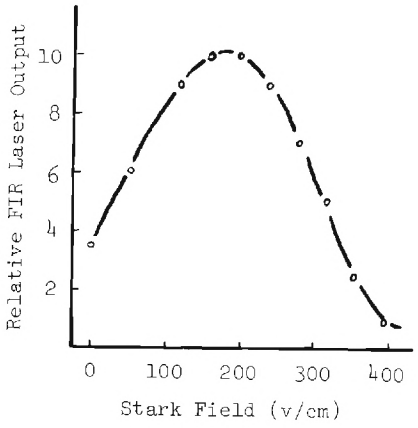

Figure 1. FIR Laser Output vs. Stark Field

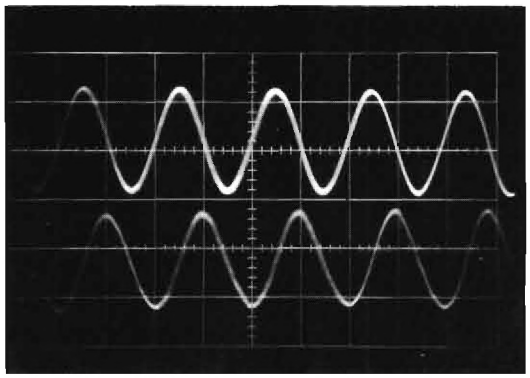

Figure 2. Modulation of FIR Laser Output. Upper trace is modulating sine wave. Laser trace is modulated FIR laser output.

FAR INFRARED SPECTRUM OF $CoCO_3$: HIGH FREQUENCY MODE OF ANTIFERROMAGNETIC RESONANCE AND TWO-MAGNON ABSORPTION

V.M.Naumenko, V.V.Eremenko, A.I.Maslennikov, A.V.Kovalenko,
Physico-Technical Institute of Low Temperatures,
The Ukrainian Academy of Sciences, Kharkov, U.S.S.R.

Abstract. A high-frequency mode of antiferromagnetic resonance and two-magnon absorption at 34.6 and 54.7 cm^{-1} (at $T \to 0$ K), respectively, have been observed. From the experimental data we have calculated H_A=115 kOe, $g_z = 7 \pm 2$ (at H_E=160 kOe and $g_\perp$=3.3). The two-magnon absorption is treated as a simultaneous excitation of two magnons near the Brillouin-zone boundary, one of which belongs to the low-frequency gapless branch and the other - to the weak dispersion high-frequency branch.

Cobalt carbonate $CoCO_3$ has a rhombohedral calcite type structure and the space group D_{3d}^6. At T=18.1 K $CoCO_3$ becomes a weak ferromagnet[1]. The sublattice magnetic moments lie in the basal plane[2]. The g-factor at $H \perp C_3$ ($g_\perp = 3.3 \pm 0.2$) and Dzyaloshinsky field ($H_D = 51.5 \pm 8$ kOe) were determined from the resonance measurements of low frequency (l.f.) mode of antiferromagnetic resonance (AFMR)[3]. Other parameters of the crystal and characteristic features of the dispersion curves could be determined from the study of the high frequency (h.f.) mode of AFMR and two-magnon absorption measurements.

To this end we performed a study of the absorption spectrum of $CoCO_3$ in the frequency range from 12.5 to 100 cm^{-1} using a diffraction spectrometer. Temperature of the sample placed in the cryostat and cooled by the thermal exchange gas could be varied from 5 to 300 K. The crystals were grown by Dr. N.Yu.Ikornikova by the hydrothermal synthesis and revealed good conoscopic figures that indicated the lack of blocks.

At 34.6 and 54.7 cm^{-1} (at $T \to 0$ K) the absorption lines were observed (Fig.1). Absorption coefficient, as usually, was calculated from the ratio of the transmission at $T \approx T_N$ to that at given temperature. As temperature is raised the lines get progressively weaker and broader until near T=14 K they merge with the background without noticeable shifts in position (Fig.2). The both lines shift in magnetic field (Fig.3). While the line at 34.6 cm^{-1} is roughly Lorentz-shaped the line at 54.7 cm^{-1} is asymmetric. Line parameters are listed in the Table including the line shape function and the "truncation".

Table (T=5 K)

Frequency at maximum (cm^{-1})	Polarization	Intensity at maximum (cm^{-1})	Width at half maximum (cm^{-1})	Integral intensity (cm^{-2})
34.6 ± 0.3	$h \perp m$	120	1.4	270
54.7 ± 1	$e \perp C_3$	6	10	100

Here e and h are electric and magnetic vectors of the high frequency field, respectively, is a weak ferromagnetic moment. Intensity of the line at 34.6 cm^{-1} is given for the case when the domain structure was removed by the magnetic field (H=1 kOe) applied parallely to the basal plane.

The calculation [4] of crystal field of cobalt carbonate shows that the separation between the lowest doublets is 163 cm^{-1}. Therefore, the lines found cannot be attributed to electron transitions. The lines at 34.6 and 54.7 cm^{-1} we interpreted as h.f. AFMR mode and two magnon absorption line, respectively.

As known, the resonance frequencies of a $CoCO_3$ type uniaxial weak ferromagnet are

$$\left.\begin{aligned} \omega_1 &= \gamma_\perp (H^2 + HH_D)^{1/2} \\ \omega_2 &= \gamma_\perp (H_{AE}^2 + HH_D)^{1/2} \end{aligned}\right\} H \perp C_3 \quad (1)$$

$$\left.\begin{aligned} \omega_1 &= 0 \\ \omega_2 &= \gamma_\perp \left(H_{AE}^2 + \frac{\gamma_z}{\gamma_\perp} H^2\right)^{1/2} \end{aligned}\right\} H \parallel C_3 \quad (2)$$

$$\hat{g}_{1,2} = \begin{vmatrix} g_\perp & \pm g_{xy} & 0 \\ \mp g_{xy} & g_\perp & 0 \\ 0 & 0 & g_z \end{vmatrix}$$

where ω is the cyclic frequency; $\hat{\gamma} = \hat{g} \frac{e}{2mc}$; $H_{AE} = (2H_E H_A + H_A^2)^{1/2}$

$\gamma_z = (\omega_2^2 - \omega_{20}^2)/\gamma_\perp H^2$

$\omega_2 = \omega_{20}$ at H=0, and H_E, H_A and H_D are the exchange, anisotropy and Dzyaloshinsky fields, respectively. Using the obtained experimental data (see Figs.1 and 3), H_E=160 kOe and $g_\perp$=3.3 available from [3], we have calculated the parameters H_A=115 kOe and $g_z = 7 \pm 2$. The exchange field H_E=160 kOe has been determined from the relation $2H_E = M_0/\chi_\perp$, using the data on the perpendicular susceptibility[1] and assuming the saturation magnetization per mole to be pure spinous, i.e. the specific value of $M_0 = gN\mu S$ =16.8·10 emu/mol,

where g=2, N is the Avogadro number, μ is the Bohr magneton, S=3/2. It is seen that the anisotropy field is close to the exchange one; thus, the nontrivial magnetic properties of $CoCO_3$ can be expected. However, the value of H_E is not known precisely and the above-mentioned estimation of H_E is very rough. But it should be noted that the magnetization approaches a saturation $m/M_0=0.9$ in the field $H=2H_E=320$ kOe, i.e. the value $H_E=160$ kOe is quite reasonable (without the Dzyaloshinsky interaction the complete saturation of the magnetization had to be observed in the field $2H_E$).

It is of interest to estimate the Dzyaloshinsky field from the AFMR data because static measurements[1,5] yield $H_D=27$ kOe but from the l.f. mode data[3] $H_E=51.5$ kOe. Our measurements in fields up to 50 kOe yield $H_D=113$ kOe ($H_D=(\omega_2^2-\omega_{20}^2)/\gamma^2 H$). The weak temperature dependence of the frequencies (Fig.2) can be explained by the high value of the anisotropy field. From this point of wiev $CoCO_3$ approaches to Ising-type magnetics. As it seems to us there is another peculiarity which arises from the high anisotropy field and results in a weak dispersion of one of the spin-wave branches. This comes from the following. The magnon energy of l.f. branch at the Brillouin zone boundary is about 15 cm^{-1} (estimated from T_N). The line at 54.7 cm^{-1} can be attributed to the two-magnon absorption when one magnon is excited from the l.f. branch (≈ 15 cm^{-1}) and the other one - from the h.f. branch (see Fig.4). Then the h.f. branch energy at the Brillouin zone boundary is about 40 cm^{-1}, i.e. dispersion of this branch is small.

In conclusion we want to point out that the lines at about 36 and 57 cm^{-1} were observed independently in the Raman spectra [6].

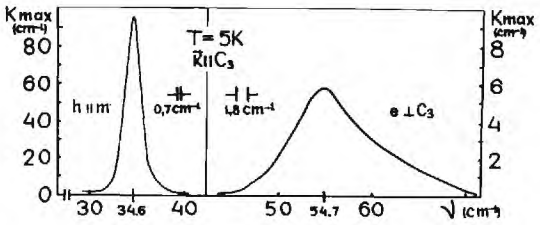

Fig.1. Absorption spectrum of $CoCO_3$ (the observed contours).

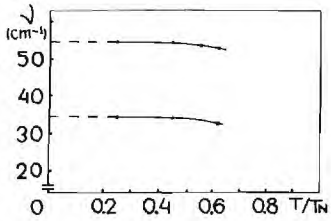

Fig.2. Temperature dependence of the observation line frequencies.

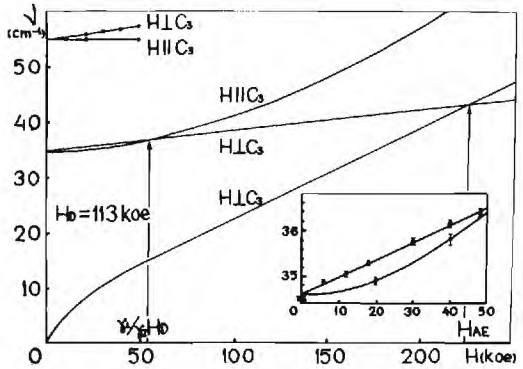

Fig.3. Dependence of frequencies of AFMR and two-magnon line on external magnetic field. Solid lines are the results from the expressions (1)-(2) at H =113 kOe. • - our experimental data.

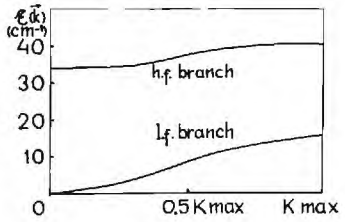

Fig.4. Spin-wave dispersion curves for $CoCO_3$ (qualitative curves).

References

1. A.S.Borovik-Romanov and V.I.Ozhogin, Sov.Phys.-JETP, 39, 27, 1960.
2. B.J.Brown, P.J.Welford and J.B.Forsyth, J.Phys.C6, 1405, 1973.
3. G.D.Bogomolov, Yu.F.Igonin, L.A. Prozorova and F.S.Rusin, Sov.Phys., JETP, 54, 1069, 1968.
4. Yu.A.Popkov, A.P.Mokhir, N.A.Sergienko, in: Proceeding of the Third Intern.Conf.on Light Scatt.in Solids, Flammarion Sciences ed. (France, Paris, 1976), p.317.
5. V.I.Ozhogin. Thesis on Research for the Degree of Doctor of Physical and Mathematical Sciences (1974), Fig.41.
6. Yu.A.Popkov, V.V.Eremenko and A.P. Mokhir, to be published.

FAR INFRARED ABSORPTION AND ZEEMAN EFFECT IN CaF_2, BaF_2 AND CdF_2 DOPED WITH RARE EARTH AND TRANSITION IONS

A. HADNI, G. VILLERMAIN-LECOLIER, G. MORLOT, P. STRIMER and J.P. AUBRY
University of Nancy I
Nancy, France

Electronic transitions and localised vibrations of the compensation F^- ion have been found in the case of rare earth ions, while resonant modes are observed in the case of several transition ions.

We have studied the far infrared absorption of BaF_2, CaF_2 and CdF_2 doped with Tb, Sm, Nd, Pr, Dy, Ho, Er from room temperature down to 1.4 K. The background absorption induced by the rare-earth (R) impurity is too high in the case of CdF_2 for any electronic transition to be seen. It is low enough for CaF_2 and BaF_2 doped crystals. In the case of all $BaF_2 : R^{3+}$ crystals considered, we have found a common absorption band at 131 cm^{-1}. The structure is explained by localized vibrations of the compensation F^- ions, in three different sites : cubic, tetragonal, and trigonal, where the R^{3+} ions are distributed in different proportions : 4 %, 46 %, 50 % respectively [1]. We have also found specific bands sensitive to magnetic fields [2] in the case of Dy^{3+} (41.2 cm^{-1}), Ho^{3+} (37 cm^{-1}), and Er^{3+} (69.2 and 70.3 cm^{-1}). The Zeeman effect gives information on the Lande g factors g_1 and g_2 for ground and excited levels, respectively and shows that for Er^{3+} the observed lines correspond to two different sites. It is shown that $g_1 = g_2 = 3.6$ for one site and $g_1 = g_2 = 0.98$ for the other one. For $BaF_2 : Dy^{3+}$, $g_1 = 3.2$, $g_2 \simeq g_1$; for $BaF_2 : Ho^{3+}$, $g_2 - g_1 = 7.6$. In both these crystals the tetragonal and the trigonal sites have not been distinguished.

References

[1] G. MORLOT, A. HADNI, G. VILLERMAIN-LECOLIER et P. STRIMER - Modes de résonance du Fluorure de Baryum contenant des éléments de la famille des terres rares - C.R. Acad. Sc. Paris t.281 (1975) B-599.

[1] G. VILLERMAIN-LECOLIER, G. MORLOT, P. STRIMER, J.P. AUBRY and A. HADNI - Far Infrared Stark and Zeeman splitting of trivalent rare earth ions in barium, calcium and cadmium fluoride - Physical Review B (1976 to be published).

THE TEMPERATURE DEPENDENCE OF THE DIELECTRIC RESPONSE OF PSEUDO DISPLACIVE FERROELECTRICS BY DISPERSIVE FOURIER TRANSFORM SPECTROSCOPY[†]

K. F. Pai, T. J. Parker* and R. P. Lowndes[+]
Department of Physics
Northeastern University
Boston, Massachusetts 02115

The anharmonic interactions of the ferroelectric mode in both the pseudo displacive and hydrogen bonded ferroelectrics are generally considered to be very strong, and an understanding of the anharmonic self-energies associated with these modes should lead to a better understanding of the nature of the ferroelectric transition. If it is assumed that in these materials the frequency dependent lattice contribution to the complex dielectric constant is determined primarily by the summation term associated with the ferroelectric mode, and contributions from other $q \gtrsim 0$ modes are ignored, then an estimate can be made of the frequency dependence of the anharmonic self-energy over a limited frequency range from experimental measurements of the dielectric response together with a measurement of the thermal strain self-energy shift of the mode arising from the thermal expansion of the crystal.

The difficulties of obtaining adequate values for the dielectric functions of these materials, especially at low frequencies in the region of the ferroelectric mode, by measuring the power reflection spectrum and then calculating the phase spectrum using a Kramers-krönig analysis are well known. With this in mind we have measured the amplitude and phase reflection spectra of several pseudo displacive ferroelectric crystals, such as TlBr, $KTaO_3$ and $SrTiO_3$, in the frequency range $\sim$ 20 - 400 cm^{-1} and at temperatures of 100, 200 and 300K using the relatively new technique of dispersive Fourier transform spectroscopy. The experiments were performed on a phase modulated Fourier spectrometer which employs a division of the field of view technique to obtain absolute phase measurements by metallising part of the specimen surface to provide a convenient phase reference. These results will be discussed in terms of the dielectric functions and the frequency dependence of the anharmonic self-energies associated with the ferroelectric soft modes as indicated above.

Acknowledgment

We wish to thank Professor E. H. Bellamy for permission to borrow the dispersive Fourier transform spectrometer from Westfield College, University of London, and we would also like to thank Dr W. G. Chambers for providing the Fourier transform computer programs.

[†]Research supported by a grant from the U.S. Army Research Office and by a grant from the Research Corporation.

*On leave of absence from Westfield College, University of London during 1975-76.

[+]On sabbatical leave at Westfield College, University of London, during 1976-1977.

SUBMILLIMETER SPECTROSCOPY OF TO-PHONON MODE SOFTENING IN PbTe

G. Bauer, H. Burkhard
I. Physikalisches Institut der Rheinisch-Westfälischen Technischen Hochschule Aachen, Germany

A. Lopez-Otero[+]
Institut für Physik, Experimentalphysik II,
Universität Linz, Austria

Introduction. In IV-VI compounds there is a possibility for a structural instability due to a transition from a high temperature NaCl to a low temperature rhombohedral structure. Whereas in GeTe and in mixed crystals $Ge_{1-x}Pb_xTe$, $Pb_{1-x}Sn_xTe$ this transition takes place at finite temperatures in pure PbTe until now no positive Curie temperature has been reported. It is,however, well established that the static dielectric constant is temperature dependent, i.e. PbTe exhibits a paraelectric behaviour.

Several authors have pointed out the importance of the carrier concentration on the extrapolated negative value of the Curie temperature. From recent magnetoplasma measurements Kawamura et al. [1] deduced such a dependence. The phase transition through TO-phonon mode softening was explained by strong interband electron TO-phonon coupling. Recently also an influence of the compensation (i.e. the ratio of the Pb to Te vacancies) on the values of the static dielectric constant has been reported [2] as deduced from capacitance measurements using Schottky barriers on p-PbTe. We report on investigations of the temperature dependence of the TO-phonon frequencies which were deduced from far infrared reflectivity measurements by Fouriertransformspectroscopy.

Experimental. Epitaxially PbTe single crystalline films of 1...27 µm thicknesses grown on BaF_2 and NaCl substrates were investigated. The free carrier concentration ranged from $0.3...5.10^{17}cm^{-3}$ and the mobilities had values up to $2.10^6cm^2/Vs$.

Like in ref. [2] no direct information on the vacancy compensation ratio is available. However, from the growth conditions ofthe various samples at least a general trend might be expected (with increasing growth temperature the number of native defects and thus the compensation will increase). In addition there is one further problem, namely that of sample thickness. It can be expected that crystalline perfection of the films depends on the film thickness especially for $d \leq 2$ µm. Some of the samples which we report on in this study had thicknesses of 1...2 µm.

For an evaluation of the TO-phonon mode frequency the reflectivity spectra were fit by using an oscillator model for the dielectric function:

$$\varepsilon(\omega) = \varepsilon_\infty + \frac{(\varepsilon_s-\varepsilon_\infty)\,\omega_{TO}^2}{\omega_{TO}^2-\omega^2-i\omega\Gamma} - \frac{\omega_p^2}{\omega(\omega+i\omega_\tau)} \qquad "1"$$

where ε_s and ε_∞ are the static respectively the high frequency dielectric constants; ω_{TO} is the TO-phonon mode frequency and Γ the damping parameter; ω_p is the plasma parameter and ω_τ is the free carrier collision frequency.

The reflectivity R has been calculated for an absorbing film on an absorbing substrate, taking into account multiple reflections and interference effects in the film substrate sandwichs [3]. The plasma parameter ω_p was taken from measurements at higher wavenumbers, and ω_{TO}, Γ and ω_τ were varied for the best fit.

Results. In figure 1. fits (solid lines) according to this procedure together with measured values of reflectivity (dots) are shown for a thin n-PbTe film of 1.4 µm thickness on NaCl substrate for 3 lattice temperatures. Whereas at 300 K the reflectivity shows only a broad maximum at $32cm^{-1}$ (the systematic shift of the measured data to lower reflectivities above the TO-frequency as compared with the fit is due to a 2 phonon process, which can be separated) and falls

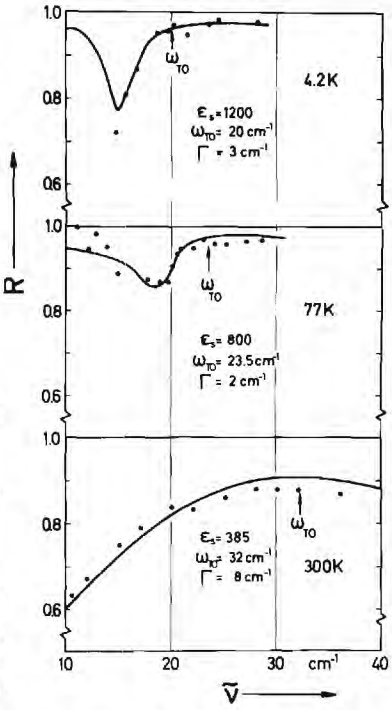

Figure 1. Reflectivities of a thin PbTe film on NaCl substrate with carrier concentration of $n=3.10^{17}cm^{-3}$ vs. frequency for 3 temperatures.

off monotonically to lower wavenumbers, at lower temperatures a pronounced minimum in reflectivity occurs shifting to lower wavenumbers according to the softening of the TO-phonon frequency.

Figure 2. presents a reflectivity curve fit (solid line) together with measured data (dots) of a thick n-PbTe film (d = 14 μm, T = 4.2 K) on BaF_2 substrate. The TO-phonon frequency is about 2 cm^{-1} lower than in the film of 1.4 μm thickness on NaCl. Although the carrier

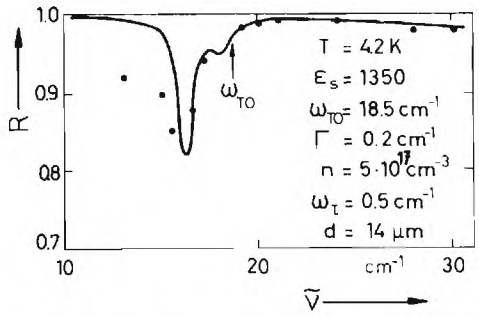

Figure 2. Reflectivity of a thick PbTe film on BaF_2 vs. frequency. The carrier concentration is $n = 5 \cdot 10^{17}$ cm^{-3}, the collision frequency ω_τ is 0.5 cm^{-1}.

concentrations of the two samples are nearly the same we suppose that the defect concentration differs strongly. Especially thin PbTe films on NaCl have more defects and lower mobilities than those on BaF_2 (which may be due to the different thermal expansion coefficients). The assumption of a higher defect concentration is supported by the fact that for PbTe films of only 1 μm thickness on NaCl substrates the TO-phonon frequencies are even higher, namely at 22, 27 and 32 cm^{-1} for the temperatures 4.2, 77 and 300 K. But at the moment we cannot conclusively decide wether there is a similar dependence of the Curie temperature on the defect concentration as shown in ref. [2].

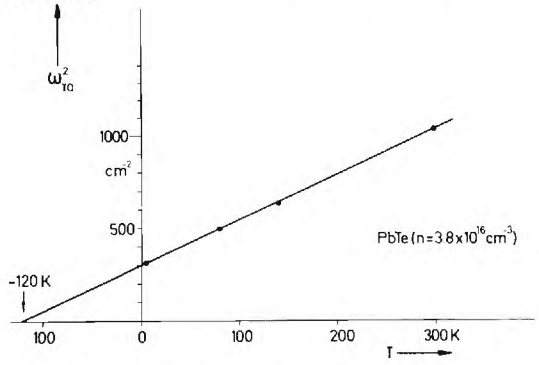

Figure 3. TO-phonon mode frequency squared vs. temperature for an n-PbTe film on NaCl substrate.

Figure 3. shows the temperature dependence of ω^2_{TO} of a thick PbTe film. The linear shape of the curve demonstrates that a Curie-law of the static dielectric constant is well established. The resulting Curie temperature is - 120 K.

References

[1] H. Kawamura, K. Murase, S. Nishikawa, S. Nishi, S. Katayama Solid State Commun. 17, 341 (1975)
H. Kawamura et al., Progr. Theor. Phys. 57, 156 (1975)
S. Katayama, Solid State Commun. 19, 381 (1976)

[2] W. Jantsch, A. Lopez-Otero, XIII International Conference on the Physics of Semiconductors, Roma, 1976

[3] H. Burkhard, G. Bauer, A. Lopez-Otero, Solid State Commun. 18, 773 (1976)

+supported in part by the "Fonds zur Förderung der wissenschaftlichen Forschung, Österreich".

FAR INFRARED MEASUREMENTS ON KH_2PO_4 USING AN ASYMMETRIC POLARIZING INTERFEROMETER

D.A. Ledsham,* W.G. Chambers+ and T.J. Parker*
Departments of Physics and Mathematics+
Westfield College,
(University of London)
Kidderpore Avenue,
London, NW3 7ST

Introduction

In 1964 Barker and Hopfield [1] presented a coupled mode theory to describe the infrared spectra of KH_2PO_4 [KDP] type ferroelectrics. Since that date a great amount of work, both experimental and theoretical, has been done in this field. The experimental techniques employed have been chiefly those of Raman scattering [2,3,4] and infrared power spectroscopy [5,6,7].

In recent years, a new experimental technique has been developed for infrared spectral measurement, that of dispersive Fourier transform spectroscopy [DFTS]. We have built a polarizing interferometer for dispersive rlection studies in the range 5→235cm^{-1} and early measurements with it included the room temperature spectra of CsI, ferroelectric KDP and antiferroelectric ADP [8].

In order to investigate the coupled mode picture of KDP, we have performed dispersive reflection measurements on the 'c' axis of KDP, using the polarizing interferometer, from 300°K to 150°K [9].

Experimental Method

A few improvements have been made to the polarizing instrument that was described in a previous article [8]. These include the use of all-reflecting output optics to replace the polythene lenses which absorbed much of the infrared radiation, and a change to a more flexible form of phase modulation as used by Birch et al [10]. This latter modification was important because it is planned to use a liquid Helium detector to improve the low frequency performance of the instrument below ~30cm^{-1}.

To overcome the chief problem that arises in dispersive reflection spectroscopy, that of exact replacement of the fixed mirror by the sample, the technique of division of the field of view was again used [11].

A cooling system consisting of a liquid nitrogen dewar, a cryogenic temperature control unit and an arrangement of heaters and thermo-couples was used for the low temperature measurement. A working pressure of less than 10^{-5}Torr ensured that the crystal surface did not ice-up whilst results were being recorded.

Theory and Results

The coupled mode formation was originally developed by Barker and Hopfield in order to explain data obtained from infrared measurements on $BaTiO_3$, which could not be interpreted by superposition of independent oscillators.

Other workers, employing Raman scattering [2,3,4], power spectroscopy [5,6,7] and dispersive spectroscopy [12], used this coupled mode theory to explain results obtained from measurements on KDP. This followed the discovery that in KDP the soft mode is strongly coupled to an optic phonon mode of the same symmetry.

Using the notation of Barker and Hopfield, we consider two particles of unit mass with effective charges e, and e_2 coupled mutually by a spring of constant k_{12} and to fixed points by springs of constants k_1 and k_2.

The dielectric function is then given by [9]

$$\varepsilon(\omega)-\varepsilon_\infty = \frac{e_1^2G_1+e_2^2G_2+2e_1e_2k_{12}G_1G_2}{1-k_{12}^2G_1G_2} \qquad (1)$$

where $G_j = \dfrac{1}{-\omega^2+i\omega\Gamma_j+(k_j+k_{12})}$ $\quad [j = 1,2]$ (2)

is the response of the uncoupled mode.

To fit our experimental curves using the seven parameter model of (1) we chose the following set of parameters (k_1+k_{12}), (k_2+k_{12}), k_{12}, Γ_1, Γ_2, e_1, $-e_2$ following Barker and Hopfield.

This model describes the case of reactive spring coupling between the two modes. There are, in fact, an infinite number of possible models each with its corresponding set of seven parameters [1]. We prefer to use the model as above for reasons stated in another article [9]. This article also presents the experimental curves and the resulting parameter fitting values.

These parameter values were compared to those of She et al [4] who chose the same type of coupling. The essential difference is that our values for ω_1^2, the square of the soft mode frequency, are consistently larger. This is probably due to a lack of accurate data below ~40cm^{-1}. The model is also shown to be sensitive to small shifts in the phase spectrum, hence the importance of accurate phase measurement.

Concluding Remarks

Future dispersive reflection work on the 'c' axis of KDP will be directed towards the low

frequency end of the spectrum below ~40cm^{-1}. The ε'' band, associated with the ferroelectric transition, peaks at ~50cm^{-1} at room temperature and moves to lower frequencies as the temperature is lowered towards that at which the ferroelectric transition occurs. It is important to resolve this band if accurate fits to data are to be obtained. The use of a liquid Helium detector should enable results to be obtained down to ~5cm^{-1} or lower.

Similar low temperature reflection measurements on the 'a' axis of KDP are in progress.

References

1. Barker, A.S. and Hopfield, J.J.; Phys Rev 135, A1732 (1964)

2. Lagakos, N. and Cummins, H.Z.; Phys Rev B 10, 1063 (1974)

3. Katiyar, R.S., Ryan, J.F. and Scott, J.F.; Phys Rev B 4, 2635 (1971)

4. She, C.Y., Broberg, T.W.,Wall, L.S. and Edwards, D.F., Phys Rev B 6, 1847 (1972)

5. Kawamura, T., Mitsuishi, A. and Yashinaga, H.; J Phys Soc Japan 28, Supp 227 (1970)

6. Sugawara, F. and Nakamura, T.; J Phys Soc Japan 28, 158 (1970)

7. Onyango, F., Smith, W. and Angress, J.F.; J Phys Chem Solids 36, 309 (1975)

8. Ledsham, D.A., Chambers, W.G. and Parker, T.J.; Infrared Phys 16, 515 (1976)

9. Ledsham, D.A., Chambers, W.G. and Parker, T.J.; Infrared Phys (to be published)

10. Birch, J.R., Price, G.D. and Chamberlain, J.; Infrared Phys 16, 311 (1976)

11. Parker, T.J. and Chambers, W.G.; IEEE Trans MTT 22, 1032 (1974)

12. Gauss, K.E., Happ, H. and Rother, G.; Phys Stat Sol (b) 72, 623 (1975)

RESULTS, POTENTIALS AND LIMITATIONS OF JOSEPHSON MIXER RECEIVERS AT MM AND LONG SUBMM WAVELENGTHS

J. Edrich
University of Denver, Colorado

D.B. Sullivan and D.G. McDonald
Cryogenics Division, National Bureau of Standards
Boulder, Colorado

Josephson mixers with a conversion loss $L_c \leq$ 13 db and a noise temperature $T \sim 100$ K are reported for $\lambda \geq 0.95$ mm. Their potentials and limitations in noise, bandwidth, drive power and stability are discussed.

Introduction

Josephson effect devices using point contacts are ideally suited as ultra-sensitive mm-wave mixers. Their noise temperatures have been measured to be less than 100 K for frequencies up to 100 GHz [1-3]. No quantitative mixer data are available for the upper mm-wave and the submm-wave range, where these devices are particularly attractive because of their low intrinsic noise, their wide bandwidth and their low local oscillator (LO) power requirements. We report here on a Josephson mixer which is tunable over the entire wavelength range 0.92 mm $< \lambda <$ 1.36 mm (220 to 325 GHz). Based on these results certain potentials and limitations of these mixers for $\lambda \lesssim 0.92$ mm are presented.

Description of the 1 mm Josephson Receiver

Figure 1 shows a block diagram of the system which was designed for use as a spectral line receiver on a mm-wave antenna. The beam of the 300 GHz signal is focussed by a dielectric lens into a scalar horn. The LO signal is injected via a cross guide coupler. Following are the Nb point contact Josephson mixer and the if amplifier, an X-band maser. One side of the Josephson junction consists of a chemically sharpened Nb whisker of 0.15 mm length and 50 μ diameter. This whisker extends across the reduced-height waveguide (0.15 mm x 0.86 mm). The other side consists of an insulated 0.13 mm thick Nb wire which is flattened at one end to form the contact anvil. This wire serves as the adjustable member of the junction as well as coaxial line feeding the IF signal through a radial choke into the X-band waveguide.

Junction Bias and System Noise at λ = 1 mm

Best mixing results were usually obtained with junctions that exhibited a normal state resistance $R_N \sim 30$ ohms and a supercurrent $I_c \sim 25$ μA. This amounts to a product $I_c R_N = 750$ μV which is about one third of the theoretically possible value of $\pi\Delta/2e$, where $2\Delta/e$, the superconducting gap voltage, is 2.8 mV for niobium. It was found that the lowest conversion loss occurs for a supercurrent depression of only 9% which refers to an LO level of less than 10 μW. Simplified theories [4] as well as experimental evidence [1] at lower frequencies would suggest that the optimum LO level results in a supercurrent suppression of 50 %. The reason for our lower value is not fully understood. The optimum dc bias point was found to be near 50 % of the first-step voltage consistent with earlier results [1].

Despite the smaller LO level, the relatively low double-sideband noise temperature, T_{sys}=1500 K was measured for the system shown in Figure 1 utilizing the hot-cold (300-77 K) method.

Noise Contribution of Josephson Mixer at $\lambda \sim 1$ mm

The If noise temperature T_{IF} at the first slip fit was measured to be 20 K; this includes the contributions of the components shown in Figure 1 ahead* and behind the maser. The maser exhibits a bandwidth of 20 MHz and a gain of 36 db; it is followed by a two-stage tunneldiode amplifier with a noise temperature of 700 K** and a relatively wide bandwidth of 1 GHz. Table I lists the loss and noise contributions of important components. The loss measurements were performed with a 300 GHz carcinotron.

In the following calculations the simplified model of a reciprocal, resistive mixer is used in order to obtain an upper limit for the conversion loss L_c and an approximation for the mixer noise temperature T_M. Subtracting the noise contributions of all external components results in a single-sideband conversion loss L_c = 12.1 db for the Josephson mixer [5]. Using this L_c value one can obtain for the "net" single-sideband noise temperature of the Josephson mixer

$$T_M = (L_c - 2)\ 4\ K = 57\ K. \qquad (1)$$

These results are consistent with earlier estimates which suggested that the conversion and noise properties of Josephson mixers are nearly frequency independent up to the submm range [6]. It should be noted that the conversion loss L_c represents a conservatively high value since the lowest possible noise contributions of some of the cooled components like the horn and the input waveguides were used for these calculations. The T_M and L_c values contain also noise contributions caused by fm noise of the LO.

Potentials and Limitations

It is worthwhile noting that later tests of the cooled scalar horn used for the 1 mm receiver revealed an especially lossy vane section. Removal of this section resulted in a reduction of the

*) Loss of waveguide, switches, adapter and semi-rigid line L = 1.45 db.

**) T_{TDA}=900 K referred to cold output of maser

insertion loss by ∿1 db (at 4 K). Although the noise was not reevaluated with this change, it is instructive to note that this change, along with elimination of an unnecessary protective mylar film and a narrowing of the bandwidth of the tunneldiode amplifier to 100 MHz, results in an estimated noise temperature (SSB) T_{sys}=823 K. This latter noise temperature represents an improvement by an order of magnitude over the best uncooled mixer receivers [7].

The observed rounding of the rf biased I-V curves in the vicinity of the first zero-voltage step was relatively small suggesting that even for frequencies above 300 GHz, perhaps even above 600 GHz, good mixing efficiencies can be expected. For λ<1 mm the relatively small required LO power of less than 10^{-5} W can still be obtained via multiplication from 100 GHz. An LO coupler similar to the above mentioned one should be usable up to 600 GHz ; this method of LO injection results in good directionality of the LO signal and little loss in the signal line. Based on our experience with the 300 GHz system it appears quite feasible to use the same waveguide construction together with a simpler, not corrugated, conical horn up to 600 GHz. The instantaneous bandwidth of such receivers is presently limited by the bandwidth of existing low-noise if masers or paramps to 140 MHz or 600 MHz, respectively. The rf tuning range is limited by the tunability of the fundamental drive oscillators, such as 100 GHz klystrons, to about 15 %.

In order to improve the instantaneous bandwidth of our 300 GHz receiver and to make it field-usable it is presently being equipped with a 140 MHz wide C-band maser, a closed-cycle helium refrigerator and a stable, permanent Josephson junction similar to the ones successfully tested at 47 GHz [3].

This work was supported by a National Science Foundation Grant.

References

[1] Y.Taur, J.H.Claassen and P.L.Richards, IEEE Trans.Microw.Theory Tech., MTT-22, 1005 (1974).
[2] H.Kanter, Rev.Phys.Appl. 9, 255 (1974).
[3] J.Edrich, "A Low-Noise 47 GHz Mixer Using a Permanent Josephson Junction", accepted for IEEE Trans.Microw.Theory Tech. MTT-24 (Nov.76).
[4] F.Auracher and T.Van Duzer, Proc.1972 Appl. Supercond.Conf., IEEE Publ.No. 72CH0682-5-TABSC, 603 (1972).
[5] W.W.Mumford and E.H.Scheibe, Horizon House Microw., Inc., Dedham, Mass. (1968).
[6] C.A.Hamilton, J.Appl.Phys. 44, 2371 (1973).
[7] M.V.Schneider and G.T.Wrixon, Dig. 1974 IEEE S-MTT Symp., IEEE Publ.No. 74CH0838-3MTT, 120-123 (1974).

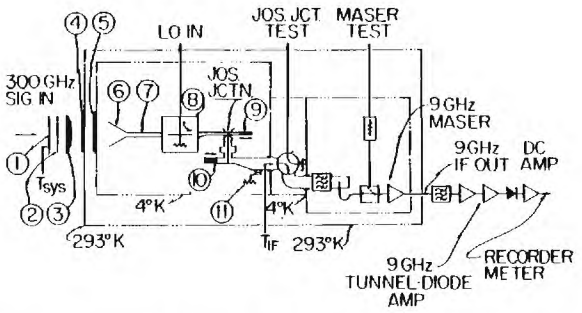

Figure 1: Blockdiagram of 300 GHz Josephson Mixer Receiver. Component numbers refer to Table I.

Table I: Significant noise contributions in 300 GHz Josephson mixer receiver.

No.[α]	Component Description	Loss L_R Refl. db	Loss L_D Diss. db	Loss L_T Tot. db	SSB[β] Noise Contrib. K
1	Protect. Mylar film, 0.075 mm thick	0.4	0.25	0.65	474
2	Screen filter (gold plated 2 mm holes)	0.7	0	0.7	489
3	Lens (1 cm Rexolite)	0.45	1.5	1.95	1293
4	Vacuum Window (high-dens.polyeth.1.5mm)	0.4	0.1	0.5	352
5	Helium window (1.5mm polyethylene)	0.4	0.1	0.5	338
6	Corrugated horn with trans. circ./rect. guide & cond. vane	2.3	0.2	2.5[γ]	1358
7	RG139 guide between horn & LO coupler (5 cm Cu, 5 cm Ag)	0	0.15	0.15	106
8	LO cross coupler	0.14	0.02	0.16	112
9	Movable red.-height waveguide short	1.5	0	1.5	906
10	Movable X-band short	0.2	0	0.2	121
11	X-band coupler with 4 K termination	0.4	0	0.4	237

Notes: α. Component numbers refer to fig.1
β. Defined as the difference between the system noise temperature with and without one particular component [5].
γ. Using 2 horns and 2 lenses a loss of 8 db was measured at 300 K (incl. reflections and spillover) which extrapolates to a loss of 4.45 db for one uncooled lens and one cooled horn.

THE JOSEPHSON SELF OSCILLATOR MIXER AS A SUBMILLIMETER AND FAR-INFRARED DETECTOR

G. Vernet, J-C. Hénaux and R. Adde
Institut d'Electronique Fondamentale, Université Paris-Sud,
91405 - Orsay - (France).

The Josephson self oscillator-mixer has potential detector applications at submillimeter frequencies. A quantitative investigation of noise effects and of its physical origin is performed with measurements in the frequency range 145 GHz - 891 GHz.

Recent publications [1,2] show that the Josephson mixer with external LO has performances which compare favorably in the millimeter range with Schottky diodes. In this frequency domain where tunable radiation sources are easily available, the local oscillator is not a problem and it does not appear that the Josephson oscillator mixer presents a very interesting alternative. The situation is different in the submillimeter and far infrared region where the availability of an internal oscillator easily tunable in a wide frequency constitutes a considerable advantage.

The Josephson oscillation has already been used for frequency conversion [3,4] and it has been demonstrated that it could be used up to the far-infrared [5]. The main source of difficulty of this mode of operation in a practical device is the important linewidth of the frequency converted signals which is directly related to the Josephson oscillation linewidth [6]. This difficulty way be overcome is several ways :
i/ The Josephson oscillation linewidth Δf_o may be decreased by coupling to a cavity tuned at the h.f. or at the i.f. [3], ii/ alternatively a decrease of Δf_o may be obtained with low impedances junctions ($<1\Omega$) since Δf_o is related to the dynamic junction resistance at the operating point, iii/ the selection of wide if bandwidths B to make full use of the frequency converted signals ($B \gtrsim f_o$).

The first two methods do not appear to allow the realization of an easily tunable receiver, well coupled to the external radiation source which impedance is often a few 10^2 Ohms. This point is particularly crucial in a low noise receiver. We have selected the third method for the detection of hf signals in the frequency range 145 GHz - 981 GHz with superconducting point contacts.

An exact experimental knowledge of the Josephson oscillation linewidth at these frequencies is an important question since it determines the junction parameters (practically the normal resistance R_N) and the bandwidth B which will have to be chosen for the device operation.

On the other side the main physical origin of the internal noise in a point contact is still an opened question. In the case of the Josephson mixer with external LO, the internal noise is responsible of the noise temperature T_M referred to the input. In the Josephson oscillator-mixer it is also responsible of the linewidth of the fundamental oscillation. Some of the already existing results [7,8] are well explained with the theory developped for oxide tunnel junctions where the noise is mostly due to the fluctuations of the dc pair and quasiparticle current components in the junction. Other results [9] have been interpreted assuming that the only source of noise is the thermal noise due to the junction normal resistance, the observed excess noise being attributed to complex non linear mixing processes. Direct measurements at very high frequencies such that $\Omega = \omega_S/\omega_c \gtrsim 1 (\omega_c = \frac{2e}{\hbar} RI_c)$ seem to be very useful as in these conditions the above non linear processes are negligible and linewidth measurements allow to reach directly with a good precision the internal noise level of the junction.

We present results of self-mixing 5 in a JJ with 145 GHz or 891 GHz (HCN laser) radiation signals. The i.f. which have been used have the following passbands 460-640 MHz, 100-600 MHz, 100-1000 MHz. Compared to previous experiments [6], the gain in sensitivity is considerable and linewidths measurements are possible with signal powers much lower than the levels at which the induced step appears in the VIC. In these conditions the Josephson oscillation is not perturbed by the external radiation and parasitic effects such as phase-locking or photon-assisted tunneling are practically eliminated.

Figure 1 shows a typical result at 891 GHz. The experimental linewidth $\Delta f_o \simeq 7$ GHz, with a $\simeq 1$ GHz contribution from the i.f. system. Then, $(\Delta f_o)_{eff} = 6$ GHz $\pm$ 1 GHz.

These results have been obtained with a point contact with the following characteristics :

$R_N I_c = 500\ \mu V$ $\quad R_N = 9\ \Omega$
$I_o = 225\ \mu A$ $\quad R_d = 10\ \Omega$
$V_o = 2$ mV

The theoretical linewidths are :

- SIS tunnel junction model : (Scalapino [10], Stephen [11]) :

$$f_o = 2\pi \left(\frac{2e}{h}\right)^2 e\, I_o R_d^2 = 5{,}3 \text{ GHz}$$

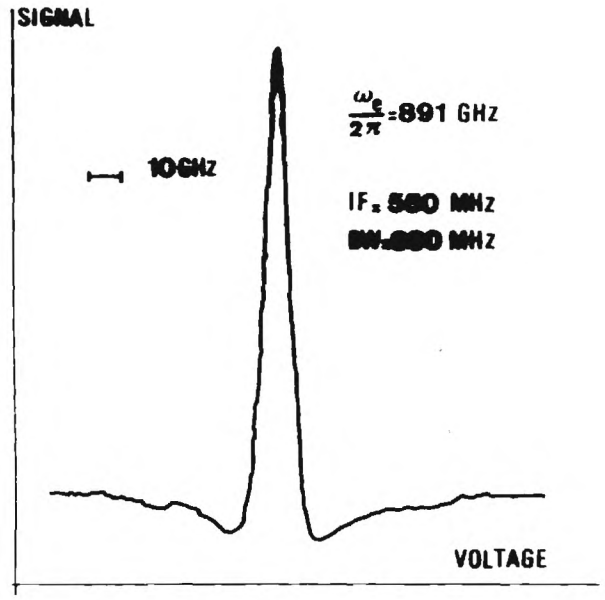

Figure 1. Heterodyne detection of a FIR signal (895 GHz HCN laser) using the internal oscillation of a Josephson point contact as local oscillator. The linewidth of the Josephson ac current deduced from this experiment is attributed to shot noise in the junction.

- Thermal noise from the normal resistance (Likharev [12]):

$$\Delta f_o = 2\pi \frac{2kT}{R_N} \left(\frac{2e}{h}\right)^2 R_d^2 = 1{,}9 \text{ GHz}$$

which compared to experiment show that the tunnel junction model gives a much better agreement. Many other experimental results give a similar conclusion.

These results confirm previous observations [7, 8] at lower frequencies. The Josephson oscillation linewidths in point contacts are better explained assuming shot noise proportional to the junction current while thermal noise related to its normal resistance R_N gives lower linewidth values independent of the dc bias.

These results may be well understood if the physical mecanism in a point contact is related to tunneling. The existence of tunneling effects is confirmed by the observation of the Riedel singularity [13, 14] in the devices. However it is necessary to find a model able to explain these results as well as the results at lower frequencies.

In a practical device the broad linewidth of the Josephson oscillation ($\sim$ GHz) may limit its use. We discuss the possibility to reduce the linewidth with a resistive shunt.

1. Y. Taur, J.H. Claassen and P.L. Richards, IEEE MTT 22, 1005 (1974).

2. P.L. Richards, J.H. Claassen and Y. Taur, Int. Conf. LT14, Otaniemi, Finland p. 238, Aug. 1975.

3. A. Longacre, 1972 Applied Superconductivity Conf., Annapolis, Maryland (IEEE, New-York 1972, p. 603).

4. G. Vernet and R. Adde, J. Appl., Phys. 45 2678, 1974.

5. G. Vernet, J-C. Hénaux and R. Adde, Journées Nationales Microondes, Limoges, Mars 1976.

6. G. Vernet and R. Adde, Rev. de Phys. Appliquée, 9, 275 (1974).

7. H. Kanter and F.L. Vernon, Phys. Rev. Lett. 25, 588 (1970).

8. G. Vernet and R. Adde, Appl. Phys. Lett. 19 195 (1971).

9. J.H. Claassen, J.H. Taur and P.L. Richards, Appl. Phys. Lett., 25, 759 (1974).

10. D.J. Scalapino, Proceedings of the Symposium on the Physics of Superconducting Devices, 1967, University of Virginia, Charlottesville, p. G-1 (unpublished).

11. M.J. Stephens, Phys. Rev. 182, 531 (1969).

12. K.K. Likharev and V.K. Semenov J.E.T.P. Letters 16, 442 (1972).

13. G. Vernet and R. Adde Appl. Phys. Lett. 28, 559 (1976).

14. Thomé and Couder, Int. Conf. Low Temp. Physics, LT 14, Otaniemi, 1975.

HETERODYNE SPECTROSCOPY IN THE THz REGION WITH A LASER LOCAL OSCILLATOR

B.F.J. Zuidberg and A. Dymanus
Fysisch Laboratorium
Katholieke Universiteit
Toernooiveld
Nijmegen, The Netherlands

1. Introduction

A sensitive heterodyne receiver has been constructed for use in the submillimeter wave region. The application of a laser as a local oscillator (LO) in the fundamental mixing mode greatly improves the sensitivity compared to systems with klystron LO's in the harmonic mixing mode, especially in the 1 THz region. The possibilities for application in submillimeter spectroscopy are demonstrated with a tunable receiver for the region around 891 GHz employing an HCN laser as a LO. The high sensitivity obtained with this system shows good prospects for spectroscopy in the 1-5 THz region.

2. Experimental arrangement

The diagram of the experimental set up is shown in Fig. 1. In the present application the detector was used to detect harmonic signals obtained from a klystron driven harmonic generator. In case of spectroscopy a variable IF is generated when tuning the signal frequency. The variable IF is converted to a fixed frequency IF' using a second LO coupled to the frequency stabilizing system in such a way that its frequency changes synchronously with the signal frequency.

The mixer in which the laser LO-power and the signal (harmonic) power obtained from a klystron driven harmonic generator are mixed, is a crossguide structure. The harmonic signal enters through a T-band waveguide, while the laser radiation enters through a 0.6 mm diameter circular waveguide extending into a small conical horn. The radiation is focused into this horn with a polyethylene lens. The crystal is placed in the circular guide.

The point-contact (PC) diode consists of an n-type GaAs crystal and an Au/Cu whisker. This combination is chosen because of its superior performance in a harmonic mixing experiment at 891 GHz [1] . The intermediate frequency (IF) signal is extracted via a 50 Ω coaxial line.

For the LO we use an 8 m HCN laser with a semiconfocal configuration. The laser utilises a Michelson type output coupling [2] providing a highly polarized beam and continuous variation of the extracted power. The laser was adjusted to the stable discharge, which is the absolute necessity in this experiment. Invar rods were used to reduce the thermal fluctuations in the resonator length. The maximum power output under the stable discharge conditions was in the order of 60 mW.

3. Measurements

In the first experiment we tried to detect the ninth harmonic of a 3 mm klystron at a fixed IF of 150 MHz. The mixing signal was so strong, that it could be directly displayed on the scope, despite the large bandwidth of the system. A result is shown in Fig. 2, obtained by applying a voltage upon the klystron reflector voltage. The origin of the signal was confirmed by placing a waveguide filter with the cut-off frequency of 500 GHz between mixer and generator.

The LO power, required for optimum detection was in the order of 30 mW, slightly varying for the different contacts. An experiment with an external bias showed that the required LO power can considerably be reduced by the application of a small bias current without upsetting the signal to noise (S/N-) ratio.

4. Sensitivity

The noise equivalent power (NEP) of our system has been obtained by measuring the total noise factor F, given by

$$F = L(F_{IF} + t - 1) \qquad (1)$$

where L represents the conversion loss, F_{IF} is the noise figure of the IF amplifier and t is the noise temperature ratio of the mixer diode (including the LO contribution). The conversion loss was found to be (32 ± 5) dB. The large error quoted here is due to uncertainty in the power generated in the ninth harmonic, which is estimated to be about 10^{-8} W. For the noise temperature ratio values of $t \simeq 2$ were obtained. Combining these values with a value of 4.8 dB for the noise figure of the IF amplifier used at 150 MHz, a value of 6.5×10^3 is obtained for the total noise factor, yielding an NEP of about 5×10^{-17} W/Hz. At an IF of 365 MHz an amplifier with a noise figure of 0.9 dB was available, resulting in an improvement of the NEP to 3×10^{-17} W/Hz.

5. High resolution spectroscopy at 891 GHz

The high sensitivity of the heterodyne detection enabled the extension of microwave gas spectroscopy with a harmonic generator to the region around 891 GHz, with the spectrometer, shown in Fig. 1. A 20 cm long piece of T-band waveguide is used as an absorption cell.

The first transition we measured was the $6_{15} \rightarrow 6_{24}$ transition in D_2O, calculated to be about 367 MHz away from the laser center frequency [3] . This means that an IF around 367 MHz had to be used, for which an IF amplifier with 0.9 dB noise figure was available. The transition has a relatively high intensity and could be observed directly on the scope. High S/N values

could be obtained when using synchronous detection. The transition was found to be at 890 396.03(0.30) MHz, in good agreement with an earlier value, obtained by high resolution Stark spectroscopy [4].

References

[1] B.F.J. Zuidberg and A. Dymanus, to be published in Appl.Phys.Letters

[2] K.M. Evenson, J.S. Wells, L.M. Matarrese and D.A. Jennings, J.Appl.Phys. 42, 1233 (1971)

[3] W.S. Benedict, S.A. Clough, L. Frenkel and T.E. Sullivan, J.Chem.Phys. 53, 2565 (1970)

[4] A.H. Brittain, A.P. Cox, G. Duxbury, T.G. Hersey and R.G. Jones, Mol.Phys. 24, 843 (1972)

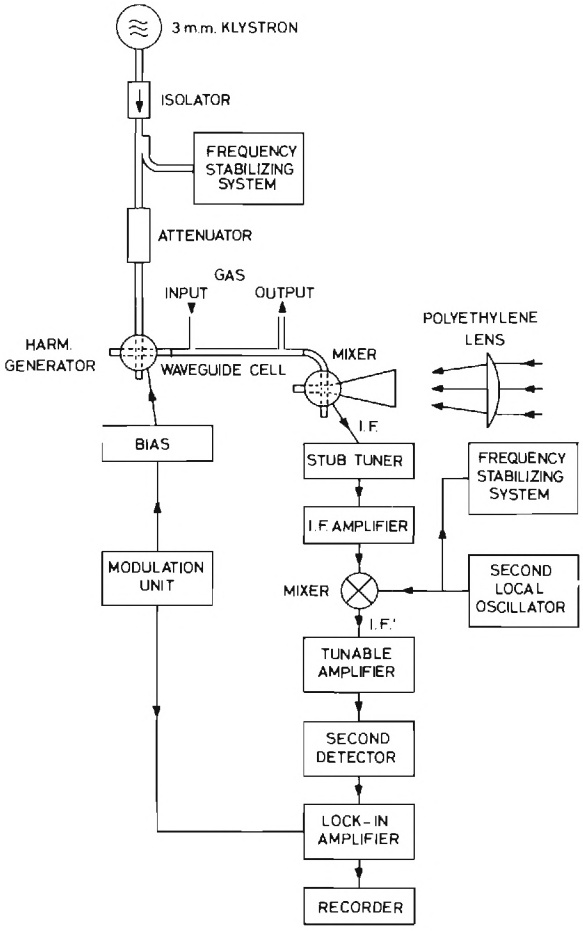

Fig. 1. Spectrometer for submillimeter heterodyne spectroscopy

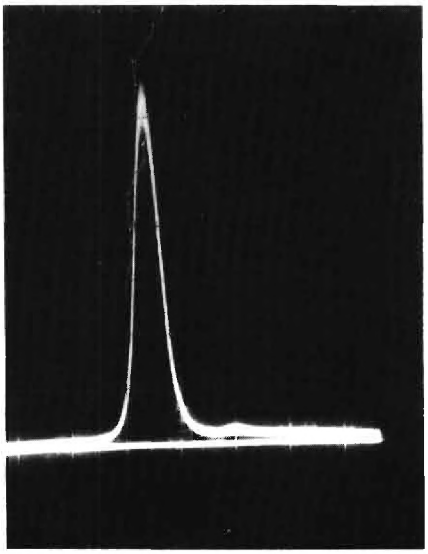

Fig. 2. Oscilloscope display showing the ninth harmonic from a 3 mm klystron

HETERODYNE DETECTION IN THE FAR INFRARED USING SHALLOW IMPURITY STATES IN SILICON

P. Norton*, R. E. Slusher and M. Sturge
Bell Laboratories
Murray Hill, New Jersey 07974

We present a study of far infrared heterodyne detection using the bulk photoconductivity associated with negative donor ion states (D^- centers) in n-type silicon at temperatures near 2K. A measured quantum efficiency η of 1% and a response time τ of 1nsec indicate that this detector provides an increase in sensitivity and bandwidth compared with other presently available detectors (e.g. GaAs) in the 120 to 500μm wavelength region.

The FIR photoconductivity in n-type Si is due to excitation of electrons weakly bound to neutral donor sites to form D^- centers at temperatures below 4K. A wide spectrum of FIR radiation, whose spectral width depends on both donor concentration and temperature [1], will excite the electrons from D^- centers to the conduction band. Electrons bound at D^- centers are supplied by ionization of neutral donors by near infrared radiation. In the experiment reported here this near infrared radiation was the 300K thermal radiation from the detector dewar window. This near infrared pump radiation does not add significantly to the noise for heterodyne detection since the recombination rate for electrons at D^+ centers is small compared to the pumping rate for electrons from D^- centers due to the FIR local oscillator.

The experimental arrangement for heterodyne detection is shown in Fig. 1. The detector D

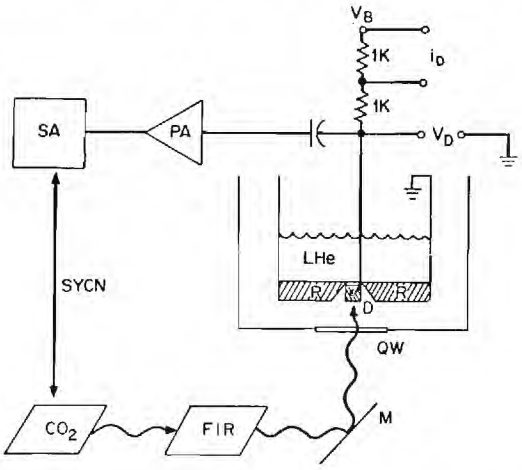

Figure 1. The FIR local oscillator, Si detector D mounted in a liquid He dewar and the bias and preamplifier networks are shown schematically.

has dimensions of 0.5 x 0.5 x 0.2cm and the bulk phosphorus donor concentration is $8.5 \times 10^{15}cm^{-3}$. One contact of the detector is In soldered to the cold finger and the other contact is connected with 50Ω coaxial cable to the bias network and preamplifier PA. The reflecting surfaces labelled R directed the near infrared radiation, required to supply electrons for the D^- centers, onto the sides of the detector.

Far infrared local oscillator radiation was obtained from a CO_2 laser pumped methyl alcohol gas laser operating at a peak power of 60mW in a 0.2msec pulse and a wavelength of 118.8μm. With a detector bias field E of 50V/cm and a bias current of 400μA the measured FIR current responsivity R_I was $4 \times 10^{-3}A/W$.

Heterodyne operation of the detector was confirmed with the observation of beats in the detector current in the range from 5 to 20MHz due to the FIR laser operating on several transverse modes simultaneously. The response time of the detector was estimated to be 1nsec at 2K from the current decay after a weak burst of CO_2 laser radiation. A similar Si detector has resolved 5nsec structure in the superradiant 496μm radiation from methyl floride pumped by a mode locked CO_2 laser [2]. These results confirm the detectors fast response in the FIR. A response time of 1nsec implies a heterodyne detection bandwidth of 150MHz.

A quantum efficiency of 1% at 118μm is obtained for the detector described above using the relation

$$\eta = \frac{R_I L hf}{e\tau\mu E} \qquad (1)$$

where L is the length between electrodes, hf is the energy of the incident FIR photon, e is the electron charge, and μ is the mobility. The mobility was $4 \times 10^4 cm^2/V$ sec and the lifetime τ was 1nsec from the measurement described above. This efficiency is probably not optimized with the detector dimensions used in the present experiment. The sample dimensions should be matched to the FIR and near infrared pump absorption lengths for optimum efficiency. We found that the detector responsivity was not sensitive to the intensity of the near IR pump.

The limiting noise for heterodyne detection with the detector and local oscillator described above was the preamplifier input noise. The 2.5db noise figure of the preamplifier limited the NEP in the heterodyne mode to $3 \times 10^{-16}W/Hz$ at a wavelength of 118.8μm. If the shot noise voltage due to the local oscillator could be made the dominant noise source, the NEP would be reduced to $4 \times 10^{-19}W/Hz$. Since the shot noise voltage is inversely proportional to the electrode separation L, it can be shown that the shot noise should be dominant if L is reduced to 0.5mm [3]. This

dimension is of the order of the FIR wavelength and still allows coupling the FIR radiation to the detector by focusing with a lens.

The spectral response of the detector sample used here and other similarly doped samples over a range of concentrations has been studied as a function of temperature [1]. In general, a broad spectral response is found in the FIR from 100 to 500 μm and the sensitivity is a sharply increasing function of inverse temperature. Due to the random distribution of impurities in the crystal, there exists a range of binding energies for an extra electron bound to a group of neutral donor atoms. At the lowest temperatures the most weakly-bound configurations will be stable against thermal ionization, while at higher temperatures only the more tightly-bound centers will be available for photoexcitation. The donor concentration of $8.5 \times 10^{15} cm^{-3}$ was chosen for the detector studied here to optimize the quantum efficiency and sensitivity over the range of wavelengths from 120μm to 500μm where fast sensitive detectors have not previously been available. The spectral response of the detector described here is shown at two temperatures in Fig. 2

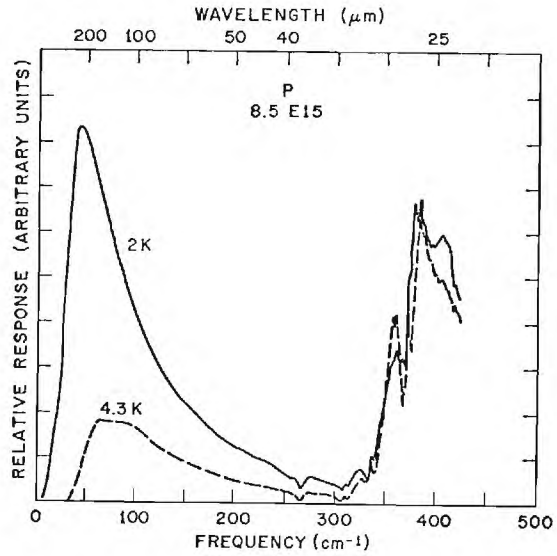

Figure 2. Spectral response of the phosphorus-doped Si detector is shown at constant FIR power for two temperatures.

These spectra were normalized to constant incident power as monitored with a Ge bolometer. The peak at $380 cm^{-1}$ is due to photoexcitation of electrons from neutral donors and the peak at $50 cm^{-1}$ at 2K is due to D^- centers. The ratio of the detector response at the two peaks is also a measure of the detector efficiency in the FIR. Using this ratio from Fig. 2 and a quantum efficiency at $380 cm^{-1}$ of 50% yields a peak FIR quantum efficiency of 6% in agreement with the result obtained above at 118μm.

Heterodyne detection with high quantum efficiencies and wide bandwidths in the FIR should be useful for a wide range of research applications. For example, the detector can be used for studies of molecular line radiation from interstellar clouds. This application is restricted at present because of the lack of a tunable or fixed frequency laser local oscillator with a frequency sufficiently near a molecular line of interest (e.g. transitions between the high lying rotational levels of CO). A second interesting research application for this detector involves detection of FIR laser radiation scattered from high temperature toroidal plasma devices. The detector described above and a FIR laser with a wavelength between 200 and 500 μm could provide a localized measurement of plasma turbulence, ion temperatures and impurity concentrations in prototype fusion reactors [4].

References

1. P. Norton, J. Appl. Phys. 47, 308(1976) and P. Norton, Phys. Rev. Letters 37, 164 (1976).
2. T. A. DeTemple, Univ. of Ill., Champagne-Urbana, Ill. (private communication).
3. See for example, F. R. Arams, E. W. Sard, B. J. Peyton and F. P. Pace in Semiconductors and Semimetals, ed. by R. K. Willardson and A. C. Beer (Academic Press, New York, 1970) 5, pp. 409-434.
4. B. Lax and D. R. Cohn, IEEE Trans. MTT-22, 1049(1974).

*Present address: Honeywell Corp. Research Center, Bloomington, Minn. 55420

DETECTION OF PASSIVE SUB-MILLIMETER WAVE RADIATION

Geert J. Wijntjes
Block Engineering, Incorporated
19 Blackstone Street
Cambridge, Massachusetts 02139

Heterodyne detection at the quantum level of sub-millimeter wave radiation has been demonstrated on numerous occasions. At this time sufficient local oscillator power to reach this limit has only been available at the discrete wavelength of existing lasers in the mid-IR. It is, however, reasonable to expect that in the near future sufficient powerful sources tunable over useful bands will become available for the whole region classified as sub-millimeter wave. In the sensing of low levels of radiation, receivers of this kind can thus provide the experimentor with an alternative to sensors of the classic kind, consisting of a quantum counter or power detector preceeded by some form of optical filtering device as exemplified by narrow band filters, Fabry-Perot resonators and transform devices such as Fourier transform spectrometers and Hadamard encoders.

In itself, the fact that quantum limited performance can be obtained for a heterodyne receiver is not particularly significant since the same is true for many detectors from the visible to submillimeter regions. For example, in the case of a photo multiplier operating in the visible, it is well known that a single photoelectron per second can readily be detected. Similarly, in the IR from 1 to 100 μm, detectors cooled to sufficiently low temperatures are background limited for as much as 10^8 to 10^{10} reductions in background flux below that due to a 300°K background.

The potential advantage of a heterodyne receiver results then from the fact that since its bandwidth is determined in the electrical frequency domain, it can be easily controlled and hence the background contribution reduced until signal power is lost. On the negative side is the heterodyne receiver's small light gathering power or étendue, which for a single channel is limited to a single diffraction mode. Also, since it is essentially a single channel device, the multiplex advantage available from a Fourier spectrometer is not normally present. Hence in order to make a valid comparison between a heterodyne receiver and a direct detection receiver their respective sensitivities should be evaluated in terms of the nature of the particular source of radiation, be it an extended or a point source, its wavelength, its optical bandwidth (e.g., a continuum source or line source), and the properties of the medium it is observed through, i.e., its transmission and stability (scintillation effects). Other factors which may affect this equation are acquisition and pointing considerations as well as aspects such as mechanical stability, vibration, etc. Last but potentially important, are physical or weight limitations. For example, a Michelson interferometer with a 10 m stroke may just be out of the question on a spacecraft while a mixer followed by an electrical filter can easily be accommodated.

SUBMILLIMETER PLASMA DIAGNOSTICS IN CONTROLLED THERMONUCLEAR FUSION RESEARCH*

Daniel R. Cohn

Francis Bitter National Magnet Laboratory†
Massachusetts Institute of Technology
Cambridge, Massachusetts 02139

*Supported by ERDA
†Supported by the National Science Foundation

The characteristic parameters of plasma in the tokamak, the mirror and the bumpy torus devices used in controlled thermonuclear fusion research are such that submillimeter wavelengths are required for a number of important diagnostics. These diagnostics include measurements of plasma density, electron cyclotron radiation levels, ion temperature, and impurity concentration. It may also be possible to use submillimeter radiation to measure transverse thermal conductivity in a tokamak plasma by local heating and to determine the poloidal magnetic field by cyclotron absorption and measurements.

A 337 μm HCN laser interferometer is being used to measure the temporal dependence of plasma density on the French tokamak TFR [1]. High resolution and the unambiguous determination of the sign of the plasma density change are obtained by modulation of the laser radiation. The modulation is produced by use of a rotating grating. A 119 μm CH_3OH laser interferometer has recently been installed on the Alcator tokamak at MIT [2,3]. Measurements of the density dependence of the particle confinement time in Alcator have been made using this system. Modulation in the CH_3OH laser interferometer system is obtained by mixing the radiation from two lasers separated in frequency by 1 MHz. The 119 μm wavelength of the CH_3OH laser is very well suited to measurement of plasma density in high density ($n > 5 \times 10^{14}$ cm^{-3}) tokamak devices; at longer wavelengths such as the 337 μm HCN laser line, plasma refraction effects decrease the quality of the measurement.

Measurements of electron cyclotron emission at harmonics of the electron cyclotron frequency have been used to determine the presence of a very large amount of nonthermal radiation in low density tokamak plasmas [4]. The third harmonic of the electron cyclotron frequency occurs at 892 μm at a magnetic field of 40 kG. Because of the inhomogeneity of the magnetic field in a tokamak cyclotron emission can also be used to measure continuously in time the electron temperature at a given spatial point [5].

It has been proposed to use submillimeter radiation to measure ion temperature and impurity concentration by Thomson scattering [6, 7]. Thomson scattering will provide the only definitive means of measuring ion temperature in future tokamak devices. The ion temperature is determined by measurement of the linewidth of the Thomson scattered radiation. In the proposed diagnostic the linewidth of the scattered radiation would be measured by a heterodyne detection system employing a Schottky barrier diode [8]. Submillimeter laser pulse energies on the order of 100 millijoules and power levels on the order of 1 MW are required. A further requirement is that the laser radiation be narrow in bandwidth ($\leq$ 50 MHz full width half maximum). A number of high power submillimeter laser systems have been developed in order to produce high power narrow linewidth radiation [9, 10, 11, 12, 13]. At present, 12 millijoule, 200 kW level radiation has been produced at 496 μm from a CH_3F oscillator amplifier system and at 385 μm from a D_2O oscillator amplifier system [12, 13].

High power millimeter and submillimeter radiation could be used to measure thermal conductivity in a tokamak plasma by local heating at a harmonic of the electron cyclotron frequency [6]. The thermal transport coefficient would be determined by measurement of the decay of heat in the locally heated region. Sensitive x-ray techniques could be used to measure small temperature changes [14]. The development of a 1 MW level laser in the 1200 μm - 700μm range is required. A 1220 μm $C^{13}H_3F$ laser which produces 5 kW when pumped with 10 MW of CO_2 laser radiation has recently been developed [15]. At this wavelength the laser frequency is equal to the second harmonic of the electron cyclotron frequency in the presence of a 44 kG magnetic field. It should be possible to scale the power of the $C^{13}H_3F$ laser up to the MW level by increasing the CO_2 pump power to the 2 GW level.

References

1. D. Veron, Optics Commun. 10, 95 (1974).
2. S.M. Wolfe, K.J. Button, J. Waldman and D.R. Cohn, Appl. Optics, Vol. 15, no. 11, November 1976.
3. S.M. Wolfe, K.J. Button, J. Waldman and D.R. Cohn, Proc. of this Conference.
4. A.E. Costley, R.J. Hastie, J.W. M. Paul and J. Chamberlain, Phys. Rev. Lett. 33, 758 (1974).
5. R. Cano, Seventh European Conference on Plasma Physics and Controlled Fusion, Lausanne, 1975.
6. D.L. Jassby, D.R. Cohn, B. Lax and W. Halverson, Nucl. Fusion 14, 745 (1974).
7. D.E. Evans and M.L. Yeoman, Phys. Rev. Lett. 33, 76 (1974).
8. H.R. Fetterman, B.J. Clifton, P.E. Tannenwald, C.D. Parker, and H. Penfield, IEEE Trans. Microwave Theory and Tech. MTT-12, 1013 (1974).

9. Z. Drozdowicz, R.J. Temkin, K.J. Button and D.R. Cohn, Appl. Phys. Lett. 28, 328 (1976).

10. F. Brown, P. Hislop, and S. Kronheim, Appl. Phys. Lett. 28, 654 (1976).

11. A. Semet and N.C. Luhmann Jr., Appl. Phys. Lett. 28, 659 (1976).

12. D.E. Evans, L.E. Sharp, W.A. Pebbles and G. Taylor (to be published in IEEE Journal of Quantum Electronics).

13. Z. Drozdowicz, P. Woskoboinikow, K. Isobe, D.R. Cohn, R.J. Temkin, K.J. Button and J. Waldman, Proc. of this Conference.

14. D.R. Cohn, D.L. Jassby and J.E. Hosea, San Francisco APS meeting, November 1976.

15. M.P. Hacker, Z. Drozdowicz, D.R. Cohn, K. Isobe and R.J. Temkin, Phys. Lett. 57A, 328 (1976).

STIMULATED RAMAN EMISSION IN INFRARED EXCITED GASES*

S. J. Petuchowski and A. T. Rosenberger
Department of Physics
University of Illinois
Urbana, Illinois 61801

and

T. A. DeTemple
Department of Electrical Engineering
University of Illinois
Urbana, Illinois 61801

ABSTRACT

Intense (kW) stimulated Raman emission has been observed from D_2O vapor at 50.3 μm. The process was identified by measuring the frequency difference between the emitted radiation and the rotational transition center frequency using an external absorption cell technique.

In this paper we report the first observation of stimulated Raman emission in gases excited by CO_2 lasers. Intense far infrared (FIR) emission has previously been observed from optically pumped D_2O using MW infrared excitation pulses [1,2, 3]. By analogy with FIR pulses observed in optically excited HF and CH_3F experiments, the D_2O system was thought to be superradiant. Recent spectroscopic studies have shown that for the strongest FIR transition, the infrared pump line (P(32) 9.6 μm) is ∿ 750 MHz above the D_2O ν_2 band transitions $J_T = 6_5 \rightarrow 5_5$, $6_6 \rightarrow 5_4$ [4]. In Fig. 1 is shown a partial energy level diagram showing the pump transition and the observed FIR transitions. The observed signal strength was ordered 66 > 50 >> 83 μm. In what follows, we present evidence that the 50 μm signal is due to stimulated Raman emission with a characteristic frequency shift equal to the pump detuning to within the limits introduced by the uncertainty in the relevant pressure broadening coefficients.

The experiment was composed of a grating tuned high-pressure CO_2 laser and an external 3.5 m long D_2O cell. The CO_2 laser produced ∿ 1 MW, 150 nsec pulses on a single transverse and longitudinal mode obtained with the use of a low-pressure intercavity CO_2 gain cell [1]. Using this technique, the CO_2 pulse oscillates on line center ±30 MHz with a single pulse spectral width of < 10 MHz, including chirp. The D_2O cell contained Si Brewster windows and an external Au coated flat was used as a back reflector. The CO_2 pulse was injected into the cell by reflecting off the internal surface of the back Si Brewster window which also had an internal infrared dielectric coating (> 95% transmission in the FIR) to raise the reflectivity to > 90% for the P-polarization. Spectral identification was carried out with a 0.5 m grating monochrometer using various FIR gratings in higher orders. Temporal and energy measurements were performed with a pyroelectric joule meter, a disc calorimeter, a photon drag detector, a Ge:Ga (4°K) detector and recently developed Si (2°K) photoconductor.

The key characteristic of a Raman effect is the shift in scattered frequency which should be proportional to the pump detuning. In order to measure this small shift, a second D_2O cell was used as a spectrometer and the magnitude and pressure dependence of the apparent FIR absorption coefficient was measured and compared with calculated values. For a homogeneously broadened transition, the absorption coefficient in the wings becomes $\alpha = mp^2/\Delta^2$, where Δ is the detuning, p is pressure and m is a calculable material parameter. Only the magnitude and not the sign of Δ can be determined by this method. In Fig. 2(a) is shown the quadratic pressure dependence measured for the P(32) absorption. Also shown in the calculated behavior for a detuning of 750 MHz which essentially confirms the offset value. Here the weaker 7_{34}-6_{25} absorption is neglected, and a broadening coefficient of 26 MHz/torr from Ref. 2 is assumed.

Prior to propagating through the D_2O absorption cell, the intense (∿ kW) FIR pulses were filtered through a monochrometer and attenuated to low levels (< W) to prevent saturation. The apparent absorption coefficient was then measured as a function of pressure in both the source and absorption cell. In Fig. 2(b) is shown the result for the 50 μm signal which corresponds to a detuning of ∿ 1.1 GHz, which is somewhat greater than the pump detuning. The 66 μm signal was also off resonance, but uncertainties in the excited-state spectroscopic data preclude a reasonably precise determination of its detuning at the present time. The 83 μm signal was absorbed strongly at all

pressures and appeared to be near resonance.

Since it is known that other laser-like transitions involving pure rotational and vibrational-rotational states are pumped in an off-resonant manner, it is interesting to consider how many of these may actually be due to the stimulated Raman effect. For example, a number of transitions in the ν_2 band of $^{14}NH_3$ which are offset $\sim$ 1 GHz from CO_2 pump lines produce FIR emission which might be likely candidates for stimulated Raman emission.

*Supported by Army Research Office - Durham and the University of Illinois Industrial Affiliates Program.

References

1. T. K. Plant, L. A. Newman, E. J. Danielewicz, T. A. DeTemple and P. D. Coleman, IEEE Trans. on Microwave Theory and Tech., MTT-22, 988 (1974).

2. F. Keilmann, R. L. Sheffield, J.R.R. Leite, M. S. Feld and A. Javan, Appl. Phys. Lett., 26, 19 (1975).

3. D. E. Evans, et al., Opt. Commun., to be published.

4. C. L. Lin and J. Shaw, 31st Symposium on Molecular Spectroscopy, June 1976, Columbus, Ohio, Paper FC-10.

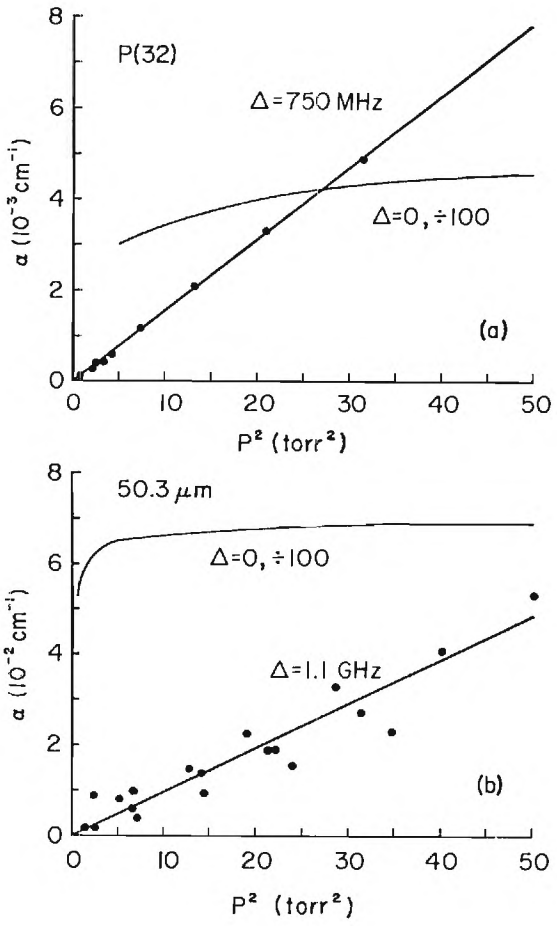

Figure 2. Small signal D_2O absorption coefficients at a) P(32) 9.6 μm and b) 50.3 μm. Solid lines are the calculated behavior for the indicated detunings.

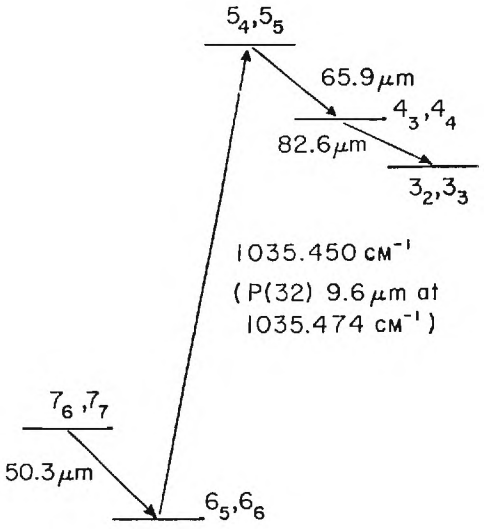

Figure 1. Partial energy level diagram of D_2O showing observed far infrared transitions. Not shown is the nearby 000, 7_{34}-010, 6_{25} transition.

ABSORPTION MEASUREMENTS ON VERY DILUTE SOLUTIONS IN THE 10 TO 120CM^{-1} RANGE

H. Kilp
Institut für Physik
Universität Mainz
D-6500 Mainz, West Germany

Dispersion and absorption measurements on polar liquids can give information on the rotation of molecules and their interaction in dense phase. The relaxation spectrum even for simple liquids is very broad and extends from microwaves into the far infrared (FIR). In order to obtain details of the orientational motion this spectrum must be measured accurately.

Measurements in the FIR, in particular, are related to the short time behaviour (<1ps) of the orientation, and only after the development of Fourier transform spectroscopy (FTS) this range of the spectrum has been extensively investigated. Most of the work, however, has been done on pure liquids, and despite a basic understanding of the molecular processes contributing to the observed absorption, a model with reasonable parameters is still needed.

The study of very dilute solutions of polar molecules in non-polar solvents, on the other hand, has the advantage of being a simpler system theoretically. Dipole-dipole interaction is essentially absent, and the possibility to compare the behaviour of different polar molecules in the same solvent or one molecular species in different solvents can give information on the relevant parameters. This technique has been widely used in the microwave region, but in the FIR there are some experimental difficulties.

Firstly, generators with sufficient power and stability and sensitive detectors are less readily available. Secondly, non-polar solvents have considerably loss in the FIR and the absorption of a very dilute solution is often only slightly higher than the absorption of the solvent. This absorption difference, however, is the relevant quantity for the investigations envisaged. For that reason, a method has been developed to observe the absorption difference directly and thus obtain higher accuracy.

Measurements to test this method have been made with coherent sources at fixed frequencies of 9.5, 30 and 85cm^{-1} and with an incoherent source in the 25 to 120 cm^{-1} range by means of Fourier transform spectroscopy.

The liquid cell

The absorption difference $\Delta\alpha$ between solution and solvent is obtained from the transmission of an unguided parallel beam through a two-chamber cell (see Fig. 1). A moveable window in the middle allows the two liquid thicknesses x_1 and x_2 to be varied in such a way that $x_1 + x_2$ remains constant. The transmitted power is then given by

$$P = P_o\, T \exp(-2\alpha_2 L) \exp(-2\,\Delta\alpha\, x_1), \quad (1)$$

where P_o is the incident power, T the combined transmission coefficient of the window and the two lenses, $\Delta\alpha = \alpha_1 - \alpha_2$, $L = x_1 + x_2$, and α_1 and α_2 are the absorption coefficients (amplitude) of solvent and solution, respectively.

The expression (1) shows the detector signal P to be a simple exponential function of the window position, and this is also verified experimentally. The absence of signal variations from multiple reflections in the cell, even when monochromatic radiation is used,is explained by the near match of the refractive indices of the liquids and the lens and window materials. The much higher reflection from the spherical surfaces of entrance and exit lens, on the other hand, is not focussed onto the detector.

Coherent sources

Measurements were made at three FIR frequencies using 1) at 9.5 cm^{-1} a harmonic generator driven by a 70 GHz Klystron, 2) at 30 cm^{-1} an HCN gas laser, and 3) at 85 cm^{-1} the same laser run on an H_2O discharge. Since none of these sources was stable to better than a few percent a fraction of the power was directed to a second detector by a beam splitter in front of the cell. Then, this signal was fed as reference into a logarithmic ratio meter together with the signal from the beam transmitted by the cell. A double beam method is thus

realised and $\Delta\alpha$ is read directly from the slope of the linear relation between output of the ratio meter and window position.

Fourier transform spectroscopy

A cell of the same principle as described above was adapted to a Fourier spectrometer of the modular type developed at the National Physical Laboratory in England [1] . This spectrometer was equipped with a 25 μm Mylar beam splitter to cover the frequency range from 25 to 120 cm^{-1}. Other features of the instrument included a water cooled Hg-lamp, Golay detector with quartz window, phase modulation [2] and a stepping mirror drive. Double sided interferograms were recorded for a resolution of 4 cm^{-1} and the Fourier transforms were computed off-line.

The absorption difference $\Delta\alpha(\tilde{\nu})$ as function of the frequency is given by

$$\Delta\alpha(\tilde{\nu}) = (x_a - x_b)^{-1} \ln\left[F\{I_a(\Delta)\}/F\{I_b(\Delta)\}\right] \quad (2)$$

where $I_a(\Delta)$ and $I_b(\Delta)$ are interferograms as function of the path difference Δ, recorded for two different window positions x_a and x_b, respectively. $F\{\}$ symbolizes the Fourier transform.

Results

Measurements have been made on dilute solutions of chlorobenzene and benzophenone in cyclohexane at 20°C because microwave data [3] are available for both systems. The absorption difference $\Delta\alpha$ between solution and solvent was determined for four different concentrations of each system. For molar fractions c below .05 $\Delta\alpha$ was found to be proportional to c at all frequencies indicating that there is no dipole-dipole interaction.

At present, the accuracy of $\Delta\alpha/c$ is about ± 2% for the measurements with coherent sources and about ± 5% for the FTS data. The low power output of thermal sources is the main reason for higher FTS errors. In each case, further improvement by a factor of 2 should be obtainable without difficulties.

The FIR spectra connect smoothly to the microwave data and show the expected deviations from a Debye line shape. These are due to librational motions of the polar molecules and to inertial effects. With these FIR measurements it is now possible to observe the complete relaxation spectrum also for dilute solutions.

Acknowledgements

This work was supported by the Deutsche Forschungsgemeinschaft. The FTS measurements have been made at the National Physical Laboratory in England.

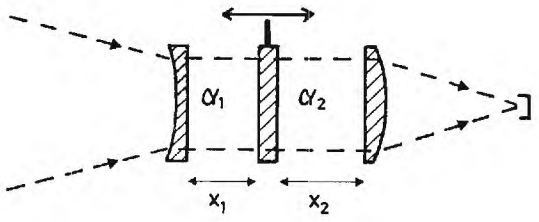

Figure 1. Schematic of the two-chamber liquid cell.

References

[1] G.W. Chantry, H. Evans, J. Chamberlain, and H.A. Gebbie, Infrared Physics Vol. 9, 85 (1969)

[2] J. Chamberlain, Infrared Physics Vol. 11, 25 (1971)

[3] H. Kilp, G. Klages, and W. Noerpel, in "Molecular Motions in Liquids", pp. 123, D. Reidel, Dordrecht 1974.

STARK SHIFT LASER SPECTROSCOPY AT SUBMILLIMETER WAVELENGTHS FOR CHEMICAL ANALYSIS*

L. W. Hrubesh and D. C. Johnson
Lawrence Livermore Laboratory
P. O. Box 808
Livermore, California 94550

Edgar A. Rinehart
University of Wyoming
Laramie, Wyoming

Very high sensitivity and spectrometric resolution have been obtained for gaseous paramagnetic molecules by using fixed-tuned submillimeter lasers and tunable magnetic fields [1-4]. This technique, commonly called laser magnetic resonance spectrometry (LMRS), has an electric analogy, Stark shift laser spectrometry [5,6], which, in addition to providing ultra high resolution for molecular spectroscopy also holds considerable promise as an analytical tool for gases. The same technique at longer wavelengths has been successfully applied to chemical analyses [7,8] but with less sensitivity than that expected with submillimeter lasers. Work is currently underway at the Lawrence Livermore Laboratory to develop Stark shift spectrometry at submillimeter wavelengths with emphasis toward characterizing its analytical capabilities.

A large number of laser source lines are made available for Stark shift spectrometry at submillimeter wavelengths by optically pumped waveguide lasers with many more expected to result from continued work. Near coincidences are expected to exist between these source lines and pure rotational absorption transitions (usually in their ground vibrational state) of asymmetric polar molecules. The additional frequency offset can be made up by the application of a field to the gas which frequency shifts its Stark components in proportion to some power of the applied field. A Stark shift absorption spectrum can be obtained by detecting the laser power transmitted through a gas sample which is simultaneously being subjected to a swept voltage. The distinct pattern of absorption lines, and in some cases, the frequency locations of select Stark lines, can be used to identify the presence of particular gases in a mixture. Quantitative information can be obtained from the absorption intensities.

A spectrometer, constructed for the purpose of investigating the analytical potential of this technique is shown in Fig. 1. The CO_2 pumped FIR waveguide laser is similar to that described by Hodges and Hartwick [9]. The CO_2 laser frequency is stabilized at the peak of the FIR pump transition by using a separate Stark cell and servo loop to control the CO_2 cavity length. Most of our current work is with CH_3F and CH_3OH as the submillimeter laser medium but future work will make use of any available laser lines that can be optically pumped by the CO_2 laser. The analytical Stark cell is 50 cm long and has a plate spacing of 0.215 cm. Breakdown limits the applied voltages to less than 10 KV in the pressure range from 0.01 to 0.1 Torr. Field intensities from zero to approximately 50 KV/cm can be applied to the gas in either a continuous sweep or at selected constant values. Either a Golay cell or a helium cooled bolometer is used as a detector. The absorptions are observed as derivative spectra because slight field modulation and phase sensitive detection is used. Although a mixture of several gases gives a very complicated spectrum, several variables can be used to help interpret the complex spectra in a real analysis. For example, different spectra for the same compound can be obtained by using different laser lines available from the optically pumped waveguide laser. Also, because the laser radiation is polarized, two distinctly different spectra are observed from a compound depending upon the orientation of the applied electric field with respect to the laser radiation electric field (these are the $\Delta M = 0$, and $\Delta M = \pm 1$ sets of Stark transitions).

Work is continuing at this laboratory to characterize the technique as an analytical tool, to catalog spectra with currently available laser lines and to develop computer techniques to both control the spectrometer as well as to deconvolute and quantify the spectral data. Potentially, this type of spectrometer has advantages over other analyzers because of its very high resolution, high sensitivity (theoretically capable of detecting 10^8 molecules/cc) and its multiple gas capability. On the other hand, some of its limitations include instrumental complexity, complex spectra and requirements for reduced pressure samples. In future work we intend to modify the FIR waveguide laser for intra-cavity absorption detection to further enhance the sensitivity. Our objective is to apply this technique as a compliment to other gas analyzers for routine sample analyses at LLL. We expect this technique to considerably enhance our analytic capability for organic solvents, chlorinated and fluorinated compounds, and moderately reactive molecular species.

*Prepared for U.S. Energy Research & Development Administration under contract No. W-7405-Eng-48.

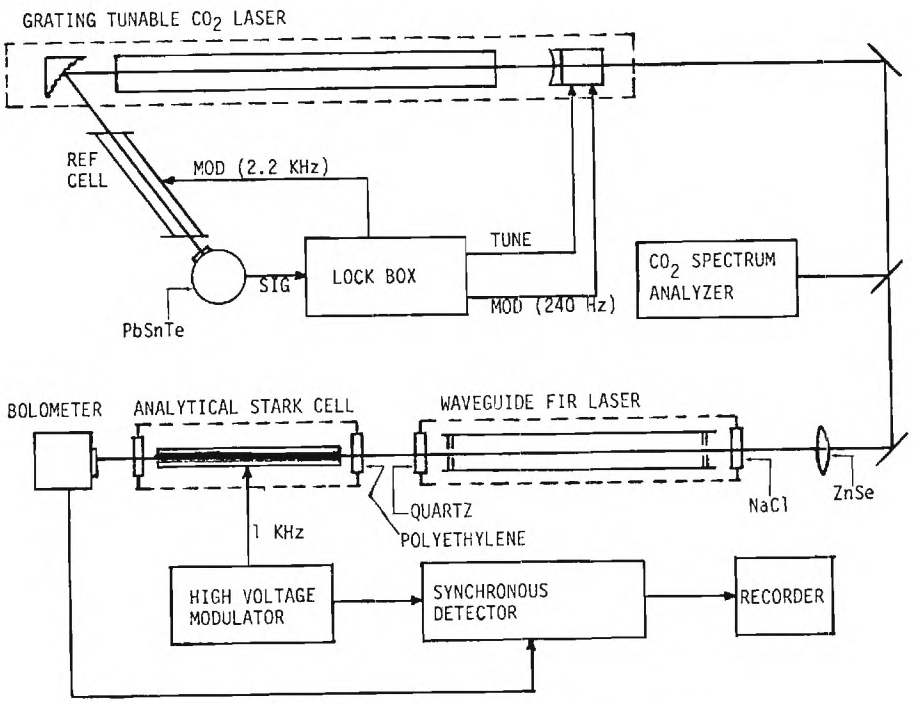

FIG. 1 SUBMILLIMETER LASER ANALYTICAL SPECTROMETER

References

[1] K. M. Evenson, H. P. Broida, J. S. Wells, R. J. Mahler and M. Mizushima, "Electron Paramagnetic Resonance Absorption in Oxygen with the HCN Laser," Phys. Rev. Lett. 21, 1038 (1968).

[2] K. M. Evenson, J. S. Wells and H. E. Radford, "Infrared Resonance of OH with the H_2O Laser: A Galactic Maser Pump ?," Phys. Rev. Lett. 25, 199 (1970).

[3] H. E. Radford, K. M. Evenson, and Carleton J. Howard, "HO_2 Detected by Laser Magnetic Resonance," J. Chem. Phys. 15, 3178 (1974).

[4] P. B. Davies, D. K. Russell, B. A. Thrush, and F. D. Wayne, "Detection of the Amino Radical NH_2 by Laser Magnetic Resonance Spectroscopy," J. Chem. Phys. 62, 3739 (1975).

[5] G. Duxbury and R. G. Jones, "High Resolution Submillimeter Stark Spectroscopy using an HCN Maser," Molec. Phys. 20, 721 (1971).

[6] A. H. Brittain, A. P. Cox, G. Duxbury, T. G. Hersey and R. G. Jones, "The Dipole Moment of Water: Stark Effects in D_2O and HDO," Molec. Phys. 24, 843 (1972).

[7] H. Uehara, M. Tanimoto and Y. Ijuuin, "A Stark-Sweep Microwave Cavity Spectrometer for Zeeman Effect Studies and for Pollutant Monitoring," Chem. Phys. Lett. 26, 578 (1974).

[8] M. Tanimoto and H. Uehara, "Detection of Acrolein in Engine Exhaust with Microwave Cavity Spectrometer of Stark Voltage Sweep Type," Environ. Sci. and Technology 9, 153 (1975).

[9] D. T. Hodges and T. S. Hartwick, "Waveguide Laser for the Far Infrared (FIR) Pumped by a CO_2 Laser," Appl. Phys. Lett. 23, 252 (1973).

EXTENSION OF ELECTRIC RESONANCE SPECTROSCOPY TO THE SUBMILLIMETER WAVELENGTH REGION

J. J. Gallagher
and
W. M. Penn
Georgia Institute of Technology
Atlanta, Georgia

Abstract

The requirements for the performance of molecular beam electric resonance experiments at wavelengths shorter than one millimeter are discussed. Examples relevant to current experiments are presented, and comparisons made with millimeter and near IR experiments.

Introduction

Electric resonance spectroscopy in molecular beams originated as a form of radio frequency spectroscopy, and more recently was extended to the millimeter wavelength region. It is the electric analogue to magnetic resonance spectroscopy. The large number of molecules both stable and unstable which can be treated by electric resonance techniques and have transitions in the submillimeter wavelength region warrant consideration for investigation. In order to perform this type of spectroscopy, experimental requirements exist which until recently have been difficult to achieve. It is the purpose of this paper to discuss these limitations and to indicate the application of this spectroscopic tool to molecules of interest to astronomy and atmospheric investigations.

Electric Resonance Molecular Beam Techniques

The electric resonance molecular beam technique employs two inhomogeneous electric fields for deflection of the molecular beam and eventual separation of the energy states, and a homogeneous electric field region in which the interaction with an electromagnetic field occurs. This interaction results in the molecular transition, which is indicated by a beam detector. In the original millimeter wave investigation, the interaction with the electromagnetic field was performed in either a single resonator or a double resonator scheme (the Ramsey pattern technique). The latter method provides greater resolution, but, in turn, requires greater precision at the higher frequencies. The single resonator technique was, in addition, employed for extending the electric resonance technique to the submillimeter wavelength region by observing the $4_0 \rightarrow 4_2$ transition of H_2S at 369 GHz [1]. While the need for improvements in this observation were evident, the investigation did demonstrate the capability of using the technology in the submillimter wavelength region. A short-wavelength limit for molecular beam spectroscopy was not evident in this study as long as phase-locked, spectrally pure excitation sources are available. It is desirable to employ the two resonator separated-field method in the submillimeter region in order to provide resolution which cannot be obtained by any other method. However, as shorter wavelength investigations are performed, a system of narrow beams will be required for the separated-field method. This is necessary in order to confine the beam to regions of approximately equal amplitude in the two resonators. The effect of a large single beam, as used in the initial experiments (0.006 in. wide), would be to cause molecules to cut regions of different field amplitudes at higher frequencies (e.g., $\lambda/2$ = 0.010 in. at 600 GHz).

For high resolution interest, the Ramsey pattern can be compared with the use of the Lamb dip in optical spectra. The requirement for stable sources is probably the most vigorous requirement for the performance of high resolution molecular beam spectroscopy, and this has, until recently, been the major limiting factor in the performance of this type of investigation. Although phase-locking and harmonic generation methods provide stable sources to high frequencies, there is an upper limit to this technique so that submillimeter sources are required for operation well into the submillimter wavelength region. Power is not the problem, since approximately 10^{-8}W would result in saturation of the resonance in the measurements performed thus far. Stable submillimeter wave lasers have been demonstrated by phase-locking an HCN laser at 890 GHz to a radio frequency standard [2]. The availability of optically pumped lasers, although fixed in frequency, provides sources across the submillimeter band for performance of electric resonance spectroscopy. Stability and spectral purity of these sources will be required. Recent observations by Oka [3] have been performed in the 10 μm region with stable lasers.

Applications of the Technique

The electric resonance technique is particularly useful for hyperfine structure high resolution applications and in the observation of unstable molecules which will dissociate or combine with others upon collision. As a result, the submillimeter wavelength region is an ideal region for the application of these techniques.

In this respect, it is appropriate to consider application of the technology to the following cases:

1) Free radicals, of interest to radio astronomy, upper atmospheric phenomena and plume diagnostics, are often difficult to form and extremely unstable under collisions. The mass spec-

trometer in the detection system also serves the purpose of identification of the molecular species being formed. The free radical, with both electric and magnetic dipole moments, can interact with the electromagnetic field through either the electric or magnetic moment. Because of the lack of tunability of optically pumped lasers, coincidence of the molecular transitions with the laser transition is not always a likely situation but tuning the molecular transition by means of the Stark effect or Zeeman effect can solve this problem for the case of free radicals or unstable molecules. Several radicals, sufficiently light to have rotational transitions only in the submillimeter wavelength region, are appropriately treated by this technique. Among the radicals which can be investigated by the method are CH, OH, NH, HCO, NH_2, CN, HO_2, SO, BaO, and CℓO.

2) Molecules with low vapor pressures, not detectable with conventional vapor spectroscopic methods, are formed in high temperature reactions. Oxides and hydrides can be investigated by this method.

3) Of interest to the understanding of atmosphere propagation is the formation of molecular dimers of H_2O. Recent observations in an electric resonance apparatus has been made on the water dimer $(H_2O)_2$. Extension of these measurements to the submillimeter wavelength region will allow comparison with observations made in the atmosphere.

4) Resolution of electronic transition spectra and vibrational spectra is often limited by optical line overlays or spectroscopic resolution limitations. The use of double resonance spectroscopic methods involving laser excitation and submillimeter electric resonance can contribute to the analysis of metastable and excited electronic or vibrational states. The stability of the pump laser is a determining factor in this application.

5) It has recently been shown that the use of a supersonic free molecular jet, expanded into a low pressure region, will produce ultra-cooled molecules in the gas phase without condensation [4]. The method is an appropriate technique for inclusion in double resonance molecular beam experiments. It has been shown [4] that, with the cooling that can be achieved, only two rotational levels of the molecule are substantially populated so that both spectral analysis and line intensity are improved.

Conclusions

Several applications of submillimeter electric resonance spectroscopy to molecular species of interest to atmospheric studies, radio astronomy, high temperature reactions, flames and plumes have been discussed. The availability of submillimter sources and components will allow the performance of this important form of spectroscopy at higher frequencies than previously possible.

REFERENCES

1. R. E. Cupp, R. A. Kempf and J. J. Gallagher, "Hyperfine Structure in the Millimeter Spectrum of Hydrogen Sulfide: Electric Resonance Spectroscopy on Asymmetric—Top Molecules," Phys. Rev. 171, 60 (1968).

2. V. J. Corcoran, R. E. Cupp, and J. J. Gallagher, "Frequency Lock of the Hydrogen Cyanide Laser to a Molecular Frequency Standard," IEEE Journ. Quant, Elect., QE-5, 424 (1969).

3. B. M. Landsberg, T. Oka, and A. J. Merer, "Laser Electric Resonance of HCO," presented at 31st Symposium on Molecular Spectroscopy, The Ohio State University, Columbus, Ohio, June 14-18, 1976.

4. R. E. Smalley, L. Wharton, and D. H. Levy, Journ. Chem. Phys, 61, 4363 (1974).

SPECTROSCOPIC DETECTION OF METHOXY (CH_3O)

H. E. Radford
Center for Astrophysics
Harvard College Observatory and
Smithsonian Astrophysical Observatory
Cambridge, Massachusetts 02138

and

D. K. Russell
Department of Physical Chemistry
University of Cambridge
Cambridge, England CB2 1EP

Methoxy (CH_3O) is symmetric rotor free radical, a rara avis never before detected by spectroscopic means. It is a reactive trace constituent of the atmosphere and probably is also present in the interstellar gas, where radio astronomers have in recent years found large quantities of its close chemical relatives methanol (CH_3OH) and formaldehyde (H_2CO)

Because of its orbitally degenerate ground state, methoxy can exhibit several effects unusual in polyatomic molecules, in particular large fine structure, strongly anisotropic magnetism and hyperfine structure, and Jahn-Teller distortion. The submillimeter spectra presented here illustrate these effects, with the possible exception of the last, but span too narrow a wavelength range to permit more than a qualitative analysis for the present.

The spectrometer is an optically-pumped submillimeter laser, with an intracavity absorption cell that is located in a variable magnetic field. It will operate at 50 different wavelengths between 0.1 mm and 0.75 mm. The same spectrometer has been used in studies of several other molecular radicals, and a description of it may be found in reference [1]. The absorption sample was generated by mixing methanol vapor with the products of an electric discharge in a flowing helium $-CF_4$ mixture, at a total pressure of 0.35 Torr. New spectra appeared at 5 wavelengths near 0.5 mm. They were identified with CH_3O by their hyperfine structure and by chemical substitution tests.

Molecular orbital calculations [2] show that the unpaired 2e electron of CH_3O is non-bonding, and is localized on the oxygen nucleus, mainly in a 2p atomic orbital. It is thus rather far away from the perturbing potential of the methyl group, a conclusion that is also suggested by the smallness of hyperfine splittings in the observed spectra. In consequence, quenching of the orbital angular momentum of the 2e electron by the three-fold potential of the methyl group may be small, and a first-order spin-orbit interaction could split the spin-doublet levels of CH_3O by as much as ~100 cm^{-1}. The Zeeman effect of such levels will be linear to a good approximation, and characteristic of Hund's case (a) coupling of the electron spin. A preliminary analysis of the observed spectra confirms the expected linear Zeeman effect.

We acknowledge helpful discussions with J. M. Brown, R. F. Curl, and M. M. Litvak.

1. F. D. Wayne and H. E. Radford, J. Mol. Spectroscopy (to be published).

2. D. R. Yarkony, H. F. Schaefer III, and S. Rothenberg, J. Am. Chem. Soc., 96, 656 (1974).

COLLISION INDUCED FAR INFRARED ABSORPTION IN ARGON-HELIUM MIXTURES AND NITROGEN AT HIGH PRESSURE*

R. P. Lowndes and A. Rastogi
Department of Physics
Northeastern University
Boston, Massachusetts 02115

The simplest kind of collision induced far infrared absorption occurs for binary mixtures of rare gases, such as for instance, in an equimolar mixture of argon and helium. In collisions of such unlike atoms, under high pressures for instance, the respective electron clouds of the atoms are deformed and an induced dipole moment persists during the time the two atoms are sufficiently close to each other. The presence of this dipole moment leads to a strong far infrared absorption which is associated with pure translational transitions and this was first reported on by Bosomworth and Gush [1] for various inert gas mixtures.

A more complicated collision induced phenomena is that found in homonuclear diatomic gases. A free homonuclear diatomic molecule possesses no permanent dipole moment and consequently transitions in its vibrational, rotational or translational states cannot be observed. Collectively, however, for instance if put under high pressures, such molecules can acquire dipole moments induced by clusters of two or more interacting molecules and this can be utilized to probe the transitions of the characteristic molecular motions. The dipole moment induced in a collision between two homonuclear diatomic molecules, for instance of nitrogen, has a component arising from the short-range overlap forces and a component resulting from the polarization of one molecule by the quadrupole field of the other. Such a dipole moment can lead to the appearance of induced vibrational, rotational and translational transitions; in the presence of noncentral intermolecular forces the vibrational and rotational motions are inherently coupled, as are the translational and rotational motions, giving rise to vibrational-rotational and translational-rotational transitions. For nitrogen gas the induced translational-rotational transitions appear as a broad band in the far infrared and this is well separated from the induced vibrational-rotational absorption occurring in the near infrared. The collision induced translational-rotational absorption in nitrogen gas was first observed in the far infrared by Heastie and Martin [2] and later more completely by Gebbie et al. [3] and Bosomworth and Gush [1].

In all of these studies the collision induced absorption was studied at comparatively low densities below 300 amagats where the absorption was well described by that arising from binary collisions alone. The far infrared studies were not extended to measurements at higher densities because of the technical difficulty of performing far infrared spectroscopy at high pressures. The requirements of high pressure containment and far infrared spectroscopy are mutually conflicting because the former requires small apertures for maximum strength whilst the latter requires large apertures to provide maximum energy throughput from the comparatively weak far infrared sources. These requirements are further complicated because of the scarcity of readily available window materials which satisfy the competing demands of strength and transmissivity in the far infrared. We have recently developed a high pressure far infrared cell which has largely overcome these difficulties [4,5] and in this paper we report on the use of this cell to 7 kbar to study the collision induced translational far infrared absorption in helium-argon mixtures and the collision induced translational-rotational far infrared absorption in nitrogen gas for densities as high as 800 amagats. In addition to absorption arising from binary collisions, this work reveals evidence for absorption from both ternary and quaternary collisions.

*Research supported by a grant from the Army Research Office and by a grant from the Research Corporation.

References

[1] J.R. Bosomworth and H.P. Gush, Can. J. Phys. 43, 751 (1963).
[2] R. Heastie and D.H. Martin, Can. J. Phys. 40, 122 (1962).
[3] H.A. Gebbie, N.W.B. Stone and D. Williams, Mol. Phys. 6, 215 (1963).
[4] R.P. Lowndes, Proc. 4th Int. Conf. on High Pressure (Physico-Chemical Society: Kyoto 1975), p. 805.
[5] R.P. Lowndes and A.K. Rastogi, Phys. Rev. B (in press 1976).

STARK MEASUREMENTS OF H_2S IN THE MILLIMETER/SUBMILLIMETER WAVELENGTH REGION

R. E. Cupp
National Oceanic and Atmospheric Administration
Boulder, Colorado

and

J. J. Gallagher
Engineering Experiment Station
Georgia Institute of Technology
Atlanta, Georgia

Abstract

A parallel plate Stark cell has been used for measurements on millimeter wave transitions of the hydrogen sulfide molecule. With this cell and phase matched sources, high precision values for molecular dipole moments are achieved.

Stark Effect of Hydrogen Sulfide

The dipole moment of hydrogen sulfide has been previously determined by employing rotational constants available at that time and line strengths obtained from linear interpolation between values given in tables [1]. More recently, improved rotational constants have been determined from infrared data and additional microwave lines, from which it has been possible to calculate energy levels and line strengths [2]. As a result, the dipole moment of H_2S has been remeasured with a parallel plate Stark cell and phase-locked multiplying chains.

Table I gives the rotational constants of H_2S, used by S. A. Clough [2] to calculate the energy levels and line strengths. If the Stark energy is given by

$$W_{J K_{-1} K_1} = (\alpha + \beta M^2)\ \mu^2 E^2 \times 10^{-6} \text{ MHz},$$

where μ is in debye units and E is in volts/cm, then the coefficients, α and β (in MHz/debye^2 (volts/cm)$^{-2}$), as used in this work, are given in Table II. The dipole moment determinations were made for the three rotational transitions:

$1_{01} \rightarrow 1_{10}$	168,762.762 MHz
$2_{11} \rightarrow 2_{20}$	216,710.436 MHz
$3_{21} \rightarrow 3_{30}$	300,505.519 MHz

The parallel plate Stark cell was arranged so that $\Delta M = 0$ and $\Delta M = \pm 1$ transitions could be observed, and both types of transitions were observed for the $1_{01} \rightarrow 1_{10}$ rotational transition. A total of twenty-eight measurements has been made for the determination of the H_2S dipole moment. Table III gives the moment values for the individual transitions and the value obtained from the averaging of all values. The average dipole moment of H_2S is given as 0.9766 ± 0.0003 debye. No systematic variation of the dipole moment is evident for different transitions as in the case of H_2O. As a result, higher order Stark effect terms have not been necessary for the present determination. For the transitions, $2_{11} \rightarrow 2_{20}$ and $3_{21} \rightarrow 3_{30}$, $\Delta M = \pm 1$ components were observed but were not sufficiently consistent to include in the dipole moment determination. From thirteen measurements of the $2_{11} \rightarrow 2_{20}$, $\Delta M = \pm 1$ transitions, the average dipole moment is $\mu = 0.9769 \pm 0.0013$ debye. In the case of the $2_{11} \rightarrow 2_{20}$, $\Delta M = \pm 1$ transitions, a slight voltage variation of the dipole moment was evident, but improvement in these measurements is necessary before such an effect can be theoretically included.

In the previous determination, the error in this measurement ($\mu(H_2S) = 0.974(5)$) was underestimated by approximately a factor of two. The effects of the superposition of dc and ac (modulating) Stark voltages which may result in a difference between the applied and the effective Stark voltage was overlooked. In the measurements upon which the present calculations are based, account was taken of the modulation field by averaging the sine wave modulation with the dc Stark voltage. The effective Stark field was given by $E_{eff} = E_o\ (1 + 1/2\ (E_{ac}/E_o)^2)$ where E_{ac} is the amplitude of the modulation field and E_o is the applied dc field.

The parallel plate cell was constructed with optically polished quartz spacers, which were measured to be 0.5004 ± 0.0001 cm. The dc supply, which was used, was calibrated to be accurate within $\pm$ 3 parts in 10^5. The sources employed for these measurements were phase-locked to a frequency standard so that stabilities and accuracies on the order of at least 1 part in 10^8 were available. The major sources of error in this system are the quartz spacers, which were only checked to $\pm$ 0.0001 cm even though they were optically lapped to a greater accuracy, and the experimental accuracy of determining the center frequency of each Stark component. Only resolved components were employed, although no account was taken of line overlap [3].

The difference in the results obtained from our measurements and previous work is approximately 0.002 debye units. This difference is not entirely attributable to the neglect of the superposition effect of the dc and ac voltages as this effect in our case would result only in an average shift of approximately 0.0005 debye from our measured value. The difference results apparently from the difference in α and β which exists for the two works.

The calculations have been performed with the second order Stark effect. At the low voltages employed, higher order effects and molecular polarizability effects were not observable. The lack of centrifugal distortion for the stated accuracy has been questioned, but it has not been evident that these effects are observed in contrast to the work on H_2O.

The observations on $\Delta M = \pm 1$ components of the $2_{11} \rightarrow 2_{20}$ and $3_{21} \rightarrow 3_{30}$ transitions produced a wide spread in the dipole moment determined from these transitions. This can probably be traced to the loss in intensity and alignment at higher frequencies when the polarization of the millimeter wave signal is rotated perpendicular to the Stark plates.

TABLE I

Rotational Constants of H_2S (MHz)

($\kappa = -0.522676$)

A	310,590.997
B	270,312.998
C	141,825.000
D_J	14.859
D_{JK}	-4.066
D_K	8.597
δ_J	8.708
R_5	8.657
R_6	-2.000

TABLE II

Stark Coefficients for H_2S

($MHz/debye^2(volts/cm)^2$)

State	α	β
1_{01}	-0.06889	-0.35829
1_{10}	-0.04726	0.38733
2_{11}	-0.026696	-0.055367
2_{20}	-0.009108	0.082215
3_{30}	-0.001747	0.023055
3_{21}	-0.013099	-0.003561

TABLE III

Dipole Moment of H_2S

$J'_{K_{-1}, K, M'} \rightarrow J_{K_{-1}, K, M}$	μ (debye units)
$1_{01}, \pm 1 \rightarrow 1_{10}, \pm 1$	0.9766 ±0.0004
$1_{01}, 0 \rightarrow 1_{10}, \pm 1$	0.9764 ±0.0002
$1_{01}, \pm 1 \rightarrow 1_{10}, 0$	0.9765 ±0.0002
$2_{11}, \pm 1 \rightarrow 2_{20}, \pm 1$	0.9797 ±0.0001
$2_{11}, \pm 2 \rightarrow 2_{20}, \pm 2$	0.9769 ±0.0003
$3_{21}, \pm 3 \rightarrow 3_{30}, \pm 3$	0.9768 ±0.0004
$3_{21}, \pm 2 \rightarrow 3_{30}, \pm 2$	0.9764 ±0.0005
Average:	0.9766 ±0.0003

This work was supported in part by the Air Force Cambridge Research Laboratories.

References

1. R. H. Schwendeman and V. W. Laurie, "Tables of Line Strengths," Pergamon Press, New York, N. Y. (1958)

2. S. A. Clough (private communication)

3. Y. Beers and G. P. Klein, Journal Research (NBS) - A. Physics and Chemistry 76A, #5,521 (1972)

PLASMA DENSITY MEASUREMENTS BY USING A MODULATED SUBMILLIMETER LASER INTERFEROMETER SYSTEM*

S.M. Wolfe†, K.J. Button, J. Waldman‡ and D.R. Cohn

Francis Bitter National Magnet Laboratory‡
Massachusetts Institute of Technology
Cambridge, Massachusetts 02139

*Supported by ERDA.
†Also Physics Department, M.I.T.
‡University of Lowell.
‡Supported by the National Science Foundation

INTRODUCTION

We have measured the electron-density, n_e, of the plasma confined by the magnetic field in a tokamak (in particular, the M.I.T. Alcator) by using a submillimeter interferometer. The interferometer, shown in Fig. 1, contains twin optically pumped waveguide lasers. The twin lasers operate at a wavelength of 118.8 micrometers (CH_3OH) but are detuned with respect to each other by approximately one MHz for modulation purposes. This wavelength is appropriate for measurement of electron densities $\geq 10^{14}$ cm^{-3}.

INTERFEROMETER

Electron density can be measured by observing the phase shift, ϕ, of electromagnetic radiation which passes through the plasma; this phase shift is proportional to the integral of the electron density along the optical path. The frequency of the radiation must be considerably larger than the plasma frequency ω_{pe} if reflection and refraction effects are to be avoided, that is, $\omega > \omega_{pe} = (n_e e^2/\epsilon_0 m)^{1/2}$, where e and m are the electronic charge and mass. While millimeter waves were appropriate for this purpose in the lower densities ($n_e \leq 10^{14}$ cm^{-3}) formerly achieved in tokamak devices, the higher frequencies of submillimeter wave radiation are now required. We have chosen the 118.8 μm line of methyl alcohol to operate on the Alcator device, which achieves plasma densities in the range 10^{14} cm$^{-3} < n_e < 1 \times 10^{15}$ cm^{-3}; at this wavelength, a phase shift $\phi = 2\pi$ (one fringe) corresponds to an average density of 1×10^{14} cm^{-3} over a parabolic density profile of 9 cm radius.

PHASE MODULATED INTERFEROMETRY

A simple interferometer, such as the common Michelson and Mach-Zender configurations, is limited in resolution by amplitude fluctuations. Furthermore, since the output $I \propto (1 - \cos\phi)$, the resolution $dI/d\phi \propto \sin\phi$ is a function of the value of the fringe shift and for $\phi = m\pi$ the resolution is zero. The situation may be improved considerably by introducing a time dependent phase modulation into one arm of the interferometer, such that the output is of the form $I \propto \cos(\Delta\omega t + \phi)$, where $\Delta\omega$ is the modulation frequency, which can be compared to a reference signal proportional to $\cos(\Delta\omega t)$. The phase shift is then obtained directly from the time lag between the two signals, since $\phi = \Delta\omega\Delta t$ where Δt is the time lag between the two. The technique is insensitive to amplitude variation and gives a resolution which is independent of phase.

The modulation scheme used in the present system is shown in Fig. 1. Two CW optically pumped CH_3OH lasers are located on a single granite base and pumped by a single CO_2 laser. The cavities are tuned such that the two oscillate at frequencies differing by Δf of the order of 1 MHz. A reference signal $\underline{x}$ at the difference frequency is then generated by mixing a portion of the two beams in a detector D1; similarly a phase shifted signal $\underline{y}$ is obtained in the second detector D2, where one of the beams has passed through the plasma before entering the detector. The phase lag between the two signals, $\underline{x}$ and $\underline{y}$, is then obtained electronically.

The time resolution of the system is in principle given by the period of the beat signal or by the bandwidth of any filters used in the detection system. Here the value of 1 MHz was chosen to be fast enough to follow the evolution of the density during fast instabilities and also to resolve density fluctuations due to MHD phenomena, while remaining low enough to permit convenient analysis and to be small compared to the approximate 10 MHz gain bandwidth of the laser oscillator.

The CH_3OH waveguide lasers [1] provide 2 mW each at 118.8 μm with beam divergence $\leq$ 20 mrad and frequency stability of $\sim$25 kHz. Cavity tuning is accomplished manually by means of a differential screw type translation stage. The low beam divergence is permitted by use of a capacitive grid [2,3] as an output coupler. This device is fabricated by depositing a 2500 Å thick aluminum coating through a metal mesh structure onto a z-cut crystal quartz substrate. For a grid constant of 76 μm and square separation of 20.8 μm, the coupler is 80% reflecting to the 118.8 μm radiation and effectively traps the 9.69 μm pump radiation inside the cavity.

The Ga-doped Ge photoconductive detectors provided by K. Shivanandan [4] have an NEP of 10^{-12} W/Hz$^{1/2}$ which is considerably lower than required in the present application. Signal-to-noise ratios are observed in excess of 10^2 at the one MHz modulation frequency even in the absence of careful filtering and baffling of the incident beam.

The plasma density is obtained from a simple phase comparator circuit consisting essentially of a single flip-flop. The zero-crossing transition of the reference detector, $\underline{x}$, sets the output high, while the next transition of the signal detector, $\underline{y}$, resets the state to zero. The output of the flip-flop is therefore a pulse train with the same period τ as the modulation frequency and pulse width equal to the time delay, Δt, between zero crossings of the two signals. This pulse

train is then integrated on a low pass filter; the resulting signal is then proportional to the ratio $\Delta t/\tau = \phi/2\pi$ which is the fractional phase shift due to the plasma. With this circuit the output voltage rises to its maximum value as ϕ increases to 2π and then resets to zero as ϕ passes through each fringe. The result is shown in the display in Fig. 2. Here the density rises rapidly in the first 2 msec, then begins to fall; at about 10 msec, gas is pulsed into the chamber and the density again rises, reaching a value of $\sim 2.9 \times 10^{14}$ cm^{-3} at 80 msec into the discharge. The density then falls rapidly as the current decays during the final 25 msec of the discharge.

The system we have described has been designed as a single path interferometer to measure the integrated column density in the present Alcator device. In machines with larger size and greater diagnostic access it will be desirable to employ a multi-path system capable of determining, with Abel inversion techniques, the evolution of the density profile in time. For such measurements higher powers than those employed here will be required, and construction of a system which should provide at least an order of magnitude increase in power levels is now in progress.

References

1. S.M. Wolfe, K.J. Button, J. Waldman and D.R. Cohn, Appl. Optics Vol. 15, no. 11, November, 1976.

2. S.M. Wolfe, to be published.

3. R. Ulrich, Infrared Phys. 7, 37 (1967).

4. K. Shivanandan, D.P. McNutt, M. Daehler, and P.D. Feldman, "Far Infrared Photometer System for Airborne Infrared Astronomy", Naval Research Lab Report 7879.

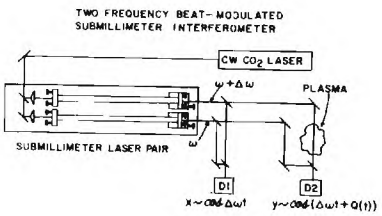

Figure 1. Dual Beam Modulated Interferometer System. Two optically pumped lasers are operated at frequencies differing by $\Delta\omega$. Mixing the two outputs in detector D 1 provides a modulated signal $x \sim \cos(\Delta\omega t)$, while detector D 2 sees a similar signal $y \sim \cos(\Delta\omega t + \phi)$ with an additional phase shift due to the plasma. The magnitude of this phase shift is then obtained directly from comparison of the two signals.

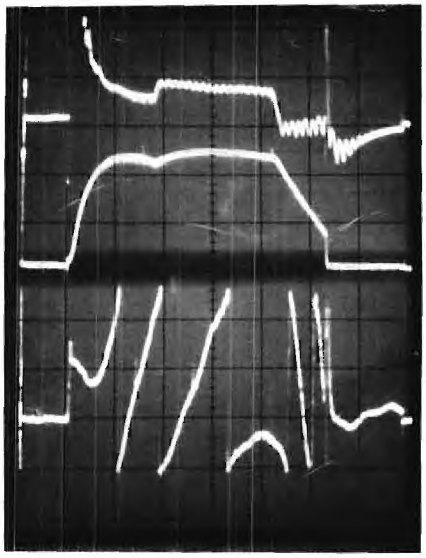

Figure 2. Interferometer Operation. Top trace shows loop voltage, V = 4V/div. Middle: plasma current I = 55 kA/div. Lower trace: interferometer output, $\bar{n}_e \approx 2.5 \times 10^{13}$ cm^{-3}/div., time: 20 msec/div.

HCN INTERFEROMETER FOR ELECTRON DENSITY MEASUREMENT OF A TOKAMAK PLASMA

D. Véron, J. Certain, J.P. Crenn.

ASSOCIATION EURATOM-CEA SUR LA FUSION
Département de Physique du Plasma et de la Fusion Contrôlée
Centre d'Etudes Nucléaires
Boîte Postale n° 6, 92260 FONTENAY-AUX-ROSES (FRANCE)

Principle of the apparatus

The principle of the interferometer built for the Tokamak in operation at Fontenay-aux-Roses (T.F.R.) is as follows : the frequency of the reference beam of the interferometer is slightly Doppler shifted with the aid of a cylindrical grating which rotates at a constant speed. This beam is then recombined with the probing beam. The resulting beat signal is monitored by a square law (pyroelectric) detector. The phase shift φ experienced by the probing beam upon traversing the plasma is thus transferred to this low frequency signal. The value of φ is then deduced from the time interval Δt elapsing between the zero crossings of this signal and the corresponding zero crossings of a reference signal which have the same frequency but with a fixed phase. The time Δt is measured by an electronic clock whose frequency exceeds that of the beat signal by three orders of magnitude.

Description

To avoid any feedback to the laser source, and subsequent signal cross-talk between channels, a Mach-Zehnder type arrangement seemed preferable to the Michelson type [2]. The whole assembly is attached to a frame independent from the machine to minimize mechanical vibrations of the set up.

The eight channels are feeded by a single HCN waveguide laser [3] with a 3 meter long discharge and having a maximum output power of 150 mw. The eight channels are divided in two sets of four channels placed in two separate ports. All the informations given in this paper are related to one set of four channels, unless otherwise specified.

A single matching concave mirror is used to transform the divergent beam extracted from the laser into a convergent beam, which is then divided into four probing beams. The path length between the focussing mirror and the median plan of the plasma is made equal for each channel so as to place the beam waists of the four probing beams in the median plan of the plasma. The reference signal is obtained from a fifth channel which is not crossing the plasma. The size of the optical components has been calculated from the gaussian beam theory [4] which has been proved to be applicable to HCN laser beams [3,5]. Reflecting and focussing elements are made of aluminized glass mirrors, which have a loss coefficient of the order of .01.Windows and most of the beam splitters are made of crystal quartz, whose measured loss coefficient is .04 ± .01. The beam splitters used to recombine the probing and the reference beams are tungsten wire grids.

Performances and results

The time resolution of the interferometer, set by the frequency of the beat signal, is typically 100 µs. It can easily be changed by varying the rotational speed of the grating. The value of the phase shift is stored in a ferrite memory for every period of the beat signal, and displayed on an oscilloscope screen (Fig.1, right). An on line computer gives the line density variation, versus time, for each channel, as a continuous curve (Fig.1, left).

The sensitivity of the actual apparatus, defined as the standard deviation of the measured value of a constant phase shift, is better than 10^{-2} fringe. This means that line density variations as small as 5.10^{12} cm^{-2} can be measured (one fringe corresponds to a line density of $6.62\ 10^{14}$ cm^{-2}).

This unique device has been used reliably on TFR for nearly one year to determine electron density profiles.

References

|1| P.BLANC, D.VERON, Proc. Int. Conf. on Fusion Technology, Grenoble 1972.

|2| D.VERON, Opt. Commun. 10, 95 (1974)

|3| P.BELLAND, D.VERON, L.B.WHITBOURN, J. Phys. D. 8, 2113 (1975)

|4| H.KOGELNIK, Bell Syst. Tech. J.44, 455 (1965).

|5| J.P.LESIEUR, M.C.SEXTON, D.VERON, J. Phys. D. 5, 1212 (1972).

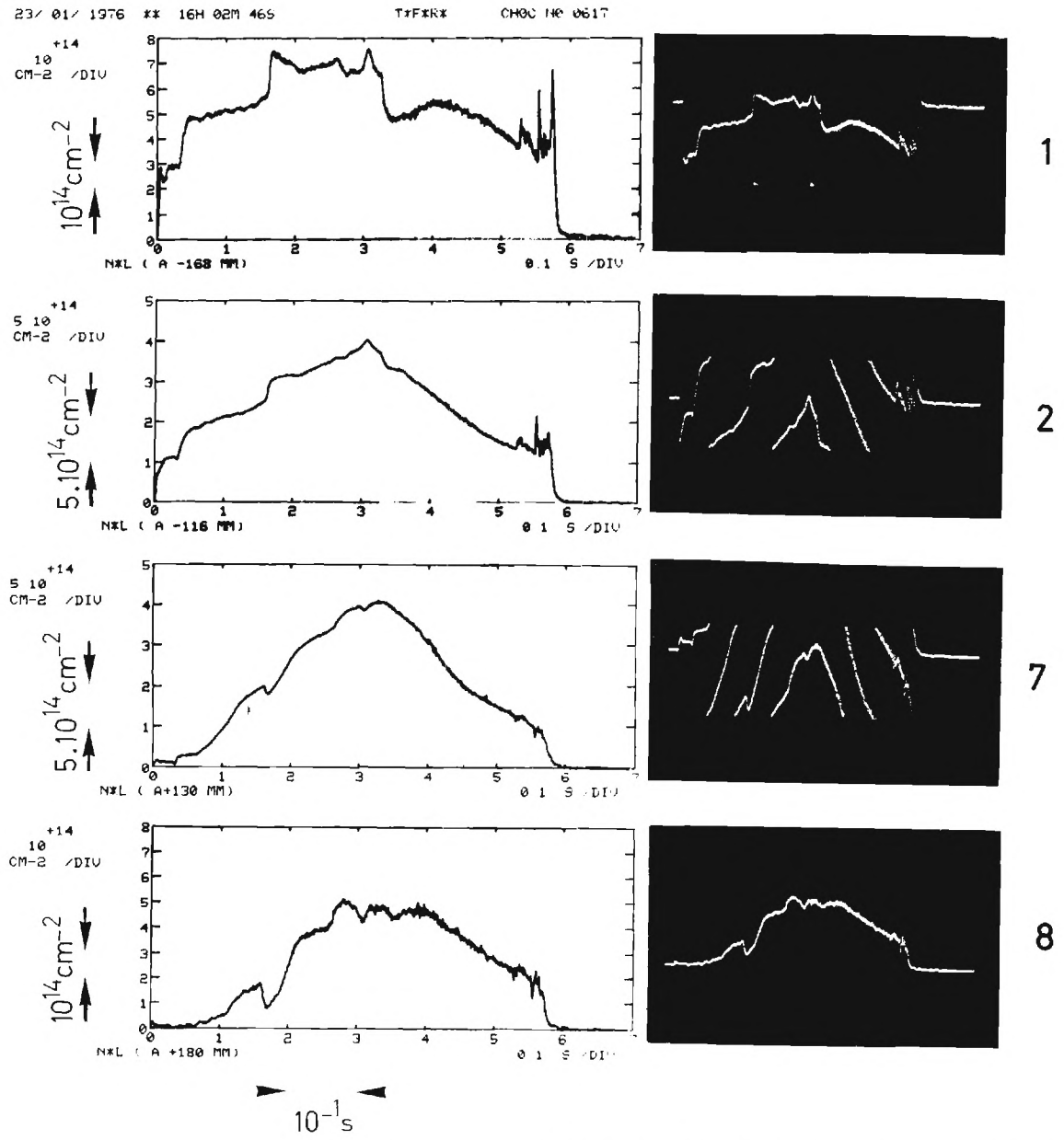

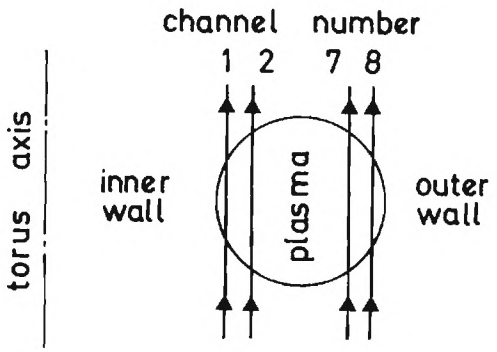

Figure 1. Typical display of the line density variation on channels 1, 2, 7 and 8 (from top to bottom, before (right) and after processing by the on-line computer (left). Channels 1 and 2 are probing the inner part of the plasma column, while channels 7 and 8 are probing the outer part of it (see drawing at lower left). The fast increase of the line density on channels 1 and 2, which occurs about .17s after the starting point, is accompanied by a decrease of the line density on channels 7 and 8. This clearly indicates that the plasma column moves, at that time, towards the inner wall of the vacuum chamber.

EVAPOROGRAPHIC AND PYROELECTRIC IMAGE RECORDING FOR TWO-DIMENSIONAL PLASMA INTERFEROMETRY IN THE FAR INFRARED

G.Dodel and W.Kunz

Institut für Plasmaforschung der Universität Stuttgart, Pfaffenwaldring 31, D7 Stuttgart 80, Germany,F.R.

1. Introduction

Plasma interferometry in the submillimeter far infrared (FIR) spectral range ($50\,\mu m \lesssim \lambda \lesssim 1mm$) is becoming a well established method for electron density(n_e) measurement in the regime $10^{13}cm^{-3} \lesssim n_e \lesssim 10^{16}cm^{-3}$ [1-4]. With all the interferometers cited the phase shift is measured as an average over the cross section of the radiation beam. To obtain phase information in a direction perpendicular to the beam, the plasma either has to be scanned with one beam or probed with several beams[5], analogous to multichannel microwave interferometry.

A different way to obtain this information could be the recording of two-dimensional interferograms, analogous to optical interferometry. In the FIR the feasability of two-dimensional interferometry first of all depends on the availability of two-dimensional detection schemes sufficiently sensitive to compensate for the relatively modest FIR laser powers. We report here some experiments and considerations concerning the recording of two-dimensional FIR interferograms by means of evaporography and pyroelectric imaging.

2. General Considerations

We characterize the sensitivity of the two-dimensional thermal detector (no quantum detector arrays or line scan cameras are available for the FIR until now) by the minimum radiation energy per unit area q_{min} that must fall on it to form an image. The sensitivity required to record an interferogram depends on the laser power P, the exposure time τ, the area G^2 of the object under investigation, the scale M at which the object is imaged on the detector and on the fractional loss L in the interferometer via the relation

$$q_{min} \leq \frac{P\,\tau\,(1-L)}{G^2\,M^2} \qquad (1)$$

In a stationary experiment with a cw laser source being used, τ is limited by the specific thermal properties of the detector (e.g. by the characteristic time for the lateral thermal spread within the detector which causes the image to be smeared out). Therefore, in the stationary case the quantity τ_{max}/q_{min} may be considered as a figure of merit for the detector, τ_{max} denoting the maximum tolerable exposure time. In a pulsed experiment τ is given by the pulse length of the laser source which, in general is much less than any thermal time constant of the detector. The quantity $1/q_{min}$ has therefore to be considered as figure of merit in the pulsed case.

Note that, since τ_{max} is determined by thermal effects, it also depends on the highest spatial frequency occurring in the image, i.e. on the fringe distance if the image is an interferogram. As a consequence, image reduction, i.e. making M small, in general only reduces the requirements for the sensitivityof the detector in a pulsed experiment. In the stationary case, a smaller M also reduces τ_{max},because higher spatial frequencies are then present in the image. (For example, one can show that the advantage of small M is just compensated by the reduction of τ_{max} if it is lateral heat conduction that smears out the image.)

In the FIR, in any case, image reduction to a size substantially smaller than the detector is not desirable because of diffraction. The diffraction limited local resolution R for coherent illumination is [6]

$$R = \frac{G}{Y} = \frac{1}{1.54}\cdot\frac{G}{\lambda}\cdot\frac{1}{F}\cdot\frac{M}{M+1}$$

(Y-minimum resolvable distance in the image; λ - wavelength; F -"F number" of the optical element used for imaging) If we denote the linear dimension of the detector by D, the maximum resolution achievable is (putting M=D/G)

$$R_{max} = \frac{1}{1.54}\cdot\frac{1}{\lambda}\cdot\frac{1}{F}\cdot\frac{D}{D/G+1} \leq \frac{1}{1.54}\cdot\frac{1}{F}\cdot\frac{D}{\lambda}$$

In the following table the upper limit of resolution (which is achieved if $G \gg D$) is listed for several FIR wavelengths and the two detector sizes of interest (D=16mm,dia. of the pyroelectric tube and D=80 mm, dia. of evaporographic membrane). F=5 is assumed.

laser	wavelength (μm)	upper limit of resolution	
		pyroel.tube	evaporograph
CH_2F	496	4	20
HCN	337	6	30
D_2O	94	22	110
D_2O	66	31	155

It is evident from these numbers that no further loss in spatial resolution due to image reduction is tolerable. Two-dimensional interferometry makes sense only if $R_{max} \gg 1$. In terms of a wavelength requirement this condition may be written

$R_{max} \gg 1$, $F = 5$ $\Rightarrow$ pyroel.cam.: $\lambda \ll 2mm$; evaporograph: $\lambda \ll 10mm$

3. Evaporography

The evaporograph we used has been described in detail in Ref.[7]. Its principal may be briefly summarized as follows: a thin film of oil is made to condense on an extremely thin (several $0.1\,\mu m$) nitrocellulose membrane which is coated with an absorbing metal oxide layer and stretched in an evacuated chamber. Radiation of an infrared image absorbed in the coated membrane causes the oil film to evaporate at different rates. Illumination with white light makes the intensity distribution of the infrared image visually observable as a distribution of different interference colours.

As an example Fig.1 shows the evaporographic record of a $337\,\mu m$ interferogram of a 10 A carbon arc. The fringe distance is 3mm, the FIR exposure time 5 sec, a 10 mW cw HCN laser being used. Fig.2 shows an interferogram of the same arc, the Mach-Zehnder interferometer being adjusted to "infinite" fringe distance .

The minimum energy necessary per unit area to

form an image was determined to be 0.4 mJoule/cm^2 for our evaporograph. The maximum tolerable exposure time for a fringe distance of 3 mm was in the range of several 10s of seconds. It is difficult to give a precise number for τ_{max} and an idea of its dependance on the fringe distance, because image formation in an evaporograph is a very complex dynamic process. A systematic experimental investigation of this question remains to be done. A theory of the evaporograph which takes the dynamics of the process into account -to our knowledge- does not exist.

4. The Pyroelectric Camera

For about two years pyroelectric cameras [8,9] have been commercially available. The essential element is a TV vidicon tube, the sensitive layer of which consists of a thin ($\approx$ 20/um) pyroelectric target 16mm in diameter. An infrared image is transformed on the target by absorption to a temperature"image" and the latter, via the pyroelectric effect, appears as a surface charge"image". The charge image is scanned by an electron beam and the signal processed as in normal TV technique.

We used a Heimann pyroelectric camera to check its applicability to two-dimensional FIR interferometry. The q_{min} value we measured at 337/um is 0.01 mJoule/cm^2. An even better value of q_{min}=0.6/uJoule/cm^2 was measured with a CO_2 laser (λ=10.6/um). We ascribe this to better target absorption and lower window losses, the Ge window of the standard tube being bloomed for optimum transmission in the 10/um region.

The low q_{min} values of the pyroelectric camera make it especially suited for p u l s e d FIR interferometry. From Eq.(1) -putting M=D/G- it can be seen that FIR laser pulses of several millijoules will be sufficient. Optically pumped superradiant FIR lasers achieve such pulse energies already at moderate energies (1 to 10 Joule) of the CO_2 laser pump.

Figs. 3 and 4 show two interferograms which were recorded behind Fresnel biprisms of TPX using a 94/um optically pumped D_2O laser. The FIR exposure time corresponds to the 70 nsec pulse length of the laser. Note that the interferograms do not appear uniformly illuminated. There is some evidencethat this is not due to nonuniform intensity distribution of the laser beam but to internal interferences occurring within the pyroelectric tube. This phenomenon which would be a serious drawback for the FIR application of standard pyroelectric tubes is being investigated at present.

When a stationary interferogram was produced on the tube, the maximum exposure time tolerable was about 0.2 sec for a fringe distance of 3 mm. This relatively low value possibly could be improved for special stationary applications by image storing techniques or by scanning the pyroelectric target not at normal TV rate but only once after a certain time of thermal integration.

5. Conclusion

Evaporography has been shown to be well suited for two-dimensional FIR interferometry of stationary plasmas with moderate power cw FIR lasers. Because of the large tolerable exposure time it can -in stationary applications- even compete with pyroelectric recording.

The pyroelectric camera appears especially suited for pulsed two-dimensional FIR interferometry. Slight modifications of the standard tube (e.g. to avoid internal reflections) may be necessary, however. Because of the small tube diameter a satisfactory spatial resolution can be achieved with readily available optics only at wavelengths below, say, 200/um.

References:

1. Chamberlain J. et al., J. Plasma Phys. 16(1969)75
2. Petrov G.D. et al., High Temperature 10(1972)154
3. Heckenberg N.R. et al., J. Appl. Phys. 44(1973)4522
4. Véron D., Opt. Comm. 10(1974)95
5. Véron D. et al., Report EUR-CEA-FC-799(1975) Fontenay-aux-Roses
6. Born and Wolf, Principles of Optics, p.424 Pergamon Press, Oxford
7. Dodel G. et al., Infrared Physics 16(1976)237
8. Holeman B.R. et al., J. Phys. D 4(1971)1898
9. Felix P. et al., Optics and Laser Techn. 8(1976)75

Fig.1

Fig.2

Evaporographic record of 337/um interferograms of a 10 A carbon arc (Fig.1: fringe distance 3mm; Fig.2: "infinite" fringe distance) Exposure time 5 sec.

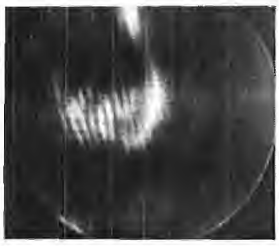

Fig.3

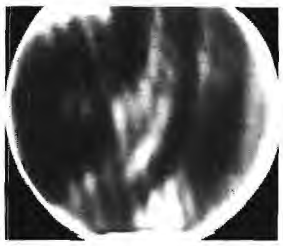

Fig.4

Pyroelectric recordings of 94/um interferograms behind TPX biprisms. Exposure time 70 nsec. The diameter of the picture corresponds to the 16mm tube diameter.

CO_2 LASER SCATTERING FROM TURBULENCE IN TOKAMAKS

R. E. Slusher and C. M. Surko
Bell Laboratories
Murray Hill, New Jersey 07974

We report a study of electron density fluctuations in the Adiabatic Toroidal Compressor (ATC) Tokamak using heterodyne detection to study the small angle scattering of CO_2 laser radiation. The scattering apparatus described below allows us to study fluctuations with wavelengths from 1 to 10^{-3}cm, frequencies from 10kHz to 1GHz and fluctuation amplitudes $\tilde{n}/n$ as low as 10^{-5} (where $\tilde{n}$ is the total fluctuation amplitude and n is the electron density)[1]. We observed scattering due to density fluctuations at frequencies $\omega/2\pi$ below 2MHz and wavelengths λ from 0.3 to 1cm These fluctuations are predicted to be driven in contained plasmas by density and temperature gradients The observed turbulence may play an important role in electron transport phenomena in prototype fusion reactors similar to the ATC.

A schematic diagram of the scattering apparatus is shown in Fig. 1. A 200W cw CO_2 laser beam, I, is directed through the plasma

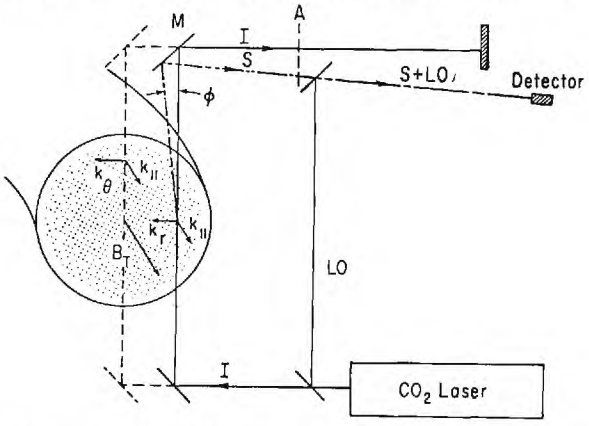

Figure 1. CO_2 laser and scattered beam paths are shown through the toroidal plasma (dotted region).

in a direction perpendicular to the major plane of the torus. Scattered radiation, S, oriented at a small angle φ with respect to I is directed with mirrors to the Ge:Cu:Sb detector where a photocurrent is produced which is proportional to the square of the sum of the electric fields of S and a local oscillator beam LO. The scattering angle φ is related to the CO_2 laser wavelength λ_I of 1 06 × 10^{-3}cm by the Bragg condition that φ is approximately λ_I/λ. The mirror M can be moved to study the components of the fluctuation wavevectors $\vec{k}$ perpendicular (k_θ and k_r) and parallel ($k_{||}$) to the torodial magnetic field B_T. Using a 10m beam path from the plasma to the detector we are able to obtain a k resolution of 5.5cm^{-1}(HWHM).

The ATC plasma had a center density of 2.2 × $10^{13}cm^{-3}$, an average density n in the region of turbulence of 1 × $10^{13}cm^{-3}$, an electron temperature of 800eV, a plasma current of 70kA, a B_T of 16kG and an effective charge of 5. The filling gas was H_2.

The frequency spectra of the observed fluctuations are shown in Fig. 2.

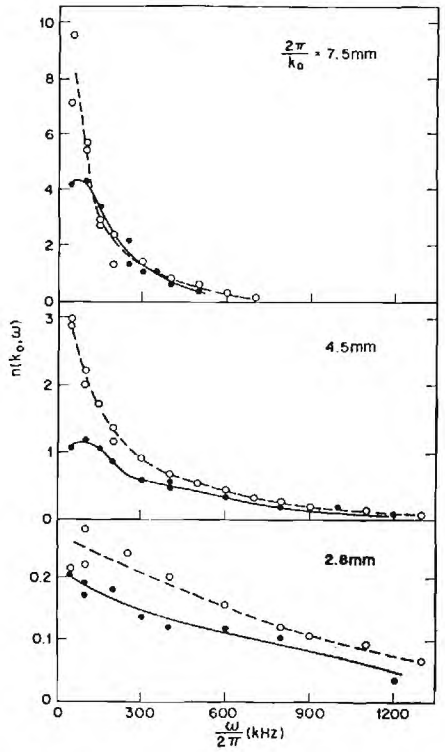

Figure 2. The frequency spectrum of the fluctuations at fixed wavevector is shown. The solid and dashed curves are guides to the eye.

The observed scattering was nearly constant throughout the 45msec ATC discharge and the points in Fig. 2 are averaged between 25 and 35msec from the beginning of the discharge. The solid circles were taken with the beam I through the center of the discharge and thus correspond primarily to poloidally directed fluctuations with wavevectors k_θ. The open circles were taken with I at the outer edge of the plasma and correspond to radially directed fluctuations with wavevector k_r. No scattering was observed in the $k_{||}$ direction. Integrating the spectra in Fig. 2 over frequency and wavevector we obtain a total fluctuation level $\tilde{n}/n$ of 3 × 10^{-2}.

The data shown above indicate that the turbulence is nearly isotropic in a plane perpendicular to B_T. A given wavevector fluctuation is found to be associated with a broad range of frequencies which could be explained by large growth or damping coefficients for the turbulent waves.

The thermal ion feature in the scattered spectrum due to collective scattering from the electrons which shield the ions is predicted to be at a frequency of 400MHz for 1mm waves in the ATC plasma. A negative search for this feature implies the absence of any ion-acoustic wave turbulence during the ATC discharge at levels larger than ten times the thermal level. This important spectral feature can be used to determine the ion temperature and ion-impurity content of plasma. Using the apparatus described above this feature should be observable with sufficient signal to noise ratio to yield an ion temperature measurement averaged over the duration of the discharge for the high density phases of the Alcator Tokamak at MIT.

Ohmic heating in Tokamak plasmas is not sufficient to achieve ion temperatures required for fusion reactors. Several auxillary heating methods are under study at present including injection of high energy neutral beams and rf input into the plasma near the ion-cyclotron frequency and the lower hybrid frequency. An important diagnostic capability of laser scattering is the measurement of the directly driven density fluctuations in rf heating experiments near the lower hybrid frequency. For example, an 800MHz wave (near the lower hybrid frequency) was launched into the ATC at the edge of the plasma with a four-port waveguide array at incident powers up to 150kW. The driven 800MHz wave in the plasma is expected to have an associated electron density modulation $\tilde{n}/n$ of 5×10^{-3} and a radially directed wavelength of 1.5mm at the CO_2 laser interaction volume which was located 135° around the torus from the waveguide. We searched for scattering associated with wavelengths from 1mm to 1cm at positions of I throughout the outer half of the plasma and did not observe the driven wave. The estimated sensitivity was greater than the predicted level of fluctuation by a factor of five. This negative result is not understood at present.

References

1. C. M. Surko, R. E. Slusher, D. R. Moler and M. Porkolab, Phys. Rev. Letters 29, 81(1972); R. E. Slusher, C. M. Surko, D. R Moler and M. Porkolab, Phys. Rev. Letters 36, 674(1976).

CYCLOTRON RESONANT LASER INDUCED GAS BREAKDOWN AT 496 MICRONS*

M.P. Hacker†, R.J. Temkin, and B. Lax†

Francis Bitter National Magnet Laboratory‡
Massachusetts Institute of Technology
Cambridge, Massachusetts 02139

ABSTRACT

A pulsed 496 μm CH_3F laser has produced breakdown in various gases in a magnetic field at cyclotron resonance. Resonance lineshapes in helium, hydrogen and oxygen are compared and related to properties of these gases.

*Work supported by National Science Foundation, Division of Engineering
†Also Physics Department, M.I.T.
‡Supported by National Science Foundation

In a recent paper[1], the authors reported the observation of laser-induced breakdown of helium gas, using a pulsed mirrorless CH_3F laser at 496 μm, in a variable magnetic field near the electron cyclotron resonant value of 216 kG. We present here new data on submillimeter laser breakdown of hydrogen and oxygen gases; observed differences in the resonance lineshapes for these gases when compared to helium, are explained qualitatively in terms of the properties of the gases. Additional data for helium, argon, and nitrogen gases have also been obtained.

The experimental setup is depicted schematically in Fig. 1. The 496 μm laser radiation was focused to a ~4 mm diameter spot in the target gas, which was contained in a cell in the bore of a Bitter solenoid magnet. A small DC glow discharge provided the preionization necessary for avalanche breakdown[2]. Visible light emission from the gas was measured in order to assess the relative magnitude of breakdown as a function of such parameters as pressure, magnetic field, and laser intensity. More detailed descriptions of the breakdown experiment and the CH_3F laser may be found in previous papers[1,3].

The intensity of visible-light emission is plotted as a function of magnetic field in Fig. 2, for helium, hydrogen, and oxygen gases at a fixed pressure of 3 Torr. Laser pulse energy was 0.3 mJ total, in a ~60 nsec pulse length, with a peak focused intensity of about 40 kW/cm^2 at 496 μm (about 1/2 the total intensity). The main resonance at B = 216 kG corresponds to the 496 μm line, while the subsidiary peak at B = 198 kG is due to a weaker laser line at 541 μm. The data have been scaled to the same peak, on-resonance values in order to emphasize differences in resonance lineshape among the three gases. Actual peak intensities for oxygen, hydrogen, and helium were in the approximate ratio .06:.45:1 .

A conventional equilibrium theory of breakdown in the presence of a magnetic field[4] predicts an avalanche ionization rate ν_i given by

$$\nu_i \propto S \frac{\nu_c}{(\omega - \omega_c)^2 + \nu_c^2} \qquad (1)$$

where ν_c is the electron-atom collision frequency, $\omega_c = eB/mc$ is the cyclotron frequency, S the laser intensity, and ω the laser frequency. This Lorentzian form, with halfwidth ν_c, is valid for gases such as helium and hydrogen, where ν_c does not depend strongly on electron velocity; for other gases the lineshape will be altered, but the linewidth will still be of order ν_c, evaluated at the mean electron velocity.

The data presented here concern the visible light emission, rather than direct measurement of ionization rate ν_i. However, at pressures of the order of 100 Torr and greater, the dependence of light intensity on magnetic field is in fact Lorentzian, and the width is in quantitative agreement with Eq. (1). At lower pressures, however, such as for the data of Fig. 2 (p = 3 Torr), the lineshapes are not Lorentzian; the widths are very much larger than predicted by Eq. (1), and also increase with increasing laser intensity. Even so, the linewidth in Fig. 2 is largest for oxygen, smaller for hydrogen, and smallest for helium, and the peak intensities have the opposite ordering. This is in qualitative agreement with Eq. (1), which predicts larger linewidths and smaller peak values for larger collision frequencies. The collision frequencies ν_c/p are 2.4×10^9 sec^{-1} Torr^{-1} for helium, 5.9×10^9 for hydrogen, and 1.3×10^{10} (for 50 eV electrons) in oxygen[5]. On the basis of these collision frequencies, the expected resonance linewidths (HWHM) at p = 3 Torr are .4 kG, 1 kG, and 2 kG for helium, hydrogen, and oxygen respectively.

At the low pressure and high laser intensity considered here, the mean energy gained by an electron in the interval between collisions exceeds the mean thermal energy. For this case, the equilibrium theory does not apply[4]. Moreover at low pressures the fractional ionization becomes large enough that Coulomb collisions with ions must be taken into account. Both effects tend to broaden the resonance at low gas pressures and high laser intensities.

REFERENCES

1. M.P. Hacker, D.R. Cohn, and B. Lax, Appl. Phys. Lett. 29, 146 (1976).

2. M.P. Hacker, D.R. Cohn, and B. Lax, Appl. Phys. Lett. 23, 392 (1973).

3. R.J. Temkin, D.R. Cohn, Z. Drozdowicz, and F. Brown, Opt. Commun. 14, 314 (1975).

4. A.D. MacDonald, Microwave Breakdown in Gases (Wiley, New York, 1966).

5. S.C. Brown, Basic Data of Plasma Physics (Wiley, New York, 1959).

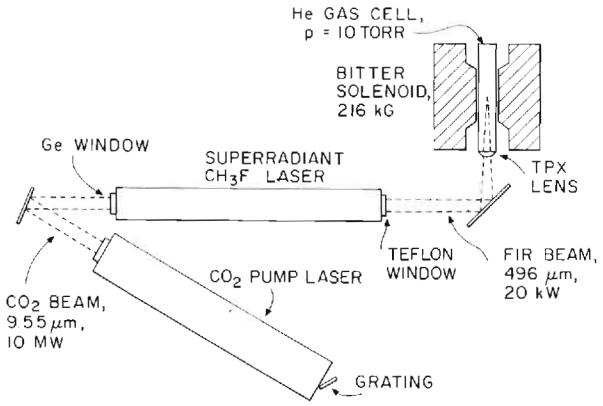

Figure 1. Experimental setup (schematic).

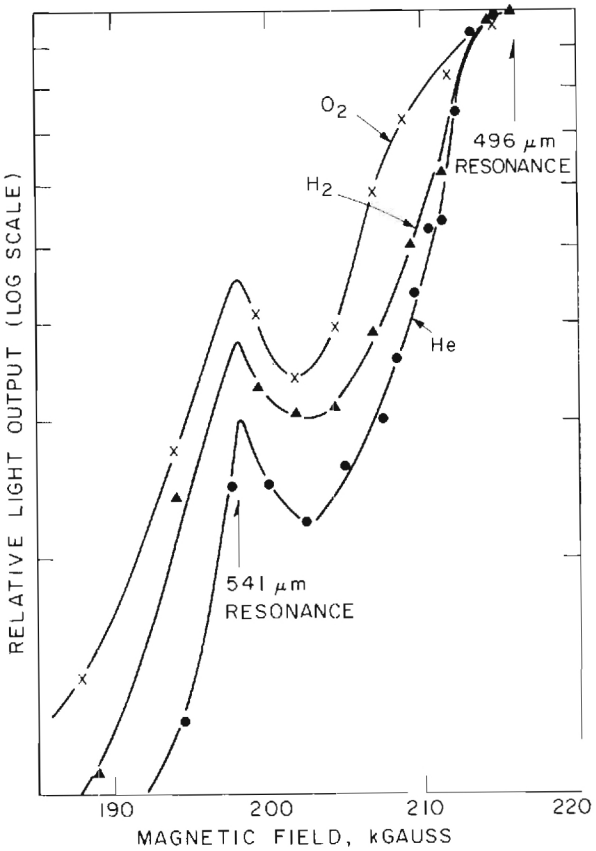

Figure 2. Visible light intensity vs. magnetic field.
X : O_2 gas
▲ : H_2 gas
● : He gas

QUARTZ BEAM SPLITTERS FOR FAR INFRA-RED (FIR) DIAGNOSTICS*

Alan M. Frank
Lawrence Livermore Laboratory
Livermore, California 94550

Abstract

Crystalline quartz resonant reflectors are an extremely useful and versatile component for use in FIR diagnostic systems. The low absorptivity and high index of refraction allow beam splitters with a wide range of reflectivities. Design, construction, and operating considerations will be discussed.

Summary

Crystalline quartz and its optical properties in the Far Infra-Red is well represented in the literature [1,2]. Its most important properties are a relatively high index of refraction and low absorption (Fig. 1). The high rigidity and low absorption allow the fabrication of microphonic free components. Acoustically stable components are essential in the severe shock environment of a pulsed magnetic fusion experiment.

The resonant reflector, as suggested by D. Veron et al. [3], uses the multiple reflections between the front and back surfaces of a parallel plate. The high index of quartz results in a substantial Fresnel reflection from the surfaces. The phase angle, between front and back surface reflections, can be varied by adjusting the thickness of a component. By tuning the phase angle, the total reflectivity of a parallel quartz plate can be adjusted from nearly zero to well over 50%.

The exact closed form solutions for a resonant reflector accounting for absorption and multiple reflections are given in Born and Wolfe [4]. There are substantial differences in the solutions for the two polarizations which become important at nonnormal angles of incidence. Only in the S-polarization, that is with the $\vec{E}$ vector normal to the plane of incidence, can a reflectivity of 50% be achieved.

Quartz is strongly birefringent. Therefore, to prevent rotation of the plane of polarization, the crystalline axis must be oriented parallel to the face of the crystal. The extraordinary ray is preferred because of its higher refractive index and lower absorption. Therefore, the $\vec{E}$ vector of the radiation must be parallel to the axis.

We have used the exact solution for a resonant reflector to examine the fabrication and operational tolerances and requirements. For example, thickness variations of ± 2 μm can cause a 5% variation of reflectivity in a beam splitter.

A resonant beam splitter is quite sensitive to angular variations. Therefore, with a small adjustment of incident angle, the resonant splitter reflectivity can be tuned over the entire range of 0 to > 50% (Fig. 2). This result is useful in a multibeam interferometric system where several splitters of differing reflectivities are necessary. This also allows the tuning of signal and reference beam intensities for maximum fringe contrast.

The greatest drawbacks of crystalline quartz are its cost and scarcity. Synthetically grown crystalline material is available in diameters to about 75 mm. Natural crystals of optical grade are generally imported from Brazil on a haphazard basis. Although occasionally crystals are available for components as large as 200 mm, it is difficult to find and quite costly. Taken in the context of an entire diagnostic system, the costs are not prohibitive.

References

1. R. B. Sosman, The Properties of Silica, American Chemical Society, New York, 1927.

2. Amer. Inst. of Physics Handbook, McGraw-Hill, New York, 1972.

3. D. Veron, J. Certain, J. P. Crenn, Association Euratom-CEA sur la Fusion, EUR-CEA-FC-799, Dec. 1975.

4. M. Born & E. Wolfe, Principles of Optics, Pergamon Press, Oxford, 1975.

* Work performed under the auspices of the U.S. Energy Research and Development Administration under Contract No. W-7405-Eng-48.

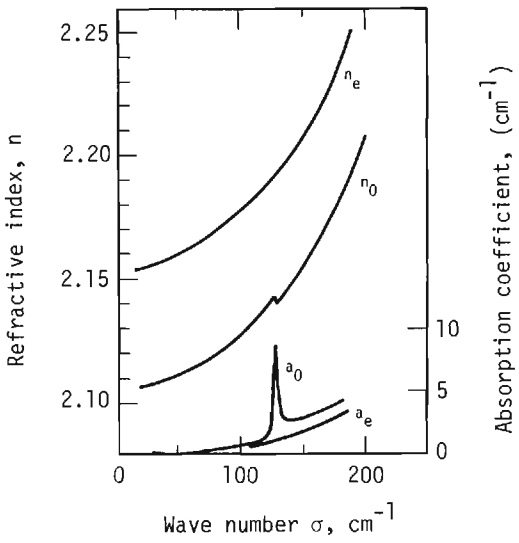

Fig. 1. Optical constants of crystal quartz from 20 to 200 cm^{-1}. [E.E. Russell and E.E. Bell, J. Opt. Soc. Am. 57, 341 (1967).]

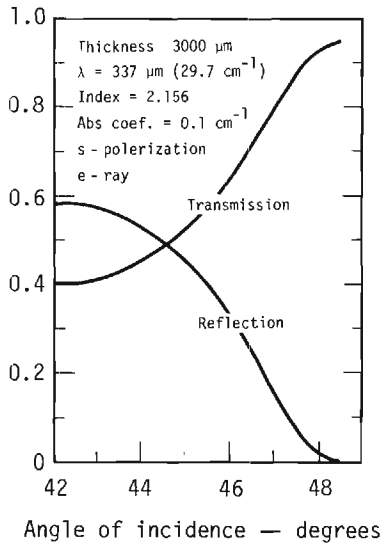

Fig. 2. Transmission and reflection vs. angle of incidence for crystal quartz beam splitter (calculated).

SURFACE POLARITON STUDIES IN THE FAR INFRARED

R. T. Holm
Naval Research Laboratory
Washington, D.C. 20375

Surface polaritons are electromagnetic modes that propagate along the interface separating two media and whose fields decay exponentially away from the interface [1,2]. Surface polaritons exist in spectral ranges in which one of the media has a negative dielectric constant while the other medium has a positive dielectric constant. The negative (positive) dielectric-constant medium is referred to as the active (inactive) medium. The "source" for a surface polariton is provided for by a surface polarization charge at the interface due to the active medium.

The nature of surface polaritons is probably most easily visualized by describing their electromagnetic fields. The fields must be solutions of Maxwell's equations throughout both media and must satisfy the field continuity requirements across the interface. For a semi-infinite active medium occupying the half space $z < 0$ contiguous with a semi-infinite inactive medium, the field components can be expressed in the form

$$E_{A,I} = E_o\left[1, 0, \mp \frac{ik}{\alpha_{A,I}}\right] e^{\pm\alpha_{A,I} z}\, e^{i(kx - \omega t)} \tag{1}$$

$$H_{A,I} = \frac{\omega}{c} E_o \left[0, \pm \frac{i\varepsilon_{A,I}}{\alpha_{A,I}}, 0\right] e^{\pm\alpha_{A,I} z} e^{i(kx - \omega t)}$$

where the subscripts A and I refer to the active and inactive media, respectively. The component of the wave vector parallel to the interface, $k_{//}$, is given by the dispersion relation

$$k_{//} \equiv k = \frac{\omega}{c}\left(\frac{\varepsilon_A \varepsilon_I}{\varepsilon_A + \varepsilon_I}\right)^{1/2} \tag{2}$$

where ε is the dielectric constant. The perpendicular component, $k_\perp$, is given by

$$(k_\perp)_{A,I} \equiv i\alpha_{A,I} = \left(\frac{\omega^2}{c^2}\varepsilon_{A,I} - k^2\right)^{1/2} \tag{3}$$

As evident from Eqs. (1), a surface polariton is a transverse magnetic wave propagating in the x-direction with its electric field elliptically polarized in the x-z plane

As mentioned before, surface polaritons exist in frequency regions where $\varepsilon_A(\omega) \leq -\varepsilon_I$. In the far infrared this condition can be satisfied by optic phonons and/or free carreirs. Under these circumstances, surface polaritons are sometimes referred to as surface optic phonons and/or surface plasmons and have been studied on a variety of materials, such as GaAs, InSb, NaCl, LiF, SiO_2, etc.

As a consequence of their exponential damping away from the interface, surface polaritons are nonradiative, and, as such, cannot be excited by light directly incident onto the active medium. As a result, one must use some coupling technique. The most common technique, referred to as attenuated total reflection, utilizes a prism whose base is separated from the sample surface by a small gap, usually air. Light (p-polarized) internally incident at the base of the prism at an angle greater than the critical angle is totally reflected, thus establishing an evanescent wave in the air gap with fields similar to those of a surface polariton. Holding the angle of incidence (frequency) fixed and varying the frequency (angle of incidence) of the incident light leads to an attenuation of the totally reflected light when the frequency and wave vector of the prism evanescent wave equal those of the surface polariton. The attenuation of the incident light corresponds to the excitation of a surface polariton.

[1]. E. Burstein, W.P. Chen, Y.J. Chen and A. Hartstein, J. Vac. Sci. Technol. 11, 1004 (1974).

[2]. A. Otto, Festkorperprobleme XIV, edited by O. Madelung and H.J. Queisser (Pergam Oxford, 1974), p. 1.

FAR INFRARED PROPERTIES OF III-V AND IV-VI SEMICONDUCTOR SYSTEMS*

P. M. Amirtharaj, B. L. Bean and S. Perkowitz
Physics Department
Emory University
Atlanta, Georgia 30322

The simple two-oscillator model, which works well for bulk semiconductors in the far infrared (FIR)[1], can also be applied to epitaxial film / substrate systems with the assumption of an abrupt interface. This picture is not wholly satisfactory. Tennant and Cape [2] had to assume that the free carriers at the interface had a smooth spatial variation to fit FIR reflection data for a PbSnTe film on a PbSnTe substrate. Here we report on and compare three systems—PbSe on NaCl, PbSnTe on PbSnTe, and InAs on GaAs—which should have different kinds of interface behavior.

FIR reflectivity data were taken with a modified Grubb-Parsons Fourier spectrometer at room temperature with a resolution of 8 cm^{-1}. Quartz and diamond window Golay cells gave good spectral coverage to 350 cm^{-1}. Transmission data were obtained with a pumped FIR laser spectrometer which provided seven methyl alcohol lines between 8.2 and 103.6 cm^{-1}. The laser data agreed with Fourier results and had much smaller errors. Both systems have been described in detail elsewhere [1,3].

The reflectivity data were fitted to expressions derived from the standard two-oscillator dielectric function with the abrupt interface assumption [2]. The computer fits gave values for the lattice and free carrier parameters for both film and substrate including the TO phonon frequency ω_T, the carrier concentration N and mobility μ, and the film thickness; and also gave values of chi square to evaluate the goodness of the fit.

The results for PbSe/NaCl are given in Fig. 1. With a semiconductor film on an ionic substrate the abrupt interface model should be suitable. In fact the fit with this model over the entire frequency range shown is nearly as good as those obtained for bulk samples. The fit parameters for PbSe agree with published or grower's values. Two values have been reported for ω_T in PbSe, 44 [4] and 39 cm^{-1} [5]. The present result of 45 cm^{-1} confirms the higher value.

Figure 2 shows the results for $Pb_{0.79}Sn_{0.21}Te/Pb_{0.79}Sn_{0.21}Te$, a more complex system. In fitting the data it was assumed that the film and substrate had the same lattice parameters but different free carrier parameters. The fit over the entire frequency range was poor in the region 110-240 cm^{-1}, where the small interference fringes are free carrier dependent. A separate good fit could be made to the high frequency region but this fit failed badly at low frequencies. Further, although the fit values of N and μ for the film agreed with the grower's estimates, the results for the substrate did not agree with known values in either of the fits. These results suggest that the kind of behavior seen by Tennant and Cape is occurring, although some features of the present fits indicate that the carrier variation at the interface is not very smooth.

The results for the third system, InAs on high resistivity GaAs, are given in Fig. 3. Features in the reflection spectrum include interference fringes at low frequencies and lattice resonances between 200 and 300 cm^{-1}. The fit is complicated by the need to include two different lattices. It was not possible to make a good overall fit, although the main features are obtained, and even limited range fits were not very good. There are indications that these difficulties are due to interface effects. First, all the fits returned values near 10^{16} cm^{-3} for the substrate carrier concentration. Such a value is unreasonable for high resistivity GaAs. If the substrate did have such a concentration the FIR transmission through the system would be too small to measure. As the figure shows, however, the transmission is as large as 12%. A tentative conclusion here is that the value of 10^{16} cm^{-3} is associated with a thin layer at the interface.

The high frequency data give further evidence for interface effects. Previous FIR work has shown that the ternary alloy $In_xGa_{1-x}As$ is a two-mode system for $x > 0.2$ where the LO and TO mode frequencies differ from those in InAs and GaAs [6]. In an In-rich alloy ω_T for the InAs-like mode would be about the same as for pure InAs, 220 cm^{-1}; but ω_T for the GaAs-like mode would be less than the pure GaAs value of 270 cm^{-1}. The values for the two high frequency peaks seen here, 220 and 256 cm^{-1}, could therefore arise from an In-rich ternary compound forming at the interface.

The measurements of Tennant and Cape and the present results suggest that FIR reflection and transmission are sensitive to interface effects in systems of basic and applied interest. Although the quantitative analysis of such effects is difficult, recent work shows that the use of recursive computer fitting schemes may provide a way to extract from optical data actual spatial profiles of interface variations [7].

Samples for this study were supplied by E. D. Palik, NRL; S. G. Parker, Texas Instruments; and H. H. Wieder, NELC.

* Work supported by ONR Contract No. N00014-76-C-0429.

References

1. S. Perkowitz, Phys. Rev. B 12, 3210 (1975); S. Perkowitz and R. H. Thorland, Phys. Rev. B 9, 545 (1974); S. Perkowitz and J. Breecher, Infrared Phys. 13, 321 (1973).

2. W. E. Tennant and J. A. Cape, Phys. Rev. B 13, 2540 (1976).

3. B. L. Bean and S. Perkowitz, Appl. Opt., Nov., 1976 (to be published). See also B. L. Bean and S. Perkowitz, this conference.

4. E. Burstein, R. Wheeler, and J. Zemel, in Proc. of the Seventh Int. Conf. on the Physics of Semiconductors, Paris, 1964 (Dunod, Paris, 1964), p. 1065.

5. H. Burkhard, R. Geick, P. Kastner, and K. H. Unkelbach, Phys. Stat. Sol. (B), 63, 89 (1974).

6. G. Lucovsky and M. F. Chen, Solid State Commun. 8, 1397 (1970).

7. N. S. Kochneva and V. M. Kochetkov, Sov. Phys. Semicond. 9, 1200 (1976).

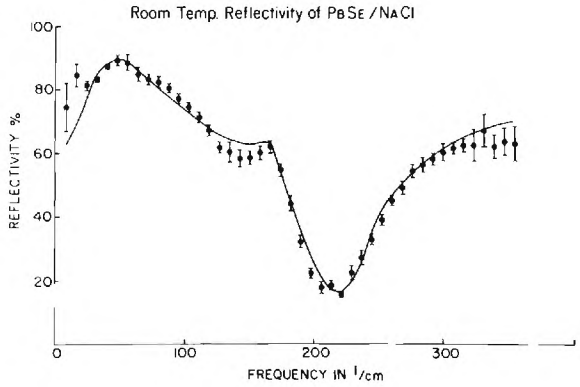

Figure 1. FIR reflectivity of a 2μm thick epitaxial layer of PbSe on an NaCl substrate. Data points are shown with associated errors. The solid curve represents the best fit using the two oscillator abrupt interface model.

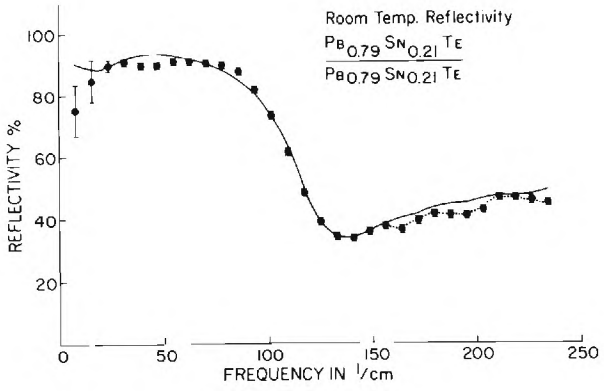

Figure 2. FIR reflectivity of a 21μm thick epitaxial layer of $Pb_{0.79}Sn_{0.21}Te$ on a $Pb_{0.79}Sn_{0.21}$ Te substrate. The solid curve is the best fit over the entire frequency range. The dotted curve is the fit to the region 110-240 cm^{-1} only.

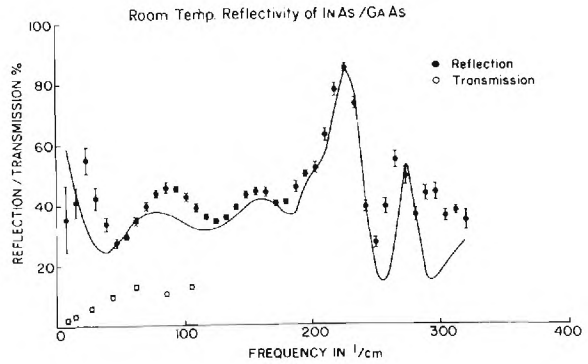

Figure 3. FIR reflection and transmission for a 12μm thick epitaxial layer of InAs on a substrate of high resistivity GaAs. The best fit curve was determined using only the data from 8 to 240 cm^{-1}. Note that the error bars for laser spectrometer data (O, transmission) are much smaller than those for Fourier spectrometer data (●, reflection), especially at very low frequencies.

FAR INFRARED PROPERTIES OF SHALLOW IMPURITY STATES IN HEAVILY DOPED p-TYPE GERMANIUM

K. Yoshihiro, J. Kinoshita and C. Yamanouchi
Electrotechnical Laboratory
Tanashi, Tokyo, 188 Japan

Abstract

Measurements of absorption coefficient and photoconductivity have been made at sub-mm wavelengths in Ga-doped Ge single crystals with concentrations around the metal to nonmetal transition at temperatures down to 1.4K. The photoconductivity associated with A^+ states is nearly 3 times as large as that associated with D^- states of n-Ge for the concentrations studied.

Introduction

Optical properties of shallow-donor negative ions and shallow-acceptor positive ions produced in Ge and Si at low temperatures have been investigated by several authors [1-3]. Gerschenzon, Gol'tsman and Ptitsina observed the binding energy of the electron or hole with the neutral donor or acceptor from the sub-mm photoconductivity in Ge and Si samples containing 10^{12}-10^{15} impurities/cm^3. These investigations were confined to the concentrations where the impurity atoms were considered to be of isolated hydrogen-like states, D^- or A^+.

For heavily doped samples, it is expected that the wave functions of D^- (or A^+) states are overlapped and the charge carriers are transfered through a so called D^- (or A^+) band. The optical properties in the heavily doped samples are not sufficiently studied as yet. We reported previously the result of optical measurements of heavily Sb-doped n-Ge [4] and P-doped n-Si [5] at a wavelength of 337 μm and showed that the activation energy ε_2 which had been observed in the resistivity at temperatures between 20 and 4 K [6] was the energy required for the transition from the donor ground state to the D^- band. One of the aims of the present work is to study whether the optical properties associated with the A^+ band in p-type samples are similar to those associated with the D^- band in n-type samples when the ionizastion energies of the donor and the acceptor are equal. In this conference we will present the measurements of absorption coefficient and photoconductivity in Ga-doped p-type Ge single crystals for radiations produced by an HCN laser and a Carcinotron. We will also discuss the difference between the dynamical characters of A^+ and D^- band probably caused by the difference in correlations [7] between electrons and holes.

Experimental Results and Discussions

The samples studied were of concentrations ranging from 2×10^{16} to 6×10^{17} Ga atoms/cm^3 and were $10 \times 1.4 \times (0.05 - 1.0)$ mm^3 in size. The compensation ratio N_D/N_A was estimated at less than 5%. The activation energy ε_2 for the samples studied was obtained from the resistivity measurements below 20K and is shown in Fig. 1, together with the ε_2 values of Sb-doped Ge samples. The $|N_A-N_D|$ was obtained from the Hall coefficient R_{300} measured at room temperature with the magnetic field of 20 kOe and the relation $N_A - N_D = 1/R_{300}e$. Figure 1 indicates that the ε_2 is only a function of the carrier concentration if the impurity ionization energy is given and the concentration of compensating impurity is negligible.

Figure 2 shows the photoconductive response $-\Delta\rho/\rho$ of 337 μm radiation plotted against ε_2 for various Ga-doped samples and various temperatures. The previous result for Sb-doped Ge is also shown for comparison. The photoconductive response of Ga-doped samples is nearly 3 times as large as those of Sb-doped samples. The photoconductive threshold for Ga-doped Ge shifts to the lower ε_2 side compared with that for Sb-doped Ge. Figure 3 shows the absorption coefficients of both the p- and n-type samples as a function of concentration. The absorption coefficient depends little on temperature. Since the concentration dependence of absorption coefficient for Ga-doped Ge almost coincides with that for Sb-doped Ge except for the structures seen in Sb-doped Ge, the larger photoconductive response observed in p-type samples suggests that the energy relaxation time of the photocarriers in A^+ band is longer than that in D^- band. The differences between p- and n-type Ge in the magnitude of photoconductive response and the

absorption coefficient can be understood provided that the Coulomb interaction between holes in the A^+ band and negatively ionized acceptors is weaker than that between electrons in the D^- band and positively ionized donors. The effect of the magnetic field and the incident photon energy will also be discussed.

References

[1] R.A.Brown and M.L.Bruns, Phys. Lett. 32A 513 (1970).

[2] D.D.Thornton and A.Honig, Phys. Rev. Lett. 30 909 (1973).

[3] E.M.Gerschenzon, G.N.Gol'tsman and N.G. Ptitsina, Sov. Phys. JETP 37 299 (1973); E.M.Gerschenzon, Proc. 12th Int. Conf. Physics of Semiconductors 355 (1974).

[4] K.Yoshihiro, M.Tokumoto and C.Yamanouchi, IEEE Trans. MTT MTT-22 1072 (1974).

[5] J.Kinoshita, C.Yamanouchi and K.Yoshihiro, J. Phys. Soc. Japan 36 1493 (1974).

[6] H.Fritzsche, J. Phys. Chem. Solids 6 69 (1959).

[7] M.Okazaki, M.Inoue, Y.Toyozawa, T.Inui and E.Hanamura, J. Phys. Soc. Japan 22 1349 (1967).

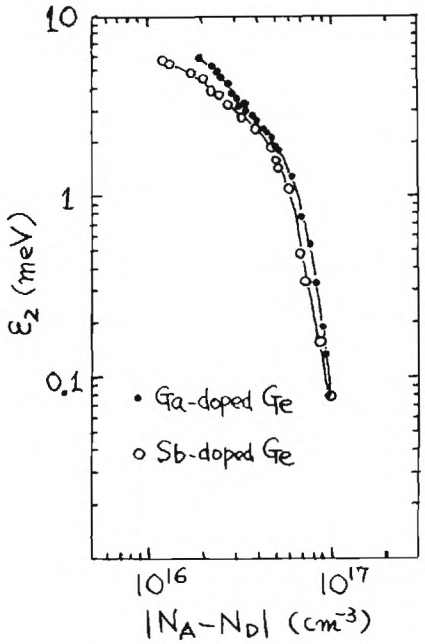

Fig.1 The activation energy ε_2 for various Ga- and Sb-doped Ge samples obtained from d.c. resistivity measurements.

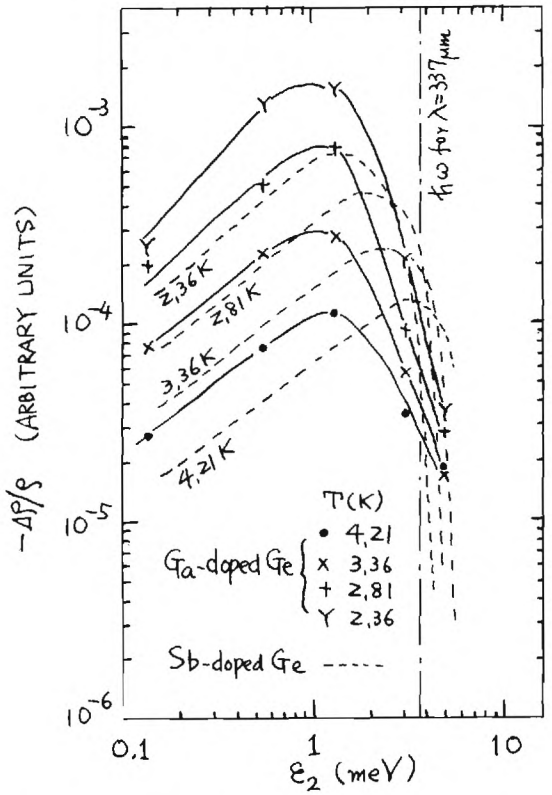

Fig.2 Photoconductive response $-\Delta\rho/\rho$ vs. ε_2 for various samples. $\lambda = 337$ μm.

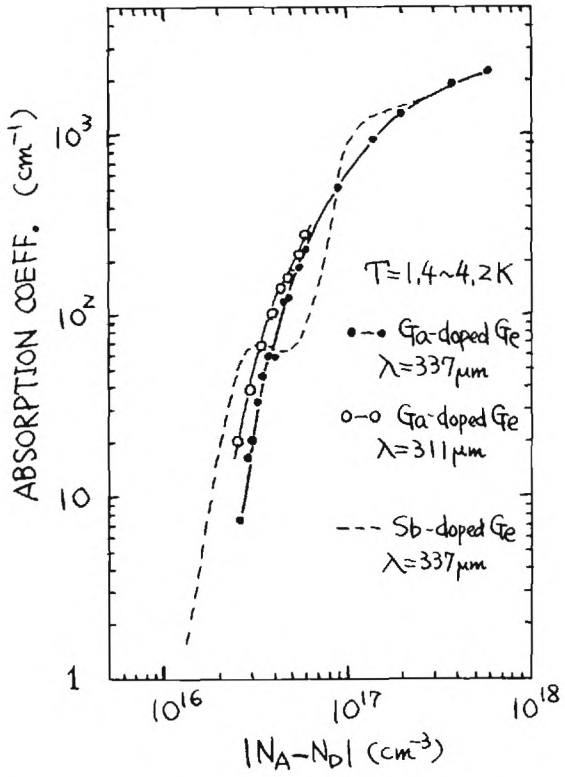

Fig.3 Absorption coefficient vs. concentration.

FAR-INFRARED STUDY OF EXCITONS, ELECTRON-HOLE DROP AND IMPURITY SYSTEM IN GERMANIUM

E. Otsuka, T. Ohyama, H. Nakata and Y. Okada*
Department of Physics, College of General Education,
Osaka University, Toyonaka, Osaka 560, Japan

Decay-kinetics of exciton and electron-hole drop systems in highly photoexcited germanium crystal are investigated by observing time-resolved far-infrared laser magneto-absorption. Magnetospectroscopy of doped material is also studied over 48 - 220 μm.

INTRODUCTION

Excitons, electron-hole drops (EHD) and impurity systems in germanium are accessible for far-infrared laser investigation in the sense of magneto-optical absorption. Especially important is the coexistence system of excitons and EHD, in which excitons are considered to have evaporated from the surface of EHD. Absorption arising from transition between the discrete levels of exciton and that arising from magnetoplasma resonance of EHD are readily distinguishable through changing wavelength, temperature, excitation power and delay-time after photoexcitation. Time-resolved analysis of these two kinds of absorption leads to a new type analysis of the decay-kinetics of the short-lived coexistence system. Impurity absorption, on the other hand, is steadily observable, since the lifetime of impurity is infinite. A simple magneto-spectroscopy measurement is carried out for indium-doped germanium just by using various wavelengths of laser.

EXCITONS AND EHD

Pure germanium crystal is photoexcited either by xenon flash-lamp or by Q-switched YAG laser at liquid helium temperatures. Typical traces of magneto-absorption are shown in Fig. 1 for the wavelength of 84.3 μm (D_2O laser) at various delay-times. The lowest field 1s → 2p_ type transition of exciton is sharply defined on top of the broad EHD background absorption. The EHD absorption decays steadily with time, while the excitonic absorption seems to stay nearly flat for a certain period of time. This feature is shown in Fig. 2 as obtained for 3.6 K. A simple interpretation is that during the existence of EHD free excitons are provided from EHD through evaporation, thus tending to keep the amount of excitons from decreasing. The rapid decay of excitonic absorption after 40 μs then indicates disappearance of EHD.

The decay-kinetics can be written:

$$\dot{n}_d = -n_d/\tau_o - aT^2 n_d^{2/3}\exp(-\phi/kT) + bn_d^{2/3}n_{ex},$$

$$\dot{n}_{ex} = aNT^2 n_d^{2/3}\exp(-\phi/kT) - n_{ex}/\tau_{ex} - bNn_d^{2/3}n_{ex}$$

with conventional notations [1]. A simple analysis valid only for the region in which n_{ex} is constant yields

$$n_{ex} = (a/b)T^2\exp(-\phi/kT),$$

$$n_d = n_{do}\exp(-t/\tau_o) + n_{ex}\tau_o[\exp(-t/\tau_o) - 1]/N\tau_{ex}.$$

These relations are guaranteed under the condition

$$1/\tau_{ex} \ll bNn_d^{2/3}.$$

Since $b \propto \langle v_{ex}\rangle \propto T^{1/2}$, where $\langle v_{ex}\rangle$ is the thermal velocity of the exciton, one may expect

$$n_{ex} \propto T^{3/2}\exp(-\phi/kT).$$

Comparison with experimental observation yields the value of 14.7 K for the work function ϕ.

The apparent decay-time of the EHD signal varies from 11.5 μs at 4.2 K to 24 μs at 3.3 K. This is not the internal electron-hole recombination time τ_o but contains the effect of the term which is proportional to n_{ex}. The relative abundance of excitons at higher temperatures tends to shorten the apparent decay-time of EHD.

One feature worth noting is the approximate constancy of n_d at the critical point where n_{ex} starts to decay after being time-independent; namely, it is independent of temperature and excitation power.

Whenever n_d is small, τ_{ex} is directly observable through time variation of the exciton signal. The evaporation from EHD, however, cannot entirely be neglected at higher temperatures and this tends to make τ_{ex} longer. One finds, for example, τ_{ex} = 6 μs at 3.3 K and 10 μs at 4.2 K. It should be mentioned that the exciton signal is rather hard to observe below 3 K, since the density of excitons coexistent with EHD becomes very small at low temperatures.

As a rule, the EHD signal strongly depends on the excitation power, while the exciton signal depends on it very little.

IMPURITY SYSTEM

As an example of laser spectroscopic study of the impurity system, use of various wavelengths (48 - 220 μm) is made for investigating the indium impurity in germanium. The indium concentration is 3.7 x 10^{14} cm^{-3}, with negligible donor compensation. So far as the prominent spectral peaks observed are concerned, no difference is found between 1.7 and 4.2 K, indicating that they are the transitions originating from the deep-lying lowest electronic state of the impurity. Out of the most outstanding absorption peaks, two representative 1s → 2p_ type transitions are identified. It turns out that the tentative association model of the acceptor states with the Landau levels; namely, 1s with N = 0 and 2p with N = 1, is basically good even for weak and intermediate magnetic fields. A picture of magneto-

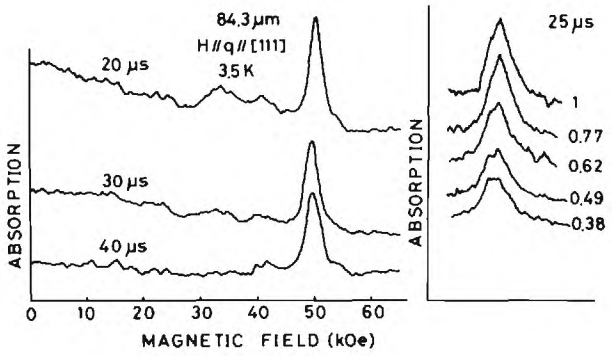

Figure 1. Absorption traces of the exciton signal at different delay-times after photoexcitation, on top of the plasma absorption due to EHD. Only the EHD absorption is changing around for the delay-times shown. The exciton signal shows little change for varying excitation power as indicated on the right. The relative excitation powers are shown in numbers.

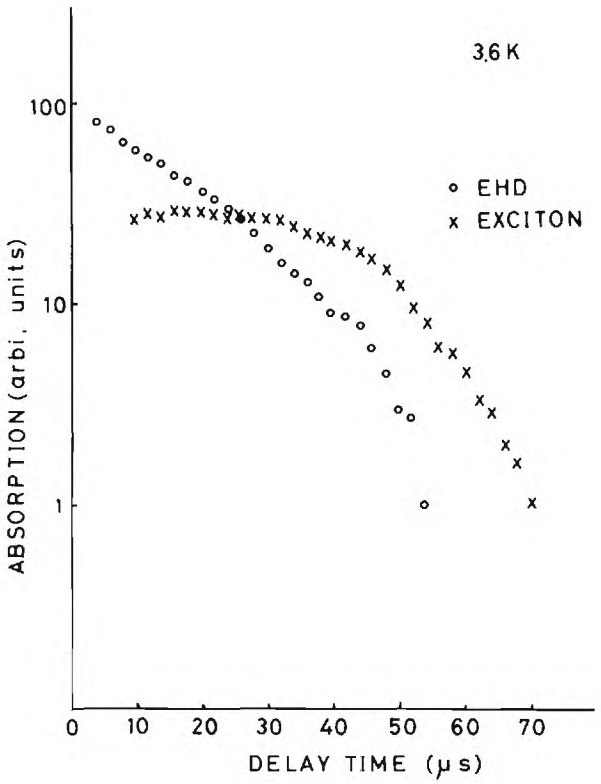

Figure 2. Decay profiles of exciton and EHD absorption signals. EHD absorption is measured at the fool of the exciton signal. One may note the nearly time-independent n_{ex} between 10 and 40 μs of delay-time.

optical transition for H // [111] with various wavelengths is presented in Fig. 3. The solid lines indicated A through E correspond to the "prominent peaks". The dashed-lines are the result of a variational calculation based upon the Yafet-Keyes-Adams type approach [2]. The lines A and B are assigned to be the $1s \rightarrow 2p_-$ type transitions as indicated. The numbers with suffix in the parentheses are the Landau levels (after the Hensel-Suzuki notations [3],[4]) with which the discrete states are associated. For longer wavelengths not shown, only a broad line is observed near 50 kOe for 172 μm and no clearly discernable peaks for 220 μm.

* Now at the Horiba Ltd., Kyoto.

1. T. Ohyama, T. Sanada and E. Otsuka: Phys. Rev. Lett. 33, 647 (1974).
2. Y. Yafet, R. W. Keyes and E. N. Adams: J. Phys. Chem. Solids 1, 137 (1956).
3. K. Suzuki and J. C. Hensel: Phys. Rev. B9, 4184 (1974).
4. J. C. Hensel and K. Suzuki: Phys. Rev. B9, 4219 (1974).

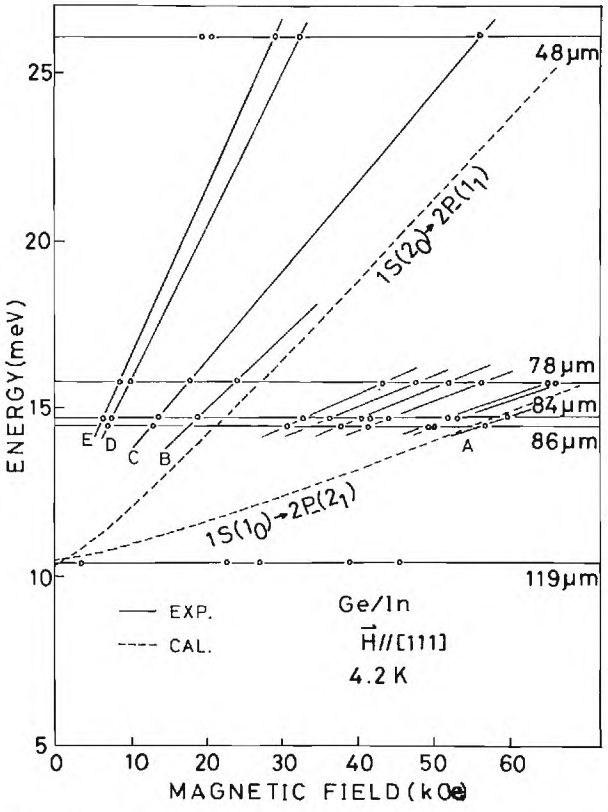

Figure 3. Laser magneto-spectroscopic result for indium in germanium. Meanings of the notations are described in the text.

SUBMILLIMETER-CYCLOTRON RESONANCE OF ELECTRONS IN ACCUMULATION LAYERS ON INDIUMANTIMONIDE SURFACES

M. v.Ortenberg and U. Steigenberger
University of Würzburg
D-8700 Würzburg, GFR

Abstract:

We report of the submillimeter-laser-magneto transmission of pure n-type InSb in a MIS-arrangement as function of the applied gate voltage. From the recorded data we derive a strong dependence of the surface-cyclotron mass in accumulation layers on InSb surfaces on the electric surface field and henceforth on the surface density of electrons. The influence of the surface potential on the kp Hamiltonian is discussed in detail.

Indiumantimonide is a narrow-gap semiconductor with strongly nonparabolic energy bands. In the presence of an external magnetic field the cyclotron mass depends not only on the magnetic field intensity, but also on the wavevector parallel to the magnetic field orientation [1]. This wavevector can be changed considerably by a quantizing electric field perpendicular to the sample surface. Therefore we observe a definite electric field dependence of the cyclotron mass. The explicit variation of the mass with the electric field intensity depends, of course, on the definite shape of the electrostatic surface potential. This potential, however, is affected by the involved screening mechanism and is different for inversion and accumulation layers. After the study of the surface-cyclotron resonance of electrons in InSb inversion layers by Därr et al. [2] the principal objective of the present experiments was to investigate the surface cyclotron resonance in accumulation layers on n-type InSb and to discuss the present results in comparison with those of the inversion layers.

The quantizing electric field was produced in a metal-insulator-semiconductor-, - short in a MIS- -, arrangement [2-4]. To monitor the dc-surface properties during the experiment the sample was provided with electrical contacts suitable for the measurements of the field effect and the magnetoresistance. In fig. 1 we have plotted the field-effect curve of a MIS-device with a pure n-type InSb sample for different parameters of the external magnetic field intensity. For positive values of the gate voltage up to 1000 V corresponding to a surface field of $2.9 \cdot 10^5$ V/cm an accumulation of electrons is generated. For negative polarization surface holes in inversion are induced. In the slope of the field-effect curve magneto-quantum oscillations are observed. For zero magnetic field no field effect is observed because of the high residual free carrier concentration of the sample, which is drastically reduced by magnetic freeze-out with increasing magnetic field intensity.

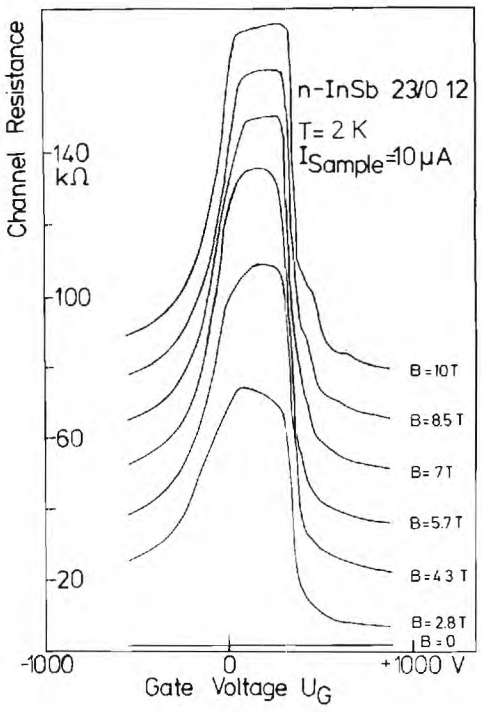

Fig. 1 The field-effect curves of a InSb-MIS device for different parameters of the external magnetic field intensity exhibit the strong influence of the electric field on the dc-properties.

In fig. 2 we have plotted in the upper part the electric field induced transmission change as function of the magnetic field intensity. The spectra were obtained by square-wave modulation of the gate voltage from the threshold up to the voltage indicated by the parameters. In the lower part the relative transmission of the device for zero electric field is plotted. This spectrum is completely dominated by the magnetoresonances of the electrons in the bulk of the InSb substrate. This volume resonance, of course, modifies the broad surface resonance in the upper part. There is a definite shift of the flat extremum to higher magnetic field intensities with increasing gate

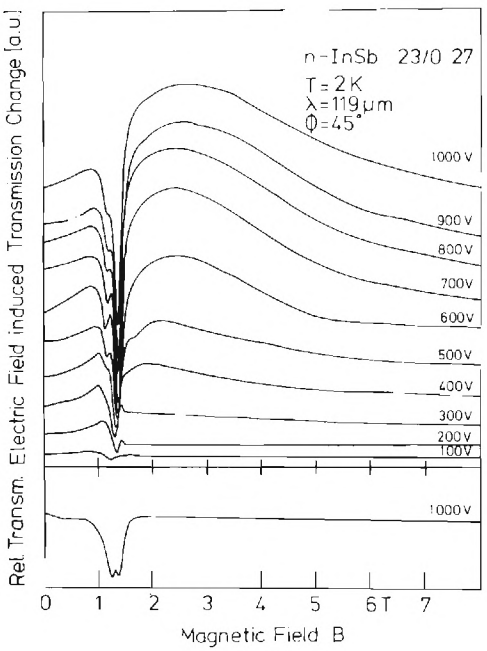

Fig. 2 The extrema of the surface cyclotron resonance of electrons in an accumulation layer on InSb are shifted to higher magnetic field intensities with increasing gate voltage as given by the parameter.

voltage. This indicates the strong dependence of the surface-cyclotron mass on the electric field. From the detailed invesigation we conclude that our experimental data in accumulation can be explained bv only one electric subband, which corresponds to the lowest subband in inversion as found by Därr et al. [2].

References

[1] E.O. Kane, J.Phys.Chem.Solids 1, 249 (1957)

[2] A. Därr, J.P. Kotthaus and J.F. Koch Solid State Commun 17, 455 (1975)

[3] M. v.Ortenberg and R. Silbermann Solid State Commun. 17, 617 (1975)

[4] M v.Ortenberg, S Merz and A. Schlachetzki, Proceedings of the 13th International Conference on the Physics of Semiconductors, Rome, 1976.

LINE SHAPE OF CYCLOTRON RESONANCE IN N-TYPE GERMANIUM AT 337μm IN THE TEMPERATURE RANGE 15-100 K

F. Kuchar
Angewandte Physik, University of Vienna, A-1090 Vienna
L.Boltzmann Institut für Festkörperphysik, A-1060 Vienna

Introduction

Recently, an influence of the non-parabolicity of the conduction band of n-type Ge on the position of the transvers-mass cyclotron resonance was observed in far-infrared experiments [1,2]. Like in a magnetopiezotransmission experiment [3] the results seemed indicate that the non-parabolicity is stronger than calculated [3]. In the calculations only two bands - the L_1 conduction band and the L_3,valence band - were taken into account. A more refined theory [4] including 15 bands did not yield significant corrections. So, it was difficult to understand what might cause the strong non-parabolicity as observed in the experiments.

It is the purpose of this work to show that the inclusion of the k_H dependence in the a.c. conductivity which has been neglected so far removes the discrepancy. Furthermore, we show that it is necessary to take into account the non-parabolicity for an exact interpretation of cyclotron resonance line shapes although this effect is much smaller than in semiconductors like n-InSb.

Experimental Arrangement

Our cyclotron resonance experiments were performed in Faraday geometry using the 337 μm line of an HCN laser and a superconducting magnet in a temperature variable cryostat with mylar windows. The radiation was linearly polarized. Two differently doped germanium crystals were investigated; N_D-N_A was 1.5×10^{15} cm^{-3} (sample 1) and 5×10^{13} cm^{-3} (sample 2). The orientation of the samples was [111] parallel to the magnetic field direction; the deviation from the desired orientation was less than ±2 degrees.

Theoretical Considerations

At the HCN laser frequency, $\hbar\omega$ equals kT at about 40 K. Therefore, a quantum-mechanical treatment [5] is necessary for an interpretation of cyclotron resonance data in the temperature range up to about 100 K. For the calculation of the transmittivity one has to take into account the non-parabolicity of the conduction band in the a.c. conductivity [6]. Here, we will treat only the case of the transverse-mass resonance.

In Faraday geometry, the relevant quantity for describing cyclotron resonance absorption is σ_+. The correct quantum-mechanical expression was given by Burkhard et al.[6] :

$$\sigma_+ = \frac{2e^2}{h^2\omega}\sum_n (n+1)\int_{-\infty}^{\infty} dk_H \times \frac{\left\{f\left[\varepsilon(n,k_H)\right] - f\left[\varepsilon(n+1,k_H)\right]\right\}(\Delta\varepsilon)^2}{i(\Delta\varepsilon - \hbar\omega) + \hbar\Gamma} \qquad (1)$$

The energy level spectrum of the [111] valley for B parallel to its long axis is given by [3]

$$\varepsilon(n,k_H) = -0.5\varepsilon_G(L_1,L_3,)\left\{1 - \left[1+4\frac{(n+1/2)\hbar eB/m_t(0)+\hbar^2k_H^2/2m_H}{\varepsilon_G(L_1,L_3,)}\right]^{1/2}\right\} \qquad (2)$$

Spin splitting is neglected in Eqs.(1) and (2) because of the small g factor of free electrons in n-Ge.$\Delta\varepsilon$ is the energy difference of two adjacent Landau levels. k_H is the wave vector parallel to the magnetic field direction, m_H is the electron mass in this direction (m_l). $\varepsilon_G(L_1,L_3,)$ is the minimum direct gap at the L point. $m_t(0)$ is the zero-field transverse mass at the band edge. The population probabilities $f[\varepsilon(n,k_H)]$ in Eq.(1) are calculated using the measured electron concentration n_c.Γ is the damping parameter and will be compared with the relaxation time appearing in the d.c. mobility ($\Gamma = 1/\tau$).

Results and Discussion

In the interpretation of our experimental cyclotron resonance data, we assume that interference effects are absent. This is justified by the observation of symmetric resonance curves at low temperatures (15-20 K); interferences could be avoided by lapping the samples with rough grinding powder.

Line Shape

In Fig.1 we show a comparison of transmittivity line shapes for linearly polarized radiation which are calculated by taking into account a non-parabolic and a parabolic conduction band, respectively. These curves show: (i) A parabolic interpretation of experimental resonance positions yields higher values of the transvers mass m_t. (ii) In the non-para-

bolic case, transitions at $k_H \neq 0$ and between higher Landau levels are important particularly at high temperatures where several Landau levels are populated significantly. This causes asymmetric line shapes and a shift of the resonance position with temperature which will be discussed below. The asymmetry of the lines can be obscured in heavier doped samples (e.g. sample 1) because of the large electronic contribution to the refractive index and consequently to the reflectivity.

A comparison of experimental and theoretical line shapes including non-parabolicity is shown in Fig.2 for sample 1. In the calculations experimental values of n_c and τ are used: n_c is 1×10^{15} cm^{-3} at 40 K and 1.4×10^{15} cm^{-3} at 80 K, the corresponding values of τ are 3.6×10^{-12} sec and 2.3×10^{-12} sec; thickness is 50 μm. Experimental transmission values are fitted to theoretical transmittivities far below the resonance.

Resonance Position

The temperature dependent position of the transmission minimum of the transverse-mass resonance is plotted for both samples in Fig.3. The theoretical curves are obtained with $\varepsilon_G(L_1,L_3)$= 2.16 eV [7] and the experimental data of n_c and τ. The reason for the shift is the same as for the asymmetric line shapes: Resonance transitions at $k_H \neq 0$ and $n \neq 0$ occur at higher magnetic fields since the Landau levels are not equally spaced due to non-parabolicity (cf. Eq.(2)).

The best fit performed at low temperatures yielded $m_t = (0.0818 \pm 0.0004) m_o$. Because of the good agreement between theory and experiment in Fig.3, we conclude that the $\vec{k}.\vec{p}$ treatment [3] yielding Eq.(1) is correct. (Taking into account k_H=0 transitions only, the calculated mass changes were up to 85% too small [1,2]).

References

[1] F.Kuchar and K.Veigl,J.Phys.C 9, 2797 (1976).

[2] J.C.Ousset et al.,J.Phys.C 9, 2803 (1976).

[3] R.L.Aggarwal et al.,Phys.Rev. 180, 800 (1969).

[4] M.Cardona, Modulation Spectroscopy, Solid State Phys.,Suppl.11,p.319.

[5] A.Ron,Phys.Rev. 134, 1770 (1964).

[6] H.Burkhard et al., Proc.13th Int. Conf.Phys.Semicond.,Rome 1976.

[7] D.E.Aspnes and J.E.Rowe, Phys.Rev.B 7, 887 (1973).

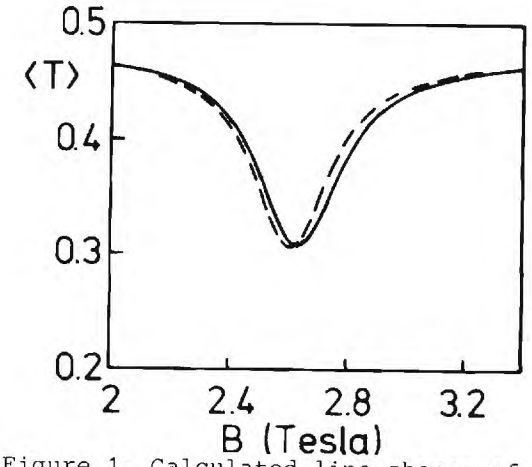

Figure 1. Calculated line shapes of the m_t resonance for a non-parabolic (full curve) and a parabolic band (dashed). $n_c=5\times10^{13}cm^{-3}$, $\tau=4\times10^{-12}$sec, d=300μm, 50K.

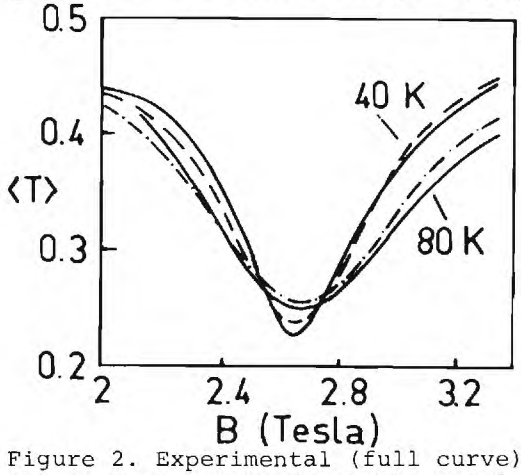

Figure 2. Experimental (full curve) and theoretical curves (dashed), sample 2.

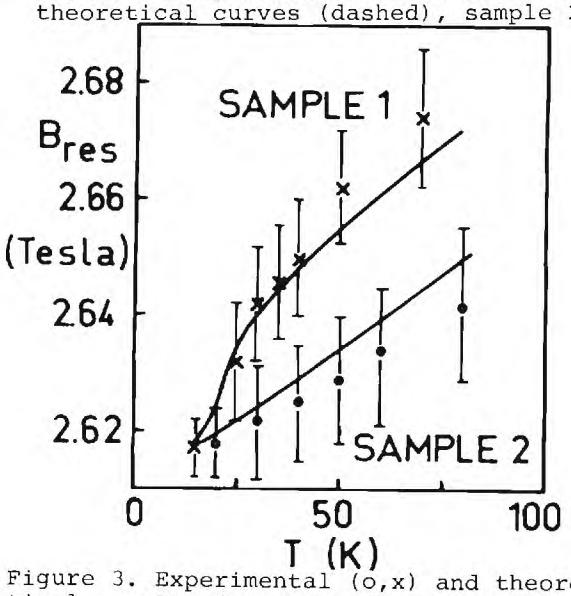

Figure 3. Experimental (o,x) and theoretical results (curves) of the temperature dependence of resonance position B_{res}.

VOLTAGE TUNABLE FAR-INFRARED SOURCE BASED ON ELECTRONIC TRANSITIONS IN Si-INVERSION LAYERS

D. C. Tsui and E. Gornik*
Bell Laboratories
Murray Hill, New Jersey 07974, *Holmdel, New Jersey 07733

Abstract

For the first time gate voltage tunable narrowband far-infrared radiation from Si inversion layers is observed. The radiation is emitted by electronic transitions between the two-dimensional subbands. Population of the excited-state subband is obtained with an electric field along the channel.

In the inversion layer of a Si-MOS structure the energy levels of the electrons being discrete for their motion perpendicular to the interface and continuous for their motion parallel to the interface, form two-dimensional subbands.[1] The energy splitting of the subbands is a function of the electron density in the inversion layer and also weakly dependent on the impurity concentration of the Si-substrate. The electron concentration and thus the subband splitting can therefore simply be tuned by varying the gate voltage (V_G) on the Si-MOSFET. Radiative transitions of electrons between subbands previously demonstrated in absorption[3] and photoconductivity[4] experiments provide the basis for a voltage tunable radiation source.

In this paper we report the observation of far-infrared radiation emitted by electronic transitions between subbands of an inversion layer. We used n-channel Si-MOSFETs on p-type (100) Si. The radiation was generated by heating up the electron distribution with an electric field along the channel.

Figure 1 shows an illustration of the energy structure of the inversion layer together with the hot electron distribution function. On a Si(100) surface the inversion layer has two sets of subbands namely the light mass $E_o, E_1 \ldots$ subbands, which are shown in Fig. 1, and the heavy mass E_o', E_1', ... subbands. E_o lies lowest in energy, while E_1 and E_o' lie close together.[1,2] Far-infrared radiation is emitted by electrons in the E_1 subband as they relax into the E_o subband as indicated by the arrow in Fig. 1.

The gate oxide of the Si-MOSFETs were thermally grown at 1100°C and subsequently annealed in H_2 at 380°C. We have studied samples made on 6 to 12 Ωcm Si-substrate with oxide thicknesses varying from 0.1 μm to 1.0 μm and the peak mobility at 4.2 K varying from 8000 to 20000 cm^2/Vs. The gate are of the devices was either 2.5 x 2.5 mm^2 or 0.25 x 0.25 mm^2. The emission measurements were made at 4.2 K and no dependence on T was noticed by going down to 1.6 K. The sample and the detector were mounted in a brass light pipe with closed ends, so that all the emitted radiation could be collected. A photoconductive Ga:Ge detector with well-known spectral response[5] was used to detect the radiation. The radiation was analyzed with the help of narrowband As:Ge[6] and crystalline quartz filters which have sharp absorption lines at 100 cm^{-1} and 132 cm^{-1} respectively.

Figure 2 shows the detector response as a function of the gate voltage (or the electron concentration n_s in the inversion layer) for two different electric fields E_D along the channel. The device has a channel length of 2.5 mm. For the lower electric field (16 V/cm) the photosignal is plotted for both positive and negative channel field while the averaged signal is shown for E_D = 20 V/cm. For this device the channel voltage required to generate sufficient intense radiation is an appreciably fraction of V_G. In this case the detector signal becomes dependent on the polarity of E_D as demonstrated in Fig. 2. However we find that the averaged signal always yields to a detector spectrum identical to that obtained from a device with ten times shorter channel length. On such a device the signal is independent of the polarity of E_D. Qualitatively the curves in Fig. 2 reflect the spectral response of the Ga:Ge detector indicating a narrowband emission tunable by changing the gate voltage. With the aid of the narrowband filters we determine a linewidth in the range of 6 cm^{-1}.

The emission intensity at 100 μm wavelength for a 2.5 x 2.5 mm^2 gate device is estimated to be about 3 x 10^{-12} W for E_D = 20 V/cm. The intensity increases exponential with increasing channel field to about 10^{-9} W at E_D = 150 V/cm showing a saturation tendency for higher fields.

In this experiment tuning of the emission was observed from ∿ 130 μm to 60 μm with gate voltages between 15 V and 40 V for a device with 6000 Å oxide thickness by using the Ga:Ge detector. Since the subband splitting is a continuous function of the gate voltage tuning from 300 μm to 15 μm is expected for radiation from E_1 to E_o transitions. Transitions from other subbands and the use of hole as well as electron inversion and accumulation layers on other Si surfaces can extend this tunable range even further. With big devices having gate areas of about 1 cm^2 and oxide thicknesses of several μm intensities up to 10^{-7} W can be expected.

We thank G. Kaminsky and W. N. Wittnebert for technical assistance and V. T. Nguyen and J. M. Rowell for helpful discussions.

1. F. Stern and W. E. Howard, Phys. Rev. 163, 816 (1967).
2. A. B. Fowler, F. F. Fang, W. E. Howard and P. J. Stiles, Phys. Rev. Lett. 16, 901 (1966).
3. A. Kamgar, P. Kneschaurek, G. Dorda and J. F. Koch. Phys. Rev. Lett. 32, 1251 (1974).
4. R. G. Wheeler and H. S. Goldberg, IEEE Trans. on Elec. Dev. ED-22, 1001 (1975).
5. W. J. Moore and H. Shenker, Infrared Physics 5, 99 (1965).
6. J. H. Reuszer and P. Fisher, Phys. Rev. 135, A 1125 (1966).

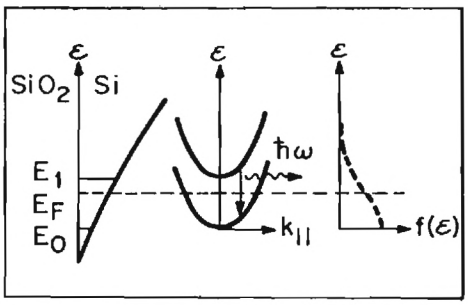

Fig. 1 - Illustration of the energy structure of the Si-inversion layer perpendicular and parallel to the surface, the electron distribution and the radiative transition between the E_1 and E_0 subband.

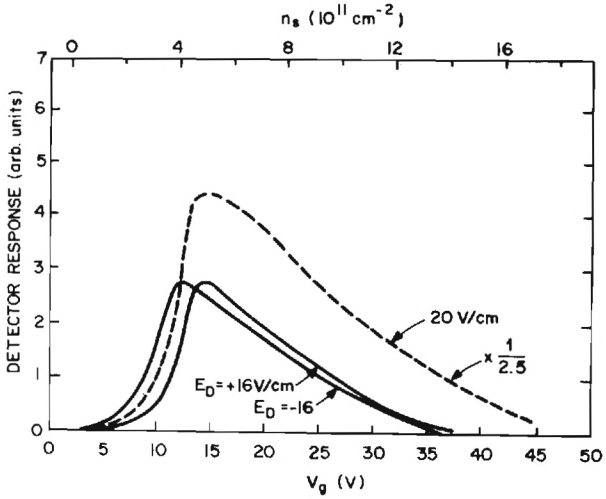

Fig. 2 - Detector response versus gate voltage (V_G) (or electron concentration ns) for different electric fields along the channel.

SUBMILLIMETER SYSTEM FOR IMAGING THROUGH INCLEMENT WEATHER

Richard L. Hartman
US Army Missile Command
Redstone Arsenal, Alabama 35809

and

Paul W. Kruse*
Honeywell Corporate Research Center
Bloomington, Minnesota 55420

If the US Army is to operate well during inclement weather, including fog, rain, snow, and low-lying clouds, it must have a transportable system which will provide a visual image at ranges of 1-5 kilometers consistent with direct-fire weapons. The combined requirements of limited antenna aperture, small beam divergence, reasonable atmospheric absorption, and low scattering from aerosols drive us to the submillimeter portion of the spectrum.

We envisage a system employing a submillimeter source feeding an antenna (mirror) about 1 meter in diameter. The illumination beam is scanned over the target area at TV frame rates. The receiver probably uses the same antenna, with the receiving element slightly displaced to compensate for the transit time during the dwell time on a resolution element. The return signal is used to paint a TV-like image on a CRT.

In 1974 Kruse performed an initial analysis [1, 2] of such a system. The range equation for an optical heterodyne system which provided spotlight illumination of the target was shown to be

$$R_I^2 \exp\left[2(\alpha_c + \alpha_I)R_I\right] = \frac{P \rho A \eta \lambda \tau}{\pi hck}$$

where, R_I = inclement weather range, α_c = clear air attenuation, α_I = inclement weather attenuation, ρ = target reflectivity, h = Planck's constant, λ = wavelength, η = quantum efficiency of detector, P = output power, τ = dwell time on resolution element, and A = receiving area.

Using the assumptions of Table I, the performance of an 850 micron system is predicted in Figure 1.

Because atmospheric attenuation dominates, range is weakly dependent on transmitter power. The predicted performance was good enough to arouse Army interest, and marginal enough to require a detailed experimental assessment. This paper describes the beginning of that assessment.

There are two key issues: (1) does submillimeter radiation, in fact, penetrate the atmosphere as assumed, and (2) do tactical targets, in fact, provide sufficient return of a type usable to develop images? Based on recent experiments, the answer to both questions is affirmative. Some calculations and measurements predicted attenuation coefficients higher than those used in the 1974 analysis. However, recent work [3] shows the two-way, clear-weather outdoor attenuation of an 890 micron FIR laser to be at least as good as the value used in the 1974 analysis.

The second question has been addressed experimentally. One concern has been that radar pictures usually consist of a few bright specular reflections. The solution to this problem is nonlinear processing. The specular returns are subdued, either by a hard-limiting circuit or by a logarithmic response. Figure 2 shows the improvement in an image made in collimated laser light by switching from linear to logarithmic processing.

Spectral reflectance of painted armor plate was measured with a Fourier spectrometer. The results are complex and not yet well characterized. We speculate that in the submillimeter regime the thickness of the coat of paint is important. Nonetheless, the reflectivity is consistent with the 1974 assumption.

To provide a complete test of question (2), active scanned images were taken of real tactical vehicles, using a 3 mm wavelength radar [4]. The operating range of the proposed submillimeter system was simulated by having the target close to the radar and focusing the antenna. One resulting image, processed in a nonlinear manner, is shown in Figure 3.

Many questions remain. There is a major issue in the trade-off of image quality, operating range, and antenna size. Speckle effects degrade the image but can be mitigated by adding diverse images. Experimental data on bad weather degradation of submillimeter beams is lacking. The possibility of enhancing the system operation with Doppler signature recognition must be explored. The specific case of image resolution enhancement in a diffraction-limited, common aperture, active scanned, coherent system should be addressed. Submillimeter sources and detectors have progressed far in the last few years and provide excellent laboratory and breadboard tools, but have a long way to go to provide the compact, efficient, easy to operate devices needed for field operation.

To provide the Army an ability to operate in inclement weather will require a comprehensive program of magnitude comparable to that which led to present FLIR technology, or to laser rangefinder/designator technology. It will take a decade to develop operational capability. If current studies prove that the Army needs can be satisfied with a submillimeter system, the system requirements will have a major impact on submillimeter technology over the next decade.

*Member, Army Scientific Advisory Panel

TABLE I. Assumptions and Characteristics of Inclement Weather Imaging System

Frequency	850 microns
Antenna Aperture	1 meter
Quantum Efficiency	50%
Display S/N	50/1
Resolution/Frame	100 x 100 elements
Frame Rate	30 per second
Target Reflectivity	0.1
Clear Attenuation	10 dB/km
Rain Attenuation	15 dB/km
Fog Attenuation	2 dB/km
Visibility in Fog	270 meters at 0.1 gm/m^3 H_2O

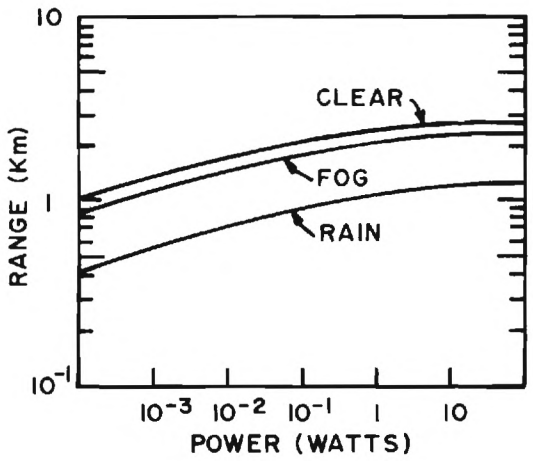

Figure 1. Predicted Performance of the Submillimeter Radar [Specified in TABLE I]

Figure 2. Nonlinear Recording Allows Imaging in the Presence of Specular Reflections

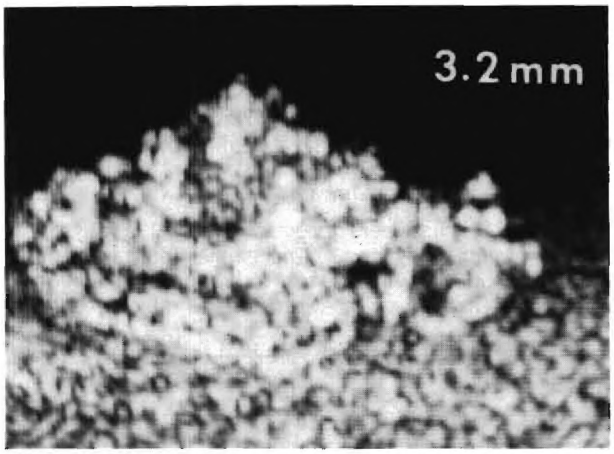

Figure 3. An M-48 Tank Imaged with a 3.2 mm Radar

REFERENCES

1. A System Enabling the Army to See Through Inclement Weather, Paul W. Kruse, Army Scientific Advisory Panel Report, June 1974

2. Technology for Battlefield Target Recognition in Inclement Weather, Paul W. Kruse and V. Garber, Proc. IRIS (23) [in press]

3. Submillimeter Laser Propagation, W. L. Gamble and Bobby D. Guenther, Paper C102 this conference

4. Millimeter and Infrared Image Scans of Military Vehicles, J. Mark Baird, Hughes Res Laboratory Final Task Rpt on Contract F-30602-73-C-0191, 1976. Further analysis is in progress at the US Army Missile Command

SUBMILLIMETER LASER WAVE PROPAGATION

W. L. Gamble and B. D. Guenther
U. S. Army Missile Command
Redstone Arsenal, Alabama 35809

This paper will describe primarily the apparatus, techniques, goals and some preliminary results of the U. S. Army Missile Command submillimeter wave program. The chief goal is to fill some of the most critical data gaps identified by Hartman and Kruse [1]. The basic question is: what range and effective angular resolution can scanned submillimeter radar systems achieve, in particular, during meterological conditions of severely limited visibility. The most critical propagation issues are water vapor absorption, extinction due to aerosols, and beam degradation effects, if any, due to atmospheric turbulence. Of course the reflectance properties of cultural targets, as well as general terrain, are also of importance to the potential operating effectiveness of radar systems.

A program has been designed which will, hopefully, supply much needed basic information on the important atmospheric extinction effects and mechanisms while simultaneously supplying a body of engineering data on the effects a wide variety of meterological conditions have on the performance of certain types of radar systems operating at submillimeter wavelengths. The program will explore the entire spectral region between 700 and 1,300 microns. Two monostatic submillimeter radar sets have been constructed. These consist of: sources, the necessary off-axis parabolas for forming 30 cm diameter collimated beams, video detectors with beam splitter signal pick-offs and 40 cm diameter flat mirrors in scanning mounts for directing the beam. Except where noted below, the two radars are identical.

The beam is scanned over a set of carefully spaced targets of known cross-section on a meterologically, well-instrumented propagation range. One radar operates pulsed for measuring backscattering while the other operates cw. The cw system will be utilized primarily for absorption and beam degradation measurements. An aerial view of the range is sketched in Figure 1. Each target consists of a corner cube with a chopped aperture. The three choppers run at different frequencies so that there can be no ambiguity as to which target the beam is illuminating. Reference signals from the choppers allow synchronous detection when desired. The corner cubes are housed in heated, portable "dog houses" designed to keep them dry and relatively clean. This is necessary in order that good propagation measurements can be made during rainy, foggy, and dusty conditions.

Calibration will be achieved by moving the targets to positions of equal range from the transmitter for cross-section measurements and verification. The corner cubes will be sized and positioned to remove the r^4 dependence in the range equation. The relative returns are then a direct measure of extinction

The size and condition of beam wave front, after propagation to the targets, can be investigated by scanning the beam over the corner cubes if the corner cubes are somewhat smaller than the beam. It may be desirable to illuminate two such corner cubes simultaneously with their choppers synchronized in order that the output of a synchronous detector would be a direct measure of extinction. Reflective optics are used in order to avoid the severe losses in currently available fast lenses.

The detectors currently in use are Golay cells for cw operation and InSb, Putley detectors operating in the video mode. Conversion to heterodyne detection is underway. The decision to use CO_2 pumped FIR lasers for sources was made primarily on the basis of the prohibitive costs of currently available tubes. It is entirely reasonable to believe that optimum system wavelengths can be predicted on the basis of a good set of propagation and target signature data at a set of discrete wavelengths between 700 and 1,300 microns, plus high resolution spectroscopic data on the materials affecting the data taken at discrete wavelengths. The lasers are essentially identical to those described by Hodges et al [2].

Meterological instrumentation monitors, on a continuous basis, such factors as rain rate, temperature, humidity, atmospheric pressure, solar radiation levels, visibility, wind velocity profiles and turbulence. The major weakness in meterological instrumentation on the propagation range is an inadequate capacity, at the present time, to characterize particle size distributions in rain and fog.

The entire system including transmitter, receiver, and all meterological sensors are interfaced to a minicomputer. Scanned A to D converters located at the downrange meterological towers are connected by digital data links to the central processor. The state of the atmosphere as well as propagation effects will be monitored on an essentially continuous basis for a year in order that a meaningful and representative sample of different types of weather conditions are encountered.

Short range imaging experiments are being conducted on military vehicles as well as test targets using the same equipment. Ranges for such experiments will be extended to a kilometer and greater when the receivers have been converted to heterodyne operation. Such issues as the effects of speckle, atmospheric scintillation, and aerosol scattering on scanned imaging radar systems will

be addressed under realistic conditions. A limitation of some potential importance should be noted, however, in that we will not be able to scan an image in a short time compared to atmospherically-induced scintillation times, especially during rain. If the results of the current program are promising in terms of Army applications, a system with a faster scan rate will be set up in the future.

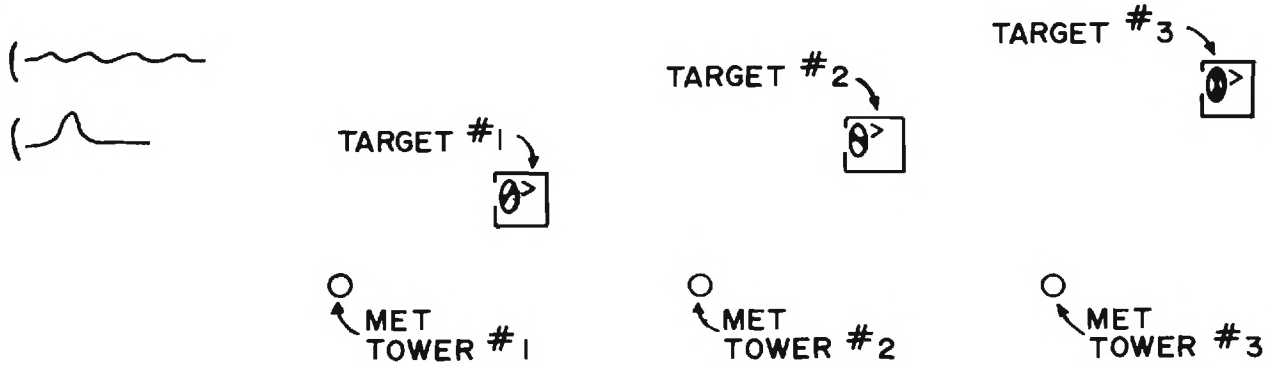

Figure 1. Schematic of Submillimeter Propagation Range

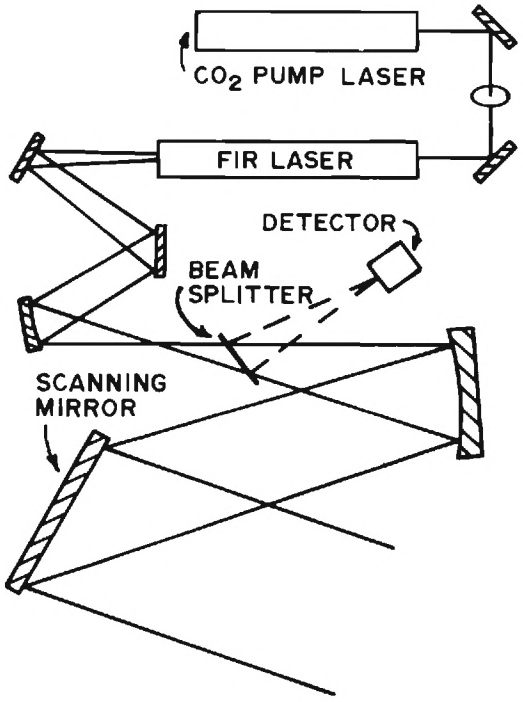

Figure 2. Submillimeter Radar

REFERENCES

1. Submillimeter System for Imaging Through Inclement Weather, Richard L. Hartman and Paul W. Kruse, Paper C-101 this conference.

2. D. T. Hodges, F. B. Foote, and R. D. Reel, Efficient High Power Operation of the CW FIR Waveguide Laser, Appl. Phys. Letters (in press).

SPECKLE AND SPECULAR EFFECTS IN SUBMILLIMETER IMAGING

V. J. Corcoran

Institute for Defense Analyses
400 Army-Navy Drive
Arlington, Va. 22202

Abstract

Speckle effects and specular reflections from non-diffuse surfaces affect the ability of active submillimeter systems to image scenes. These effects and techniques to circumvent the associated problems with respect to recognition and identification are investigated.

Introduction

An active system which scans a scene with a laser boresighted to a scanning receiver is under investigation for imaging in inclement weather. The submillimeter region has been chosen as a compromise between the far infrared wavelengths where good resolution can be obtained and the millimeter region where good atmospheric transmission can be obtained.

Imaging implies the ability of the observer to recognize and/or classify objects in a scene. One of the factors that limits the usefulness of the image of a scene, in addition to an unsatisfactory signal level, is the resolution of the system relative to the size of the objects of interest in the scene.

Speckle effects caused by the coherent illumination of rough surfaces and specular reflections from non-diffuse surfaces also affect the ability of submillimeter systems to produce useable images of illuminated scenes. These effects and techniques to circumvent the associated problems with respect to recognition and indentification are investigated in this paper.

Laser speckle has been studied since the first visible CW laser was demonstrated. Considerable work has been done on the statistical properties of the speckle under the assumption that the deviations from the mean obey Gaussian statistics and that the correlation distance is zero; i.e., the surface consists of zero width deviations that can deviate an infinite amount from the mean. Considerably less work has been devoted to studying more realistic approximations to the problem of determining the characteristics of radiation reflected from rough surfaces. Even in these studies, the approximations have been somewhat idealized.

Methods for reducing speckle have also been studied. The generic techniques for decreasing speckle include spatial and temporal reduction of coherence, aperture integration with the aperture considerably larger than the speckle size and time averaging with a moving aperture.

In the submillimeter region, the surfaces of most man-made objects are usually not rough. In fact, a surface often consists of a composite of a number of smooth surfaces. The properties of the speckle pattern, therefore, can be expected to be different from those caused by a rough surface, and specular effects must be included. In an imaging system, the image quality is important, not the statistics of the radiation incident in the image plane unless the statistics provide an evaluation of the image. It is evident that atmospheric turbulence will affect the speckle pattern produced by illuminating a rough surface and should also be considered in the complete analysis of a problem.

The important questions are (1) what is the output, (2) is it satisfactory, and (3) what can be done to improve the image?

The imager might be a single element line scanner, a scanning array (either parallel or serial) or a mosaic (CCD, etc.). In each case, the speckle size and the contrast is of interest, and these values for ideal situations can be obtained from previous work.

In this paper, an attempt is made to expand the previous work to the real problem that must be faced in a submillimeter imager. To achieve the objectives of the paper, the output current of a detector is first determined for propagation in a vacuum. Optics and turbulence effects are later included. The specular and speckle effects are both contained in the complete expression for the output current.

Analysis

When light impinges upon a rough surface, the scattered radiation consists of a specular component and a diffuse component. The relative amounts of radiation in each depend upon the fluctuations in the surface relative to the wavelength of the incident radiation and on the spatial frequency content of the waves. For submillimeter radiation, the fluctuations that exist in a man-made surface can be comparable to a wavelength of radiation so that the rough surface approximation may not hold. A more detailed analysis is then required.

For an envelope detection system, the quantity of interest is the power that is collected by the receiver and imaged on the detectors as a function of angle, since the current is proportional to the incident power. For a two-dimensional perfectly conducting surface with a normal spatial distribution illuminated by radiation incident at

an angle θ_1 with respect to the normal to the mean surface, the mean scattered power is given by

$$\langle \rho\rho^* \rangle = F^2 e^{-g}\left(\rho_o^2 + \frac{\sqrt{\pi T}}{2L}\sum_{m=1}^{\infty}\frac{g^m}{m!\sqrt{m}}\, e^{-v_x^2 T^2/4m}\right) \qquad (1)$$

where

$$F = \sec\theta_1 \frac{1 + \cos(\theta_1 + \theta_2)}{\cos\theta_1 + \cos\theta_2}$$

$$g = \left[2\pi\frac{\sigma}{\lambda}(\cos\theta_1 + \cos\theta_2)\right]^2$$

$$\rho_o = \frac{\sin v_x L}{v_x L}$$

$$v_x = \frac{2\pi}{\lambda}(\sin\theta_1 - \sin\theta_2)$$

θ_1 is the angle of incidence

θ_2 is the scattering angle which is measured in the opposite sense from θ_1

L is the length of the surface

and

T is the correlation length of the surface.

Equation 1 is limited by the following conditions:

- The surface is perfectly conducting.
- Shadowing and multiple scattering may be neglected.
- The incident wave is plane and linearly polarized with the E vector either in the plane of incidences, xz, or perpendicular to it.
- The observation point is in the far field.
- The radius of curvature of the scattering elements is greater than the wavelength of the incident radiation.

The expression for the mean scattered power consists of two terms; the first is a specular term which is a maximum for a smooth surface (g=0) and the second is a diffuse term which is zero for a smooth surface and becomes dominant for a very rough surface (g≫1). The specular term is highly directional as would be expected for the reflection from a smooth surface. Because of conservation of energy, the increase in the specular component as the surface becomes smooth requires a corresponding decrease in the total diffuse component, which causes the speckle. In principle, therefore, a speckle image is always available if the specular component is filtered.

The expression for the speckle size depends upon the receiver aperture. In the limit when the statistics are Gaussian and the correlation length is zero, the speckle size is given by the equation

$$\text{Spot Size} = \lambda\, f/\# \qquad (2)$$

where f/# is the f-number of the optics. For the submillimeter region, the speckle size is a fraction of a millimeter.

A number of specific techniques for reducing speckle have been suggested; however, many of these methods, which usually involve mechanical motion, would probably be impractical for the application involved in which the source is either pulsed or is a CW device which dwells on a resolution element for a limited time. Techniques using integration with a detector whose size is much larger than speckle spots have also been suggested. Finally, time averaging techniques have been suggested.

The specific techniques that may be of some value for the submillimeter system include multifrequency operation, frequency modulation, time delay and integration, and frame-to-frame integration.

In the multifrequency operation, it is necessary to choose at least two wavelengths whose spacing is such that constructive interference at one wavelength would result in destructive interference at another. If the spectral width were sufficient, operation with a multimode source would suffice; however, this may not be possible in the submillimeter region.

Changing the frequency within the pulse or the dwell time is effectively reducing the temporal coherence of the source, or the process can be considered to be the integration of many pulses of varying frequency. Regardless of the viewpoint, the contrast in the speckle pattern can be reduced with this technique if a rapid modulation scheme can be devised.

Time delay and integration would employ an array of detectors each of which would sample the same resolution element at different times. The outputs would then be summed to produce the signal for a given resolution element. This technique, which is used in some FLIRs, would reduce the contrast by the temporal integration.

By using frame-to-frame integration, the phase changes that occur in the period of 1/30 sec, the normal frame time, would be integrated to reduce the speckle. This also is a temporal integration technique, but the integration intervals are different from those used in the time delay and integration method.

Summary

The analysis has shown that the signal on a detector from an illuminated surface consists of two components--a specular and a diffuse component. The specular component can be ignored so that a speckle pattern, albeit reduced in value, is always obtained. The size of the speckles is on the order of a wavelength. Techniques such as frequency diversity or temporal integration can be used to reduce the speckle.

REFLECTIVITY OF COMMON MATERIALS IN THE SUBMILLIMETER REGION

M. D. Blue
Georgia Institute of Technology, Atlanta, Georgia

and

S. Perkowitz
Emory University, Atlanta, Georgia

Abstract

The appearance of an illuminated scene at submillimeter wavelengths is determined by surface reflectivity. Reflectivities of some man-made and natural materials have been measured. The results provide some insight for evaluating possible applications of submillimeter radiation.

Introduction

The gradual realization of practical submillimeter wave sources including optically pumped lasers throughout the submillimeter region [1], and relativistic electron beam devices [2], gives rise to the possibility of practical terrestial systems operating within the atmospheric windows. Systems calculations are handicapped by a lack of data concerning dielectric properties of common materials in this spectral region. Recent transmission data and active imaging experiments indicate the potential utility of this technology [3]. The work reported here represents an initial attempt to characterize the FIR-submillimeter reflectivity of common materials, and can be used as a guide for initial estimates of system performance.

Experimental Methods

The room temperature reflectivity measurements employed a modified Grubb Parsons Mark II Fourier transform spectrometer [4]. Light pipe optics carried the radiation to a sample holder which was open to the atmosphere so that the sample could be studied under natural conditions. Conventional desiccant and a constant flow of dry nitrogen gas were used to eliminate water vapor absorption from the sample light pipe and holder and the remainder of the spectrometer was evacuated. The radiation impinged on the samples at an angle of 12°, negligibly different from normal incidence. The sample holder was mounted horizontally to accomodate loose samples such as sand. The detector was a Unicam quartz window Golay cell with the usual polyethylene filtering. All data were taken at a resolution of 8 cm^{-1}. A sample in/sample out method was used to obtain the reflection coefficient, with the reference value supplied by a polished stainless steel mirror. Such a mirror has a nearly constant far infrared reflectivity of about 97% and so can be treated as a 100% reflector with little error.

Experimental Results

A list of materials used in this study is presented in Table 1. Both natural and man-made materials were considered. Natural materials include typical surfaces as seen in earth backgrounds. Man-made materials include asphalt and concrete as well as metal surfaces.

The normal reflectivities for several metal surfaces as well as for grass are shown in Figure 1. It can be seen that flat black paint on aluminum reduces the reflectivity to a value below that of a normally oxidized aluminum surface surface in the FIR. Similarly, flat olive drab paint reduces reflectivity of clean brass which, like all high conductivity materials, has very high reflectivity throughout this region. However, the paints have quite different spectra.

For many natural surfaces, it is likely that the surface scattering effects dominate the reflectivity. For example, the reflectivity of concrete closely parallels rusty iron over this spectral region. As these materials are quite different, it is possible that the normal reflectivity is dominated by surface roughness effects. Fresh grass shows a reflectivity typical of our organic samples. Normal reflectivity of dry grass was similar, going from 20% at 20 cm^{-1} to 3% at 200 cm^{-1}. For a fresh maple leaf, reflectivity decreased monotonicaly from 13% to 5% over this range, while a dry maple leaf showed a modest peak of 16% at 100 cm^{-1} dropping to 10% at 50 cm^{-1} and 150 cm^{-1}.

In general, all organic samples along with sand, mud, asphalt, and concrete have lower reflectivities than the painted metal surfaces examined within the limited scope of this study. The organic material did not show strong structure at 200 cm^{-1} as observed in chlorophyll transmission spectra [5].

Summary

This study examined normal reflectivity for a small group of natural and man-made samples from 20 cm^{-1} to 200 cm^{-1} at room temperature. Many interesting questions are raised by these data which suggest several directions for further work. Among these are extension to longer wavelengths, off-axis reflection, temperature effects, and additional samples.

The most significant result to date appears to be the clear separation in the value of normal

reflectivity between metal surfaces and typical natural materials representative of terrestial backgrounds. This result suggests that detection and imaging systems operating in this wavelength region can distinguish man-made objects from their backgrounds.

This study was supported by the Army Research Office.

References

1. J. J. Gallagher, M. D. Blue, B. Bean, and S. Perkowitz, Infrared Physics, in press.

2. H. H. Fleischmann, Physics Today 28, 35 (May 1975), and V. L. Granatstein, M. Herndon, Y. Cramer, and J. A. Nation, Plasma Physics 11, 23 (1975).

3. T. S. Hartwick, D. T. Hodges, D. H. Barker, and F. B. Foote, Appl. Optics 15, 1919 (1976).

4. S. Perkowitz and J. Breecher, Infrared Physics 13, 321 (1973).

5. S. Perkowitz and B. Bean, Bull. Am. Phys. Soc. 21, 371 (1976).

TABLE I. Far Infrared Reflectivity Of Some Common Materials

Natural Materials	
Sand	< 2% (overall reflectivity 20-200 cm^{-1})
Mud (soil)	< 2% (overall reflectivity 20-200 cm^{-1})
Wood	
Oak, Mahogany, Fir	< 2% (overall reflectivity 20-200 cm^{-1})
Rosewood	< 5% (overall reflectivity 20-200 cm^{-1})
Leaf	
Maple - fresh, dry(green); Grass - fresh, dry(green)	See text, < 20%(at 100 cm^{-1})
Man-Made Materials	
Asphalt	∿ 5% (overall reflectivity 20-200 cm^{-1})
Painted metal, Flat black on Al, Army OD on brass; Rusted iron; Oxidised Al	Refer to Figure 1.
Concrete	Similar to rusted iron

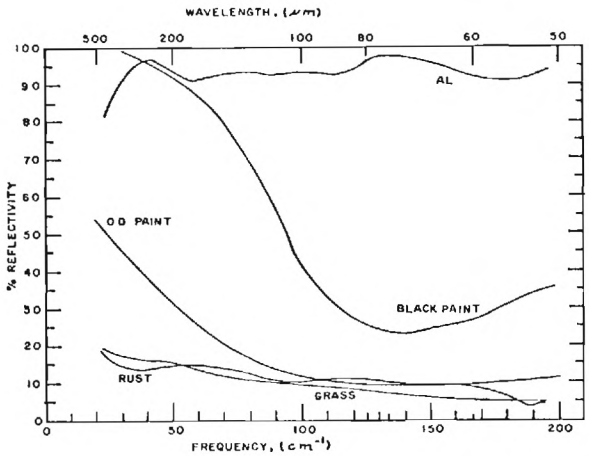

Figure 1. Normal reflectivity of common materials. Included are a normally oxidized aluminum surface (Al), Aluminum sprayed flat black (Black Paint), olive drab paint on brass (OD Paint), a freshly cut blade of grass (Grass), and a rusty iron surface (Rust).

INDIRECT INTERACTION FREQUENCY SHIFT OF RADIATION

J. Cooney
Department of Physics and Atmospheric Science
Drexel University
Philadelphia, Pennsylvania 19104

This paper discusses a form of parametric interaction of radiation with matter. What seems novel about this interaction is that a change is brought about in the temporal spectrum of scattered flux of radiation that arises from physical properties of matter with which the field does not directly interact.

To begin with imagine a finite, uniformly spaced linear array or matrix, of identical entities, static and of equal size. Clearly the size of these entities must be less than the array spacing or the idea of the array would itself lose meaning. Next let this array be embedded in a second or background material which itself is continuous. Now imagine a flux of radiation (called type I) falling on the matrix. It must be supposed to interact with (e.g. scatter off of) the discrete material of the array but not to interact with the continuous background material. Also imagine a second flux of radiation (called type II) falling on the matrix. Type II radiation must be supposed to interact with the background material as well as the discrete array elements.

Both fluxes of radiation may be electromagnetic. However in a specific application detailed in another paper, type I radiation is electromagnetic and type II radiation is acoustic. In the remainder of this paper it will be useful, for concreteness, to view the two fluxes of radiation in this manner. Thus, for specificity, let it be assumed that the lattice array is illuminated by a pulse of acoustic radiation, but that the speed of its propagation though the array is controlled by the acoustic properties of the continuous or background material. In addition for array element with the appropriate mechanical properties, let it be supposed that internal vibrations are set into oscillation by interaction with the acoustic pulse. Because of the free boundary, the mechanical vibrations can alter the shape of the array elements. Thus if it is assumed that the embedding material is say, air, then the lattice elements are set progressively into oscillation at time intervals corresponding to the lattice spacing divided by the acoustic speed in air.

Simultaneously with the acoustic pulse (type II), let the array be illuminated by a flux of electromagnetic radiation (type I). The electromagnetic radiation can consist of such frequencies as to have its interaction with the background material be of negligible proportions. On the other hand let the properties of the lattice elements be such as to provide significant interaction with the electromagnetic radiation. Thus for the electromagnetic radiation, if the electric polarization of the array entity, is among other things shape dependent, then the internal vibrations arising from the acoustic radiation will modulate the shape of the lattice element in such a way as to impose a modulation on the scattered electromagnetic flux through the shape dependent polarizability.

Imagine a plane wave $E_o = E_{oo} \exp[i(k_o \cdot x - wt)]$ incident on the matrix array. Simultaneously let an acoustic pulse fall on the array as shown in Fig. 1.

Let
$$P_\ell = \alpha_\ell E_o \tag{1}$$

where P_ℓ is the polarization of the individual (ℓth) lattice element and α_ℓ its polarizability.

Imagine the acoustic pulse to contain appropriate frequency components with enough amplitude to set up oscillations in the individual array elements. Suppose as noted above that such oscillations induce shape changes which cause a change in the polarization P.

For these circumstances α_ℓ becomes a function of time. Hence for a given array element

$$\alpha_\ell = \alpha_\ell^s + [\alpha_\ell^E(t) - \alpha_\ell^s]\, H(t-t_\ell) \tag{2}$$

where α_ℓ^s is the undistorted lattice element polarizability and $\alpha_\ell^E(t)$ is the portion of the polarizability due to the distortion of the lattice element. $H(t-t_\ell)$ is the Heaviside function. t_ℓ is the arrival time of the acoustic pulse at the ℓ^{th} array element.

If the array is of finite length the scattered electromagnetic field in the dipole approximation is

$$E_{sc} = \frac{E_{oo}}{\varepsilon_o} \sum_{\ell=1}^{N} \frac{k^2 \alpha_\ell(t)}{r - x_\ell} \exp[i(k\cdot(r-x_\ell) - wt)] \tag{3}$$

where N is the number of the lattice elements. r is the distance to the point of observation. x_ℓ is the distance to ℓ^{th} element. As usual k is the spatial and w the temporal frequency.

Putting (2) in (3) one has

$$E_{sc} = \frac{E_{oo}}{\varepsilon_o} \sum_{\ell} \frac{k^2}{r-x_\ell} [\alpha^s_\ell + (\alpha^E_\ell(t) - \alpha^s_\ell)H(t-t_\ell)] \quad x$$

$$\exp[i(k\cdot(r-x_\ell)-wt)]$$

$$= {}^sE_{sc} + \frac{E_{oo}}{\varepsilon_o} \sum_{\ell} \frac{k^2}{r-x_\ell} (\alpha^E_\ell - \alpha^s_\ell)H(t-t_\ell) \quad x$$

$$\exp[-i(k\cdot(r-x_\ell)-wt)] \qquad (4)$$

where

$${}^sE_{sc} = \frac{E_{oo}}{\varepsilon_o} \sum_{\ell} (k^2\alpha^s_\ell / r-x_\ell) \exp[i(k\cdot(r-x_\ell)-wt)] \qquad (5)$$

${}^sE_{sc}$ would be the total scattered field were there no mechanical oscillations of the array elements.

Now anticipating a spectral analysis let

$$H(t-t_\ell) = \frac{1}{2\pi i} \int_{-oo}^{oo} \frac{\exp[i(t-t_\ell)]y}{y} dy \qquad (6)$$

Furthermore let the individual polarizability element when it is distorted be expressed as a series expansion over the normal modes of the internal mechanical oscillation of the array element.

Thus let

$$\alpha^E_\ell = \alpha^s_\ell + \sum_m \alpha_{\ell_m} \exp iw'_m t \qquad (7)$$

(Since damping is present w'_m is complex. Let $w'_m = w_m + i\beta_m$.

Now rewriting (4) including (5) (6) and (7)

$$E_{sc} = {}^sE_{sc} + \frac{E_{oo}}{\varepsilon_o} \frac{k^2}{2\pi i} \int_{-oo}^{oo} \frac{dy}{y} \sum_{\ell=1}^{N} \sum_{m=o}^{oo} \quad x$$

$$\exp[ik(r-x_\ell)] \frac{\alpha_{\ell m}}{r-x_\ell} \exp[it(w+w'_m+y)]\exp[-iyt_\ell] \qquad (8)$$

To examine the spectral content of E_{sc} we evaluate its fourier transform.

$$\varepsilon_{sc}(w') = \frac{1}{(2\pi)^{\frac{1}{2}}} \int_{-oo}^{oo} E_{sc}(t')\exp[iw't']dt' \qquad (9)$$

This yields, letting $t_\ell = \frac{\ell d}{V_s}$ for equal spacing and size to

$$\varepsilon_{sc}(w') = {}^s\varepsilon_{sc}(w') + \frac{E_{oo}}{\varepsilon_o(2\pi i)} (2\pi)^{\frac{1}{2}} \quad x$$

$$\frac{\exp[ikr]}{r} \sum_{m=o}^{oo} \frac{\alpha_m}{\Gamma_m + i\beta_m} \Bigg\} \Bigg\} \qquad (10)$$

where

$$\Bigg\}\Bigg\} = \frac{\exp[\frac{d}{2V_s}\{[\Gamma_m - kV_s)+i\beta_m\}]\{1-\exp[i\frac{Nd}{V_s}[(\Gamma_m - kV_s)+i\beta_m]]\}}{\sin[\frac{d}{2V_s}[\Gamma_m - kV_s)+i\beta_m]\}}$$

Now as $k = \frac{w}{c}$, $\Gamma - kV_s = w'-w-w_m-w\frac{V_s}{c}$.

Clearly when the term $\Gamma - kV_s$ goes to zero a resonance occurs at $w' = w_m + w(1 + \frac{V_s}{c})$. The magnitude of the resonance is of order N. For one case of practical interest $w_{m=2} \simeq 100$ Hertz and $w\frac{V_s}{c} \simeq 10^4$ Hertz. Thus as a result of the acoustically shifted frequency one has side bands. One clearly expects the presence of β_m to broaden the frequency band of the return signal and a side band at w_m. However this sideband frequency shifted fractionally from the incident electromagnetic field in the additional amount of the ratio of V_s/c is clearly unexpected as there is no translatory motion such as would be required by the Doppler effect. Only a phase of mechanical oscillation is propagating through the array at the speed V_s. From this arises the parametric interaction which gives rise to the frequency shift high-lighted here.

Atmospheric applications will be discussed.

SUBMILLIMETER WAVE PROPAGATION MEASUREMENT TECHNIQUES

Stephen L. Johnston
Professional Engineer
4015 Devon Street, S. E.
Huntsville, Alabama - 35802

Introduction

Exploration and utilization of a new part of the electromagnetic spectrum requires knowledge of the propagation characteristics of that region. Theoretical studies are necessary to predict what is to be expected; however, experimental propagation measurements are needed to verify the validity of the theoretical studies. Experimental measurements require that adequate apparatus for the region under study be available. While fully adequate apparatus is desirable, frequently valuable (although limited) data can be obtained from very rudimentary apparatus. Many years before the microwave region achieved adequate apparatus, Hertz through his classical experiments in 1889 generated 60 centimeter waves using a spark gap transmitter.

The submillimeter region (variously defined as wavelengths in the region of about 1 mm to 10um) is the last electromagnetic frontier. Several theoretical studies have been conducted on propagation characteristics of this region. Experimental measurements have been beset by two problems; apparatus availability and the nature of the region itself. Both detector (receiver) and RF signal sources have been a problem. While considerable progress has been made in each of these areas, currently available apparatus still does not permit making all the propagation measurements that are needed for this region. This region is characterized by much higher attenuation than the centimeter region. Greater receiver sensitivity and/or power output of RF sources are needed in this region. Present apparatus characteristics have permitted a number of propagation measurements to be made however. While several papers have addressed comparison of theoretical and experimental SMM propagation data, usually the various measurement techniques have been described only in individual papers on measurement results. However, measurement techniques are important both as a guide in assessment of resulting data and in the planning of additional measurements to be made. Measurement conditions, e.g., path description, and technical characteristics of the measurement apparatus are of further interest. This paper will survey SMM measurement techniques used by various workers, to date, and will discuss various aspects of their techniques.

Data Base and Frequency Region

During the performance of a recent SMM radar preliminary design study, propagation data from experimental measurements of others were needed for use in the radar performance analysis and in selection of the radar frequency. A literature search by Dr. Dorathy Stewart identified over 50 papers on SMM wave propagation. This included both theoretical computations and experimental measurements from 1.4 mm to 100 um wavelength. From this collection, only those papers containing experimental measurements in the frequency region that are anticipated for the experimental radar were selected.

Lasers have been operated at many discrete lines in the submillimeter region with average powers at some lines on the order of 10mW. While that power is adequate for some purposes, higher power is desirable. About 20 dB greater power output has been achieved from RF tubes in the vicinity of 1 mm.

RF sources at 280 GHz (Varian Extended Interaction Oscillator - proposed 1W CW, 10W pulsed) and 290 GHz (Thompson - CSF Carcinotron, 1W CW with lesser powers up to 600 GHz) and 5 mW at 220 GHz (Varian Klystron) caused interest to be centered in the 200-300 GHz region. For convenience, the octave 180-360 GHz was chosen for this paper. Techniques have been used in this region which have not been used yet in the shorter wavelength portions of the SMM band.

Twenty-six references pertaining to propagation measurements/apparatus in this octave were identified. Even though this is a relatively small number of papers, it is believed to be representative of work done in this region. Review of these papers indicated that they could be classified either by measurement purpose or by measurement techniques. The former included atmospheric attenuation, rain attenuation, snow attenuation, solar spectrum, H_2O absorption, etc.

Measurement Techniques

Measurement techniques were used of four basic types - outdoor direct, outdoor reflectivity, indoor chamber and radiometer. A graph showing measurement frequencies and measurement techniques used for these 26 measurements is contained in the accompanying figure. Frequencies which have been allocated in this octave by the World Administrative Radio Conference on Space Telecommunications (WARC/ST) are also on the chart.

This paper will discuss these measurement techniques, and will give characteristics of apparatus used along with factors to be conwidered in using these techniques. Some special implementation of these techniques will be shown. Finally, certain propagation measurements which are needed for the submillimeter region will be cited.

This paper represents the individual views of the author only and specifically should not be considered a position of the U. S. Army Missile Command or the United States Army.

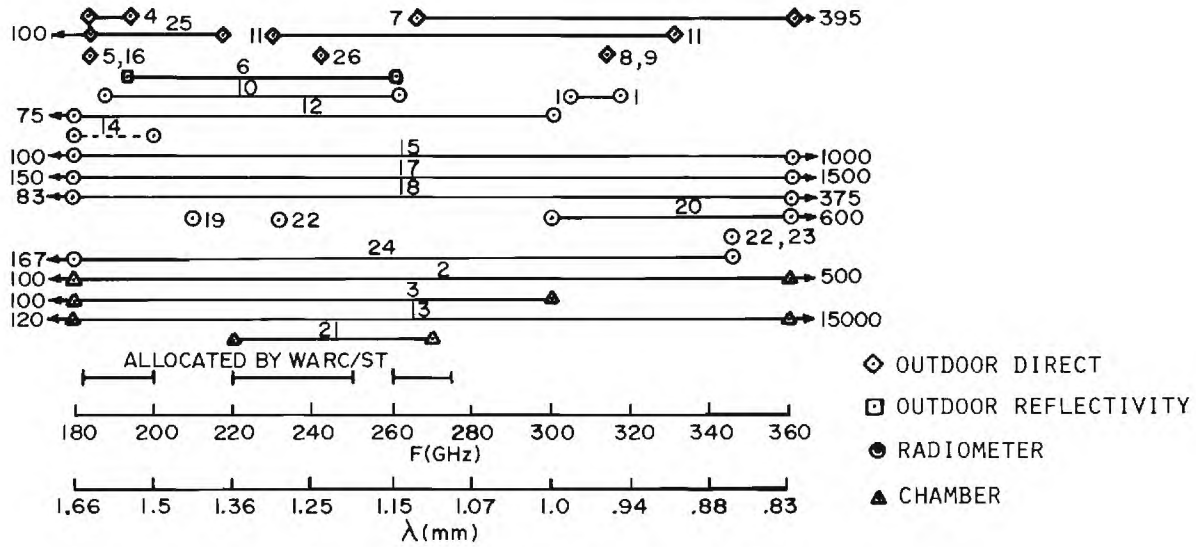

FREQUENCIES AND TECHNIQUES USED IN SUBMILLIMETER ATMOSPHERIC ATTENUATION MEASUREMENTS

References

1. Shurman Y. Chang and James D. Lester, "Performance Characteristics of a 300 GHz Radiometer and Some Atmospheric Attenuation Measurements," IEEE Trans. AP, Vol. AP-16, No. 5, pp 588-591, Sept. 1968.

2. R. Emery, "Atmospheric Absorption Measurements in The Region of 1mm Wavelength," Infrared Phy., Vol. 12, pp 65-79, 1972.

3. L. Frankel and D. Woods, "The Microwave Absorption by H_2O Vapor and Its Mixtures With Other Gases Between 100 and 300 Gc/s," IEE Proc. (G.B.), Vol. 54, pp 498-505, 1966.

4. G. T. Coats, R. A. Bond and C. W. Tolbert, "Propagation Measurement In The Vicinity of the 183 Gc/s Water Vapor Line," Electr. Eng. Res. Lab U. of Tx., Report 7-20, Feb. 5, 1962.

5. T. W. Whaley, Jr. and B. M. Fannin, "Characteristics of Free Space Propagation Near The 183 GHz H_2O Line," IEEE Trans. AP, Vol. AP-17, pp 682-684, Sept. 1969.

6. V. Ya Ryadov and N. I. Furashov, "Investigation of The Spectrum of Radiowave Absorption by Atmospheric Water Vapor in The 1.15 - 1.5mm Range," Radiophys. & Quantum Electron, Vol. 15, No. 10, pp 1124-1128, October 1, 1974.

7. V. Ya Ryadov and N. I. Furashov, "Measurement of the Atmospheric Absorption of Radio Waves in the Range 0.76 - 1.15mm," Radiophys. and Quantum Electron, Vol. 9, No. 5, pp 504-507, 1966.

8. Yu.S. Babkin, et al, "Measurement of Attenuation in Rain Over 1Km Path At a Wavelength of 0.96mm," Radio Eng. and Electron Phys., Vol. 15, No. 12, pp 2164-2166, 1970.

9. Yu.S. Babkin, et al, "Attenuation of Radiation at a Wavelength of 0.96mm in Snow," Radio Eng. and Electron. Phy., Vol. 15, No. 12, pp 2171-2174, 1970.

10. A. S. Vardanyan et al, "Measurements of the 980-1600um Atmospheric Absorption by Radioastronomical Means," Radio Eng. and Electron. Phys., Vol. 18, No. 2, pp 163-165, 1973.

11. Yu. I. Malyshenko and I. Kh. Vakser, "Measurement of the Attenuation Coefficient of 1.3 and 0.86mm Radio Waves in Rain," Radiophys., Vol. 14, No. 6, pp 755-757, June 1971.

12. J. A. Bastin et al, "Spectroscopy at Extreme Infrared Wavelengths III Astrophysics and Atmospheric Measurements," Proc. R. Soc., Vol A 278, pp 543-573, 1964.

13. N. G. Yaroslavsky and A. E. Stanevich, "The Long Wavelength Infrared Spectrum of H_2O Vapor and the Absorption Spectrum of Atmospheric Air in the Region 20-2500u (500-4cm^{-1})," Opt. and Spectrosc., Vol. 7, pp 380-382, 1958.

14. Georgia Tech Radiometer Program, NASA Grant NSG 5012, 1975.

15. H. A. Gebbie, W. J. Burroughs, "Observations of Atmospheric Absorption in the Wavelength Range 2mm to 300uM," Nature, Vol.217,pp 1241-1242, 1968.

16. Yu. I. Malyshenko, "Measuring the Parameters of the 183.31 GHz Water-Vapor Absorption Line in the Surface Atmosphere," Ukr. J. of Phys., Vol.12, No. 8, pp 1317-1322, 1967.
17. J. N. Gaitskell and A. E. Gear, "Solar and Lunar Observations at Submillimeter Wavelengths," Icarus, Vol. 5, pp 237-244, 1966.
18.H.M. Thiessing and P. J. Caplan, "Measurement of the Solar Spectrum," J. Opt. Soc. Am., Vol. 46, pp 971-978, 1956.
19. W. M. Sinton, "Observations of Solar and Lunar Radiation at 1.5 Millimeters," J. Opt. Soc. Am., Vol. 45., pp 975-979, 1955.
20. R. A. Williams, W. S. C. Chang, "Observation of Solar Radiation From 50u to 1mm," Proc. IEEE, Vol. 54, No. 4, pp 462-470, April 1966.
21. J. E. Harries, W. J. Burroughs and H. A. Gebbie, "Millimeter Wavelength Spetroscopic Observations of the Water Dimer in the Vapour Phase," J. Quant. Spectrosc. and Radiat. Trans., Vol. 9, pp 799-807, 1969.
22. Paul F. Goldsmith et al, "Measurement of Atmospheric Attenuation at 1.3 and 0.87 mm with an Harmonic Mixing Radiometer," IEEE Trans., MTT Vol. MTT-22, NR 12, pp 1115-1116, Dec. 1974.
23. V. Ya. Ryadov, N. I. Furashov and G. A. Sharonov, "Measurement of the Atmospheric Transparency to 0.87mm Waves," Radio Eng. and Electr. Phys., Vol. 9, pp 773-778, 1964.
24. L. M. Kukin, L. V. Lubyako and L. I. Fedoseev, "The Measurement of Atmospheric Absorption in the Wavelength Range 1.8 - 0.87mm," Radiophys. and Quantum Electron., Vol. 10, No. 6, pp 407-412, 1967.
25. Yu. A. Dryagan et al, "Measurement of the Atmospheric Absorption of Radio Waves in the Range 1.36 - 3.0mm," Radiophysics and Quantum Electronics, Vol. 9, No. 6, pp 624-627, 1966.
26.Yu. I. Malyshenko, "Measurement of Absorption Coefficient of Water Vapor in the Transparency Window at 1.3mm, Radio Eng. and Electron. Phys., Vol. 14, No. 3, 1969, pp 447-448, 1969.

INFRARED OPTO-ACOUSTIC SPECTROSCOPY OF THE ATMOSPHERE AND THE STRATOSPHERE

C. K. N. Patel
Bell Telephone Laboratories, Incorporated
Murray Hill, New Jersey 07974

SUMMARY

Opto-acoustic spectroscopy - the technique of measuring spectral absorption characteristics of materials by calorimetric means - has come of age with the availability of tunable lasers producing reasonably high powers. Solids, liquids and gases have been studied with this technique in the range from near ultraviolet to the infrared. However, in the present review I shall restrict the discussion to the opto-acoustic spectroscopy of gaseous materials in the infrared region only.

Identification of a gaseous species by the measurement of its infrared absorption spectrum is an established technique. However, generally the absorption measurements involve the determination of the power that is incident into a gas cell and the power that emerges from the cell at a particular wavelength. In this straightforward absorption measurement technique, the smallest fractional absorption, $(P_{in}-P_{out})/P_{in}$ that can be measured is $\approx 10^{-3}$. Thus to identify a gaseous species that is present in very small concentration or to measure the spectra arising from a very weak absorption bands, very long path lengths (tens of meters) are required. The technique of opto-acoustic spectroscopy is characterized by a direct measurement of the quantity $\Delta P = P_{in}-P_{out}$ rather than the measurement of P_{out} and P_{in} from which ΔP is inferred. This well known technique of calorimetry is readily applied to gaseous media when most of the absorbed radiation in the gas is lost by its conversion to translational energy of the gas, i.e. heat, rather than reradiation, a condition that is easily met in the infrared region. The resultant gas pressure increase is detected by using a sensitive microphone. The advantage of the opto-acoustic technique becomes evident when the pressure induced by the absorbed power, ΔP, is large compared to the thermal fluctuations in the gas. Since $\Delta P = P_{in}(1-e^{-\alpha l})$ where α is the absorption coefficient and l is the path length in the cell, ΔP can be made arbitrarily large, for a given αl, by increasing P_{in}. Thus with the advent of high power tunable lasers, measurement of small αl has become considerably easier than that was possible earlier. It is now possible to measure absorption arising from very small concentrations of molecules and spectra arising from weak absorption bands using gas cell path lengths of 10-20 cms.

Infrared opto-acoustic spectroscopy has been carried out with continuously tunable lasers as well as with step tunable lasers. I will discuss both of these techniques and their applications to the problem of spectroscopy and detection of pollution in the atmosphere and stratosphere. The spectroscopic studies involve use of tunable spin flip Raman lasers and have yielded high resolution spectra[1] of molecular species such as NO, H_2O etc. Infrared opto-acoustic spectroscopy of gases is being extended to include 1) the presence of strong magnetic fields to study Zeeman spectra, 2) the presence of strong electric fields to study Stark spectra, 3) high pressures to look for weak pressure induced absorption, and 4) low temperatures to improve the resolution available in the case of Doppler limited spectroscopy.

Infrared opto-acoustic spectroscopy has had a significant impact in the field of pollution detection because of the inherent capability of measuring small αl. Earlier we had shown[2] that NO concentration as small as 10^8 molecules cm^{-3} can be detected (volumetric mixing ratio of 1 part in 3×10^{11} at atmospheric pressure). This capability has been used to study NO concentration on ground[3] as well as in the stratosphere[4]. In the stratosphere our experiments provided the first measurements which have put the theoretical models[5] of catalytic destruction of ozone by nitric oxide on an observational basis.

Step tunable infrared lasers have been used in the infrared opto-acoustic spectroscopy primarily in the area of pollution detection. Because of the intrinsic nature of the tuning method, this scheme is not particularly useful in high resolution spectroscopy (Doppler limited case) since the probability of an exact coincidence between a fixed frequency laser line and an absorbing transition is very small. But for pollution detection on ground, one can take advantage of the pressure broadening of absorption lines to obtain a measurable absorption on a laser line even in absence of good coincidence between the laser line and a nearby absorbing line of the pollutant. The most significant measurements of these types deal with the detection of HCN and NH_3 during the reduction of NO over platinum catalysts[6]. Under certain experimental conditions, very high HCN concentrations have been detected in the bench scale reactor effluent. The results of these bench scale experiments may have some bearing on the problem of catalytic treatment of automobile exhausts.

Finally, I will briefly describe some of the very recent[7] advances in the construction of the opto-acoustic cells which have considerably eased the fabrication difficulties and increased the signal to noise ratio as compared to the earlier versions. I will also discuss the relative merits of other schemes, e.g. wavelength modulation scheme, for detection of small αl.

REFERENCES

1. C. K. N. Patel in *Coherence and Quantum Optics*, ed. L. Mandel and E. Wolf (Plenum Press, 1973) pp. 567-593.

2. C. K. N. Patel in *Laser Spectroscopy*, ed. R. G. Brewer and A. Mooradian (Plenum Press) pp. 471-491.

3. L. B. Kreuzer and C. K. N. Patel, *Science* **173**, 45 (1971).

4. C. K. N. Patel, *Optical and Quantum Electronics* **8**, 145 (1976).

5. P. J. Creutzen, *J. Geophys. Research* **76**,7311 (1971); H. Johnston, *Science* **173**, 517 (1971).

6. R. J. H. Voorhoeve, C. K. N. Patel, L. E. Trimble and R. J. Kerl, *Science* **190**, 149 (1975); *J. Catalysis* (to be published).

7. C. K. N. Patel and R. J. Kerl (unpublished).

SHORT AND INTENSE SUBMILLIMETER PULSES PRODUCED BY REFLECTION OF MICROWAVES ON THE FRONT OF AN INTENSE RELATIVISTIC ELECTRON BEAM

H.J. Doucet
Laboratoire de Physique des Milieux Ionisés
Groupe de Recherche du C.N.R.S.
Ecole Polytechnique, Palaiseau, 91120, France

Introduction

Relativistic Doppler effects have been proposed several years ago for conversion of centimetric electromagnetic waves to millimetric or submillimetric waves by reflection on a mirror at a velocity close to the speed of light [1].

Electron beams have been used to produce such a fast moving mirror under particular conditions to be able to reflect the incident electromagnetic wave : the Compton effect have been suggested as a scattering mechanism [2] [3], but this yields an extremely weak reflection probability, and thus an inefficient device. Collective properties of intense relativistic electron beams can provide more efficient mechanisms : nonlinear processes such as Raman scattering enhanced by a resonance effect at the cyclotron frequency have been used in an attempt to explain the observed emission of intense infrared light [4]. Such nonlinear processes still yield a too small reflection probability and thus it seems difficult to design any pratical device based upon this phenomenon.

A more promising mechanism could be based on a linear reflection from the fast refractive index variation of the beam front of an intense R.E.B. [5]. Experimental evidence of such processes have already been demonstrated by a frequency conversion of microwaves [6], [7]. In the present talk we will discuss beam parameters and limiting factors in view of producing practical generators of very intense and short submillimeter and infrared pulses.

Relativistic Doppler Effect

The relativistic Doppler frequency shift resulting from the reflection of an electromagnetic wave on a beam front is well known. The frequency and photon energy are enhanced by a factor $(1 + \beta)^2 \gamma^2$, the pulse power is enhanced by a factor $(1 + \beta)^4 \gamma^4$ and the pulse length is reduced by the frequency ratio [1], [5], [6].

Cut-off mechanisms in infinite medium

When the beam diameter is much larger than the wavelength in the beam frame, the conditions of reflection can be described as for an infinite medium.

1. Plasma frequency cut-off. Such a cut-off can be used without external magnetic fields. Beam parameters and diffraction effects are such that this yields a rather good diagnostic of beam foccus sing but no practical device. Charge and current neutralisation can be very useful [8] if a low pressure gas is used.

2. Right-mode cut-off. In the presence of an intense external magnetic field, the frequency band between the cyclotron frequency and the cut-off of the right hand mode can be used. The effect of the self magnetic field of the beam has to be included. The reflection generally occurs on a small part of the beam and finite size effects have to be taken into account.

Interaction length and signal coherence

The elementary description of a fast moving front of refractive index variation needs to be corrected for important effects : the classical refractive index of a cold plasma is a description of the asymptotic response of the plasma to a given field perturbation but transient plasma behavior also has to be included. The interaction length is computed and found to be compatible with most of the beam conditions. The coherence of the reflected signal is also described in terms of density gradient effects which decrease the reflection probability, and diffraction effects which limit the interest of the possible use of beam focusing.

Reflection via a REB traveling in a waveguide

The introduction of an electron beam into a waveguide modifies the dispersion relation and can yield reflection [6]. Perturbation theories have been intensively used to predict the behavior of an electron filled waveguide [9]. An interesting and simple image of the waveguide behavior with a high density electron beam can be found by using a coaxial waveguide picture where the inner conductor is an electron beam considered as a perfect conductor. This description show the interest of TE modes and takes into account the electron beam-front velocity decrease due to magnetic energy production in the waveguide. Optimum conditions can be found with reasonable eam beam parameters.

Conclusions

Despite the rather crude theory of the reflection of an electromagnetic wave at a beam front, the frequency conversion due to the relativistic Doppler effect seems to be a very promising way of producing short and intense pulses of

millimeter, submillimeter and infrared electromagnetic waves.

The recent experimental evidence for this phenomenon show the need for a better description including the calculation of the reflection probability and frequency spectrum for realistic beam conditions.

This technique could yield in a near future the possible generation of tunable Gigawatt or Terawatt for a very short pulse (a few ps) in the far infrared (10 μ to 100 μ). The limiting factor would be mostly due to the beam rise time and no really coherent and monochromatic wave can be seriously expected for large frequency conversion despite the coherence of the microwave source signal used.

Références

1 - K. Landecker, Phys. Rev. 86, 852 (1952)

2 - R.H. Pantell, G. Soncini and H.E. Puthoff, IEEE, J. Quantum Electronics, QE - 4, 11, 905 (1968)

3 - G. Mourier, Brevet : 7218034 - May 1972
US. Patent : 360416 - May 1973

4 - Granatstein et al. IEEE Trans. MTT 22, 1000, (1974)

5 - H.J. Doucet - Advisory group meeting on experimental aspects of laser - electron beam produced thermonuclear plasmas. Trieste, 25-29 August 1975

6 - V.L. Granatstein, R.K. Parker, P. Sprangle, International Topical Conference on Electron Beam Research and Technology, Vol. II p 401, SAND 76-5122, (1976)
V.L. Granatstein et al. - private communication from S.P. Schlesinger - to be published in Phys. Rev. (1976)

7 - H.J. Doucet - H. Lamain - C. Rouillé - J.L. Faure - J.M. Buzzi and N. Camarcat Bull. Am. Phys. Soc. 20, 1290 (1975)

8 - H.J. Doucet - Brevet D. 10966 janv. 1976

9 - E. Ott and W.M. Manheimer NRL Report 2687 (dec. 1973)

EXPERIMENTAL EVIDENCE OF RELATIVISTIC DOPPLER FREQUENCY CONVERSION ON A RELATIVISTIC ELECTRON BEAM FRONT

J.M. Buzzi, H.J. Doucet, J.C.Faure*, H.Lamain, C.Rouillé
Laboratoire de Physique des Milieux Ionisés
Groupe de Recherche du C.N.R.S.
Ecole Polytechnique, Palaiseau, 91120 France

and

J.C.Cabé, J.Delvaux, J.C.Jouys, C.Peugnet, M.Roche
Commissariat à l'Energie Atomique
Centre d'Etudes de Valduc, Is sur Tille, 21120 France

Relativistic Doppler frequency shift by a relativistic mirror of intense microwaves pulses appears as an efficient process for the generation of submillimeter waves at high energy level. The ability of electron beams to be used as a relativistic mirror for microwaves has been studied experimentally in two different situations : (a) in the case of a high impedance REB device (43Ω) and (b) with a low impedance REB machine (2Ω). The REB being an interesting and very powerful microwave generator is used as well as the microwave pulse source and as the relativistic mirror.

Experiment with a high impedance device

The first serie of experiment is performed on a synchrotron maser [1] using a 43 Ohms line delivering an electron beam (Physics International, Pulserad 110A). The electron energy is variable from 0.5 to 1.5 MV. The synchrotron maser is used as a source of intense microwave pulse (1 to 10 MW, 5 to 10 ns), in 3 cm wavelength and also as a relativistic mirror. The complete process of the frequency conversion experiment is understood as follow :

A microwave single pulse or sometimes series of successive microwaves short pulses are produced in a circular 5cm diameter waveguide of the synchrotron maser during the erection time of the current (5 to 10 ns). The microwave is emitted through a teflon window and transmitted to free space via a large conical horn. The microwave pulse is then reflected on a metallic sheet at a variable distance from the source. Part of the reflected signal comes back into the synchrotron maser waveguide at the arrival time of a higher beam density. A second reflection associated with a Doppler relativistic frequency shift is then expected to occur.

The reflection mechanism on the electron beam is understood as an increase of the cut-off frequency of the waveguide as a function of time. The emission starts with a frequency ω slightly higher than the cut-off frequency of the empty waveguide ω_∞ [2] :

$$\omega = \gamma_{//}\, \omega_\infty \text{ with } \gamma_{//}=(1-\beta_{//}^2)^{-\frac{1}{2}} \text{ and } \beta_{//}=v_{//}/c$$

where $v_{//}$ is the parallel electron velocity. When the beam density increases, the cut-off frequency ω_∞' reaches the initial emission frequency ω. Therefore, when the microwave pulse is reflected back in the waveguide, it can be reflected by the beam if a proper delay is given between the emission and the reflection, by adjusting the position of the external mirror.

The frequency ω_1 of the reflected pulse is shifted by the relativistic Doppler effect : [3]

$$\omega_1 = \omega\,(1+\beta_{//})^2\,\gamma_{//}^2$$

Moreover the duration τ_1 of the reflected pulse is reduced with respect to the duration τ of a short emission pulse

$$\tau_1 = \tau\,\frac{\omega}{\omega_1}$$

Conversion frequency from the X band to the Ka band have been observed in qualitative agreement with the expected beam front velocity. Moreover, the pulse compression has been qualitatively observed from correlation between the pulse shapes of the X band signals and of the Ka band signals. The emission in the X band appears as series of a few spikes. Very similar spikes succession is observed in the Ka band but with a shorter time delay between spikes. The ratio between these time delays in the X band and in the Ka band is approximatively equal to the frequency ratio as expected. This ratio is also found to be the same for the corresponding spikes widths in the two bands.

Experiment with a low impedance device

The second set of experiments is performed with a 2 Ohms line generator with electron energy of 400 kV. The electron beam is injected in a 5cm diameter pipe in a gaz at low pressure (air, 5 microns to 1 Torr). In this configuration a very intense, narrow band emission, is observed around 10 GHz. This strong emission, as in the previous experiment, is used as a microwave source and is then reflected back in the device. One fraction of the emitted 10 Ghz signal is transmitted to free space through a conical horn. This signal is detected by an antenna and measured using a dispersive delay line in the X band. The second fraction of the emission is transmitted to a rectangular regular waveguide via a circular to rectangular 3db coupler. While observing the emission, the rectangular waveguide is connected to a matched load and introduces no reflection in the circular waveguide. While observing the reflection on the electron beam, the rectangular waveguide of variable length is terminated by a short circuit. When a proper length is used (approximatively 2 m), the observed spectrum on the delay line contains new frequencies shifted from the emission frequencies by a factor of about 1.1. This frequency shift is compatible with the expected beam front velocity observed in other experiments [4] in gases for pressure below 0.1 Torr where ion acceleration occurs. Therefore this Doppler frequency shift appears as a new diagnostic tool for beam propagation studies among the classical diagnostics used in this experiment : B_0 probes, X rays fluorescence and calorimetry.

Conclusions

These preliminary results indicate that the reflection of microwaves by relativistic electron beams is an interesting possibility for frequency conversion and could be used for generating high power pulses of submillimeter waves.

In our experiments, the use of the same REB as a microwave source and as a relativistic mirror is a limiting factor in the observation of large frequency change because the conditions for emission are obviously not optimum for the reflection.

References

-1- V.L. Granatstein, P. Sprangle, R.K. Parker, and M. Herndon, Journ. of Appl. Physics, 46, 2021, (1975)

-2- E. Ott and W.M. Manheimer
NRL Report 2687 (dec. 1973)

-3- K. Landecker, Phys. Rev. 86, 852 (1952)

-4- C.L. Olson, Phys. Fluids 18, 585 and 598 (1975).

SUBMILLIMETER OSCILLATOR-AMPLIFIER SYSTEMS

D. P. Hutchinson
Oak Ridge National Laboratory*
Oak Ridge, Tennessee 37830

The topics which will be considered by the Oscillator-Amplifier Discussion Group will include suppression of spurious oscillator output, i.e. ouput at adjacent K levels, suppression of superradiance in a pulsed FIR amplifier and control of FIR pulse shape. Because of its verified high power output, emphasis will be placed on CH_3F lasers; however, due to the rapidly expanding nature of FIR research transitions of other gases will also be discussed.

---

*Operated by Union Carbide Corporation for the U.S. Energy Research and Development Administration.

DESIGN AND FABRICATION OF SCHOTTKY-BARRIER DIODES FOR SUBMILLIMETER WAVE APPLICATIONS**

G.T.Wrixon
Department of Electrical Engineering
University College, Cork
Ireland

ABSTRACT

Factors that play a role in the realization of Schottky-barrier diodes for use as low noise,low conversion loss elements at submillimeter wavelengths are discussed. Fabrication techniques including the use of plasma processing,ion-beam milling and electron beam lithography are also covered.

The cut-off frequency $f_c\{=(2\pi R_s C_o)^{-1}\}$ of a Schottky-barrier diode varies as r^{-n}, where usually $n \gtrsim 1$. In order to use these diodes at submillimeter wavelengths the radius r must be reduced. As r is reduced,however,R_s increases. This leads to a number of undesirable effects: (a) More signal and LO power is dissipated in R_s,leading to heat production and excess thermal noise; (b) good impedance matching,necessary for low conversion loss, becomes difficult to achieve[1]; (c) scattering noise,which varies as the current density increases[2].

It has been found experimentally[3] that an R_s of greater than $\sim 10\Omega$ leads to unsatisfactory noise figure performance of diodes in millimeter mixer circuits. With GaAs epilayers of $\sim 2 \times 10^{17}$/cc doping and 0.2μM thickness,an R_s of 10Ω is achieved when the diode diameter is $\sim 1.5\mu M$. This results in an f_c of about 3000 GHz*. Although higher cut-off frequency can be made by further reduction of the diode diameter, such diodes will have degraded noise and conversion loss performance because of the factors listed above.

Alternative methods of increasing f_c above this value,which do not result in degraded performance,include the use of electron beam lithography,to distribute the diode area. This cuts down on current crowding and decreases R_s. Increases in f_c of up to 40% have been obtained using this technique[4]. Use of a higher mobility material such as InSb can also be considered; however severe technical difficulties in the diode fabrication first need to be overcome.

When electron beam lithography is used in diode fabrication it is necessary to etch strips of width 0.2μM. Conventional chemical techniques are inadequate for this purpose as undercutting of the electron resist leads to a large increase in etched area. Under these conditions, the use of energetic ion etching techniques,either plasma or ion-beam, is imperative. Use of plasma etching techniques is particularly attractive because of their flexibility, different gases,e.g. Freon 12 and 14, being used to etch the native GaAs oxide and SiO_2 respectively, while an O_2 plasma is used for organic ashing. Plasma etching gives vertically etched sidewalls with no undercutting. This not only reduces diode contacting capacitance but decreases diode noise by eliminating any thin interfacial dielectric layer.

*In order not to be conversion loss limited,one should not operate the diodes at frequencies greater than $f_c/10$. However, with proper impedance matching,it is possible to operate the diodes up to frequencies as high as f_c with only a 3 to 4 dB degradation in conversion loss.

References

1. F.Bernues,H.J.Kuno and P.A.Crandell, Microwaves,March 1976,p.46.
2. A.R.Kerr and R.J.Mattauch,private communication.
3. G.T.Wrixon, IEEE Trans.MTT,Vol. MTT-22,No.12,December 1974.
4. G.T.Wrixon and R.F.W.Pease,Inst.of Physics Conference,Series No. 24 (1975)

**This work is supported by the European Millimeter Diode Laboratory.

SUBMILLIMETER MIXERS*

G.T.Wrixon
Department of Electrical Engineering
University College, Cork
Ireland

ABSTRACT

Mixer performance at submillimeter wavelengths is currently limited by insufficient LO pump power. The use of subharmonically pumped mixers incorporating low capacitance diodes appears to offer a solution.

*This work was carried out at the Engineering Experiment Station,Georgia Institute of Technology,Atlanta,Ga. under NASA Grant No.NSG-5012

A number of factors combine to impede the realization of low noise,low conversion loss mixers at submillimeter wavelengths. Chief among these is the lack of suitable sources of local oscillator (LO) power. In addition,methods of conveying the LO power to the non-linear mixing element,either by injection cavity, directional filter or balancing scheme, are difficult to implement because of the extremely small dimensions of submillimeter circuits.

Subharmonic mixers[1] have a decided advantage over conventional mixers operating at these wavelengths for the following reasons.

(i) The local oscillator frequency is one-half (or one-quarter) that needed in conventional mixers.

(ii) No high-Q injection system or mechanically difficult balancing scheme is needed.

(iii) A small amount of local oscillator power, 10-15 mW,is sufficient[2].

(iv) The local oscillator AM noise sidebands are suppressed[3].

(v) No d.c. return path is needed in order to apply bias to the diode.

As an example of (iv),Fig.1 shows the calculated noise improvement η (in dB) for a subharmonic mixer at 183 GHz over a fundamental mixer at 183 GHz, using local oscillator with similar AM noise characteristics.

Up to now subharmonic mixers have been built using beam-lead diodes,as these are conveniently incorporated into the stripline integrated circuits which comprise the mixer. The use of beam lead devices,however,limits the use of subharmonic mixers to applications at frequencies less than 100 GHz. At higher frequencies,the unavoidable overlay capacitance of the beam lead ($\sim$.02-.03 pF) gives rise to a low impedance path in parallel with the non-linear diode resistance.

In order to use the subharmonic mixer concept at higher frequencies,low capacitance ($\sim$.007 pF) diode chips must be incorporated directly into the circuit and be contacted by a low capacitance (<.001 pF) pressure type etched contact. Fig.2 shows one way in which this can be implemented. The two diodes are mounted and contacted across the signal waveguide on three pieces of quartz in a manner similar to that used by Kerr[4] in his fundamental cryogenic mixer. The quartz also acts as a substrate for the suspended stripline circuits used in the mixer. Between the LO waveguide and the diodes there is a band-pass filter for the LO power and a band-stop filter for the signal. Between the diodes and the IF output there is a low pass filter for the intermediate frequency (IF) output. The device shown in Fig.2 is currently being modelled at lower frequencies to finalize the design of the transitions,filters and matching networks and,when complete,scaling of the mixer up to 400 GHz (.75 mm) will be possible.

Above 400 GHz a waveguide mount is not feasible and Fig.3 shows a preliminary quasi-optical version of a subharmonic mixer currently also under investigation.

References

1. M.V.Schneider and W.W.Snell,Jr.,IEEE Trans.,MTT,Vol.MTT-23,pp.271-275, March 1975.

2. T.F.McMaster,M.V.Schneider & W.W.Snell Jr., Proc.Int.Microwave Cong.,Cherry Hill,N.J.,1976.

3. P.S.Henry,B.S.Glance and M.V. Schneider, IEEE Trans.,MTT,May 1976.

4. A.R.Kerr, IEEE Trans.,MTT,Vol.MTT-23 No.10,October 1975.

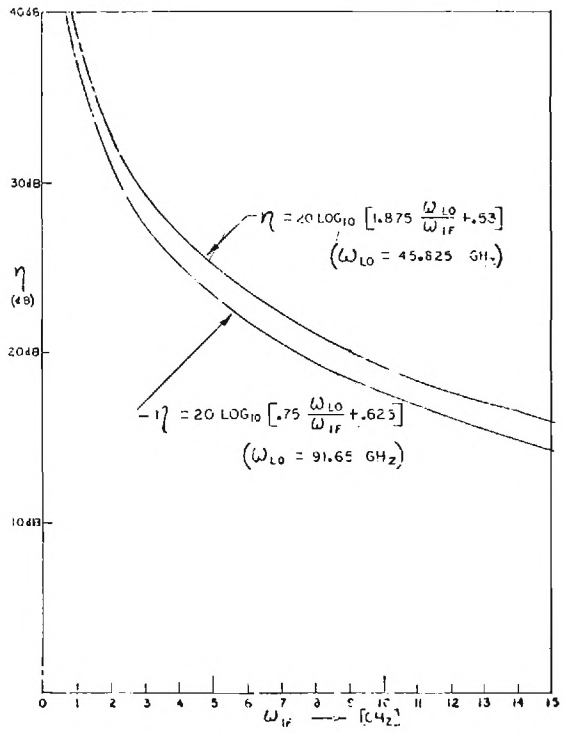

Fig.1: Calculated noise improvement of a subharmonic mixer at 183 GHz pumped at either one half or one quarter its fundamental frequency as a function of intermediate frequency (IF). The relevant formulae can be derived from material contained in Ref.3.

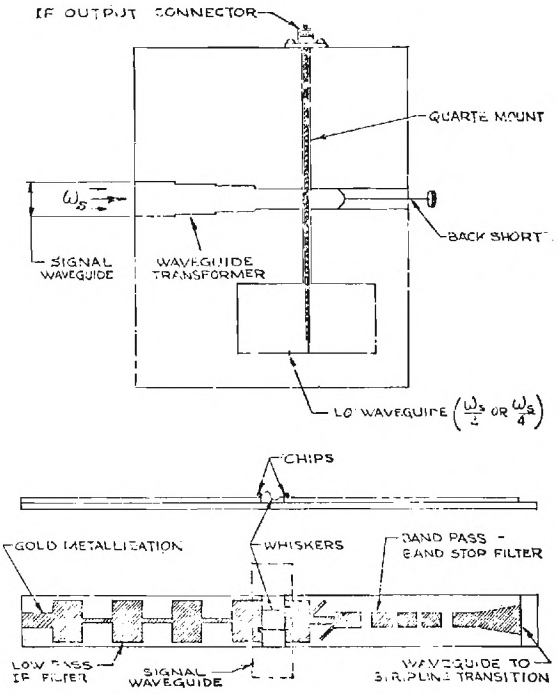

Fig.2: Section through the E-plane of the signal waveguide of a subharmonic mixer which is operable down to a wavelength of 0.75 mm.

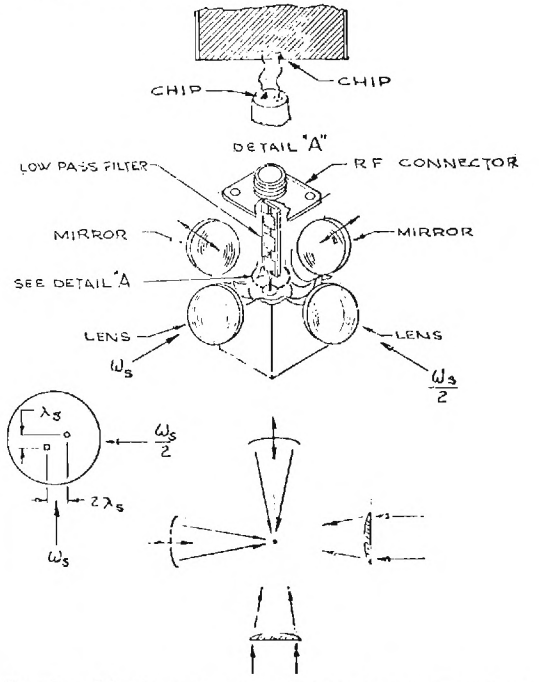

Fig.3: Preliminary quasi-optical version of subharmonic mixer.